JMRI

Journal
of Magnetic
Resonance
Imaging

Published by the Society for Magnetic Resonance Imaging

1993 Annual Meeting Printed Program

Guest Editors
Laurence P Clarke, PhD
Walter Kucharczyk, MD
Jeffrey S Ross, MD
Michael L Wood, PhD

A Supplement to JMRI March / April 1993 Issue, Volume 3(P)

Hitachi. Outstanding in our fields.

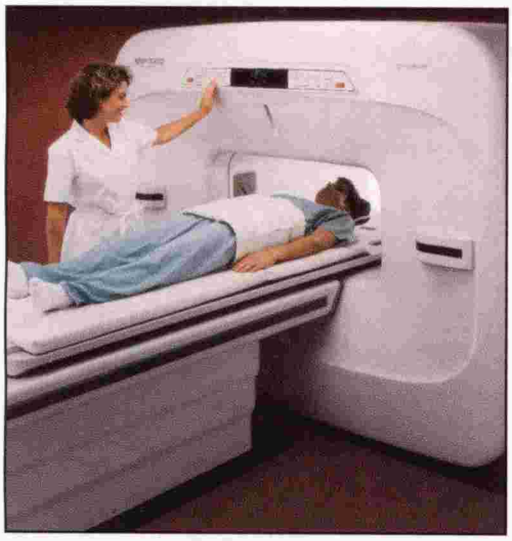

Mid-field

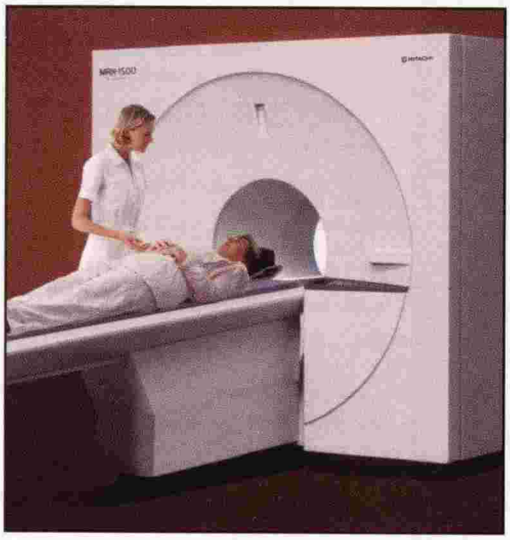

High-field

In both mid-field and high-field magnetic resonance imaging, Hitachi brings a technological capability second to none in the world. In fact, Hitachi is recognized as a premier technology company in the world today. That expertise provides the results you want: superb clinical performance in remarkably cost-effective MRI systems.

Our mid-field MRP-5000 and MRP-7000 systems offer maximum operational flexibility for a broad range of clinical applications and diagnostic procedures. A vertical magnetic field and the latest in Hitachi computer architectural design provide high image quality and maximum throughput for excellent return on investment.

The Hitachi MRH-1500 features 1.5 Tesla field strength using the latest in superconductive magnet technology combined with innovative RF, gradient and computer electronics. Whole-body imaging is accomplished with an extremely efficient system that offers minimal cost of operation.

In either field, you receive all the traditional Hitachi benefits: assured reliability backed by our "98% Uptime Guarantee," easy siting, system upgradeability, and maximum patient comfort. Put the technological strength of Hitachi to work in your facility. Call 1-800-800-3106 for more details about the entire line of Hitachi MR systems.

HITACHI

Hitachi Medical Systems America, Inc.
1963 Case Parkway
Twinsburg, Ohio 44087 USA
Tel: (216) 425-1313
1-800-800-3106
Fax: (216) 425-1410

Hitachi Medical Corporation
Hitachi Hagoromo Bldg.
1-2-10 Uchi-Kanda
Chiyoda-Ku, Tokyo 101, JAPAN
Tel: 033-294-3851
Fax: 033-294-3860

MRH-1500 availability pending FDA 510(k) pre-market clearance.

"Convince them something's needed, and you get the chance to make it happen."

GREGG KURITA
Asst. Mgr./Program Director
Radiology Department
Kaiser Richmond

"I suggested we start a training program for Radiologic Technologists. Now, I'm administrating the program," said Gregg.

We are constantly improving by listening to our people. So as a Radiologic Technologist at Kaiser Permanente in Northern California, you'll have the same opportunity for input — to make suggestions, criticism: to play a major role in shaping our future services.

You'll be part of a team working closely with doctors, nurses and therapists, expanding your knowledge — enjoying a wide choice of opportunities, comprehensive benefits, including tuition reimbursement, and generous vacation.

"People think I'm crazy. But I love my job. I get up in the morning and I want to go to work," said Gregg. "It happens when you work at Kaiser Permanente."

To learn more about our opportunities, benefits, and highly competitive salaries, please call Pamela Woods at 1-800-522-0045. Or write to her at Kaiser Permanente Medical Care Program, Regional Recruitment Services, 1814 Franklin, 5th Floor, Oakland, CA 94612. We are EEO/AA employer.

KAISER PERMANENTE®
Good People. Good Medicine.

A defense against cancer can be cooked up in your kitchen.

There is evidence that diet and cancer are related. Follow these modifications in your daily diet to reduce chances of getting cancer:

1. Eat more high-fiber foods such as fruits and vegetables and whole-grain cereals.
2. Include dark green and deep yellow fruits and vegetables rich in vitamins A and C.
3. Include cabbage, broccoli, brussels sprouts, kohlrabi and cauliflower.
4. Be moderate in consumption of salt-cured, smoked, and nitrite-cured foods.
5. Cut down on total fat intake from animal sources and fats and oils.
6. Avoid obesity.
7. Be moderate in consumption of alcoholic beverages.

No one faces cancer alone.

AMERICAN CANCER SOCIETY®

How to live with someone who's living with cancer.

When one person gets cancer, everyone in the family suffers.

Nobody knows better than we do how much help and understanding is needed. That's why our service and rehabilitation programs emphasize the whole family, not just the cancer patient.

Among our regular services we provide information and guidance to patients and families, transport patients to and from treatment, supply home care items and assist patients in their return to everyday life.

Life is what concerns us. The life of cancer patients. The lives of their families. So you can see we are even more than the research organization we are so well known to be.

No one faces cancer alone.

AMERICAN CANCER SOCIETY®

JMRI Journal of Magnetic Resonance Imaging

Owned and published by the Society for Magnetic Resonance Imaging, and produced with the assistance of the Radiological Society of North America.

Gary D. Fullerton, PhD, Editor-in-Chief
UNIVERSITY OF TEXAS HEALTH SCIENCE CENTER AT SAN ANTONIO

Lou Jean Floyd, PhD, Assistant to the Editor-in-Chief
UNIVERSITY OF TEXAS HEALTH SCIENCE CENTER AT SAN ANTONIO

● ASSOCIATE EDITORS

William G. Bradley, Jr, MD, PhD
Memorial MRI
Long Beach Memorial Medical Center
403 E Columbia St
Long Beach, CA 90806

E. Mark Haacke, PhD
Department of Physics
Case Western Reserve University
Cleveland, OH 44106

Steven E. Harms, MD
Department of Radiology
Baylor University Medical Center
3500 Gaston Ave
Dallas, TX 75246

Anton N. Hasso, MD
Section of Neuroradiology
Loma Linda University Medical Center
Loma Linda, CA 92354

R. Edward Hendrick, PhD
Department of Radiology C278
University of Colorado Health Science Center, Denver, CO 80262

R. Mark Henkelman, PhD
Department of Medical Biophysics
Sunnybrook Health Science Centre
2075 Bayview Ave
North York, Ont
Canada M4N 3M5

Charles B. Higgins, MD
Department of Radiology C-309
UCSF Medical Center
San Francisco, CA 94143

Francis W. Smith, MD
Department of Radiology
Aberdeen Royal Infirmary
Foresterhill, Aberdeen
Scotland

David D. Stark, MD
Department of Radiology
Massachusetts General Hospital
Boston, MA 02114

Michael W. Weiner, MD
Department of Radiology
UCSF Medical Center
San Francisco, CA 94121

Michael L. Wood, PhD
Department of Diagnostic Imaging
St Michael's Hospital
30 Bond St
Toronto, Ont
Canada M5B 1W8

● PULSE AND BOOK REVIEW EDITOR

Jeffrey L. Duerk, PhD
MetroHealth Medical Center
Cleveland

● CONSULTING EDITOR

Stanley S. Siegelman, MD
The Johns Hopkins University School of Medicine and Johns Hopkins Hospital
Baltimore

● EDITORIAL BOARD

Scott W. Atlas, MD
University of Pennsylvania Hospital
Philadelphia

Michael N. Brant-Zawadzki, MD
Hoag Hospital/Newport Harbor
Newport Beach, Calif

R. Nick Bryan, MD
The Johns Hopkins University
School of Medicine, Baltimore

Graeme M. Bydder, MB, ChB
Hammersmith Hospital, London

Laurence P. Clarke, PhD
University of South Florida, Tampa

Mark S. Cohen, PhD
Massachusetts General Hospital
Charleston, Mass

John V. Crues III, MD
Cottage Hospital, Santa Barbara, Calif

Jacques D. DeCertaines, PhD
Laboratoire De RMN, Rennes, France

W. Thomas Dixon, PhD
Emory University School of Medicine
Atlanta

Richard L. Ehman, MD
Mayo Clinic, Rochester, Minn

Margaret A. Foster, PhD
University of Aberdeen
Aberdeen, Scotland

Jens Frahm, PhD
Max Planck Institute
Göttingen, Germany

J. Randy Jinkins, MD
University of Texas Health Science Center, San Antonio, Texas

Peter M. Joseph, PhD
University of Pennsylvania
Philadelphia

Denis Le Bihan, MD, PhD
National Institutes of Health
Bethesda, Md

David N. Levin, MD, PhD
University of Chicago Hospital, Chicago

Robert B. Lufkin, MD
UCLA School of Medicine, Los Angeles

James R. MacFall, PhD
Duke University, Durham, NC

Kenneth R. Maravilla, MD
University of Washington, Seattle

Donald G. Mitchell, MD
Thomas Jefferson University Hospital, Philadelphia

Ponmada A. Narayana, PhD
University of Texas Medical School
Houston

Ray L. Nunnally, PhD
Otsuka Electronics, Fort Collins, Colo

C. Leon Partain, MD, PhD
Vanderbilt University Medical Center
Nashville, Tenn

Roderick I. Pettigrew, MD, PhD
Emory University Hospital, Atlanta

Ronald R. Price, PhD
Vanderbilt University Medical Center
Nashville, Tenn

Stephen J. Riederer, PhD
Mayo Clinic, Rochester, Minn

Peter A. Rinck, PhD
University of Trondheim
Trondheim, Norway

Val M. Runge, MD
University of Kentucky, Lexington, KY

Derek Shaw, PhD
International General Electric Company
Slough Berks, England

Peter M. Som, MD
Mount Sinai Medical Center
New York, NY

Mutsumasa Takahashi, MD
Kumamoto, Japan

Stephen R. Thomas, PhD
University of Cincinnati, Cincinnati

Jeffrey C. Weinreb, MD
NYU Medical Center, New York, NY

Ian R. Young, PhD
GEC Hirst Research Centre, London

MARCH/APRIL 1993 ▪ Volume 3 (P)

1993-1994 MResource Guide

Did you miss out in 1992?

Include yourself in the 1993-1994 Edition…

If you know about specialized MR products, accessories or services, share your sources with MR colleagues by providing this data for publication in the MResource Guide. Please complete the box below and fax this form to the **SMRI** Central Office at 312/951-6474. The information you provide will be published in the MResource Guide in the JMRI September/October 1993-1994 issue.

Product description:

How do you use this product?

Model Number:

Product Manufacturer:

Manufacturer's Address:

Manufacturer's Phone Number and/or Contact Person:

SMRI

Society for Magnetic Resonance Imaging

213 West Institute Place, Suite 501, Chicago, Illinois 60610, Phone 312/751-2590, Fax 312/951-6474

JMRI Journal of Magnetic Resonance Imaging

EDITORIAL

SMRI '93 PROGRAM ABSTRACTS

PLENARY SYMPOSIA

Sunday Morning

Sunday Afternoon

Monday Morning

Monday Afternoon

Tuesday Morning

Tuesday Afternoon

Wednesday Morning

Wednesday Afternoon

PROFFERED PAPER ABSTRACTS

Sunday Morning

Monday Morning

Monday Afternoon

Continued

MARCH/APRIL 1993 ▪ Volume 3 (P)

Proffered Paper Abstracts continued

Tuesday Morning

Tuesday Afternoon

Wednesday Morning

Wednesday Afternoon

POSTER EXHIBIT ABSTRACTS

Sunday

Monday

Tuesday

Wednesday

Contrast Agent Special Issue Order Form

JMRI, the critical link between pharmaceutical manufacturers and the clinical user of medicine, provides yet another important and helpful tool...
the Contrast Agent Special Issue.

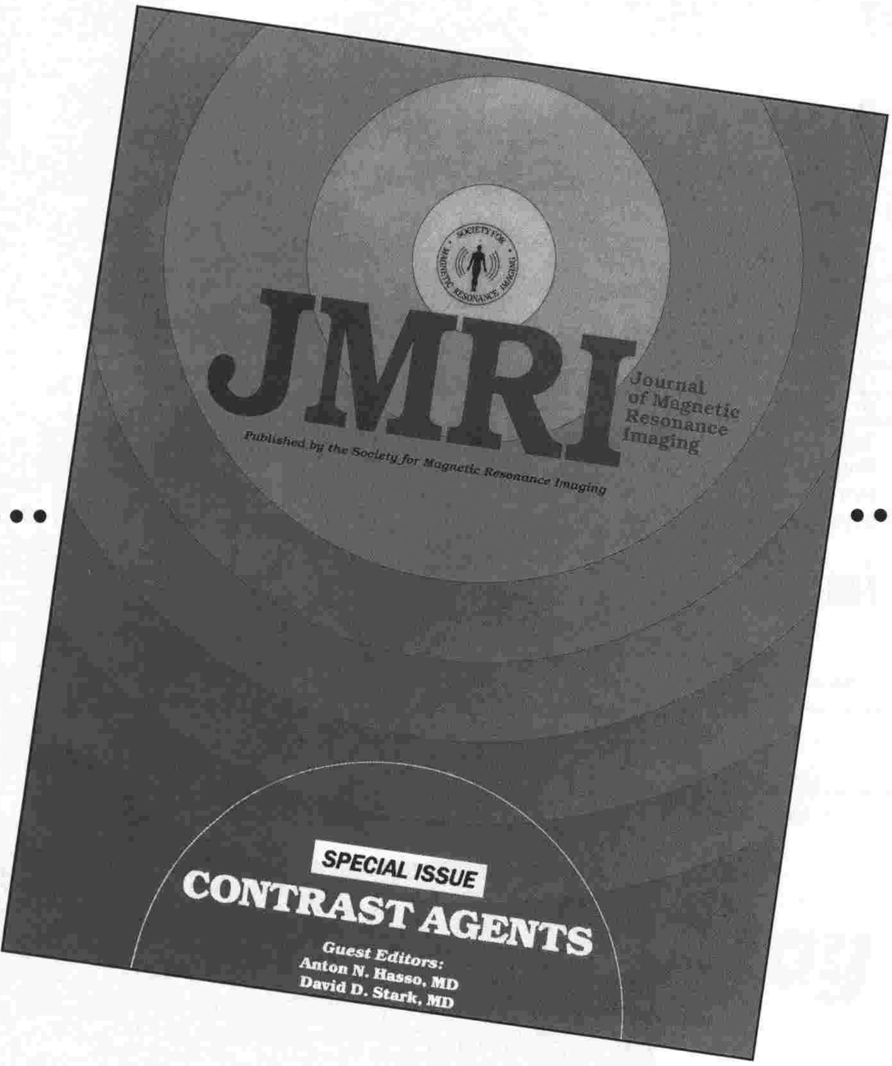

The Contrast Agent Special Issue will be published in the January, 1993 **JMRI** double issue. Additional copies of the issue will be available and may be ordered by faxing this Order Form to the **SMRI** Central Office at 312/951.6474. If questions, call 312/751·2590.

Take *control of a critical variable in magnetic resonance...order your Contrast Agent Special Issue today.*

Number of Issues ☐
@ $25.00 each $
Payment enclosed (U.S. funds only) ☐
MasterCard/Visa ☐

Name
Address

City/State/Zip Code
Country
Phone

Name
Account #/Exp. date

JMRI
Journal of Magnetic Resonance Imaging
213 West Institute Place, Suite 501, Chicago, Illinois 60610, Phone: 312/751.2590 FAX: 312/951.6474

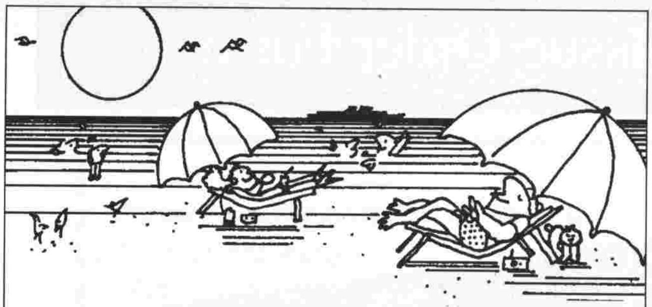

Keep your MRI practice up and running, even when you're not.

Let one of our fully credentialed, experienced MRI specialists step in to cover your practice when you step out… for vacation, CME, or while you recruit a new permanent associate.

We'll pay for malpractice insurance and coordinate all the details like scheduling, licensing, and hospital privileges. Plus, we'll make sure the provider we send is a good match for your particular practice and facility.

Stop by booth #914 (or call us toll-free anytime) to hear more about CompHealth's exclusive services and MRI coverage options.

1-800-328-3085

CompHealth
RADIOLOGY STAFFING

PLEASE VISIT US AT BOOTH #914
Ask about our reduced rate schedule for extended or repeat coverage

The Time Has Come…

…to send for the latest copy of the free Consumer Information Catalog.

It lists more than 200 free or low-cost government publications on topics like money, food, jobs, children, cars, health, and federal benefits.

Send your name and address to:

Consumer Information Center
Department TH
Pueblo, Colorado 81009

A public service of this publication and the Consumer Information Center of the U.S. General Services Administration

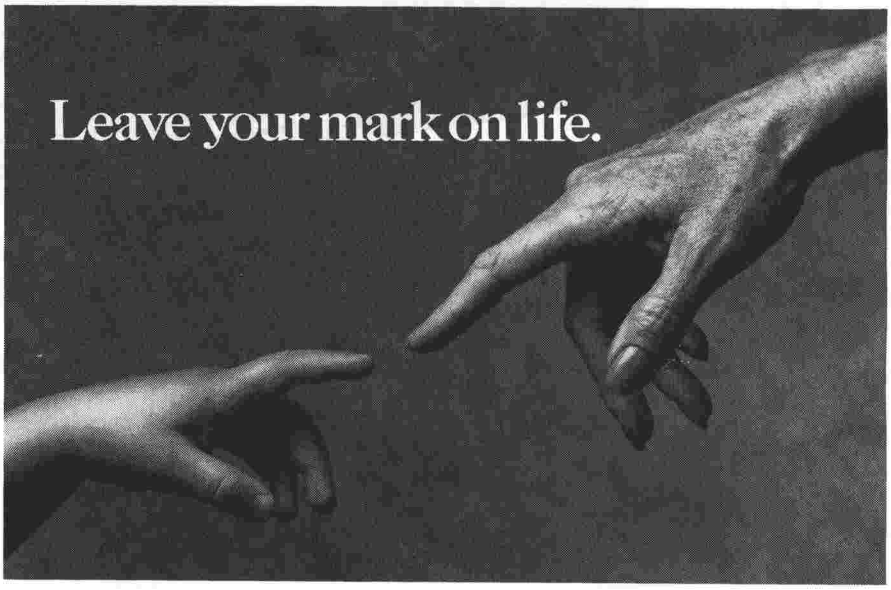

You don't have to move mountains to make a difference on this earth.

By leaving even the smallest legacy to the American Cancer Society in your will, you can leave a loving and lasting impression on life.

And giving life is the greatest way of leaving your mark on it.

AMERICAN CANCER SOCIETY®

For more information, call your local ACS Unit or write to the American Cancer Society, 4 West 35th Street, New York, NY 10001.

VERSA

0.1 mmol/kg ProHance

For Routine Brain & Spine Enhancement

Increases Diagnostic Yield vs. Unenhanced Images

In a multicenter phase III clinical study[1–4] involving 411 patients, ProHance at 0.1 mmol/kg provided:

- Improved lesion detection (36%)[1]
- Improved definition of lesion borders (56%)[1]
- Improved visualization of lesions (63%)[1]

when compared with precontrast brain or spine images.[1]

Proven Safety

During clinical trials, at recommended doses and injection rates, ProHance caused no clinically or statistically significant changes in serum iron or bilirubin.[1] The most common adverse events observed were nausea (1.4%) and taste perversion (1.4%). There were no clinically or statistically significant differences in incidence or intensity of adverse events between recommended doses or injection rates.

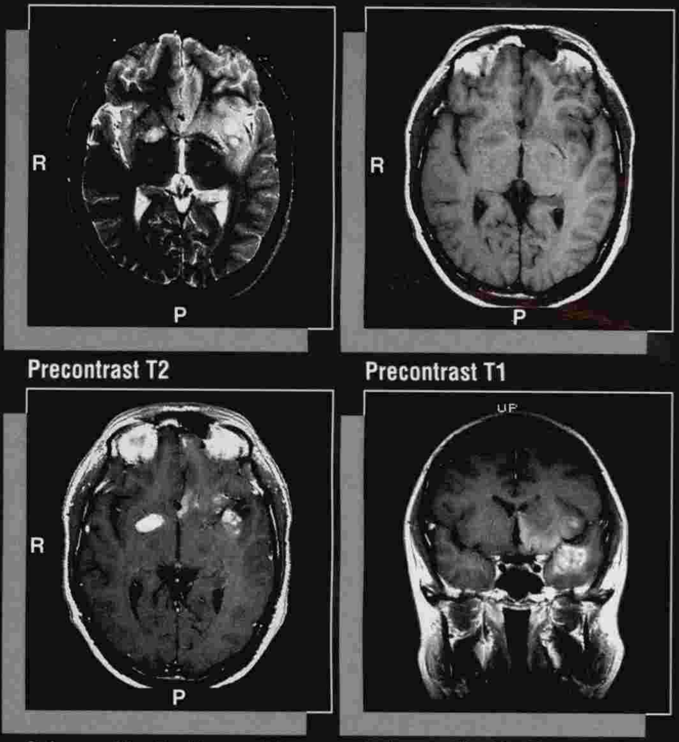

Precontrast T2

Precontrast T1

0.1 mmol/kg ProHance, T1 (axial)

0.1 mmol/kg ProHance, T1 (coronal)

Male, 37 years old with a 1-week history of expressive dysphasia and auras of acrid smell. Postcontrast images show a lesion in the left temporal lobe extending across sylvian fissure into frontal lobe (axial), and a second, apparently detached tumor focus in left temporal region (axial), as well as subependymal spread along 3rd ventricle (coronal). With discovery of extent and location of lesions, open craniotomy was ruled out and stereotactic biopsy was performed. Tumor was multifocal glioblastoma multiforme.[5]

TILITY

Cumulative Administered Dose of 0.3 mmol/kg ProHance*

For Poorly Enhancing Lesions, Negative or Equivocal Scans

Can Further Increase Diagnostic Yield vs. 0.1-mmol/kg ProHance Images

A study of 68 patients highly suspected of having cerebral metastases was conducted to evaluate the efficacy of a cumulative administered dose of 0.3 mmol/kg of ProHance versus a 0.1-mmol/kg dose.[1] Of these 68 patients, 64 yielded evaluable images at both dose levels. A total of 16 patients were judged by the blinded neuroradiologist to have no MR evidence of cerebral metastatic disease at either dose.

- A cumulative administered dose of 0.3 mmol/kg of ProHance increased detection of cerebral metastases by an additional 32% when compared with 0.1-mmol/kg images (N = 48).

*0.1 mmol/kg followed by an additional 0.2 mmol/kg up to 30 minutes after the first dose.

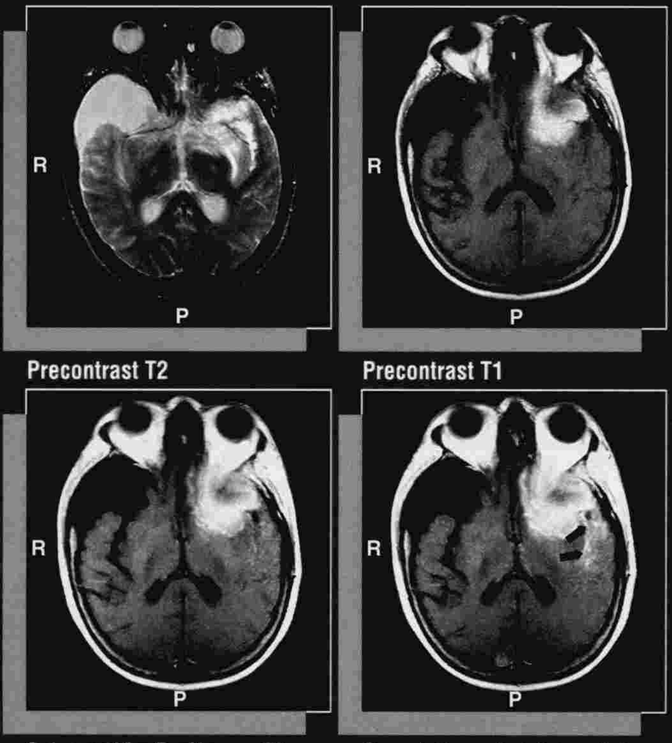

Precontrast T2 **Precontrast T1**

0.1 mmol/kg ProHance, T1 **Cumulative administered dose of 0.3 mmol/kg ProHance, T1**

Female, 61 years old with a previous history of breast cancer presented with a two-month history of headache and recently diagnosed right hilar mass. Postcontrast (0.1 mmol/kg ProHance) T1-weighted image shows a left frontal lobe mass and a subarachnoid cyst near the temporal lobe. T1-weighted image following a cumulative administered dose of 0.3 mmol/kg ProHance revealed a second lesion in the right occipital lobe, confirming a diagnosis of metastatic disease and avoiding the necessity of a biopsy.[1,6]

Unique Versatility

ProHance®

Gadoteridol Injection

Please see adjacent page for brief summary of full prescribing information.

Unique Versatility

ProHance®

Gadoteridol Injection

- Unique dosing versatility: 0.1 mmol/kg and cumulative administered dose of 0.3 mmol/kg in select patients
- Proven safety for all recommended dosing options
- Unique non-ionic, macrocyclic chelate

CAUTION: FEDERAL LAW PROHIBITS DISPENSING
WITHOUT PRESCRIPTION

ProHance®
(Gadoteridol Injection)

Brief Summary of the full text of the latest Official Package Insert dated November 1992 (J4-450A).

DESCRIPTION

PROHANCE® (Gadoteridol Injection) is a non-ionic contrast medium for magnetic resonance imaging (MRI), available as a 0.5 M sterile clear colorless to slightly yellow aqueous solution in vials for intravenous injection.

Gadoteridol is the gadolinium complex of 10-(2-hydroxypropyl)-1,4,7,10-tetraazacyclododecane-1,4,7-triacetic acid with a molecular weight of 558.7, an empirical formula of $C_{17}H_{29}N_4O_7Gd$ and has the following structural formula:

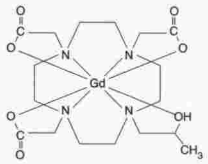

Each mL of PROHANCE® contains 279.3 mg gadoteridol, 0.23 mg calteridol calcium, 1.21 mg tromethamine and water for injection. PROHANCE® contains no antimicrobial preservative.

PROHANCE® has a pH of 6.5 to 8.0. Pertinent physicochemical data are noted below:

Parameter		
Osmolality (mOsmol/kg water)	@37°C	630
Viscosity (cP)	@20°C @37°C	2.0 1.3
Specific Gravity	@25°C	1.140

PROHANCE® has an osmolality 2.2 times that of plasma (285 mOsmol/kg water) and is hypertonic under conditions of use.

CONTRAINDICATIONS

None known.

WARNINGS

Deoxygenated sickle erythrocytes have been shown in *in vitro* studies to align perpendicular to a magnetic field which may result in vaso-occlusive complications *in vivo*. The enhancement of magnetic moment by PROHANCE® may possibly potentiate sickle erythrocyte alignment. PROHANCE® in patients with sickle cell anemia and other hemoglobinopathies has not been studied.

Patients with other hemolytic anemias have not been adequately evaluated following administration of PROHANCE® to exclude the possibility of increased hemolysis.

Patients with history of allergy or drug reaction should be observed for several hours after drug administration.

PRECAUTIONS

General-Diagnostic procedures that involve the use of contrast agents should be carried out under direction of a physician with the prerequisite training and a thorough knowledge of the procedure to be performed. In a patient with a history of grand mal seizure, the possibility to induce such a seizure by PROHANCE® is unknown.

Since gadoteridol is cleared from the body by glomerular filtration, caution should be exercised in patients with severely impaired renal function. An alternate route of excretion frequently observed in patients with severe renal impairment receiving iodinated contrast media, is the hepatobiliary enteric pathway, although this has not been demonstrated with PROHANCE® (Gadoteridol Injection). However, caution should be exercised in patients with either renal or hepatic impairment.

The possibility of a reaction, including serious life threatening or fatal anaphylaxis or cardiovascular reactions or other idiosyncratic reactions, should always be considered, especially in those patients with a history of a known clinical hypersensitivity.

When PROHANCE® is to be injected using nondisposable equipment, scrupulous care should be taken to prevent residual contamination with traces of cleansing agents. After PROHANCE® is drawn into a syringe, the solution should be used immediately.

Repeat Procedures-Data for repeated examinations are not available. If in the clinical judgment of the physician, repeat examinations are required, a suitable interval of time between administrations should be observed to allow for normal clearance of the drug from the body.

Information for Patients-Patients scheduled to receive PROHANCE® should be instructed to: 1) Inform their physician if they are pregnant or breast feeding; 2) Inform their physician if they have anemia or diseases that affect the red blood cells; 3) Inform their physician if they have a history of renal or hepatic disease, seizure, asthma or allergic respiratory diseases.

CARCINOGENESIS, MUTAGENESIS, AND IMPAIRMENT OF FERTILITY

No animal studies have been performed to evaluate the carcinogenic potential of gadoteridol or potential effects on fertility.

PROHANCE® did not demonstrate genotoxic activity in bacterial reverse mutation assays using *Salmonella typhimurium* and *Escherichia coli*, in a mouse lymphoma forward mutation assay, in an *in vitro* cytogenetic assay measuring chromosomal aberration frequencies in Chinese hamster ovary cells, nor in an *in vivo* mouse micronucleus assay at intravenous doses as high as 5.0 mmol/kg.

PREGNANCY CATEGORY C

PROHANCE® administered to rats at 10 mmol/kg/day (33 times the maximum recommended human dose of 0.3 mmol/kg) for 12 days during gestation doubled the incidence of postimplantation loss. This may have been related to maternal toxicity.

When rats were administered 6.0 or 10.0 mmol/kg/day for 12 days, an increase in spontaneous locomotor activity was observed in the offspring.

PROHANCE® increased the incidence of spontaneous abortion and early delivery in rabbits administered 6 mmol/kg/day (20 times the maximum recommended human dose) for 12 days during gestation. This may have been related to maternal toxicity.

There are no adequate and well-controlled studies in pregnant women. PROHANCE® should be used during pregnancy only if the potential benefit justifies the potential risk to the fetus.

NURSING MOTHERS

It is not known whether this drug is excreted in human milk. Because many drugs are excreted in human milk, caution should be exercised when PROHANCE® is administered to a nursing woman.

PEDIATRIC USE

Safety and effectiveness of PROHANCE® in children have not been established.

ADVERSE REACTIONS

The most commonly noted adverse experiences were nausea and taste perversion with an incidence of 1.4%. These events were mild to moderate in severity.

The following additional adverse events occurred in fewer than 1% of the patients:

Body System	Adverse Events
Body as a Whole	Facial Edema; Neck Rigidness; Pain at Injection Site; Chest Pain; Headache; Fever; Itching Watery Eyes; Abdominal Cramps; Tingling Sensation in Throat; Flushed Feeling
Cardiovascular System	Prolonged P-R Interval; Hypotension; Elevated Heart Rate; A-V Nodal Rhythm
(continued)	
Digestive System	Edema–Tongue; Gingivitis; Dry Mouth; Loose Bowel; Vomiting; Itching Tongue
Nervous System	Anxiety; Dizziness; Paresthesia; Mental Status Decline; Loss of Coordination in Arm; Staring Episode; Syncope
Respiratory System	Dyspnea; Rhinitis; Cough
Skin and Appendages	Pruritus; Rash; Rash Macular Papular; Urticaria; Hives; Tingling Sensation of Extremity and Digits
Special Senses	Tinnitus

OVERDOSAGE

The minimal lethal single dose of PROHANCE® (Gadoteridol Injection) in mice was found to be between 7 and 10 mmol/kg (23 to 33 times the maximum recommended human dose of 0.3 mmol/kg). Overt clinical signs noted prior to death included ataxia, convulsions, collapse, bloody exudate from nares, and decreased activity. PROHANCE® was not lethal to rats at single doses up to 10 mmol/kg.

DOSAGE AND ADMINISTRATION

The recommended dose of PROHANCE® is 0.1 mmol/kg (0.2 mL/kg) administered as a rapid intravenous infusion or bolus. However, in patients suspected of having cerebral metastases or other poorly enhancing lesions, in the presence of negative or equivocal scans, after 0.1 mmol/kg injection, at the clinician's discretion, a second dose of 0.2 mmol/kg (0.4 mL/kg) can be administered up to 30 minutes after the first dose for further evaluation. Any unused portion must be discarded.

To ensure complete injection of the contrast medium, the injection should be followed by a 5-mL normal saline flush. The imaging procedure should be completed within 1 hour of the first injection of PROHANCE®.

Parenteral products should be inspected visually for particulate matter and discoloration prior to administration. Do not use the solution if it is discolored or particulate matter is present.

Squibb Diagnostics
Princeton, New Jersey 08543

3022-802
Printed in U.S.A.

For full prescribing information consult package insert.

References

1. Data on file, Squibb Diagnostics.
2. Runge VM, Dean B, Lee C, et al. Phase III clinical evaluation of Gd-HP-DO3A in head and spine disease. *JMRI.* 1991;1:47–56.
3. Runge VM, Bradley WG, Brant-Zawadzki MN, et al. Clinical safety and efficacy of gadoteridol: a study in 411 patients with suspected intracranial and spinal disease. *Radiology.* 1991; 181:701–709.
4. Runge VM, Bronen RA, Davis KR. Efficacy of gadoteridol for magnetic resonance imaging of the brain and spine. *Invest Radiol.* 1992;27(Suppl 1):S22–S32.
5. Case provided courtesy of Lou Rosa, MD, Georgetown University Hospital, Washington, DC.
6. Yuh WTC, Engelken JD, Muhonen MG, et al. Experience with high-dose gadolinium MR imaging in the evaluation of brain metastases. *Am J Neuroradiol.* 1992;13:335–345.

Squibb Diagnostics
A Bristol-Myers Squibb Company
Princeton, NJ 08543
U.S.A.

Letter from the President

The **Society for Magnetic Resonance Imaging** invites you to attend the 1993 Annual Meeting in San Francisco. The 11th Anniversary Meeting of the **SMRI** begins with the traditional Educational Program on Saturday, March 27 and extends to Sunday, March 28. The Educational Program provides an excellent faculty group covering all aspects of clinical MR. Parallel to the Educational Session on Saturday, March 27 will be a Technologist Workshop co-sponsored with the SMRT.

The 1993 **SMRI** Scientific Program promises to be one of the most exciting ever. A variety of excellent plenary speakers reinforces a program of outstanding scientific papers. The Scientific Program special Topical Conference this year focuses on MR Contrast and Contrast Agents and will be held on Sunday, March 28. The balance of the Scientific Program will begin on Monday, March 29 at 8:00 AM and conclude on Wednesday, March 31 at 4:30 PM. Parallel to the Scientific Program on Monday, the **SMRI** will host the third annual MR Economics Symposia, a major addition to the Society's Annual Meeting.

An expanded Technical Exhibits Area will provide access to the latest in MR equipment and accessories. Start your review of the exhibit area with the Technical Exhibits Opening Reception on Saturday, March 27 (5:00 PM-7:00 PM). Poster presentations are again included in the Scientific Program and are displayed adjacent to the Technical Exhibits Area. Posters may be viewed daily from 8:00 AM - 8:00 PM or, more leisurely, during the daily discussion period over the luncheon hour. In addition, you may view award winning posters during the Poster Exhibit Reception scheduled on Sunday, March 28 (5:00 PM-7:00 PM). The **SMRI** Gala Reception will be held on Monday, March 29 (7:30 PM-10:30 PM). As usual, these receptions will provide you with an opportunity to informally visit and share information with your colleagues.

The **Journal of Magnetic Resonance Imaging**, launched in 1991 by the **SMRI**, has become a major force in the dissemination of information in our field. We encourage you to submit your clinical and technical papers to **JMRI**. The journal will occupy booth #902 where papers may be submitted for consideration.

The **SMRI** looks forward to the most exciting and rewarding Annual Meeting ever!

See you in San Francisco!

Sincerely,

Steven E Harms, MD
SMRI *President*

The Society for Magnetic Resonance Imaging

About the Society...

Society Mission

1993 marks the eleventh anniversary of the Society for Magnetic Resonance Imaging (**SMRI**). The Society was chartered in November, 1982 to:

o provide an equal opportunity to clinical and basic scientists to contribute to the development of MRI.

o offer an international multidisciplinary forum for the advancement of magnetic resonance imaging.

o promote the applications of magnetic resonance techniques to medicine and biology, with specific emphasis on imaging.

o prepare and disseminate technical and product information related to research techniques, equipment and clinical applications of magnetic resonance.

o develop educational and training material and methods for the application of magnetic resonance to medicine and biology.

Since its inception, the **SMRI** has grown to an international association of over 2,000 clinical and basic scientists dedicated to research and the application of MR as a diagnostic technique in medicine. The professionalism and experience of its members has guided the Society to its current position as the major resource for the clinical MRI practitioner.

Annual Meeting

Since 1982, the Annual Meeting of the **SMRI** has grown to be the most comprehensive forum for the exchange of scientific, technical and product information related to research techniques, equipment and clinical applications of magnetic resonance.

The Scientific Program consists of more than 26 plenary symposia and 480 peer-reviewed papers, works in progress presentations and scientific posters. Additionally, a three-day Educational Program provides an introduction to MRI basics and an in-depth analysis of MR Economics. Also, a one-day SMRT Workshop and a Morning Tutorial Basic/Clinical Science Workshop are included in the scientific agenda.

An integral component of the Annual Meeting is the technical exhibition of MRI products, accessories and services. Over 35 leading companies from around the world participate in presenting over 12,000 square feet of technical exhibits. The Meeting provides a forum for the discussion and exchange of ideas between clinical and basic scientists, technologists, radiology business managers and administrators, purchasing agents and manufacturers.

Publications

Journal of Magnetic Resonance Imaging (JMRI)

1993 marks the third year of self-publication of the Society's official journal, the Journal of Magnetic Resonance Imaging (**JMRI**). Owned by the **SMRI**, **JMRI** is produced in collaboration with the Radiological Society of North America, publisher of **Radiology** and other radiology-related journals.

JMRI, under the direction of Gary D Fullerton, PhD, Professor and Chief of Radiological Sciences at the University of Texas Health Science Center, San Antonio, presents a balance of technical and clinical articles on MR imaging and spectroscopy research. **JMRI** bi-monthly publishes 120 pages of peer-reviewed original research, works in progress, review articles, educational articles, **SMRI** reports and other special features, with more than 100 manuscripts published annually. **JMRI** expanded its scope in 1992 to launch production of an MResource Guide, a directory of MR equipment, service and accessory manufacturers, coupled with a compendium of MR definitions, pulse sequences and acronyms.

Echoes

1993 introduces the fourth volume of **Echoes**, the Society's self-published newsletter. Distributed three times annually, the newsletter provides important Society updates as well as state-of-the-art technical notes and clinical protocols to the membership. Edited by Paul T Weatherall, MD, Director of Clinical MRI, Rogers MR Center of the University of Texas, the newsletter provides an open communications forum to the membership.

Future Meetings

Upcoming Annual Meetings for the Society will include:

1994: 12th Annual Meeting in Dallas, TX, March 5-9
1995: 13th Annual Meeting in Washington, DC, March 25-29
1996: 14th Annual Meeting in Vancouver, BC, April 20-26.

Attendance at these meetings is sure to provide you with the critical link between science and the clinical application of magnetic resonance.

PAST ANNUAL MEETINGS

'82	'83	'84	'85	'86	'87	'88	'89	'90	'91	'92	'93
1982 Organizational Meeting Houston	**1983** 1st Annual Meeting Broadmoor Hotel Denver	**1984** 2nd Annual Meeting Greenlefe Hotel Orlando	**1985** 3rd Annual Meeting Town and Country Hotel San Diego	**1986** 4th Annual Meeting Wyndham Franklin Plaza Philadelphia	**1987** 5th Annual Meeting Palacio del Rio San Antonio	**1988** 6th Annual Meeting Westin Copley Place Boston	**1989** 7th Annual Meeting Century Plaza Hotel Los Angeles	**1990** 8th Annual Meeting Washington Hilton and Towers Washington, DC	**1991** 9th Annual Meeting Hyatt Regency Hotel Chicago	**1992** 10th Annual Meeting New York Hilton and Towers New York	**1993** 11th Annual Meeting San Francisco Hilton and Towers San Francisco

SMRI at Work

1992-93 Officers

Steven E Harms, MD
President

E Mark Haacke, PhD
Past President

Stephen J Riederer, PhD
President-Elect

Michael L Wood, PhD
Treasurer

John V Crues III, MD
Secretary

1993 Annual Meeting Organizing Committee

Organizing Committee Chairmen
Walter Kucharczyk, MD
Michael L Wood, PhD

Scientific Program Chairmen
Laurence P Clarke, PhD
Jeffrey S Ross, MD

Scientific Poster Program Chairmen
Richard L Ehman, MD
Perry Sprawls, PhD

Scientific Program: Morning Tutorial Program Chairmen
Scott W Atlas, MD
Stephen J Riederer, PhD

Educational Program Chairmen
Paul J Keller, PhD
William Sattin, PhD
William T C Yuh, MD, MSEE

Educational Program: MRI Economics Symposium Chairmen
Bruce J Hillman, MD
Stuart W Young, MD

SMRT Workshop Program Chairmen
Rodney Bell, RT
Luann Culbreth, MEd

Board of Directors

Scott W Atlas, MD (1994)
William G Bradley, Jr, MD, PhD (ex-officio, 1993)
Michael J Bronskill, PhD (1994)
Richard L Ehman, MD (1994)
Jens Frahm, PhD (1994)
Gary D Fullerton, PhD (editor)
Gary H Glover, PhD (1995)
R Edward Hendrick, PhD (ex-officio, 1994)
J Bruce Kneeland, MD (1994)
Robert B Lufkin, MD (ex-officio, 1995)
James R MacFall, PhD (1994)
Kenneth R Maravilla, MD (1993)
Michael E Moseley, PhD (1995)
Dwight G Nishimura, PhD (1995)
Bruce R Rosen, MD, PhD (1995)
Frank G Shellock, PhD (1993)
Perry Sprawls, PhD (1993)
David D Stark, MD (1995)
Jeffrey C Weinreb, MD (1994)
Ian R Young, PhD (1994)
Stuart W Young, MD (1994)
William T C Yuh, MD, MSEE (1995)

1993 SMRI HONORARY MEMBER AWARD RECIPIENT

About the Award..
Honorary membership in the Society for Magnetic Resonance Imaging is conferred on an individual who has rendered unusual service to the science of Magnetic Resonance Imaging. It is the highest honor the Society can bestow upon an individual.

Past Honorary Member Award Recipients

1992:
Graeme E Bydder, MD

1990:
Francis W Smith, MD

1989:
Ian R Young, PhD

1988:
Paul C Lauterbur, PhD

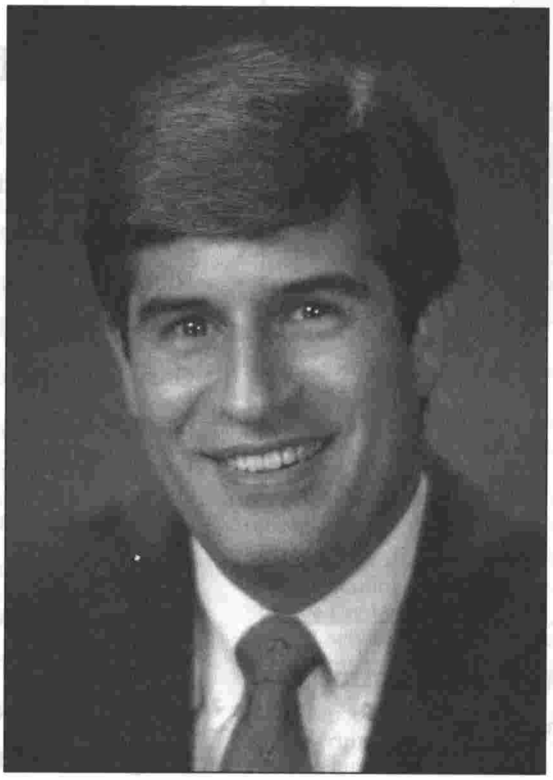

William G Bradley, Jr, MD, PhD, FACR

William G Bradley, Jr, MD, PhD, FACR, joined the staff at Long Beach Memorial Medical Center on January 1, 1990 as Director of MR Imaging and Radiology Research. Prior to joining Long Beach Medical Center, Dr. Bradley served as Director of MR at the Huntington Medical Research Institutes and was a staff radiologist at the Huntington Memorial Hospital, both in Pasadena. In 1977, Dr. Bradley received his medical degree from the University of California, San Francisco. In 1974, he earned a PhD in Chemical Engineering from Princeton. Dr. Bradley has published over 100 articles, is currently working on his eleventh medical textbook, is an internationally renowned MR lecturer, serves on the faculties of the University of California, San Francisco, Irvine, Los Angeles and the California Institute of Technology and was awarded the Gold Medal by the Society of Magnetic Resonance in Medicine in 1989. His book, *Magnetic Resonance Imaging*, Volume 1 (co-authored with David D Stark, MD of Boston, MA) was awarded best Scientific Book for 1988. Dr. Bradley is an active member and serves on various committees of the American College of Radiology, Society for Magnetic Resonance Imaging (past president), Society of Magnetic Resonance in Medicine, California Radiological Society, Los Angeles Radiological Association, Western Neuroradiological Society, Radiological Society of North America and the American Roentgen Ray Society. He also serves as a reviewer for several radiology publications as well as serving on the editorial boards of many of the publications. Dr. Bradley lives in Pasadena, California, with his wife, Rosalind B Dietrich, MB, ChB and four children, David, Kristin, India and Felicity.

1993 FELLOW OF THE SOCIETY AWARD RECIPIENTS

About the Award...

Fellow of the Society awards are conferred on those individuals who have made both a significant contribution to the science of MRI and rendered outstanding service to the Society.

Past Fellow of the Society Award Recipients

1992:

E Mark Haacke, PhD
Kenneth R Maravilla, MD
Jeffrey C Weinreb, MD
Michael L Wood, PhD

1991:

Graeme Bydder, MD
R Mark Henkelman, PhD
Robert B Lufkin, MD
Felix W Wehrli, PhD

1990:

C Leon Partain, MD, PhD
Val M Runge, MD
David D Stark, MD

1989:

Sharad R Amtey, PhD
Paul A Bottomley, PhD
William G Bradley, Jr, MD, PhD
Gary D Fullerton, PhD
John C Gore, PhD
Carlton T Hazlewood, PhD
R Edward Hendrick, PhD
Andre Luiten, PhD
William J MacIntyre, PhD
Ray L Nunnally, PhD
Francis W Smith, MD
Luis E Todd, MD

Jeffrey L Duerk, PhD

Dr. Duerk is Assistant Professor in the Departments of Radiology and Biomedical Engineering, MetroHealth Medical Center and Case Western Reserve University in Cleveland. He received his Bachelor's degree in Electrical Engineering at Purdue University in 1981, his Master's degree in Electrical Engineering at Ohio State University in 1983 and his PhD in Biomedical Engineering at Case Western Reserve in 1987. Dr. Duerk has served as a Research Fellow and Clinical Scientist at Picker International (NMR Division), an Assistant and Adjunct Professor of Radiology at Indiana University Medical Center and an Imaging Scientist and Assistant Professor of Radiology and Biomedical Engineering at Case Western Reserve University. Jeff is active in the **SMRI**, Institute of Electronic and Electrical Engineers (IEEE), SMRM, and the American Association of Physicists in Medicine (AAPM). His primary research interests include the theoretical analysis of the effects of motion in MRI, development of motion compensation techniques, including gradient waveform design, in addition to other interests in local coil design, reconstruction, processing and cardiac applications of MRI. He is an author on 20 technical journal articles in MRI, 3 book chapters, and over 40 conference abstracts. Dr. Duerk served as the editor of **SMRI**'s **Echoes** newsletter and also serves on the Editorial Board of **JMRI**. In addition, he is editor of **JMRI**'s "Pulse" section and is a member of the **SMRI** Publications Committee.

Steven E Harms, MD

Dr. Harms is Director of Magnetic Resonance in the Department of Radiology at Baylor University Medical Center in Dallas, Adjunct Associate Professor of Radiology (Division of Diagnostic Radiology) at M.D. Anderson Cancer Hospital in Houston, and is presently Clinical Assistant Professor of Radiology (Department of Radiology), University of Texas Southwestern Medical School in Dallas. Steve received his MD at the University of Arkansas in Little Rock and also completed his residency in Radiology at the University of Arkansas. He is currently serving as President of the **SMRI**. His past professional experience includes a Post-Doctoral Research Associate position in the Physical Chemistry Department, State University of New York, working directly with Dr. Paul Lauterbur, and Assistant Professor and Instructor in the Departments of Diagnostic Radiology and Biophysics at M.D. Anderson Cancer Center. His research interests include three-dimensional imaging applications, development of new fast scanning sequences, and musculoskeletal, TMJ, body, ophthalmological and breast applications of MRI. He is the author of over 80 papers, patents, and published abstracts and over 20 book chapters. In addition to serving as President of **SMRI**, Steve has served on the Board of Directors, co-chaired Evening Tutorial, Educational and Scientific Programs of past Annual Meetings and currently serves as an Associate Editor of **JMRI**.

Accreditation for Category I

The Radiological Society of North America is accredited by the Accreditation Council of Continuing Medical Education to sponsor Continuing Medical Education of Physicians.

The Radiological Society of North America designates this continuing medical education activity of the Society for Magnetic Resonance Imaging for a maximum of 36.25 credit hours in Category 1 of the Physician's Recognition Award of the American Medical Association.

Accreditation for ECE

Technologists wishing to record ECE credits will receive 1993 SMRT Workshop accreditation forms upon registering. Upon completion of the Workshop, return forms to the **SMRI** Registration desk located in the Grand Ballroom Foyer, Ballroom Level. A record of these attendance forms will be forwarded to the ASRT for accreditation.

Announcement Board

An area is set aside in the Registration Area for posting announcements of future meetings and seminars and for publicizing events during the **SMRI** Meeting. Announcements may not be larger than 8-1/2 x 11 inches.

Annual Meeting Printed Program: A How-To-Guide

This Program contains a complete listing, with abstracts, of all scientific courses, sessions, and exhibits. Material is organized by category (Plenary Symposia, Proffered Papers, Scientific Poster Exhibits and Awards Presentation) and ordered chronologically within each category.

The Sections and Symbols throughout these pages are guides to information you wish to locate. Beginning with Plenary Symposia and continuing with Indices and Information, each section is preceded by a divider page. Please review the text on each divider page for important information and announcements relating to that particular section.

A designates an Awards presentation. The Awards Ceremony will be held in the Imperial Ballroom on Monday (*8:00 AM-8:45 AM).*

EP designates an Educational Session. Educational Program material will be distributed on-site to Educational Program attendees. The Educational Program will be presented in the Plaza Room on Saturday and Sunday and the California Room on Monday.

PS designates Scientific Program Plenary Symposia. Plenary Symposia will be presented in the Imperial Ballroom.

MT designates a Scientific Program: Morning Tutorial presentation. Morning Tutorial sessions will be presented in the Franciscan A and Franciscan B Rooms.

P designates a Poster Scientific Paper. Poster Papers will be presented in the Poster Exhibit Area, located in the Grand Ballroom on the Ballroom Level. Posters will be on display Sunday-Wednesday.

Attendance Record

Personalized bar codes will be presented to each attendee upon registering. Evaluation/CME Attendance Forms will be distributed at the beginning of each session; at the conclusion of each session, attendees are instructed to complete the Evaluation Form and affix a personalized bar code to the Form so that CME credit may be received. A Deposit Box will be located outside of each meeting room; forms may be deposited in the box at the conclusion of each session. Evaluations will be tabulated for use in future meeting planning while CME credits will be tabulated and forwarded to the Radiological Society of North America (RSNA) to register each attendee's credit hours. Please note, if an attendee requires CME credit, an attendee must follow the above instructions.

Bank

To exchange foreign currency or US-denominated travelers checks, visit the Front Desk of the San Francisco Hilton and Towers. An automated teller machine (ATM) is also available on the lobby level of Building Three. This ATM will honor American Express, Discover, Visa, MasterCard, American Express/Express Cash, Exchange, 1st Interstate, Armed Forces Financial Network, Money Network, Cirrus, The Plus and the Star System.

Business Center

The hotel Business Center, located on the 4th Floor of Building Three (Hotel Guest Extension 6135), offers the following services: photocopying, FAX transmissions, UPS, Federal Express (priority and economy), word processing and typing.

Emergency Information

In case of an emergency, please contact the hotel Assistant Manager on any house telephone at extension 6105 or 444.

Food Service

Complimentary pre-session coffee service is available in the Registration Area, 7:00 AM-8:00 AM on Saturday and Sunday and 6:30 AM-7:30 AM thereafter. In addition, complimentary coffee breaks and luncheon service will be provided daily. Saturday's morning coffee service and afternoon soda breaks will be provided in the Ballroom Foyer while luncheon service will be provided in the Imperial and Franciscan Ballrooms. Thereafter, all breaks will be in the Technical Exhibits Area. Please refer to the following "Walk Through **SMRI '93**" for specific service schedules.

Job Bulletin

Technologist job listings may be posted in SMRT booth #910, the booth of the Combined Section of Magnetic Resonance Technologist (SMRT). All other job listings may be posted on the Job Bulletin Board set aside in the Registration Area. Posted materials regarding positions available and positions sought may not exceed 8 1/2 x 11 inches.

Lost and Found

Lost and Found articles will be presented to the Hotel Security service for safekeeping. Please contact the Security Office on any house telephone at extension 6200.

Message Center

A Message Center Board is set aside in the Registration Area for posting messages during the **SMRI** Annual Meeting. Notepads and pencils will be available for message deposit and retrieval.

Post Office

Should attendees require postal services, a stamp machine and mailbox are located in the hotel lobby.

GENERAL INFORMATION

Presenters of Papers

- **Last minute concerns** about a presentation, call the **SMRI** Central Office at (312)751-2590 before March 25. After this date, call the San Francisco Hilton/**SMRI** Registration area at 415/771-1400.

- **Contact authors** of abstracts listed in the Printed Program by writing to the **SMRI** Central Office at 213 West Institute Place, Suite 501, Chicago, Illinois 60610. Requests will be forwarded to the author.

- **The Slide Preview Room** is located in the Green Room, adjacent to the Registration Area on the Ballroom level. The hours are as follows:

Saturday, March 27-Sunday, March 28
7:00 AM - 6:00 PM

Monday, March 29-Tuesday, March 30
6:30 AM - 6:00 PM

Wednesday, March 31
6:30 AM - 3:30 PM

Registration

All meeting registration will take place in the Grand Ballroom Foyer, located on the Ballroom Level of the San Francisco Hilton and Towers, according to the following schedule:

Friday, March 26
3:00 PM - 6:00 PM

Saturday, March 27
7:00 AM - 5:00 PM

Sunday, March 28
7:00 AM - 6:00 PM

Monday, March 29
6:00 AM - 6:30 PM

Tuesday, March 30
6:00 AM - 6:00 PM

Wednesday, March 31
6:00 AM - 3:30 PM

Registration Entitlements

In completing the Registration Form, please use the following guide in selecting a Program to attend:

Educational Program

Entitled to attendance at the Educational Program (including the Economics Symposium) or SMRT Tech Workshop. Those who wish to attend only the Economics Symposium may register on-site.

Scientific Program

Entitled to attendance at Scientific Program (including the MR Contrast and Contrast Agents Topical Conference and Morning Tutorial Program).

Scientific/Educational Program

Entitled to attendance at both Educational and Scientific Programs.

Schedule of Events

For alumni groups and other **SMRI**-affiliated committees and organizations that have made meeting arrangements through the **SMRI** Central Office, a schedule of events is available for review at the Registration Desk, Grand Ballroom Foyer, Ballroom Level of the San Francisco Hilton and Towers.

Scientific Poster Exhibit Hours

Scientific Poster Exhibits are located in the Grand Ballroom, Ballroom Level of the San Francisco Hilton and Towers. Exhibit hours are Sunday-Tuesday 8:00 AM - 8:00 PM and Wednesday 8:00 AM - 1:00 PM.

SMRI Membership Services

Membership applications will be available at the Registration Desk, Grand Ballroom Foyer, Ballroom Level, for all non-member attendees wishing to join the Society. Due to the review process required, membership applications may not be approved on-site. However, you will be notified of your acceptance within six weeks following the Annual Meeting. Membership inquiries by current members may also be addressed at the Registration Desk.

SMRI Business Meeting

All **SMRI** members are encouraged to attend the Annual Business Meeting of the Society to be held Monday, March 29, 10:00 AM-10:30 AM in the Imperial Ballroom.

SMRI Publications

For subscription or manuscript information regarding the **Journal of Magnetic Resonance Imaging (JMRI)**, visit booth #902 in the Technical Exhibits Area. Manuscripts for submission to **JMRI** may be submitted to the booth.

Social Program

The **SMRI** cordially invites all attendees (single day registrants must visit the Social Program Desk to purchase tickets) to join in an evening of fellowship at the following receptions:

Technical Exhibits Opening Reception

Technical Exhibits Area
Saturday, March 27
5:00 PM - 7:00 PM

Poster Exhibit Reception

Poster Exhibit Area
Sunday, March 28
5:00 PM - 7:00 PM

SMRI Gala Reception

Imperial Ballroom
Monday, March 29
7:30 PM - 10:30 PM

A Social Program Desk will be staffed in the Registration Area for participants wishing to purchase tickets for accompanying guests.

Technical Exhibits

The **SMRI** Technical Exhibits Program will display the latest in MR equipment, supplies, and services in Grand Ballroom, Ballroom Level, beginning with a reception on Saturday, March 27 from 5:00 PM to 7:00 PM. Thereafter, the exhibits will be on display Sunday, March 28, through Tuesday, March 30, 9:30 AM - 4:00 PM, and Wednesday, March 31, 9:30 AM - 1:00 PM.

Who's Who—Official Badges

Badges are color-coded as follows:

Blue: Member SMRI/SMRT
Red: Non-member
Green: Accompanying Guests
Brown: Technical Exhibitors

SAT 3/27

7:00 AM - 5:00 PM
General Registration

Educational Program

8:00 AM - 10:00 AM
- ☐ Intro. to MRI: Show & Tell
- ☐ How to Diagnose & Resolve Imaging Problems
- ☐ Protocol & Technique
- ☐ FAST Imaging

10:00 AM-10:30 AM
Break

10:30 AM - 12:00 PM
- ☐ Brain Tumor
- ☐ Sellar, Parasellar, & Skull Base
- ☐ MR of Stroke

12:00 PM - 1:30 PM
Luncheon

1:30 PM - 3:00 PM
- ☐ White Matter Disease & Miscellaneous
- ☐ Congenital Brain Disease
- ☐ Head and Neck

3:00 PM - 3:30 PM
Break

3:30 PM - 5:00 PM
- ☐ Tumor of the Spine
- ☐ Degenerative Disk Disease
- ☐ Congenital Spine Disease

SMRT Technologist Workshop

8:30 AM - 10:00 AM
- ☐ Vascular Anatomy
- ☐ Time of Flight/Inflow Principles & Applications

10:00 AM - 10:30 AM
Break

10:30 AM - 12:00 PM
- ☐ Phase Contrast Principles & Applications
- ☐ Post Processing MRA

12:00 PM - 1:00 PM
Luncheon

1:00 PM - 2:30 PM
- ☐ MRI Contrast Principles
- ☐ Neuro Applications
- ☐ Abdominal Applications

2:30 PM - 3:00 PM
Break

3:00 PM - 4:30 PM
- ☐ Breast Applications
- ☐ Musculoskeletal Applications
- ☐ Contrast Enhanced MRA

TECHNICAL EXHIBITS RECEPTION
5:00 PM - 7:00 PM

SUN 3/28

7:00 AM - 6:00 PM
General Registration

9:30 AM - 4:00 PM
Technical Exhibits

8:00 AM - 8:00 PM
Poster Sessions

Educational Program

8:00 AM - 10:00 AM
- ☐ Vascular Imaging: CNS & Body
- ☐ Protocol & Technique for MR in the Body
- ☐ Liver
- ☐ Kidney, Adrenal & Retroperitoneum

10:00 AM - 10:30 AM
Break

10:30 AM - 12:00 PM
- ☐ Pelvis
- ☐ Pediatric Abdomen
- ☐ Cardiac and Thoracic Images

12:00 PM - 1:30 PM
Luncheon
Scientific Poster Discussion Period: Physics I: Flow, Motion, Perfusion, Artifacts

1:30 PM - 3:00 PM
- ☐ Shoulder: Surgeon's Perspective
- ☐ Shoulder: Instability
- ☐ Shoulder: Impingement/ Rotator Cuff Disease

3:00 PM - 3:30 PM
Break

3:30 PM - 5:00 PM
- ☐ Knee: Menisci & Cruciates
- ☐ Knee: Non-Meniscal Pathology
- ☐ Foot/Ankle

Scientific Program Topical Conference: MRI Contrast and Contrast Agents

8:00 AM - 10:00 AM
- ☐ Basics of Image Contrast
- ☐ Basics of Contrast Agents
- ☐ CNS Applications of Contrast
- ☐ Contrast Agents in the Spine

10:00 AM - 10:30 AM
Break

10:30 AM - 12:15 PM
- ☐ Proffered Papers: Contrast Agents/MTC

12:15 PM - 1:30 PM
Luncheon
Scientific Poster Discussion Period: Physics I: Flow, Motion, Perfusion, Artifacts

1:30 PM - 3:00 PM
- ☐ Hepatobiliary Agents
- ☐ Perfusion Imaging
- ☐ Diffusion

3:00 PM - 3:30 PM
Break

3:30 PM - 5:00 PM
- ☐ MTC/Protein Contrast & Mechanisms
- ☐ Calcium Contrast Mechanisms
- ☐ Iron/Susceptibility Contrast

POSTER RECEPTION
5:00 PM - 7:00 PM

PERSONAL ITINERARY:

Morning	Afternoon

MON
3/29

6:00 AM - 6:30 PM
General Registration

9:30 AM - 4:00 PM
Technical Exhibits

8:00 AM - 8:00 PM
Poster Sessions

Educational Program: MRI Economics Symposium

8:00 AM - 10:15 AM
☐ New Initiatives for Funding MRI & MRS Research at NCI
☐ Pitfalls in Acquiring MRI Equipment: Operational Experience
☐ Evaluating New Technologies for Policy Purposes

10:15 AM - 10:45 AM
Break

10:45 AM - 12:30 PM
☐ Financial Structuring & Dissemination of MRI Facilities in the '90's
☐ Contrast Media Research: Implications for MRI Reimbursement

12:30 PM - 1:30 PM
Luncheon
Scientific Poster Discussion Period:
Clinical MRI: Head, Spine, Body

1:30 PM - 3:00 PM
☐ Managed MRI Scan Referrals: Economic Impact
☐ Self-Referral & Conflict of Interest for Diagnostic Imaging

3:00 PM - 3:45 PM
Break

3:45 PM - 5:30 PM
☐ Rate Regulation, Decreasing Reimbursement & Strategies for Adaptation
☐ Competitive Strategies & Reimbursement in MRI

Scientific Program: Morning Tutorial

6:45 AM - 7:45 AM
☐ k-Space & Fast Scan MRI:
Basic Concepts
Clinical Applications
☐ Musculoskeletal Imaging:
MRI of the Shoulder
MRI of the Wrist

Scientific Program

8:00 AM - 8:45 AM
☐ Awards Presentation

8:45 AM - 10:00 AM
MRI Breast: Imaging & Interventional Strategies
☐ Imaging Management of Breast Carcinoma
☐ MRI of the Breast
☐ Minimally Invasive Therapy in Breast Cancer

10:00 AM - 10:45 AM
Break

10:45 AM - 12:30 PM
☐ Proffered Papers

12:30 PM - 1:30 PM
Luncheon
Scientific Poster Discussion Period:
Clinical MRI: Head, Spine, Body

1:30 PM - 3:00 PM
Cardiac MRI: Functional & Clinical Applications
☐ Adult Cardiac Evaluation
☐ Functional Cardiac Imaging
☐ Wall Motion & Image Processing

3:00 PM - 3:45 PM
Break

3:45 PM - 5:30 PM
☐ Proffered Papers

GALA RECEPTION
7:30 PM - 10:30 PM

TUE
3/30

6:00 AM - 6:00 PM
General Registration

9:30 AM - 4:00 PM
Technical Exhibits

8:00 AM - 8:00 PM
Poster Sessions

Scientific Program: Morning Tutorial

6:45 AM - 7:45 AM
☐ Surface Coils:
New Advances
Applications in the Pelvis
☐ MR Angiography:
Nuts & Bolts of Pulse Sequences
Current Limitations

Scientific Program

8:00 AM - 9:30 AM
MRA: Technical Advances & Clinical Efficacy
☐ CNS Time-of-Flight
☐ CNS Phase Contrast
☐ Body Applications

9:30 AM - 10:30 AM
Break

10:30 AM - 12:15 PM
☐ Proffered Papers

12:15 PM - 1:30 PM
Luncheon
Scientific Poster Discussion Period:
Physics II: Rapid Imaging, Pulse Sequences, Image Processing

1:30 PM - 3:00 PM
MR Flow: Quantitative & Clinical Applications
☐ CSF Flow
☐ Cardiac Applications & Bolus Tracking
☐ Phase Contrast Applications

3:00 PM - 3:45 PM
Break

3:45 PM - 5:30 PM
☐ Proffered Papers

WED
3/31

6:00 AM - 3:30 PM
General Registration

9:30 AM - 1:00 PM
Technical Exhibits

8:00 AM - 1:00 PM
Poster Sessions

Scientific Program: Morning Tutorial

6:45 AM - 7:45 AM
☐ Motion Compensation:
Basic Physics
Clinical Applications
☐ Functional Brain MRI:
Physiological Issues
Functional Brain Imaging

Scientific Program

8:00 AM - 9:30 AM
Fast Scan Techniques in the Abdomen: Clinical Efficacy
☐ Limitations of Fast Scan
☐ Advantages of Fast Scan

9:30 AM - 10:30 AM
Break

10:30 AM - 12:15 PM
☐ Proffered Papers

12:15 PM - 1:00 PM
Luncheon
Scientific Poster Discussion Period:
Contrast Agents, Spectroscopy, Other Nuclei

1:00 PM - 2:30 PM
MRI Segmentation: Interventional & Stereotactic Strategies
☐ Interventional MRI
☐ Deformable Anatomic Atlases & Validation of Segmentation
☐ Segmentation Techniques

2:30 PM - 2:45 PM
Break

2:45 PM - 4:30 PM
☐ Proffered Papers

PERSONAL ITINERARY:

Morning

Afternoon

SMRT Technologist Workshop: California Room

SAT
3/27

Moderators: R Bell, BSRT, L Culbreth, MEd

8:30 AM - 10:00 AM

Vascular Anatomy	L Culbreth, MEd
Time-of-Flight/Inflow Principles and Applications	M Totina, RT

10:00 AM - 10:30 AM

Break	Ballroom Foyer

10:30 AM - 12:00 PM

Phase Contrast Principles and Applications	W H Faulkner, RT
Post Processing MRA	B Burrows, RT

12:00 PM - 1:00 PM

Luncheon	Franciscan and Imperial Ballrooms

1:00 PM - 2:30 PM

MRI Contrast Principles	R E Lenkinski, PhD
Neuro Applications	M A Soloman MD
Abdominal Applications	M E Bernardino, MD

2:30 PM - 3:00 PM

Break	Ballroom Foyer

3:00 PM - 4:30 PM

Breast Applications	R Clemens, RT
Musculoskeletal Applications	J J Busch, MD
Contrast Enhanced MRA	D D Stark, MD

SOCIETY OF MAGNETIC RESONANCE IN MEDICINE • SOCIETY FOR MAGNETIC RESONANCE IMAGING •

S M R T

Educational Program: Plaza Ballroom

SAT
3/27

8:00 AM - 10:00 AM
Introduction to MRI Scanning
Moderator: J P Keller, PhD

Intro to MRI: Show and Tell.................................P L Davis, MD
How to Diagnose & Resolve
Imaging Problems..J P Keller, PhD
Protocol and Technique....................................E K Fram, MD
FAST Imaging...S W Atlas, MD

10:00 AM - 10:30 AM
Break...Ballroom Foyer

10:30 AM - 12:00 PM
Brain Diagnostics I
Moderator: W T C Yuh, MD, MSEE

Brain Tumor..R N Bryan, MD
Sellar, Parasellar,
and Skull Base...............................W G Bradley, Jr, MD, PhD
MR of Stroke......................................W T C Yuh, MD, MSEE

12:00 PM - 1:30 PM
Luncheon...Franciscan and
Imperial Ballrooms

1:30 PM - 3:00 PM
Brain Diagnostics II
Moderator: R B Lufkin, MD

White Matter Disease
and Miscellaneous..B P Drayer, MD
Congenital Brain Disease.................................W S Ball, MD
Head and Neck..R B Lufkin, MD

3:00 PM - 3:30 PM
Break...Ballroom Foyer

3:30 PM - 5:00 PM
Spine Diagnostics
Moderator: G K Sze, MD

Tumor of the Spine..G K Sze, MD
Degenerative Disk Disease..................................J S Ross, MD
Congenital Spine Disease...........................A J Barkovich, MD

SUN
3/28

8:00 AM - 8:30 AM
Vascular Imaging
Moderator: A N Hasso, MD

CNS..A N Hasso, MD
Body..J P Finn, MD

8:30 AM - 10:00 AM
Body MR Diagnostics I
Moderator: P J Fritzsche, MD

Protocol and Technique......................................D D Stark, MD
Liver...M E Bernardino, MD
Kidney, Adrenal & Retroperitoneum..................P J Fritzsche, MD

10:00 AM - 10:30 AM
Break...Grand Ballroom

10:30 AM - 12:00 PM
Body MR Diagnostics II
Moderator: R J Herfkens, MD

Pelvis..H Y Kressel, MD
Pediatric Abdomen.................................R B Dietrich, MB, ChB
Cardiac and Thoracic Images...........................R J Herfkens, MD

12:00 PM - 1:30 PM
Luncheon..Grand Ballroom

1:30 PM - 3:00 PM
Shoulder MR Imaging
Moderator: J B Kneeland, MD

Shoulder: The Surgeon's Perspective..................M S Shapiro, MD
Shoulder: Instability..M Rafii, MD
Shoulder: Impingement/Rotator Cuff Disease...J B Kneeland, MD

3:00 PM - 3:30 PM
Break...Grand Ballroom

3:30 PM - 5:00 PM
Other Musculoskeletal MR Diagnostics
Moderator: L L Seeger, MD

Knee: Menisci & Cruciates..................................L L Seeger, MD
Knee: Non Meniscal Pathology.........................J V Crues III, MD
Foot/Ankle...R M Kerr, MD

Educational Program—MRI Economics Symposium: California Room

MON
3/29

Moderator: B J Hillman, MD, S W Young, MD

8:00 AM - 10:15 AM
New Initiatives for Funding MRI & MRS
Research at the National Cancer Institute.............F Shtern, MD
Pitfalls in Acquiring
MRI Equipment: Operational Experience....................H Salmon
Evaluating New Technologies for
Policy Purposes..B J McNeil, MD, PhD

10:15 AM - 10:45 AM
Break...Grand Ballroom

10:45 AM - 12:30 PM
Financial Structuring and Dissemination
of MRI Facilities in the 90's..................................C Farnsworth
Contrast Media Research:
Implications for MRI Reimbursement............G L Wolf, PhD, MD

12:30 PM - 1:30 PM
Luncheon..Grand Ballroom

1:30 PM - 3:00 PM
Managed MRI Scan Referrals:
Economic Impact...J V Crues III, MD
Self-Referral and Conflict
of Interest for Diagnostic Imaging....................B J Hillman, MD

3:00 PM - 3:45 PM
Break...Grand Ballroom

3:45 PM - 5:30 PM
Rate Regulation, Decreasing
Reimbursement and Strategies
for Adaption...M L Silbiger, MD, MBA
Competitive Strategies and
Reimbursement in MRI.......................................S W Young, MD

Scientific Program: Imperial Ballroom

SUN 3/28

Topical Conference: MRI Contrast and Contrast Agents

8:00 AM - 10:00 AM
Basics of Contrast
Moderator: G K Sze, MD

Tissue Contrast in MRI: Basic Principles and
Abdominal Applications ....D G Mitchell, MD
Basics of MR Contrast Agents ....R Brasch, MD
CNS Applications of Contrast.................M N Brant-Zawadzki, MD
Contrast Agents in the Spine.................................M T Modic, MD

10:00 AM - 10:30 AM
Break...Grand Ballroom

10:30 AM - 12:15 PM
Proffered Papers: Contrast Agent I: Abdomen/Chest
Moderators: P A Rinck, PhD, C E Spritzer, MD

001 10:30 AM 003 10:54 AM 005 11:18 AM 007 11:42 AM
002 10:42 AM 004 11:06 AM 006 11:30 AM 008 11:54 AM

12:15 PM - 1:30 PM
Luncheon...Grand Ballroom
Scientific Poster Discussion Period

1:30 PM - 3:00 PM
Functional and Hepatobiliary Imaging
Moderator: D LeBihan, MD, PhD

Hepatobiliary Contrast Media.................................D D Stark, MD
Functional MRI of the Brain.........................B R Rosen, MD, PhD
Diffusion..M E Moseley, PhD

3:00 PM - 3:30 PM
Break...Grand Ballroom

3:30 PM - 5:00 PM
Endogenous Contrast Mechanisms
Moderator: R M Henkelman, PhD

Magnetization Transfer Contrast in MRI ....R S Balaban, PhD
Calcium Contrast Mechanisms........................W Kucharczyk, MD
Susceptibility Contrast and Brain Iron....................E K Fram, MD

MON 3/29

Morning Tutorial Program

6:45 AM - 7:45 AM

k-Space and FAST Scan MRI
Franciscan Room A

k-Space: Basic Concepts ....J Listerud, MD, PhD
k-Space: Clinical Applications................................S W Atlas, MD

Musculoskeletal Imaging
Franciscan Room B

MR Imaging of the Shoulder ....M E Schwitzer, MD
MR Imaging of the Wrist ....T H Berquist, MD

Scientific Program

8:00 AM - 8:45 AM
Awards Presentation
Moderator: S E Harms, MD

Awards Presentation..S E Harms, MD
W S Moore Award Presentation......................R H Mohiaddin, MD
I I Rabi Award Presentation..............................L P Panych, MEng

8:45 AM - 10:00 AM
MRI Breast: Imaging and Interventional Strategies
Moderator: S E Harms, MD

Imaging Management of Breast Carcinoma ....W P Evans, MD
Potential Clinical Roles for Breast MRI.................S E Harms, MD
Minimally Invasive Therapy in
Breast Cancer ....S G Bown, MD, FRCP

10:00 AM - 10:45 AM
Break...Grand Ballroom

10:45 AM - 12:30 PM
Proffered Papers

12:30 PM - 1:30 PM
Luncheon...Grand Ballroom
Scientific Poster Discussion Period

1:30 PM - 3:00 PM
Cardiac MRI: Functional and Clinical Applications
Moderator: K M Link, MD

Adult Cardiac Evaluation.......................................R D White, MD
Functional Cardiac Imaging..............................R J Herfkens, MD
Heart Wall Motion and Image Processing.....................L Axel, MD

3:00 PM - 3:45 PM
Break...Grand Ballroom

3:45 PM - 5:30 PM
Proffered Papers

Scientific Program: Imperial Ballroom

TUE 3/30

Morning Tutorial Program

6:45 AM - 7:45 AM
Surface Coils
Franciscan Room A

New Advances in Surface Coils ....R E Lenkinski, PhD
Surface Coil Applications in the Pelvis ....M D Schnall, MD, PhD

MR Angiography
Franciscan Room B

MR Angiography: Nuts and Bolts of Pulse Sequences ....D L Parker, PhD
MR Angiography: Current Limitations ....P Ruggieri, MD

Scientific Program

8:00 AM - 9:30 AM
MRA: Technical Advances and Clinical Efficacy
Moderator: A W Litt, MD

MRA: CNS Time-of-Flight ....T J Masaryk, MD
Phase Contrast MRA: Neurological Applications.....P A Turski, MD
MRA in the Body ....P J Finn, MD

9:30 AM - 10:30 AM
Break........................Grand Ballroom

10:30 AM - 12:15 PM
Proffered Papers

12:15 PM - 1:30 PM
Luncheon........................Grand Ballroom
Scientific Poster Discussion Period

1:30 PM - 3:00 PM
MR Flow: Quantitative and Clinical Applications
Moderator: E M Haacke, PhD

CSF Flow ....D Enzman, MD
Cardiac Applications and Bolus Tracking ....R R Edelman, MD
Phase Contrast Applications ....N Pelc, PhD

3:00 PM - 3:45 PM
Break........................Grand Ballroom

3:45 PM - 5:30 PM
Proffered Papers

WED 3/31

Morning Tutorial Program

6:45 AM - 7:45 AM
Motion Compensation
Franciscan Room A

Basic Physics of Motion Compensation Techniques ....M L Wood, PhD
Clinical Applications of Motion Compensation in Body MRI........................D G Mitchell, MD

Functional Brain MRI
Franciscan Room B

Physiological Issues in Functional Brain Imaging ....K R Thulborne, MD, PhD
Functional Brain Imaging with MRI..............B R Rosen, MD, PhD

Scientific Program

8:00 AM - 9:30 AM
Fast Scan Techniques in the Abdomen: Clinical Efficacy
Moderator: J C Weinreb, MD

Limitations of Fast Scan ....S J Riederer, PhD
E Delang, MD
Advantages of Fast Scan........................J P Mugler III, PhD
D Johnson, MD

9:30 AM - 10:30 AM
Break........................Grand Ballroom

10:30 AM - 12:15 PM
Proffered Papers

12:15 PM - 1:00 PM
Luncheon........................Grand Ballroom
Scientific Poster Discussion Period

1:00 PM - 2:30 PM
MRI Segmentation: Interventional and Stereotactic Strategies
Moderator: L P Clarke, PhD

Interventional MRI ....R B Lufkin, MD
Deformable Anatomic Atlases and Validation of Segmentation........................M W Vannier, MD
MRI: Automatic Segmentation Techniques...........L P Clarke, PhD

2:30 PM - 2:45 PM
Break........................Grand Ballroom

2:45 PM - 4:30 PM
Proffered Papers

Scientific Program Proffered Papers

MON

3/29

10:45 AM - 12:30 PM

Papers 101-108 **Head and Neck I** Franciscan Room B	**Papers 109-116** **Contrast Agent II: Experimental I** Franciscan Room C	**Papers 117-124** **MRA: Clinical I** Plaza A	**Papers 125-132** **Rapid Imaging Techniques I** Plaza B	**Papers 133-140** **Breast** Imperial Ballroom
Moderators: *A N Hasso, MD* *W R K Smoker, MD*	***Moderators:*** *W G Bradley, Jr, MD, PhD* *D D Stark, MD*	***Moderators:*** *R A Clark, MD* *P J Fritzsche, MD*	***Moderators:*** *M S Cohen, PhD* *S R Thomas, PhD*	***Moderators:*** *R Kikinis, MD* *M L Silbiger, MD*
101 **10:45 AM**	109 **10:45 AM**	117 **10:45 AM**	125 **10:45 AM**	133 **10:45 AM**
102 **10:57 AM**	110 **10:57 AM**	118 **10:57 AM**	126 **10:57 AM**	134 **10:57 AM**
103 **11:09 AM**	111 **11:09 AM**	119 **11:09 AM**	127 **11:09 AM**	135 **11:09 AM**
104 **11:21 AM**	112 **11:21 AM**	120 **11:21 AM**	128 **11:21 AM**	136 **11:21 AM**
105 **11:33 AM**	113 **11:33 AM**	121 **11:33 AM**	129 **11:33 AM**	137 **11:33 AM**
106 **11:45 AM**	114 **11:45 AM**	122 **11:45 AM**	130 **11:45 AM**	138 **11:45 AM**
107 **11:57 AM**	115 **11:57 AM**	123 **11:57 AM**	131 **11:57 AM**	139 **11:57 AM**
108 **12:09 PM**	116 **12:09 PM**	124 **12:09 PM**	132 **12:09 PM**	140 **12:09 PM**

3:45 PM - 5:30 PM

Papers 141-148 **Cardiac I** Franciscan Room A	**Papers 149-156** **Pulse Sequence I** Franciscan Room B	**Papers 157-164** **Flow Velocity I** Franciscan Room C	**Papers 165-172** **Angiography Techniques I** Plaza A	**Papers 173-180** **Musculoskeletal I** Plaza B	**Papers 181-188** **Perfusion/ Diffusion I** Imperial Ballroom
Moderators: *M R Fisher, MD* *R J Herfkens, MD*	***Moderators:*** *J R MacFall, PhD* *M S Silver, PhD*	***Moderators:*** *C Dumoulin, PhD* *D G Nishimura, PhD*	***Moderators:*** *J A Arrington, MD* *M S Cohen, PhD*	***Moderators:*** *J V Crues III, MD* *R Kier, MD*	***Moderators:*** *R R Edelman, MD* *P M Joseph, PhD*
141 **3:45 PM**	149 **3:45 PM**	157 **3:45 PM**	165 **3:45 PM**	173 **3:45 PM**	181 **3:45 PM**
142 **3:57 PM**	150 **3:57 PM**	158 **3:57 PM**	166 **3:57 PM**	174 **3:57 PM**	182 **3:57 PM**
143 **4:09 PM**	151 **4:09 PM**	159 **4:09 PM**	167 **4:09 PM**	175 **4:09 PM**	183 **4:09 PM**
144 **4:21 PM**	152 **4:21 PM**	160 **4:21 PM**	168 **4:21 PM**	176 **4:21 PM**	184 **4:21 PM**
145 **4:33 PM**	153 **4:33 PM**	161 **4:33 PM**	169 **4:33 PM**	177 **4:33 PM**	185 **4:33 PM**
146 **4:45 PM**	154 **4:45 PM**	162 **4:45 PM**	170 **4:45 PM**	178 **4:45 PM**	186 **4:45 PM**
147 **4:57 PM**	155 **4:57 PM**	163 **4:57 PM**	171 **4:57 PM**	179 **4:57 PM**	187 **4:57 PM**
148 **5:09 PM**	156 **5:09 PM**	164 **5:09 PM**	172 **5:09 PM**	180 **5:09 PM**	188 **5:09 PM**

PERSONAL ITINERARY:

Morning

Afternoon

Scientific Program Proffered Papers

TUE
3/30

10:30 AM - 12:15 PM

Papers 201-208 **Cardiac II** California Room	Papers 209-216 **Abdomen** Franciscan Room B	Papers 217-224 **Brain** Plaza A	Papers 225-232 **Rapid Imaging Techniques II** Plaza B	Papers 233-240 **Contrast Agent III: Experimental II** Imperial Ballroom
Moderators: *L Eastwood, PhD* *C B Higgins, MD*	***Moderators:*** *D G Mitchell, MD* *P Y Poon, MD*	***Moderators:*** *K R Maravilla, MD* *A S Smith, MD*	***Moderators:*** *J Listerud, MD, PhD* *S J Riederer, PhD*	***Moderators:*** *T J Brady, MD* *R L Nunnally, PhD*
201 **10:30 AM**	209 **10:30 AM**	217 **10:30 AM**	225 **10:30 AM**	233 **10:30 AM**
202 **10:42 AM**	210 **10:42 AM**	218 **10:42 AM**	226 **10:42 AM**	234 **10:42 AM**
203 **10:54 AM**	211 **10:54 AM**	219 **10:54 AM**	227 **10:54 AM**	235 **10:54 AM**
204 **11:06 AM**	212 **11:06 AM**	220 **11:06 AM**	228 **11:06 AM**	236 **11:06 AM**
205 **11:18 AM**	213 **11:18 AM**	221 **11:18 AM**	229 **11:18 AM**	237 **11:18 AM**
206 **11:30 AM**	214 **11:30 AM**	222 **11:30 AM**	230 **11:30 AM**	238 **11:30 AM**
207 **11:42 AM**	215 **11:42 AM**	223 **11:42 AM**	231 **11:42 AM**	239 **11:42 AM**
208 **11:54 AM**	216 **11:54 AM**	224 **11:54 AM**	232 **11:54 AM**	240 **11:54 AM**

3:45 PM - 5:30 PM

Papers 241-248 **Spectroscopy: Human** California Room	Papers 249-256 **Pelvis** Franciscan Room A	Papers 257-264 **Head and Neck II** Franciscan Room B	Papers 265-272 **Angiography Techniques II** Plaza A	Papers 273-280 **Musculoskeletal II** Plaza B	Papers 281-287 **Perfusion/ Diffusion II** Imperial Ballroom
Moderators: *P A Narayana, PhD* *R R Price, PhD*	***Moderators:*** *R C Smith MD* *J C Weinreb, MD*	***Moderators:*** *W P Dillon, MD* *R B Lufkin, MD*	***Moderators:*** *E M Haacke, PhD* *B D Pressman, MD*	***Moderators:*** *J Beltran, MD* *J B Kneeland, MD*	***Moderators:*** *M J Bronskill, PhD* *M E Moseley, PhD*
241 **3:45 PM**	249 **3:45 PM**	257 **3:45 PM**	265 **3:45 PM**	273 **3:45 PM**	281 **3:45 PM**
242 **3:57 PM**	250 **3:57 PM**	258 **3:57 PM**	266 **3:57 PM**	274 **3:57 PM**	282 **3:57 PM**
243 **4:09 PM**	251 **4:09 PM**	259 **4:09 PM**	267 **4:09 PM**	275 **4:09 PM**	283 **4:09 PM**
244 **4:21 PM**	252 **4:21 PM**	260 **4:21 PM**	268 **4:21 PM**	276 **4:21 PM**	284 **4:21 PM**
245 **4:33 PM**	253 **4:33 PM**	261 **4:33 PM**	269 **4:33 PM**	277 **4:33 PM**	285 **4:33 PM**
246 **4:45 PM**	254 **4:45 PM**	262 **4:45 PM**	270 **4:45 PM**	278 **4:45 PM**	286 **4:45 PM**
247 **4:57 PM**	255 **4:57 PM**	263 **4:57 PM**	271 **4:57 PM**	279 **4:57 PM**	287 **4:57 PM**
248 **5:09 PM**	256 **5:09 PM**	264 **5:09 PM**	272 **5:09 PM**	280 **5:09 PM**	

PERSONAL ITINERARY:

Morning

Afternoon

Scientific Program Proffered Papers

WED 3/31

10:30 AM - 12:15 PM

Papers 301-308	Papers 309-316	Papers 317-324	Papers 325-332	Papers 333-340
Spectroscopy II	**MRI: General**	**Flow Velocity II**	**MRA: Clinical II**	**Contrast Agent IV: Brain and Miscellaneous**
California Room	Franciscan Room B	Plaza A	Plaza B	Imperial Ballroom
Moderators: *G B Matson, PhD* *J A Sorenson, PhD*	***Moderators:*** *M R Fisher, MD* *N J Pelc, ScD*	***Moderators:*** *R S Hinks, PhD* *S R Thomas, PhD*	***Moderators:*** *C Dumoulin, PhD* *T R McCauley, MD*	***Moderators:*** *S B Peterman, MD* *G K Sze, MD*
301 **10:30 AM**	309 **10:30 AM**	317 **10:30 AM**	325 **10:30 AM**	333 **10:30 AM**
302 **10:42 AM**	310 **10:42 AM**	318 **10:42 AM**	326 **10:42 AM**	334 **10:42 AM**
303 **10:54 AM**	311 **10:54 AM**	319 **10:54 AM**	327 **10:54 AM**	335 **10:54 AM**
304 **11:06 AM**	312 **11:06 AM**	320 **11:06 AM**	328 **11:06 AM**	336 **11:06 AM**
305 **11:18 AM**	313 **11:18 AM**	321 **11:18 AM**	329 **11:18 AM**	337 **11:18 AM**
306 **11:30 AM**	314 **11:30 AM**	322 **11:30 AM**	330 **11:30 AM**	338 **11:30 AM**
307 **11:42 AM**	315 **11:42 AM**	323 **11:42 AM**	331 **11:42 AM**	339 **11:42 AM**
308 **11:54 AM**	316 **11:54 AM**	324 **11:54 AM**	332 **11:54 AM**	340 **11:54 AM**

2:45 PM - 4:30 PM

Papers 341-348	Papers 349-356	Papers 357-364	Papers 365-373	Papers 374-381	Papers 382-388
Chest/Cardiac	**Relaxometry**	**Pulse Sequence II**	**Image Processing**	**Musculoskeletal III: Spine**	**Perfusion/ Diffusion III**
California Room	Franciscan Room A	Franciscan Room B	Plaza A	Plaza B	Imperial Ballroom
Moderators: *J L Duerk, PhD* *R D White, MD*	***Moderators:*** *G D Fullerton, PhD* *S W Young, MD*	***Moderators:*** *W Sattin, PhD* *F G Shellock, PhD*	***Moderators:*** *L P Clarke, PhD* *D N Levin, MD, PhD*	***Moderators:*** *B D Flannigan-Sprague, MD* *E Kanal, MD*	***Moderators:*** *S Majumdar, MD* *V M Runge, MD*
341 **2:45 PM**	349 **2:45 PM**	357 **2:45 PM**	365 **2:45 PM**	374 **2:45 PM**	382 **2:45 PM**
342 **2:57 PM**	350 **2:57 PM**	358 **2:57 PM**	366 **2:57 PM**	375 **2:57 PM**	383 **2:57 PM**
343 **3:09 PM**	351 **3:09 PM**	359 **3:09 PM**	367 **3:09 PM**	376 **3:09 PM**	384 **3:09 PM**
344 **3:21 PM**	352 **3:21 PM**	360 **3:21 PM**	368 **3:21 PM**	377 **3:21 PM**	385 **3:21 PM**
345 **3:33 PM**	353 **3:33 PM**	361 **3:33 PM**	369 **3:33 PM**	378 **3:33 PM**	386 **3:33 PM**
346 **3:45 PM**	354 **3:45 PM**	362 **3:45 PM**	370 **3:45 PM**	379 **3:45 PM**	387 **3:45 PM**
347 **3:57 PM**	355 **3:57 PM**	363 **3:57 PM**	371 **3:57 PM**	380 **3:57 PM**	388 **3:57 PM**
348 **4:09 PM**	356 **4:09 PM**	364 **4:09 PM**	372 **4:09 PM**	381 **4:09 PM**	
			373 **4:21 PM**		

PERSONAL ITINERARY:

Morning

Afternoon

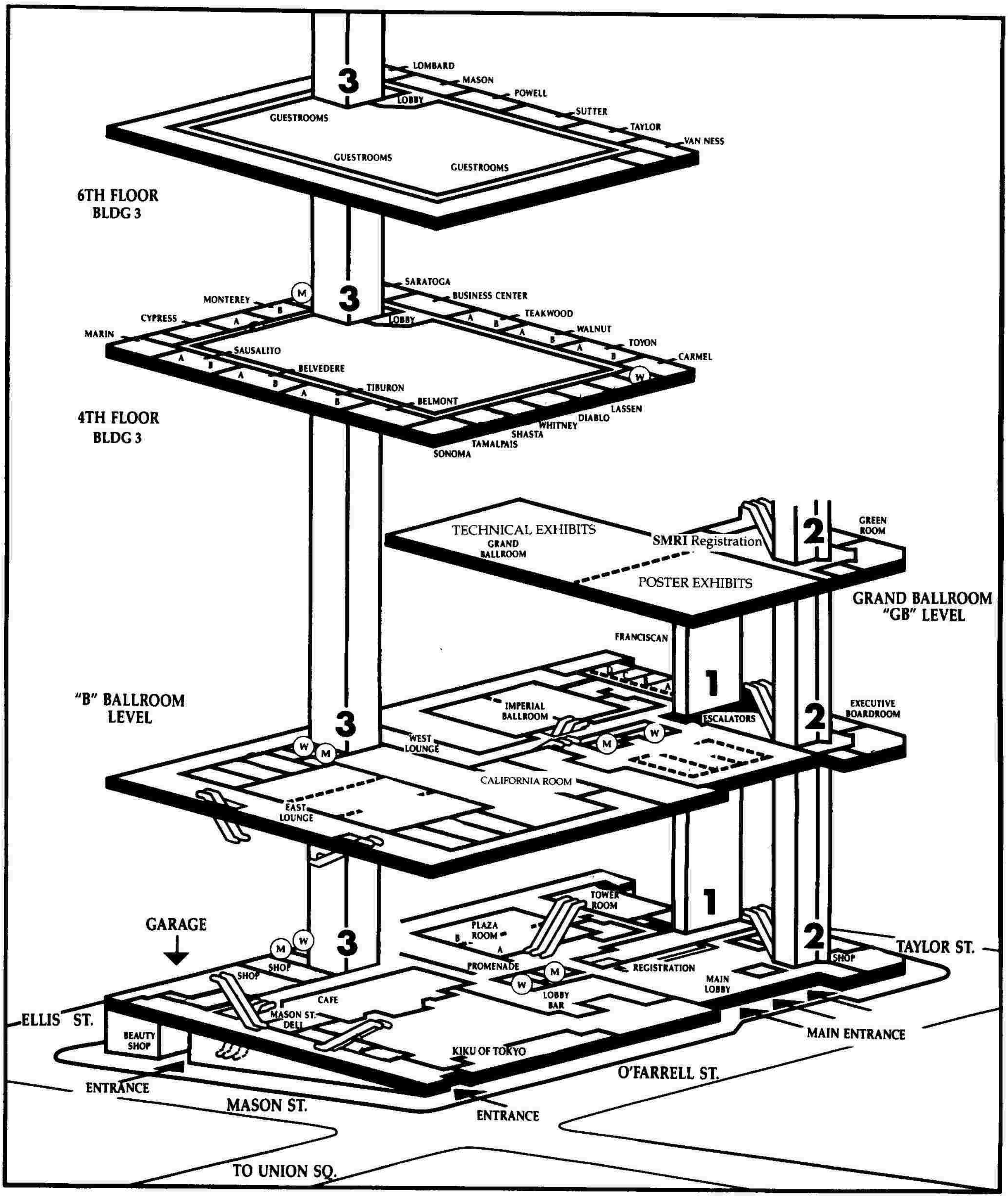
3
LOMBARD
MASON
POWELL
SUTTER
TAYLOR
VAN NESS
LOBBY
GUESTROOMS
GUESTROOMS
GUESTROOMS
6TH FLOOR
BLDG 3
SARATOGA
BUSINESS CENTER
TEAKWOOD
WALNUT
TOYON
CARMEL
MONTEREY
CYPRESS
MARIN
M
3
LOBBY
SAUSALITO
BELVEDERE
TIBURON
BELMONT
W
LASSEN
DIABLO
WHITNEY
SHASTA
TAMALPAIS
SONOMA
A
B
4TH FLOOR
BLDG 3
TECHNICAL EXHIBITS
GRAND
BALLROOM
SMRI Registration
POSTER EXHIBITS
2
GREEN
ROOM
GRAND BALLROOM
"GB" LEVEL
FRANCISCAN
1
"B" BALLROOM
LEVEL
IMPERIAL
BALLROOM
ESCALATORS
2
EXECUTIVE
BOARDROOM
3
W
M
WEST
LOUNGE
CALIFORNIA ROOM
EAST
LOUNGE
GARAGE
TOWER
ROOM
PLAZA
ROOM
1
2
M
W
3
SHOP
SHOP
PROMENADE
REGISTRATION
MAIN
LOBBY
SHOP
TAYLOR ST.
LOBBY
BAR
CAFE
MASON ST.
DELI
ELLIS ST.
BEAUTY
SHOP
KIKU OF TOKYO
MAIN ENTRANCE
O'FARRELL ST.
ENTRANCE
MASON ST.
ENTRANCE
TO UNION SQ.

SMRI

Society for Magnetic Resonance Imaging

MEMORANDUM

DT: March 4, 1993
TO: SMRI Membership
FR: Steven E. Harms, MD, SMRI President
RE: 1993 Annual Business Meeting Call to Attendance

****

Detailed below please find a preliminary agenda for the 1993 Annual Business Meeting of the Society for Magnetic Resonance Imaging scheduled on Monday, March 29, 10:00 am - 10:30 am in the Imperial Ballroom of the San Francisco Hilton and Towers.

Annual Business Meeting Preliminary Agenda

1. REPORT FROM THE PRESIDENT

1.1 Educational Structure Reorganization

- Ad Hoc ACCME Committee Status Report
- Annual Meeting and Education Coordination Council (AMECC) Reorganization

1.2 Merger Discussions with the Society of Magnetic Resonance in Medicine (SMRM)

2. REPORT FROM THE PAST PRESIDENT

2.1 Journal of Magnetic Resonance Imaging (JMRI) Status Report
2.2 Combined Section of MR Technologists (SMRT) Status Report

3. REPORT FROM THE SECRETARY

3.1 Results of the 1993 - 1994 Elections
3.2 Review of Proposed Constitution and Bylaws Revisions
3.3 Thank You to Members Interested in Participating on Society Committees

4. REPORT FROM THE TREASURER

4.1 June 30, 1992 Year End Audit Report
4.2 1993 Fiscal Year Status Report

5. TRANSFER OF OFFICE TO INCOMING PRESIDENT

As you will note, in addition to reviewing Society activities during the past year, the Meeting will address two very important issues relative to the Society's future: a reorganization of the Society's educational structure and a possible Society merger with the SMRM. Your attendance at the Meeting is strongly urged as the Society's future direction is determined by the membership and thus, your input is essential to the SMRI's continued growth and development.

Should you be unable to attend the meeting, please forward your comments/concerns regarding the educational restructuring (as detailed in the proposed Constitution/Bylaws revisions of the pre-Meeting membership mailing) and/or a potential merger with the SMRM to an SMRI Officer/Board member prior to the Meeting so that your comments may be addressed in that forum.

The Society looks forward to reviewing its accomplishments during the past year and discussing its goals for the future with you in San Francisco.

213 West Institute Place • Suite 501 • Chicago, IL 60610 • 312-751-2590 • FAX 312-951-6474

Editorial

SMRI 1993: Annual Meeting Overview

WE PRESENT AN OVERVIEW of the Eleventh Annual Meeting of the Society for Magnetic Resonance Imaging (SMRI) to help you appreciate the wide range of activities being offered. This year, the Annual Meeting has been organized with a mandate similar to that of the previous meetings, namely to provide a comfortable forum for clinicians, clinical scientists, basic scientists, and technologists to discuss problems and share ideas. It is the product of the efforts of many people, including members of the Annual Meeting Organizing Committee, corporate sponsors, abstract reviewers, session moderators, presenters, the staff at the SMRI Central Office, and, we hope, more participants than ever. The Annual Meeting includes the Scientific Program, Poster Program, Morning Tutorial Program, Educational Program, MRI Economics Symposium, Combined Section for Magnetic Resonance Technologists (SMRT) Technologist Workshop, extensive technical exhibits, and social activities.

The Scientific Program is the forum for presentation of work at the forefront of magnetic resonance (MR) research. The Scientific Program begins on Sunday morning, March 28, and continues until Wednesday afternoon, March 31. Each day includes both plenary symposia and proffered-paper sessions. Similarly to the past five Annual Meetings, the first day is devoted to a topical symposium; this year it will be on the subject of contrast and contrast agents. The remainder of the Program attempts to accommodate the wide spectrum of MR research. The plenary symposia aim to consolidate knowledge on particularly relevant topics. This year, the plenary symposia feature contrast agents, breast imaging, heart imaging, MR angiography and flow, fast imaging, and image segmentation. These topics should appeal to essentially everyone involved in the MR field. We thank Laurence P. Clarke, PhD, and Jeffrey S. Ross, MD, for organizing the Scientific Program.

Posters have proved to be an effective format for presenting MR research. Certain work can be communicated better through a poster than an oral presentation. Other posters consist of research that could not be presented orally because of insufficient space or unavailability of a suitable proffered-paper session. Clearly, poster presentations are an important channel for communicating scientific research. Richard L. Ehman, MD, and Perry Sprawls, PhD, deserve credit for organizing the Poster Program.

Ever since the first SMRI Annual Meeting, many participants have welcomed tutorials and clinical case reviews, even when these sessions followed a full day of lectures. This year, the tutorials are in the morning rather than the evening. It is hoped that the rescheduling will ease the transition from the business of the day into the social events of the evening, for which the SMRI Annual Meeting is well known. Credit for planning the morning tutorials belongs to Scott W. Atlas, MD, and Stephen J. Riederer, PhD.

Also, since the first SMRI Annual Meeting more than a decade ago, participants have responded favorably to the Educational Program. The Program continues to evolve, thanks to experience and also to the comments on evaluation forms submitted by the participants. This year, the Educational Program promises to be as effective and well received as its predecessors. It has been organized by Paul J. Keller, PhD, William Sattin, PhD, and William T. C. Yuh, MD, MSEE.

Two years ago, the Educational Program was expanded to include a symposium on economics and reimbursement issues. Such a symposium has been part of the Annual Meeting ever since. Bruce J. Hillman, MD, and Stuart W. Young, MD, are to be congratulated for their efforts in organizing this year's MRI Economics Symposium.

The SMRT is holding a workshop at the Annual Meeting. We expect that this workshop will be as impressive as those of previous regional meetings, which have demonstrated enthusiastic support for this new organization of MR technologists. Rodney Bell, RT, and Luann Culbreth, MEd, deserve credit for organizing the workshop.

Two of the most visible aspects of the Annual Meeting are audiovisual services and local arrangements, for which Dwight G. Nishimura, PhD, and Michael E. Moseley, PhD, respectively, deserve thanks.

The staff at the SMRI Central Office have become indispensable in organizing the Annual Meeting. Kristen Q. Coe, who is the Executive Director, has been with the SMRI through five Annual Meetings. Karen Bacidore, who also has several years of experience, coordinated the various preparations for the Scientific Program. Kimberley Poff, who joined the Central Office recently after four years with the Convention Service Department of the Hyatt Regency Hotel in Chicago, coordinated most of the other preparations. The experience and hard work of these Central Office staff members are the main reasons that the SMRI can produce a well-organized Annual Meeting.

Index terms: Editorials • Radiology and radiologists, education • Society for Magnetic Resonance Imaging • Society for Magnetic Resonance Imaging, annual meeting

JMRI 1993; 3(P):19–20

Finally, we express our appreciation to Steven E. Harms, MD, who, as President of the SMRI, asked us to serve as Annual Meeting Organizing Committee Co-Chairmen. Comments about this year's Annual Meeting or suggestions for improving future Annual Meetings are encouraged. They should be directed to the SMRI Central Office at (312) 751-2590 and (FAX) (312) 951-6474. We hope that we have helped create a meeting that will uphold the impressive tradition of the first 10 SMRI Annual Meetings—relevant, informative, and stimulating.

MICHAEL L. WOOD, PhD
WALTER KUCHARCZYK, MD
Co-Chairmen of the Annual Meeting Organizing Committee and Guest Editors

Notes

Notes

MR

1 9 9 3

PLENARY SYMPOSIA

From the Contrast Agent Topical Symposium on Sunday through the MRI Segmentation session on Wednesday, the Plenary Symposia, spaced throughout the week, highlight the Annual Meeting's educational programming. The Plenary Symposia also provide the opportunity to recognize Society Award recipients and to honor individuals who have made important contributions to MRI.

SUNDAY, MARCH 28

8:00 AM - 10:00 AM
Basics of Contrast

1:30 PM - 3:00 PM
Functional and Hepatobiliary Imaging

3:30 PM - 5:00 PM
Endogenous Contrast Mechanisms

MONDAY, MARCH 29

8:00 AM - 10:00 AM
Award Presentations
MRI Breast: Imaging and Interventional Strategies

1:30 PM - 3:00 PM
Cardiac MRI: Functional and Clinical Applications

TUESDAY, MARCH 30

8:00 AM - 9:30 AM
MRA: Technical Advances and Clinical Efficacy

1:30 PM - 3:00 PM
MR Flow: Quantitative and Clinical Applications

WEDNESDAY, MARCH 31

8:00 AM - 9:30 AM
Fast Scan Techniques in the Abdomen: Clinical Efficacy

1:00 PM - 2:30 PM
MRI Segmentation: Interventional and Stereotactic Strategies

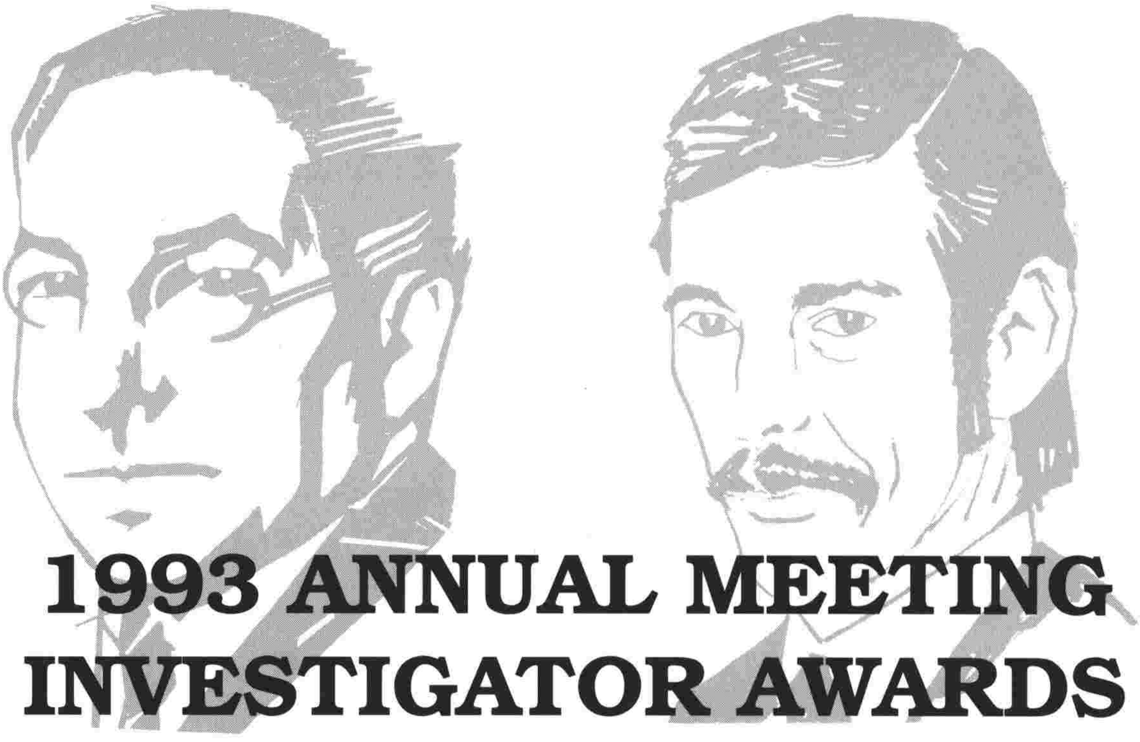

1993 ANNUAL MEETING INVESTIGATOR AWARDS

Isidor I Rabi Award

This award is named in memory of Isidor Isaac Rabi, physicist, statesman, and pioneer of modern science. During the 1930's, Rabi and his co-workers at Columbia University developed and used nuclear magnetic resonance methods to measure, with extreme accuracy, the magnetic properties of nuclei. This work earned Rabi the 1944 Nobel prize in physics and directly stimulated research on collective nuclear magnetic resonance in solids and liquids, which has led to magnetic resonance spectroscopy and imaging. I I Rabi died in 1988 at the age of 89.

Lawrence P Panych

Mr. Panych is a research assistant at Brigham and Women's Hospital, Harvard Medical School, Department of Radiology, and a graduate student in Radiological Sciences at the Massachusetts Institute of Technology. His current PhD research thesis is in the area of the development of adaptive imaging technique based upon wavelet transform encoding. He is a native of Alberta, Canada, having attended college at the University of Alberta and was graduated with a Bachelor's degree in philosophy. A second Bachelor's degree was earned in biomedical engineering from McGill University and a Master's degree from the University of British Columbia. During that time, Mr. Panych worked for five years as a research engineer with the reknowned neurologist, Dr. J A Wada, in the development of an automated unit for long term monitoring of intractable seizure patients. The work involved biological signal processing and pattern recognition and some work with expert systems. He has been in Boston since 1988 and his current interests are in basic imaging principles and novel applications of magnetic resonance imaging.

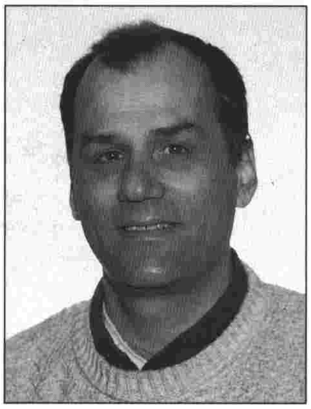

William S Moore Award

This award is named in memory of William Stanley Moore, physicist and Past President of the **SMRI**. William S Moore was born in 1936 in Ardrossan, Scotland and was educated at Merchiston Castle School in Edinburgh. He won an open scholarship to Caius College Cambridge where he was graduated with a BA degree in physics in 1958 and a MA in 1961. Thereafter, he moved to Nottingham University where he obtained his PhD for research in electron paramagnetic resonance. From 1961 to 1983, he served on staff at Nottingham University before moving to Boston as Director of NMR Physics at the Brigham and Women's Hospital. In 1984, Dr. Moore was elected President of the Society and died shortly afterwards on the 25th of March at the age of 47.

Raad H Mohiaddin, MD

Dr. Mohiaddin received his MD degree from Mosul University, Iraq, in 1981 where he received his training as a cardiologist. Since 1984, he has been working at the magnetic resonance unit of the Royal Brompton National Heart and Lung Hospitals in London, England, and has been involved in the development and clinical use of cardiovascular magnetic resonance imaging. Currently, he is heading the clinical sciences group of this department. His main interest is in functional MRI as applied to congenital and acquired cardiovascular disease.

SMRI '93 Eleventh Annual Meeting
Plenary Symposia

Sunday Morning • Imperial Ballroom
Plenary Symposia 001–004

BASICS OF CONTRAST

MODERATOR: GK Sze, MD
8:00 AM–10:00 AM

PS 001 • 8:00 AM

Tissue Contrast in MR Imaging: Basic Principles and Abdominal Applications

DG Mitchell, MD
Department of Radiology, Thomas Jefferson University Hospital, Philadelphia, PA

The greatest strength of MR imaging lies in its versatile depiction of tissue contrast. The variety of abdominal tissues and pathologic processes provide an especially challenging model for development of a comprehensive examination to potentially replace a battery of other tests. T1, T2, chemical shift, and flow contrast can be achieved with spin-echo, inversion-recovery, gradient-echo, RARE, and echo-planar techniques. The liver and pancreas have shorter T1 than most other nonfatty tissues, possibly due to high intracellular surface area. Damaged parenchyma and most tumors have longer T1, rendering them conspicuous on T1-weighted MR images, while well-differentiated hepatocellular tumors may have similar or even shorter T1. T2-weighted images depict most inflammatory or neoplastic abnormalities as hyperintense. Iron overload in the liver, pancreas, and spleen can be identified, excluded, and/or quantified on T2- and T2*-weighted images, allowing diagnosis and grading of and distinction between iron-overload states, potentially obviating biopsy. The chemical shift between triglyceride and water allows the accurate identification or exclusion of lipid by fat/water opposed-phase or signal suppression techniques. Suppression of lipid signal also reduces lipid-induced image degradation and increases the conspicuity of tissues enhanced by paramagnetic contrast agents. Flow can be detected and measured by physical displacement of protons or by phase changes relative to static tissue. MR angiographic techniques can help assess suspected vascular pathology, including aortic disease or stenosis/occlusion of many abdominal arteries and veins. Comprehensive MR imaging can help diagnose or exclude a greater range of diseases than any other modality.

PS 002 • 8:30 AM

Basics of MR Contrast Agents

RC Brasch, MD
Department of Radiology, University of California, San Francisco, CA

The purpose of this presentation is to familiarize and update the practicing diagnostician on MR contrast media, including modes of action, current indications, safety, dose considerations, and new applications. Similarities and potential differences in available or "soon-to-be-released" gadolinium chelate formulations will be discussed. Current indications for using intravenously infused paramagnetic contrast media for central nervous system (CNS) diagnosis include leptomeningeal disease, metastases, distinction of residual tumor from postoperative changes, pituitary microadenomas, acoustic neuromas, and epidural fibrosis versus herniated disk. Relatively newer applications of small-molecular gadolinium complexes, outside the CNS, include characterization of breast masses, evaluation of the female pelvis, and musculoskeletal enhancement. Differences between the modes of action of paramagnetic and magnetic susceptibility agents will be detailed. The strategies for the design of newer agents that have unique distribution and enhancement patterns will be explained. These include oral agents for the gastrointestinal tract, macromolecular agents for perfusion and capillary integrity imaging, and particulates for imaging the reticuloendothelial system (liver, spleen, and lymph nodes). The potential utility for liver imaging with small-molecule chelates with specific uptake by the hepatocyte can be shown from preclinical studies. The potential of a new generation of smaller superparamagnetic nanoparticles (MIONs) that can be linked to a variety of bioactive carriers will also be demonstrated.

PS 003 • 9:00 AM

Central Nervous System Applications of Contrast Agents

MN Brant-Zawadzki, MD
Department of Radiology, Hoag Memorial Hospital, Newport Beach, CA

Approximately 35% of all clinical MR studies of the central nervous system (CNS) use contrast agents. The first of the paramagnetic agents approved for use was gadopentetate dimeglumine. Millions of doses of this agent have been used worldwide. Recently, 2 nonionic agents have been clinically tested and approved for human use (gadodiamide, gadoteridol). These agents have a theoretically improved safety margin, particularly with higher doses, given the lower osmolar load they present. Preliminary experience suggests that a double or triple dose (up to 0.3 mmol/kg) of these agents can improve sensitivity in the detection of metastatic disease (and potentially other lesions). The most widespread use of paramagnetic contrast agents in MR imaging of the CNS involves screening and following up patients with metastatic disease involving the brain or the spinal canal. Leptomeningeal disease can easily be missed without the use of intravenous contrast agents. Contrast agents can be used to differentiate the effects of therapy from new, recurrent, or residual disease. In the spine, the most common use for these agents is the differentiation of postsurgical epidural granulation tissue from residual or recurrent disk herniation. New uses of contrast agents exploit the magnetic susceptibility effects of these agents, particularly on their first pass through the intracranial circulation, for perfusion imaging of the brain. Also, these agents can enhance MR angiography, particularly in the venous circulation. Finally, 3D image rendition of MR imaging studies benefits from the use of these agents, making segmentation of lesions easier. This plenary session will serve to summarize the clinical utility of paramagnetic contrast agents in the CNS and focus on the newer developments in this arena.

PS 004 • 9:30 AM

Contrast Agents in the Spine

MT Modic, MD

Cleveland Clinic Foundation, Cleveland, OH

Contrast-enhanced MR imaging has emerged as an important adjunct technique for the diagnosis of both intrinsic and extrinsic lesions of the spine. The common pathway for enhancement in both normal and abnormal structures relates to a prominent vasculature, a permeable capillary endothelium, and a capacious extravascular space. In healthy subjects, enhancement can be identified in the epidural venous plexus, basivertebral veins, and both cartilage and ossification centers in children. Enhancement within the vertebral body in an adult, however, is usually abnormal. Data to date would suggest that contrast-enhanced MR imaging is becoming routine in patients with suspected intramedullary disease, neoplasms, infection, vascular abnormalities, and in the postoperative lumbar spine. Its use in the nonoperated spine for degenerative disease, while interesting, is not yet established. This presentation will summarize the known limitations and potential benefits of the use of contrast agents in the spine.

Sunday Afternoon • Imperial Ballroom
Plenary Symposia 005–007

FUNCTIONAL AND HEPATOBILIARY IMAGING

MODERATOR: D Le Bihan, MD, PhD

1:30 PM–3:00 PM

PS 005 • 1:30 PM

Hepatobiliary Contrast Media

DD Stark, MD

University of Massachusetts Medical Center, Worcester, MA

Intensive efforts to improve the diagnostic utility of body MR imaging have resulted in a variety of specialized methods for pharmaceutical manipulation of contrast and tissue signal-to-noise ratios. Paramagnetic ions such as gadolinium (III), iron (III), and manganese (II) have unpaired outer-shell electrons that align (magnetic susceptibility) with an externally applied magnetic field (B_0). Fluctuations in the orientation of these electrons relative to adjacent water protons produce electron-proton dipole-dipole interactions that enhance (increase) the rate of longitudinal (T1) relaxation. Crystalline iron oxides are related to the particles that serve as recording materials on magnetic tapes. Ferro- or ferrimagnetic crystal structures pool the unpaired electrons of constituent atoms and therefore have a net magnetic susceptibility that is approximately a hundredfold larger than the sum of individual paramagnetic atoms. Transverse relaxation (T2) is enhanced to a greater degree than possible with paramagnetic materials. Paramagnetic complexes and composite particles have been designed to target specific cellular receptors or transport proteins located on the cell surface. Examples of such cell-specific targeting mechanisms include the hepatocyte anionic receptor targeted by Gd-BOPTA, the hepatic-binding protein targeted by galactose-linked macromolecules, and phagocytosis of opsonized particles by reticuloendothelial cells (hepatic Kupffer cells). While much of this work is in experimental stages, Mn-DPDP, targeted to hepatocytes and excreted in bile, was the first paramagnetic hepatobiliary MR agent to begin clinical trials. Superparamagnetic iron oxide is undergoing clinical trials in several countries. Both classes of contrast agents have shown enhanced detection of liver cancer in humans.

PS 006 • 2:00 PM

Functional MR Imaging of the Brain

BR Rosen, MD, PhD

NMR Center, Massachusetts General Hospital, Charlestown, MA

Fundamental aspects of brain function can be investigated by using the well-established interrelationship between cerebral activity, metabolism, and regional hemodynamics. Several techniques have been proposed to measure changes in regional hemodynamics with MR imaging. Of these, magnetic susceptibility contrast is one of the most powerful means of affecting tissue signal intensity. Dynamic paramagnetic contrast techniques, based on exogenous or endogenous agents, have shown considerable promise in providing the ability to generate maps of hemodynamic parameters. Exogenously administered contrast agents, after intravenous injection, produce significant signal changes during first-pass cerebral transit. Because cerebral transit times are on the order of seconds, a rapid imaging technique is needed to resolve the passage of an intravascular agent through the capillary bed. Several groups have employed high-speed echo-planar imaging (EPI) methods to evaluate the time course and regional distribution of injected contrast agents. For endogenous (deoxyhemoglobin) contrast agents, the intrinsic hemodynamic response time to changes in brain activation state is under 2 seconds. The use of high-speed techniques is again required to provide 3D coverage of the brain with adequate temporal resolution. Noninvasive measurement of cerebral blood volume and flow and blood oxygenation has been shown to have significant impact on the diagnosis and management of patients with ischemia, neurodegenerative disorders, and cerebral neoplasms and will play a fundamental role in improving our understanding of normal brain function. With ischemic disease, functional MR imaging data offer the potential to both detect hypoperfusion well before conventional MR studies and to quantify the degree of hypoperfusion within the central lesion and the surrounding ischemic penumbra. The unique ability of MR imaging to show tissue microvasculature may allow MR imaging to directly show the phenotypic expression of tumor angiogenic growth factor genotypes. Microvascular insult may also lie at the heart of neurodegenerative disorders such as Alzheimer disease. Direct imaging of cortical activation will have a direct effect on cognitive and behavioral neuroscience and also opens new clinical possibilities for presurgical planning, improved specificity in evaluating dementias, and development of quantitative tools for studying neuropsychiatric disorders at a functional level.

PS 007 • 2:30 PM

Diffusion

ME Moseley, PhD

Department of Radiology, University of California, San Francisco, CA

Diffusion-weighted MR imaging (DWI) has had a dramatic effect in neurophysiology through the mapping of information relating to the molecular environments of cerebral water. Measurements of the apparent diffusion coefficient (ADC) of water are determined by normal as well as pathologic translations of water populations along specific anatomic planes averaged over distances smaller than or larger than cell sizes, depending on the operator-selected observation parameters. Within the last 4 years, DWI has provided unique tissue contrast in differentiating lesions from normal tissues, in determining the spatial orientation of white matter tracts, and in the creation of "MR neurograms" for the rapid and noninvasive determination of the degree, severity, and status of stroke-induced brain damage in a variety of experimental models and clinical studies and in the observation of status epilepticus. It is becoming clear that decreases in the measured ADC observed in pathologic tissues follow similar time and severity scales with correlated histopathology, potentially linking changes in the physical environment of water to the loss of ion homeostasis. Sudden increases in ADC measured in these tissues appear to be related to a loss of cellular integrity or necrosis. It is anticipated that quantitation of the changes in the biophysical environments of water will lead to a better understanding of the mechanisms involved in pathologic brain damage. As high-speed MR methodologies mature, DWI will find further applications in noncerebral tissues such as muscle, kidney, the eye, and tumors.

Sunday Afternoon • Imperial Ballroom
Plenary Symposia 008–010

ENDOGENOUS CONTRAST MECHANISMS

MODERATOR: RM Henkelman, PhD
3:30 PM–5:00 PM

PS 008 • 3:30 PM

Magnetization Transfer Contrast in MR Imaging

RS Balaban, PhD
National Institutes of Health, Bethesda, MD

Magnetization transfer contrast (MTC) is the result of selectively observing the dipolar interaction of bulk water protons (H_f) with the protons contained in macromolecules (H_r) of a tissue. The extent of the dipolar interaction of H_f and H_r has been shown to be dependent on the molecular dynamics and surface chemistry of the macromolecules contributing to the selectivity of MTC. MTC is generated by combining saturation transfer techniques with standard MR imaging procedures. Generally, MTC is produced by selectively saturating H_r with RF energy off resonance from H_f. The specific practical and theoretical aspects of saturation transfer between H_r and H_f is an area of current debate. Of major importance is the specificity and power deposition of the irradiation scheme used to saturate H_r to generate MTC. By the appropriate choice of frequency and power for H_r irradiation, the power deposition for generating MTC can be reduced by factors of 10. In addition, the specific lineshapes of H_r and H_f is important in the interpretation of the magnetization transfer results. H_r has been shown to have a complex lineshape composed of both Gaussian and Lorentzian characteristics that can change with molecular dynamics, providing unique information on tissue structure. In the last 3 years, MTC has been applied in clinical MR imaging with useful applications in the study of the knee, eye, brain, breast, and heart. The application of MTC to accentuate MR angiography and contrast agent studies has also been demonstrated. Thus, MTC is quickly becoming another tool in maximizing the quality and diagnostic potential of MR imaging.

The U. S. government holds a patent on the MTC approach discussed in this presentation.

PS 009 • 4:00 PM

Calcium Contrast Mechanisms

W Kucharczyk, MD, RM Henkelman, PhD
Department of Radiology, University of Toronto, Toronto, Ontario, Canada

Tissue calcification occurs in many diseases. The ability of an imaging modality to ascertain the presence of calcification may enable detection of lesions that are otherwise occult or indicate the type of disease process that is present. It follows therefore that the ability to detect calcification is diagnostically important. However, in contradistinction to the well-characterized effect of calcification on x-ray attenuation, the effect of calcium on MR signal intensity is not as well understood. The purpose of this presentation is to review the mechanisms through which calcium affects MR signal intensity and explain how image contrast is dependent on operator-controlled pulse sequence parameters. Finally, the detectability of calcification with CT and various MR imaging methods will be compared. This will be done through a review of the literature as well as presentation of original work. A series of 2% agarose gel phantoms were made containing different calcium salts at various concentrations. Gradient-echo (GRE) and SE MR imaging were performed while systematically altering TR, TE, and flip angle, with and without the use of spoilers. Relaxation times were determined from the appropriate MR images. The surface area of the calcium salts was determined by an analytic method known as BET analysis, wherein a layer of inert gas is adsorbed on the crystal surface and subsequently quantitated. CT attenuation was independently measured for each type of calcium sample. T1 and T2* relaxivity were found to be directly linearly related to the BET surface area. The image contrast that occurred depended on whether the pulse sequence highlighted the T1 or T2* shortening effect. T1-weighted SE sequences showed high surface area samples as hyperintense, whereas T2 SE and T2*-weighted GRE sequences demonstrated hypointensity. The hypointensity could be emphasized by using long TE and flip angles close to the Ernst angle. Visually apparent high signal intensity on T1-weighted images occurred at calcium concentrations between 5 and 30 g% by weight; this was always apparent on CT scans as hyperattenuation, as were calcium concentrations below 5 g%. T2*-weighted imaging showed visually apparent hypointensities at calcium concentrations well below 5 g% but not as sensitively as CT. T1 and T2* shortening occurs with tissue calcification. This may result in hyperintensity on T1-weighted SE images or hypointensity on T2- and T2*-weighted images. The T1 shortening is due to relaxation enhancement of bulk water at the calcium salt surface. T2* shortening can be partially explained by the same surface effect, but a more important mechanism is susceptibility-induced signal loss. The hypointensity that T2* shortening creates can be best accentuated on GRE sequences with long TE. T2*-weighted images depict calcium more sensitively than do T1-weighted images, but neither is as sensitive as CT.

PS 010 • 4:30 PM

Susceptibility Contrast and Brain Iron

EK Fram, MD
Barrow Neurological Institute, St. Joseph's Hospital and Medical Center, Phoenix, AZ

The effects of iron and susceptibility will be discussed. Pulse sequences will be compared, including gradient-echo, SE, and fast SE sequences. Gradient-echo pulse sequences provide high sensitivity for detecting susceptibility gradients generated by iron because, unlike SE imaging techniques, they fail to correct for field inhomogeneities. The deposition of nonheme brain iron will be discussed in both normal aging as well as various disease states. The evolution of hemorrhage will be reviewed with its MR imaging correlates.

Monday Morning • Imperial Ballroom Plenary Symposia 011–013

PRESIDENT'S SESSION: MRI of the Breast: Imaging and Interventional Strategies

MODERATOR: SE Harms, MD
8:00 AM–10:00 AM

A 001 • 8:15 AM (WS Moore Award)

Visualization of Flow by Vector Analysis of Multidirectional Cine MR Velocity Mapping: Technique and Application

RH Mohiaddin, GZ Yang, PJ Kilner, DB Longmore
Magnetic Resonance Unit, Royal Brompton Hospital, London, England

Purpose: The authors describe a noninvasive method for visualization of flow and demonstrate its application in phantoms and in the great vessels of healthy volunteers and of patients with aortic and pulmonary arterial diseases. The technique uses multidirectional MR velocity mapping acquired in selected planes. Maps of orthogonal velocity components were then processed into a graphic form immediately recognizable as flow.
Methods: Cine MR velocity maps of orthogonal velocity components in selected planes were acquired in a rotating disk and flow phantoms, 10 healthy volunteers, and 11 patients (aortic aneurysm, 4; pulmonary hypertension, 3; aortic coarctation, 4). Velocities were represented by multiple computer-generated streaks whose orientation, length, and movement corresponded to velocities in the chosen plane.
Results: Computer graphic representation of MR velocity data as moving "particles" allowed visualization of complex patterns of secondary flow. The technique revealed coherent, helical forward blood movement in the normal thoracic aorta and pulmonary arteries during midsystole and reverse flow during early diastole. Abnormal flow patterns with secondary vortices are seen in patients with dilated arteries.
Conclusions: The technique achieved clear visualization of flow patterns in phantoms. Normal and abnormal flow in the aorta and pulmonary arteries were demonstrated. The authors now have a reliable method for the investigation of the nature and hemodynamic significance of primary and secondary flow structures in health and disease.

A 002 • 8:30 AM (II Rabi Award)

An Implementation of Wavelet-encoded MR Imaging

IP Panych, PD Jakab, FA Jolesz
Radiology Department, MRI Division, Brigham and Women's Hospital, Boston, MA

Purpose: Wavelet transform encoding has been previously proposed by Weaver and Healy as an alternative to Fourier transform phase encoding of MR images, although, to the authors' knowledge, there has been no published report of an implementation of this technique. The authors recently succeeded in implementing wavelet transform encoding to produce single-section images.
Methods: Wavelet encoding was implemented by manipulation of RF pulse shapes to generate excitation profiles that are basis functions of a wavelet transform. Individual sections were selected with section-selective 180° pulses along the direction orthogonal to both the frequency- and wavelet-encoded directions. After inverse Fourier reconstruction in the frequency-encoding direction, data values are coefficients of a wavelet expansion. These can be inverse transformed with a very efficient digital wavelet transform algorithm to reconstruct the final images. For comparison, T2-weighted images were made by using wavelet and phase encoding and care was taken to keep SNR and T2 weighting constant for both types of encoding.
Results: Comparison of wavelet-encoded and phase-encoded images of phantoms and biologic samples shows that the wavelet-encoded images compare favorably with phase-encoded images.
Conclusions: Wavelet encoding of MR images is feasible with wavelet-shaped selective excitation profiles. More averages are required for wavelet encoding to achieve an SNR ratio similar to that of phase encoding. However, when the time factor is included, SNR ratios for the two encoding techniques are more comparable because wavelet encoding can be much faster than phase encoding.

PS 011 • 8:45 AM

Imaging Management of Breast Carcinoma

WP Evans, MD
Susan G. Komen Breast Center, Sammons Cancer Center, Baylor University Medical Center, Dallas, TX

For many years, the treatment of breast cancer involved only surgery. However, modern management of the disease is multidisciplinary, and breast imaging procedures (mammography and US) have become increasingly important. Mammographic screening is the most significant method for early detection. A screening-detected abnormality is usually evaluated with diagnostic mammography and/or US to determine its location and significance. With a palpable lesion, breast imaging is necessary not only to characterize the lesion but also to screen the remaining breast tissue. Once a lesion has been characterized, it can be histologically diagnosed by using stereotaxic digital or US-guided core biopsy techniques. If appropriate, tissue for hormone receptors and flow cytometry can be obtained at the same time. For surgical excision of a nonpalpable lesion, needle localization and radiography of the specimen are mandatory. When malignant calcifications are found and breast conservation is considered, postlumpectomy magnification mammography can determine if all suspicious calcifications have been excised. Finally, mammographic surveillance for local recurrence is crucial for women treated with breast conservation. From diagnosis through follow-up care, breast imaging procedures play a significant role in the treatment of the breast cancer patient.

PS 012 • 9:10 AM

Potential Clinical Roles for Breast MR Imaging

SE Harms, MD, DP Flamig, PhD
MRI Department, Baylor University Medical Center, Dallas, TX

The three major categories for clinical breast MR imaging application are outlined: (1) specificity, (2) sensitivity, and (3) silicone. MR imaging can be used to improve the specificity of conventional breast imaging and is designed to reduce the number of biopsies for benign disease. Low-resolution dynamic MR imaging is a commonly used method. Competing with this technology is the imaging-guided needle biopsy. MR imaging may be used to improve the sensitivity of breast imaging for lumpectomy staging and identification of disease in patients with compromised conventional imaging evaluations. Since the primary reason for this role is accurate treatment staging, identification of lesion margins and extent is the major issue. To achieve this high level of sensitivity, the technologic requirements are 3D acquisition for improved resolution, fat suppression with heavy T1 weighting for improved contrast, and fast imaging time (around 5 minutes) to obtain adequate tumor-parenchymal contrast. Detection of free silicone in patients with silicone augmentation implants is a potential role for MR imaging. Conventional MR imaging (T1- and T2-weighted SE) has been used to identify areas with signal intensity characteristics that indicate probable free silicone. Competing with this approach is US, which is more available and similar in specificity. Alternatively, special silicone suppression pulse sequences may be employed that provide chemically specific information based on the unique chemical shift or T1 of silicone. Silicone-specific sequences provide information not available with conventional imaging. With technologic improvements on the horizon, MR imaging is expected to have an expanded role in the clinical management of breast abnormalities in the future.

PS 013 • 9:35 AM

Minimally Invasive Therapy in Breast Cancer

SG Bown

National Medical Laser Centre, Department of Surgery, University College London, The Rayne Institute, London, England

Screening programs identify many patients with small cancers localized to the breast. Local excision, with adjuvant therapy if appropriate, can give results comparable to radical surgery. Nevertheless, even a lumpectomy leaves a scar and some cosmetic deformity. Interstitial laser photocoagulation (ILP) is a new technique that can destroy tumors deep within the breast less invasively. The concept is simple. One or more needles are inserted into the tumor and thin (0.4-mm) laser fibers are inserted through the needles so their bare tips rest in the target tumor. All fibers are then activated simultaneously from a diode laser (wavelength, 805 nm; 2–3 W down each, 500-sec exposure). The cancer is destroyed in situ with gentle thermal coagulation and the dead tissue resorbed by normal healing mechanisms. ILP is still evolving, the real challenge being to match the extent of laser-induced necrosis to the full extent of the cancer being treated. Current work images small cancers before and after ILP in patients scheduled for surgery, so the images can be correlated with microscopic examination of the resected specimen. The simplest imaging for fiber insertion is US, but this is inaccurate for monitoring therapy. Contrast-enhanced CT defines the necrosed area well, but not before 24 hours after treatment. MR imaging is the most promising modality both for defining lesions and monitoring therapy. Recent reports identify cancers down to a few millimeters and experimental studies show MR imaging can pick up temperature changes during ILP. Nevertheless, much must be done to correlate real-time MR images with the final biologic effect of ILP to establish the true role of this promising new treatment.

Monday Afternoon • Imperial Ballroom
Plenary Symposia 014–016

CARDIAC MRI: Functional and Clinical Applications

MODERATOR: KM Link, MD
1:30 PM–3:00 PM

PS 014 • 1:30 PM

Adult Cardiac Evaluation

RD White, MD

Cleveland Clinic Foundation, Cleveland, OH

The strength of MR imaging in the evaluation of acquired adult cardiovascular disease is in its ability to provide a diversity of information normally requiring multiple other imaging techniques to be performed. Within a busy routine-clinical and clinical-research center (Cleveland Clinic Foundation), the exploitation of the multiple capabilities of MR imaging has led to a large experience with cardiovascular MR imaging for evaluation of adult disease. Data on the use of MR imaging in the clinical setting for evaluating adult cardiovascular disease will be presented. The presentation will focus on the three most common adult cardiovascular conditions evaluated with MR imaging at our institution: thoracic aortic disease, diastolic dysfunction, and nonischemic myocardial disease. Examples demonstrating the value of static "dark-blood" (ie, SE), dynamic "bright-blood" (ie, cine gradient-echo), flow-mapping (ie, phase velocity mapping), ultrafast near-real-time (ie, first-pass turbo gradient-echo), 3D imaging (ie, MR angiography), and myocardial tagging (ie, SPAMM) techniques will be shown. The multipotentiality of MR imaging to evaluate several anatomic and physiologic abnormalities associated with adult cardiovascular disease is presently its strongest attribute.

PS 015 • 2:00 PM

Functional Cardiac Imaging

RJ Herfkens, MD

Department of Radiology, Stanford University School of Medicine, Stanford, CA

The sensitivity of MR imaging to flow has been both a blessing and a curse as MR imaging techniques have developed. The artifacts generated by motion during imaging times have been destructive, yet the functional information recently generated with dynamic imaging is capable of providing important information about cardiac and vascular function. The development of cine MR imaging techniques has allowed the acquisition of four-dimensional data sets that encompass the entire cardiac volumes and the cardiac cycle. The extraction of volume information over time for both right and left ventricles provides an extremely powerful tool for noninvasive evaluation of cardiac diseases. Velocity information has been encoded in the cine techniques, allowing the direct and accurate measurement of flow in vascular structures. These motion-sensitive techniques have also been applied to analysis of cardiac motion. The dynamic velocity information provides data about myocardial thickening, stress, and strain.

PS 016 • 2:30 PM

Heart Wall Motion and Image Processing

L Axel, PhD, MD

Hospital of the University of Pennsylvania, Philadelphia, PA

Assessment of heart wall motion is an important part of diagnosis and treatment of cardiac disease. Although MR imaging still plays a relatively minor role in clinical wall motion studies, it has some unique strengths that may lead to its playing a more major role in the future. The use of image processing techniques will play an important part in exploiting the capabilities of MR imaging for wall motion assessment. In common with other rapid or cardiac synchronizable tomographic imaging techniques, MR imaging can provide both global measures of wall motion (eg, stroke volume and ejection fraction) and local measures of wall motion and wall thickening. The clinical utility of this depends on the ease of performing the analysis. Robust and rapid automated analysis methods for defining the ventricular cavities and measuring their function will speed clinical acceptance of cardiac MR imaging. MR imaging also provides unique methods for detailed analysis of regional wall motion. The same methods useful for MR imaging of fluid motion, magnetization tagging, and motion-induced phase shifts are also useful for studying the motion of the myocardium. Regular patterns of altered magnetization can be created within the myocardium at one phase of the cardiac cycle, which will serve as visible tags on images obtained at later phases of the cardiac cycle. Motion of the heart will result in a corresponding motion of the tag images. Myocardial velocity can be calculated from suitable sensitized phase images; it must be integrated to find displacements. Again, efficient analysis is needed for clinical utility.

Tuesday Morning • Imperial Ballroom
Plenary Symposia 017–019

MRA: Technical Advances and Clinical Efficacy

MODERATOR: AW Litt, MD
8:00 AM–9:30 AM

PS 017 • 8:00 AM

MR Angiography: Central Nervous System Time-of-Flight Technique

TJ Masaryk, MD
Department of Radiology, Cleveland Clinic Foundation, Cleveland, OH

MR angiography can provide significant additional information to complement the routine spin-echo MR examination of the brain. The idea of a combined study has gained favor, as it provides a noninvasive alternative for the complete study of patients with suspected cerebrovascular disease. In particular, because of their relatively short time of acquisition, time-of-flight (TOF) MR angiographic sequences can be easily added to the traditional parenchymal study without significantly prolonging the overall examination time. TOF techniques create vascular contrast through the inflow of blood protons into a region of interest previously prepared by an RF excitation, inversion, or saturation pulse. The most popular techniques consist of relatively simple gradient-echo pulse sequences in which the inflow of spins produces exceptionally high signal intensity within the vessels on the basis of the TOF effects known as "entry slice phenomenon" or "flow-related enhancement." Angiographic images can then be derived from such data sets through the use of computer postprocessing techniques, which obviate the need for mask acquisitions to create a subtraction angiogram. Since TOF MR angiography requires only a single data set, the acquisition is less susceptible to problems such as patient motion and eddy currents, which arise with longer examination times and multiple data sets. TOF techniques are considered less vulnerable to the phase dispersion (and signal loss) that accompanies complex motion typically seen in regions of arterial flow (ie, tortuous vessels, stenoses). Hence, TOF MR angiography has been successfully applied to the clinical evaluation of carotid atherosclerosis (2D and 3D methods), intracranial aneurysms, and arterial occlusions (3D techniques), as well as dural sinus occlusion (2D TOF venograms). Disadvantages of the TOF studies include the potential for saturation of slowly moving spins in areas far "downstream" within the volume or distal to a severe stenosis. Potential solutions to this problem include the use of reordered k-space acquisition to maximize signal intensity prior to saturation, variable flip angles over the volume of acquisition, or thin overlapping, stacked 3D volumes. Another important factor contributing to artifact of the vessel lumen is the intravascular phase dispersion secondary to complex motion. Reduction of the minimum TE limits the motion-induced dephasing and is possible through truncated RF pulses and asymmetric data sampling, innovative image reconstruction (eg, spiral k-space acquisition), and new high-performance gradient systems. Large, carefully controlled, prospective clinical trials must still be conducted to more clearly define the role MR angiography will play in the evaluation of patients with clinically suspected cerebrovascular disease. Accurate and strict data analysis using criteria established with clinical outcome studies (eg, NASCET) in conjunction with the latest technologic innovations will continue to expand the role of MR angiography in the treatment of such patients.

PS 018 • 8:30 AM

Phase-Contrast MR Angiography: Neurologic Applications

PA Turski, MD
Department of Radiology, University of Wisconsin Medical School, Madison, WI

Phase-contrast (PC) MR angiography is a versatile angiographic technique in which flow direction, flow velocity, and hemodynamic effects are incorporated into the vascular image. Bipolar flow-encoding gradients are used to encode a range of velocities and a particular flow direction. The 2D PC angiograms can be acquired as a section, slab, or cardiac-gated cine acquisition. The cine PC technique not only provides the opportunity to assess hemodynamics (rheology) but is also the platform for quantitative measurements of velocity and volume flow rates. The PC data can also be acquired as a 3D volume acquisition to permit reprojection of the data in a fashion analogous to 3D time of flight. In this presentation, the techniques of PC MR angiography will be reviewed and their role in the evaluation of patients with occlusive vascular disease, arteriovenous malformations, central nervous system neoplasms, venous thrombosis, and aneurysms will be presented. The evolving role of quantitative measurements of volume flow rates for patients with vascular occlusive disease and vascular malformations will also be discussed.

PS 019 • 9:00 AM

MR Angiography in the Body

JP Finn, MD
Department of Radiology, New England Deaconess Hospital, Boston, MA

The technical challenges for MR angiography in the body are greater than those in the head and neck. However, important clinical questions can often be fully addressed with available techniques. The range of techniques is becoming such that strict clinical comparison of all of them is a formidable task, and new developments in 2D and 3D imaging are occurring rapidly. Clinical experience to date suggests that MR angiography has a definite role in venous disease, and conventional angiography can usually be avoided. Several factors contribute to the success of MR venography: Flow in veins is fairly steady and flow patterns tend to be less disturbed than in arteries; veins are usually bigger than arteries and when obstructed have a greater tendency to recruit collaterals rather than develop high flow velocities. Numerous clinical applications for MR imaging of arterial disease have been proposed, and initial reports, though encouraging, stress the limitations of currently available techniques. Arterial flow can be rapid and highly pulsatile, resulting in ghosting artifact and signal loss due to phase incoherence. In these circumstances, the radiologist must have additional tools to help offset these effects. Shorter TEs are possible with faster and stronger gradients, and cardiac-gating maneuvers can substantially improve image quality for pulsatile flow. Imaging of narrowed branch vessels, however, imposes demands on spatial resolution that may require the use of specialized surface coils. In the limit, techniques based on imaging blood flow will have difficulty distinguishing slow flow from thrombus, and fast sequences, which employ relaxation time weighting, can increase the diagnostic yield in problem cases. The potential for noninvasive flow quantification with MR offers unique advantages over other modalities, and methods for rapid flow evaluation based on the amplitude or phase of the MR signal are now available. In this presentation, a range of established and promising techniques for MR angiography in the body will be reviewed, and their strengths and weaknesses discussed.

Tuesday Afternoon • Imperial Ballroom
Plenary Symposia 020–022

MR FLOW: Quantitative and Clinical Applications

MODERATOR: EM Haacke, PhD
1:30 PM–3:00 PM

PS 020 • 1:30 PM

Cerebrospinal Fluid Flow

DR Enzmann, MD

Department of Radiology, Stanford University Medical Center, Stanford, CA

Cine phase-contrast (PC) MR imaging provides an accurate method for investigating cerebrospinal fluid (CSF) flow. This method was used to measure CSF flow at strategic locations in the neuraxis to delineate timing and flow during the cardiac cycle. The cine PC MR technique (TR/TE = 54/9) generates 16 images per cardiac cycle, showing both direction and velocity of CSF flow. These measurements can be converted to volume flow measurements in milliliters per minute or milliliters per cardiac cycle. These flow measurements were obtained at the following sites: the incisura, the aqueduct, and the C-2 to C-3 level. They were also obtained in syringomyelia. CSF flow shows an oscillating pattern within all the major CSF pathways with ventricular system oscillation (ie, the aqueduct, being slightly out of phase with the subarachnoid space [SAS]). Flow in the aqueduct is delayed compared with that in the SAS. In healthy individuals, oscillatory aqueductal flow is low, approximately 1.7 mL/min. Flow at the C-2 to C-3 level, which reflects CSF displaced from the cranium, is higher, approximately 39 mL/min. In patients with syringomyelia, the syrinx fluid acts similar to SAS CSF, and the total volume of fluid is displaced (ie, SAS CSF and syrinx fluid is equivalent to that normally displaced in the SAS only). The total amount of CSF oscillatory flow in syringomyelia is in the normal range. Cine PC MR techniques for measuring CSF flow provide valuable baseline information about normal CSF flow and also allow characterization of abnormal CSF flow such as in syringomyelia.

PS 021 • 2:00 PM

Cardiac Applications and Bolus Tracking

RR Edelman, MD

Department of Radiology, Beth Israel Hospital, Boston, MA

In this session, clinical applications of quantitative methods in the heart will be surveyed. Fast imaging techniques such as echo-planar, segmented TurboFLASH, and spiral imaging have proved helpful for avoiding artifacts from cardiac pulsation and respiratory motion. With variations in these techniques, flow quantification can be applied in the heart. Bulk flow can be measured in coronary arteries and veins by using phase or bolus tracking methods. In principle, capillary flow (myocardial perfusion) can be quantified by using the central volume principle in conjunction with administering a paramagnetic contrast agent. Molecular motion (diffusion) has been quantified in the brain but, until recently, never in the heart. Flow velocities in the coronary arteries at rest and with pharmacologic augmentation have been quantified by using a rephased-dephased image acquisition and segmented TurboFLASH sequence to compute a phase map. Alternatively, flow velocities can be measured by using bolus tracking approaches with segmented TurboFLASH or echo-planar imaging. At present, volume flow measurements are inaccurate because an insufficient number of pixels span the coronary artery lumen. Quantification of cardiac perfusion is not yet possible because the bolus of contrast material is not instantaneous and existing contrast agents rapidly diffuse into the interstitium; however, qualitative evaluation appears promising. Motion-resistant pulse sequences show promise for determining the apparent diffusion coefficient of myocardium. Quantitative methods for measuring flow in the heart require further development but potentially have considerable clinical value.

PS 022 • 2:30 PM

Phase-Contrast Applications

NJ Pelc, ScD

Lucas MRS Imaging Center, Stanford University, Stanford, CA

The purpose of this presentation is to discuss the fundamental aspects of phase-contrast (PC) MR imaging and its flow-related applications, with emphasis on quantitative measurements. PC techniques are based on the fact that spins that move in the presence of magnetic field gradients experience time varying fields that differ from those of static spins. For constant velocity motion, the phase of the net transverse magnetization is shifted by an amount proportional to the first moment of the gradient waveform. To isolate motion effects from other sources of phase shifts, measurements with multiple gradient moments are used. In the simplest method, two sequences are used and the phase shift is $\gamma \Delta M_1 v$, where ΔM_1 is the change in first moment (which is selectable) and v is the velocity. Ungated, cardiac-gated, and real-time imaging techniques employing PC have been implemented. For imaging all three velocity components, four measurements are needed. The flexible and reliable relationship between phase shift and velocity can be exploited for quantitative applications. In one important application, through-plane velocity is measured. The integral of velocity within a vessel lumen is the volume flow rate through the vessel. While the flow need not be perpendicular to the imaging plane, this condition is preferred. PC flow measurements have been validated in vitro and in vivo and are being exploited for a variety of research and clinical applications. Careful technique is needed to guarantee accuracy and reproducibility, including sufficient spatial resolution and flow-encoding strength.

Wednesday Morning
Imperial Ballroom
Plenary Symposium 023

PRESIDENT-ELECT SESSION: Fast Scan Techniques in the Abdomen—Clinical Efficacy (A Debate)

MODERATOR: JC Weinreb, MD
8:00 AM–9:30 AM

PS 023 • 8:00 AM

Fast Imaging Techniques in Diagnostic Abdominal Imaging: Advantages and Limitations

SJ Riederer, PhD, EE de Lange, MD, CD Johnson, MD, JP Mugler, III, PhD
MR Research Lab, Mayo Clinic, Rochester, MN

Fast imaging methods as applied to abdominal imaging have undergone considerable technical and clinical study over the last several years. However, except in a limited number of institutions, such methods have not yet replaced conventional T1- and T2-weighted SE imaging for diagnosis. The purpose of this plenary session is to explore the feasibility of fast abdominal imaging. This will be done in a panel discussion in which the following hypothesis will be debated: *Fast imaging techniques will replace conventional SE methods within the next 3 years for diagnostic imaging of the abdomen.* In this context, a "fast" technique is defined as one that can be performed within a single or a limited series of breath holds. Both panel teams are composed of a radiologist and physicist experienced in the topic, and the hypothesis will be explored from both technical and clinical viewpoints. At the beginning of the session, the various fast abdominal imaging methods will be briefly reviewed. These include spin-echo, gradient-echo, and echo-planar techniques. Next, specific aspects of the hypothesis will be discussed. The topics will include plausible advantages of fast imaging such as reduction of motion artifacts and reduced examination time. Additionally, potentially major limitations will be reviewed such as reduced resolution, degraded signal-to-noise ratio, sensitivity to artifacts specific to fast imaging, or inability of the techniques to image certain pathologies. Case presentations will be used extensively for illustration, and the panelists will draw on their respective clinical experience. Predictions will be made as to the requirements for and likelihood of the eventual widespread clinical use of fast imaging techniques in diagnostic abdominal imaging.

Wednesday Afternoon
Imperial Ballroom
Plenary Symposia 024–026

MRI SEGMENTATION: Interventional and Stereotactic Strategies

MODERATOR: LP Clarke, PhD
1:00 PM–2:30 PM

PS 024 • 1:00 PM

Interventional MR Imaging

RB Lufkin, MD
Department of Radiological Sciences, University of California Los Angeles Medical Center, Los Angeles, CA

Many of the advantages of MR imaging that make it such a powerful clinical imaging tool are also valuable during interventional procedures. The lack of ionizing radiation and oblique and multiplanar imaging capabilities are particularly useful during invasive procedures. Perhaps the greatest advantage of MR imaging is the high soft-tissue contrast resolution, which allows the early and sensitive detection of tissue changes during interventional procedures. One of the first applications of MR imaging–guided procedures has been for fine-needle aspiration cytology. Several approaches are also currently under evaluation for the treatment of pathology with MR guidance. Interstitial laser or RF may be applied to deep tissues to deposit thermal energy in a well-defined fashion, with minimal damage to adjacent structures. This technique has been used for lesions in brain, gasserian ganglia, liver, or the conductive pathway to the heart. Other investigators have already demonstrated the possibility in human studies of MR-guided catheter placement for intramural alcohol and chemotherapy injections. Interventional MR imaging is clearly in the early stages of development. While the value of MR-guided aspiration cytology and MR imaging evaluation of deep cerebral electrode implantation has already been confirmed with human clinical studies, the ultimate future role for MR-guided interstitial therapy remains to be defined.

PS 025 • 1:30 PM

Deformable Anatomic Atlases and Validation of MR Segmentation

MW Vannier, MD, MI Miller, PhD, D McKeel, MD
Mallinckrodt Institute of Radiology, St. Louis, MO

The segmentation of MR image data sets into regions of like tissue characteristics is a complex problem that can be approached by using a deformable anatomic atlas of the body and a suitable matching algorithm. This approach has been implemented with pattern theoretical methods, namely, deformable templates that are matched both globally and locally to normal anatomy. The validation of segmentation methods requires independent knowledge of ground truth and a means of comparing the calculated and actual class maps. The authors segmented MR brain images automatically and validated the results by using direct comparison with cadaver brain tissue slices. A global template matching procedure was implemented on a massively parallel processor (DEC MPP) to segment unknown normal MR brain images with an electronic anatomic atlas of the brain. This procedure has been validated by using cadaver brains that were MR imaged, sectioned, and photographed in the same orientation. Intra- and interobserver variations were determined for MR brain sections analyzed manually. These outlines of tissue regions were compared with automatically segmented data sets. Errors were greatest at the surface cortical mantle, where section thickness was 5 mm. Best results were obtained with 1.5-mm sections. This segmentation procedure and its validation produced results that compare favorably with manual segmentation methods (eg, outlining of MR scenes by using manual region of interest generation).

PS 026 • 2:00 PM

Automatic Segmentation Techniques in MR Imaging

LP Clarke, PhD, LO Hall, PhD, RP Velthuizen, MS,
AM Bensaid, MS, JC Bezdek, PhD
Radiology Department, University of South Florida, Tampa, FL

MR imaging segmentation can be used for (*a*) intelligent image fusion of multispectral 3D images for more efficient reading, (*b*) improved tumor volume as required for 3D RTP, (*c*) electronic surgery simulation, and (*d*) calculation of normal tissue volumes. Gray-scale approaches such as seed-growing or edge-detection methods, including wavelet approaches to outline tissue boundaries, are inherently limited for tumor volume detection because they are applied to single gray-scale images. Pattern recognition methods applied to multispectral data sets should provide better differentiation of pathology and normal tissues. A number of supervised parametric and nonparametric methods will be reviewed initially, including neural networks with different architecture. The various strategies of segmentation techniques will be reviewed on the basis of their relative performance in segmenting both normal and abnormal tissues. Finally, the advantages of these methods over gray-scale approaches or singular methods such as the eigenvector method will be discussed, particularly in terms of reproducibility of segmentation. Clinical models will include brain gliomas and recent work on breast imaging. Automatic segmentation methods such as unsupervised or semisupervised fuzzy clustering are needed to yield stable segmentation across several tissue classes and subjects imaged.

This research was supported in part by Siemens and Sun Microsystems.

1993 ANNUAL MEETING COMMENTS

The 1993 Annual Meeting Organizing Committee would appreciate receiving your comments regarding the 1993 Annual Meeting in San Francisco. Those comments will be collated and forwarded to the 1994 Annual Meeting Organizing Committee for possible incorporation in next year's educational programming. While your comments may also be provided on the Evaluation/CME Accreditation Form distributed at each session, please let us know your thoughts regarding the following:

1. Which Program did you attend? ____________________

2. Did it meet its stated objectives? _____ Yes _____ No. Why? ____________________

____

____

3. What should have been included in the Program that was not? ____________________

____

4. What should have been excluded from the Program? ____________________

____

5. What Program revisions would you like to see implemented next year? ____________________

____

____

____

6. General Comments: ____________________

____

____

Please return this form to the **SMRI** Registration Area, Ballroom Level, of the San Francisco Hilton and Towers by Wednesday, March 31, or mail it to the **SMRI** Central Office at the following address:

Society for Magnetic Resonance Imaging
213 West Institute Place, Suite 501
Chicago, Illinois 60610 USA

Notes

Notes

MR 1993

PROFFERED PAPERS

The **SMRI** Program Commitee has assembled a fine selection of scientific paper presentations from the more than 570 abstracts submitted this year. The final program offers a total of 270 papers in 33 parallel sessions during the week. Additional Works-in-Progress papers will also be presented; they may be found in a Works-in-Progress Supplement to be distributed on-site.

Seating for the scientific sessions is on a space-available basis. You are invited and encouraged to move from one meeting room to another during a time block to hear different presentations. Please, however, be sensitive to the presenter and the other attendees while implementing your itinerary.

1993 Scientific Abstract Reviewers

John A Arrington, MD
University Diagnostic Institute

Scott W Atlas, MD
Hospital of the University of Pennsylvania

Michael Barany, PhD
University of Illinois/College of Medicine

Javier Beltran, MD
Hospital for Joint Diseases

William G Bradley, Jr, MD, PhD
Long Beach Memorial Medical Center

Thomas J Brady, MD
Massachusetts General Hospital/NMR Center

Michael J Bronskill, PhD
Sunnybrook Health Science Center

Toni Ceckler, PhD
National Institutes of Health

Robert A Clark, MD
H Lee Moffit Cancer Center

Laurence P Clarke, PhD
University of South Florida College of Medicine

Mark S Cohen, PhD
Massachusetts General Hospital/NMR Center

John V Crues III, MD
Santa Barbara Cottage Hospital

Rosalind B Dietrich, MB, ChB
University of California/Irvine

William P Dillon, MD
University of California/San Francisco

Jeffrey L Duerk, PhD
MetroHealth Science Center

Linda Eastwood, PhD
Picker International, Inc

Robert R Edelman, MD
Beth Israel Hospital

Richard L Ehman, MD
Mayo Clinic

Barry Engelstad, MD
Diablo Valley Radiology Group

Madeline R Fisher, MD
Hospital of Good Samaritan

Jens Frahm, PhD
Max-Planck Institut fur Biophysikalische Chemie

Peggy J Fritzsche, MD
Riverside MRI Center

Gary D Fullerton, PhD
University of Texas Health Science Center/San Antonio

J Mark Fulmer, MD
Baylor University Medical Center

E Mark Haacke, PhD
University Hospitals of Cleveland

Steven E Harms, MD
Baylor University Medical Center

Anton N Hasso, MD
Loma Linda University

Robert J Herfkens, MD
Stanford University School of Medicine

Charles B Higgins, MD
University of California/San Francisco

G Allan Johnson, PhD
Duke University Medical Center

Peter M Joseph, PhD
University of Pennsylvania

Emanuel Kanal, MD
University Health Center of Pittsburgh

Ruben Kier, MD
Yale University School of Medicine

Ron Kikinis, MD
Brigham and Women's Hospital

J Bruce Kneeland, MD
Hospital of the University of Pennsylvania

David N Levin, MD, PhD
University of Chicago Hospital

John Listerud, MD, PhD
Hospital of the University of Pennsylvania

Robert B Lufkin, MD
University of California/Los Angeles

James R MacFall, PhD
Duke University Medical Center

Kenneth R Maravilla, MD
University of Washington

Sharmila Majumdar, MD
University of California/San Francisco

Shirley McCarthy, MD, PhD
Yale University School of Medicine

Donald G Mitchell, MD
Thomas Jefferson University Hospital

Ponnada A Narayana, PhD
University of Texas Medical School at Houston

Dwight G Nishimura, PhD
Stanford University

Ray L Nunnally, PhD
Molecular Biosystems, Inc.

Mary Osbakken, MD, PhD
Hospital of the University of Pennsylvania

Peter Y Poon, MD
British Columbia Cancer Agency

Barry D Pressman, MD
Cedars Sinai Medical Center

Ronald R Price, PhD
Vanderbilt University Medical School

Stephen J Riederer, PhD
Mayo Clinic

Peter A Rinck, PhD
University of Trondheim

Val M Runge, MD
University of Kentucky Medical Center

Frank G Shellock, PhD
Tower Imaging

Michael S Silver, PhD
Philips Medical Systems
North America, Inc

Alison S Smith, MD
University Hospitals of Cleveland

Wendy R K Smoker, MD
Medical College of Virginia

Dirk H Sostman, MD
Duke University Medical Center

Bonnie D Flannigan-Sprague, MD
Southern California Orthopedic Institute

Charles E Spritzer, MD
Duke University Medical Center

David D Stark, MD
University of Massachusetts
Medical Center

Stephen R Thomas, PhD
University of Cincinnati

Jean A Tkach, PhD
Cleveland Clinic Foundation

Patrick A Turski, MD
University of Wisconsin

Felix W Wehrli, PhD
Hospital of the University of Pennsylvania

Jeffrey C Weinreb, MD
New York University Medical Center

SMRI '93 Eleventh Annual Meeting
Scientific Paper Abstracts

Sunday Morning • Imperial Ballroom
Papers 001–008

CONTRAST AGENT I: Abdomen/Chest

MODERATORS: PA Rinck, PhD
CE Spritzer, MD

001 • 10:30 AM

Comparison of Dynamic CT and Dynamic MR Imaging for Characterization of Primary Liver Tumors

S Paris, M Lüning, C Dewey, A Muehler
Charité-Hospital Berlin, Germany

Purpose: Dynamic CT with iodinated contrast agents and dynamic MR imaging with Gd-DTPA are accepted methods in clinical routine for characterization of liver lesions. The methods were compared for enhancement characteristics and for their sensitivities in detecting diagnostically relevant criteria.
Methods: The study investigated histologically proved primary liver tumors in 31 patients (19 focal nodular hyperplasia, 11 hemangiomas, 7 hepatocellular carcinomas, 4 hepatic adenomas). Dynamic CT was performed (Somatom DR 2, Somatom Plus) by using a bolus administration of 1.5 mL/kg contrast agent (6 mL/sec). Four to six scans were taken in the first minute, thereafter 1–2 scans up to 10 minutes. Dynamic MR imaging was performed (Gyroscan S15, 1.5 T) by using a bolus injection of 0.1 mmol/kg Gd-DTPA (4–5 mL/sec). Twelve images (gradient echo, TR/TE = 28/14, 60°, total imaging time 6 seconds) were acquired in the first 2 minutes; thereafter, 1–2 images were acquired up to 10 minutes. Images were analyzed retrospectively by 3 radiologists who used uniform criteria for both techniques.
Results: Time-density (dynamic CT) and time-intensity (dynamic MR imaging) curves of contrast enhancement were roughly similar. However, dynamic MR imaging commonly showed a longer persistence of enhancement compared with that of dynamic CT. Additionally, there were some significant differences ($P < .05$) in the detection of diagnostic criteria between CT and MR imaging. Dynamic CT was found to be superior in the detection of surrounding irregular blood vessels, whereas dynamic MR imaging was more sensitive for the diagnosis of fibrotic pseudocapsules and septations within the lesion.
Conclusion: Although both iodinated agents and Gd-DTPA are exclusively distributed throughout the extracellular compartment, dynamic CT and dynamic MR imaging were shown to differ in their sensitivities for detection of diagnostic criteria. These differences are probably related to different techniques (eg, spatial resolution, time resolution, adherent tissue contrast, etc) as well as to different volumes of contrast agent to achieve sufficient enhancement. Dynamic MR imaging may prove to be more sensitive for characterizing liver lesions, but this has to be shown in larger, controlled studies.
A. Muehler is an employee of Schering AG.

002 • 10:42 AM

Dynamic Contrast-enhanced MR Imaging of Pancreatic Transplant

HD Nguyen, WTC Yuh, DJ Fisher, ET Tali, V Douzdjian, PF Argibay, JL Cooper, MM Abecassis, RJ Corry
Radiology, MR Division, University of Iowa Hospitals and Clinics, Iowa City, IA

Purpose: To investigate the utility of dynamic contrast-enhanced MR imaging and automated quantitative computer analysis in the evaluation of pancreatic transplant graft functions.
Methods: Dynamic contrast MR images were obtained in 10 dual pancreatic/renal transplant patients by using spoiled gradient-echo imaging (25/13, NEX = 1–2, flip angle = 50°) after bolus injection of 0.1 mmol/kg Gd-DTPA either by hand or with an MR imaging compatible injector (Medrad, Pittsburgh, Pa). The pancreas and kidney enhancement sequences were qualitatively assessed by two radiologists. Computerized time-intensity curves were generated for the pancreas and kidney by using region-of-interest image statistics. These curves were fitted to the logistic dose response curve, $y = (a + b)/[1 + (x/c)^d]$.
Results: There were 5 normal and 5 rejected grafts, 4 with biopsy proof. Normal grafts qualitatively showed prompt and intense enhancement, while rejected grafts demonstrated diminished and delayed enhancement. Quantitative analysis showed that the slope of normal grafts ($m = 7.3$) was significantly higher ($P = .0315$) than that of rejected grafts ($m = 4.2$). The rise time of normal grafts (13.8 sec) also was found to be significantly shorter ($P = .0569$) than that of the rejected grafts ($m = 21.2$ sec). In 2 of 4 biopsy proof cases, graft dysfunction was only evident with quantitative analysis.
Conclusion: Contrast-enhanced dynamic MR imaging appears to be useful in the evaluation of pancreatic rejection. Quantitative analysis appears to be more sensitive in the detection of early subtle changes of graft dysfunction.

003 • 10:54 AM

Oral Contrast Agent for MR Imaging Evaluation of Pancreatic Masses

JS Kriegshauser, CD Johnson
Mayo Clinic Scottsdale, Scottsdale, AZ

Purpose: To evaluate the usefulness of positive oral contrast agent (OMR) for MR imaging of patients with known or suspected pancreatic masses.
Methods: Of 30 patients included in an evaluation of OMR at the Mayo Clinic's Rochester and Scottsdale facilities, 28 were evaluated for known or suspect pancreatic masses. Twenty-three patients had abnormalities in the pancreas; 5 were normal. The authors evaluated the pre- and post-OMR MR images for lesion detection, lesion conspicuity, ability to separate the lesion from the gastrointestinal tract and determine organ of origin, and overall anatomic display. They also rated the stomach, duodenum, and proximal small bowel on each image as to how well each was depicted.

Results: OMR improved lesion conspicuity in 11 of 23 cases and improved the ability to separate the lesion from the gastrointestinal tract or determine organ of origin in 16 of 23 cases compared with pre-OMR images. Overall, post-OMR images were better than pre-OMR images. The fast breath-hold T1-weighted sequence (snapshot) with OMR was best overall. OMR did not allow or facilitate detection of new lesions.
Conclusion: OMR improves MR imaging of pancreatic masses. With further refinement of breath-hold techniques and the timing of administration of oral contrast agents, MR imaging should continue to improve for evaluation of the pancreas.

004 • 11:06 AM

Initial Clinical Experience with Gadobenate Dimeglumine: A New MR Contrast Agent for Liver Imaging

MW Bourne, A Giovagnoni, CE Williams, M Misericordia, PC Rowlands, GH Whitehouse, F Amici
Department of Radiodiagnosis, Royal Liverpool University Hospital, Liverpool, England

Purpose: To establish the safety and efficacy of gadobenate dimeglumine.
Methods: Forty-four patients were studied at two institutions. Thirty patients were randomized to receive gadobenate dimeglumine (0.25 mol/L solution) at a dose of either 0.05 or 0.1 mmol/kg at an infusion rate of 10 mL/min. Fourteen patients were randomized to receive the contrast agent at an infusion rate of 0.5 mL/min at the same doses. Imaging was performed at 2 field strengths. Twenty patients were examined at 1.5 T and 24 patients at 1.0 T. T1-weighted SE acquisitions were acquired before and at 0, 10, 20, 30, 40, 60, and 120 minutes after administration of contrast material. T2-weighted SE acquisitions were acquired before administration of contrast material and, in 20/45 patients, at 120 minutes after administration of contrast material. Adverse events were assessed and recorded for a period of 24 hours.
Results: No significant clinical or laboratory adverse events were recorded. A strong and prolonged (up to 120 minutes) enhancement of hepatic parenchymal signal intensity was observed at both dose levels. During the vascular phase, lesion/liver C/N decreased with a subsequent reduction in lesion conspicuity and detection. At 60–120 minutes, washout of contrast material from the lesions led to an increase in lesion/liver C/N to values exceeding precontrast levels. The number of lesions detected on the postcontrast T1-weighted images exceeded that of precontrast T1-weighted and T2-weighted images at both field strengths. In the slow infusion group, no advantage was seen in comparison with the bolus injection group.
Conclusion: These initial results suggest that gadobenate dimeglumine is both a safe and efficacious contrast agent for magnetic resonance imaging of the liver. Further prospective, phase 3 studies are warranted.

005 • 11:18 AM

MR Imaging with Mn-DPDP: Enhancement of Primary Liver Lesions

TJ Vogl, B Schnell, B Hamm, C McMahon, J Lissner
Department of Radiology, University of Munich, Munich, Germany

Purpose: The purpose of this phase II study was to evaluate the diagnostic value and differentiation ability of the new hepatobiliary contrast agent Mn-DPDP with regard to the morphologic appearance and differentiation of liver tumors of hepatocellular origin.
Methods: Forty patients with suspected focal liver tumors were examined before and after intravenous injection of 5 or 10 μmol/kg Mn-DPDP. Routinely, T1- and T2-weighted SE sequences and a GRE sequence (breath-hold FLASH, T1-weighted) were used. Eight patients with liver lesions of hepatocellular origin (hepatocellular carcinoma [HCC] [*n* = 5]; cirrhosis with regenerative nodules [*n* = 2], focal nodular hyperplasia [FNH] [*n* = 1]) were evaluated separately regarding the detectability, determination, and diagnostic differentiation of these lesions.
Results: In all 8 patients, Mn-DPDP significantly increased the signal-to-noise ratios of liver parenchyma and lesions. The HCC lesions were either homogeneous hyperintensive (*n* = 2) or inhomogeneous hyperintensive (*n* = 3) on the T2-weighted SE images. On the T1-weighted images, they were either hypo- or hyperintensive and could not be differentiated from liver metastases. The substantial Mn-DPDP enhancement allowed better demarcation and improved the differential diagnosis. In one of two patients with liver cirrhosis, multiple regenerative nodules could be detected only after injection of Mn-DPDP. In the patient with FNH, only one lesion was detected on the plain images, but after injection of Mn-DPDP, three homogeneous lesions with strong enhancement could be differentiated. One of these lesions showed a characteristic central scar.
Conclusion: Specific enhancement of liver tumors of hepatocellular origin with Mn-DPDP revealed that more lesions could be detected and internal structures, such as a pseudocapsule or a central scar, could be identified.

006 • 11:30 AM

Superparamagnetic Iron Oxide Enhanced Hepatosplenic MR Imaging: Safety and Diagnostic Efficacy

PR Ros, C Stoupis, DA Allen, GM Torres
Department of Radiology, University of Florida College of Medicine, Gainesville, FL

Purpose: To assess the safety and diagnostic efficacy of a superparamagnetic iron oxide, AMI-25 (Advanced Magnetics, Cambridge, Mass), as an intravenous contrast agent for hepatosplenic magnetic resonance (MR) imaging compared with contrast-enhanced computed tomography (CECT).
Methods: Fifty-two patients with known or suspected focal lesions of the liver (*n* = 46) and/or spleen (*n* = 6) were studied at 1.0 T. T1- and T2-weighted images were obtained before and after drip infusion of 10 μm/kg AMI-25. Qualitative and quantitative analyses were prospectively performed. MR imaging findings were compared with those of CECT, which was performed within 10 days of MR imaging.
Results: Only 6 mild adverse reactions (11%) occurred, requiring no therapy. Postcontrast T2-weighted images demonstrated marked (> 60%) decrease in signal intensity in liver (96%) and in spleen (78%). Postcontrast T2-weighted images provided improved liver/lesion visualization and diagnostic confidence compared not only with that of precontrast T2-weighted images (81% and 86%), but also with that of CECT scans (70% and 77%). Postcontrast T1-weighted images were inferior to precontrast T1-weighted images (53%) and CECT scans (49%). Postcontrast T2-weighted images revealed, in 37% of cases, lesions not detected on either precontrast T2-weighted images or CECT scans. AMI-25 uptake was not seen in malignant lesions but only in benign ones (focal nodular hyperplasia [*n* = 2], adenoma [*n* = 1], and focal fat [*n* = 2]).
Conclusion: MR imaging with AMI-25 enhancement has the potential to be the noninvasive method of choice in hepatosplenic imaging, since it appears to enable detection of additional malignant lesions not seen with plain MR imaging or CT.

This research was supported in part by a scientific grant from Advanced Magnetics, Inc.

007 • 11:42 AM

OMR, a Positive Bowel Contrast Agent for Abdominal MR Imaging: Phase 2/3 Clinical Trials

RM Patten, AA Moss, P Ang, J Bova, S Bowman, R Entel, R Halvorsen, J Hampsey, R Herfkens

Rainier Medical Imaging Center, University of Washington, Kirkland, WA

Purpose: In a multicenter clinical trial, 222 patients with suspected or documented abdominal pathology were studied to evaluate the efficacy and safety of OMR—an effervescent solution of ferric iron—as a positive MR bowel contrast agent.

Methods: Spin-echo T1-weighted axial imaging of the upper abdomen was performed at 0.35–1.5 T in 222 patients before and after ingestion of 600 mL of oral contrast agent containing either 6 or 12 g of OMR. Laboratory parameters and vital signs were monitored, and subjective reaction to OMR was assessed for each patient. The effect of the contrast agent on bowel marking and organ delineation was assessed by investigators and blinded reviewers.

Results: No statistically significant changes in mean vital signs or laboratory values were seen after administration of OMR. Mild diarrhea was the most common adverse event, seen in 15% of patients. Investigators found moderate-to-significant improvement in opacification (94%), signal intensity (94%), distention (93%), and delineation (91%) of the upper gastrointestinal tract after ingestion of OMR. Blinded noncomparative review confirmed statistically significant improvement in these parameters. Additionally, OMR provided improved delineation of pancreatic margins in 36% (investigators' review) to 53% (blinded review) of cases. Compared with unenhanced studies, enhancement with OMR provided additional radiologic information in 64% of cases, specific additional information on a detected abnormality in 21%, and information valuable in changing a diagnosis or patient management in 10%.

Conclusion: OMR is a safe oral MR contrast agent that effectively marks the upper gastrointestinal tract. Use of this agent may assist the diagnostic efficacy of abdominal MR imaging in a small but substantial number of patients.

008 • 11:54 AM

Initial Human Evaluation with a Magnetic Susceptibility Contrast Agent Dy-DTPA-BMA for Myocardial Perfusion with Fast Gradient-Echo Imaging

H Sakuma, M O'Sullivan, J Lucas, MF Wendland, M Saeed, MC Dulce, KL Krayl, A Watson, CB Higgins

Department of Radiology, University of California, San Francisco, CA

Purpose: Prior studies in rats with use of subsecond MR imaging have demonstrated the effectiveness of Dy-DTPA-BMA for assessing regional myocardial perfusion. In the current human study, T2*-weighted fast gradient echo and spin echo imaging were applied to demonstrate the passage of Dy-DTPA-BMA through normal human myocardium.

Methods: Images were acquired with a GE 1.5-T Signa. A fast GRASS sequence (10.8/4.2) with driven equilibrium (DE) preparation pulse was used to produce T2*-weighted contrast. DE preparation time was 40 msec and k-space data were filled centrically. Dy-DTPA-BMA (Sanofi-Winthrop and Nycomed) was injected at doses of 0.05, 0.1, 0.2, 0.4, and 0.6 mmol/kg in 12 healthy volunteers. In addition to the fast dynamic imaging, pre- and postcontrast T2-weighted SE images (3RR/60) were obtained.

Results: T2*-weighted dynamic images showed a temporal decrease in myocardial signal at doses of Dy-DTPA-BMA from 0.2 to 0.6 mmol/kg. The maximal reduction (30%–50% decrease) in the signal of myocardium was delayed compared with that of chamber blood. There was no rapid recovery of the myocardial signal intensity. Postcontrast T2-weighted SE images demonstrated a myocardial signal attenuation (30%–45% decrease) at a dose of 0.4 mmol/kg or higher.

Conclusion: T2*-weighted dynamic MR imaging with magnetic susceptibility contrast media could be used to monitor the first passage of contrast media through human myocardium by using a conventional MR imaging system.

A. Watson and K. L. Krayl are employees of Sanofi-Winthrop.

Monday Morning • Franciscan B Papers 101–108

HEAD AND NECK I

MODERATORS: AN Hasso, MD
WRK Smoker, MD

101 • 10:45 AM

In Vivo P-31 Spectroscopy of Salivary Gland Tumors: Results and Differential Diagnosis

TJ Vogl, A Dadashi, A Jassoy, C Becker, S Ihrler, J Lissner

Department of Radiology, University of Munich, Munich, Germany

Purpose: The in vivo metabolism of salivary gland tumors through the application of P-31 MR spectroscopy is analyzed in this study. The aim of this prospective study was to assess whether P-31 MR spectroscopy can help distinguish benign from malignant tissue in salivary gland lesions.

Methods: P-31 MR spectroscopy investigations were performed in 14 healthy subjects (control) and 20 patients with salivary gland processes (13 malignant masses, 4 benign tumors, and 3 inflammations). MR images (T1-, T2-weighted sequences) were obtained on a 1.5-T Magnetom by application of a head coil or a Helmholtz surface coil, specially designed for investigations in the neck region. The MR spectra were obtained with a 50-mm double-tuned surface coil, centered on the region of interest. P-31 MR spectroscopy was performed with a TR of 1 second and accumulation of 512 FIDs. Thus, it was possible to differentiate the peaks of phosphomonoester (PME), inorganic phosphorus (Pi), phosphodiester (PDE), phosphocreatine (PCr), and ATP and ADP.

Results: In two large squamous cell carcinomas of the parotid gland and in five patients with metastasis, the P-31 spectrum of the tumor determined at a transmitter amplitude of 5 V showed an enlarged PME peak (3.74) and PDE peak (5.58), an elevated Pi peak (2.39) and a decreased PCr peak (−10%). The pH was 7.08. The spectral characteristics of a patient with pleomorphic adenoma and two patients with cystadenolymphoma of the parotid gland showed slightly increased PME, Pi, and PDE. PCr and ATP were slightly decreased (−30%). The calculated pH displayed a smaller value in the necrotic center of the tumor (7.10) in comparison to the periphery (7.24). The spectra of benign masses in chronic inflammatory diseases showed a minimal elevation of PME (0.34 ± 0.15), Pi (0.35 ± 0.05) and PDE (0.75 ± 0.2).

Conclusion: The spectras of malignant tumors showed a dramatic decrease in phosphocreatine and accompanying increases in Pi, PDE, and PME with slight changes in the ATP levels. Initial expectation to differentiate tumor histology with P-31 MR spectroscopy is only valid for differences between benign and malignant lesions.

102 • 10:57 AM

MR Imaging and MR Angiography in Patients with Paragangliomas of the Jugular Bulb and Carotid Body

TJ Vogl, JO Balzer, MF Juergens, J Lissner
Department of Radiology, University of Munich, Munich, Germany

Purpose: The findings of 118 patients with suspected carotid, tympanic, and jugular paragangliomas are presented, and the value of new MR imaging techniques such as TurboFLASH and MR angiography is discussed.
Methods: From 1988 to 1992, 118 patients with clinically suspected paragangliomas were examined with conventional MR imaging—plain T2 and plain and enhanced T1-weighted spin-echo sequences (gadopentetate dimeglumine, dose: 0.1 μmol/kg body weight). Time dependence of contrast medium enhancement was recorded using the TurboFLASH sequence. From 1990 to 1992, each patient with paraganglioma additionally underwent time-of-flight MR angiography. It was performed as an add-on scan prior to contrast medium application, using 3D FISP and 2D FLASH gradient-echo sequences. MR findings and available CT and DSA correlation were prospectively evaluated by three independent observers.
Results: Seventeen carotid body tumors, 25 tympanic, and 47 jugular paragangliomas were detected. Four patients with suspected tumor of the carotid body had an aneurysm of the carotid artery. Enhancement factor in all paragangliomas was 1.8 with maximum enhancement at 150 sec after injection. Correlation of MR imaging with CT revealed that MR was superior to CT in 81% and equal in 19% of the cases. MR angiography was performed in 52 patients and correlated with DSA findings in 19 cases. Additional information concerning topographic relationship of vascular structures, vessel displacement, occlusion or infiltration by tumor could be gained through MR angiography. Correlation with DSA findings revealed that MR angiography was able to visualize all vessels down to a diameter of 1.5 mm, but failed in imaging of small feeding vessels of paragangliomas.
Conclusion: In comparison to CT, MR has a higher spatial resolution, a better soft-tissue and soft tissue-bone differentiation. The recording of enhancement-time pattern is helpful in the differential diagnosis. MR angiography contributed to the diagnosis of paragangliomas by giving topographic information about vascular structures and enabling visualization of vessel occlusion or infiltration by tumor. A major advantage of MR angiography is the possibility of distinguishing between prominent jugular bulb and glomus tumor.

103 • 11:09 AM

Three-dimensional MR Reconstruction Technique for Surgical Planning of Acoustic Neuroma

TJ Vogl, J Assal, T Wustrow, C Bergman, J Lissner
Department of Radiology, University of Munich, Munich, Germany

Purpose: To evaluate the value of 2D SE and 3D GRE MR imaging sequences and 3D reconstruction for preoperative planning of surgical approaches to acoustic neuromas of the skull base.
Methods: Twenty-two patients with acoustic neuromas were prospectively examined with T1- and T2-weighted SE sequences before and after administration of contrast media, 3D GRE sequences, and a newly developed 3D reconstruction with window technique (1.5-T Magnetom) (TurboFLASH, 10/4, flip angle 15°, 128 partitions). After postprocessing of the 3D data cube on an integrated unit, the window technique allowed a surgical approach step by step from any desired direction, from the surface to the region of the tumor. Interactive software and video were prepared in a way that the user could slice through the 3D computer model and inspect cross-sectional images. All patients underwent surgical correlation with histopathologic evaluation, and the accuracy of the 3D view was confirmed by means of intraoperative inspection of the soft tissue.
Results: Intraoperative correlation revealed an intra-extracanalicular acoustic neuroma in 14 patients and 7 intracanalicular, and 1 extrameatal lesions. Three observers independently analyzed the results of 2D SE MR imaging, 3D sequences, and 3D window technique. The evaluation of the C/N of muscle to fat revealed nearly equal values for the 2D ($x = 7.8$) and 3D ($x = 6.9$) techniques. Preoperative diagnosis revealed true-positive findings in all patients. Standard 2D SE examinations before and after administration of contrast media showed best values for the 3 evaluated parameters. For the subsequent 3D examination, optimal contrast and high spatial resolution were provided by the 3D reconstruction technique.
Conclusion: Standard postcontrast SE techniques allow an optimal diagnostic evaluation of acoustic neuromas; the 3D reconstruction technique proved optimal for direct intraoperative planning in skull base lesions.

104 • 11:21 AM

Pituitary Screening in Children with Growth Hormone Deficiency: Use of High-Resolution 3D Spin-Echo, Gradient-Echo, and Turbo Field-Echo Sequences

C Leutner, KC Seelos, C Brack, G Reinheimer, M Reiser
Department of Radiology/Neuroradiology, University of Bonn, Bonn, Germany

Purpose: Growth hormone (GH) replacement in children with GH deficiency is an expensive and long-term treatment. The presence of morphologic abnormalities may have impact on treatment planning and decision making. In this study, pituitary screening was done by comparing contrast characteristics and diagnostic value of 3 different 3D sequences.
Methods: T1-weighted 3D MR imaging was performed in 29 children with GH deficiency at 0.5 T (Philips, Gyroscan T5-II) with SE, gradient-echo (FFE), and turbo field-echo (TFE) sequences. TR/TE was 300/25 msec for SE, 50/7.5 msec for FFE, and 16/5.2 msec for TFE sequences. Anisotropic data (256 × 205 matrix, FOV = 180, 1.5-mm sagittal and 2.0-mm coronal sections) were acquired in all and isotropic data (128 × 128 matrix, FOV = 128, 1-mm sections) in some children.
Results: With 3D TFE, 64 overcontiguous sections were obtained in 3 minutes compared with 6 minutes for 3D FFE or 13 minutes for 3D SE sequences. The 3D SE images were best with respect to C/N and edge definition, but few children tolerated the long imaging time, and thus motion artifacts occurred. The 3D FFE and 3D TFE sequences proved to be an excellent alternative, with tolerable imaging times. Although lower in C/N, they provided the same diagnostic information, with some overaccentuation of edges by chemical shift artifacts. The morphologic abnormalities found included a lack, asymmetry, or ectopy of pituitary gland or stalk and hypothalamic lesions.
Conclusion: High-resolution 3D MR imaging revealed abnormalities in 30% of children with GH deficiency. With short 3D FFE and 3D TFE sequences available, successful routine pituitary screening can be done even in less cooperative children. Isotropic data acquisition with multiplanar reformatting capability is an additional advantage.

105 • 11:33 AM

Retrospectively Gated Steady-State Free Precession Imaging of Cerebrospinal Fluid Motion in Patients with Syringomyelia

BC Sander, C Siewert, JC Böck, N Hosten, P Schubeus, R Felix
Department of Radiology, University Hospital Rudolf Virchow, Berlin, Germany

Purpose: To study cerebrospinal fluid (CSF) motion in patients with primary syringomyelia.

Methods: MR imaging was performed on a 1.5-T Siemens Magnetom. Ten volunteers and 10 patients with primary syringomyelia were examined. In midsagittal section position, a 2D steady state free precession sequence (SSFP) (20/10, flip angle of 80°, 5-mm section thickness, 256 × 256 matrix, 230-mm field of view, 4-minute acquisition time) was applied. With retrospective gating, 16 images were obtained, each representing CSF motion at 1 phase of an averaged cardiac cycle. CSF motion could be displayed in a cine loop. Semiquantitative results were obtained with signal intensity measurements of the syrinx and CSF spaces.

Results: The SSFP sequence yielded high signal intensity for stationary CSF and low signal intensity for moving CSF. Low signal intensities of CSF were normally present in the spinal subarachnoid space and in the prepontine cistern. In 6 cases, the fluid within the syrinx was displayed with high signal intensity. In these patients septa could be identified within the syrinx. An opposite pattern with pronounced motion in the syrinx was found in 4 patients. The pulsations within the syrinx were phase shifted compared with the CSF pulsations in the subarachnoid space.

Conclusion: The retrospectively gated SSFP sequence allows differentiation between syringomyelia with moving or stationary fluid. Further investigations will show if these results are helpful in planning and control of surgical therapy of syringomyelia.

106 • 11:45 AM

Tissue Contrast in MP-RAGE Imaging of the Skull Base and Neck Compared with Conventional T1-weighted Imaging

AW Litt, RA Holliday
MRI Department, New York University Medical Center, New York, NY

Purpose: Alteration of the relative contrast of extracranial soft tissues has been incidentally noted on magnetization-prepared rapid gradient echo (MP-RAGE) images of the brain despite preservation of typical T1-weighted gray matter/white matter contrast. The purpose of this study is to further characterize and assess the potential utility of these alterations in imaging of the skull base and neck.

Methods: Ten patients with suspected pathology of the skull base or neck were studied with conventional T1-weighted images (600/15) and with MP-RAGE (10/4/15°, 160-mm slab thickness, 128 partititions). The MP-RAGE data sets were reconstructed into axial images comparable with the conventional study.

Results: Relative tissue contrast on the MP-RAGE images was different from that on the T1-weighted images. The parotid gland was of the same signal intensity as the adjacent muscles on the MP-RAGE images rather than of higher intensity. Fat/muscle contrast was similarly reduced. Certain "cystic" masses, such as lymphovascular lesions, were hypointense to muscle with MP-RAGE, while mildly hyperintense on the T1-weighted images. Lesion localization was often superior on the MP-RAGE images compared with the conventional T1-weighted images. This was believed to be secondary to the alteration of relative tissue intensity as well as to the multiplanar reconstruction capability.

Conclusion: While the anatomic detail achieved with MP-RAGE imaging is better than that of conventional T1-weighted studies, the relative contrast between tissues is altered. Characterization of pathology must therefore be performed with an understanding of the different contrast relationships in this technique.

107 • 11:57 AM

MR Imaging of the Skull Base: Evaluation of Cerebrospinal Fluid Leaks and Cavities

LM Levy, S Rajan, D LeBihan, J Gulya, M Morris, D Schellinger
Georgetown University Hospital, Columbia, MD

Purpose: To evaluate patients with diseases involving the skull base by using MR flow imaging.

Methods: Over 20 cases with congenital, neoplastic, inflammatory, and postsurgical abnormalities affecting the skull base were reviewed. These abnormalities included cerebrospinal fluid (CSF) leak, postoperative defects and fluid cavities, mass lesions, atrophic changes, and inflammatory meningitis. A steady state gradient-echo sequence sensitized to slow flow by additional gradient pulses was used. In some cases, cine phase-contrast and diffusion-weighted spin-echo images were also obtained.

Results: The extent and location of CSF leakage were demonstrated with slow-flow and diffusion-weighted imaging. Abnormal CSF exit pathways could clearly be observed in cases with significant CSF leaks. In postoperative cavities, the slow-flow images helped to differentiate loculated or trapped fluid collections from freely communicating CSF spaces. No flow was observed in solid masses, including those with cystic or necrotic centers. Normal CSF flow was decreased or absent in regions of inflammatory meningitis. In general, cine phase-contrast and magnitude imaging were less sensitive in the detection of complex flow effects than were slow-flow or diffusion-weighted imaging.

Conclusion: MR flow imaging can be useful in further evaluating the location and nature of abnormalities involving the skull base.

108 • 12:09 PM

Utility of PET Imaging with FDG for Assessing Cervical Lymph Nodes: Comparison with MR Imaging

Y Anzai, S Rege, L Chaiken, E Abemayor, T Lee, B Jabour, R Hawkins, R Lufkin
Radiology Department, UCLA Medical Center, Los Angeles, CA

Purpose: The presence of lymph node metastases has a strong influence on treatment planning and prognosis of patients with head and neck cancers. MR imaging is relatively nonspecific in differentiating benign from malignant nodes. In this study, PET and MR imaging correlation of neck lymph nodes was performed to evaluate the utility of these two modalities.

Methods: PET scans were obtained with a Siemens/CTI 931/08-12 scanner. After a 4-hour fast, patients were injected with 10 mCi of 2-[18F]fluoro-2-deoxy-D-glucose (FDG) intravenously. MR imaging was performed with a 0.3-T permanent unit and 1.5-T superconducting units. T1- and T2-weighted axial images were mainly used for PET correlation. Nine patients who had squamous cell carcinoma and underwent radical neck dissections were evaluated for this study. Both PET and MR imaging were performed in all patients prior to the surgery.

Results: Two hundred fifty-six lymph nodes were removed from 9 patients; of these, 34 were found to be metastatic. Only 24 of 35 metastatic lymph nodes greater than

1.5 cm were considered positive with MR imaging. PET scans showed high uptake in 25 of 34 metastatic lymph nodes. PET depicted 3 nonenlarged metastatic lymph nodes. However, with PET, 9 false-negative lymph nodes were detected. Possible reasons for this included low glucose metabolism in the area of necrosis and partial volume effect of PET, causing underestimation of small lymph nodes.
Conclusion: PET imaging with FDG provides information about the status of glucose metabolic rate and has potential for assessing lymph nodes in the head and neck region, adding specificity.

Monday Morning • Franciscan C
Papers 109–116

CONTRAST AGENT II: Experimental I

MODERATORS: WG Bradley, Jr, MD, PhD
DD Stark, MD

109 • 10:45 AM

In Vivo Assessment of the Severity of Postischemic Myocardial Injury with Superparamagnetic Agents and Dynamic MR Imaging

E Canet, D Revel, N de Lorgioril, R Ferrat, L Sebbag, C Porcher, N Amiel
Hôpital Cardiovasculaire et Pneumologique, Lyon, France

Purpose: Superparamagnetic iron oxide particles (SPIO), more often described as T2 and T2* contrast agents, are able to express in certain conditions T1 enhancement. Moreover, during their intravascular phase, these agents might be useful for assessing tissue perfusion. In this study, myocardial transit of SPIO and ultrafast inversion recovery T1-weighted MR imaging were used to evaluate the severity of myocardial injury in a closed-chest canine model of ischemia-reperfusion.
Methods: Radiolabeled microsphere technique was used to assess the severity of ischemia during occlusion, expressed as a ratio of ischemic subepicardial blood flow versus nonischemic flow in a dog model of ischemia-reperfusion. Infarct sizing (IS) was performed by ex vivo TTC staining and planimetry and expressed as a percentage of left ventricular (LV) size (IS/LV). Low-dose SPIO was injected into a femoral vein (brief bolus) after 2-hour ischemia and 5-hour reperfusion. MR signal intensity was dynamically acquired in a midventricular short axis section for 40 sec. Time-density curves of signal intensity enhancement (SIE) after SPIO were performed by computer-assisted measurements of mean SI in 3 regions of interest of 32 pixels, positioned on the left ventricular cavity, and preceding ischemic and nonischemic zones. Myocardial perfusion defect was then evaluated by maximum SI enhancement following SPIO (SIE) in I normalized to SIE in NI (normalized to SIE in %) and related to blood flow (in %) and infarct size (IS/LV).
Results: After IS, 2 groups of subjects could be clearly defined: one with moderate insult (IS $\leq$ 10%, group I), and the other with severe damage (IS $>$ 10%, Group II), the second group corresponding to subjects with profound alteration of subepicardial blood flow during occlusion. MR signal intensity in the left ventricular cavity and nonischemic myocardium enhanced rapidly after SPIO injection and peaked at 9 sec. In ischemic areas, delayed upslope and difference in peak signal intensity could be related to the ischemic damage remaining after 5 hours of reperfusion. In addition, there was a strong, significant inverse relationship between normalized SIE and infarct size ($r^2 = 0.607$, $P = .0001$).
Conclusion: SPIO and dynamic MR T1-weighted imaging may be a promising approach for assessing the severity of myocardial injury after ischemia.

110 • 10:57 AM

Clearance and Biodistribution Studies of Mn-EDTA-DDP Liposomes (Memsomes): A New Class of Liver MR Contrast Agents

TA Fritz, D Shen, EC Unger, B Kulik, GL Wu
Department of Radiology/MRI, University of Arizona, Tucson, AZ

Purpose: To evaluate the clearance and biodistribution of Mn-EDTA-DDP memsomes.
Methods: Clearance was performed by using 5 Sprague Dawley rats injected via tail vein with 30 μmol/kg Mn^{+2} as Mn-EDTA-DDP (1.1 μCi of Mn-54 per rat). The animals were then returned to metabolism cages, and feces and urine were collected daily for 7 days. On the last day, the animals were killed; organs of interest were removed and rinsed with saline, and weights were recorded. All feces, urine, and organs were counted for radiation accumulation. Biodistribution was studied in male ICR mice. Six time points were evaluated: 5, 15, and 30 minutes and 1, 4, and 24 hours with 3 mice per time point. All animals were given 1 μCi of Mn-EDTA-DDP memsomes via the tail vein. At the time points, the animals were killed, and organs were harvested, weighed, and measured for radiation accumulation.
Results: Clearance was entirely by the fecal route; cumulative mean clearance was 91.09% ± 9.46. Only the liver retained any radioactivity (mean, 1.0% ± 0.24). Of the radiolabel recovered, 90% was cleared in the first 24 hours (estimated half-life of 6 hours). Biodistribution showed far greater uptake of Mn^{+2} by the liver than any other organ at 5, 15, and 30 minutes. The small intestine, large intestine, and pancreas showed steady increase at 15 and 30 minutes and 1 and 4 hours. By 24 hours, the majority of material had cleared ($>$90%). This is in strong agreement with clearance data and supportive of our estimated 6-hour half-life.
Conclusion: Mn-EDTA-DDP memsomes appear to be liver-specific MR contrast agents with rapid hepatobiliary clearance.
The authors are stockholders of ImaR$_x$ Pharmaceuticals.

111 • 11:09 AM

Reduction of Magnetic Susceptibility Artifacts with Iron Oxide-containing GI Contrast Agents: Importance of Optimizing Formulation

DL Rubin, HH Muller, MK Sidhu, SW Young, WA Hunke, WG Gorman
Department of Radiology, Stanford University, Stanford, CA

Purpose: Iron oxide-containing gastrointestinal (GI) contrast agents cause magnetic susceptibility artifacts. Even though some agents have produced good image quality with SE pulse sequences, severe artifacts have still occurred with gradient-echo and fat-saturation sequences. To reduce these artifacts, the authors optimized the concentration and viscosity of the formulation.
Methods: Phantom and canine studies ($n = 39$) were performed with an iron oxide contrast agent (WIN 39996, Sterling Winthrop) consisting of monodisperse 3.5-μm polymer particles coated with iron oxide. A concentration range of 25 to 250 μg iron per milliliter was prepared in 25 μg/mL increments. Viscosities of 1, 25, 50, 100, 150, 300, 450, and 600 cp were prepared. Imaging was performed at 1.5 T by using spin-echo (300/15 and 2,000/35, 70) with and without fat saturation, and gradient-echo

sequences (25–40/13, 30° flip angle), initially and after 1 hour.

Results: In the phantom and canine studies, susceptibility artifacts were seen at 1 and 25 cp. For formulations exceeding 50 cp, the 125–150 μg/mL concentrations yielded excellent negative contrast with the same susceptibility changes as air. No susceptibility artifacts were observed on SE, gradient-echo, and fat-saturation pulse sequences, even after 1 hour. However, concentrations greater than 150 μg/mL did produce artifacts.

Conclusion: The formulation of WIN 39996 has been optimized to provide negative contrast without producing susceptibility artifacts, even with gradient-echo and fat-saturation pulse sequences.

112 • 11:21 AM

Complementary Use of T2-, Postcontrast T1- and Perfusion-weighted MR Images for the Sequential Monitoring of a Focal Ischemic Lesion in the Rat Brain

D Lanens, M Spanoghe, J Van Audekerke, R Dommisse, A Van der Linden, A Øksendal

Research Group for Biomedical NMR, University of Antwerp, Wilrijk, Belgium

Purpose: The extent of the penumbra as a threatened zone of reversible ischemia is the target area for all cerebral-protective treatments. By using a combination of functional MR imaging procedures, the authors focused on the ability to discriminate areas of threatened from areas of dead cells.

Methods: A small focal cerebral infarction was photochemically induced in male Wistar rats. The resulting infarction was monitored with SE MR imaging (1.9 T; T2-weighted: 3,000/100; T1-weighted: 320/36) before and 20 minutes after contrast agent administration (Gd-DOTA, 0.5 mmol/kg) starting immediately after induction (1–5 hours) and on subsequent days (day 1, 3, 5, and 10). Perfusion-weighted imaging (2,500/130, 128 × 64) was performed by using the susceptibility agent Dy-DTPA-BMA injection (Nycomed, Norway) (1 mmol/kg).

Results: From 1 to 3 days after the insult, the hyperintense area on T2-weighted images, corresponding to edema, coincided well with the areas of reduced cerebral blood flow on perfusion-weighted images. The area of blood-brain barrier (BBB) disruption, as assessed with postcontrast T1-weighted imaging, was approximately half of this area. Five to 10 days after the insult, the hyperintense area on T2-weighted images decreased dramatically, while the nonperfused zone and BBB disrupted zone decreased to a much smaller extent.

Conclusion: A good correlation exists between the information obtained from T1-, postcontrast T1-, and perfusion-weighted images and pathologic and histologic findings in this animal model. The combined information from these 3 types of MR images may indicate the extent of the penumbra.

A. Øksendal is an employee of Nycomed.

113 • 11:33 AM

Paramagnetic Manganese-incorporated Hydroxylapatite Particles for Liver Imaging

DL Nosco, JB Wilking, LA Meeh, MR Hynes, KP Galen, WP Cacheris

Mallinckrodt Medical, Inc, St Louis, MO

Purpose: This study was conducted to develop a novel MR imaging contrast agent for the liver. The particle-based T1 agent is derived from the biocompatible material hydroxylapatite (HA).

Methods: Mn(II)-HA was produced by incorporation of paramagnetic Mn(II) salts into the solid structure during HA synthesis. The percentage of the Mn(II) can be varied from 0.1% to 100%. The relaxivity of the particles depends on synthetic conditions such as temperature, percentage of Mn(II), and coating agent. The parameters of this reaction were investigated to optimize the size and relaxivity of the particles.

Results: R1 was found to vary between 2 and 40 L · $\text{mmol}^{-1} \cdot \text{sec}^{-1}$, depending on the method of synthesis. Acute toxicity in mice (in doses of Mn[II]) decreased significantly as the percentage of manganese in the particles was increased. The Mn(II)-incorporated HA particles showed rapid uptake by the liver (RES) with immediate image enhancement on T1-weighted images. At a dose of 10 μmol/kg, up to 65% signal intensity enhancement was observed in rat liver and remained sustained for at least 4 hours. Administration of Mn(II)-incorporated HA particles to tumor-bearing rats improved the detection of the lesions.

Conclusion: Mn(II)-incorporated HA particles are potent T1 relaxation agents. These particles have been shown to be effective T1 contrast agents for enhancing the liver and for improving the detection of lesions in the liver.

114 • 11:45 AM

Quantification of First-Pass Distribution of MR Contrast Media in the Myocardium with Echo-Planar Imaging

M Saeed, MF Wendland, KK Yu, N Derugin, CB Higgins

Department of Radiology, University of California, San Francisco, CA

Purpose: To determine the first-pass extraction of the new nonionic MR contrast medium Dy-DTPA-BMA (Nycomed Salutar, Sterling Winthrop, Nycomed), by comparing residue curves with those obtained with a macromolecular intravascular agent Dy-DOTA-polylysine108 (Nycomed Salutar).

Methods: Gradient-recalled echo-planar imaging was used in the current study to monitor the first-pass dynamics of Dy-DTPA-BMA and Dy-DOTA-polylysine in normal rat hearts ($n = 8$). Sets of 32 consecutive electrocardiogram-gated images (1,000/10) were acquired. Each animal received a bolus injection of each agent at 0.05 and 0.1 mmol dysprosium per kilogram to compare directly the transit profile of the two agents.

Results: Administration of 0.1 mmol/kg of both agents caused equivalent maximal diminution in myocardial signal 46% ± 5 for Dy-DTPA-BMA and 40% ± 6 for Dy-DOTA-polylysine. However, the residue curves after administration of the extravascular agent were broader than those of the intravascular agent, with substantially greater tissue retention after clearance of the bolus. The extraction for Dy-DTPA-BMA was 30% ± 1 and 32% ± 6 for 0.05 and 0.1 mmol/kg doses, respectively.

Conclusion: Extraction of low-molecular-weight agents causes measurable alteration in the apparent transit profile, allowing one to estimate the extraction fraction by rapid imaging techniques. Furthermore, the extraction of low-molecular-weight agents produces unreliable results in uncorrected MR-based perfusion measurements in the heart.

115 • 11:57 AM

Initial Human Experience with the Magnetic Susceptibility Contrast Agent Dy-DTPA BMA, for MR Imaging Evaluation of Cerebral Perfusion

IH Cox, LM Prayer, ME Moseley, J Kucharczyk, WP Dillon, K Bleyl, A Watson

Department of Radiology, Neuroradiology Section, University of California, San Francisco, CA

Purpose: The optimum dose of Dy-DTPA-BMA for observing cerebral perfusion in relation to efficacy and safety was determined in healthy human volunteers.

Methods: GRASS images (34/25, 128 × 256, 0.75 NEX, 24 FOV, 1.5 T) were obtained through the basal ganglia of 10 volunteers during intravenous injection of Dy-DTPA-BMA at doses ranging from 0.05 to 0.6 mmol/kg, all administered at a constant infusion rate. Time-enhancement curves and peak signal loss (PSL) were determined from basal ganglia (BG), cortical white matter (WM), cortical gray matter (GM), and whole brain (WB). Each dose was administered to 2 subjects, between whom PSLs were averaged. In 2 additional subjects, injections were timed to coincide with the center of k space for T2-weighted SE images.

Results: PSLs of whole brain were 5%, 15%, and 30% at 0.05, 0.1, and 0.2 mmol/kg contrast agent, respectively. At 0.4 and 0.6 mmol/kg, PSL reached 39% and 42%, respectively. The duration of the bolus peak was prolonged at the 0.6 mmol/kg dose, which may be of importance in detecting subtle abnormalities of cerebral perfusion. Vascular enhancement dominated signal loss on WB analysis. Regional PSL reflected tissue blood supply: BG, 33%; WM, 22%; GM, 32% at 0.6 mmol/kg. T2-weighted conventional SE images obtained during contrast bolus peak revealed BG PSL of only 15%–20% at doses of 0.4 and 0.6 mmol/kg.

Conclusion: Fast GRE images enhanced with 0.4 mmol/kg of Dy-DTPA-BMA demonstrated cerebral perfusion through mean signal intensity decreases of 22% (WM) to 39% (WB). Higher doses did not increase signal loss but prolonged the duration of the bolus peak. Conventional T2-weighted SE imaging was relatively insensitive to contrast perfusion effects, even when timed to coincide with the bolus peak.

The authors are affiliated with Sterling-Winthrop, Inc, and Salutar/Nycomed Imaging.

116 • 12:09 PM

Gadolinium Phosphonates as MR Imaging Agents: Physiologic Effects in Normal Rabbits

IK Adzamli, H Weinstein, JA Leppo

Department of Radiology, University of Massachusetts Medical Center, Worcester, MA

Purpose: Sodium salts of Gd-DTPA-HPDP (a 3-amino-propane-1-hydroxo-1,1-diphosphono–modified Gd-DTPA) for infarct-specific MR imaging are potentially toxic when rapidly injected at MR imaging useful doses. This study investigates the hemodynamic functional responses to Na$^+$,Gd-DTPA-HPDP (and Na$^+$,Gd-EDTMP, a bound phosphonate) in intact rabbits, and explores safe administration.

Methods: Anesthetized rabbits were catheterized (carotid artery) to permit monitoring of left ventricular-developed pressure (LVP) (peak-systolic pressure − end-diastolic pressure), the first derivative (LVdP/dt), and heart rates. The agents were injected intravenously at either 1 mL/kg per minute (rapid) or 1 mL/kg per 5 minutes (slow), and also co-injected with added CaCl$_2$.

Results: When 50 μmol/kg (maximum tolerated rapid dose) Na$^+$,Gd-DTPA-HPDP was injected ($n = 3$), the LVP dropped from 125 ± 22 to 21 mmHg ± 2, and LVdP/dt from 2,270 ± 260 to 210 mmHg/sec ± 50 (83% and 91%, respectively). The heart rate was less responsive (from 285 ± 10 to 251 beats per min ± 10). All parameters recovered within 3 minutes with no intervention. Slow injection ($n = 3$) or coadministration of CaCl$_2$ (50 μmol/kg, $n = 3$) prevented adverse hemodynamic effects. A rapid 25 μmol/kg Na$^+$,Gd-DTPA-HPDP dose produced a smaller effect ($n = 3$, a reversible 20% LVP loss; ie, systemic calcium recruitment was effective at low dose rates). Na$^+$,Gd-EDTMP (50 μmol/kg, $n = 4$) elicited 18% loss in LVP; however, this agent precipitates with added calcium, hence is equivocal.

Conclusion: High doses of the sodium salts of phosphonate-modified Gd-DTPA can be used safely as slow infusions or by co-injection with an equivalent of CaCl$_2$. Administration as infusions need further exploration in MR imaging of infarcts.

Monday Morning • Plaza A
Papers 117–124

MRA: Clinical I

MODERATORS: RA Clark, MD
PJ Fritzsche, MD

---

117 • 10:45 AM

Preoperative Cortical Venous Mapping

KE Withers, O Boyko, M Agabright, R Helsper

Duke University Medical Center, Durham, NC

Purpose: To relate intraparenchymal pathology to cortical venous anatomy for the preoperative localization of lesions.

Methods: Axial T1- and T2-weighted images of the brain were acquired on a research-capable General Electric 1.5-T MR imaging system. MR angiography was then performed with a 2D time-of-flight imaging sequence with a TR of 45 msec, TE that was system specified, 60° flip angle, flow compensation, 1.5-mm section thickness, and a 20-cm field of view. Sections should cover from the middle cerebral artery to the superior vertex. These vertex sections of the cortical veins were obtained by means of postprocessing and collapsing the most superiorly acquired sections.

Results: In 9 cases, the preoperative determination at MR angiography of the cortical vein in the closest proximity to the underlying pathology was confirmed at surgery. Verification of the venous system seen with MR angiography proved to have a 100% correlation with surgically important cortical veins. (Two of the cases had lesions of less than 2 cm.)

Conclusion: The use of 2D MR angiography with a 3D display provides the ability to localize pathology in SE imaging onto MR angiograms of the cortical veins. This venous mapping provides the neurosurgeon with an accurate reference and important venous landmarks, which are valuable for surgery.

118 • 10:57 AM

MR Imaging Analysis of the Renal Arteries with Phase-Contrast Cine Studies

JM Silverman

Department of Radiology, Cedars-Sinai Medical Center, Los Angeles, CA

Purpose: Multiple MR imaging strategies have been used to evaluate the renal arteries with varying degrees of success. The author chose to analyze phase-contrast cine sequences with their cardiac gating and respiratory compensation advantages to determine if this method is efficacious for evaluating the renal arteries.

Methods: Ten healthy volunteers and 20 patients were enrolled in the study. Coronal and axial T1-weighted SE imaging was performed for localization of the renal arteries and for detection of mass lesions of the adrenal glands or kidneys. Coronal and axial phase-contrast cine imaging of the renal arteries was then performed by using 15-mm-thick, slightly overlapping slabs. In general, 3 slabs were needed in the coronal plane and 2–4 in the axial plane. The individual as well as collapsed images were analyzed for patency and pulsatility of the renal arteries and compared with radionuclide renal scans and/or angiograms when possible. All images were interpreted without knowledge of the results of the other imaging methods.
Results: All images were judged to be diagnostic. No respiratory misregistration was present. Qualitative pulsatility of the renal arteries was assessed and found to be decreased in atherosclerotic vessels. Compared with renal images and angiograms, the phase-contrast cine images correlated well with respect to patency of the extrarenal renal arteries. The majority of the cases demonstrated large intrarenal vessels as well.
Conclusion: MR imaging evaluation with a phase-contrast cine data base shows promise as an accurate, noninvasive imaging method for evaluating the renal arteries.

119 • 11:09 AM

Prospective Evaluation of Breath-Hold Pulmonary MR Angiography

ML Schiebler, G Holland, J Listerud, H Palevsky, H Hatabu, T Foo, W Gefter
Department of Radiology, Philadelphia, PA

Purpose: To prospectively evaluate the efficacy of a new MR angiography technique for the diagnosis of pulmonary embolism in patients suspected clinically of having either acute or chronic pulmonary emboli.
Methods: Fifteen patients suspected clinically of having pulmonary embolic disease were prospectively enrolled in an MR imaging protocol that included the following pulse sequences: (1) transverse SE 500–700/25, 5-mm-thick sections, 256 × 128 matrix, interleaved, 2 averages, electrocardiogram (ECG) gated; (2) transverse cine SPAMM TR 60/12, 5-mm sections, 5-mm skip, 256 × 128 matrix, 2 averages, ECG gated; (3) Sagittal breath-hold 9/2.5, 8-mm sections, 256 × 128 matrix, 2 averages, 3-mm overlap, with the receive-only 4-coil array positioned over the right lung. All patients underwent operative, angiographic, or high probability ventilation-perfusion imaging to confirm the presence or absence of emboli. The studies were independently and blindly read by 3 radiologists unfamiliar with the cases.
Results: There were 12 patients with pulmonary embolic disease (chronic or acute) and 3 patients without evidence of disease with angiography. Breath-hold MR angiography was the most sensitive (0.83) and specific (1.0) of the three sequences tested. Combining all the MR studies, the positive predictive value was 1.0 and the negative predictive value was 0.6. The 2 false-negative cases were of peripheral emboli. No central emboli were missed.
Conclusion: These preliminary results are encouraging for the further use of breath-hold MR angiography as a new noninvasive method for the primary diagnosis of central pulmonary arterial emboli.

120 • 11:21 AM

MR Angiographic Guidance for Placement of Transjugular Portosystemic Stent Shunt

MF Mueller, JP Finn, KR Stokes
Department of Radiology, MRI, Beth Israel Hospital, Boston, MA

Purpose: Transjugular intrahepatic portosystemic shunt (TIPS) placement is a new radiologic technique to achieve portal decompression percutaneously in patients with variceal bleeding. Complication rates correlate with the number of needle passes required to puncture the portal vein. The purpose of this study was to determine whether MR angiography can map the optimal course for bridging the hepatic and portal veins in TIPS procedures and, hence, decrease the complication rate.
Methods: Sequential 2D time-of-flight angiography was used to plan catheter placement for TIPS procedures in 6 of 15 patients, and the results were compared with those of 9 patients who did not have prior vascular mapping. The largest patent hepatic vein was chosen, and the pathway from this to the closest branch of the portal vein was estimated by reference to the scale on the MR images.
Results: Fourteen of 15 attempted TIPS procedures were successful and resulted in rapid shunting from the portal to the hepatic venous system. Of the patients who did not undergo MR angiographic guidance, 2 died due to complications of the procedure, and 2 more patients had nonfatal hemorrhage. Procedure time in this group was, on average, 2.8 hours (range, 1.75–4 hours), and in these, there was a high number of intrahepatic needle passes (mean, 12.1; range, 2–23). The 6 patients who underwent the TIPS procedure with MR angiographic guidance had no complications. The procedure time was shorter (mean, 1.7 hours; range, 1.5–2 hours), and the average number of needle passes was fewer (mean, 2.2; range, 1–4).
Conclusion: Findings to date suggest that MR angiography is very useful for preoperative mapping in TIPS, and planning based on MR angiographic findings can significantly decrease the length of the procedure and the rate of complications.

121 • 11:33 AM

Evaluation of Thoracic Outlet Syndrome with MR Imaging and MR Angiography

MB Esposito, JA Arrington, R Clark, FR Murtagh, ML Silbiger, W Blackshear
University of South Florida, Tampa, FL

Purpose: MR imaging and MR angiography demonstrate well the degree of vascular compression and the relationship of the vessel to the adjacent structures in thoracic outlet syndrome.
Methods: A baseball player presented complaining of thoracic outlet syndrome symptoms in his throwing arm. Imaging of the brachial plexus and the thoracic outlet region was performed with 2D time-of-flight technique in the sagittal plane. MR angiography was performed with the symptomatic arm in 2 positions: at the patient's side and over the patient's head. Ten other patients (5 of whom were professional baseball players and heavily muscled, and 5 of whom were nonathletic and not heavily muscled) were imaged by using the same protocol.
Results: In the symptomatic player, MR angiography demonstrated normal flow in the axillary and subclavian veins with the arm at the patient's side but complete subclavian vein occlusion at the level of the first rib with the patient's arm over his head. MR imaging also demonstrated marked hypertrophy of the subclavius muscle. The occlusion was confirmed with venography and surgery.
Conclusion: The degree of compression of the subclavian vein is clearly shown with MR angiography, while sagittal spin-echo MR imaging clearly demonstrates the relationship of the vessels to the adjacent structures that are causing the obstruction.

122 • 11:45 AM

Global Mesenteric Perfusion: Assessment with Cine Phase-Contrast Flow Volumetry of the Portal Venous System

DJ Burkart, CD Johnson, RL Ehman
MR Research Lab, Mayo Clinic, Rochester, MN

Purpose: There is a need for a noninvasive method of screening patients with suspected mesenteric ischemia. The purpose of this study was to assess the accuracy of volumetric flow rates in the portal venous system as a measure of global mesenteric blood flow.
Methods: Eleven volunteers and 2 patients with suspected mesenteric ischemia were studied by using the commercially available cine phase-contrast (CPC) pulse sequence. Volumetric flow rates (VFR) were obtained in the celiac axis (CA), superior mesenteric artery (SMA) and vein (SMV), and portal vein (PV) in the volunteers. Flow measurements in the PV and SMV were acquired in the patients.
Results: The ratio of the measured mesenteric perfusion (sum of CA and SMA flow) and PV flow was 1.15 ± 0.04. In the volunteers, the mean volumetric flow rates in the CA, SMA, SMV, and PV were 9.9 mL/min/kg ± 3.2, 6.0 mL/min/kg ± 1.8, 5.7 mL/min/kg ± 2.0, and 13.7 mL/min/kg ± 1.8, respectively. The linear regression of the comparison of VFR in the SMA and SMV was $\mathrm{VFR}_{\mathrm{SMV}} = -0.88$ mL/min/kg + 1.09 $\mathrm{VFR}_{\mathrm{SMA}}$ ($r = .97$, $P = .00002$, SEE = 0.41 mL/min/kg). At conventional mesenteric angiography, 1 patient had severe mesenteric ischemia and the other patient was normal. MR flow measurements in the PV were 9.1 and 15.0 mL/min/kg, respectively.
Conclusion: The results suggest that flow measurements in the PV and SMV are a useful noninvasive method of assessing mesenteric blood flow, thereby permitting identification of patients with mesenteric ischemia.

123 • 11:57 AM

Image Processing for 3D Steady-State MR Angiography of the Lower Extremities

A Rao, P Schmalbrock
Magnetic Resonance Imaging Facility, Ohio State University, Columbus, OH

Purpose: MR angiography presents an alternative to contrast angiography and Doppler US for evaluation of peripheral vascular disease, but time-of-flight and phase-contrast methods are problematic because of the need to cover a large region with high resolution and the large variability of peripheral arterial flow. The authors evaluated 3D steady-state high-resolution-yielding black-blood images based on loss of coherence for flowing spins.
Methods: Coronal images of volunteers acquired in 2–6 minutes on a 1.5-T GE Signa with the body coil by using the 3D gradient-echo sequence with TR/TE/α of 21/5/30° (28–60 sections with 1–2-mm thickness; 40–48-cm FOV with 512 × 384 or 25-cm FOV with 256 × 192) were transferred to a SUN workstation and reformatted into axial images with IDL (Interactive Data Language, Boulder, CO). A seed-point within an artery was manually selected, and its neighboring 26 pixels were checked. Pixels below a selected threshold were included as part of the vessel. Next, selected pixels were chosen as new seed-points and 8 neighbors within and 9 corresponding pixels in the adjacent section were examined. In this way, a decision regarding pixel inclusion was made for all axial sections and the intensity for included pixels was set to a value exceeding all surrounding regions. Maximum intensity projection yielded angiographic displays.
Results: High-quality images depicting both arteries and veins with low signal intensity can be generated. Initial tests of the connectivity algorithm allowed extraction of major vessels. A detailed evaluation of the behavior of the algorithm at branches and for smaller vessels is currently under way.
Conclusion: Three-dimensional steady-state black-blood imaging is a promising technique for fast high-resolution evaluation of the entire lower extremity.

124 • 12:09 PM

Combined Black and White Blood MR Angiography of Stenoses

JN Oshinski, DN Ku, JW Peifer, RI Pettigrew
George W. Woodruff School of Mechanical Engineering, Georgia Institute of Technology, Atlanta, GA

Purpose: A major problem with 2D inflow angiography is signal loss in the turbulent flow field distal to stenoses. On the other hand, black-blood images consistently show the flow as black even in the turbulent flow field past stenoses. This study was undertaken to assess the viability of imaging stenotic flows by using a combination of inflow and black-blood MR angiography.
Methods: A 2D inflow MR angiographic sequence (TR/TE/α = 7/26/60°) was conducted on an in vitro human umbilical vein graft containing a 90% stenosis at a Reynolds number of 500. Transverse black-blood sections were acquired distal to the stenosis, where inflow images experienced signal loss. The signal intensity values from the black-blood sections were inverted and filtered to match the intensity of the inflow sections. These black-blood sections were then substituted for the sections that contained signal loss in the inflow images.
Results: The maximum-intensity projection views of the stenosis phantom from the inflow MR angiogram showed an 8-mm region of complete signal loss distal to the stenosis throat. The projection views of the stenosis phantom reconstructed with the inverted and filtered black-blood sections inserted in the area of signal loss visualized the complete flow field within the stenosis phantom. A comparison between an x-ray angiographic image of the stenosis and the combined inflow/black-blood image showed that the combined method depicted stenosis severity accurately.
Conclusion: This study showed that excellent images of stenosis can be obtained by using a procedure that combines inflow and black-blood sections.

Monday Morning • Plaza B
Papers 125–132

RAPID IMAGING TECHNIQUES I

MODERATORS: MS Cohen, PhD
SR Thomas, PhD

125 • 10:45 AM

Spiral Scan Imaging of Cortical Activation

DC Noll, CH Meyer, JD Cohen, W Schneider
University of Pittsburgh, Carnegie Mellon University, Pittsburgh NMR Institute, Pittsburgh, PA; Stanford University, Stanford, CA

Purpose: In the human brain, changes in levels of blood oxygenation in response to a stimulus or task can be imaged by using conventional MR imaging, but imaging times can be long. The authors investigated the use of spiral-scan imaging as a method for rapidly acquiring T2*-weighted images for high-resolution mapping of cortical activity by using a conventional 1.5-T imager.
Methods: The multisection, spiral-scan pulse sequence used had an echo time of 43 ms to achieve the desired T2* contrast. The gradient waveforms were designed to use 20 interleaved spirals of length 17.6 ms to acquire a 203 ×

203 Fourier matrix with a 24-cm FOV (theoretical resolution of 1.18 × 1.18 mm). The stimulus or task is repeated 10 times in each of 2 states, after which percent difference and Student *t* test images are generated.
Results: Activation in the motor and visual cortices was imaged with spiral-scan imaging by using fist-clenching and flashing checkerboard stimuli, respectively. Regions of activity typically demonstrated percent changes in signal intensity of 3%–40%, with the latter likely being due to veins draining the areas of activity. The standard deviation in nonactivated tissues was typically 1.25%.
Conclusion: Spiral-scan imaging is demonstrated as a robust method for recording functional information from the human brain. When compared with standard spin-warp imaging, the spiral-scan method seems more robust to the effects of brain motion. This is important, since all methods, including echo-planar, are likely to require multiple acquisitions or interleaving to achieve high resolution.

126 • 10:57 AM

Chemical Shift Imaging with RARE

K Oshio, RV Mulkern

Department of Radiology, Children's Hospital, Harvard Medical School, Boston, MA

Purpose: To implement and test 3DFT chemical shift imaging sequences based on RARE techniques to decrease spectroscopic imaging times.
Methods: Section-selective CPMG sequences, with 32-msec echo readouts performed in the absence of imaging gradients and in-plane spatial mapping, performed with orthogonal phase-encode gradients, were implemented on a 1.5-T imaging system. One of the phase-encode gradients was incremented from echo to echo to increase the data acquisition rate.
Results: A 4-echo sequence repeated 1,024 times with a 1-second TR was used to generate 64 × 64 spatial matrices at 128 spectral frequencies separated by 32 Hz each in 17.1 minutes; this is 4 times faster than achievable with conventional chemical shift imaging. The minimum effective TE obtainable was 43 msec.
Conclusion: The present study demonstrates that RARE methods may be used to gainfully decrease conventional imaging times for 2D spatial maps over a moderately resolved spectral range (32 Hz/pixel). This spectral resolution is suitable for quantitative fat/water studies at 1.5 T. Full 2D mapping of long T2 brain resonances like NAA, Cho and PCr/CR, however, will require improved spectral resolution with longer echo readouts and, subsequently, longer effective echo times. Assuming a spectral resolution of 8 Hz/pixel is sufficient for brain metabolite studies at 1.5 T, the minimum effective TE achievable with our methods is 135 msec. Such a sequence would produce 64 × 64 spatial matrices of selected metabolites in reasonable examination times, considerably enhancing the clinical applicability of proton spectroscopic imaging.

127 • 11:09 AM

Simultaneous-Multisection Ultrafast FLASH with a Hard Pulse

S Singh, WR Brody

Department of Radiology-MRI, The Johns Hopkins University School of Medicine, Baltimore, MD

Purpose: For many applications of MR imaging, it would be desirable to image simultaneous multiple sections, especially with high temporal resolution. This will be particularly useful for cardiac functional imaging, bolus-tracking-based perfusion/diffusion imaging, and MR angiography. Here we present simultaneous-multisection ultrafast FLASH MR imaging.
Methods: The strategy for multisection FLASH is to first saturate/null the volume outside the sections of interest (SOIs) during the preparation period, and then apply a train of short, hard pulses, instead of section-select pulses, to acquire FLASH MR imaging data from all the sections simultaneously without increasing TR, and complete in a time window selected about the null point. In order to separate sections, an additional readout gradient is applied orthogonal to the plane of the SOIs.
Results: Pulse sequences for the selection of multiple SOIs for FLASH MR imaging are extensions of the methods 1–3 used for defining a single SOI (submitted to this meeting) and were implemented on our 1.5-T GE Signa system. For example, using spatially selective 90° sinc saturation pulses followed by nonselective inversion (method 1), seven bands of thickness 3.2 cm each with interband spacing of 1.2 cm were nulled in a 20-cm-diameter sphere ($T_1 \sim 600$ msec), thus simultaneously defining 6 SOIs (the regions between the saturation bands) of thickness 1.2 cm each. Similarly, multiple SOIs of thickness 3.5 mm were isolated by first saturating the SOIs with spatially selective sinc/DANTE pulses (tip angle $\geq 90°$) followed by nonselective inversion (method 2) or vice-versa (method 3), and then nulling the magnetization outside the SOIs. The FLASH MR imaging data acquisition was started by using a train of short, hard pulses and an additional readout gradient and completed within a time window selected about the null point (methods 1–3), thus imaging multiple SOIs simultaneously with a TR of ≤ 2 msec on 4.7-T GE CSI hardware. Phantom as well as in vivo data demonstrate the efficacy of these methods.
Conclusion: Simultaneous multisection FLASH in the same imaging time as single-section FLASH ($TR < 2$ msec) is possible.

128 • 11:21 AM

High-Resolution, Ultrashort-Echo-Time MR Angiography with a Whole-Body EPI Imager

PA Wielopolski, RR Edelman, JP Finn, FX Schmitt

Department of Radiology, MRI, New England Deaconess Hospital and Beth Israel Hospital, Boston, MA; Siemens Medical Engineering Group, Erlangen, Germany

Purpose: Our goal is to evaluate ultrashort echo times for the acquisition of MR angiograms with and without velocity compensation by using a whole-body EPI imager.
Methods: Phantom and patient studies have been performed with a prototype Siemens 1.5-T EPI whole-body imager using short echo times of 1.5 msec without velocity compensation and 2.5 msec with velocity-compensated sequences with a minimum field of view of 200 mm for a 256^2 matrix and evaluated in regions with stenosis. Lower bandwidth sequences with slightly increased echo times and velocity compensation were also compared. In patients and volunteers, magnetization transfer pulses were included to improve the vessel contrast in the cerebral circulation.
Results: Short echo times without velocity compensation demonstrated minimal dephasing due to flow, compared with the velocity-compensated version with the same readout bandwidth. The high readout bandwidth compromises the signal-to-noise ratio; sequences with slightly longer echo times with velocity compensation and reduced readout bandwidths can be used at the expense of increased sensitivity to flow dephasing. With TE = 2.5 msec, the fat signal was reduced and vessel depiction near the carotid bifurcation was improved.
Conclusion: The use of ultrashort echo times reduces extensively the dephasing effects of higher-order-motion terms in stenotic and increased turbulence regions, dramatically improving the quality of MR angiograms.

129 • 11:33 AM

Volumetric Measurement of the Substantia Nigra with High-Resolution 3D Gradient-Echo Imaging

P Schmalbrock, DW Chakeres, VA Hacker
Magnetic Resonance Imaging Facility, Ohio State University, Columbus, OH

Purpose: Evaluation of the brain stem with standard 2D SE imaging and attempts to quantify the volume of the substantia nigra in patients with Parkinson disease had limited success (1,2). The major reason is the 3–5-mm minimal section thickness available with SE imaging. Furthermore, the iron content in some of these tissues may lead to variable T2 and low signal on T2-weighted images. We evaluated high-resolution 3D gradient-echo imaging with very short TE/TR, with a flip angle near the Ernst angle yielding high signal (3).

Methods: Axial images were acquired on a 1.5-T GE Signa system by using the spoiled 3D gradient-echo (3D-SPGR) sequence with TR/TE/α of 50/5/15° and the standard quadrature head coil. Spatial resolution achievable in 10–14 minutes ranged from 0.8 × 1.0 × 2.0 mm to 0.8 × 1.5 × 1.5 mm. Initial measurements of the substantia nigra volume were obtained by manual tracing.

Results: The substantia nigra yields the highest signal due to higher PD and longer T1, compared with the red nucleus, the cerebral peduncle and the cerebellar decussation. The substantia nigra could be seen in 5 to 7 sections, and the initial analysis of 4 patients (aged 25–64 years) resulted in similar volumes on both sides in the range of 300–450 mm^3.

Conclusion: Our initial results indicate that 3D-SPGR imaging near the Ernst angle is a promising technique for high-resolution studies of the brain stem and volumetric measurements. The signal-to-noise ratio of the head coil could be overcome by using phased arrays, for example, to further improve image quality and resolution.

1. Drayer B, Burger P, et al. AJNR 1986; 147:103–110. 2. Huber SJ, Chakeres DW, et al, Arch Neurol 1990; 47:735. 3. Schmalbrock P, Chakeres DW, SMRM 1992, 1726.

130 • 11:45 AM

Single-Shot GRASE Imaging with an Enhanced Gradient System (Comparison with EPI)

K Oshio, C von Weymarn, G McKinnon
Department of Radiology, Brigham and Women's Hospital, Harvard Medical School, Boston, MA

Purpose: The GRASE sequence has been developed on unmodified clinical imagers. Single shot T2-weighted imaging is possible, however, on enhanced (faster) gradient systems. The purpose of this study was to test the actual performance of the sequence on an enhanced gradient system, and to compare it with the EPI technique by using the same hardware.

Methods: The GRASE sequence was implemented on a 1.5-T imager with an enhanced gradient amplifier (GE Signa with a gradient speedup circuit developed at GE Medical Systems). Both GRASE and EPI sequences were tested on this system by using the same ramp time, readout time, field of view (FOV), and so forth.

Results: The maximum resolution obtained with the GRASE sequence was 128 × 120 with a 24 × 24-cm FOV. The effective TE was 120 msec, and the total imaging time was 220 msec. With EPI, we could acquire a single-shot image with a matrix of 256 × 128 and 36 × 18-cm FOV. TE was set to 40 msec for half NEX (8 overscans) and 120 msec for full NEX. Imaging time was 80 msec and 140 msec, respectively. In the 256 × 128 mode, EPI images were distorted. Image distortion was much less in the 128 × 64 mode. In GRASE images, there was no noticeable distortion.

Conclusion: EPI and GRASE had comparable maximum resolution. In higher resolution, however, EPI images tended to be more distorted. The disadvantage of GRASE is longer imaging time (200 vs 40 msec) and a relatively long effective TE.

131 • 11:57 AM

POMP (Phase Offset Multiplanar) Imaging with the RARE Sequence

K Oshio, H Hayano, S Kosugi
Department of Radiology, Brigham and Women's Hospital, and Harvard Medical School, Boston, MA

Purpose: POMP (phase offset multiplanar) imaging is a type of 3D imaging technique in which the phase encoding in the section direction is done by specially designed RF pulses, rather than phase-encoding gradient pulses. Compared with Fourier 3D, it is more efficient, with a small number of section encodings (< 8), since it does not have the aliasing problems at the excitation slab edges. The purpose of this study was to investigate the feasibility of applying the POMP technique to the RARE sequence.

Methods: Since RARE imaging uses the CPMG echo train, the phase relations between 90° and 180° pulses have to be kept while phase encoding. For this reason, both 90° and 180° pulses have to be phase-encoded with the same section profile. The pulse sequence was implemented on a clinical imager (0.5 T Vectra, YMS/GE).

Results: Up to three sections were excited with each 90° pulse, yielding 3 times as many sections per acquisition. There were no noticeable intersection intensity variations.

Conclusion: POMP can be implemented with the RARE sequence by phase-encoding both 90° and 180 pulses with the same section profile. This can be used to compensate for the RARE sequence limitation in the number of sections.

K. Oshio is a consultant to Yokogawa Medical Systems.

132 • 12:09 PM

Imaging of Silicone Breast Implants at 1.0 T

PJ Fritzsche, D Atkinson, WG Bradley, Jr
Riverside MRI Center, Riverside, CA

Purpose: A number of studies have evaluated MR imaging in patients with suspected rupture of silicone breast implants at 1.5 T. Because S/N, field inhomogeneities, and chemical shift artifact change with field strength, the authors investigated a number of strategies for optimizing breast imaging at 1.0 T.

Method: The authors examined 15 volunteers and 10 patients referred for suspicion of silicone implant rupture. Images were obtained on a standard 1.0-T Siemens Magnetom with a dedicated bilateral breast coil. A STIR method was used to image silicone with reduced background fat signal (TR/TE/TI = 4,500/18/75, section thickness = 5 mm, gap = 0 mm). Transverse images were obtained with a 384 × 512 matrix and 380 FOV and sagittal orientation with a 192 × 256 matrix and 210 FOV. A saturation band was used to decrease artifacts from the heart. TI was adjusted to 300 msec to null silicone. To produce thin sections with adequate S/N, a 3D gradient-echo sequence (PSIF) was performed in the coronal plane (30/20, 128 × 256 matrix, 320 FOV).

Results: The dedicated coil produced diagnostic image quality in the anterior portion of all breasts; however, the axillary areas outside the coil were not as well appreciated. The combination of fat nulling and a limited-FOV coil reduced most motion artifact. In contrast, the silicone-nulling sequence, with its bright fat, demonstrated considerable artifact. The 3D imaging provided thin sections and high spatial resolution that proved beneficial in illustrating contained ruptures and small circumferential folding of the envelope over multiple sections. Compared to 1.5-T studies with similar parameters, these studies exhibited negligible S/N differences but noticeably less chemical shift artifact. The latter point was useful in cases in which the chemical shift of silicone obscures small circumferential defects.

Conclusion: Acquisition and display parameters known to be successful for MR imaging of the breast at 1.5 T can be modified for practical imaging at 1.0 T. With these optimized techniques, diagnostic information and image quality were found to be comparable with results from 1.5 T.

Monday Morning • Imperial Ballroom
Papers 133–140

BREAST

MODERATORS: R Kikinis, MD
ML Silbiger, MD

---

133 • 10:45 AM

Silicone Breast Implants: Comparison of MR Diagnosis and Surgical Findings

J Lichman, DJ Atkinson, GD Gillan, RS Hurwitz
Department of Radiology, Hoag Memorial Hospital, Newport Beach, CA

Purpose: Conventional mammography is limited in its ability to help detect rupture of silicone breast implants. MR imaging, with its capability of multiplanar cross-sectional imaging of the entire prosthesis, offers the potential for a more accurate evaluation of implant integrity.

Methods: The authors examined 25 patients who were referred for suspicion of silicone implant rupture. Imaging was performed with a standard 1.5-T Siemens Magnetom system by using a dedicated bilateral breast coil. With this coil, patients lay prone with breasts unrestrained. In the interest of reducing overall imaging time and nulling fat, a dual-echo TurboSE (FastSE) sequence incorporating a preparatory inversion recovery pulse was used. The TR/TE/TI was 4,612/17–109/100; section = 5 mm; gap = 2 mm. Transverse, sagittal, and coronal planes were imaged with a matrix of 384 × 512 and field of view of 380 mm. The absence of fat signal minimized respiratory motion, as did the use of a dedicated coil. Motion artifacts from the heart were minimized by a saturation band. Given a slightly longer T1 for the implant, silicone appeared relatively brighter than fat, with an intermediate signal from muscle and fibroglandular tissue. The later echo (TE = 109) was useful in reducing fat signal and producing higher silicone/fat contrast.

Results: In the group of 25 patients, surgical removal and replacement of prostheses was performed in 16 breasts. Implant rupture was diagnosed at surgery in 7 of 16 breasts. Prospective comparison of the MR diagnosis and the surgical findings gave a true-positive predictive value of 86% and a true-negative value of 89%. One case of extensive gel bleed showed no abnormality on MR images.

Conclusion: Fat-nulled, dual-echo MR imaging in a dedicated breast coil is an accurate and easily implemented technique for evaluation of silicone breast implant rupture.

D.J. Atkinson is an employee of Siemens Medical Systems.

134 • 10:57 AM

Gadolinium-enhanced Breast MR for Characterization of Suspicious Breast Lesions

F Kelcz, GE Santyr, EJ Fairbanks, SJ Mongin
University of Wisconsin, Madison, WI

Purpose: The positive predictive value for mammography is typically only 15%–30%. The purpose was to determine if the gadolinium enhancement profile could be used to differentiate benign from malignant breast lesions and so reduce the number of negative biopsies.

Methods: In women being sent for breast biopsy, dynamic, gadolinium-enhanced MR imaging was performed in either a single- or multiple-section format by using a spoiled, gradient-recalled echo sequence. The data were fit to a generalized form of a saturation curve described by 4 parameters: the initial signal intensity (SI), the increase in SI after gadolinium enhancement, the number of seconds after contrast agent infusion at which the SI was midway between its starting and final value, and M, the normalized kinetic order of the rise rate of SI.

Results: The study included 27 women with the following diagnoses: 3 carcinomas, 9 fibroadenomas, and 15 other benign breast lesions. In 12 women, no enhancing lesions were detected; in none was a malignancy diagnosed. Fifteen enhancing lesions were subjected to the curve-fitting algorithm. The parameter most accurate in distinguishing malignancy was M. A threshold value of M = 4.5 permitted correct classification of 3 of 3 malignancies and 14 out of 15 benign lesions.

Conclusion: Dynamic, gadolinium-enhanced MR imaging was far more accurate in distinguishing benign from malignant lesions than traditional breast examination methods. The mathematical model employed virtually eliminated false-positive results from enhancing fibroadenomas. Had MR imaging results been used to help determine the necessity for surgical intervention, 23 of 24 unnecessary biopsies could have been avoided.

135 • 11:09 AM

Contrast-enhanced Breast MR Imaging with Dynamic and Fat-Suppression Techniques

CW Piccoli, DG Mitchell, GF Schwartz, S Vinitski
Thomas Jefferson University Hospital, Philadelphia, PA

Purpose: To examine the potential of dynamic contrast-enhanced breast MR imaging in detecting and differentiating benign and malignant disease.

Methods: Breast MR imaging was performed at 1.5 T by using a dedicated breast surface coil in 33 women with abnormal mammographic, sonographic, or clinically palpable findings. The examination included T1- and T2-weighted sequences with and without fat suppression and a dynamic multiplanar spoiled gradient echo series following administration of 0.1 mmol/kg Gd-DTPA, by using either out-of-phase (TE = 2.3) or in-phase (TE = 4.2) imaging, acquired every 30 seconds for 3 to 5 minutes. Histopathologic correlation is available for 20 cases. The remaining patients are being followed clinically and with imaging.

Results: Excisional biopsy helped to identify benign lesions in 12 patients and malignancies in 8. Dynamic enhancement curves reflect a tendency for more rapid enhancement of malignancies compared to benign disease, although there was gradual enhancement of 1 colloid carcinoma. No lesions were found in 7 patients, and cysts, but no enhancing masses, were found in 2 with mammographic or sonographic abnormalities. Follow-up of these 9 patients with negative MR imaging findings has shown no evidence of malignancy. Abnormalities were found in 4 patients who chose follow-up with MR imaging and mammography. Out-of-phase imaging helped to delineate masses but partially obscured small lesions. Fat suppression increased the conspicuity of breast lesions.

Conclusion: MR imaging appears useful for evaluating patients with equivocal mammographic or sonographic findings. Dynamic enhancement patterns may be of diagnostic value, although overlap of benign and malignant lesions occurred. Fat suppression improves lesion conspicuity, but out-of-phase imaging may obscure small masses.

136 • 11:21 AM

Silicone-specific MR Imaging of the Breast

RA Jensen, SE Harms, DP Flamig, MD Meiches, WP Evans
MRI Department, Baylor University Medical Center, Dallas, TX

Purpose: A silicone-specific MR method was used to distinguish free silicone from other lesions in patients with silicone breast augmentation.
Methods: The rotating delivery of excitation off resonance (RODEO) pulse sequence selectively eliminated signal from the narrow range of $(CH_3)_4Si$ resonance. This method preserved a high-resolution, silicone-specific 128 × 256 × 256 3D set acquired in approximately 5 minutes. Thirty-seven breasts in 24 patients were evaluated with both a fat-suppressed, 3D MR sequence and a silicone-suppressed, 3D MR sequence to distinguish free silicone from masses. Twenty-four of these breasts were imaged both before and after gadolinium administration. Conventional breast imaging methods were also performed in all patients.
Results: In all patients, silicone implants and injections demonstrated a unique appearance compared to normal breast tissue. MR identified free silicone in 10 breasts, 5 of which were confirmed pathologically. No free silicone was present on MR images in 27 breasts; 7 of these were confirmed by biopsy or mastectomy as showing no evidence of free silicone. In these 7 breasts, 2 infiltrating lobular and 1 infiltrating ductal carcinomas were found, which were interpreted as being suggestive of malignancy on MR images on the basis of enhancement. The remaining cases were fibroadenomas ($n = 2$), an apocrine cyst ($n = 1$), and localized fibrosis and inflammation ($n = 1$). Thus, in the 12 cases in which pathologic evaluation was performed, there was no discrepancy with MR findings.
Conclusion: Silicone-specific MR imaging of the breast can distinguish free silicone from masses in patients who have undergone problematic conventional imaging.

137 • 11:33 AM

MR Imaging in Diagnosing Breast Carcinoma

M Megido-Ravid, Y Itzchak, M Shabtai, M Koller, J Kopolovic
Sheba Medical Center, Tel Aviv, Israel

Purpose: To evaluate the accuracy of MR imaging with Gd-DTPA in the diagnosis of breast pathology.
Methods: During the last 3 years, 250 women aged 20–89 years were examined. All mammographic results were suggestive of masses and were sampled for biopsy after the MR imaging examinations. One hundred twenty-two (48.8%) had lumps; 128 (51.2%) had calcifications. Images were obtained with the Elscint Gyrex 2T instrument. Field strength was 1.9 T. A transmitter/receiver H-1 surface coil 16 cm in diameter and specially designed for breast examinations was used. A spin-echo pulse sequence was applied. Gd-DTPA was administered intravenously at a dose of 0.1 mmol/kg.
Results: By applying the T2-weighted sequence, it was possible to eliminate all the cysts. Fibroadenomas were seen in 18 women. Usually no pathology was seen when using the T1-weighted sequence. After the injection of Gd-DTPA, T1 was shortened in 85 of the cases; 18 of them were recognized previously as fibroadenomas. The pathologic results from the biopsies showed complete correlation between histologically normal tissue and normal MR images. Sixty-nine percent of the 67 cases with shortened T1 were histologically diagnosed as carcinoma. Thirty-one percent were diagnosed as premalignant changes, such as papillary hyperplasia, apocrine metaplasia, and atypical intralobular hyperplasia. The sensitivity of the technique was 98.53% for carcinoma and precarcinomatous states. The specificity was 100%.
Conclusion: MR imaging with Gd-DTPA is a nontraumatic, noninvasive, accurate technique for differentiating between normal and pathologic breast tissue.

138 • 11:45 AM

Microcalcifications in Clinically Normal Breast: The Value of High-Field, Surface Coil, Gd-DTPA–enhanced MR Imaging

JD Tesoro-Tess, A Amoruso, E Turrini, L Balzarini, E Ceglia, D Rovini, R Musumeci
Istituto Nazionale Tumori, Milan, Italy

Purpose: After routine screening mammography, several patients had results suggestive of clusters of microcalcifications not clearly classified as benign or malignant. Gd-DTPA-enhanced MR imaging demonstrated high values of accuracy and sensitivity as a possible imaging approach to breast cancer and proved to be a valuable technique both for benign and malignant lesions.
Methods: During a 12-month period, 30 patients had nonsignificant clinical breast examination results suggestive of microcalcifications. SE (500/17) and gradient echo (320/14/80°) sequences were taken before and after a bolus injection of Gd-DTPA (0.2 mmol/kg). Four-mm-thick sections with a 10% gap were acquired in sagittal and transverse planes. A rapid (less than 3 min) focal signal enhancement was considered positive for malignancy. All patients underwent surgery within 5 days after MR imaging.
Results: In 18 of 30 patients, histology disclosed malignant disease. The total number of correctly diagnosed cases included 13 positive and 11 negative, with 80% accuracy. Only 1 false-positive result (an abscessed chronic mastitis) was encountered, whereas 4 of 5 false-negative results were in situ carcinomas (3 intraductal microfocus and 1 lobular plurifocal), and 1 was an infiltrating tubular adenocarcinoma. All lesions with a slight and delayed signal enhancement were correctly interpreted as benign (fibroadenoma or dysplasia). Gradient echo images were always more adequate than SE images because of their higher contrast enhancement. Tumor size is the major limit of this method, and in 4 of 5 diagnostic errors, the tumor's diameter was less than 5 mm.
Conclusion: Patients with uncertain mammographic findings (mainly microcalcifications) and negative clinical examination results can be treated either with frequent clinical and mammographic examinations or surgery, since mammographic diagnostic accuracy is not always high (60%). The high values of accuracy (80%) and positive predictive value (92.8%) of Gd-DTPA-enhanced MR imaging suggest the mandatory use of exeresis only in those patients with positive MR imaging results.

139 • 11:57 AM

Selective Silicone Imaging for Breast Implant Patients

S Mukundan, WT Dixon, BD Kruse, RC Nelson, D Monticciolo
Department of Radiology, Emory University School of Medicine, Atlanta, GA

Purpose: To develop a pulse sequence that will show silicone while suppressing all tissues, to detect silicone implant leakage.
Methods: Relevant protons fall into 3 groups: silicone methyl protons, lipid protons, and water protons. Silicone in implants and water in most tissues have a T1 several times as long as that of fat. T1-based suppression is therefore used for fat. Silicone and fat have about the same chemical shift, but water has a considerably higher reso-

nant frequency (about 0.2, 1.2, and 4.5 ppm, respectively). Chemical shift-based suppression is therefore used for watery tissues. STIR suppresses fat. A $1\underline{3}3\underline{1}$ pulse centered on silicone has little effect on silicone; however, it appears as a 90° pulse to water. Therefore, followed by a spoiler gradient, it suppresses water signals. The effects of STIR on water and $1\underline{3}3\underline{1}$ pulses on fat are irrelevant. Typically, an 8-section SE mode was used, giving an imaging time under 7 minutes. Surface coils were used for good sensitivity.
Results: By using this pulse sequence, the authors have imaged double-lumen implants, double-lumen stacked implants, ruptured implants with both intra- and extracapsular leaks, and direct silicone injections. Images obtained in both the axial and sagittal planes clearly depicted all surfaces of the implants. Images of pathologic specimens with direct injections correlated well with images taken in vivo.
Conclusion: This silicone-only sequence yields high-quality images of all surfaces of breast implants and has excellent clinical potential for diagnosing silicone leakage.

140 • 12:09 PM

Can MR Imaging be the Gatekeeper for Surgical Breast Biopsy?

TJ Turkat, BD Klein, RH Richman, RL Polan
Conego Medical Magnetic Resonance Systems, Thousand Oaks, CA

Purpose: Breast biopsy is often required for further evaluation of abnormalities detected at physical examination or at mammography. The positive biopsy rate is relatively low, on the order of 30%. We have undertaken a project to determine if MR imaging can be used to significantly elevate the positive biopsy rate.
Methods: Twenty-four patients who were scheduled for surgical biopsy, due to either abnormal mammographic findings or abnormal findings at physical examination, underwent MR imaging. The findings were not used in clinical decision-making. All patients subsequently underwent surgical breast biopsy. A General Electric 1.5-T Signa System with a dedicated receive-only breast coil (Medical Advances) was utilized. Gradient-echo, fat-suppressed images were obtained before and after injection of a standard dose of gadolinium. Percentage change in signal intensity was calculated in the area of interest. The ratio of signal intensity within the lesion compared with adjacent fat was also measured.
Results: Eighty percent (8/10) of the positive MR imaging results proved to be cancer at surgical biopsy. The positive biopsy rate (without MR analysis as a factor) was 33% (8/24). No false-negative MR examination results were obtained.
Conclusion: The preliminary data suggest that MR imaging is highly accurate in distinguishing between benign and malignant lesions of the breast. The number of biopsies could be significantly reduced by including MR imaging in the work-up of breast lesions prior to surgical biopsy. The study is ongoing.

Monday Afternoon • Franciscan A
Papers 141–148

CARDIAC I

MODERATORS: MR Fisher, MD
RJ Herfkens, MD

141 • 3:45 PM

Atrial Function Assessed with MR Imaging in Healthy Volunteers and in Patients with Myocardial Infarction

RH Mohiaddin, M Hasegawa, R Underwood, DB Longmore
Magnetic Resonance Unit, Royal Brompton Hospital, London, England

Purpose: In the past 2 decades, there has been considerable interest in the evaluation of atrial volumes and atrial function in a variety of heart diseases. We used MR imaging to help measure atrial volumes and emptying fractions in healthy volunteers and in patients with myocardial infarction.
Methods: Fourteen healthy volunteers (mean age ± SD = 47 years ± 13) and 14 patients (age, 56 years ± 9) with previous myocardial infarction were studied. All patients were in a sinus rhythm, had competent cardiac valves, and had no heart failure. Atrial (LA, RA) and ventricular (LV, RV) volumes were measured from a set of transverse SE images acquired at end ventricular systole (ESV) and diastole (EDV). Percentage of ventricular ejection fraction (EF) (EDV-ESV)/EDV × 100 and atrial emptying fraction (EF) (ESV-EDV)/ESV × 100 were calculated.
Results: In patients with myocardial infarction, LA EDV and ESV were significantly higher ($P < .001$), and EF was significantly lower ($P < .001$) than in the control group.
Conclusion: Changes in atrial and ventricular volumes can be measured noninvasively with MR imaging. We have established normal ranges and have demonstrated abnormalities in patients with myocardial infarction.

142 • 3:57 PM

Left Ventricular Diastolic Regional Wall Motion Assessment with MR Velocity Mapping: Comparison of Coronary Artery Disease with Controls

SP Karwatowski, RH Mohiaddin, GZ Yang, DN Firmin, SR Underwood, DB Longmore
Royal Brompton Hospital, London, England

Purpose: Current noninvasive techniques for assessment of diastolic function focus on global measures. Long-axis ventricular wall motion is an early marker for IHD. We have used cine magnetic resonance velocity mapping to study regional long-axis diastolic ventricular wall motion.
Methods: Eighteen normal volunteers (10 men) and 21 patients with IHD (17 men, 13 with a previous infarct) were studied when not taking cardiac medication. Magnetic resonance cine velocity information was acquired through a basal short-axis plane. This short-axis ring was divided into 16 sectors and velocity-time curves were constructed. The peak early-diastolic wall velocity during early diastole was identified, and maximum and minimum velocities were measured. These were used to give a range of velocities standardized to the peak velocity.
Results: The mean velocity in millimeters per second (comparison with control values) for maximum velocity in the control group was 100; it was 78 ($P = .06$) for those with angina and 71 ($P = .02$) for those with infarcts. The mean velocity for minimum velocity in the control group was 52; it was 29 ($P = .04$) for those with angina and 13 ($P = .02$) for those with infarcts. The range of velocities in the control group was 50; for the group with angina it was 62 ($P = .6$), and for the group with infarct it was 84

($P = .02$). In normal patients, peak wall velocities were greater in early diastole than in systole; posterior wall velocities were consistently the highest, and peak velocity decreased with age.
Conclusion: Magnetic resonance velocity mapping of long-axis ventricular wall motion provides unique regional information not available with other techniques. It can detect resting abnormalities of diastolic regional long-axis wall motion in patients with IHD.

143 • 4:09 PM

Differentiation of Myocardial Injuries by Contrast-enhanced Echo-Planar Imaging

M Saeed, MF Wendland, KK Yu, K Lauerma, HT Li, F Cavagna, CB Higgins
Department of Radiology, University of California, San Francisco, CA

Purpose: To compare the dynamic effects of bolus injection of Gd-BOPTA/Dimeg (Bracco SpA, Milan, Italy) on both T1 and T2* shortening of myocardial signal by using inversion recovery (IR) and gradient recalled (GR) echo-planar imaging (EPI) in rats subjected to (1) reversible myocardial injury, (2) irreversible myocardial injury, or (3) occlusive infarcts.
Methods: Animals were divided into 3 groups (9 rats per group). Reperfused reversible and irreversible myocardial injuries were produced by placing a reversible occluder around the left coronary artery to allow reperfusion (1 hr) after 15 or 60 minutes of occlusion. Group 3 rats were subjected to 2 hours of permanent occlusion. ECG-gated EPI images (TR = 2 sec, TE = 10 msec, TI = 0.7 sec for IR-EPI, and TR = 1 sec for GR-EPI) were acquired in sets of 32 consecutive images. Two doses of Gd-BOPTA/Dimeg were injected: 0.025 mmol/kg for IR-EPI and 0.25 mmol/kg for GR-EPI.
Results: In all groups, normal myocardial signal was increased on IR-EPI and decreased on GR-EPI images during the first pass of Gd-BOPTA/Dimeg. In reversibly injured myocardium, normal and injured myocardium were indistinguishable. In irreversibly injured myocardium, enhancement of the injured zone was delayed but steadily increased to a higher value than normal on IR-EPI images; on GR-EPI images, the diminution in signal of the injured region after the injection was much less than in normal myocardium. In occlusive infarcts, the signal intensity of the injured region did not change with either pulse sequence.
Conclusion: Gd-BOPTA/Dimeg in conjunction with T1 and T2* sensitive EPI has the potential to (1) delineate infarcted regions (both occlusive and reperfused infarcts), and (2) discriminate reversible from irreversible injuries and occlusive from reperfused infarcts.

144 • 4:21 PM

Assessment of Myocardial Tendency to Infarction of Hypertrophied versus Normal Hearts with Gadoteridol-enhanced MR Imaging

K Lauerma, M Saeed, MF Wendland, N Derugin, KK Yu, CB Higgins
Department of Radiology, University of California, San Francisco, CA

Purpose: Previous studies have indicated that the outcome of a coronary ischemic event tends to be more severe in the presence of left ventricular hypertrophy (LVH). Therefore, the current study was designed to detect and compare the ischemic regions in normal and hypertrophied hearts following brief occlusion of the left coronary artery (LAD) and reflow in rats by using the new nonionic MR contrast medium gadoteridol (ProHance; Bristol-Myers Squibb).
Methods: Two experimental groups were designed: normal rats ($n = 11$) and rats subjected to LVH by suprarenal aortic banding ($n = 10$). After 8 weeks, the LAD was occluded for 25 minutes and reperfused for 1 hour before the acquisition of the first image. Three transaxial images at different levels (ECG-gated, TR = 250 msec, TE = 20 msec) were acquired with a GE Omega 2T MR system before and for 30 minutes after the injection of gadoteridol (0.3 mmol/kg). Area at risk and infarction size were determined in the same 3 sections by using blue dye injection and histochemical staining, respectively.
Results: There was no significant difference in SI between normal (0.45 ± 0.03) and ischemic (0.45 ± 0.03) regions before administration of gadoteridol. After injection, SI of the ischemic region (1.72 ± 0.17 was higher than in normal myocardium (1.02 ± 0.06; $P < 0.05$). Enhancement of reperfused hearts persisted for at least 30 minutes after injection. There was no significant difference in the area at risk between normal rats (46% ± 2) and rats with LVH (46% ± 3). On MR images, the hyperintense area was substantially larger in rats with LVH (34% ± 5) than in normal hearts (11% ± 3). By using histochemical staining, the infarction size was significantly greater in rats with LVH (23% ± 5) compared to normal rats (5% ± 2). The apparent injury appeared larger on MR images versus histochemical staining.
Conclusion: Reperfused myocardial infarcts are considerably larger in hearts with LVH versus normal hearts. This difference can be determined noninvasively by using MR contrast media.

145 • 4:33 PM

Anatomic MR Imaging of the Cardiovascular System with 3D Black Blood Acquisition

D Li, EM Haacke, CB Paschal
Department of Radiology (MRI), University Hospitals of Cleveland, Cleveland, OH

Purpose: Two-dimensional SE anatomic cardiac imaging has thick sections and section misregistration. In this work, we use a single 3D acquisition to cover a 40–80-mm-thick volume of the heart, creating thin and contiguous sections with high contrast between cardiac cavities and myocardium and excellent great vessel wall delineation.
Methods: Double-inversion pulses (the first nonselective and the second selective) were applied immediately after an ECG trigger to invert the magnetization of the flowing blood outside the region of interest (ROI) while preserving that of the surrounding tissue. The inversion time (TI) allows blood with inverted magnetization to flow into the ROI. After TI, 16 or 32 3D section-encoding steps (with central reordering) were acquired for each in-plane phase-encoding loop. TI was chosen so that the zero 3D section-encoding line was collected when the longitudinal magnetization of the inflowing blood was nearly zero. The data acquisition window for each cardiac cycle was 200–300 msec in diastole with short TR (9–12 msec) RF-spoiled FLASH. Averaging 4 acquisitions suppresses respiratory motion effects and enhances the signal-to-noise ratio. With 128 phase-encoding lines, the acquisition time was 6–9 minutes.
Results: With this double-inversion 3D imaging technique, blood signal was greatly suppressed with little or no effect on the stationary tissue, creating high contrast between blood and the surrounding structures. High resolution in the section-select direction allowed better depiction of fine structures, such as trabeculae carnae, papillary muscles, and valves, than with 2D SE sequences.
Conclusion: This method could be useful in defining congenital anatomic abnormalities of the cardiovascular sys-

tem. The contrast is also good enough for end systolic and end diastolic ventricular volume calculations.

146 • 4:45 PM

Three-dimensional MR Imaging of the Coronary Arteries with Fat Saturation

D Li, CB Paschal, EM Haacke, RD White, LP Adler
Department of Radiology, University Hospitals of Cleveland, Case Western Reserve University, Cleveland, OH

Purpose: A 3D approach can overcome the problems of thick sections, low signal-to-noise ratio, and misregistration associated with 2D breath-hold coronary artery imaging. With thick-slab 3D imaging, however, blood signal becomes partially saturated, and the surrounding fat may be isointense with coronary arteries. In this work, we use fat saturation (FS) to reduce fat signals, allowing clear coronary artery delineation.
Methods: The FS pulse was applied during the trigger delay time (TD) of the imaging sequence. After TD, 32 3D section-encoding steps (with central reordering) were acquired for each in-plane phase-encoding loop with RF-spoiled FLASH (TR = 8.5 msec; matrix size = 150 × 256; number of signals averaged = 4; section thickness = 2 mm; region of interest = 64 mm; acquisition time = 7–10 minutes). A CP body coil was used, and the patients were put in a supine position. The original images were then postprocessed by multiplanar reconstruction (MPR) after transverse acquisition, to display the coronary arteries in oblique planes.
Results: Ten volunteers and 2 patients were studied on a 1.5-T imaging system. Fat signals were greatly suppressed, allowing visualization and tracking of the coronary arteries over the imaging volume in all studies. MPR images were able to display 4–5-cm proximal portions of the coronary arteries in most cases. A congenitally abnormal left coronary system was characterized in 1 patient and was confirmed by conventional angiography.
Conclusion: The advantages of 3D acquisition include high resolution, contiguous spatial coverage with complete image registration, and postprocessing capability. There is no need for surface coils, lying in the prone position, or breath hold, which makes it more robust and more acceptable to patients.

147 • 4:57 PM

Fast 3D Cardiac Imaging with MTC to Enhance Contrast for Ventricular Volume Calculation

D Li, EM Haacke, LP Adler, S Kaushikkar
Department of Radiology (MRI), Case Western Reserve University, University Hospitals of Cleveland, Cleveland, OH

Purpose: Ventricular volume can be determined by 2D techniques, but relatively thick sections are required to cover the entire heart in a single-scan session. A single, thick-slab, 3D scan can cover the whole heart with contiguous thin sections. Blood signal tends to be partially saturated, however, reducing the contrast between cardiac cavities and myocardium. In this work, magnetization transfer contrast (MTC) pulses were used to enhance the contrast in 3D techniques.
Methods: Twenty-five MTC pulses were applied during the trigger delay time (TD) of the fast 3D cardiac imaging sequence. Each pulse had a duration of 8.192 msec, offset frequency of 3 kHz, and magnitude of 10 μT with a Gaussian pulse shape. After TD, 32 3D section-encoding steps were acquired for each in-plane phase-encoding loop. Centrally reordered 3D encoding was used to take advantage of the blood inflow. The data acquisition window for each cardiac cycle was 270 msec with short TR (8.5 msec) RF-spoiled FLASH, which could be placed at end systole or end diastole. One 3D scan covered over 130 mm with each section 4 mm thick. With 128 phase-encoding lines and 4 acquisitions, the imaging time was 6–9 minutes. The local SAR was below 4 W/kg for all studies.
Results: Without MTC pulses, blood and myocardium were nearly isointense for some sections because of their similar T1. MTC pulses suppressed the myocardial signal by about 40%, increasing the blood/myocardium contrast by up to a factor of 10.
Conclusion: Single, fast, 3D, thick-slab whole-heart coverage greatly reduces the imaging time compared to multiple thin-slab 3D or thick-slab 2D cine images. It also eliminates the misregistration artifacts associated with the other 2 methods and the partial volume effects of the thick-slab 2D technique. Blood/myocardium contrast enhancement with MTC proves to be sufficient for the determination of the ventricular volume through segmentation.

148 • 5:09 PM

Submillimeter Imaging of Coronary Arteries with Angiographic and Phase-Contrast Velocity-encoding MR Methods

RM Peshock, JR Kowal, LG Wilbert, WA Erdman, DE Gutekunst, M NessAiver, GD Clarke
Mary Nell and Ralph B. Rogers Magnetic Resonance Center, University of Texas Southwestern Medical Center, Dallas, TX

Purpose: Accurate, noninvasive MR imaging evaluation of coronary artery anatomy and flow would have considerable application in the assessment of coronary artery disease.
Methods: A Picker HPQ 1.5-T MR imaging system with a body insert gradient coil was used for rapid, high-resolution imaging. A single breath-hold phase-encoding grouping (PEG), cine MR imaging sequence was developed to image the left coronary arterial tree with a pixel size of 0.49 mm^2 to 0.81 mm^2 and 6-mm section thickness. A TR/TE = 13/9, velocity sensitized/compensated PEG sequence produced submillimeter images of coronary flow velocity with a section thickness of 10 mm. Studies of transient regional myocardial ischemia by using a balloon occluder were performed in a canine model. Cine images of the left anterior descending coronary artery (LAD) were obtained in long- and short-axis views. Acquisition sets were obtained with and without presaturation pulses to accentuate inflowing signal in the coronary arteries.
Results: Breath holds of 20–35 seconds were required. The LAD was easily visualized before coronary occlusion. Typical flows in the left anterior descending artery and vein were 30–60 mL/min. Following occlusion, the LAD was not visualized on the images, although the great cardiac vein was still apparent. In those animals that survived reperfusion, the LAD was again observed. Identification of the coronary structures was verified with a postmortem radiographic contrast study.
Conclusion: These initial studies suggest that PEG cine MR imaging using presaturation and velocity sensitization may provide a rapid and sensitive means for the noninvasive assessment of coronary artery anatomy and flow.
M. NessAiver is an employee of Picker International.

Monday Afternoon • Franciscan B
Papers 149–156

PULSE SEQUENCE I

MODERATORS: JR MacFall, PhD
MS Silver, PhD

149 • 3:45 PM

Slew Rate Reduction in 2D Pulse Design with Nonuniform K-Space Sampling

BS Hu, JM Pauly, GA Wright, DG Nishimura

Departments of Electrical Engineering and Medicine, Stanford University, Stanford, CA

Purpose: The design of multidimensional excitation pulses for localization of small volumes has been principally limited by the finite gradient slew rate. Time-bandwidth constraints restrict RF pulse duration to a few milliseconds, limiting the time for k-space coverage by the gradient. As the slew-rate constraint is dictated primarily by the exact k-space trajectory chosen, our aim is to examine alternative k-space trajectories that are more slew-rate efficient.

Methods: If the sampling trajectory is altered to nonuniformly emphasize the lower k-space frequencies, more of the gradient amplitude changes will occur at a lower absolute amplitude, leading to a reduced slew rate. This sampling leads to trade-offs in the aliasing structures of the resultant profile. As a prototype, we investigated k-space spirals with the general form $\theta \sim r^{\beta}$ in polar coordinates. β controls the nonuniformity in the k-space trajectory. Keeping the number of turns and the extent of k-space coverage constant, decreasing β significantly reduces the slew rate.

Results: A 2D selective Gaussian RF pulse with $\beta = 0.5$ reduces the required slew rate to 55% of the uniformly sampled pulse ($\beta = 1$). Experimentally, on a GE 1.5-T Signa imager (peak slew rate = 2 G/cm/msec), a 3-cm-diameter cylinder can be excited with a pulse duration of 5.12 msec. This represents a reduction in diameter of 40% from a similarly specified, but uniformly sampled, RF pulse of equal duration. Alternatively, very small volumes can be excited. A 7.5-mm-diameter cylinder can be selected in approximately 10 msec. Aliasing side lobes peaked at about 5% but did not greatly affect the overall quality of the image, as they are small and more uniformly smeared.

Conclusion: Nonuniform sampling can greatly reduce the slew-rate requirement of multidimensional pulses. The relaxed slew-rate requirement can be traded off for reduced volume selection or pulse duration. Experimental results agree well with theory.

150 • 3:57 PM

MT Measurement of T_{2r} with a Whole-Body System

J Hua, GC Hurst

Department of Radiology, MetroHealth Medical Center, Cleveland, OH

Purpose: T_{2r}, an important parameter in standard 2-pool models of magnetization transfer (MT), can be interpreted as an index of the degree of "rigidity" of the restricted pool. T_{2r} is difficult to measure directly, particularly for whole-body systems. An indirect measurement method using MT "z-spectra" has been demonstrated on a small-bore system (Grad and Bryant. J Magn Reson 1990; 90:1). The findings reported here follow our study of MT methods for whole-body systems.

Methods: Algebraic expressions were derived from Wu's analytic solution for steady-state magnetizations with MT (Wu. J Magn Reson 1991; 94:186). Since the similarity of CW and shaped, pulsed MT methods has been established, we used Gaussian-shaped MT pulses in the experiments. Boiled eggs and $MnCl_2$-doped water were used as samples, with observable T1 and T2 measured by using standard methods. The RF power was calibrated and system RF compressions were considered.

Results: A linear function was found to be $\Delta\omega^2 = A^*\omega_1^2 - 1/T_{2r}^2$, where $\Delta\omega$ represents offset frequency of a z-spectrum measured at a reasonable z value, ω_1 is the B_1 amplitude of MT excitation, and A is a constant. This is greatly different from expressions given by Grad and Bryant, and was well validated by findings using boiled egg white. Boiled egg white T_{2r}, obtained from the (negative) intercept of the function above, was found to be 151 μsec ± 3.

Conclusion: T_{2r} can be measured by an MT technique using a whole-body MR imaging system.

151 • 4:09 PM

Novel Technique for the Construction of 180° Refocusing RF Pulses

TP Roberts, ME Moseley, J Kucharczyk, TA Carpenter, LD Hall

Department of Radiology, University of California, San Francisco, CA

Purpose: The authors present a method for the construction of 180° refocusing pulses by the symmetrization of suitably optimized 90° excitation pulses. These 180° pulses have sharply band-selective properties and are applicable to a range of MR pulse sequences, such as fast spin-echo (FSE) and double spin-echo volume localization (PRESS). Because of its sharply selective frequency response, spatial definition is improved while spurious echoes arising from imperfect flip angles are minimized.

Methods: Any RF pulse that results in a 90° rotation can be used as the starting point for this technique. The authors chose to use a self-refocused pulse, which is asymmetric in time and causes a band-selective rotation of magnetization from the z axis to the y axis. If, however, it is applied to magnetization initially aligned along the y axis, it disperses the spin isochromats in the xz plane. If a second pulse is applied at this point, with a modulation envelope formed by the time reversal of the original pulse, isochromats within the selected band will be rotated from their position in the xz plane to align along the y axis. This result is derived by consideration of rotation operators.

Results: Band-selective refocusing pulses are generated from self-refocusing 90° excitation pulses. The peak RF level of the composite pulse is the same as that of each 90° pulse, if the overall duration of the 180° pulse is twice that of the original 90° subpulses. This facilitates pulse power calibration. The excitation bandwidth of such a 180° pulse is also equal to that of the original 90° pulses. Pulses were applied to the double spin-echo volume localization sequence to achieve sharp region-of-interest delineation and also to the fast spin-echo sequence to improve section definition.

Conclusion: A simple method for the construction of band-selective 180° refocusing pulses is proposed. Such pulses are applicable to a variety of pulse sequences for MR imaging and localized spectroscopy.

152 • 4:21 PM

Magnetization Transfer Contrast Imaging of Hepatic Neoplasms

MD Hollett, AM Aisen, HN Yeung, IR Francis, R Bree

Department of Radiology/MRI, University of Michigan Hospitals, Ann Arbor, MI

Purpose: A method of performing magnetization transfer contrast (MTC) by using a pulse sequence based on a series of on-resonance binomial pulses appended prior to a conventional spin-echo sequence has been recently described. We investigated the use of this technique in the detection and characterization of focal hepatic neoplasms on a 0.5-T imager.

Methods: SE imaging utilizing T1- and T2-weighted axial sections was performed in 17 patients with hepatic neoplasms, 14 with primary or metastatic hepatic malignant neoplasms, and 3 with hemangiomas. After the SE imaging, a T1-weighted MTC sequence was performed in 7 patients, and in the remaining 12 patients, a proton-density (PD) MTC sequence was performed. (Two patients underwent both sequences.)

Results: As expected, muscle showed the greatest signal drop (to 25% of control in the 12 patients with proton-density-weighted MTC), and fat the least. Liver and neoplasms behaved similarly (60%–70% signal loss). The average lesion-to-liver contrast ratios were as follows: For the group with T1-weighted images (n = 7), control was 0.87 ± 0.26 and the corresponding MTC images were 1.04 ± 0.23. For the group with PD-weighted images and nonhemangiomas (n = 9), control was 1.10 ± 0.16 and MTC was 1.23 ± 0.28. For the 3 patients with hemangiomas who had proton-weighted MTC, control was 1.21 ± 0.06 and MTC was 1.64 ± 0.70. There were no statistically significant differences between the MTC and control images.

Conclusion: In this series, MTC imaging using a binomial saturation pulse did not greatly improve contrast between malignant hepatic neoplasms and normal liver parenchyma and did not improve sensitivity for lesion detection.

153 • 4:33 PM

Contrast Optimization in Pulsed Magnetization Transfer Imaging

RW de Boer, H Kooijman, LH Hofland, M Beese
MR Clinical Science, Philips Medical Systems, Best, The Netherlands

Purpose: The image contrast due to magnetization transfer between mobile and restricted H-1 pools can be generated either by relatively long off-resonance RF irradiation or by short, intense RF pulses with zero effect on resonance (pulsed MTC). For pulsed MTC, a $90_x\ 90_{-x}\ 90_{-x}\ 90_x$ pulse with 0.5 msec duration of each of the elements has been used by others (Chan TW, Schneider E. SMRM book of abstracts, 1992; 327).

Methods: The authors investigated the effectiveness of a general $a_x\ a_{-x}\ a_{-x}\ a_x$ pulse independent of the pulse angle α and the pulse duration. Experiments were performed on a Philips Gyroscan T5 at 0.5 T by using both spin-echo and gradient-recalled-echo sequences.

Results: A value of the pulse angle α of 170° was optimal for this purpose. For this angle, the MTC is stronger, and unwanted direct saturation of the long T2 mobile H-1 pool is minimized. Numerical simulation showed that the frequency range over which the pulse has a zero effect on the long T2 species is increased from 200 Hz to over 800 Hz compared to α = 90°, whereas the magnetization of the short T2 pool is more effectively saturated (M_z equals 0.82 for α = 90° compared with M_z equals 0.49 for α = 170° for T2 = 0.01 msec).

Conclusion: In volunteer and patient studies, a contrast improvement and a marked increase of insensitivity to field inhomogeneities was achieved by using a pulse angle α = 170° instead of α = 90°.

R.W. de Boer is an employee of Philips Medical Systems.

154 • 4:45 PM

Evaluation of a CSF-nulled, Heavily T2-weighted Inversion-Recovery Technique in the Brain

WG Bradley, Jr, R Gullapalli, J Mano, NR Bucciarelli, SR Kapelov, WJ Mullin, DM Murakami
Memorial Magnetic Resonance Center, Long Beach Memorial Medical Center, Long Beach, CA

Purpose: At the 1992 SMRI meeting, Bydder et al introduced a CSF-nulled inversion recovery technique called prolonged inversion echo time inversion recovery (PIETIR). The technique utilized a TR of 6,000 msec and produced heavily T2-weighted images with black CSF. Although the technique was shown to detect lesions not seen on traditional T2-weighted spin-echo images, the acquisition times were excessive due to the TR of 6,000 msec. The purpose of this study was to modify the PIETIR sequence to shorten the acquisition time and to maintain the heavy T2 weighting for lesion detection.

Methods: By shortening the TR to 4,500 msec (keeping the TI at 2,000 msec and the TE at 160 msec), acquisition time is reduced by 25% and CSF is made to be isointense with brain. By using a 128 × 256 matrix over a rectangular FOV, reasonable spatial resolution in reasonable acquisition times (9.6 min) is achieved. Twenty patients with suspected CNS disease were imaged by using this technique, which was compared with routine spin-echo imaging (TR = 3000, TE = 30 and 80 msec) on a Picker 1.5 HPQ imager.

Results: Like the original technique of Bydder et al, the short PIETIR sequence provides more T2 weighting for the detection of parenchymal lesions without the problem of partial-volume artifact from high-intensity CSF at brain-CSF interfaces. Thus, it was particularly useful for the evaluation of subependymal lesions (MS, ischemia, or infection in AIDS), as well as the subtle cortical infarcts.

Conclusion: By utilizing a combination of shorter acquisition times, rectangular matrix, and rectangular FOV, a technique that is more sensitive to the presence of parenchymal disease than the traditional T2-weighted spin-echo sequence has been developed that provides images in clinically reasonable acquisition times.

This research was supported in part by a scientific grant from Picker International.

155 • 4:57 PM

MR Mammography: Improved Techniques for Imaging of Breast Implants

NR Bucciarelli, D Atkinson, LM Teresi, WJ Mullin, DM Murakami, SR Kapelov, S Roux, WG Bradley, Jr
Memorial Magnetic Resonance Center, Long Beach Memorial Medical Center, Long Beach, CA

Purpose: The inherent ability of MR imaging to image along arbitrary planes of section offers the potential for considerable improvement in imaging of patients with silicone breast implants. MR imaging is limited, however, by the necessary compromises of imaging time, spatial resolution, coverage, tissue contrast, minimization of artifact, and magnetic field (B_0 and B_1) inhomogeneities. To address these issues in a clinical setting, the authors tested 2 promising high-speed imaging methods.

Methods: The authors attempted to null either silicone or fat by using spectroscopic-selective saturation techniques and turbo STIR techniques on a standard Siemens 63SP with a dedicated bilateral breast coil. Off-resonance pulses, 150 Hz (for fat saturation) or 400 Hz (for silicone saturation), were added to a 3D FISP module. Ten volunteers and 15 patients with suspected implant ruptures were studied. To null fat, a modified turbo STIR technique was employed. An inversion pulse was inserted prior to the standard turbo SE sequence, offering good T1 contrast with a reduced acquisition time. Two echoes were acquired, offering a combination of proton-density and T2 weighting with fat or silicone nulling. To null fat, interleaved sequence parameters were: TR/TI/TE = 4,700/100/19-103, FOV = 300, matrix 128 × 256, 5-mm sections (0-mm gap). By selecting a slightly longer TI (400), silicone nulling was possible with the same technique. To view the breasts with higher spatial resolution, a faster 3D PSIF sequence (TR/TE of 17/7) was employed with a coronal acquisition to reduce cardiac motion artifact and produce voxel dimensions of 1 × 1.2 × 1.2 mm in less than 3 minutes.

Results: The fat-nulling was successful in demonstrating the presence of high-intensity silicone against a darkened background. Silicone envelope ruptures within the surgical capsule were seen as wavy or linear low-intensity structures ("linguini sign") within the silicone. Owing to their long T2, cysts were better appreciated on the second echo. Silicone nulling was useful in characterizing questionable areas, but bright fat produced more motion artifact. The 3D sequence proved useful in demonstrating irregular silicone envelope contours and small defects within the capsule. The MR techniques using spectral presaturation to null fat or silicone were limited by B_0 and B_1 nonuniformity.

Conclusion: Combined, these techniques have proved useful by demonstrating implant leakage in a number of clinical cases. Based on their experience, the authors believe that these techniques offer a promising, clinically robust method for imaging of breast implants.

156 • 5:09 PM

MR Mammography: Initial Clinical Experience in Imaging of Breast Implants

NR Bucciarelli, S Roux, D Atkinson, LM Teresi, DM Murakami, WJ Mullin, SR Kapelov, WG Bradley, Jr

Memorial Magnetic Resonance Center, Long Beach Memorial Medical Center, Long Beach, CA

Purpose: Conventional mammography is limited in patients with breast implants, as the high intensity of silicone obscures intracapsular ruptures and the surrounding breast parenchyma. A poor definition of envelope circumference and extent of leakage along the chest wall and axilla also presents problems. In this initial clinical study, we evaluated the role of MR imaging in the diagnostic workup of patients with known and suspected breast implant rupture.

Methods: A fast IR technique was employed with a dedicated bilateral breast coil on a conventional MR imager (Siemens 63SP). A modified turbo SE sequence incorporating a preparatory inversion pulse was used. This produced 2 fat-nulled echoes; TR/TI/TE = 4700/100/19 and 103, FOV = 300, 128 × 256 matrix, 5-mm sections, 0-mm gap. Silicone nulling was possible by using the same technique (TI = 400). A 3-minute volume PSIF sequence (TR/TE = 17/7) was employed coronally, producing a high-resolution study with voxel dimensions down to 1 × 1.2 × 1.2 mm. These techniques were tested in 5 asymptomatic volunteers and 25 patients with suspected implant rupture.

Results: Of the 30 patients studied, 22 demonstrated evidence of intracapsular or extracapsular rupture. Surgical follow-up has been obtained in 5 of the 22 patients thus far, with additional follow-up expected in the near future. From our experience, normally occurring radial folds in implants can be distinguished from intracapsular rupture by recognizing double- versus single-layered portions of envelope, respectively. In addition, chemical shift artifact adjacent to portions of the envelope suggests radial folds rather than rupture.

Conclusion: MR mammography is a novel technique for evaluating breast implants. Its ability to detect ruptures (especially those that are "silent") is extremely promising.

Monday Afternoon • Franciscan C
Papers 157–164

FLOW VELOCITY I

MODERATORS: C Dumoulin, PhD
DG Nishimura, PhD

157 • 3:45 PM

Quantification of the Coronary Flow with Time-of-Flight Echo-Planar Imaging in Normal and Stress Test Conditions

BP Poncelet, HL Kantor, RM Weisskoff, G Holmvang, MS Cohen, TJ Brady, VJ Wedeen

MGH-NMR Center, Massachusetts General Hospital, Charlestown, MA

Purpose: To validate an echo-planar imaging (EPI) time-of-flight technique for flow quantification of the left anterior descending (LAD) coronary artery in normal and "exercised" conditions.

Methods: The authors extended a time-of-flight (TOF) model described by Wehrli et al (1), to derive flow velocities from measured wash-in curves (2). Short-axis cardiac studies were performed with a gated, flow-compensated, gradient-echo (GRE) EPI pulse sequence (retrofitted Signa 1.5 T-ANMR, TE = 29 msec, 1.5 × 3 × 5–10 mm, surface coil, fat suppression). A series of 20 GRE EPI images were collected, each acquired at the same cardiac delay within a breath hold. A 3-cm presaturating slab was applied, with the saturation delay progressively incremented at successive heartbeats. Three reference images were collected without presaturation within each series.

Results: Flow velocity was measured in the proximal portion of the LAD coronary artery in 11 healthy volunteers (age range, 25–45 years). The sensitivity to detect cyclic velocity changes was tested at rest and in stress test conditions. Reproducible data were obtained that showed the characteristic LAD phasic flow pattern (Vmax = 6 cm/sec ± 5 in systole and 26 cm/sec ± 3 in diastole). In 9 subjects, a mean velocity change of 42% ± 12 was seen, when performing an isometric leg/hand exercise, in agreement with expected flow change for this mild stress test.

Conclusion: When combined with EPI, TOF flow quantification can measure coronary flow velocity.

1. Wehrli et al, Radiology 1986; 160:781–785. 2. Poncelet et al, SMRM proceedings 1992, 604.

158 • 3:57 PM

Phase-Contrast Fast Spin-Echo Imaging

RS Hinks, MA Bernstein

GE Medical Systems, Milwaukee, WI

Phase-contrast (PC) MR angiography is well known as a method of sensitizing the MR signal to flowing material based on MR signal phase shifts (1,2). Conventional PC MR angiography involves the use of gradient-recalled echoes, low flip angles, and short TRs. In a typical PC MR angiography sequence, at least 2 examinations are performed that are identical except for a difference in their gradient first moments. Since the gradient first moment is a velocity sensitizing moment, flowing spins experience different phase shifts in the 2 experiments and may be displayed by subtracting out signal from static spins, which have identical signal on the 2 experiments. In the present investigation, the principles of PC MR angiography have been applied to the fast spin echo (FSE) sequence to sensitize it to flowing spins. The key to properly encoding spins for flow in FSE is that the first moments must be set up to keep the stimulated echo and primary echoes in phase at all echoes. This is done by nulling the first moment at least at the RF pulses and serves to maintain signal coherence throughout the echo train. In the first of at least 2 experiments, the gradient pulses are designed so that the first moment has some value N at each echo, while in the second of 2 experiments the first moment has some different value M at each echo. In both experiments, the static material has the same phase, while the phase from flowing material changes due to the difference in first moments. Subtraction of the echo signals from the 2 experiments gives cancellation of the signal from static material, resulting in an image that represents the flowing material. The signal processing methods used for conventional PC MR angiography are applicable to the present method. PC FSE has been evaluated with both phantom and volunteer studies.

1. Dumoulin CL, Souza SP, Walker MF, Wagle W. Three dimensional phase contrast angiography. Magn Reson Med 1989, 9:139–149. 2. Pelc NJ, Bernstein MA, Shimakawa A, Glover GH. Encoding strategies for three-direction phase-contrast MR imaging of flow. JMRI 1991, 1:405–413. 3. Hinks RS. Flow compensation in fast spin echo imaging.

159 • 4:09 PM

Flow Measurements with Dynamic Gd-DTPA–enhanced MR Imaging

RJ Massoth, AA Tzika, RS Dunn, WS Ball, S Majumdar
Department of Radiology/Medical Physics Division, University of Cincinnati, Cincinnati, OH

Purpose: To develop and validate flow and volume measurements with dynamic, Gd-DTPA–enhanced MR imaging for assessing brain hemodynamics in pediatric patients.

Methods: Dynamic T2*-weighted MR imaging with spoiled gradient echo (TR msec/TE msec/flip angle = 24/15/10°, 256 × 128 matrix, NEX = 0.75, FOV = 26 cm, 10-mm sections, 2.5 sec/image) during intravenous bolus injection of Gd-DTPA (0.1 mmol/kg) was performed on a 1.5-T GE Signa. Laminar flow phantoms were used to validate relative cerebral blood volume (rCBV), relative cerebral blood flow (rCBF), and mean transit time (MTT) calculations over physiologic ranges. Calculations include moment analysis (MTT), numerical integration (rCBV) of concentration-time curves for $\Delta R2^*$ ($R2^* = 1/T2^*$), Stewart's equation to calculate MTT (cMTT) for phantoms, and MR estimated flow (Gd-DTPA quantity injected/rCBV).

Results: Measured voxel size was 1.2 × 1.2 × 10.5 mm, corresponding to 0.015 mL/voxel. Flow measurements of 500–1000 mL/min, encompassed physiologic flow rates for brain. The ratio of measured flow to MR estimated flow was $(1.55 \pm 0.29) \times 10^6$. Thus, cortical gray matter rCBV = 36.6 mL ± 13.8 and white matter rCBV = 15.4 mL ± 6.3 for 52-voxel ROIs ($n = 20$); flow (CBV/MTT) was 325.1 and 137.0 mL/min, respectively, for the same brain regions.

Conclusion: Corrected flow measurements and hemodynamic parameters were performed in a clinical setting. Their significance must be addressed in patient populations. Faster imaging techniques will facilitate independent measurement of arterial input functions, thereby improving accuracy.

160 • 4:21 PM

Cerebrospinal Fluid Flow Quantification: Comparison of Three Measurement Methods

WJ Mullin, D Atkinson, R Hashemi, J Yu, WG Bradley, Jr
Memorial Magnetic Resonance Center, Long Beach Memorial Medical Center, Long Beach, CA

Purpose: MR imaging of cerebrospinal fluid (CSF) flow abnormalities has been shown to be an effective clinical tool for the diagnosis of different hydrocephalic conditions. Current methods for assessment of flow have largely relied on phase-contrast methods to demonstrate the effect of CSF pulsations. To the authors' knowledge, the corroboration with external standards (ie, pulsatile flow phantoms) has never been done. In this study, they created a physiologic pulsatile CSF flow phantom and used it to verify the MR imaging methods.

Method: Our flow phantom consisted of a small animal ventilator (Harvard pump) system, with pulsatile flow generated from an oscillating piston/cylinder arrangement through 3-mm inside diameter polyethylene tubing simulating the cerebral aqueduct. The range of stroke volumes tested varied from 1.0 to 50.0 μL. Simultaneous in-line measurements of average volumetric flow were obtained with a transit time US flow meter (Transonic Systems, Ithaca, NY). The mean diastolic and systolic velocities were calculated by dividing the average volumetric flow by the cross-sectional area and ranged from ± 0.5 to 23 mm/sec. With a phase sensitive MR sequence, the authors acquired a series of measurements over the entire "cardiac" cycle. To avoid problems of missing data from the late-diastolic flow period, they used retrospective cardiac gating to acquire data over the entire cycle. The spatial resolution in this study was 0.32 × 0.32 mm, with axial section thicknesses ranging from 2 to 4 mm and aliasing velocities ranging from 20 to 40 mm/sec.

Results: Excellent correlation was found between measurements from the piston/cylinder method and the flow probe. Similarly, there was an excellent corroboration between the MR method and the other two techniques over this physiologic range of velocities.

Conclusion: Given the correlation between these measurement techniques, true clinical quantitative measurements of CSF flow are possible. On the basis of these data and qualitative studies to date, the inclusion of a clinical quantitative method may have a significant impact on the management of patients with hydrocephalus and other CSF flow abnormalities.

161 • 4:33 PM

Phase-Contrast Cine MR Imaging Determination of Renal Blood Flow in the Transplanted Kidney

FG Sommer, KCP Li, N Pelc, B Myers, R Jamison,
E Pagtalunan, L Newton, C McDonnell
Department of Radiology, Stanford University Medical Center, Stanford, CA

Purpose: To evaluate the ability of a technique of cine phase-contrast (PC) MR imaging to measure blood flow in normally functioning renal allografts.

Methods: Seventeen patients with renal allografts, for which no rejection episodes had ever occurred, had renal blood flow measured with a technique of PAH clearance, followed by a determination of renal blood flow with a cine PC technique the same day. MR imaging was performed on a 1.5-T system; preliminary GRASS images in sagittal and axial planes were employed to define acquisition planes perpendicular to the transplant veins in which flow was measured. Electrocardiogram gating, respiratory compensation, TR = 25, TE = 12, 4-mm section thickness, and maximum flow-encoding velocity of 50 cm/sec were employed in the cine PC acquisition. A total of 4 studies were deemed unsatisfactory due to technical factors or patient claustrophobia.

Results: Comparison of renal blood flow values for the 13 transplants successfully evaluated with the 2 techniques showed a high degree of correlation ($r = .92$, $P < .001$).

Conclusion: It appears possible to measure blood flow in renal transplant veins with quite a high degree of accuracy by using cine PC MR imaging. This technique may prove useful to evaluate complications, such as rejection, affecting blood flow in renal transplants.

162 • 4:45 PM

Segmented K-Space Velocity Mapping Sequence for Quantification of Renal Artery Blood Flow during Breath Holding

C Thomsen, M Cortsen, L Søndergaard, F Ståhlberg, O Henriksen

Danish Research Center for MR, Hvidovre Hospital, Hvidovre, Denmark

Purpose: MR measurements of renal artery flow are hampered by the necessity for double-oblique imaging, the occurrence of artifacts due to pulsatile blood flow and respiratory motion, and the possibility for occurrence of complex flow patterns. Recently, velocity mapping techniques have been used together with retrospective gating to study renal artery flow in tilted imaging planes (1,2). To reduce the effects of respiratory motion and complex flow patterns, the authors designed an electrocardiogram (ECG)-triggered velocity mapping sequence with short velocity-encoding gradient duration to be executed during breath holding, by using a segmented k-space signal sampling technique (1). The sequence was tested in vivo in a healthy volunteer.

Method: A 1.5-T MR imaging unit (Siemens SP63/84) was used throughout the study. Velocity mapping was performed by using two gradient-echo sequences. To achieve velocity sensitivity with minimum encoding of higher-order-motion terms, the flow-encoding gradient duration was minimized by using sequences with reversed gradient polarity (3). K space was segmented with 16 phase-encoding steps per cardiac cycle repeated with a 10-msec time interval, giving an acquisition window of 160 msec in every heartbeat. Fourier lines encoding low spatial frequencies were concentrated to create a narrow effective time window. The total acquisition time was 16 heart cycles, and temporal resolution was obtained by repeated execution with different trigger delays.

Results: With a TE of 6 msec, the flow-encoding gradient duration was 1.5 msec giving a velocity sensitivity of 3.9 R/m/sec and a sensitivity to second-order motion of 0.001 R/m/sec^2. In an initial healthy volunteer, peak flow in the right renal artery was 1.3 L/min, giving an average-minute volume of 450 mL/min.

Conclusion: The proposed sequence was successfully executed both in phantoms and in vivo. The flow values obtained in the volunteer are in agreement with literature values obtained by using invasive techniques. The authors conclude that ECG-gated MR velocity mapping with breath holding can be used for accurate determination of renal artery flow.

1. Edelman R, et al, Radiology 1990; 177:515–521. 2. Lundin B, et al, Lancet 1992; 339:373. 3. Thomsen C, et al, Proc of Soc Magn Reson Med 1992; 2,924.

163 • 4:57 PM

Rapid Measurement of Renal Blood Flow by Using Breath-Hold Cine MR Imaging with Phase-encoding Grouping

LG Wilbert, JR Kowal, WA Erdman, RM Peshock, HF Li, M NessAiver, GD Clarke

Mary Nell and Ralph B. Rogers Magnetic Resonance Center, UT Southwestern Medical Center, Dallas, TX

Purpose: Measurement of renal blood flow (RBF) can be important in evaluating patients with renal disease. MR imaging with flow encoding typically requires acquisitions lasting several minutes and can be degraded by motion artifacts. Phase-encoding grouping (PEG) substantially reduces the time required for flow measurements. Thus, the authors examined the accuracy and reproducibility of rapid, breath-hold PEG MR imaging to measure flow in phantom models and in the renal arteries of healthy volunteers.

Methods: High-resolution PEG flow studies were acquired on a Picker International 1.5-T HPQ system with a single axis gradient inset. Voxel size was 1 × 1 × 10 mm with an acquisition time of 25–40 seconds for 6–12 frames per cardiac cycle. Phantom studies used a pulsatile flow pump triggered by a simulated cardiac waveform. In human studies, flow was measured in the proximal portion of both renal arteries and in the lumbar aorta above and below the renal artery origins. Total renal artery flow was compared with the difference in aortic flow.

Results: There was excellent agreement between MR imaging assessment of pulsatile flow and timed volume measurements ($r = .99$) and ultrasonic measures of velocity in the phantom. In human studies, the mean RBF for 6 measurements was 978 mL/min ± 141. There was good agreement between the total RBF and the difference in aortic flow. Interobserver variability was small with a mean percentage difference of 15%.

Conclusion: Studies in phantoms and healthy volunteers indicate that breath-hold velocity-sensitized MR imaging with phase-encoding grouping can be used to obtain rapid, reproducible measurements of renal blood flow.

M. NessAiver is an employee of Picker International.

164 • 5:09 PM

Quantitative Comparison of MR Velocity Measurements with Bolus Tracking versus Phase Technique: Studies in a Pulsatile Flow Phantom and in Humans

D Chien

UCSF Department of Radiology, VA Medical Center, San Francisco, CA

Purpose: The goal of this project is to compare the accuracy of bolus tracking versus phase-contrast technique for flow quantification.

Methods: Comparison was done in a pulsatile flow phantom and in humans by using a 1.5-T Siemens whole-body system. The authors have a phantom model with known pulsatile velocity waveforms determined with a laser Doppler velocimeter (1). The two techniques were optimized separately prior to doing the quantitative comparison. Triggered bolus track images were acquired with a flow-compensated gradient-echo sequence (60/80). With the phase technique, the phase shifts were obtained by subtracting pairs of triggered phase images acquired with a flow-sensitive and a flow-compensated sequence. Velocity measurements in humans were performed at the carotid arteries with electrocardiogram triggering.

Results: The velocities measured by the 2 approaches were in close agreement with each other and with the laser Doppler values (< 2% deviation). The accuracy of each technique depended on specific sequence parameters including the choice of delay time between the flow tag and

data readout in bolus tracking and the choice of velocity sensitivity in phase acquisitions.
Conclusion: While both techniques can be optimized to give accurate flow quantification, our study demonstrated the link between measurement accuracy and the proper choice of specific sequence parameters in each of the 2 approaches studied.

1. Selby K, Saloner D, Anderson C, Chien D, Lee R. SMRM proceedings 1992, 2903.

Monday Afternoon • Plaza A
Papers 165–172

ANGIOGRAPHY TECHNIQUES I

MODERATORS: JA Arrington, MD
M Cohen, PhD

165 • 3:45 PM

Volume Dynamic MR Angiography Studies of the Heart, Great Vessels, and Lungs

PM Margosian, M NessAiver
Picker International, Inc, Highland Heights, OH

Purpose: The goal was to make volume dynamic images of the heart, great vessels, and lungs, by using gated acquisitions with phase encode grouping (PEG), a raw data segmentation technique, and volume projection techniques to derive the desired 3D views, and to do it in a reasonable time.
Methods: Numerous gated studies were done with a Picker HPQ imager equipped with software to support PEG acquisitions and cine maximum-intensity projections (MIP). Most cardiac acquisitions were obtained in volunteers as a series of 12–20 contiguous coronal sections, each 3–4 mm thick, typically starting just in front of the aorta and progressing in the posterior direction. Cine MIP projections provided the desired volume viewing of the blood flow dynamics. Volume studies of the great vessels were typically parasagittal, while examinations of the lungs were done at a variety of orientations, normally just grazing the heart.
Results: A number of cine MIP views of heart, lungs, and great vessels were obtained that demonstrated the capability of providing dynamic volume appreciation of major flow patterns in these areas.
Conclusion: Volume dynamic views (cine loops) of up to 8 frames can be acquired in 15–20 minutes for heart, lungs, and great vessels by means of a series of 10–20 sequential 2D gated PEG measurements. One outcome is the ability to show a contraction wave passing over the surface of the heart or of the aorta. A test of clinical efficacy is planned.
P.M. Margosian is an employee of Picker International.

166 • 3:57 PM

High-Resolution MR Angiography: Use of Magnetization Transfer Contrast and Static Reprojection Data Processing Technique

AN Shetty, AM Wang, J Taft, DP Wesolowski, R Manjakuppam, J Farah
William Beaumont Hospital, Royal Oak, MI

Purpose: To describe improved techniques of acquiring and processing MR data for providing high resolution images of intracranial and extracranial vessels.
Methods: The conventional time-of-flight technique relies on inflow of unmagnetized spins in a selected slab and a good background suppression. The predominant relaxation is cross-relaxation between free and bound water. The presence of macromolecules in tissues provides an efficient means of cross-relaxation for producing high background signal intensity. Thus, by using magnetization transfer contrast (MTC) technique, the cross-relaxation contribution is reduced and the contrast in a tissue may be manipulated. Traditionally, a standard discrete Fourier transform (DFT) is used in which some of the information is lost. The authors have instead used a static reprojection algorithm (SRA), which is a non-Fourier method of reconstruction to provide MR images. The k-space data is used without data padding, interpolation, or any original modeling techniques, such as maximum entropy spectral estimation. Instead, it employs techniques derived from multidimensional system theory to project the raw data into a space of inherently greater density (in the functional analytic sense) than the DFT can. Thus, the SRA is capable of resolving finer details than the DFT method can, without generating any artifacts.
Results: Intracranial and extracranial vessels were studied in 6 volunteers and 2 patients to determine the improvements caused by the MTC together with the new processing algorithm.
Conclusion: The vessel resolution and lumen definition are far improved when the MTC technique used in conjunction with the new processing method.

167 • 4:09 PM

Cardiac-Phase–specific Study of Poststenotic Signal Loss

K Selby, D Saloner, CM Anderson
Radiology Services, VA Medical Center, San Francisco, CA

Purpose: MR angiograms are known to overestimate the degree and extent of stenotic lesions. This is due to intravoxel phase dispersion in the highly disturbed poststenotic flow. By acquiring MR data during that phase of the cardiac cycle when flow disturbance is least severe, poststenotic signal loss should be minimized. The authors have used cardiac-phase–specific data acquisition to study the behavior of poststenotic signal loss as a function of cardiac phase.
Methods: Pulsatile flow was generated through a 6-mm-diameter tube containing a 2-mm-diameter "stenosis" of 6-mm length. Cardiac-phase selective prospective gating was used to acquire MR angiograms of 2-mm in-plane sections. For the low-frequency phase-encoding lines, data was acquired only within a controlled time window corresponding to a chosen portion of the pulsatility cycle. During the remainder of the cycle, phase-encoding steps were not advanced and echoes were discarded. The high-frequency lines were acquired continuously throughout the pulsatility cycle. By varying the position of the time window, images corresponding to all phases of the pulsatility cycle were acquired.
Results: Poststenotic signal loss was greatest when data were acquired during peak systole and was minimized for diastolic acquisition.
Conclusion: Poststenotic signal loss is decreased by acquiring the low-frequency image lines in diastole. This technique may improve the assessment of in vivo stenoses.

168 • 4:21 PM

Improved MR Angiography of Pulsatile Blood Flow with Gated, Segmented Acquisition

JP Finn, JR Moore, RR Edelman
Department of Radiology, New England Deaconess Hospital, Boston, MA

Purpose: Flow velocity in arteries varies greatly during the cardiac cycle. Flow enhancement and the tendency toward turbulence are therefore periodic and can be maximized or minimized by gating appropriately. The purpose of the present study was to develop techniques for single-phase and multiphase gated arteriography in the body by using k-space segmentation and reordering.

Methods: The authors implemented a flow-compensated, 2D, RF-spoiled FLASH sequence with segmented interleaved data acquisition. Eight to 24 lines per segment were acquired depending on the heart rate and the desired number of phases per acquisition. The flip angle was typically 50°, and a prepulse was employed to suppress stationary background signal. The time per Ky line was 32 msec and TE was fixed at 10 msec. Gated, breath-hold images were acquired of the aorta, renal, visceral, and iliac arteries in healthy subjects and in 7 patients with atherosclerotic disease. The vascular contrast-to-noise ratio (C/N) of gated images was compared with that of ungated images with similar voxel sizes and sequence parameters.

Results: With 16 lines per segment or more, 192 × 256 matrix images were acquired within a comfortable breath hold. Consistently higher vascular C/N was obtained with the segmented sequences than with the nonsegmented ones. For the aorta and renal arteries, C/N values were increased by a factor ranging from 1.4 to 3.2. Multiphase acquisition showed marked variation in arterial signal intensity during the cardiac cycle, and typically 1 of 3 frames showed no flow contrast in the vessel.

Conclusion: Gated, breath-hold angiography consistently improves arterial flow enhancement. Further studies are required to define its clinical performance.

169 • 4:33 PM

Coronary Artery MR Angiography with a Prototype Whole-Body Echo-Planar Imaging System

RR Edelman, P Wielopolski, L Simonetti, W Li, F Schmitt
Department of Radiology, Beth Israel Hospital, Boston, MA

Purpose: The feasibility of depicting the coronary arteries by using a TurboFLASH method with k-space segmentation was recently shown, but with limited spatial and temporal resolution. The authors hypothesized that the approach could be improved with an MR imaging system with enhanced gradient capabilities.

Methods: Imaging was performed on a 1.5-T prototype whole-body echo-planar system (Siemens Medical Systems, Iselin, NJ). Two versions of the segmented TurboFLASH sequence were compared: (1) a conventional version with 10 mT/m gradients switched in 1 msec, TR/TE = 13/8, and first-order flow compensation, 8 lines per segment for a segment duration of 104 msec, minimum FOV of 20 cm; and (2) an accelerated version with TR/TE = 3.5/1.5, 14 lines per segment for a segment duration of 49 msec, minimum FOV of 13 cm. Signal-to-noise ratio was enhanced by using a planar quadrature surface coil.

Results: By using the accelerated sequence, temporal resolution was improved by about a factor of 2 compared with the conventional version, giving less blurring of coronary arteries in healthy volunteers; moreover, breath-hold time was reduced nearly twofold. At the TE of 1.5 msec, flow compensation was not required. The short TE eliminated magnetic susceptibility artifacts at the heart-lung interface and improved depiction of pulmonary vessels.

Conclusion: The use of a whole-body echo-planar system with enhanced gradient capabilities improves image quality and temporal and spatial resolution for MR angiography of the coronary arteries.

170 • 4:45 PM

Temporary Variable TR/Excitation Flip Angle 3D Time-of-Flight MR Angiography of the Intracranial Vasculature

JA Tkach, W Lin, EM Haacke, TJ Masaryk, JD Dillinger
Cleveland Clinic Foundation, Cleveland, OH

Purpose: The objective of this study was to investigate the efficacy of the use of temporal modulation of TR and flip angle (α) to minimize blood signal saturation in 3D time-of-flight (TOF) MR angiography of the intracranial vasculature.

Methods: All studies were performed on a Siemens 1.5-T SP system by using a circularly polarized transmit-receive head coil. A high-resolution, short FE/TE, velocity compensated, RF spoiled 3D ROAST sequence served as the template. TR and α remained constant in the control. Reverse centric section-select phase encoding (k_z) was employed. A frequency selective fat saturation pulse and an off-resonance magnetization transfer saturation pulse were applied to reduce background signal. TR and α either remained constant or were temporally varied independently or together within the k_z loop. Total acquisition time was held constant, equal to that of the control. The control and modified techniques were tested in 5 healthy volunteers. The base images and associated maximum-intensity projections were compared.

Results: The control MR angiograms showed the greatest amount of blood saturation. The conspicuity and continuity of the small vessels were appreciably improved when TR was increased with decreasing k_z. The reduction of α with decreasing k_z provided similar but less marked improvements. The highest quality MR angiograms were obtained when these 2 schemes were implemented simultaneously.

Conclusion: 3D TOF MR angiographic techniques incorporating temporal modulation of TR and α within the section-select loop are effective in reducing the amount of blood saturation. The associated MR angiograms of the intracranial vasculature exhibit a marked increase in small vessel information.

171 • 4:57 PM

Improvements in 3D Time-of-Flight MR Angiography of the Renal Arteries

PA Hardy, JA Tkach, GK Lammert, MG Zelch
Cleveland Clinic Foundation, Cleveland, OH

Purpose: In MR angiography, contrast between flowing blood and stationary surrounding tissue should be improved by acquiring the data with minimum signal from the background tissue at low spatial frequencies and maximum signal from the flowing blood at high spatial frequencies. A 3D time-of-flight MR angiographic sequence was developed to test this hypothesis.

Methods: The sequence was developed on a 1.5-T Siemens SP63 whole-body imager. The sequence permitted arbitrary variation of the order of acquiring the partition (k_z) phase-encode lines and the excitation flip angles (α_n). A flow phantom and healthy volunteer subjects were used to test 3 phase-encode acquisition schemes: normal ($-k_z$ increasing to $+k_z$ monotonically); centric ($k_z = 0$ proceeding alternately to $+k_z$ and $-k_z$); and reverse centric ($+k_z$ and $-k_z$ proceeding to $k_z = 0$). For each phase-encoding scheme, different methods of altering the excitation flip angles were tested. Measurement of contrast between the flowing and stationary materials was used to evaluate the resulting MR angiograms.

Results: In the flow phantom, the contrast was increased by a factor of 3 over that of standard FISP 3D MR angiograms by using the flip angle strategy $\sin(\alpha_{n+1}) = \tan(\alpha_n)$ combined with centric phase-encode reordering. In volunteers, the increase was smaller perhaps due to the pulsa-

tility of the flow, producing signal loss subsequent to intravoxel dephasing.
Conclusion: Improved contrast on renal artery MR angiograms can be obtained by strategically manipulating the k_z phase encode and excitation flip angle scheme to alter the distribution of signal in k_z space.

172 • 5:09 PM

Analysis and Display of Renal Perfusion and Vasculature

NS Negin, RS Mezrich, LM Brand-Abend
Laurie Imaging Center, New Brunswick, NJ

Purpose: MR renal perfusion studies provide information on flow to the kidneys. MR renal angiograms allow the visualization of stenosis. Diminished perfusion and renal arterial stenosis are indications of renal vascular hypertension. The authors intend to image the structure and function of the renal arteries to provide a diagnosis of renal vascular hypertension.
Methods: MR angiography was performed on a GE Signa 1.5-T magnet with a thoracic/lumbar coil. Perfusion images were acquired during gadolinium injection. Prior to renal angiography, velocity encoding checks were performed that helped determine optimal velocity for maximum signal from renal arteries. Velocity checks minimally vary from 40 to 60 cm/sec. Then a 2D phase-contrast angiogram was obtained with the following parameters: 45° flip angle, TR = 40 msec, 2 NEX, and a 256 × 128 matrix. A final image that again measured uptake of gadolinium was obtained. Phase-contrast images were reconstructed and viewed on a 3D-rendering machine. Perfusion images were analyzed with custom software. Regions of interest were assigned, and an intensity profile plot versus time was generated.
Results: Successful MR angiograms have allowed visualization of proximal renal arteries. Completed perfusion studies provide information for objective measurement of renal function. These results are correlated with those of arteriography and nuclear medicine studies.
Conclusion: Analysis of renal arteries through MR angiography and perfusion studies allows a comprehensive view of renal structure and function. For renal vascular hypertension, this is useful in obtaining a pre- and postoperative renal survey.

Monday Afternoon • Plaza B
Papers 173–180

MUSCULOSKELETAL I

MODERATORS: JV Crues, III, MD
R Kier, MD

173 • 3:45 PM

MR Imaging Assessment of Abnormalities of Articular Cartilage in the Knee: A Blinded and Unblinded Analysis of Available Techniques

MP Recht, J Kramer, S Marcelis, M Pathria, D Trudell, P Haghighi, DJ Sartoris, D Resnick
Cleveland Clinic Foundation, Cleveland, OH

Purpose: In an attempt to improve the detection of chondral abnormalities by using MR imaging, a fat-suppressed (FS) 3D SPGR sequence was optimized and then compared with 5 other pulse sequences in the assessment of naturally occurring cartilage abnormalities of the patellofemoral compartment of the knee.
Methods: Optimization of the FS SPGR sequence was performed by using 5 cadaveric knees. The optimized sequence was then performed in 5 additional knee specimens. The following sequences were also obtained in all 10 cadaveric knees: T1-weighted SE (TR msec/TE msec = 500/14), multiecho T2-weighted SE (2,000/20, 70), a 3D GRASS (40/10, 30° flip angle), and 3D SPGR (40/5, 30° flip angle). Imaging was conducted at 1.5 T. After imaging, the specimens were sectioned and inspected for the presence of chondral lesions. For each of the sequences, representative MR images were evaluated by 1 of the authors who was blinded to the macroscopic findings.
Results: Cartilage appeared as a high-signal-intensity structure compared with fluid and bone marrow on the FS SPGR sequences. In addition, normal articular cartilage consistently demonstrated a trilaminar structure. Regions of cartilage fibrillation or focal loss of thickness demonstrated loss of at least the superficial layer of this trilaminar appearance. The sensitivity, specificity, and accuracy of the FS SPGR sequence in the blinded evaluation of the MR images were 96%, 95%, and 95%, respectively, which were significantly better ($P < .02$) than the other tested sequences.
Conclusion: The FS SPGR sequence performed significantly better in the depiction of chondral lesions than any of the other 5 tested sequences. Although the histologic correlation of the trilaminar appearance of cartilage is uncertain, its presence or absence may prove to be a reliable indicator of early cartilage abnormalities.

174 • 3:57 PM

Patterns of Tarsal Ossification in the Pediatric Foot

AM Hubbard, JS Meyer, S Mahboubi, MP Harty
Children's Hospital of Philadelphia, Philadelphia, PA

Purpose: The bones of the foot are partially ossified at birth. Assumptions about the position of the tarsals that can affect surgical treatment of foot deformities are made from the position of ossification centers on radiographs. This study evaluated the normal patterns of ossification in individual tarsals.
Methods: A retrospective review of pedal MR imaging studies was done in 42 children aged 3 months to 6 years (mean, 2.5 years). The calcaneus, talus, cuboid, and navicular were defined on 3–4-mm-thick sagittal and axial T1-weighted images. The location of the centers of ossification within the cartilaginous anlage were recorded, and the axes of those centers were compared with the axes of the anlage.
Results: Ossification of the talus begins in the neck, progressing anteriorly and posteriorly, the posterior aspect ossifying last. The long axis of the ossified segment differed by 5°–15° from the cartilaginous axis. Ossification of the calcaneus begins at the junction of the anterior and middle thirds of the anlage, the posterior aspect ossifying last. The long axes of the ossified segment and anlage were the same. Ossification of the navicular begins in the middle or lateral third of the cartilaginous anlage on axial images and centrally on sagittal images. The cuboid ossifies concentrically from its cartilaginous center.
Conclusion: Ossification centers of all tarsals do not develop centrally in the cartilaginous anlage, and knowledge of these patterns may affect the treatment of the incompletely ossified foot.

175 • 4:09 PM

Can Quantitative MR Imaging Help Diagnose Osteoporosis?

FW Wehrli, JC Ford, JG Haddad, M Attie, FS Kaplan
Department of Radiology, University of Pennsylvania Medical Center, Philadelphia, PA

Purpose: Current methodology for diagnosing osteoporosis includes bone densitometry and US. This work reports the results of a study to evaluate the effectiveness of quan-

titative MR imaging for the differentiation of healthy volunteers from patients with osteoporosis based on a procedure developed by the authors.
Methods: Sixty-three women (48 healthy and 17 with osteoporosis) were subjected to a protocol from which lumbar vertebral bone marrow T2* was measured as a figure of merit of trabecular plate density. Patients with osteoporosis are characterized as having abnormally low bone mineral density and/or spinal compression fractures. T2* was measured by fitting the region of interest decay curve sampled at successive maxima of the fat-water interferogram (1,2) assuming exponential decay. Means and standard deviations were computed for the 2 populations after correcting for age-related changes in T2* derived from the behavior found for healthy volunteers. Fractures were determined on the basis of midline sagittal images of the thoracic spine.
Results: Patients with osteoporosis had higher mean T2* measured for L-5 than did the healthy volunteers: (mean ± SE) 20.8 msec ± 1.3 versus 16.2 msec ± 0.7 (P = .002). When computed as an average from L-1 to L-5, discrimination was improved: 22.5 msec ± 1.7 versus 16.8 msec ± 0.5 (P = .0001).
Conclusion: Compared with the preliminary work on a smaller sample (1) performed in a more complex protocol involving full interferogram analysis, the new study provides improved statistical significance. Quantitative MR imaging may prove to be an alternative to bone densitometry provided (*a*) it can be shown to be a better predictor of fracture risk and (*b*) the procedure cost can be lowered.
1. Wehrli FW, Ford JC, Attie M, Kressel HY, Kaplan FS. Radiology 1991; 179:615–621. 2. Ford JC, Wehrli FW. JMRI 1992; 2(P):103.

176 • 4:21 PM

MR Imaging in the Diagnosis of Morton Neuroma: Use of Gadolinium and Fat Suppression

MR Terk, PK Kwong, B Horvath, PM Colletti
Department of Radiology, USC School of Medicine, Los Angeles, CA

Purpose: To evaluate the use of contrast-enhanced, fat-suppressed MR imaging in suspected Morton neuroma.
Methods: Twenty-one patients with suspected Morton neuroma were studied. All underwent close clinical follow-up with subsequent surgery, with pathologic correlation in 10 cases. Patients were selected for surgery by demonstration of a discrete mass on MR images. T1-weighted images (short TR/TE) before and after the administration of Gd-DTPA, multiecho sequences (long TR/short TE; long TR/TE), T1-weighted fat-suppressed images before and after administration of contrast agent, and T2-weighted fat-suppressed images were evaluated in this study. The fat-suppression technique employed was selective presaturation with inversion recovery (SPIR), a technique employing chemically selective inversion pulses (Philips S15/ACS).
Results: Morton neuromas were best seen on the T1-weighted SPIR images after administration of Gd-DTPA. All 10 surgical specimens corresponded closely with the MR images. In no case was surgery undertaken in the absence of MR findings, precluding evaluation of false-negative results. Nonenhanced T2-weighted SPIR images provided almost equal conspicuity. Enhancement was not sufficiently intense to be useful with T1-weighted non-fat-suppressed sequences. Only the larger neuromas could be seen on nonenhanced T1-weighted images. Improved conspicuity with the combination of fat suppression and gadolinium was noted in all cases. T2 weighting without fat suppression was the least successful technique in demonstrating these lesions.
Conclusion: The use of T1-SPIR imaging in the axial plane combined with the administration of Gd-DTPA allowed for correct prediction of Morton neuroma and its anatomic depiction in 100% of cases examined.

177 • 4:33 PM

Dynamic Studies of the Temporomandibular Joint with Subsecond GRASS MR Imaging

JM Tyszka, PM Colletti, N Suminski
Imaging Science Center, University of Southern California, Los Angeles, CA

Purpose: MR imaging with surface coils has become the preferred modality for imaging of the temporomandibular joint (TMJ) (1,2). The acquisition of "dynamic" images of the TMJ during articulation has commonly relied on the use of a mechanical device to articulate the jaw (3,4). The use of such devices can be uncomfortable for the patient and is less convenient than a "free" study, in which the jaw is articulated without assistance. The authors' purpose was therefore to test subsecond imaging techniques in free TMJ studies.
Methods: Proprietary high-speed GRASS software (GE Signa 5x 1.5-T system) was used to acquire 256 × 128 and 256 × 192 pixel images (7.4/2.7, 60°, 1 excitation) of the TMJ by using a dual receive coil TMJ phased array. Up to 60 images of the jaw were acquired at a rate of approximately 1 image per second (128 phase encodings) as the jaw was slowly articulated by the volunteer or patient.
Results: Dynamic studies were viewed both singly and as a cine loop. The subsecond GRASS images were shown to contain sufficient diagnostic information with little motion artifact, when compared with conventional gradient- and spin-echo sequences with the same resolution and signals averaged.
Conclusion: The use of a subsecond imaging sequence for studying the kinematics of the TMJ has proved convenient and has greatly reduced the time necessary for a dynamic study while maintaining the useful information of a mechanically controlled dynamic study. Image contrast modifications are possible by pre-preparing the longitudinal magnetization with additional RF pulses.
1. Casselman JW, et al. Dynamic MRI of temporomandibular joint: technique and application. Ann de Radiologie 1990; 33:379–389. 2. Bogini A, et al. The role of MRI in the anatomic and functional assessment of the temporomandibular joint. Minerva Stomatologica 1990; 39:769–776. 3. Shellock FG, et al. Kinematic magnetic resonance imaging of the joints: techniques and clinical applications. Magn Reson Q 1991; 7:104–135. 4. Vogl TJ, et al. MR tomographic diagnosis of the internal derangement of the temporomandibular joint. Radiologie 1991; 31:537–544.

178 • 4:45 PM

MR Imaging of the Shoulder by Using Fast SE with Fat Suppression

G Lee, TW Chan, RS Sherry
Department of Radiology, University of Chicago, Chicago, IL

Purpose: The diagnosis of important shoulder pathologies is primarily based on abnormal high signal intensity (ie, fluid seen on T2-weighted images). Since fat suppression has an additive effect with fast SE (FSE) in enhancing fluid or edema because of the incidental magnetization transfer effect of multisection FSE, this sequence may be useful clinically.
Methods: Thirty-seven patients with suspected rotator cuff tears or shoulder instabilities were imaged on a 1.5-T unit. Coronal oblique FSE T2-weighted images (TR 3,500, effective TE 84) with and without chemical shift selective fat suppression with 15-cm field of view, 256 × 192 matrix, and echo train length of 8 were compared in all pa-

tients. Three patients had the FSE fat-suppressed sequence repeated with a single-section acquisition. Three patients were also imaged with routine T2-weighted SE (2,500/60) with fat suppression.

Results: Fat-suppressed T2-weighted images easily enabled distinction of bursal fluid from fat in 8 patients who had equivocal findings on the routine T2-weighted FSE images in which fat remained of high signal intensity. Two of 6 complete rotator cuff tears were better visualized on the fat-suppressed images. Two patients with intermediate signal intensity within the supraspinatus tendon on the non-fat-suppressed FSE T2-weighted images suggestive of severe tendinitis had fluid-like high signal intensity on the fat-suppressed sequence, suggestive of partial tear. Signal intensity ratio between multi versus single-section acquisition was 0.63 and 0.88 for muscle and fat, respectively, probably due to incidental magnetization transfer effect as previously reported. Image quality was superior in FSE compared with that of SE with fat suppression.

Conclusion: Fat suppression with FSE T2-weighted imaging is useful clinically because it increases conspicuity of cuff tears and abnormal fluid around the shoulder.

179 • 4:57 PM

Chemical Shift MR Imaging of the Sacrum: Sex-Dependent Differences of Bone Marrow Distribution in Healthy Young Adults

SH Duda, F Schick, M Laniado, M Strayle, CD Claussen
Department of Radiology, University of Tübingen, Tübingen, Germany

Purpose: To evaluate sex-related signal differences in the sacrum of healthy subjects by chemical shift (CS) MR imaging.

Methods: Forty healthy volunteers (age range, 18–44 years) were prospectively examined with matched-pair analysis (age/sex). The sacrum was imaged with a surface coil (1.5 T). After T1- and T2-weighted images had been obtained, CS imaging was performed by using a selective nonexcitation (SENEX) sequence (TR msec/TE msec = 300, 1,000/25) (1). The signal intensity (SI) of sacral bone marrow was assigned with a grading system from 1 to 3 and compared with that of subcutaneous fat (fat image) and gluteus muscle (water image). The ratio of red to yellow marrow was visually analyzed.

Results: CS imaging allowed a much better differentiation between yellow and red marrow when compared with that of SE imaging. Selective CS images in men aged 18–25 years showed similar intensities of fat and water signals, whereas after the age of 25 years, the relative intensity of fat is higher than that of the water signal. Regardless of age, relative SI of fatty marrow in men was greater than in women (2.6 vs 2.1; $P < .05$). Analysis of local marrow distribution revealed no substantial topographic differences between sexes. A mottled, sometimes geographic pattern could be detected in 27% of volunteers without age dependence.

Conclusion: The use of selective fat-water images revealed sex-related differences in the distribution of fatty and red marrow. These data differ from those based on macroscopic and previous imaging studies and will further improve our understanding of pathologic bone marrow changes (2,3).

1. Schick F, Bongers H, Jung WI, et al. Magn Reson Imaging 1991; 9:509. 2. Kricun ME. Skeletal Radiol 1985; 14: 10. 3. Moore SG, Dawson KL. Radiology 1990; 175:219.

180 • 5:09 PM

Rheumatoid Arthritis of the Wrist: Comparison of Conventional and Fat-Saturated SE Sequences before and after Administration of Gd-DTPA

P Lang, HK Genant, J Li, S Grampp, M Stevens, C Peterfy, K Sack
Department of Radiology, University of California, San Francisco, CA

Purpose: To compare conventional and fat-saturated SE sequences before and after intravenous administration of Gd-DTPA in rheumatoid wrists.

Methods: The authors studied 20 rheumatoid wrists by using MR imaging (SE 600/20, SE fat saturated 400/20, before and after intravenous administration of Gd-DTPA). Contrast was calculated as $(SI_{Tissue1} - SI_{Tissue2})/(SI_{Tissue1} + SI_{Tissue2})$, where SI = signal intensity.

Results: Erosions and inflammatory synovial tissue demonstrated marked contrast enhancement after Gd-DTPA. Since marrow and tissue fat have high SI on conventional T1-weighted SE images, contrast between high SI fatty tissue and enhancing erosions or enhancing inflammatory tissue is low on this sequence after Gd-DTPA (mean, 0.12 and 0.12, respectively). Enhancing peritendinous inflammatory tissue was not delineated on conventional T1-weighted SE postcontrast images in 4 patients due to adjacent fat layers. On fat-saturated postcontrast images, however, fat has low signal intensity, thereby highlighting enhancing erosions and enhancing synovial or peritendinous inflammatory tissue (mean contrast to fat, 0.18 and 0.24, respectively).

Conclusion: In imaging rheumatoid soft-tissue changes, fat-saturated T1-weighted postcontrast images are markedly superior to conventional postcontrast SE images, since signal overlap of enhancing structures with marrow or fat is avoided.

Monday Afternoon • Imperial Ballroom
Papers 181–188

PERFUSION/DIFFUSION I

MODERATORS: RR Edelman, MD
PM Joseph, PhD

181 • 3:45 PM

Functional Imaging of Human Motor Cortex at 4 T

SG Kim, J Ashe, A Georgopoulous, H Merkle, JM Ellermann, RS Menon, S Ogawa, K Ugurbil
Center for Magnetic Resonance Research, University of Minnesota, Minneapolis, MN

Purpose: MR imaging has recently been used to examine human cortical function, noninvasively and without the use of exogenous contrast agents. The basis for this technique is that deoxyhemoglobin acts as an endogenous contrast agent and therefore changes in its local concentration lead to alterations on the T2*-weighted image. Neural activation within the cerebral cortex leads to a large increase in blood flow without a concomitant increase in oxygen consumption, which in turn causes a decrease in the venous deoxyhemoglobin concentrations, producing a signal increase on the T2*-weighted image. Here, the authors applied this technique at high magnetic field strength (4 T) to study the human motor cortex function.

Methods: All MR imaging experiments were performed on a 4-T whole-body system. An oblique plane between axial and sagittal planes was defined along the central sulcus.

In this study, the right hemisphere was used. Consecutive gradient-echo oblique images were acquired with TE = 35 msec and voxel resolution = 1.3 × 2.0 × 12 mm. The motor cortex activation was achieved by making repetitive opposition movements of the thumb and each of the remaining 4 fingers. A functional activation map was generated by intensity changes divided by baseline image intensity on a pixel-by-pixel basis.

Results: Experiments were performed in 6 healthy volunteers who moved right, left, and both hands in the task. A stimulus-induced localized signal intensity change was observed predominantly within a primary motor cortex, mainly finger activity area. The rise time of the activation from the background level was within the time resolution of image acquisition (10.8 seconds). The surface area of activation of the primary motor cortex with the ipsilateral hand movements (0.15 cm^2 ± 0.20 [$n = 5$]) was significantly smaller than the activation area produced by the contralateral hand (1.16 cm^2 ± 0.35 [$n = 6$]) or by both hands (1.25 cm^2 ± 0.07 [$n = 3$], $P < .001$). The area of activation did not differ between the left and both hands. Activation-induced signal change was higher in the contralateral (9.4% ± 6.5) rather than the ipsilateral hand movement (5.0% ± 2.5); activation due to both hand movements was higher than when only 1 hand moved.

Conclusion: The authors have demonstrated that motor functional mapping can be easily achieved with conventional gradient-echo imaging at the high magnetic field and the increased sensitivity and increased susceptibility effects at the higher magnetic field strength permit a higher resolution map. With respect to the tasks examined, a task involving both hands results in greater change compared with either a contralateral or ipsilateral hand task, and activation with the contralateral hand was greater than that produced by ipsilateral hand movement. Furthermore, activation area and signal change induced by hand movement are reproducible.

182 • 3:57 PM

Diffusion-weighted Imaging at 4.7 T in the Assessment of Brain Maturation in Albino Rats

DM Wimberger, TP Roberts, J Kucharczyk, AJ Barkovich, E Kozniewska, LM Prayer
Department of Neuroradiology, University of California, San Francisco, CA

Purpose: Anisotropic diffusion has been shown to occur in mature, but not in immature, white matter tracts of the brain. The aim of this study was to establish the relationship between the age-related maturation of white matter tracts in the albino rat, as detected pathologically, and anisotropic diffusion at 4.7 T.

Methods: Twelve albino rats aged from 5 days to 6 weeks were imaged with a 4.7-T GE Omega CSI system. The ongoing stage of maturity of white matter tracts was assessed by comparing images obtained with T1-weighted (400/25) and T2-weighted (3,000/20) SE sequences and heavily diffusion-weighted (2,000/80; b ~ 1,300 sec/mm^2) imaging. The MR imaging results were compared with the state of myelination as determined by histochemical and electronmicroscopic studies (1).

Results: While optical structures could be identified on all MR images, the anterior commissure, hippocampal commissure, and the corpus callosum were localized routinely only in animals older than 3 weeks. Diffusion-weighted anisotropy preceded T2-weighted signal changes due to myelination. T1-weighted images were not informative in the assessment of maturation-related changes. Although diffusion anisotropy increases as the brain matures, a direct correlation between myelination and anisotropy was not found.

Conclusion: Diffusion-weighted imaging enables serial evaluation of age-related maturation of white matter tracts earlier than SE sequences. Neither method seems to correlate well with the actual process of myelination. The visual pathways of the albino rat are a suitable experimental model for neuroimaging evaluation of ongoing maturation processes of a cerebral white matter tract in vivo.

1. Jacobson S. Sequence of myelinization in the brain of the albino rat. An introduction to the neurosciences. Philadelphia: Saunders, 1972.

183 • 4:09 PM

Phase Shift as a Measure of Tissue Concentration for Microscopically Distributed Paramagnetic Agents: Theory Assessment with Dynamic H-1 Water Spectroscopy

TE Conturo, PB Barker
Department of Radiology and Radiological Science, Johns Hopkins Hospital, Baltimore, MD

Purpose: Data are presented supporting a linear relation between tissue paramagnetic concentration and phase shift, important for perfusion quantitation. Dynamically acquired H-1 water spectroscopic data are presented that demonstrate the equivalence between reconstructed phase shift and the volume-averaged intravoxel phase shift, from which the above linear hypothesis follows.

Methods: The frequency distributions ρ_c and ρ, the frequency shift $\Delta\omega$, and the broadening function W can be assessed by acquiring dynamic H-1 water spectra under bolus paramagnetic infusion conditions similar to those of the imaging experiment. A PRESS spectroscopic pulse sequence was employed to obtain water H-1 spectra. To hasten the acquisition rate to that of gradient echo perfusion-weighted phase-shift images, the pulse sequence was cycled and spectra were reconstructed from each acquisition. A 1 × 1 × 1-cm voxel was selected centered about the globus pallidus, excluding CSF, in an anesthetized dog. The timing intervals were $TE = 50$ msec and $TR = 1.5$ sec, and 2,048 data samples were acquired for a spectral resolution of 1 Hz.

Results: Individual water spectra are generally symmetric and have slight tails in the high field region, which can be attributed to shim imperfections for the 1-cm^3 voxel. Similar line shapes occur postcontrast as in precontrast imaging, indicating that the paramagnetic bolus imposes a symmetric distribution in frequency perturbations and that $\phi_{obs} = \langle\phi\rangle$ is valid. Despite the relatively small (~4%) intravascular volume, a large portion of the spectrum shifts to higher fields. This observation may be due to two factors: perivascular field perturbations in both the positive and negative directions and transcapillary water exchange. The peak-to-peak phase shift parallels observed image phase shifts. The maximal spectral and imaging phase shifts of ~60° indicates that exchange effects are significant.

Conclusion: Dynamic bolus-enhanced H-1 water spectra in dog brain gray matter demonstrate that the frequency distribution imposed by the partitioned paramagnetic contrast agent is symmetric. From theory, this symmetry supports that the observed phase is given by the average phase, from which it can be shown that the phase shift is proportional to the average tissue concentration.

184 • 4:21 PM

MR Functional Imaging of Silent Speech

RM Hinke, X Hu, AE Stillman, S-G Kim, K Ugurbil
Center for Magnetic Resonance Research, University of Minnesota Medical School, Minneapolis, MN

Purpose: Although previous functional imaging studies of vocalized speech have revealed a myriad of bilateral cortical and subcortical activity, 2 studies revealed unilateral

left-sided activity during phonetic discrimination and silent speech. The purpose of this study is to investigate the feasibility of using T2*-weighted MR functional imaging (MRFI) based on blood oxygen level dependent (BOLD) contrast to demonstrate this lateralization of cortical activity during silent speech.
Methods: The authors studied 6 (3 male, 3 female) healthy, right-handed, English speaking volunteers, by using a 4-T Siemens/SISCo whole-body system with a gradient-recalled-echo sequence and a quadrature head coil. The tasks included silent recitation of the alphabet and silent word generation from the alphabet (ie, A-apple, B-boat, etc). Typically 15 control, 10 task, and 15 recovery axial T2*-weighted images of the perisylvian region were obtained. A percentile intensity change map was then generated, including only those pixels that passed the Student *t* test at a 99.9% confidence level. Bilateral comparisons were made based on the areas of activation.
Results: All subjects demonstrated more activated area in the Broca region (mean, 0.469 cm^2) compared with its right-side homologue (mean, 0.146 cm^2) during silent speech word generation; intensity change, however, was comparable bilaterally (left: 3.7% ± 1.6, right: 3.14% ± 1.6). During the automatic silent articulation task (silent recitation of the alphabet), however, the area of activation on the left (mean, 0.139 cm^2) was not substantially different from that on the right (mean, 0.107 cm^2).
Conclusion: The authors have successfully performed MR functional imaging of silent speech, demonstrating a clear increase in Broca area activation over its right-side homologue during word generation, and a smaller bilateral activation during an automatic silent articulatory task. These preliminary data suggest that the Broca area may not only be involved in the motor aspects of articulation, as previously known, but may also be involved in word generation. Our studies demonstrate the capability of MR functional imaging to detect language lateralization, which may eventually be used as an alternative to the Wada test.

185 • 4:33 PM

Early Detection of Hyponatremic Encephalopathy with Diffusion-weighted MR Imaging

ZS Vexler, T Roberts, J Kucharczyk, A Arieff
Neuroradiology Section, Deparmtent of Radiology, University of California, San Francisco, CA

Purpose: Hyponatremic encephalopathy is a serious metabolic disorder associated with severe symptomatic hyponatremia, which carries a substantial cerebral morbidity. The purpose of this study was to evaluate the early time course of hyponatremic encephalopathy in cats by using MR neuroimaging combined with evaluation of neuronal cell sodium transport in synaptosomes in an in vitro system.
Methods: Acute hyponatremia was induced by intraperitoneal injection of 140 mM glucose/water and arginine vasopressin. Diffusion-weighted (1,000/80, gradient strength 1–11 G/cm) images were acquired. Maps of the apparent diffusion coefficient (ADC) were generated with pixel-by-pixel logarithmic regression analysis of the diffusion-weighted images. Synaptosomes from normal and hyponatremic brain tissue were used to investigate changes in sodium transport via 3 different neuronal membrane pathways: (*a*) Na^+-K^+ ATPase system, (*b*) sodium channels, (*c*) Na+-H+ antiporter.
Results: A reduction in the plasma sodium from 153 ± 1 to 122 mM ± 6 resulted in a decrease in the ADC from 0.69 ± 0.02 to 0.61 ± 0.03 ($P < .03$) within 2–3 hours. Analysis of the brain water content (gray matter) showed elevation from the control value of 384 ± 12 to 441 ± 8 mL/100 g dry weight ($P < .01$). There was significantly increased transport of Na+ via the Na+-K+ATPase system, reflecting adaptive extrusion of Na+ from neurons. However there was no significant change in Na+ transport through either Na+ channels or the H+/Na+ antiporter.
Conclusion: The inverse relationship found between decrease in ADC and increase in brain water suggests the development of brain edema in early stages of hyponatremia. The ADC may thus be a sensitive MR imaging indicator of the presence of cytotoxic brain edema associated with hyponatremic encephalopathy. The brain, however, has adaptive extrusion of cations that serve to decrease brain osmolality and tend to minimize cerebral edema and subsequent brain damage.

186 • 4:45 PM

Spin-Echo Echo-Planar Imaging of Localized Signal Enhancement in the Human Brain during Task Activation

PA Bandettini, EC Wong, L Estkowski, RS Hinks, JS Hyde
Biophysics Research Institute, Medical College of Wisconsin, Milwaukee, WI

Purpose: Signal enhancement in active cerebral tissue, associated with decreased concentrations of deoxyhemoglobin, has been observed by using gradient-echo (1–3) and SE (4) techniques. A detailed comparison of brain activity-related signal enhancement in SE and gradient-echo echo-planar imaging (EPI) sequences is made. SE and gradient-echo brain activity images are created and compared.
Method: Single-shot SE and gradient-echo EPI sequences (field of view = 24 cm, 64 × 64 resolution, 5–15-mm section thickness) were performed on a 1.5-T Signa by using a local 3-axis gradient coil. The motor cortex activation paradigm was self-paced finger movement. Three comparisons were made between SE and gradient-echo sequences: (*a*) Brain activity-related signal enhancement dependence on TE, thus $\Delta(1/T2^*)$ and $\Delta(1/T2)$; (*b*) spatial location of the signal enhancement; (*c*) optimal TE for brain function contrast to noise.
Results: Signal enhancement is TE dependent in both sequences, with $\Delta(1/T2^*) = -0.45\ s^{-1}$ and $\Delta(1/T2) = -0.15 s^{-1}$. The spatial location of the enhancement in the brain is identical in both sequences. Given that $\Delta(1/T2)$ and $\Delta(1/T2^*)$ are small relative to the tissue 1/T2 and 1/T2*, it is readily calculated that optimal contrast to noise occurs at TE ≈ T2 and T2*. Optimal TE = 40–50 msec for gradient-echo EPI, and 90–110 msec for SE EPI.
Conclusion: The primary source of functional susceptibility-related deoxyhemoglobin contrast apparently occurs in vessels that are subvoxel in size. While static susceptibility effects dominate, diffusing spins contribute to the dephasing. Therefore, a local increase in oxygenation causes signal enhancement in gradient-echo and SE sequences.

1. Kwong KK, Belliveau JW, Chesler DA, et al. PNAS 1992; 89:5675–5679. 2. Bandettini PA, Wong EC, Hinks RS, Tikofsky RM, Hyde JS. Magn Reson Med 1992; 25:390–397. 3. Ogawa S, Tank DW, Menon R, et al. PNAS: June, 1992. 4. Bandettini PA, Wong EC, Hinks RS, Estkowski LS, Hyde JS. SMRM 11th annual meeting, works in progress: 719, 1992.

187 • 4:57 PM

Assessment of Brain Perfusion with an Ultrasmall Superparamagnetic Iron Oxide Particle

VM Runge, JE Kirsch, JW Wells, JN Dunworth, CE Woolfolk
MRISC, University of Kentucky, Lexington, KY

Purpose: The ability of MR imaging to assess cerebral perfusion by using dynamic susceptibility contrast technique was evaluated with BMS 180549 in a model of mid-

dle cerebral artery (MCA) ischemia. Results were compared with experimentation using gadoteridol.
Methods: Dynamic imaging was performed in 5 cats, 60 minutes after MCA ligation, with BMS 180549 at a dose of 1.7 mg Fe/kg, injected at 9 mL/sec. An SSFP technique with 1.5 × 1.5-mm pixel and 1-second temporal resolution was used on a conventional 1.5-T system for imaging during bolus transit. A comparative study was performed in 5 cats by using 0.5 mmol/kg gadoteridol.
Results: With BMS 180549, the change in signal intensity (SI) was 41% ± 10 and 19% ± 4 for normal gray and white matter, respectively, compared with 27% ± 6 and 9% ± 3 for ischemic gray and white matter. Conventional T1- and T2-weighted images were normal, without evidence of the acute MCA infarct. Comparative results with gadoteridol were 45% ± 5 and 27% ± 9 for normal gray and white matter, and 20% ± 2 and 11% ± 5 for ischemic gray and white matter. The paradoxical increase in SI of muscle observed with gadoteridol was not present with BMS 180549.
Conclusion: Cerebral perfusion can be assessed with either particulate agents or a gadolinium chelate; however, results with the latter suffer possible errors due to T1 effects. Evaluation of otherwise undetectable ischemic disease is thus possible, with high spatial resolution.
This research was supported in part by a scientific grant from Squibb Diagnostics.

188 • 5:09 PM

Novel Echo-shifted Gradient-recalled MR Imaging Methods for Functional Imaging Based on Dynamic Susceptibility Effects

CTW Moonen, J Duyn, J Gillen, G Liu, G Sobering, FA Barrios, R Sexton, VS Mattay, J Frank
In Vivo NMR Research Center, National Institutes of Health, Bethesda, MD

Purpose: To develop echo-shifted gradient-recalled imaging methods (ES-FLASH) to increase T2* sensitivity while maintaining a short TR period. To demonstrate the effectiveness of the new methods for functional imaging by using a conventional clinical imager and a standard head coil.
Methods: Recently, the authors have introduced a new FLASH technique where the excitation of spins and their gradient-recalled echo are separated by more than one TR period thus enhancing T2* weighting (Magn Reson Med 1992; 26:184). In the original method, strong additional gradients were used to select the desired echo. Here, the authors demonstrate that alternative gradient schemes involving all 3 principal gradients lead to the same desired effect and have the advantage that they are effective on conventional clinical imagers with low gradient strength. They also form the basis for fast 3D imaging techniques with large T2* weighting.
Results and Conclusion: The sequences were tested in phantoms, showing a signal decay according to the T2*, indicating that the gradient arrangements are sufficient to predominantly select the desired gradient-recalled echo with TE > TR. The new ES-FLASH methods show a drastically increased sensitivity to T2* effects despite equal total TR, total duration, and image resolution. Studies in human volunteers using visual stimulation confirm earlier findings with echo-planar techniques (JW Belliveau, et al. Science 1991; 254:716) and demonstrate that such measurements can be easily performed on standard imagers by using a whole-head coil and ES-FLASH methods.

Tuesday Morning • California Room Papers 201–208

CARDIAC II

MODERATORS: L Eastwood, PhD
CB Higgins, MD

201 • 10:30 AM

MR Imaging for Assessment and Follow-up of Left Ventricular Mass in Patients with Aortic Stenosis before and after Valve Replacement

FE Vanneroy, S Cleron, N Provost, G Grollier, JC Potier, JP Foucault, D Denizet
Department of General Radiology, University Hospital, Caen, France

Purpose: To determine if cardiac MR images may be applied to the assessment of a left ventricular (LV) mass in patients with aortic stenosis.
Methods: The hearts of 10 patients with severe aortic stenosis were imaged with a 1.5-T Signa GE MR imager with contiguous, 10-mm, SE T1-weighted short axis sections from apex to base, in one multisection image acquisition. Each patient was assessed before surgery and systematically at 1 month, 3 months, and 6 months after valve replacement. Total imaging time was about 30 minutes and analysis technique required about 10 minutes. MR imaging data were compared with echocardiographic results.
Results: Accurate LV mass data were obtained (medium LV mass before surgery = 138 g/m^2, extremes = 115–167 g/m^2) without assumption about shape (as the entire ventricle was visualized), without intravenous contrast agent requirement and with a low inter- and intraobserver variability (less than 20 g).
Conclusion: MR imaging permits accurate and simple assessment or follow-up of LV mass. It should be used in place of other studies, in a sufficiently short time for cost considerations.

202 • 10:42 AM

Cine MR Imaging of Hypertrophic Cardiomyopathy: Evaluation of Anatomic and Physiologic Parameters

EO Lipchik, SE Mann, RD White
Radiology Department, Medical College of Wisconsin, Milwaukee, WI

Purpose: The authors assessed the multipotentiality of dynamic gradient-echo ("cine") MR imaging for the evaluation of various important anatomic and physiologic parameters found in obstructive (O) and nonobstructive (NO) forms of hypertrophic cardiomyopathy (HC).
Methods: Cine MR imaging (prospective electrocardiogram-triggered FISP, flip angle = 30°, TE = 9 msec, section TR = 25 [1 level] or 50 [2 levels] msec, matrix = 128 × 256, acquisitions = 3–4 in the long-axis orientation through the left ventricular outflow tract [LVOT]) was used to study 22 patients (26 examinations, including 4 after septal myectomy) with established diagnoses of HC on a conventional 1.5-T System (Siemens Magnetom-SP). Anatomic details and physiologic events, including mitral valve function (eg, systolic anterior motion [SAM] of the anterior mitral leaflet) and LVOT dynamics, were evaluated and correlated with the results of echocardiography.
Results: All 14 patients with OHC demonstrated significant SAM. Of the 8 patients with NOHC, 5 had SAM to a milder degree and 3 had none. A significant quantitative difference in the signal loss due to systolic obstruction within the LVOT between the groups of patients with and without SAM was noted; no patient with SAM had an aortic:LVOT intensity ratio less than 7, whereas the ratios in all without SAM were less than 3. LVOT area, rather than

septal thickness, correlated closest with SAM. Echocardiographic correlations with MR imaging results showed close agreement for both SAM and mitral regurgitation. Other physiologic parameters are to be discussed.
Conclusion: Cine MR imaging is well suited for demonstrating anatomic abnormalities of HC, as well as associated temporal dynamic changes of the LVOT and mitral valve. This technique provides a new parameter (signal intensity ratio) to quantify LVOT obstruction, thereby differentiating O from NO forms of HC.

203 • 10:54 AM

Improved Cine MR Imaging in the Cardiac Long Axis with Gd-DTPA

DJ Pennell, SR Underwood, DB Longmore
MR Unit, Royal Brompton Hospital, London, England

Purpose: Cine MR imaging of ventricular wall motion in the long axis is clinically useful and essential for evaluation of apical contraction, but cine quality is often limited by signal loss in slow moving blood flowing predominantly in-plane caused by magnetic saturation. This study determined the role of Gd-DTPA in improving the quality of long axis cines.
Methods: Twenty subjects (17 healthy volunteers, 3 patients with inferoapical infarction) were studied before and after administration of Gd-DTPA. A 0.5-T imager was used (80/14, flip angle 45°). Contrast was defined as the signal difference between blood and myocardium. Cines were also scored from 1 to 9 according to the reviewer's ability to distinguish endocardium from blood throughout the cardiac cycle.
Results: In the vertical long axis, mean contrast between blood and myocardium increased by 62.1% at end systole, and 49.9% at end diastole, and in the horizontal long axis by 66.7% at end systole, and 25.6% at end diastole (all $P < .0001$). The mean cine score in the vertical long axis increased from 4.2 to 6.2 ($P < .0001$) and in the horizontal long axis from 3.6 to 6.0 ($P < .0001$). In the patients with inferoapical infarction, assessment of apical contraction was greatly improved.
Conclusion: Gd-DTPA has a useful clinical role in improvement of cardiac cines acquired in the long axis when adequate clinical evaluation of wall motion is hindered by magnetic saturation of slow moving blood.

204 • 11:06 AM

Diastolic Dysfunction: Dynamic MR Imaging Velocity Mapping of Related Flow Patterns in the Superior Vena Cava

RD White, PA Hardy, CW VanDyke, N Obuchowski, AL Klein
Division of Radiology, Cleveland Clinic Foundation, Cleveland, OH

Purpose: The detection of diastolic (D) dysfunction and the differentiation between restrictive cardiomyopathy (RC) and constrictive pericarditis (CP) as the source can be problematic. The use of MR imaging velocity mapping (VMAP) of flow in the superior vena cava (SVC) was assessed for its value in characterizing D dysfunction.
Methods: MR imaging (1.5-T GE Signa: 4.6-Advantage Software) with a dynamic VMAP technique (retrospective "VINNIE": 25/9 with flow and respiratory compensation; VENC = 75 cm/sec; 192 × 256 at NEX = 2; 1 level at 32 phases or 2 levels at 16 phases per cycle per acquisition) was used to study 16 cases of suspected D dysfunction and 4 healthy volunteers; both transaxial VMAP MR imaging of mid-SVC flow and standard 4-chamber MR imaging (SE and cine) of pericardial anatomy and ventricular function were performed. VMAP plots of SVC flow per cardiac cycle were analyzed (VCALC 9 Program) for their SVC flow patterns (normal: biphasic with systolic [S] > D) and the ratios of peak-S-flow:peak-D-flow were calculated. Standard images were qualitatively evaluated for evidence of early or late RC (variably impaired ventricular filling; no substantial pericardial thickening) or CP (abrupt middle-to-late D filling impairment; corresponding significant pericardial thickening). Transesophageal echo (TEE) Doppler results provided confirmation (12 cases).
Results: Among the 16 cases, D dysfunction (no significant tricuspid regurgitation) was diagnosed with standard MR imaging in 10 cases, and RC ($n = 5$), CP ($n = 4$), and mixed ($n = 1$) appearances were differentiated (confirmed with TEE Doppler in 8/8). In the 10 cases of proved D dysfunction, S:D peak-flow ratios (range, 0.17–1.14; mean, 0.54) were significantly different ($P < .01$) from those (range, 1.28–3.39; mean, 2.04) of the control group (4 volunteers and 2 rule-out cases). Compared with CP (range 0.17–0.99; mean, 0.44) ratios, ratios for both early RC ($n = 2$) (range, 0.45–0.99; mean, 0.72) and late RC ($n = 3$) (range, 0.17–0.36; mean, 0.26) stages were different. The remaining 4 cases had milder myocardial or pericardial disease and intermediate ratios (range, 0.74–1.76; mean, 1.12).
Conclusion: MR imaging with VMAP analysis of SVC flow is sensitive for the noninvasive detection of D dysfunction and aids in the differentiation between RC, including its various stages, and CP as the source.

205 • 11:18 AM

Evaluation of Left Ventricular Volume and Mass by Using Breath-Hold Cine MR Imaging

H Sakuma, N Fujita, SJ Nelson, GR Caputo, TK Foo, A Shimakawa, CB Higgins
Department of Radiology, University of California, San Francisco, CA

Purpose: Cine MR imaging has been shown to be very accurate in evaluating cardiac function. However, the lengthy imaging time is preventing its widespread clinical use. In this study, left ventricular (LV) volumes and mass were evaluated by using breath-hold cine MR imaging, and the results were compared with those of conventional cine MR imaging.
Methods: Ten healthy volunteers were imaged by using a 1.5-T GE Signa imager. The breath-hold cine MR images were acquired with a k-space–segmented fast gradient-echo sequence (9/2.8, 20° flip angle). Eight lines of k space were collected per trigger per segment. Up to 15 cardiac phases were imaged in 16 heartbeats. The breath-hold cine MR study encompassing the whole LV was completed in 12 breath holds. Conventional non-breath-hold cine MR images (22/7.5, 35° flip angle) were obtained with flow and respiratory compensation. The imaging time was 20–30 minutes.
Results: Breath-hold studies showed no ghosting artifact, and cardiac edges were clearly identified because of the reduced blurring. Measurement of LVEDV, LVESV, and LV mass by using breath-hold cine MR imaging showed very close correlation with those of conventional cine MR studies ($r = .98$, 0.97, and 0.99, respectively). The interobserver variability of volumes and mass determined with breath-hold cine MR imaging (4.0%, 8.0%, 3.7%) was equal to or less than those with conventional cine MR imaging (4.0%, 8.6%, 5.0%).
Conclusion: Breath-hold cine MR imaging is highly useful because an accurate assessment of cardiac function is obtained in less than 5 minutes.
T.K. Foo and A. Shimakawa are employees of GE Medical Systems.

206 • 11:30 AM

Cardiac Tagging with Breath-Hold Cine MR Imaging

ER McVeigh, E Atalar, EA Zerhouni
Johns Hopkins School of Medicine, Baltimore, MD

Purpose: The purpose of this work was to develop an imaging protocol to obtain tagged cine images of the heart in a single breath hold. The motivation for this was to reduce the blurring and ghosting on cardiac images from respiratory motion and to reduce the total data acquisition time for measuring myocardial strain.

Method: A GRASS pulse sequence was used with a segmented k-space data acquisition. For a field-of-view of 24 cm and a 10-mm section thickness, TR = 6.1 msec and TE = 2.1 msec. A fractional echo was used to reduce motion artifact from the blood in the heart chambers. Arbitrary oblique planes could be achieved. A reduced k-space coverage was used to sample separately generated parallel line tagging patterns. The spatial frequency components of the parallel patterns are concentrated around the axes in k space, therefore a "cross" pattern was used for k-space sampling.

Results: Two-dimensional strain data from a single imaging plane were acquired during a single breath hold of 8–32 heartbeats. The entire imaging time for 3D strain field reconstruction was less than 300 heartbeats, or approximately 5 minutes. Image quality and consistency was greatly improved over those obtained with SE techniques, principally due to the elimination of motion artifacts. The contrast between the tags and the background tissue persists well beyond end systole.

Conclusion: The authors have reduced the total data acquisition time for 3D myocardial strain mapping by more than an order of magnitude. This now makes the technique clinically viable.

207 • 11:42 AM

Assessment of Left Ventricular Function with Radial Long-Axis Multisection Gradient-Echo MR Imaging

A von Smekal, KC Seelos, C Sopora, W Fehske, M Reiser, HJ Biersack
University of Bonn, Cologne, Germany

Purpose: To optimize visualization of regional and global myocardial wall motion and left ventricular (LV) function with a radially oriented, long-axis, multisection, multiphase gradient-echo cine MR imaging method.

Methods: Ten volunteers and 40 patients with various myocardial diseases were studied on a 0.5-T Philips Gyroscan. Electrocardiogram-gated, 3 section, multiphase, radially oriented, long-axis (RELAX) gradient-echo sequences were acquired with 25–34 phases, TE = 9 msec, flip angle = 45°, field of view = 350 mm, and matrix 256 × 204. LV myocardium was visualized in the echocardiographically known long-axis, two-chamber and four-chamber views. LV functional parameters (eg, LV ejection fraction [EF]) were calculated based on 5 different approaches and compared with echocardiographic and angiographic data.

Results: The values of LV volumes and ejection fraction showed good correlation with echocardiographic and angiographic data. Correlation of LV EF with echocardiography was $r = 0.75/0.89/0.86/0.87/0.87$, and with angiography $r = 0.87/0.88/0.90/0.91/0.90$. The acquisition of 3 LV long-axis orientations with 1 imaging sequence allowed superior visualization and interpretation of regional and global myocardial wall motion. Remodeling and pathologic myocardial wall motion pattern could be visualized.

Conclusion: The combination of 3 standard LV long-axis orientations in 1 cine MR imaging sequence with high time resolution allows reliable calculation of LV functional parameters. In a regionally deformed or severely deformed left ventricle, function can be correctly evaluated due to the radial 3 section approach. Extended myocardial areas can be visualized and analyzed. This new method enhances clinical information and can therefore increase the use of cardiac MR imaging.

208 • 11:54 AM

First-Pass Myocardial Perfusion MR Imaging with an Intravascular Contrast Agent

N Wilke, J Zhong, H Merkle, J Ellermann, HJ Weinmann, RJ Bache, K Ugurbil
Center for MR Research, Siemens Medical Engineering Group, Erlangen, Germany

Purpose: The sensitivity of the MR imaging first-pass technique was evaluated by using the intravascular contrast agent polylysine Gd-DTPA as an indicator in assessing myocardial perfusion under conditions of predetermined levels of coronary stenosis.

Methods: MR imaging was performed on a 1.5-T Magnetom SP with the TurboFLASH sequence (5.9/3, voxel: 1.8 × 2.7 × 12 mm). End-systolic images were obtained with an 18-cm Helmholtz coil. One triggered image was acquired with every heartbeat during which a low dose of polylysine Gd-DTPA (Schering AG, Berlin) bolus was injected. By using an instrumented closed-chest canine model ($n = 5$), hypoperfusion was induced by partial left anterior descending (LAD) artery occlusion at different intracoronary perfusion pressures. Hyperemia was induced with dipyridamole (0.8 mg/kg intravenously, Boehringer Ingelheim). Myocardial signal intensity was measured of the LAD and left circumflex (LCx) perfusion beds and were plotted against time to generate signal intensity versus time curves (STCs), which were fitted to a gamma-variate function. The inverse mean transit time (1/t) was calculated and compared with absolute measured myocardial blood flow (MBF, milliliters per minute per gram) as calculated from injected radioactive microspheres.

Results: The myocardial STCs demonstrate a clear upslope as well as downslope according to the polylysine Gd-DTPA bolus, which hardly escaped from the capillary blood into the tissue. Different transmural and regional myocardial perfusion levels can be exactly visualized on the MR perfusion images and accurately monitored with the STCs. Transmural detection of the impairment of myocardial perfusion improves significantly after administration of dipyridamole. The 1/t proved to be a reliable flow index when correlated with MBF ($r = 0.93$ for resting and $r = 0.8$ for dipyridamole conditions).

Conclusion: The MR imaging first-pass technique in conjunction with polylysine Gd-DTPA as a myocardial perfusion indicator has the potential for the precise assessment and localization of myocardial hypoperfusion. More sophisticated perfusion models can be applied in terms of quantifying myocardial perfusion.

This research was supported in part by an educational grant from Siemens Medical Systems and Schering AG.

Tuesday Morning • Franciscan B
Papers 209–216

ABDOMEN

MODERATORS: DG Mitchell, MD
PY Poon, MD

209 • 10:30 AM

Wilson Disease: Correlation of MR Imaging and CT Findings with Clinical Status and Hepatic Copper Levels

DM Ellinger, AM Aisen, IR Francis, GJ Brewer, MT Korobkin
Department of Radiology, University of Michigan Medical Center, Ann Arbor, MI

Purpose: To study the utility of MR imaging in patients with Wilson disease in diagnosing clinically occult hepatic disease, and to investigate a possible relationship between liver copper levels measured on biopsy specimens and MR signal intensities.

Methods: Thirty-one patients with Wilson disease underwent MR imaging on a 0.35-T instrument and limited CT scanning of the upper abdomen; biopsy specimens were available in 20 of the patients; in 15, hepatic copper values were available for correlation.

Results: Radiologic evidence of portal hypertension (such as changes in hepatic architecture, splenomegaly, or varices) was seen in 10 subjects. Evidence of liver disease based on physical examination was noted in the medical charts for 2 patients, while 23 had laboratory evidence suggestive of liver disease. Of the 20 patients who underwent biopsy, 14 had cirrhosis. With this as a standard of reference, imaging was 29% sensitive, 100% specific, and 50% accurate. The combined clinical evaluation (clinical impression plus laboratory parameters) was 79% sensitive, 17% specific, and 60% accurate. Signal intensity on T1-weighted images (expressed as the ratio of liver intensity to muscle intensity) did not correlate with copper levels on biopsy samples. However, there was a slight correlation between intensity ratios on T2-weighted images or calculated T2 values and copper levels ($r^2 = .26$ and .19, respectively).

Conclusion: Imaging was specific but not sensitive in the evaluation of the liver in patients with Wilson disease. In a sense, imaging complemented clinical and noninvasive laboratory parameters, which were sensitive but not specific. There was no correlation of intensity ratios on T1-weighted images with liver copper levels; however, there was a slight correlation with parameters on the T2-weighted images. This may be coincidental or may reflect a correlation with copper levels and the degree of hepatic inflammation.

210 • 10:42 AM

Follow-up MR Imaging of Liver Metastasis during Chemotherapy

A Giovagnoni, F Terilli, E Paci, N Danese, A Greco, A Piga
NMR Centre, University of Ancona, Ancona, Italy

Purpose: A qualitative and quantitative evaluation of liver metastasis in patients undergoing chemotherapy was performed.

Methods: Fifty-one patients with liver metastasis from solid tumors underwent MR imaging of the liver before the start of treatment and monthly thereafter for a total of 4 examinations for each patient (total of 204 examinations). MR imaging investigations were performed by using a superconductive imager at 1.0 T (Magnetom). SE T1- and T2-weighted images in axial sections were acquired. A qualitative comparative analysis of the MR imaging examinations for each patient was performed; in particular, the number, size, patterns, and evolutions of the lesions were recorded. Moreover, for each patient, a quantitative study was performed to evaluate the behavior during the time of contrast-to-noise ratio (C/N) and signal-to-noise ratio (S/N) of the lesions and normal parenchyma.

Results: The results show 15 cases (29.4%) in progressive disease, 21 cases (41.1%) with stable disease, 13 cases (25.4%) in partial regression, and 2 cases (3.9%) in complete regression. Three groups relating to behavior in C/N and S/N were identified: (1) group ($n = 21$) with unchanged C/N and S/N; (2) group ($n = 18$) with increase of C/N and S/N; (3) group ($n = 12$) with decrease in C/N and S/N. The greatest response to chemotherapy (reduction of number, size, and changes in patterns of the lesions) was observed monthly in the first control in the group of responsive patients. A correlation between reduction of C/N and response to chemotherapy was observed.

Conclusion: MR imaging appeared to be a useful imaging modality in follow-up of liver metastasis with qualitative and quantitative parameters to evaluate efficacy of chemotherapy.

211 • 10:54 AM

MR Portography: Comparison with CT Portography and Conventional MR Imaging

VS Dravid, MJ Shapiro, DG Mitchell, RJ Wechsler, E Outwater, CW Piccoli, RI Feld, FE Rosato
Department of Radiology, Thomas Jefferson University Hospital, Philadelphia, PA

Purpose: To compare MR imaging with arterial portography (MRAP) to CT with arterial portography (CTAP) and conventional MR imaging (CMRI) for preoperative evaluation of hepatic masses.

Methods: In 8 patients, selective visceral arteriography was initially performed. Then, 20 contiguous 10-mm CTAP images were obtained, 2 images per 8-second breath hold with a 3.5-second interscan delay, beginning 30 seconds after the onset of a 2.5 mL/sec SMA injection of 120–150 mL of 60% Hypaque. MR images included SE T1- and T2-weighted and multiplanar spoiled GRASS (MPSPGR) techniques. For MRAP, we hand-injected 0.1 mmol/kg Gd-DTPA into the SMA. Twenty-four contiguous interleaved 8-mm MPSPGR images were acquired during 2 12-second breath holds, 12 images were acquired immediately after injecting half the dose over 10 seconds, and 12 more were acquired on completion of the injection. The first 12 images were purely portographic, while the next 12 were partially contaminated by systemic recirculation, as with CTAP. Twenty-four additional MPSPGR images were obtained within a minute of injection, analogous to those obtained after systemic (intravenous) Gd-DTPA administration. All images were interpreted by 2 readers. The lesions were classified by location, size, and confidence.

Results: The lesions were seen best on the first-pass MRAP images and were less conspicuous on the partial recirculation MRAP, CTAP, and CMRI. All visualized lesions were seen with MRAP; 4 subcentimeter lesions were seen only with MRAP.

Conclusion: Systemic recirculation of iodinated contrast material from the beginning of the bolus and from prior angiography is a potential limitation of CTAP. MRAP may be more sensitive than CTAP or CMRI for detecting small lesions. For both CTAP and MRAP, optimal results are expected if all images are obtained during a single breath hold, within seconds of the onset of administration of contrast material.

212 • 11:06 AM

Idiopathic Hemochromatosis: Spectrum of MR Imaging Findings in Cirrhotic and Noncirrhotic Patients

ES Siegelman, DG Mitchell, E Outwater, SJ Munoz, R Rubin

Department of Radiology, Thomas Jefferson University Hospital, Philadelphia, PA

Purpose: The authors reviewed abdominal MR images in pathologically proved cases of hepatic iron overload to compare patterns of iron distribution among cirrhotic and precirrhotic patients with idiopathic hemochromatosis (IH) as well as other causes of nontransfusional hepatic siderosis.

Methods: The authors reviewed MR imaging examinations of 14 consecutive patients with histologically proved significant hepatocyte iron who did not have recent blood transfusions or portosystemic shunts. Twelve patients had clinical and laboratory evidence of IH while 2 patients without IH had moderate siderotic cirrhosis. SE 2,500/50, 100 and gradient-echo 25/7–13/20 images of the abdomen were obtained at 1.5 T. The signal intensities of liver, spleen, and pancreas were considered decreased if they were less than or equal to muscle on both the T2-weighted and gradient-echo images.

Results: All patients had low-signal-intensity liver. Seven of the 8 cirrhotic patients with IH had low-signal-intensity pancreas. All 4 precirrhotic patients with IH and both cirrhotic patients without IH had normal-signal-intensity pancreas.

Conclusion: Pancreatic iron was present only in IH patients with cirrhosis. In cirrhotic patients with hepatic siderosis, normal-signal-intensity pancreas suggests an etiology of the cirrhosis other than IH. Pancreatic signal intensity is often normal in precirrhotic IH, a stage where definitive diagnosis is important because early phlebotomy treatment prevents morbitity and mortality from IH.

213 • 11:18 AM

Breath-Hold GRASE (Turbo GSE) Imaging of the Liver: Comparison with RARE (Turbo SE) and FLASH

JC Weinreb, JL Haddad, D Feinberg, B Kiefer

MRI Radiology, New York University Medical Center, New York, NY

Purpose: GRASE (Turbo GSE) uses multiple gradient echoes (GREs) refocused within each of 1 or more SEs of a Carr-Purcell-Meiboom-Gill echo train. Because GRE refocusing requires less time than selective RF refocusing, images with desired contrast can be obtained faster than with RARE (Turbo SE) on a conventional 1.0-T imager. The purpose of this study was to compare images of the liver obtained with GRASE, RARE, and FLASH techniques.

Methods: GRASE: For T1 weighting, the minimum TR = 39 msec, TE = 13 msec, 3 echoes (GRE-SE-GRE) per TR. For T2 weighting, the minimum TR = 209 msec, TE = 110 msec, 21 echoes (seven GRE-SE-GRE sets) per TR. These were compared with standard RARE and FLASH images in 25 patients.

Results: Initially, the GRASE images suffered from ringing artifacts due to significant intensity variations between the RF and GREs. However, these were mitigated with the implementation of amplitude correction. The GRASE images were also more sensitive to eddy currents. However, good quality images were obtained in about one-third of the time of RARE.

Conclusion: GRASE is a promising technique for breath-hold imaging of the liver.

214 • 11:30 AM

T2-weighted Breath-Hold Fat-suppressed RARE (Turbo SE) Imaging of the Liver with 15 mT/m Gradients at 1.0 T

NM Rofsky, JC Weinreb, JL Haddad

MRI-Radiology, New York University Medical Center, New York, NY

Purpose: RARE sequences permit hepatic imaging with T2-weighted contrast with time saving compared with conventional SE sequences. However, because data acquisition takes several minutes, respiratory motion may significantly degrade the images, even when fat suppression pulses are applied. The authors compared hepatic images obtained with T2-weighted breath-hold fat-suppressed RARE by using 15 mT/m gradients with images obtained by using RARE and fat-suppressed RARE in the liver at 1.0 T.

Methods: The breath-hold fat-suppressed RARE (Turbo SE) sequence employed in this study uses 15 SEs per TR, TR = 2,152 msec, effective TE = 120 msec, BW = 130, matrix = 150 × 256, one acquisition, and a binomial fat selective prepulse for fat suppression. With 15 mT/m gradients, 8 sections are obtained in a 23-second breath hold. Sequences are adjusted for patients who cannot breath hold for 23 seconds. Thus, with 2–3 breath holds, the entire liver is imaged with 8–10-mm axial sections. The T2-weighted RARE (Turbo SE) sequence uses 15 echoes per TR, TR = 3,500–5,000 msec, TE = 120 msec, BW = 130, matrix = 250 × 256, and two acquisitions. It provides 16 sections through the liver in 2 minutes. The fat-suppressed RARE sequence used identical parameters preceded by a 1-3-3-1 fat selective prepulse with resultant increase in imaging time or decreased number of sections. Forty patients were studied with all 3 sequences. Images were evaluated and compared.

Results: Of the 3 sequences, the breath-hold fat-suppressed RARE provided the best results both qualitatively (motion artifacts, blurring, anatomic delineation, lesion detectability) and quantitatively (contrast-to-noise ratio).

Conclusion: T2-weighted fat-suppressed breath-hold RARE eliminates some of the problems in non-breath-hold RARE and is a useful sequence for imaging of the liver.

215 • 11:42 AM

Characterization of Focal Liver Lesions: Comparison of Plain and Contrast-enhanced MR Imaging in 107 Patients

B Hamm, RFL Thoeni, RG Gould, ME Bernardino, M Lüning, S Saini, A Mahfouz, KJ Wolf

Department of Radiology, Klinikum Steglitz, Freie Universität, Berlin, Germany

Purpose: The diagnostic value of plain and dynamic contrast-enhanced MR imaging and of combining MR imaging with clinical information for the differential diagnosis of focal liver lesions was compared in a prospective study.

Methods: One hundred seven patients with proved focal liver lesions (52 malignant, 55 benign) were examined on a 1.5-T unit by using an identical examination protocol with plain sequences (T1-weighted SE [500/15] and GRE [100/5, 80°] and T2-weighted SE [2,300/15/90]) and after an intravenous bolus of 0.1 mmol/kg Gd-DTPA with dynamic sequences (breath-hold T1-weighted GRE repeated over 10 minutes). Four experienced radiologists independently read the set of plain images and the set of combined plain and dynamic images without and with knowledge of patient age, sex, and history (minimum interval between the readings, 3 months). The image set was newly randomized between readings. The diagnostic performance of the imaging techniques regarding the radiologist's ability to differentiate between benign and malignant lesions and

to make a specific diagnosis was determined by receiver operating characteristic (ROC) analysis.
Results: The addition of dynamic contrast-enhanced MR imaging to the plain examination significantly ($P < .05$) improved the differentiation of benign and malignant focal liver lesions compared with that of plain imaging alone. Clinical history further improved diagnostic accuracy ($P < .05$). The number of correct specific diagnoses of focal liver lesions was also increased by dynamic MR imaging.
Conclusion: Dynamic contrast-enhanced MR imaging in addition to plain imaging is a valuable technique for improving the differential diagnosis of focal liver lesions. The combination of MR imaging and clinical history further improves the radiologist's diagnostic accuracy.

216 • 11:54 AM

Comparison of Fast T2-weighted SE Sequences with T2-weighted SE Sequences with Fat Saturation

RF Thoeni, FG Blankenberg, GU Mueller-Lisse
Department of Radiology, University of California, San Francisco, CA

Purpose: To compare respective values of fast spin echo (FSE) and SE sequences with fat saturation (T2F), both with T2 weighting, for diagnosing focal lesions and for assessing adenopathy, anatomic detail, and the state of vasculature in liver.
Methods: Fifty-one patients with suspected focal liver lesions (48 with proved lesions) were examined on a 1.5-T unit with FSE (4,000/102, 4 NEX) and T2F (2,500/30, 80, 2 NEX). For each sequence, the number of detectable lesions and ranking of visualization of venous structures was determined. Adenopathy and anatomic detail also were assessed. Each lesion was scored definitely normal to definitely abnormal on a 5-point confidence scale.
Results: When compared with T2F, detection of lesions with FSE was equal in 14 patients, better in 20, and worse in 14. Assessment of lymphadenopathy with FSE ($n = 18$) was equal in 4 patients, better in 3, and worse in 11. For hepatic and portal veins, 18% were judged equivocal on T2F sequences and 54% on FSE, and assessment with FSE was worse in 71 of 102 interpretations. For anatomic detail, T2F tended to be superior in all instances except for the gastrointestinal tract, but the difference was not significant.
Conclusion: Both FSE and T2F are needed to detect hepatic lesions. For assessment of vasculature in liver and adenopathy, T2F was superior to FSE. For anatomic detail in the abdomen, only the gastrointestinal tract was better assessed with FSE than T2F. At present, FSE is complementary to T2F, but it is not a fast alternative that can replace T2F.

Tuesday Morning • Plaza A
Papers 217–224

BRAIN

MODERATORS: KR Maravilla, MD
AS Smith, MD

217 • 10:30 AM

Mapping Cerebral Oxygen Consumption and Blood Flow with O-17 and F-19 MR Imaging

JJ Pekar, TM Sinnwell, AS Chesnick, CTW Moonen, JA Frank, AC McLaughlin
Diagnostic Radiology Research Program, National Institutes of Health, Bethesda, MD

Purpose: To combine MR imaging techniques with tracer methods to measure cerebral oxygen consumption and blood flow in well-defined regions of the brain in vivo.
Methods: O-17 MR imaging was used to measure the rate of increase of $H_2{}^{17}O$ in 0.8-cm^3 voxels of the cat brain during inhalation of ${}^{17}O_2$ gas. F-19 MR imaging was used to measure the rate of "wash-in" and "washout" of the inhaled inert gas CHF_3 in the same voxels. The 2 sets of measurements were performed concurrently at 4.7 T, and the results were combined to calculate the cerebral blood flow and the cerebral rate of oxygen consumption.
Results: The cerebral rate of oxygen consumption in a 0.8-cm^3 voxel situated in the parietal cortex was 1.2 mmol/kg per minute; the cerebral blood flow in the same voxel was 22 mL/100 g per minute. These values are reasonable for cats under pentobarbital anesthesia.
Conclusion: The authors have combined "simultaneous" multinuclear MR imaging with tracer methods to measure classic physiologic parameters (ie, cerebral blood flow and cerebral rate of oxygen consumption). This approach should be directly applicable to human studies at high magnetic fields.

218 • 10:42 AM

Regulation of Human Cerebrospinal Fluid Production with a β-1 Receptor Antagonist: Study Using MR Velocity Mapping

F Ståhlberg, C Nilsson, C Thomsen, O Henriksen
Department of Radiation Physics, Lund University Hospital, Lund, Sweden

Purpose: Studies of cerebrospinal fluid (CSF) dynamics and regulation have previously required invasive techniques. Recently, a method for the study of CSF hydrodynamics noninvasively using MR velocity mapping has been developed (1). In a previous investigation, a pronounced circadian variation in human CSF production was demonstrated with this technique. In an attempt to elucidate the mechanism underlying this variation, the authors have studied the effect of the β-receptor antagonist Atenolol on the nocturnal rise in CSF production.
Methods: The velocity mapping sequence had a TE of 13 msec and a velocity encoding of 20 R/m per second. Flow was measured in the cerebral aqueduct, and production was calculated as net flow over the whole cardiac cycle. After 2 consecutive measurements made between 15:00 and 17:00 in the afternoon, the drug was administered orally to 6 healthy volunteers. Six hours after intake, 2 new flow measurements were performed.
Results: After Atenolol administration, the CSF production at late night was significantly decreased ($P < .05$) compared with previously obtained values in a healthy volunteer group. Average ± standard deviation CSF production ($n = 6$) was 0.36 mL/min ± 0.20 before drug administration and 0.20 mL/min ± 0.32 after drug administration. A significant decrease in heart rate (average 21%,

$P < .025$, $n = 6$) between the first and the second measurement confirmed the absorption of the drug.
Conclusion: Specially designed flow sequences may give MR imaging the potential to investigate the effects of pharmaceutical manipulation of CSF flow and production. In this study, the authors have shown that β-receptor antagonists lower or cancel an expected nocturnal rise in CSF production, indicating that the sympathetic nervous system plays an active role in CSF regulation, possibly by activation of β-1 receptors on either the choroid plexus epithelium or pinealocytes.

1. Thomsen C, et al. Radiology 1990; 177:659–665.

219 • 10:54 AM

Serial MR Imaging Characterization of New Multiple Sclerosis Lesions

CRG Guttmann, SS Ahn, FA Jolesz, L Hsu, R Kikinis, HL Weiner
Department of Radiology, Brigham and Women's Hospital, Boston, MA

Purpose: In the context of a serial MR imaging follow-up of patients with multiple sclerosis (MS), the authors characterized the appearance of white matter lesions at different stages of their evolution.
Methods: Four patients with clinically established MS underwent serial brain MR imaging examinations during 1 year. Each patient was imaged at least 22 times at weekly, biweekly, and monthly intervals with proton density, T2-weighted, and T1-weighted post–Gd-DTPA axial sections. Newly appearing white matter lesions (WMLs) were analyzed for signal intensity pattern.
Results: A total of 22 new lesions were detected in 4 patients. On long TR images, 19/22 lesions (86%) were visible when first detected and 17 of these (89%) demonstrated a central hyperintensity; typically as the lesions aged, they showed a hyperintense rim surrounding a darker center. When present, a circumferential zone of intermediate intensity (halo) surrounding the core of the MS lesions on long TR images appeared to correspond to gadolinium enhancement. All lesions showed gadolinium enhancement within 3 weeks of their first appearance. Change in the gadolinium enhancement pattern from filled disk to ring was observed on some lesions at early stages.
Conclusion: The authors believe that stage-specific characterization of WMLs in MS is possible not only on gadolinium-enhanced but also on nonenhanced SE MR images.

220 • 11:06 AM

Focal Low Signal Intensity Caused by Calcified Penetrating Arterial Branches on MR Images of the Brain

K Yoshikawa, O Abe, T Shiono, E Takenaka, M Eguchi
Department of Radiology, Kanto Rosai Hospital, Kawasaki, Japan

Purpose: Focal low signal intensity on MR images of the brain is well known to be caused by dilated vessels such as vascular malformations, tiny chronic hematomas, and so on. The authors report this spotty low signal intensity in the brain, thought to be caused by calcified penetrating arterial branches.
Methods: Subjects were 11 men and 1 woman ranging in age from 58 to 83 years (mean, 67.4 years). Eleven had cerebral ischemic disorders and another had subacute cerebral hematoma. CT was performed in all cases and angiography in 3 cases. A 1.5-T MR imaging unit (Magnetom) was used to obtain conventional SE sequences. Section thicknesses were from 4 to 8 mm.
Results: In all cases, focal low signal intensities could be seen on T1-, T2-, and also proton-density-weighted images. They were demonstrated in the lenticular nucleus (8/12), thalamus (8/12), pons (7/12), cerebellar hemisphere (4/12), midbrain (1/12), and cerebral subcortex (1/12). In all cases, arteriovenous malformation or venous thrombosis was negated with angiography or CT.
Conclusion: Although pathologic conformation was not obtained in all cases, the authors thought that these focal low signal intensities were caused by calcified penetrating arterial branches. The reason is that calcium deposits are pathologically well known in the penetrating arterial wall of the basal ganglia and brain stem of aged brains. All these patients were old and did not have cerebral hematoma except 1 whose focal low signal intensities were seen in another region and were due to hematoma. Tiny asymptomatic hemorrhages or hemorrhagic infarction, however, could not be neglected in these cases.

221 • 11:18 AM

Diffusion-weighted MR Imaging of the Brain: Effects of Reduced Cerebrospinal Fluid Signal Intensity, Use of a Long TE, and Diffusion Weighting

IR Young, A Oatridge, JV Hajnal, GM Bydder
MRI Unit, Hammersmith Hospital, London, England

Purpose: The contributions of cerebrospinal fluid (CSF) signal reduction, use of a long TE, and diffusion weighting to the appearance of pulsed gradient spin echo (PGSE) images were assessed by reference to T2-weighted SE and T2-weighted fluid-attenuated inversion recovery (FLAIR) pulse sequences.
Methods: Sequences of all 3 types were compared on a Picker HPQ 1.0-T Vista system in patients with infarction, hemorrhage, and tumor.
Results: Both PGSE and T2-weighted FLAIR sequences reduce CSF signal intensity and produce very heavy T2 weighting, allowing the specific additional contribution produced by the diffusion weighting of PGSE sequences to be recognized. Considerable advantage accrues from CSF suppression with both PGSE and FLAIR sequences through reduction in partial volume effects and artifacts. The very heavy T2 weighting with both these pulse sequences highlights certain white matter tracts and provides high sensitivity to disease. The additional diffusion weighting with PGSE sequences can enhance or reduce white matter tract signal intensity and may enhance or reduce lesion conspicuity relative to the FLAIR sequence.
Conclusion: Many of the benefits attributed to the diffusion-weighted PGSE sequence may result nonspecifically from reduction in the CSF signal intensity and the heavy T2 weighting of the sequence without a contribution from diffusion. However, additional anatomic detail, sensitivity to myelination, and increased lesion conspicuity may result from the diffusion weighting.
I.R. Young is employed by Picker International.

222 • 11:30 AM

Cystic Meningiomas: Correlation of Imaging and Histopathology

CS Zee, PM Colletti, MS Tan, S Destian, J Ahmadi, HD Segall
Department of Radiology, University of Southern California School of Medicine, Los Angeles, CA

Purpose: To document the incidence and imaging features of cystic meningiomas and to correlate imaging features of cystic meningiomas with histopathology.
Methods: The imaging studies, clinical history, and pathology of a total of 128 meningiomas were reviewed retrospectively.
Results: A total of 12 cystic meningiomas are in this series. They can be divided into 3 different groups. One group consists of a true cystic meningioma (a smooth,

thin-walled, ringlike, enhancing lesion supplied by a middle meningeal artery). A second group consists of small, irregular cystic areas within the tumor (7 cases). A case of documented cystic, necrotic change of meningioma was seen on both CT scans and MR images. A third group consists of peritumoral cysts (4 cases). Pathologic examination of cystic meningiomas revealed meningothelial and angioblastic meningiomas.
Conclusion: Cystic meningiomas compose approximately 10% of all meningiomas in this series. Histologically, they are usually of the aggressive type, which probably indicates that cystic changes may be secondary to tumor necrosis or hemorrhage. Recognition of diagnostic features of cystic meningiomas is important, since they may mimic metastatic neoplasms or primary gliomas.

223 • 11:42 AM

MR Imaging of Brain Tumors with Simultaneous Display of Relaxation Rate and Proton-Density Information by Using Color Maps

A Brunetti, B Alfano, A Ciarmiello, M Arpaia, C Caraco, G Esposito, ML Mangoni, M Salvatore
Ist. Sc. Radiologiche II Facolta Med. e Chir., Naples, Italy

Purpose: To describe the results obtained in the study of brain tumors with the application of a recently developed MR imaging processing technique based on multiparametric color images (1).
Methods: Color-coded images were obtained from routine MR studies performed at 1.0 and 1.5 T in 30 patients with different brain tumors. T1 and T2 (R1 and R2) and spin density (PD) maps were calculated from multiecho SE sequences (1,600–2,000/15–90) and partial saturation sequences (400–500/15–20). By using a personal computer with a 24-bit high-resolution graphic board, the maps were then fused into a composite color image, with R1, R2, and PD, respectively, coding 1 of the fundamental colors (red, green, or blue). Color images were comparatively evaluated with conventional T1, T2, and proton density images.
Results: The contrast between normal brain structures and tumors appears to be enhanced on color images due to the combined effect of R1, R2, and proton density data, with no loss of diagnostic information compared with conventional T1- and T2-weighted images. In particular, extension, components, and margins of the lesions as well as surrounding edema were always clearly defined.
Conclusion: Magnetic color images may permit an easier evaluation of brain tumors by using a single image rather than multiple series of images. Therefore, they could improve the diagnostic process by simultaneously providing chromatic characterization and high anatomic definition.
1. Alfano, et al. J Comput Assist Tomogr 1992; 16:634.

224 • 11:54 AM

MR Imaging in Wilson Disease

M Topcu, I Saatci, B Diren, FF Baltaoglu, G Kose, K Yalaz, Y Renda, A Besim
Hacettepe University Hospital, Ankara, Turkey

Purpose: Wilson disease is an uncommon disorder of copper metabolism characterized by abnormal deposition of copper, mostly in the liver and brain. In this report, the authors describe the MR imaging findings in the brain.
Methods: MR images of 13 patients were analyzed retrospectively, with respect to the presence of atrophy involving the basal ganglia, brain stem, and gray and white matter.
Results: Nine patients had diffuse or, less commonly, focal atrophy. Nine patients had involvement of the brain stem, including the typical "face of giant panda" appearance in tegmentum in 5 cases. In 2 patients, hyperintensity was noted in the region between the substantia nigra and red nucleus, although the "face of giant panda" appearance was not apparent. The authors believe that the "face of giant panda" appearance is seen in the severe cases. Therefore, the remaining ones may show this particular appearance in the course of the disease. In correlation with the literature, all patients with neurologic symptoms (10/13) showed symmetric signal abnormality in the basal ganglia. The putamen was particularly involved rather than the entire lentiform nucleus in all cases with basal ganglia involvement. The striking feature was the constancy of the concentric pattern recognized in the putamen and, if involved, in the thalami, which has not been mentioned before. Seven cases showed white matter and 4 cases gray matter abnormality.
Conclusion: Symmetric involvement of the putamen and less commonly the thalami in a concentric fashion and involvement of the tegmentum, which may or may not be associated with atrophy and gray and/or white matter involvement may suggest the diagnosis of Wilson disease.

Tuesday Morning • Plaza B
Papers 225–232

RAPID IMAGING TECHNIQUES II

MODERATORS: J Listerud, MD, PhD
SJ Riederer, PhD

225 • 10:30 AM

High-Performance Whole-Body Echo-Planar Imaging System at 1.5 T

FX Schmitt, G Borth, M Hagen, F Hilgermann, KH Ideler, P Wielopolski, B Edelman
Siemens Medical Systems, Erlangen, Germany

Purpose: High-speed MR imaging methods such as echo-planar imaging (EPI) have become increasingly important in the last few years. The authors have developed a prototype high-performance whole-body imager that takes advantage of this hardware and gives a large improvement also for conventional MR imaging.
Methods: The 3-axis EPI system is fully integrated into the Magnetom (Siemens Medical Systems, Erlangen, Germany) environment. There are 3 important components that make the system possible: (1) A low-inductance whole-body stimulation-optimized gradient coil is used. (2) The standard gradient amplifier is combined with a resonant power switch, allowing the generation of fast and high sine and trapezoidal-like gradient pulses. The maximum rise time Tr is determined by the resonant frequency $Tr \leq 1/4f$. (3) Data can be measured on gradient ramps, giving equidistant k-space sampling.
Results: Because the base frequency is software modulated, EPI sequences can be adjusted from 600 Hz to 1 kHz. Low bandwidth sequences give a field of view (FOV) ≤ 17 cm for 128^2 images. The high-speed gradient system is also used to gain very short TEs (eg, TE = 1.3 msec, TR = 2.8 msec, FOV = 35 cm and 256^2 matrix). Motion artifacts often seen in conventional images are eliminated. The enhanced performance of all 3 gradients permits free selection of oblique and double oblique orientations.
Conclusion: The combination of resonant and enhanced nonresonant gradient capabilities in this prototype system provides advantages for both fast and conventional MR imaging.

226 • 10:42 AM

Accurate Section-Selection Methods for Speeding Up FLASH MR Imaging

S Singh, WR Brody
Department of Radiology-MRI, Johns Hopkins University School of Medicine, Baltimore, MD

Purpose: A method (MRM 24, 391, 1992) for speeding up FLASH has been previously described. The method first uses projection presaturation (PP) to presaturate the volume outside the section of interest (SOI), then a train of rapid, hard pulses to acquire FLASH-SOI data. However, it is less suitable for short T1 values and moving objects. The methods proposed here alleviate these limitations.
Methods: (1) After 1D PP, a nonselective inversion pulse is applied and residual M_z of the outer volume is nulled, thus defining the SOI accurately, even in the presence of short T1 species. (2) Initially, the SOI itself is saturated (tip angle ≥ 90°) while leaving the remainder unperturbed. After nonselective inversion, the SOI defines the FLASH detection section while the outer volume nulls. (3) This method is similar to method 2 except inversion is performed prior to saturation. After the section selection (methods 1–3), FLASH MR imaging data can be acquired by using a hard pulse and a conventional k-space sampling scheme and completed within a time window selected about the null point. For in vivo cases, a spectral presaturation pulse is applied to saturate fat or water prior to FLASH MR imaging.
Results: Methods 1–3 were implemented on a 1.5-T GE Signa by using a 20-cm-diameter spherical phantom with T1 ~ 600 msec. With method 1 (6 pairs of sinc pulses of short saturation time of ~ 20 msec needed for moving objects), a 3-cm-thick SOI was isolated. The RF power was tuned to produce a null time of ~ 40 msec for a typical FLASH time of 80–100 ms. With methods 2 and 3 (saturation time ~ 5 msec, null time 379 msec), a thinner SOI (3.5 mm) with much sharper boundaries was isolated even when saturating a large exterior volume. For FLASH data acquisition, 4.7-T GE CSI hardware was used that allowed us to reduce TR to less than 2 msec for a 64 × 64 image with a field of view of 10 cm in phantoms as well as in vivo.
Conclusion: The proposed methods are suitable for short T1 values (subject to FLASH time) as well as moving objects.

227 • 10:54 AM

Versatility in a Quick Echo Split Imaging Technique: Multisection and Multiple Recalled Echoes

O Heid, M Deimling, B Kiefer, R Hausmann, W Huk
Haagstrasse 12, Erlangen, Germany

Purpose: Recently the authors presented a novel, ultrafast, quick-echo split imaging technique (QUEST) (1). The objective of current work is to improve the spatial resolution of single-shot versions of this imaging method and to demonstrate its multisection capability.
Methods: The basic QUEST sequence uses only N RF pulses to acquire $2 \times 3^{N-1}$ echoes without interecho gradient switching. The removal of 1 splitting pulse shortens the echo train by 2/3 but benefits in equalizing the echo amplitudes. Conversely, applying a single additional 180° RF refocusing pulse doubles the number of distinct echoes. A reduction in echo splitting thus can be compensated by repeated echo refocusing. Due to the small number of excitations, QUEST allows the use of section selective RF pulses and enables multisection imaging in a sequential mode. All measurements were performed on conventional Siemens Magnetom whole-body imagers operating at 1.0 and 1.5 T.
Results: Good results were achieved with $N = 3$ and $N = 4$ section selective splitting pulses. By using $N = 4$ excitations, a train of 54 equidistant signals with average strength 0.1 M_0 could be acquired. $N = 3$ pulses reduced the echo number to 18 and improved the average signal to 0.2 M_0. To raise the in-plane resolution to matrix sizes of up to 128 × 162, two- to eightfold additional recalling of the primary echo train was applied. The measurement times for a single section were in the 40–150-msec range, of which the sampling intervals covered up to 70%. Up to 22 sections could be acquired in 1 second.
Conclusion: By adding multisection and multiecho techniques to QUEST, the spatial resolution can be further improved with only a minor increase in imaging time. An extra parameter in manipulating image contrast is thereby introduced.

1. Heid O, Deimling M. 11th SMRM 1992, Book of abstracts 1:433.

228 • 11:06 AM

Improved T1-weighted MP-RAGE Liver Imaging by Shaping Signal Evolutions with Variable Flip Angles

FH Epstein, JP Mugler
Biomedical Engineering, University of Virginia, Charlottesville, VA

Purpose: Magnetization-prepared rapid gradient-echo (MP-RAGE) imaging with sequential phase encoding and low flip angle (10°), and with higher flip angle (30°), centric phase encoding, and dummy repetitions have been used for T1-weighted breath-hold liver examinations. The authors investigated shaping the MP-RAGE transient signal evolution with variable flip angles to increase liver signal-to-noise ratio (S/N) and liver-spleen signal difference-to-noise ratio (SD/N).
Methods: A theoretical algorithm was developed which derives flip angles that shape the MP-RAGE signal evolution. Magnetization preparation parameters that null the spleen were chosen, and the signal shaping algorithm was used to maximize the liver signal intensity at low spatial frequencies and cause it to decrease exponentially with increasing spatial frequency. Variable-flip-angle MP-RAGE was implemented in a segmented form (due to software constraints) on our imager (Siemens Magnetom 63SP). Breath-hold imaging with the 3 competing pulse sequences was performed in volunteers.
Results: Simulations indicated that our segmented variable-flip-angle sequence should provide 95% and 200% liver S/N increases, and 100% and 300% liver-spleen SD/N increases, compared with the 10° sequential and 30° centric MP-RAGE sequences, respectively. Measured values agreed closely with theoretical predictions. Theoretically, a single-shot implementation of the variable flip angle MP-RAGE sequence should lose only 10% in liver S/N compared with the 4-segment version.
Conclusion: Shaped signal evolutions provided greatly increased liver S/N and liver-spleen SD/N for breath-hold MP-RAGE imaging while maintaining strong T1-weighted contrast. This approach may potentially increase the clinical utility of MP-RAGE in the liver.

229 • 11:18 AM

Subsecond Neurocognitive Processes Measured by Integrating MR Imaging with High-Resolution Evoked Potentials

AS Gevins, J Le, B Reutter, N Martin, K Laxer
EEG Systems Laboratory and SAM Technology, San Francisco, CA

Purpose: Along with good spatial resolution, subsecond temporal resolution is needed to resolve the neural sequencing of elementary neurocognitive processes com-

prising behavior including preparatory attention, stimulus encoding, feature extraction, decision, response preparation, response execution, and so on. Evoked potentials (EPs) have the requisite temporal resolution and would seem to be an ideal complement to structural and functional MR imaging, but their heretofore poor spatial resolution has limited their utility because there is not sufficient spatial correspondence between modalities to unambiguously determine the relationship between a sequence of EP components and structures visualized with MR imaging. The authors have made progress toward overcoming this obstacle by improving the spatial resolution of the EP, registering it with anatomic information from a subject's MR images, and conducting several experiments that measured the temporal sequencing of subsecond neurocognitive processes.
Methods: EP spatial resolution has been improved by increasing the number of recording electrodes from the usual 19 to over 120, and by developing mathematical procedures that use each subject's MR images to create realistic finite element models of the head and brain to correct blur distortion produced by conduction of the EPs through the skull and other tissues. A subsecond image of superficial cortical neuronal activity is produced by registering the deblurred EPs with 3D models of the subject's cortex derived from her/his MR images.
Results: This procedure has been initially validated by comparison of computed cortical EPs with those directly measured in subdural recordings from epileptic patients. The procedure has been applied to visual, auditory, and somatosensory detection task data from 7 subjects and linguistic stimuli from 1 subject. In all cases, results are consistent with the known functional neuroanatomy of the cerebral cortex.
Conclusion: These results suggest that the combination of MR imaging and high-resolution EPs is a useful method for resolving subsecond neurocognitive processes and support the extension of the method to fast MR imaging.

230 • 11:30 AM

Imaging of Arterial Compliance with High-Resolution Cine MR Imaging

D Chien, D Saloner, G Laub, CM Anderson
Department of Radiology, University of California, San Francisco, VA Medical Center, San Francisco, CA

Purpose: A change in vessel compliance is known to be the cause and/or result of diseases such as aneurysm formation, coronary insufficiency, and hypertension. The goal of this study is to establish a noninvasive method based on MR imaging for measuring vessel distention, to determine arterial compliance.
Methods: High-resolution cine images were acquired, with electrocardiogram triggering with a 1.5-T Siemens whole-body system. The authors optimized the technique by comparing the signal-to-noise ratio obtained with different matrix size, field of view (FOV), and flip angle. After technique optimization, triggered images were acquired of the descending aorta in healthy volunteers. A gradient-echo sequence (40/8) with first order flow compensation was used (matrix = 512 × 256, FOV = 30 cm, thickness = 5 mm). A flip angle of 20° was chosen to avoid spin saturation of slow flow during diastole. Measurements were done at the level of the heart and in the lower abdomen. The change in lumen cross-sectional area and diameter was measured and plotted versus time.
Results: In healthy volunteers, a 10%–20% change in the lumen cross-sectional area was observed, which indicated vessel compliance in healthy arteries.
Conclusion: Vessel distention can be accurately quantified with MR imaging only after technique optimization. Intravoxel dephasing and saturation of slow flow at the blood-vessel wall interface can also produce a cyclical change in flow signal intensity that mimics a variation in lumen cross-sectional area. The authors have overcome these problems by using flow compensation, a small pixel size, and a small flip angle.

231 • 11:42 AM

Endogenous Contrast in Myocardium Caused by Deoxygenation of Blood during Apnea on Echo-Planar Images

MF Wendland, M Saeed, K Lauerma, A deCrespigny, ME Moseley, CB Higgins
Department of Radiology, University of California, San Francisco, CA

Purpose: Alterations in blood oxygen tension can be visualized by using high-speed, strongly T2*-weighted sequences. The current study was designed to determine whether deoxygenation of the blood during apnea causes decrease in T2* of left ventricular (LV) blood and myocardium on gradient-recalled echo-planar images.
Methods: Anesthetized rats ($n = 8$) were mechanically ventilated after tracheotomy, and the right carotid artery was cannulated for sampling of arterial blood. Gradient-refocused echo-planar images were acquired by using a GE Omega 2-T system in sets of 32 or 64 images with an approximate 5-second TR interval. Acquisition parameters were 8K data points acquired over 33 msec yielding an image matrix of 64 × 64 points and field of view of 50 × 50 mm. TE was 10 msec. Each animal was subjected to 2 periods of apnea of 45 and 90 seconds duration. Blood gases were analyzed and correlated with signal intensity changes.
Results: Apnea resulted in measurable declines in myocardial and blood pool signal intensities. No change was observed in skeletal muscle signal intensity. The major decline in signal occurred during the first 20–40 seconds, which was followed by more gradual decline in myocardial signal intensity. Increasing the duration of apnea to 90 seconds caused greater decline in oxygen tension and LV blood signal intensity but no further decline in myocardium. The magnitude of signal loss of blood was twofold greater than that in myocardium, suggesting that the potency of deoxyhemoglobin-dependent signal loss for blood is less than that for myocardium.
Conclusion: Deoxygenation of the blood during apnea causes decreased signal intensity in LV blood and myocardium on T2* sensitive echo-planar images. The alteration of vascular content of deoxyhemoglobin may provide a basis for detecting myocardial ischemia.

232 • 11:54 AM

Ultrashort TEs for Abdominal Imaging with a Whole-Body Echo-Planar Imaging System

PA Wielopolski, JP Finn, RR Edelman, F Schmitt
New England Deaconess Hospital, Boston, MA

Purpose: Breath-hold gradient-echo sequences are widely used for routine clinical imaging of the liver. However, artifact due to susceptibility gradients and chemical shift effects can degrade image quality in the upper abdomen and retroperitoneum. Also, single-shot TurboFLASH suffers from relaxation-time filtering due to long acquisition windows. The purpose of the present study was to determine whether ultrashort TEs can eliminate these unwanted side effects.
Methods: The authors implemented an ultrafast TurboFISP sequence with a TE of 1.3 msec by using a prototype 1.5-T, whole-body echo-planar imaging system (Siemens Medical Systems, Germany) in nonresonant mode. The minimum TR for the sequence was 2.8 msec with a bandwidth of 1,950 Hz per pixel, such that the acquisition window for a 128 × 256 image was 360 msec. A nonselec-

tive preinversion pulse was used to generate T1-based contrast, and a minimum field of view of 325 mm was employed for imaging the liver. Images were acquired in healthy volunteers in multiple planes with a variety of imaging matrices, inversion times, and flip angle schemes. ***Results:*** High-resolution images of the liver, pancreas, and kidneys with strong T1 weighting were obtained free of susceptibility, chemical shift, and motion artifact. ***Conclusion:*** Initial results suggest that this approach holds promise for high-contrast, high-resolution fast imaging of the abdomen, and clinical evaluation is in progress.

Tuesday Morning • Imperial Ballroom Papers 233–240

CONTRAST AGENT III: Experimental II

MODERATORS: TJ Brady, MD
RL Nunnally, PhD

233 • 10:30 AM

Tumor-specific MR Contrast Agents: Magnetite Nanoparticles Conjugated to an Antibody Directed against Carcinoembryonic Antigen

LX Tiefenauer, G Kühne, RY Andres
Paul Scherrer Institute, Villigen, Switzerland

Purpose: By using superparamagnetic particles (SMPs), contrast in MR imaging can be achieved at much lower doses than with gadolinium complexes. In addition, antibodies labeled with radioisotopes have been successfully used in the diagnosis of tumors. By combining the high efficiency of magnetite in generating image contrast with the high specificity of antibodies, tumor tissue may be detected at high resolution with MR imaging. ***Methods:*** Magnetite particles of uniform size (9.6 nm ± 0.8) are stabilized by a copolymer (PEKY) of glutamic acid, lysine, and tyrosine (6:3:1). High-affinity antibody molecules specific to carcinoembryonic antigen (CEA) were covalently bound through their hinge region to the cross-linked PEKY coat present on the surface of SMPs. The resulting conjugates have been characterized in vitro with respect to stability, physical properties, and biological activity, and in vivo by using nude mice bearing CEA tumors. ***Results:*** On average, a single magnetite crystal was stably conjugated to 1 antibody molecule. The relaxivity R2 was 305 L · mol^{-1} · sec^{-1}, the mean size as determined by size exclusion chromatography was about 30 nm, and the net charge was negative. The immobilized antibody molecules retained their full binding capacity as demonstrated by competition binding experiments. However, accumulation in tumor tissue was poor due to fast elimination from the circulation. ***Conclusion:*** The SMPs described fulfill the requirements of high relaxivity and binding capacity needed to detect tumor surface antigens. The negatively charged PEKY coat prevents aggregation of nanoparticles and provides a platform for covalent immobilization of antibody molecules and additional biomolecules needed to prevent opsonization and subsequent fast blood clearance.

234 • 10:42 AM

Gadolinium (III)-TPPS: A Novel MR Contrast Agent for Selective Enhancement of Experimental Rat Brain Tumors

K Bockhorst, K Kohno, T Els, M Hoehn-Berlage
Max-Planck-Institut für Neurologische Forschung, Köln, Germany

Purpose: In searching for new selective MR contrast agents, the relaxation changes induced by the synthetic metalporphyrin Gd-TPPS were investigated in experimental brain tumors of rat. ***Methods:*** Gd-TPPS was synthesized by complexation of gadolinium (III)-acetylacetonate with tetraphenylporphine sulfonate (TPPS). Brain tumors in rats were produced by inoculation of glioma cells. MR imaging was performed at 4.7 T before and at various times up to 2 days after intraperitoneal administration of 0.25 mmol/kg Gd-TPPS. T1 and T2 were measured simultaneously with a modified Carr-Purcell-Meiboom-Gill sequence (1). ***Results:*** Within 40 minutes after injection of Gd-TPPS, the tumors became hyperintense on T1-weighted images and hypointense on T2-weighted images. This effect persisted until the end of the observation period. After 2 days, the T1 of neoplastic tissue was reduced from 1,339 msec ± 187 to 635 msec ± 114 and T2 from 83 msec ± 6 to 57 msec ± 7. Outside the tumor, relaxation times were not altered. ***Conclusion:*** Contrast enhancement of tumors by Gd-TPPS is more rapid but persists as long as by Mn-TPPS (2). The shielding of the Gd-TPPS molecule by acetylacetonate is responsible for a reduced polarity, which may accelerate the resorption of the substance. The long contrast effect points to tight bindings between Gd-TPPS and tumor cells. Its strong effect on both relaxation times results in contrast enhancement of tumors on T1- *and* T2-weighted images.

1. Els M, et al (abstr). Soc Magn Reson Med 1991; 1214.
2. Wilmes LJ, et al. JMRI 1993; 1:5–12.

235 • 10:54 AM

Semiquantitative Evaluation of Reticuloendothelial System Activity in Experimental Hepatic Injury by Using Superparamagnetic Iron Particles

A Muehler, H Bauer, RC Brasch, HJ Weinmann
Schering AG, Berlin, Germany

Purpose: Superparamagnetic iron particles (SPIO) have been tested in models of hepatic injury, but quantification of reticuloendothelial system (RES) activity was felt to be problematic. The current study performed a semiquantitative analysis of RES function by comparing MR images before and after administration of SPIO. ***Methods:*** Two models of hepatic injury were investigated in rats: (1) single liver x irradiation, and (2) rat liver transplant with and without presence of rejection. MR imaging was performed on a 2-T GE CSI unit by using mixed-weighted sequences (850/25–30). The liver signal intensity was standardized to a corn oil phantom. A dose of 10 μmol Fe/kg SPIO was administered intravenously. A semiquantitative measure (ΔR) of hepatic iron content was derived from the evolution of transverse magnetization during the pulse sequence, resulting in the following equation: $\Delta R = R2 \times c = -\ln (SI_{post}/SI_{pre})/TE$. Relative RES activity in hepatic injury was calculated as percentage of $\Delta R_{disease}/\Delta R_{normal}$. ***Results:*** The MR signal intensity of normal livers was effectively reduced with injection of SPIO. Whereas in rejecting liver transplants and in acute irradiation injury, the efficacy of SPIO was markedly decreased, signal intensities of nonrejecting liver grafts could be effectively influenced with SPIO. By using our mathematical model, the

RES activities were calculated to be 96% in nonrejecting and 60% in rejecting liver grafts, and only 31% in hepatic irradiation injury.
Conclusion: The same approach as described above was used for semiquantitative analysis of tissue concentration changes during first-pass experiments using susceptibility agents. The parameter ΔR was shown to be proportional to the actual concentration of the contrast agent. The authors could successfully apply this method to SPIO for evaluation of functional parameters, like RES activity. MR imaging with cell type-directed contrast agents may provide functional information.

A. Muehler is an employee of Schering AG.

236 • 11:06 AM

Dynamics of Tumor MR Imaging with Blood-Pool Contrast Agents

TS Desser, DL Rubin, M Neuder, HH Muller, SW Young, DL Ladd*, JL Toner*, RA Snow*

*Department of Radiology, Stanford University, *Sterling-Winthrop Pharmaceuticals Research Division, Sterling-Winthrop, Inc, Stanford, CA*

Purpose: To evaluate gadolinium-based polymers of five different molecular weights as MR contrast agents for imaging of rabbit thigh tumor models, compared with Gd-DTPA.
Methods: V2 carcinoma cells were implanted in thigh tissues of 26 normal New Zealand white rabbits. Imaging was performed 9–12 days after implantation, when the tumors had reached approximately 1–2 cm in diameter. MR imaging (SE 300/15, 1.5 T) was performed prior to contrast agent injection, and 1, 15, 30, and 60 minutes and 24 hours after injection of 0.1 mmol/kg of five Gd-based polymers ranging in molecular weight from 12,000 to 24,800 d, as well as Gd-DTPA. Signal intensities of tumor and muscle were measured and tumor-muscle percent contrast was calculated as $[(SI_{tumor} - SI_{muscle})/SI_{muscle}] \times 100$ for the various time points.
Results: Peak tumor-muscle contrast was seen on progressively later images up to 60 minutes as molecular weight increased, compared with a peak on the 1-minute image with Gd-DTPA. At all but the 1-minute time point, tumor-muscle contrast was greater with the Gd-based polymers than with Gd-DTPA. Significant contrast remained on the 24-hour images with the polymeric agents.
Conclusion: Gd-based polymers provide excellent tumor-tissue contrast in a rabbit thigh tumor model without the need for dynamic MR imaging to optimize imaging with low-molecular-weight agents. Larger-molecular-weight polymers provide peak contrast at later time points than do smaller agents.

237 • 11:18 AM

Superparamagnetic Contrast Agents: Predicting Signal Loss in Gradient-Echo Imaging

MF Boada, EM Haacke

Case Western Reserve University, Cleveland, OH

Purpose: It is well known that signal attenuation in gradient echo (GRE) imaging is related to magnetic field inhomogeneities present over each pixel. Owing to their high susceptibility, superparamagnetic particles (spp), such as ferrite particles, can be used as a means of increasing contrast by taking advantage of their effects on GRE images. The authors' goal is to be able to predict the dephasing effects associated with the use of spp for GRE imaging.
Methods: The simplest approach is to model local field inhomogeneities by a distribution of noninteracting dipoles (the spp). The authors' model takes this 1 step further by accounting for field changes induced by many interacting particles. Specifically, a sphere of susceptibility χ_s is placed in the center of a string of equidistant dipoles that represent the fields associated with the surrounding particles. An expression for the local field ΔB is obtained by solving the Laplace equation for the scalar potential and applying the appropriate boundary conditions. A numerical evaluation of the imaging equation was performed over the pixel by using the expression for ΔB obtained with both the noninteracting and interacting models. Signal intensity was calculated as a function of TE, concentration, and particle magnetization. GRE experiments were performed with gels at 1.5 T to observe the signal loss due to the presence of the spp. Agar-gel mixtures were prepared with different concentrations of the AMI-25. Signal loss was obtained as a function of TE for 6 different concentrations from 0.006 mg Fe/mL to 0.015 mg Fe/mL.
Results: For concentrations below 0.002 mg Fe/mL, both models closely predicted signal loss values. The noninteracting model overestimated the amount of dephasing for concentrations above 0.002 mg Fe/mL and TEs longer that 10 msec. Above this limit, the interacting model better reproduced the experimental results.
Conclusion: The interacting model better reproduces the behavior of signal loss as a function of TE for high concentrations for which interaction is expected. Further improvements to this model will be possible by considering the full 3D problem.

238 • 11:30 AM

Inversion Recovery and Driven-Equilibrium Fast GRASS Imaging for Detection of First Pass of T1 and Susceptibility Contrast Media through Canine Heart

MF Wendland, W Chew, H Sakuma, M Saeed, K Lauerma, N Derugin, CB Higgins

Department of Radiology, University of California, San Francisco, CA

Purpose: To dynamically monitor the first-pass effects of T1 and susceptibility contrast media on canine heart by using inversion recovery (IR) and driven-equilibrium (DE) prepared fast GRASS imaging, respectively.
Methods: Healthy beagles (n = 5) were repeatedly studied in a protocol that entailed measurement of transit of 0.05 mmol/kg gadodiamide injection (Sanofi Winthrop, NY; Nycomed, Oslo; Salutar Inc, Calif) by using IR fast GRASS imaging with the initial inversion pulse section selective (n = 8). Later, Dy-DTPA-BMA (Sanofi Winthrop, NY; Nycomed, Oslo; Salutar Inc., Calif) was injected as a bolus at doses of 0.2 (n = 7) and 0.4 mmol/kg (n = 4) and monitored with DE fast GRASS. All experiments were conducted on a GE Signa 1.5-T system with a quadrature head resonator and the FPRCARD sequence. For IR fast GRASS, TI was 425–500 msec to nullify the myocardial signal, and the tip angle was 5°. For DE fast GRASS, the TE of the preparation period was 40 msec, and the tip angle was 12°. In all cases, TE was 4.2 msec, TR was 9.4 msec, data matrix was 128 × 256, field of view was 24 cm, and electrocardiogram-gated images were repeated every 2–3 seconds.
Results: On IR fast GRASS images, gadodiamide injection caused marked enhancement of normal myocardium (from 6% ± 3 of blood intensity to 42% ± 5) at the peak of the bolus, followed by slow clearance. With a selective inversion pulse, blood signal intensity did not change during bolus passage. On DE fast GRASS, Dy-DTPA-BMA caused signal loss in chamber blood to 34% ± 6 and 15% ± 3 of baseline after 0.2 and 0.4 mmol/kg doses, respectively, and in myocardium signal intensity decreased to 74% ± 6 and 56% ± 6 of baseline, respectively, at the peak of the bolus. While clearance from the blood was rapid (6–8 seconds), clearance from the myocardium was slow.
Conclusion: Both T1- and susceptibility-weighted fast GRASS sequences can be used to monitor first-pass dy-

namics of contrast media through the heart. This method may be useful for characterizing myocardial ischemia.

239 • 11:42 AM

Synthesis and Characterization of Memsomes: Liposomes Bearing Membrane-Bound Paramagnetic Complexes

D Shen, EC Unger, R Ramaswami*, TA Fritz, GL Wu*, P Rodgers

*Department of Radiology/MRI, University of Arizona, and *ImaRx Pharmaceutical Corporation, Tucson, AZ*

Purpose: These studies focus on the elemental and physiochemical analysis of memsomes, small unilamellar liposomes incorporating a new class of alkylated complexes in the membrane bilayer. These agents show great promise as hepatic MR contrast agents with favorable toxicity and pharmacologic profiles.

Methods: Preparation of Mn-EDTA-DDP is initiated by adding decylamine to glycidol in methanol, yielding 3 decylamino-2-hydroxy-propane, which is reacted with EDTA dianhydride in dried methanol forming EDTA-DDP. EDTA-DDP is then reacted with MnCo$_3$ to obtain Mn-EDTA-DDP. Routine structural verification was done with infrared and MR spectroscopy. Memsomes are prepared from a 1:3 mol/L ratio of Mn-EDTA-DDP to lipid and sized with microfluidizer. Size of liposomes is measured with quasielastic light scattering verified with cryotransmission electron microscopy. Manganese concentration was determined with a modified spectrophotometric assay. Phospholipid concentration was determined with modified Stewart assay. Additionally, samples prepared by this method were exposed to autoclave cycles (121°C, 32 psi) for 15, 30, and 60 minutes and recharacterized. Relaxivity of Mn-EDTA-DDP memsomes was measured at U.S. Tesla.

Results: Elemental analysis verified infrared and MR spectrophotometric analysis of the alkyl complexes. Particle characterization shows that unilamellar liposomes of uniform size (30–40 nm) can be routinely produced with microfluidics. Additionally, memsomes are stable in size and manganese content to autoclave cycles up to 30 minutes. Relaxivity of memsomes is very high with $R1 = 37.4 \pm 1.1$ and $R2 = 53.2 \pm 0.2$ per millimole manganese (sec^{-1}).

Conclusion: Current research in this area is focused at more formal structural elucidation of the alkylated compounds as well as extensive shelf-life stability studies. Those results show great promise for this agent in future clinical settings.

The authors are stockholders of ImaR$_x$ Pharmaceuticals.

240 • 11:54 AM

Mn-EDTA-DDP Liposomes: Preclinical Imaging Study of Efficacy in a Liver Tumor Model

EC Unger, TA Fritz, B Kulik, D Shen, GL Wu*

*Department of Radiology/MRI, University of Arizona, and *ImaRx Pharmaceutical Corporation, Tucson, AZ*

Purpose: To test the imaging efficacy of a new liver MR contrast agent, Mn-EDTA-DDP liposomes (memsomes), in a rat tumor model.

Methods: Fisher 344 rats were implanted with C5 epithelioid carcinoma (1×10^6 cells per milliliter) in the liver. Fourteen days after implantation, the animals were imaged before and after administration of contrast medium with a 1.5-T GE Signa unit, with TR/TE of 250/12, 3-mm section thickness with 1-mm gap, 8 acquisitions, 256 × 192 matrix, and a 16-cm field of view with a QD knee coil. After undergoing precontrast imaging, the animals were injected via tail vein with memsomes at doses of 1, 2.5, 5.0, 7.5, 10.0, 12.5, and 15.0 μmol/kg Mn^{+2} ($n = 5$ per dose, 35 rats total). MR images were obtained before administration of contrast medium, and 6, 15, 22, and 30 minutes after administration of contrast medium. Signal intensities of liver, tumor, heart, muscle, renal cortex, renal pelvis, noise, and standard deviation of noise were measured.

Results: Memsomes cause specific enhancement of liver with no significant increase in signal intensity of tumor, heart, muscle, renal cortex, or renal pelvis. Significant liver enhancement and improvements in liver/tumor contrast occur at doses of 1.0 μmol/kg manganese and higher, with maximal enhancement at 12.5 μmol/kg manganese.

Conclusion: Manganese memsomes appear to be liver-specific imaging agents. The absence of any appreciable enhancement of the other tissues is noteworthy. When comparing manganese memsomes with other MR liver imaging contrast agents, it appears that memsomes cause more hepatic enhancement per micromole of paramagnetic ion than other liver agents, either chelates or iron oxide particles.

E.C. Unger is president and chief executive officer of ImaR$_x$ Pharmaceuticals.

Tuesday Afternoon • California Room Papers 241–248

SPECTROSCOPY I: Human

MODERATORS: PA Narayana, PhD
RR Price, PhD

---

241 • 3:45 PM

Localized H-1 MR Spectroscopy for Noninvasive Differentiation of Cerebral Tumors

TJ Vogl, A Jassoy, C Becker, A Dadashi, C Hamburger, R Sauter, J Lissner

Department of Radiology, University of Munich, Munich, Germany

Purpose: To analyze the correlation between proton spectroscopy, histology, and MR imaging for evaluating vascularization and metabolic state of metastasis and gliomas.

Methods: Forty-two patients (17 men and 25 women) with different cerebral tumors were examined. Histologic sections were obtained in all patients except 1. The tumor masses included meningiomas ($n = 14$), gliomas grade I or II ($n = 11$), gliomas grade III or IV ($n = 10$), and metastasis ($n = 7$). MR imaging and MR spectroscopy were performed on a whole-body 1.5-T Magnetom (Siemens, Erlangen, Germany) by using a head coil with circular polarization. An MR examination was additionally done in all patients before and after administration of Gd-DTPA before spectroscopy. During spectroscopy, the tumor mass was localized three-dimensionally with a gradient-echo FLASH sequence. A volume of interest (VOI) varying in size from 8 to 16 cm^3 was localized. H-1 MR spectroscopy was performed by using SE sequences with TEs of 135 and 270 msec. Additionally, the stimulated echo sequence with water selective presaturation (TE = 20 msec) was used.

Results: The detected metabolites of the proton spectra of 20 volunteers and 42 patients were choline (Cho) at 3.2 ppm, phosphocreatine/creatine (PCr/Cr) at 3.0 ppm, *N*-acetylasparate (NAA) at 2.0 ppm, and lactate (Lac) at 1.3 ppm. In comparison with the spectra of healthy control subjects, the H-1 MR spectra of gliomas showed some common features including the reduction of the NAA/Cho ratio (0.6) and the Cr/Cho ratio (0.51). Depending on the histologic grading of gliomas, the group 1 (gliomas I and II) ($n = 11$) showed normal ratios for Ins/Cho, while group 2 (gliomas III and IV) ($n = 10$) had significantly ele-

vated ratios (0.21). In all metastatic tumors, the spectra contained reduced signal intensities from Cr/PCr and NAA resonances but exhibited strong contributions from Cho-containing compounds and from mobile free fatty acids. (NAA/Cho ratio: 0.44; Cr/Cho ratio: 0.23.) In all meningiomas (n = 14), H-1 spectroscopy revealed tumorous changes. H-1 MR spectra were mainly characterized by a reduction of the Cr/Cho and NAA/Cho ratios.
Conclusion: The results of this study confirm that all tumor spectra were remarkably different from spectra of normal brain tissue. Increased saturated fatty acid concentrations were observed in all metastatic lesions. Localized proton MR spectroscopy is a valuable aid in the differential diagnosis of human brain tumors when combined with MR imaging.

242 • 3:57 PM

Image-guided Brain Proton MR Spectroscopy of Pediatric Patients with Hereditary Peroxisomal Disorders

AA Tzika, DB Vigneron, RS Dunn, WS Ball
Children's Hospital Medical Center, University of Cincinnati, Cincinnati, OH

Purpose: Single-voxel, localized proton MR spectroscopy was performed to assess brain lesions identified with MR imaging in pediatric patients clinically diagnosed with hereditary peroxisomal defects.
Methods: Twenty male subjects were studied: 6 (age range, 7–18 years) with X-linked adrenoleukodystrophy (ALD), 2 newborns with Zellweger syndrome, and 12 age-matched healthy volunteers. Single voxel (1.7–8.0 cm^3) proton MR spectra were acquired with either short-echo (TE = 18 msec) stimulated echoes and/or long-echo (TE = 270 msec) spin echoes on a 1.5-T GE Signa imager.
Results: Four ALD patients with neurologic symptoms and hyperintense lesions on T2-weighted MR images exhibited proton MR spectra with 80%–90% reduced *N*-acetylaspartate (NAA), increased levels of glutamate/glutamine (Glx) and inositols (Inls), a small lactate peak, and normal creatine. Two ALD subjects, without neurologic deterioration, showed MR images or MR spectroscopy images similar to those of age-matched healthy volunteers. The Zellweger newborns showed low NAA in white matter and elevation of mobile lipids and Glx metabolites. Significantly reduced NAA, a neuronal marker, indicates loss of neurons, while normal creatine suggests presence of viable cells, maybe glia. Increased Glx and Inls metabolites may be due to accumulation of excitatory neurotransmitters and intermediates in the extracellular space, thus signaling neurotransmitter neurotoxicity suggested to occur in neurodegeneration. The findings are supported by the biochemical and histopathologic defects caused by defective peroxisomal function.
Conclusion: Proton MR spectroscopy is both technically feasible and complementary to MR imaging. Its applications for therapeutic monitoring of peroxisomal disorders appear promising.

243 • 4:09 PM

H-1 Chemical Shift Imaging and MR Spectroscopy of Brain Tumors

S Naruse, S Furuya, M Ide, Y Horikawa, C Tanaka, T Higuchi, M Umeda, S Ueda, T Maeda
Department of Radiology and Neurosurgery, Kyoto Prefectural University of Medicine, Kyoto, Japan

Purpose: It is essential to reveal the specific changes in brain metabolism by H-1 chemical shift imaging (CSI) and MR spectroscopy. The purpose of this study was to clarify the metabolic changes in brain tumors with H-1 CSI and MR spectroscopy and to make use of them for the diagnosis of tumors.
Methods: The subjects were 48 patients with brain tumors. The system used was Magnetom H15 and Gyroscan S15 (1.5 T). H-1 CSI was performed by applying 2-directional phase encoding in a field of view in which the volume of interest was selected by using an SE method with water suppression. The metabolite mapping was done with the curve-fitted area. Some tumors to which H-1 CSI could not be applied, such as pontine glioma, were examined with single-voxel MR spectroscopy.
Results: In the tumor, the increase of choline, the decrease of *N*-acetylaspartate and the increase of lactate were clearly observed in both spectra and metabolite mapping. The increase of choline is the key issue for diagnosing the extent of the tumor. The malignant tumors (eg, metastatic tumors) showed more increase in lactate than did benign ones. The amount of lactate indicates the grade of malignancy. In some cases of glioblastoma, high peaks of glycine and succinate could be detected. Those substances are specific metabolites in glioma and, therefore, may help indicate the specificity of brain tumors.
Conclusion: H-1 CSI and MR spectroscopy are useful for observing the specific changes in the metabolism of brain tumors, for differentiating tumor from other diseases, and for determining the grade of malignancy.

244 • 4:21 PM

Clinical MR Spectroscopy of the Brain with Single-Voxel Techniques: Volunteer Baseline Study

R Sauter
Siemens AG, Erlangen, Germany

Purpose: To provide statistically relevant data of proton brain spectra from healthy volunteers for a clinical trial of proton MR spectroscopy of the brain in which standardized MR spectroscopy protocols were applied to different pathologies.
Methods: Thirty-seven institutions in Europe, North America, and Japan participated in this clinical trial. During phase I, each participating institution was asked to perform 6 volunteer examinations. For each volunteer, 2 spectra had to be acquired, representing an 8 mL volume-of-interest located in the occipital lobe and in the caput nuclei caudati, respectively. A double SE (1,600/135) technique was used. In total, 202 volunteers have been examined (age range, 18–80 years; mean and standard deviation, 31 years ± 10). Relative peak areas of *N*-acetylaspartate (NAA), choline (Cho), and creatine (Cr) have been determined (a) by manual spectral integration at the specific institution where the spectra were acquired. Results, including spectra and MR images used for localization, have been sent to the organizing site. At the organizing site, each data set has been carefully reviewed with respect to correct voxel position and acceptable spectral quality. Spectra fulfilling the criteria have been reevaluated based on the original digital data (b) by manual spectral integration performed by 1 individual and (c) by automated postprocessing performed independently at a different site by using an algorithm based on the Wigner distribution.
Results: On the basis of the evaluation performed by the participants (a), the spectra fulfilling the authors' criteria yielded the following metabolite ratios (mean values and standard deviations): NAA/Cho 2.75 ± 0.61 (n = 125) for the occipital lobe (2.06 ± 0.81 [n = 96] for the caput nuclei caudati), NAA/Cr 2.20 ± 0.42 (1.98 ± .80), and Cho/Cr 0.82 ± 0.16 (0.98 ± 0.19), respectively. Independent manual postprocessing (b) resulted in similar ratios and reduced standard deviations: NAA/Cho 2.61 ± 0.55 (n = 96) (1.82 ± 0.49 [n = 72]), NAA/Cr 2.12 ± 0.37 (1.72 ± 0.37), and Cho/Cr 0.84 ± 0.17 (0.98 ± 0.19). Provisional results of the automated postprocessing

(c) are consistent: NAA/Cho 2.69 ± 0.39 (n = 39) (2.12 ± 0.40 [n = 37]), NAA/Cr 2.09 ± 0.26 (1.79 ± 0.33), and Cho/Cr 0.79 ± 0.12 (0.86 ± 0.16).
Conclusion: Single-voxel proton spectroscopy is a robust technique well suited for providing reliable data on cerebral metabolism by using clinical MR imagers. The 2 cerebral regions evaluated in this study reveal significant differences in metabolite ratios, making these baseline studies a prerequisite for any application of MR spectroscopy to patients.
R. Sauter is an employee of Siemens AG.

245 • 4:33 PM

In Vivo Proton Spectroscopy of the Brain in Patients with Parkinson Disease

RE Block, BC Bowen, J Sanchez-Ramos, D Lampman, J Murdoch
Mount Sinai Medical Center, Miami Beach, FL

Purpose: Recent postmortem studies of the brains from patients with Parkinson disease (PD), as well as in vitro studies of both an animal model and human tissues, demonstrate a mitochondrial complex I deficiency. It is the goal of this project to determine if elevated levels of lactate, presumably resulting from a complex I deficiency, and any other spectral abnormalities can be detected in vivo.
Methods: Both healthy controls and patients with PD have been studied by using a Picker 1.5-T imager. The MESA program for water-suppressed proton spectra from single voxels was used with a TE of 270 msec and 320–640 acquisitions. The relative intensities of spectral lines from the metabolites were determined by means of a computer fit.
Results: Occipital lobe data are emphasized here because this region gave much better quality spectral data than the basal ganglia. In preliminary studies, data from 13 patients with PD and 5 healthy subjects were analyzed. The spectral region around lactate may also contain contributions from lipids and compounds such as alanine or threonine. The ratio of the intensity of the lactate region signals to that of N-acetylaspartate (NAA) was typically on the order of 0.04 for healthy subjects, generally increasing with the presence of Parkinson disease and dementia to an average age of 0.2 for severely demented patients with PD. In addition, a statistically significant difference was found in the average NAA-to-choline signal intensity ratio for PD female versus PD male patients (9.1 ± 2.3 versus 5.4 ± 2.3, respectively, with P = .02) and mixed healthy controls (3.9 ± 0.4, with P = .002).
Conclusion: Proton spectral data may yield new information on the progression of dementia and gender differences in PD.

246 • 4:45 PM

H-1 Chemical Shift Imaging and MR Spectroscopy of Patients with Alzheimer Disease

M Ide, S Naruse, S Furuya, T Maeda, Y Veda, K Nakajima
Department of Radiology, Kyoto Prefectural University of Medicine, Kyoto, Japan

Purpose: Alzheimer disease (AD) is 1 of the most common types of senile dementia, but it is difficult to diagnose AD in the early stage. The purpose of this study is to observe the characteristic changes of AD in H-1 chemical shift imaging (CSI) and MR spectroscopy and to examine the advantage of H-1 CSI and MR spectroscopy for diagnosing AD.
Methods: Twenty-five cases of AD were studied with a 1.5-T magnet (Magnetom H15). H-1 CSI was performed by applying 2-directional phase encoding in a field of view in which the volume of interest was selected by using an SE method with water suppression. The metabolite mapping was done with the curve-fitted area. Single-voxel spectra were obtained from temporal and parietooccipital lobes by using the SE method.
Results: Low concentrations of N-acetylaspartate (NAA) were observed in a wide area of cerebrum in patients with AD compared with healthy volunteers. NAA decreased more in temporal gray matter than other white matter. This regional heterogeneity could be obtained only with the H-1 CSI method. Decrease of NAA in patients with AD was detected in the early stage. Since NAA is contained in neurons, decrease of that metabolite indicates the loss of neurons in this area specifically. These data imply the essential pathophysiologic change in AD.
Conclusion: Decrease of NAA in temporal gray matter is a specific finding of AD in the early stage; conventional MR imaging and CT do not show any significant changes. H-1 CSI is one of the most useful modalities for making the early diagnosis of AD and for evaluating this disease.

247 • 4:57 PM

Increased Cerebral Choline in Alzheimer Disease Supports Theory of Membrane Defect

DJ Meyerhoff, S MacKay, N Grossman, D Norman, G Fein, MW Weiner
Department of Veterans Affairs Medical Center, University of California, San Francisco, CA

Purpose: Recent findings of increased glycerophosphocholine and decreased N-acetylaspartate (NAA) in extracts of Alzheimer diseased (AD) brains are consistent with increased membrane phospholipid degradation and neuron loss, respectively. The purpose of this study was to determine if these in vitro results can be confirmed with in vivo H-1 MR spectroscopy of patients with AD.
Methods: Five patients with AD (mean age, 74 years ± 8), 9 elderly controls (mean age, 74 years ± 5), and 6 young controls (mean age, 32 years ± 10) were studied with neuropsychologic tests (MMSE, NCSE), standard MR imaging, and H-1 MR spectroscopy. H-1 MR spectroscopy used a preselected PRESS volume of a 17-mm-thick section positioned above the ventricles. Distribution maps of N-acetyl-containing metabolites (primarily NAA), choline-containing metabolites (Cho), and creatine-containing metabolites (Cr) were analyzed, and spectral information was extracted from 2.5 mL voxels of white matter and mesial gray matter.
Results: Statistically significant differences between H-1 metabolites from patients with AD compared with elderly controls were observed only in the posterior parietal brain region: Cho/NAA was increased from 0.35 to 0.53 in cortical voxels (P = .009) and from 0.38 to 0.47 in white matter voxels (P = .03), while Cr/NAA was not significantly increased. Cortical Cho/Cr was significantly increased from 0.88 to 1.21 in patients with AD (P = .0004). Elderly controls showed trends to higher Cho/NAA and Cr/NAA relative to young controls.
Conclusion: These results are consistent with in vitro findings of increased glycerophosphocholine and decreased NAA in AD brains. They support in vitro findings of neuron loss in AD brains and give in vivo evidence of a membrane defect in AD brains.

248 • 5:09 PM

Neuron Loss in Human Immunodeficiency Virus Infection with Cognitive Impairment Suggested by H-1 MR Spectroscopy

DJ Meyerhoff, S MacKay, W Dillon, G Fein, MW Weiner
University of California, San Francisco; Department of Veterans Affairs Medical Center, San Francisco, CA

Purpose: To determine if neuropathologic findings of neuron loss in human immunodeficiency virus (HIV)-infected brains can be confirmed with in vivo measurements

of brain N-acetylaspartate (NAA) in cognitively impaired HIV-positive individuals.
Methods: Study 1: 14 HIV-positive men, 7 HIV-negative controls; study 2: 21 HIV-positive men, 10 HIV-negative male controls. Opportunistic infections and neoplasms were excluded in both studies. Cognition was tested prior to standard brain MR imaging and H-1 MR spectroscopy. H-1 spectra (voxel size: 2.5 mL) were obtained from a 17-mm-thick PRESS volume positioned at the level of the centrum semiovale. The distribution of N-acetyl-containing metabolites (mostly NAA), choline (Cho), and creatine (Cr) were analyzed in gray and white matter regions, and H-1 metabolite ratios and clinical and cognitive correlates were examined.
Results: Study 2 replicated the findings of study 1; this abstract presents pooled data: (1) approximately 20% of HIV-infected individuals had abnormal MR images (not different from the control population); (2) 14% reductions in both NAA/Cho (P = .002) and NAA/Cr (P = .001) and 12% reduction in NAA signal integrals (P = .03) throughout white and gray matter in cognitively impaired HIV-positive individuals, with no significant group by location differences; (3) nonsignificant correlation between cognitive impairment and H-1 metabolite ratios; (4) trend toward reduced metabolite ratios in asymptomatic HIV-positive subjects; (5) significant negative correlations between age and NAA/Cho and age and NAA/Cr.
Conclusion: These results are consistent with neuropathologic findings of neuron loss and suggest neuron loss and/or damage in cognitively impaired HIV-infected individuals not detected with other neuroimaging modalities.

Tuesday Afternoon • Franciscan A
Papers 249–256

PELVIS

MODERATORS: RC Smith, MD
JC Weinreb, MD

249 • 3:45 PM

Dynamic Susceptibility Contrast-enhanced MR Imaging of Human Renal Transplants

T Vestring, I Braun-Anhalt, S Maurer, G Bongartz, E Rummeny, KH Dietl, S Heidenreich, B Buchholz, PE Peters
Institut für Klinische Radiologie, Westfälische Wilhelms-Universität, Münster, Germany

Purpose: Dynamic MR imaging may be useful in monitoring function of renal transplants in animals (1). The purpose of this study was to evaluate Gd-DTPA–induced susceptibility effects in the renal medulla to analyze the function of human renal transplants.
Methods: Eighty-three human renal transplants were examined at 1.5 T. Sixty-eight transplants showed impaired function due to acute rejection (n = 45), acute tubular necrosis (n = 8), chronic rejection (n = 6), cyclosporin A nephrotoxicity (n = 3), and cortical necrosis (n = 6). Fifteen transplants were normal. The diagnosis was confirmed with biopsy (n = 57), transplant nephrectomy (n = 6), or clinical course (n = 20). Dynamic MR imaging (1.5 T, spoiled FLASH: 30/12, 40) was performed with serial imaging in the same coronal plane every 10 seconds up to 5 minutes after an intravenous bolus of 0.1 mmol/kg Gd-DTPA. The relative change of signal intensity ($RSI = SI_{post} - SI_{pre}/SI_{pre}$) in the cortex and medulla was calculated over time.
Results: In all transplants with creatinine clearance greater than 40 mL/min (n = 15), medullary RSI_{max} was followed by a drop in signal intensity within 20–30 seconds, indicating the susceptibility effects of the concentrated Gd-DTPA in the renal tubules. A delayed drop in signal intensity was noted in cases with creatinine clearance between 20 and 40 mL/min (n = 19) and no drop in cases with creatinine clearance less than 20 mL/min (n = 49). All cases with cortical necrosis showed no cortical enhancement. All other transplants displayed a cortical enhancement, but no substantial differences in cortical RSI_{max}, medullary RSI_{max}, and slope of cortical and medullary enhancement could be found in these cases.
Conclusion: In human renal transplants, dynamic MR imaging provides a sensitive means of diagnosing cortical necrosis and semiquantitative monitoring of the concentrating ability.

1. Frank JA, et al. SMRM abstr 1992; 1:121.

250 • 3:57 PM

Correlation of Endorectal Coil MR Imaging, Transrectal US, and Needle Biopsy of Prostatic Carcinoma

LP Cheung, GM Roth, VGM McDermott, MD Schnall
Department of Radiology, Hospital of the University of Pennsylvania, Philadelphia, PA

Purpose: The authors correlated the appearance of the prostate gland on endorectal surface coil MR imaging in patients with histologically proved adenocarcinoma with the results of their biopsies. Transrectal US findings were also correlated.
Methods: To date, data from 114 patients who underwent both MR imaging and needle biopsy have been analyzed. The results of diagnostic transrectal US and/or US biopsy guidance were obtained in 103 of these patients. The results of these studies were reviewed, and locations of the abnormalities were recorded.
Results: MR imaging abnormalities suggestive of malignancy were found in 107 of the 114 cases (94%) analyzed so far; of these, 103 (96%) involved the side of the gland that yielded the positive biopsy result. MR imaging depicted bilateral peripheral zone abnormalities in 28 of the 41 cases with bilaterally positive biopsy results (68%). Of the 4 cases in which MR imaging suggested a unilateral lesion contralateral to the side on which the positive biopsy result was obtained, 2 subsequently underwent radical prostatectomy, which revealed bilateral disease. For comparison, US was abnormal in 84 of 103 patients (82%); of these, 74 abnormalities (88%) were on the same side as that with the positive biopsy results. US depicted bilateral abnormalities in 15 of the 39 cases with bilaterally positive biopsy results (38%).
Conclusion: Endorectal surface coil MR imaging of the prostate gland is superior to transrectal US for detecting the side or sides containing adenocarcinoma in patients with histologically proved disease.

251 • 4:09 PM

Comparison of Conventional and 3-Point Dixon Fast Spin-Echo Imaging of the Pelvis

KC Li, SE Carlsen, H Nghiem, FG Sommer, R Herfkens, RB Jeffrey, J Fredrickson
Department of Radiology, Stanford University Medical Center, Stanford, CA

Purpose: To compare conventional fast spin-echo (SE) with fat-saturation SE (FSE) and 3-point Dixon fast SE (D-FSE) in imaging of the pelvis.
Methods: Fifteen patients undergoing pelvic MR imaging were evaluated with FSE (4,000/102, 256 × 192 matrix, 2 NEX, fat saturation) and D-FSE (4,000/104, 256 × 192 matrix, 2.7 NEX equivalent) at identical image locations, on a 1.5-T GE Signa imager. Ten patients had gynecologic malignancies, and 5 had prostate cancer. The FSE and

D-FSE images were independently compared for fat suppression, anatomic detail, image quality, and lesion detectability by 3 independent radiologists.
Results: Fat suppression on the D-FSE images was superior to that on the FSE images. The anatomic details and outlines of the pelvic organs were also better delineated on the D-FSE images, leading to more accurate staging in a case of cervical carcinoma. Minor problems encountered with the D-FSE technique included poor fat and water separation posterior to the air-filled rectum in 2 patients and exaggerated motion artifacts from vessels and peristaltic bowel loops.
Conclusion: Compared with FSE images, D-FSE images provide more uniform fat suppression and better anatomic details and have great potential in increasing accuracy of staging pelvic neoplasms.

252 • 4:21 PM

MR Imaging Characterization of Hemorrhagic Adnexal Masses: Blinded Reader Study

EK Outwater, ML Schiebler, RS Owen, MD Schnall
Department of Radiology, Thomas Jefferson University Hospital, Philadelphia, PA

Purpose: A high degree of accuracy for the MR imaging diagnosis of endometrioma has been reported. The purpose of this investigation was to test the performance of 3 blinded observers for the characterization of hemorrhagic adnexal masses as either endometriomas or other adnexal masses.
Methods: A total of 74 pathologically documented lesions in 46 patients were studied by using a 1.5-T MR system with conventional T1-weighted and either T2-weighted SE or fast SE sequences. The 3 readers scored each lesion for the presence of each of several published criteria for the diagnosis of endometrioma.
Results: A mean sensitivity of 0.68 and specificity of 0.83 (accuracy 76%) for the diagnosis of endometrioma was found for the criterion of a high-signal-intensity cyst on short TR/TE images that also showed relative hypointensity on long TR/TE images. Ancillary findings such as low-signal-intensity rims, adhesions, bowel tethering, and implants were found to lack accuracy and showed low interobserver agreement. Receiver operator characteristic curve analysis of the performance of the 3 radiologists showed similar area measurements (A_z) of 0.80, 0.75, 0.73 for the diagnosis of endometrioma.
Conclusion: In this series, MR imaging had only moderate accuracy in distinguishing endometriomas from other hemorrhagic adnexal masses.

253 • 4:33 PM

Use of T1- and T2-weighted Fast Gradient-Echo Imaging and Gd-DTPA in the MR Imaging Diagnosis of Benign and Malignant Lesions of the Penis

KC Seelos, M Vahlensieck, A Heuck, K Klocke, M Reiser
Department of Radiology, University of Bonn, Bonn, Germany

Purpose: To evaluate T1- and T2-weighted fast gradient-echo sequences (FFE) with multiple single-section (MSS) acquisition for imaging of penile anatomy and pathology.
Methods: Five healthy men were studied to determine optimal FFE parameters. Eleven patients were studied at 0.5 T (T5, Philips). They had various focal lesions such as penile and urethral carcinoma, penile metastases from rectal carcinoma, and intracorporeal fibrosis. TR/TE and flip angle were 330/11 and 60° for T1 and 720/25 and 20° for T2 weighting. Contiguous 6-mm sections with a field of view of 18 cm and 176 × 256 matrix were obtained by using a flexible circular surface coil. Gd-DTPA was given at a dose of 0.1 mmol/kg body weight.
Results: Adequate T1 and T2 weighting could be achieved with only minor motion artifacts and high signal-to-noise ratios. Excellent delineation of the 3 corpora and especially of the tunica albuginea and central cavernous artery was achieved, including the attachment of the bulb of the penis to the urogenital diaphragm. In any section direction, the number of contiguous sections could be chosen with a proportional increase in acquisition time. Gd-DTPA stayed within the cavernous spaces for a long time, leading to a prominent enhancement of the corpora on T1-weighted images and thereby increasing contrast between lesion and normal cavernous spaces.
Conclusion: FFE techniques are well suited for high-resolution MR imaging of the penis with excellent T1 and T2 contrast. The MSS acquisition mode substantially decreases imaging time with a freely adjustable number of contiguous sections. Cavernous enhancement on postcontrast T1-weighted images clearly improves lesion conspicuity.

254 • 4:45 PM

Patterns of Normal Pelvic Marrow in Adults

CD Levine, ME Schweitzer, DG Mitchell
Department of Radiology, University of Medicine and Dentistry of New Jersey, Newark, NJ

Purpose: Normal pelvic bone marrow can have a highly variable appearance, even at times mimicking neoplastic disease. The authors evaluated patterns of bone marrow to provide an aid in interpreting these studies.
Methods: In 97 patients with carcinoma, T1-weighted SE images were retrospectively examined for the location, distribution, signal characteristics, and appearance of marrow. Eighty-two patients did not and 15 patients did have osseous metastases (negative and positive bone scans). In 55 of 82 patients without metastatic disease, T2-weighted sequences were also available.
Results: Hematopoietic islands appeared as islands (< 2 cm) in 41%, masses (> 2 cm) in 23%, and grossly intermixed elements in 36%. In 98% (77/79) of patients with hematopoietic islands, a focus of fatty marrow was noted centrally. One hundred fifty lesions were identified in the group of patients with proved metastases, none of which had a central focus of fat. The total percentage of hematopoietic marrow was less than 15% (28% of patients), 15%–40% (52%), 40%–65% (12%), or 65%–85% (7%). The margins were sharp in 40% and ill defined in 60%. Appearance was universally symmetrical. Periarticular residual hematopoietic marrow predominated in the sacroiliac joints (72%) but was less common in the vertebral end plates (32%), hip joints (30%), and symphysis pubis (22%). In all patients, hematopoietic marrow remained more intense than fatty marrow on T2-weighted images.
Conclusion: Hematopoietic marrow predominates in the sacroiliac region, is always symmetric, remains more intense than fat on T2-weighted images, and usually has a central focus of fat. These morphologic characteristics may aid in differentiating foci of red marrow from metastases.

255 • 4:57 PM

MR Imaging in the Diagnosis of Fistulas

GE Myhr, G Nilsen, PA Rinck, JE Thoresen, HE Myrvold
MR-Center, University Hospital, Trondheim, Norway

Purpose: The imaging evaluation of fistulas and abscesses in the perirectal and perianal region has been based on fistulography, CT, and transrectal US. The value of MR imaging has been recognized during the last few years. The purpose of this study has been to evaluate MR fistulography by using saline as a contrast agent in patients with fistulas and/or abscesses in the perineal region.

Methods: Eleven patients with fistulas underwent 14 examinations on a Philips S15 imager (1.5 T) with multisection SE techniques (460–595/20–30 and 2,000–2,550/ 20–30, 80–100). T2-weighted images were obtained before the instillation of 2–30 mL of saline into the fistulas through a thin tube. Transverse, coronal, and/or sagittal sections were obtained after the saline instillation. Three patients underwent a follow-up examination. Four patients had no secretion at the time of examination; they were examined without saline.
Results: Fistulous tracts were found in 10 patients, fluid-containing cavities in 7. The full extent of fistulas and fluid collections and their relation to important anatomic structures such as sphincters, hollow viscera, and the supralevator and infralevator compartments were better delineated after saline instillation. Collapsed parts of the fistulous system were expanded with the saline. T2-weighted images were sufficient for diagnosis.
Conclusion: MR fistulography with instillation of saline improves the delineation of fistulas and abscesses and their relation to normal anatomic structures. The high signal intensity of the saline on T2-weighted images gives excellent contrast against adjacent muscle and fat.

256 • 5:09 PM

Bull's-eyes and Halos: Useful MR Imaging Discriminators of Osseous Metastases

ME Schweitzer, CD Levine, DG Mitchell
Department of Radiology, Thomas Jefferson University Hospital, Philadelphia, PA

Purpose: One frequent indication for MR imaging is for staging of malignancies, especially prostate cancer. Although MR imaging has been proved accurate for local staging, evaluation of osseous lesions has been limited by frequent false-positive interpretations. The authors evaluated 2 signs—the "bull's-eye" and "halo" signs—in the hope of providing a more specific means for evaluating focal pelvic marrow lesions. The bull's-eye sign was defined as an area of high signal intensity within a focal region of low signal intensity on T1-weighted images. This was considered a negative predictor of metastases and was presumed to represent a focus of hematopoetic marrow. The halo sign consisted of a high-signal-intensity rim around a lower-signal-intensity lesion on T2-weighted images, corresponding in location to focal areas of decreased signal intensity on T1-weighted images.
Methods: One hundred seventy-eight pelvic bone lesions in 25 patients were evaluated at 1.5 T. These lesions included 59 control lesions (islands of hematopoetic marrow) in 13 patients without metastases as shown by negative bone scans. One hundred eighteen lesions were evaluated in 12 patients with proved metastic disease.
Results: The sensitivity of the bull's-eye was 99%, specificity 93%, and accuracy 96.5% for identifying foci of hematopoetic marrow. Only 1 control lesion occurred without a bull's-eye. Four metastatic foci had a false-positive bull's-eye sign. The sensitivity of the halo sign was 57%, specificity 88%, and accuracy 60% as a predictor of a metastatic focus. When patients with a positive bull's-eye and a negative halo were studied, there was a 94% accuracy for predicting absence of skeletal metastases.
Conclusion: The bull's-eye was both sensitive and specific in excluding metastases, with only 1 normal lesion in nearly 200 lacking this sign. The halo, although less sensitive, was a highly specific identifier of metastases. Use of both of these signs led to only 1 incorrect diagnosis and should be helpful in clinical use.

Tuesday Afternoon • Franciscan B
Papers 257–264

HEAD AND NECK II

MODERATORS: WP Dillon, MD
RB Lufkin, MD

257 • 3:45 PM

Echo-Planar MR Imaging Perfusion Study of the Microvascular Characteristics of Cavernous Angiomas

JV Hunter, R Crowell, GJ Hunter, H Aronen, T Campbell, BR Rosen
Department of Radiology, Division of Neuroradiology, Massachusetts General Hospital, Boston, MA

Purpose: To investigate and characterize the MR imaging functional anatomy of cavernoma (a pure intracerebral venous malformation) (1) as an indicator of prognosis and lesion extent.
Methods: T2-weighted (1,000/65), axial echo-planar imaging was performed starting immediately before and continuing for up to 8 minutes after an intravenous injection of 0.2 mmol/kg Gd-DTPA.
Results: Passage of contrast material was revealed by the expected T2 susceptibility change in both normal brain and the lesion. After a smaller initial drop, the lesion then exhibited a progressive increase in signal intensity, presumably due to T1 factors. This rise was not seen in normal brain. In the penumbra of the lesion, the T2 response was attenuated, with no T1 effect demonstrated.
Conclusion: The T2 patterns seen in normal brain are well characterized (2). In the penumbra of the lesion, hemoglobin breakdown products reduce the signal intensity baseline but do not alter the T2 susceptibility changes. One explanation for the observed signal changes in the cavernoma is a partial breakdown of the blood-brain barrier, resulting in progressive extravascular trapping of gadolinium and, hence, a T1 effect. An alternative is that even with an intact blood-brain barrier the chaotically interconnected, large venous lakes have such a slow transit time of blood that they act as a pseudoextravascular space and generate a significant T1 signal change over time.
1. Lasjaunias P, Berenstein A. Surg Neuro-angiography 1990; 3:248. 2. Rosen BR, Belliveau JW, Chien D. Magn Reson Q 1989; 5:263–281.

258 • 3:57 PM

Fast SE Sequences in the Evaluation of Head and Neck Tumors

R Bruening, M Naegele, K Seelos, A Heuck, V Kunze, M Reiser
Department of Radiology, University of Bonn, Bonn, Germany

Purpose: Evaluation of the diagnostic value and image quality of the fast (turbo) T2-weighted SE sequences in comparison to the standard T2-weighted sequence in patients with head and neck carcinomas.
Methods: Twenty patients were examined on a 0.5-T system (T5, Philips). The imaging was performed in the axial plane, identical sections obtained with conventional CSE (1,800/20, 90, acquisition time 7:45 minutes, 1 average) and fast (FSE) imaging (3,000/91–120, acquisition time 3:59 minutes, 6 averages). Section thickness was 5–6 mm. All images were interpreted by 5 radiologists in a blinded manner. A subjective rating was applied for grading of anatomic display, contrast of normal tissue, delineation of tumor and lymph nodes, and an overall rating (score 1–5): grade 1, nondiagnostic imaging; grade 5, optimal image quality.

Results: The delineation of the tumors was graded equally sufficient (2.08/2.08) for both sequences. The FSE was graded superior in anatomic display (3.83/3.11) and in the contrast of normal tissue (3.69/3.30). The visualization of lymph nodes was slightly better with the FSE (1.77/1.53). The subjective total rating favored the new fast SE technique (3.62/2.97), as the contrast behavior, artifacts, and the signal-to-noise ratio were summarized. The staging was limited by the concept of the study. The tumor volumes were overestimated in 4% of cases with FSE, as with CSE. An exact staging was possible in 24% with FSE and in 20% with CSE. Volume was underestimated in 17% with both sequences. No tumor staging was possible in 9% with CSE and in 5% with FSE.
Conclusion: These results indicate that for reduced imaging time and superior image quality FSE sequences will replace conventional T2-weighted imaging in head and neck imaging.

259 • 4:09 PM

Does Magnetization Transfer Contrast Result in Improved Delineation of Tumors of the Head and Neck?

AR Gillams, N Fuliehan, S Tilak, G Grillone,
J Schreibstein, A Carter
Boston University and The Imaging Foundation, Boston, MA

Purpose: Conventional MR imaging in head and neck tumors is often disappointing. Magnetization transfer contrast (MTC), a new form of MR imaging contrast, has been shown to provide improved lesion conspicuity in liver, breast, and brain. MTC is generated by probing the efficiency of the water/macromolecule interactions of different tissues. Off-resonance RF irradiation produces macromolecular saturation that is transferred to water protons via chemical exchange and/or dipolar interaction. The result is the attenuation of signal in tissues rich in macromolecules and, hence, potentially increased lesion conspicuity. Use of MTC and Gd-DTPA produces synergic enhancement.
Methods: Fifteen patients with tumors of the head and neck underwent MR imaging on a 0.1-T resistive system (Mega 4, Instrumentarium, Finland). Standard SE sequences were performed both with and without MTC, before and after intravenous administration of gadolinium. Off-resonance irradiation parameters used were amplitude, 0.125–0.25 G; duration, 50–100 msec; and frequency offset, 4–6 kHz. The maximum specific absorption rate was within FDA guidelines.
Results: Two radiologists evaluated the images independently and without knowledge of prior results. The lesion/background contrast was measured with and without MTC.
Conclusion: MTC has the potential to significantly improve contrast and thus delineation of tumors of the head and neck.

260 • 4:21 PM

Receive-Only Surface Coil for High-Resolution Orbital Imaging: Evaluation of Choroidal Lesions

EW Brown, H Cheng, K Lashkari, K Lee, K Kwong,
A Weber, R Gonzalez, T Brady
Department of Radiology, Massachusetts Eye and Ear Infirmary, Harvard Medical School, Boston, MA

Purpose: To characterize and examine small choroidal lesions with a receive-only, small-diameter surface coil.
Methods: Images were obtained on a 1.5-T system. A 3.6-cm surface coil with an 8-mm field of view, 256 × 256 (or 192) matrix, and a section thickness of 3 mm were used to produce an in-plane resolution of 0.31 × 0.31 (or 0.42) mm. Intravenous Gd-DTPA (0.1 mmol/kg) enhancement and fat-suppressed sequences were employed. Twenty-six patients with histories of choroidal lesions were examined. Nonenhanced examinations were initially performed in 13 patients. Clinical diagnosis of melanoma or nevus was based on findings from US and flourescein angiography. US was used to measure lesion thickness. Dimensional measurement software was used to determine lesion thickness on MR images.
Results: Detailed, high-resolution images of the globes were obtained. Thirteen patients were examined without the use of intravenous contrast material. They were divided into 3 groups: (1) amelanotic melanomas ($n = 2$), (2) pigmented nevi ($n = 2$), and (3) pigmented melanomas ($n = 9$). In each group, 50% of the patients showed T1 hyperintensity, suggesting that this feature is not correlated with the melanin content of these lesions as has been previously suggested. In the 26 patients who received contrast material, there was marked enhancement of all but 1 of the melanomas ($n = 15$). The only nonenhancing melanoma was an unusual melanoma of the iris. In contrast, none of the nevi ($n = 7$) showed any significant enhancement. Choroidal angiomas ($n = 2$) showed no enhancement, while both hemangiomas ($n = 2$) showed enhancement. Lesions as small as 1.2 mm were detected.
Conclusion: The authors obtained striking high-resolution images of ocular structures with their method. Because of the small diameter of the coil, they were able to obtain a marked increase in signal to noise when compared with conventional coils. On noncontrast studies, approximately 50% of the lesions showed hyperintensity, suggesting that this feature may not correlate with the presence of melanin. The preliminary results also suggest that it may be possible to differentiate pigmented nevi from choroidal melanomas based on Gd-DTPA enhancement. This may represent a significant contribution to the diagnosis of ocular melanoma.

261 • 4:33 PM

MR Imaging of the Temporomandibular Joint in Patients Treated with Orthotic Devices

MB Esposito, JA Arrington, FR Murtagh, ML Silbiger,
R Garcia
University of South Florida, Tampa, FL

Purpose: MR imaging was used to evaluate the temporomandibular joint (TMJ) in patients with orthotic devices. The information is used to assess the efficacy of treatment and to guide the orthodontist in adjusting the device.
Methods: Thirty patients who were being treated with orthotic devices for anterior subluxation of the meniscus of the TMJ were evaluated with MR imaging. Bilateral TMJ MR imaging was performed simultaneously by using coupled 3-inch surface coils on a 1.5-T GE unit. The MR imaging protocol included T1-weighted SE images (600/30), which were obtained in the sagittal plane in the closed-mouth position both with and without the orthotic device in place. A total of 60 TMJs (30 patients) were imaged.
Results: The goal of the orthotic device is to place the mandibular condyle more anteriorly in the joint space and therefore place the condyle on the posterior band of the meniscus and reduce the subluxation. In addition to facilitating diagnosis and demonstrating the degree of anterior displacement of the meniscus, MR imaging clearly demonstrated the degree of reduction achieved with the orthotic device.
Conclusion: MR imaging can be used to evaluate the TMJ in patients with orthotic devices. The orthodontist is then able to use the information in making further adjustments to the orthotic device.

262 • 4:45 PM

MR Imaging of the Temporomandibular Joint in Patients with Cervical Whiplash

MB Esposito, JA Arrington, R Garcia, FR Murthagh, ML Silbiger
University of South Florida, Tampa, FL

Purpose: The frequency of temporomandibular joint (TMJ) injury in patients with whiplash injury was evaluated with MR imaging.

Methods: Fifty-two patients (mean age, 35 years) with cervical whiplash were evaluated for TMJ injury with MR imaging. Bilateral TMJ MR imaging was performed simultaneously by using coupled 3-inch surface coils on a 1.5-T superconducting magnet. The protocol included T1-weighted SE images (600/30) in closed- and open-mouth positions as well as closed-mouth coronal images. Proton density- and T2-weighted SE images (2,000/30, 80) were also obtained in the sagittal plane in the closed-mouth position. A standard bite block was used for the open-mouth images. The TMJ MR images were evaluated for meniscal displacement, reduction of dislocation, joint effusion, and inflammatory changes in the retrodiscal tissues as well as degenerative changes of the meniscus and bone joint.

Results: A total of 52 patients or 104 TMJs were imaged. The series shows an extremely high percentage of pathologic TMJs in patients who have suffered cervical whiplash injuries. Approximately 97% had either significant anterior displacement or a joint effusion. Approximately 70% had both anterior displacement of the meniscus and a joint effusion.

Conclusion: A high percentage of patients with cervical whiplash injury have associated TMJ injury.

263 • 4:57 PM

MR Imaging of the Temporomandibular Joint: Disk Injury and Mandibular Fracture

T Watabe, HY Mizuno, H Mizuno, M Adachi, A Heshiki, S Takaku, T Sano, M Yoshida
Saitama Medical School, Saitama, Japan

Purpose: Evaluation of MR imaging disk changes encountered in mandibular fracture.

Methods: By using a 1.5-T superconducting unit (Magnetom H15 SP) and surface coil, 2-mm sagittal or coronal images of the temporomandibular joint (TMJ) were acquired with fast imaging with steady precession (FISP) 2D or 3D acquisition (30/12, 40° flip angle). With cine MR imaging using FISP 2D, functional anatomy of the TMJ was evaluated. T1-weighted SE images (300–500/15–20) were also acquired in some patients for comparison. Ten patients with history of mandibular fracture due to traffic accidents entered the study.

Results: Of the 10 patients, 4 had multiple fractures. FISP 3D images revealed increased signal intensity of the disk in 40%. The disk displacement was accompanied by condylar fracture with or without change in signal intensity. The fluid collection adjacent to the disk was also well demonstrated with FISP. The disk intensity change was related to the time interval of MR imaging after an accident.

Conclusion: FISP 2D and/or 3D MR imaging reflected well the pathologic change of the disk due to temporomandibular fracture. Increased disk intensity in 3D FISP was the most common finding and was related most strongly to condylar fracture.

264 • 5:09 PM

MR Imaging of Choroidal Hemorrhage and Retinal Detachment

JP Williams, KL Gupta
Department of Radiology, Tulane University Medical Center, New Orleans, LA

Purpose: To determine the sensitivity of MR imaging evaluation of choroidal hemorrhage and retinal detachment in comparison with clinical and US evaluation.

Methods: One hundred fifty-four orbital and intraocular tumors were evaluated with and without gadolinium enhancement by using 1.5-T Signa GE MR imager, and the results compared with those of US and clinical evaluation.

Results: Fifty-four cases of choroidal hemorrhage and retinal detachment were detected. All cases that were detected with US were detected with MR imaging and were differentiated.

Conclusion: Both US and MR imaging with enhanced and nonenhanced techniques were found to be equally sensitive in detecting choroidal hemorrhage, retinal detachment, and tumor. MR imaging signal characteristics are sufficiently different to differentiate these 3 entities accurately.

Tuesday Afternoon • Plaza A
Papers 265–272

ANGIOGRAPHY TECHNIQUES II

MODERATORS: EM Haacke, PhD
BD Pressman, MD

---

265 • 3:45 PM

3D Time-of-Flight MR Angiography with Variable Echo Time for Fat Reduction

W Lin, EM Haacke
Department of Radiology, MRI, University Hospitals of Cleveland, Cleveland, OH

Purpose: To obtain good flow compensation in 3D TOF MR angiography, a very short field echo is needed. Consequently, high signal intensity from background tissue usually results. Although an MTC pulse can be used to suppress signal from brain parenchyma, it has no effect on fatty tissue. The authors address a robust fat reduction method that is free from static field effects, requires no extra data acquisition time, and maintains good flow compensation.

Methods: A 3D FISP sequence with velocity compensation along the frequency and section-select directions was used for all 10 volunteer studies. The TEs used were 5.1 and 6.75 msec. The gradient field echo structures for both TEs are kept the same. The above 2 TEs are combined as follows: the shorter TE (5.1 msec) was used to acquire the high k-space portion, and the longer TE (6.75 msec) was used to collect the central k-space portion of the partition encoding. The ratio of the number of lines (RNL) with TE = 5.1 msec versus TE = 6.75 msec was varied to optimize the combinations of the 2 TEs. An MTC pulse was used with a bandwidth/duration/offset of 250 Hz/8.192 msec/2 kHz. Signal intensity was measured and compared in the regions of the internal carotid artery (ICA), orbital fat, and brain parenchyma. The lumen definition of the ICA in the syphon region was evaluated as a criterion to justify the degree of flow compensation with different RNLs.

Results: Signal dropout was seen in some cases in the regions of the ICA when a TE = 6.75 msec sequence was used but not in other regions. With RNL = 20/12, the variable echo time (VARIETE) sequence gave good fat signal suppression while maintaining good flow compensation

and better lumen definition when compared with the TE = 6.75 msec sequence.
Conclusion: By using a VARIETE sequence with MTC pulses, the authors were able to suppress signal from brain parenchyma and fatty tissue while maintaining good flow compensation.

266 • 3:57 PM

Retrospective Registration of X-ray Angiograms with MR Angiographic Data

N Alperin, DN Levin, R Grzeszczuk, J Prager
Department of Radiology, University of Chicago Hospitals, Chicago, IL

Purpose: To achieve retrospective registration of x-ray angiograms with volumetric MR angiographic data. Then, the 3D information in the MR angiographic data can be combined with the x-ray angiographic data, which have superior spatial and temporal resolution.
Methods: A vessel-tracking technique was used to identify the centerlines of the same "landmark" vessels on an x-ray angiogram and on a maximum-intensity projection (MIP) image of the MR angiographic data. The MIP representation of the vessel was backprojected to locate the MR angiographic voxels. These voxels were projected onto the x-ray angiogram by using an MR angiographic or x-ray angiographic perspective transformation that was interactively "steered" until the projected MR angiographic voxels and the x-ray angiographic landmark vessel were nearly congruent. The MR angiographic or x-ray angiographic transformation was then automatically adjusted by the computer until the incongruity was minimized. The authors studied an MR head phantom containing branching tubular structures ("vessels") as well as punctate structures that were visible on both MR and radiographic images. The tubular landmarks were used to achieve retrospective registration of a volume of MR imaging data with a radiograph of the phantom. The method is now being applied to MR angiographic and x-ray angiographic data from patients.
Results: The retrospectively derived transformation led to accurate projection of the phantom's punctate landmarks from the MR imaging volume onto the radiograph, thereby verifying successful registration of the 2 examinations.
Conclusion: Vascular structures, visible on both x-ray and MR angiograms, can be used to achieve fiducial-less registration of x-ray angiographic data with MR angiographic data. This makes it practical to produce multimodality displays of the complementary information in x-ray angiography, MR angiography, and associated MR imaging studies.

267 • 4:09 PM

3D Fourier Velocity-resolved Imaging with a 4-Point Acquisition and Complex-Difference Processing

JA Polzin, FR Korosec, DM Weber, CA Mistretta, PA Turski
Magnetic Resonance Imaging Center, University of Wisconsin, Madison, WI

Purpose: Diagnosis and treatment of some vascular diseases, such as arteriovenous malformations, can be made with greater certainty if the amount of blood flowing at various velocities is known. Fourier velocity-resolved imaging techniques provide this information. The authors have developed a 3D velocity-resolved imaging (3DVRI) technique that employs subtraction to enhance image quality and yield additional information.
Methods: The 3DVRI technique was implemented on a GE Medical Systems 1.5-T imager by using a modified 3D phase-contrast sequence. Modifications included eliminating the section-encoding gradient, stepping through *N* velocity-encoding gradients, and changing the TE throughout acquisition so that it was a minimum at each step. Three data sets were collected, each sensitive to flow along a different axis. A fourth data set having no velocity sensitivity also was collected and subtracted from the flow sensitive data sets. A 3D Fourier transform was then performed to yield velocity-resolved images.
Results: *N* images were constructed from each of the subtracted data sets, each representing the density of spins in a particular velocity range. The stationary tissue signal intensity was effectively eliminated, thereby preventing it from interfering with signal intensity on the images representing low velocities. As a result of having used a 4-point acquisition method and complex-difference processing, an image representing the density of all moving spins appeared on the central image of each set. The use of the minimum TE for each set of velocity-encoding gradients resulted in reduced vessel signal dropout.
Conclusion: This technique provides quantitative information over a large range of velocities. In addition, it separates the signal intensity from flowing spins into different images depending on their velocity, with no interfering signal intensity from stationary tissues. These images can then be viewed individually, or images can be combined to aid in the diagnosis and treatment of various vascular diseases.

268 • 4:21 PM

Renal Venous Flow Visualization with Breath-Hold Segmented K-Space Cine Bolus Tracking

DJ Atkinson, LM Teresi, DM Murakami, NR Bucciarelli, WJ Mullin, SR Kapelov, WG Bradley, Jr
Memorial Magnetic Resonance Center, Long Beach Memorial Medical Center, Long Beach, CA

Purpose: Current renal arterial MR angiographic techniques have had limited success due to prolonged acquisition times, distal flow saturation, pulsatile motion, and, in some cases, the presence of multiple polar arteries or multiple nonfocal stenoses (eg, fibromuscular dysplasia). Visualization of flow in the renal veins offers an attractive alternative to arterial flow in that flow is nonpulsatile and is typically confined to a single, larger vessel. However, problems of slow flow and spin saturation have limited these venous studies to date. To overcome these issues, the authors used a bolus tracking pulse to identify renal venous flow.
Methods: Their method was tested in 5 healthy volunteers and 6 patients with angiographically proved stenosis of the renal artery. The method consisted of a series of breath-hold images with a modified segmented k-space approach and bolus tracking. Sections were 5 mm with a 1-mm overlap, with a 128 × 256 matrix along a paracoronal plane. TR/TE was 11/6, with a flip angle of 20°. The acquisition was on end-expiration and lasted 17 seconds. A standard 2D time-of-flight (TOF) MR angiogram was also obtained for comparison.
Results: The imaging time was well tolerated by all patients. Visualization of renal venous flow was observed in all cases. Unlike with typical TOF MR angiography, high-intensity perirenal fat was not a problem because these images represented flow as a displacement of a low-intensity bolus against a midintensity background.
Conclusion: This breath-hold TOF method is attractive compared with other phase methods in that it is conceptually simpler and faster to acquire. Compared with the pulsatile renal arterial flow assessment, tracking venous velocity is significantly easier and faster. By using this ve-

nous velocity with measured cross-sectional area, calculation of total renal blood flow is possible.
D.J. Atkinson is an employee of Siemens Medical Systems.

269 • 4:33 PM

Improved ICV MR Angiography: Variable Flip Angle Excitation and Magnetization Transfer Suppression with 512 Matrices

DJ Atkinson, M Brant-Zawadzki, GD Gillan
Siemens Medical Systems, Irvine, CA

Purpose: Time of flight (TOF) MR angiography, while gaining acceptance as an ICV screening modality, has been restricted by 3 effects: limited flow-to-background contrast, saturation of flowing spin signals, and limited spatial resolution. To overcome these limitations, the authors implemented a new technique with two sequence modifications. An additional RF pulse was inserted to suppress background brain signal intensity. This magnetization transfer suppression (MTS) pulse reduced brain signal intensity with minimal effect on flowing blood. To avoid flowing spin saturation, they replaced the standard slab excitation with an RF pulse that varies the flip angle over the imaging slab. Given the improved flow contrast, they were able to employ small-FOV, 512 matrices with conventional maximum-intensity projection postprocessing.
Methods: These modifications were implemented on a conventional Siemens 63 SP by using a standard flow-compensated sequence. TR/TE was 42/7. Sixty-four partitions at 1.0 mm each were used. Variable flip angle (TONE) RF pulses varied the slab excitation linearly from 10° to 30° (1:3) and from 13° to 26° (1:2), with a nominal flip angle at the center of the slab of 20°. The MTS pulse was applied 1.5 kHz off resonance with a bandwidth of 250 Hz. The imaging field of view was 20 cm with an acquisition matrix of 192 × 512. All images were obtained under existing IRB guidelines. Six healthy volunteers and 6 patients with known ICV abnormalities were examined.
Results: The inclusion of MTS suppressed the background and revealed greater vessel detail compared with the standard technique. Similarly, the TONE pulses demonstrated better vessel-to-background contrast on the more distal vessels. Combined, the images showed improved vessel detail and better visualization of 3rd order branches. In 1 case of vasculitis, focal areas of flow disturbance were more accurately delineated. The 512 imaging was greatly improved with the MTS/TONE compared with the standard method.
Conclusion: 3D MTS/TONE has the potential to enhance the quality of all MR angiographic examinations. While useful when used with existing protocols, this combination may have its role in making higher-resolution matrices more widely accessible.
D.J. Atkinson is an employee of Siemens Medical Systems.

270 • 4:45 PM

Comparison of Phase-Contrast and Time-of-Flight Methods for Producing Volume MR Angiograms at Low Field Strengths

DM Kramer, N Hylton, H Chen, A Li, JD Hale, L Kaufman
Radiologic Imaging Laboratory, University of California, South San Francisco, CA

Purpose: To produce 3D volume MR angiograms by using the 2 most accepted methods in the literature and to evaluate the relative strengths and weaknesses for low magnetic field strength application in the head and neck.
Methods: By using a 0.064-T permanent magnet system, MR angiography sequences were adapted to form 3D time of flight (TOF) and phase-contrast (PC) images of the carotid bifurcations and the circle of Willis in healthy volunteers. The TOF sequence was a series of thin-slab 3D acquisitions (16 × 1 mm) with 50% overlap of adjacent slabs. In-plane resolution was 0.7 mm in each axis and the TR/TE and flip angle were 65/16 and 90°. The PC sequence was 4 iterations of TR/TE, flip angle of 60/18, 35° with flow compensation (first order) and flow encoding along each axis. The 4 acquisitions were interleaved to minimize patient motion artifacts in the phase subtraction. Contrast and signal-to-background ratios were compared. The same volunteers were imaged multiple times to check reproducibility.
Results: The results show that PC is preferable to TOF at low field strength. This is especially true for smaller vessels with slow velocities. A signal-to-background ratio of 4:1 was achieved in the middle cerebral artery, for example.
Conclusion: The authors have demonstrated that reproducible MR angiograms can be obtained at 0.064 T. By using PC 3D methods, the image quality was significantly better than that of TOF. This is explained by 2 contributing effects. The very short T1 values of most of the stationary tissues reduces the available contrast and requires high flip angles, which limits the penetration of unsaturated blood into the image volume for TOF sequences. The relative absence of motion artifacts at low field strength helps preserve the quality of the phase subtractions.
D.M. Kramer and A. Li are employees of Toshiba America MRI, Inc. D.M. Kramer, N. Hylton, H. Chen, J.D. Hale, and L. Kaufman had research supported in part by Toshiba America MRI, Inc.

271 • 4:57 PM

3D Phase-Contrast Angiography of the Carotid Arteries at 0.064 T

NM Hylton, A Li, DM Kramer, L Kaufman, H Chen
Magnetic Resonance Science Center, University of California, San Francisco, CA

Purpose: As with conventional MR imaging, the performance of MR angiography must be optimized for the field strength of operation. The authors have explored phase-contrast (PC) methods because of the greater immunity to motion demonstrated at low field strengths. A 3D-PC angiographic technique has been optimized for operation at 0.064 T and applied to imaging of the carotid arteries.
Methods: One flow-compensated (FC) acquisition and 3 flow-encoded (FE) acquisitions along each of the orthogonal axes were acquired in an interleaved fashion within a 3D gradient-echo sequence. A TR/TE and flip angle of 60/15 and 35° were used and FE gradients were adjusted for a maximum velocity of 50 cm/sec along each axis. Thirty-two coronal partitions of 3.0-mm thickness and 0.95 × 1.1-mm in-plane resolution were acquired in 20 minutes. Phase reconstructions were performed for each of the 4 components, incorporating a phase correction scheme to remove background distortions. A phase image was constructed by taking the vector sum of the differences between each FE component and the FC component. Multiplication by the magnitude reconstruction of the FC component resulted in the final PC image. Vessel anatomy was displayed by using maximum-intensity projections of the 3D data set from variable angles.
Results: PC images of the carotid arteries were produced with a view extending from the circle of Willis to 2 inches above the aortic arch. Sagittal projections clearly indicate the carotid bifurcations.
Conclusion: 3D angiographic images of the carotid arteries at 0.064 T have been successfully produced by using an optimized PC imaging technique. PC seems to be a robust low-field-strength angiographic method.

272 • 5:09 PM

Simulating Signal Response in MR Angiography for Stenotic and Laminar Flow

D Wu, EM Haacke

Department of Radiology (MRI), Case Western Reserve University, University Hospitals of Cleveland, Cleveland, OH

Purpose: The purpose of this study was to model the flow dephasing under various flow patterns by using different sequence designs. In particular, the authors looked for a practical sequence optimized for minimal signal loss under laminar flow and for vessels of different geometries (stenotic or curved vessels). Simulations were constructed for 2D flows, and streamlines and image profiles were examined.

Methods: The blood vessel was simulated in an arbitrary direction. In this work, straight, curved, and stenotic vessels were considered. Flow calculations were performed by using finite difference techniques and tested under various sequence designs for various TEs. Expected position shifts and signal changes were monitored for both compensated and noncompensated sequences. Models were constructed to agree with physiological limits. The imaging equation was numerically evaluated to determine the raw data, which were then Fourier transformed to obtain the image.

Results: Expected shift and signal changes were observed in these simulations. Modeling was dependent on pixel size and gradient strength. These results agreed with anticipated phase-shift results, while laminar flow models showed the importance of proper subpixel evaluations. Stenotic models showed that with a field echo of 4.2 msec, excellent quality images for physiological cases of stenoses and curved flow could be obtained.

Conclusion: Flow computations and display of 2D data is a simple technique that enables the user to further understand the intricacies of complex flow stenotic geometries with MR imaging. These models can be extended to incorporate more difficult types of flow patterns and geometries and to more readily study the effects of blood flow on MR imaging signal intensity.

Tuesday Afternoon • Plaza B
Papers 273–280

MUSCULOSKELETAL II

MODERATORS: J Beltran, MD • JB Kneeland, MD

273 • 3:45 PM

Treatment of Patellar Malalignment and Maltracking by Application of a Patellar Realignment Brace: Evaluation with Kinematic MR Imaging

FG Shellock, JH Mink, A Deutsch, T Molnar, J Fox, R Ferkel

Tower Imaging, Los Angeles, CA

Purpose: To use kinematic MR imaging of the patellofemoral joint (PFJ) to determine the effect of a patellar realignment brace for treatment of patellar malalignment and maltracking.

Methods: Active-movement, kinematic MR imaging with the previously described ultrafast spoiled GRASS technique was performed in 25 patients with symptomatic PFJs (6 after surgery). Seventeen PFJs had qualitatively substantial patellar malalignment and maltracking (lateral subluxation [n = 11], medial subluxation [n = 6]). A specially designed patellar realignment brace (Bauerfeind USA) was applied to these PFJs, and kinematic MR imaging was repeated.

Results: Fourteen of 17 PFJs (82%) had a qualitative correction or improvement (ie, centralization of the patella or a lessening of subluxation) in patellar malalignment and maltracking after application of the patellar realignment brace. The 3 "failures" occurred in PFJs with patella alta and/or dysplastic anatomy.

Conclusion: The application of the specially designed patellar realignment brace acutely corrected or improved patellar malalignment and maltracking in the majority of the patients studied. Kinematic MR imaging of the patellofemoral joint facilitated identification of the abnormalities and enabled assessment of the immediate effects of this conservative treatment.

This research was supported in part by a scientific grant from Bauerfiend.

274 • 3:57 PM

Distribution of Normal and Abnormal Fluid Collections in the Glenohumeral Joint

MP Recht, J Kramer, CA Petersilge, J Yu, M Pathria, D Trudell, DJ Sartoris, D Resnick

Diagnostic Radiology, Cleveland Clinic Foundation, Cleveland, OH

Purpose: Although intraarticular fluid commonly is noted on MR images of the glenohumeral joint, neither the amount of such fluid present in asymptomatic persons nor the pattern of distribution of increasing amounts of intraarticular fluid have been studied previously. In this study, cadaveric shoulder specimens were studied during progressive distention of the glenohumeral joint. The pattern of fluid distribution observed was then used to determine the amount of intraarticular fluid normally present in asymptomatic shoulders.

Methods: Six cadaveric shoulder specimens were imaged with a 1.5-T magnet during progressive distention of the glenohumeral joint with a dilute Gd-DTPA solution. The pattern of fluid distribution was evaluated simultaneously by 3 radiologists. By using information gained from the cadaveric study, the amount of intraarticular fluid present on MR images of 20 asymptomatic shoulders was determined.

Results: Although filling of the bicipital tendon sheath and the subscapularis recess was variable, filling of the axillary recess and the space between the humeral head and glenoid cavity was more uniform. With this information, all 20 asymptomatic shoulders were determined to contain 2 mL or less of intraarticular fluid.

Conclusion: The pattern of filling of the axillary recess and space between the humeral head and glenoid cavity appears to allow an accurate estimation of the amount of fluid in the glenohumeral joint. The amount of intraarticular fluid present in 20 asymptomatic persons was determined to be 2 mL or less. Therefore, although shoulder pathology need not be accompanied by an increased amount of joint fluid, the presence of more than 2 mL of fluid should make one suspect an abnormality of the glenohumeral joint.

275 • 4:09 PM

Reformatted 3DFT Data Sets in Clinical MR Imaging of the Foot and Ankle

MR Terk, PK Kwong, S James, PM Colletti

Department of Radiology, University of Southern California School of Medicine, Los Angeles, CA

Purpose: MR imaging of the ankle is made particularly difficult by the complex anatomy resulting in the desired planes for demonstration of various anatomic structures frequently being nonorthogonal. Prospective determination of the appropriate planes is predictably often unsuccessful. The authors developed an approach predicated on

the retrospective determination of section planes by using 3D data sets and a workstation for reformation.
Methods: A total of 59 consecutive patients referred for examination of the foot and ankle were studied. A routine examination was conducted. T1-weighted sagittal, multiecho coronal, and SPIR fat-suppressed axial images were obtained. Additional sequences were obtained with the following parameters: TR/TE = 29/7, flip angle 7°, field of view 27, 80–100 sections, 1 excitation, a matrix of 256 × 205, and a section thickness of 1 mm. The time for these additional sequences was approximately 8–10 minutes. The data set obtained was transferred to a Gyroview workstation and viewed interactively with multiplanar reformation. Orthogonal, oblique, and curved planes were used.
Results: In 8 cases (14%) of tendon injury, the anatomic abnormalities were better demonstrated with the 3D technique as to location and extent. This was found to be of particular importance in the evaluation of several tibialis posterior tears that could not be seen with conventional technique. In at least 4 cases (7%), the examination was salvaged by this technique. Structures either excluded from the routine examination or partially seen could be reviewed retrospectively.
Conclusion: Three-dimensional data sets with multiplanar reformation can be obtained in a reasonable amount of time and proved to be of substantial clinical value in the evaluation of the foot and ankle.

276 • 4:21 PM

MR Imaging of the Shoulder with 3D Steady-State Free Precession with Variable Bandwidth

TW Chan, DM Leifer
Department of Radiology, University of Chicago, Chicago, IL

Purpose: To evaluate the utility of steady-state free precession with variable bandwidth (VB-SSFP) in imaging of shoulder pathologies.
Methods: Two asymptomatic volunteers and 20 patients with suspected rotator cuff tears or shoulder instabilities were imaged on a 1.5-T unit. Axial multiplanar, gradient-recalled, SE proton density- and T2-weighted oblique coronal, oblique sagittal, and coronal VB-SSFP (flip angle 45°, TR = 25, 1.5-mm thickness) sequences were obtained.
Results: The image contrast characteristics of the VB-SSFP images were similar to those of the SE T2-weighted images except that fatty tissues had higher signal intensity. Contrast between fluid or tear and adjacent muscle or tendon was higher on the VB-SSFP images. The VB-SSFP images agreed with the SE T2-weighted images in diagnosing fluid in the joint space, biceps tendon sheath, and various bursae about the shoulder, as well as 5 cases of rotator cuff tears. In 2 cases, the VB-SSFP sequence demonstrated small rotator cuff tears better than the SE images. In 1 patient, subtle contusion of the humeral head was seen on the VB-SSFP and fat-suppressed T2-weighted SE images, but not on the routine T2-weighted images. Multiplanar reformatting of VB-SSFP images also helped to depict the course of ligamentous structures and clarify areas of cuff muscle overlap from pathology.
Conclusion: Three-dimensional VB-SSFP with multiplanar reformatting is useful for the detection of rotator cuff tears and abnormal fluid around the shoulder.

277 • 4:33 PM

RF Fat Saturation Gd-DTPA–enhanced T1-weighted MR Imaging of Pediatric Musculoskeletal Lesions

SA Gronemeyer, MH Pui, BD Fletcher, SB Halls
Department of Diagnostic Imaging, St. Jude Children's Research Hospital, Memphis, TN

Purpose: Gd-DTPA enhancement and T1 weighting are not used routinely in musculoskeletal tumor MR imaging because tumor/muscle contrast-to-noise ratio (C/N) is less than on T2-weighted images, and Gd-DTPA reduces tumor/fat C/N. With the advent of RF fat saturation (FATSAT), this rationale should be reexamined.
Methods: Eight patients were examined with T2-weighted (2,200–2,550/80–90, 70°), Gd-DTPA–enhanced T1-weighted (500–750/15, 70°), and FATSAT Gd-DTPA–enhanced T1-weighted (820/15, 90°) imaging. Lesions included musculoskeletal neoplasms, infection, and fracture. C/N was calculated for lesion versus tissue of origin and/or surrounding tissue.
Results: FATSAT Gd-DTPA T1-weighted image C/N was comparable with or greater than that of T2-weighted images (factor of 1.3–9.1) in 10 soft-tissue or marrow components, and less (factor of 1.0–16.5) in 4 necrotic or fluid components and a neurofibroma. FATSAT Gd-DTPA T1-weighted image C/N was greater than that of standard Gd-DTPA T1-weighted images (factor of 1.1–2.7) in 7 soft-tissue or marrow components and less (factor of 1.1–2.2) in 4 others. FATSAT had a higher C/N (factor of > 10) than that of standard T1 in 2 necrotic or fluid components and less (factor of 1.4–2.2) for 2 others.
Conclusion: FATSAT Gd-DTPA T1-weighted images may provide advantages over T2-weighted images in visualizing solid musculoskeletal lesions. They provided little additional contrast compared with standard Gd-DTPA T1-weighted images for fluid lesions.

278 • 4:45 PM

MR Imaging of Growth-Plate Injuries

PT Weatherall, KM Song, RD Welch, JG Birch, RM Peshock
Rogers MR Center, University of Texas Southwestern Medical Center, Dallas, TX

Purpose: The authors evaluated 10 patients with growth-plate injuries and 5 goat kids with surgical disruption of the physis, to determine MR imaging sensitivity to injury and measurement of involvement, and to assess its predictive ability. Physeal injury occurs in 6%–15% of children with skeletal trauma, with 10% resulting in limb length discrepancy or deformity. Surgical treatment is frequently unsuccessful due to inability to determine the area for optimal resection.
Methods: The authors assessed injury sites in 10 children and 5 goats in a total of 23 limbs. Goat injuries were created in 2 legs over a 10%–30% area. Children's abnormalities included trauma (n = 4), Blount disease (n = 2), tumor-related deformity (n = 1), and epiphysiodesis (n = 3). Radiography and MR imaging of goats was performed each week for 4 weeks and then every other week, and the goats were killed for histologic/morphometric analysis at 8, 16, and 20 weeks. Variable (2–19 months) patient follow-up has included radiography and MR imaging and surgery for bone bridge resection. T1-, proton density-, and T2-weighted, STIR, and gradient echo T2* thin (2.5–4-mm) sectioning, 0.3–0.6-mm resolution techniques, and 3DFT RF spoiled gradient echo images were acquired by using 1.5-, 0.5-, and 0.35-T systems.
Results: MR imaging depicted the abnormalities in all of these preselected patients. Radiographs did not demonstrate any of the bone bridges in goat physis that were visible on MR images after 6–8 weeks. The thin peripheral

bone layer was likely obscured by the large marrow-filled space of the bridge found at histologic examination. In the clinical study, MR imaging enabled identification of all bone bridges that were found at surgery or radiography, although one 2–3 mm bony bar demonstrated with x-ray tomography was seen only in retrospect. It was invisible on 4-mm MR images but obvious on coronally reconstructed 1.3-mm 3DFT images. The 2D areas of physeal abnormalities were measurable in all cases. A specific "marker" for irreversible damage was not demonstrated on MR images.

Conclusion: MR imaging is superior to radiographic techniques in evaluation of measurement of the injury zone and in detection of bone-marrow–filled and fibrous bridges. The degree of superiority cannot be stated due to the limited nature of this study. Thin bone bridges may escape MR imaging detection without properly oriented thin sections. MR imaging accuracy in demarcating irreversible injury zones is encouraging but has not been proved.

279 • 4:57 PM

Rotator Cuff Tears: Improved Diagnostic Accuracy of MR Imaging With Supplemental Imaging in the Oblique Sagittal Plane

RM Patten, R Spear
Rainier Medical Imaging Center, University of Washington, Kirkland, WA

Purpose: MR imaging of the shoulder is useful for detecting rotator cuff tears. Much of the literature has stressed the use of the oblique coronal (OC) plane for imaging. The authors performed this study to evaluate the diagnostic utility of supplemental imaging in the oblique sagittal (OS) plane.

Methods: Two radiologists blindly reviewed surface-coil shoulder MR images obtained at 1.5 T in 50 patients (20 with confirmed full- or partial-thickness rotator cuff tears) for rotator cuff pathology. Tears were characterized as to size, location, and extent. For each examination, the radiologist's diagnostic level of confidence (5-point scale) was tabulated. Examinations were reviewed twice, initially by using only double-echo SE images obtained in the OC plane and 1 week later by using double-echo SE images obtained in the both the OC and OS planes.

Results: Sensitivity, specificity, and accuracy of MR imaging for the presence or absence of rotator cuff tears was 85%, 80%, and 82%, respectively, when only OC MR images were available for evaluation. However, when both the OC and OS images were assessed, sensitivity, specificity, and accuracy of diagnosis increased to 95%, 97%, and 96%, respectively. Use of OC and OS images reduced the number of both false-negative and false-positive diagnoses and improved lesion characterization. Moreover, reliance on both OC and OS images resulted in an increase in confidence for the diagnosis of rotator cuff tear from 3.8 to 4.5.

Conclusion: The OS imaging plane is useful for MR imaging evaluation of the rotator cuff. Compared with OC imaging, supplemental series in the OS plane may improve accuracy for diagnosis of rotator cuff tears.

280 • 5:09 PM

Bone Marrow Dynamics in Aplastic Anemia

E Kozawa, HY Mizuno, H Mizuno, AS Heshiki
Saitama Medical School, Saitama, Japan

Purpose: Bone marrow MR images of patients with aplastic anemia were obtained with STIR with short and long TEs and were analyzed with respect to marrow dynamic changes.

Methods: By using a 1.5-T superconducting unit (Magnetom H15 SP) and a surface coil, midsagittal lumbar spine images were acquired with short and long STIR TE pulse sequences (2,000/130–160/20 and 100). Twenty-nine examinations were performed in 16 patients with aplastic anemia (6 men and 10 women). Five of 16 patients underwent pre- and posttreatment sequential studies. The MR imaging signal intensities were visually judged, and a signal intensity ratio between the highest signal intensity in the vertebra and subcutaneous fat was calculated for objective analysis. The signal intensity distribution was classified in 3 types: type A, homogeneously low; type B, focal areas of high intensity; and type C, high signal intensities in the margin of the vertebrae. MR imaging findings were compared with sternal bone marrow clot specimens.

Results: Of 5 pretreatment patients, 2 were type A and 3 were type B. All type A patients showed severe aplastic anemia, and 1 of 3 type B was a severe form. All 11 MR images obtained during treatment were classified as type B. Five posttreatment MR images were classified as type C when the treatment was judged as effective. MR imaging pattern as well as clinical features of low-grade myelodysplastic syndrome (MDS) were similar to those of aplastic anemia.

Conclusion: MR imaging with short and long TEs reflected well the bone marrow dynamics of aplastic anemia. Differential diagnosis includes low-grade MDS.

Tuesday Afternoon • Imperial Ballroom
Papers 281–287

PERFUSION/DIFFUSION II

MODERATORS: MJ Bronskill, PhD
ME Moseley, PhD

281 • 3:45 PM

Statistical Description of Microvascular Flow as Measured with MR Imaging

M Su, O Nalcioglu
Department of Radiological Sciences, Division of Physics and Engineering, University of California, Irvine, CA

Purpose: Quantification of microvascular flow can provide significant information for the functional assessment of a biologic system. In the current work, the authors investigate a method for studying the dependence of the MR signal intensity on microvascular flow. The quantitative analysis is based on the spin phase analysis technique.

Methods: A gel bead phantom (Sephadex G-50-300) was used in the experiments to simulate tissue. The signal intensity was measured with flow sensitive (FS) and insensitive (FI) pulse sequences. A simulation program based on a statistical model was designed to simulate the path of the spins in the medium. The spin's velocity phase accumulated during TE was calculated by using the model. When the voxel contains many spins, the signal reduction can be estimated from the phase distribution of the spins.

Results: The signal attenuation in the phantom at different flow velocities (0–0.4 cm/sec) was measured. The normalized signal intensity for the FS pulse sequence dropped to 0.7 when the flow velocity reached 0.1 cm/sec; the signal intensity for the FI sequence dropped to only 0.75 at 0.4 cm/sec. The agreement of the simulation results with the experimental data was excellent.

Conclusion: A realistic quantification of the signal reduction due to microvascular flow has not been proposed previously. Here, the authors describe a systematic study of the phenomenon and hope that this will shed light on the quantitative understanding of the behavior of MR signal intensity in microvascular flow.

282 • 3:57 PM

Fourier Analysis of Functional Echo-Planar Imaging Time-Course Series

PA Bandettini, EC Wong, EA DeYoe, JR Binder, RS Hinks, JS Hyde

Biophysics Research Institute, Medical College of Wisconsin, Milwaukee, WI

Purpose: A robust new method of creating brain activity images with Fourier analysis of echo-planar imaging (EPI) time-course series is presented.

Methods: On a 1.5-T Signa with a 3-axis local gradient coil of original design, the authors use blood oxygenation-sensitive gradient-echo (1,2) (< 3,000/40) or SE (3) (< 3,000/100) single-shot EPI to obtain single or multisection (thickness = 4–15 mm, field of view = 24 cm, resolution = 64 × 64) time-course series of up to 128 sequential images. During the time course, neuronal activity is modulated in a square wave manner by specific tasks. The hemodynamic response behaves as a low pass filter of the square wave, causing the MR signal intensity to approach a sinusoid at the activation frequency. The Fourier transform is then applied to the time response vector of each pixel, creating a series of spectral density images.

Results: After the Fourier transform is applied, a resonance peak is apparent in the the activated brain region. The image residing at the activation frequency peak in the transformed data set clearly delineates the periodically activated brain tissue.

Conclusion: Advantages of this method over simple subtraction of baseline images from activation images include the following: (*a*) No baseline or activation period is arbitrarily chosen. (*b*) Many tasks, oscillated at different frequencies, can be multiplexed into 1 time-course series. Different activated brain regions appear at different resonant peaks in the frequency image set. (*c*) Higher harmonics contain information about the details of the time course in specific brain regions.

1. Kwong KK, Belliveau JW, Chesler DA, et al. PNAS 1992; 89:5675–5679. 2. Bandettini PA, Wong EC, Hinks RS, Tikofsky RM, Hyde JS. Magn Reson Med 1992; 25:390–397. 3. Bandettini PA, Wong EC, Hinks RS, Estkowski LS, Hyde JS. SMRM 11th Annual Meeting, Works In Progress: 1992; 719.

283 • 4:09 PM

Projection Imaging for Suppression of Gross Motion Artifact in Diffusion-weighted MR Imaging

AF Gmitro, AL Alexander

Department of Radiology, University of Arizona, Tucson, AZ

Purpose: The purpose of this work was to develop a diffusion-weighted imaging technique that is less sensitive to gross patient motion than the conventional diffusion-weighted imaging technique.

Methods: In diffusion-weighted imaging, large balanced gradients are used to induce phase shifts due to the motion of the spins. The random nature of diffusional motion leads to a distribution of phase shifts and a concomitant reduction in signal intensity. Gross translational motion, however, causes a constant phase shift in the measured signal. When the translational motion varies from 1 TR to the next, the phase shifts vary from 1 acquisition to the next, which causes the phase-direction motion artifact of 2D Fourier imaging. The large gradients used for diffusion weighting greatly exacerbate this problem and ultimately limit the utility of diffusion-weighted imaging. This type of motion artifact can be eliminated by using a projection imaging method. The key concept is that because projections of a positive real object are positive and real, the phase shifts due to gross translational motion of the object can be corrected with a magnitude operation.

Results: This concept was tested with a stimulated-echo diffusion-weighted sequence. In vivo images of a rat obtained by using both 2D Fourier data acquisition and the projection imaging method were obtained. The motion artifact is shown to be far less severe with this projection imaging technique.

Conclusion: The projection imaging method can be used to reduce gross motion artifacts in diffusion-weighted MR imaging.

284 • 4:21 PM

Evaluation of Murine Tumor Perfusion with F-19 MR Spectroscopy by Using the Apparent Diffusion Coefficient of Intravascular Perfluorocarbon Emulsions

BJ Dardzinski, PS Hees, CH Sotak

Department of Biomedical Engineering, Worcester Polytechnic Institute, Worcester, MA

Purpose: To study tumor perfusion with F-19 MR spectroscopy by measuring the apparent diffusion coefficient (ADC) of intravascular perfluorocarbon (PFC) emulsions.

Methods: C3H mice with 0.5–1.0-cm^2 RIF-1 tumors are administered a 10 g/kg dose of F-44E PFC emulsion. A diffusion-weighted stimulated echo sequence was used to measure the ADC of the PFC at 2.0 T.

Results: The ADCs of the F-44E emulsion and the neat compound were 2.10×10^{-8} mm^{2}sec^{-1} and 4.5×10^{-4} mm^{2}sec^{-1}, respectively. Inside the tumor, diffusion coefficients ranged from 9.25×10^{-5} mm^{2}sec^{-1} ($\Delta = 22.5$ msec) to 0.85×10^{-5} mm^{2}sec^{-1} ($\Delta = 262.5$ msec). In another animal, there was evidence of a 2-component diffusion coefficient, with the fast component (8.5%) = 2.10×10^{-3} mm^{2}sec^{-1} and the slow component (91.5%) = 3.31×10^{-5} mm^{2}sec^{-1} ($\Delta = 70.5$ msec).

Conclusion: Preliminary data indicate that the ADC of PFCs arises from blood flow in the tumor. A time dependent diffusion coefficient as a function of Δ was also observed along with a 2-component diffusion process. The ADC of intravascular PFCs should provide additional insight into tumor perfusion and vascularity.

Funding for this work by The Whitaker Foundation is gratefully acknowledged.

285 • 4:33 PM

Myocardial Perfusion MR Imaging with Magnetization Transfer

PV Prasad, D Burstein, RR Edelman

Department of Radiology, MRI, Beth Israel Hospital, Boston, MA

Purpose: The authors propose a new MR imaging technique to evaluate myocardial tissue perfusion that obviates the use of extrinsic contrast agents and motion sensitizing pulses.

Methods: The technique is based on the presence of exchange between intravascular and interstitial water protons that exhibit differences in the degree of magnetization transfer (MT) effects. The authors used an isolated isovolumic (Langendorff) rat heart model to demonstrate the effect of flow on MT-weighted image intensity. The experiments were performed on a Bruker Biospec 4.7-T system, by using a single-shot TurboFLASH imaging sequence with different preparation pulses.

Results: The authors observed a 3% increase in MT-weighted signal intensity per milliliter per minute change in flow rate. They also observed a small increase in T1, measured in the presence of the MT pulse, with increasing flow rates. By using a pulse sequence with MT plus inversion recovery (IR) preparation, the authors observed synergistic changes due to both of the above effects, leading to

about a 10% change in the measured intensities per milliliter per minute change in flow rate. MT + T1-weighted images obtained after coronary artery ligation showed much better contrast compared with that of images obtained with MT weighting alone.
Conclusion: The results from these preliminary experiments appear to be promising as a potential noninvasive assessment of myocardial tissue perfusion. Since no extrinsic contrast agent is administered, these studies are repeatable several times, allowing stress studies to be performed. Further studies are needed to evaluate the sensitivity of this technique in clinical situations.

286 • 4:45 PM

Observation of Changes in the Apparent Diffusion Coefficient of Water with Changes in Membrane Permeability in Red Blood Cells

LL Latour, K Svoboda, PP Mitra, CH Sotak
Department of Biomedical Engineering, Worcester Polytechnic Institute, Worcester, MA

Purpose: During cerebral ischemia, the apparent diffusion coefficient (ADC) of water decreases by $\sim$40%. While the mechanism for the reduced ADC is unclear, 1 hypothesis suggests that changes in membrane permeability may be involved. To test this hypothesis, the authors measured the ADC of water in a red blood cell model, in which the membrane permeability can be chemically modified.
Methods: Whole red blood cells were washed and packed with centrifugation. The membrane permeability was altered with p-chloromercuribenzene sulfonate (pCMBS). The ADC of water in the cell pack and the cytoplasm was measured at 2.0 T, as a function of diffusion time (Δ), by using a modified stimulated echo technique.
Results: The water ADC at long values of Δ for untreated cells was 0.48×10^{-5} cm^2/sec compared with the cytoplasm ADC value of 1.56×10^{-5} cm^2/sec. After treatment with pCMBS, the ADC of water decreased by $\sim$30% with a corresponding reduction in the membrane permeability (calculated based on effective media theory).
Conclusion: A significantly reduced water ADC is observed with decreased membrane permeability and supports the hypothesis that this mechanism may be responsible for the reduced ADC observed during cerebral ischemia.

287 • 4:57 PM

Comparison between Scintigraphic and MR Techniques for the Assessment of Pulmonary Arterial Flow

SI Mavrogeni, RH Mohiaddin, MA Sakrana, SR Underwood, DB Longmore
Magnetic Resonance Unit, Royal Brompton Hospital, London, England

Purpose: Pulmonary perfusion scintigraphy with Tc-99m MAA is widely used in combination with ventilation scintigraphy for the detection of embolic lung disease and for the assessment of regional lung function. MR velocity mapping of flow in the right and left pulmonary arteries is an alternative method of assessing the flow to each lung. Because the quantitative information provided with MR velocity mapping is well validated, the authors have compared the 2 techniques to validate measurements of relative pulmonary perfusion made from perfusion scintigrams in patients with known or suspected lung disease.
Methods: Ten patients (mean age, 48 years; range, 20–78 years; 4 men) undergoing routine pulmonary perfusion scintigraphy were also studied with MR imaging. The diagnoses were suspected pulmonary embolism ($n = 3$), chronic airways disease ($n = 3$), pulmonary hypertension ($n = 2$), idiopathic pulmonary hemosiderosis ($n = 1$), cardiomyopathy ($n = 1$). One patient was excluded because of atrial fibrillation. The ratio of perfusion to both lungs was assessed from the ratio of the geometric means of scintigraphic counts within each lung field imaged in the anterior and posterior projections. MR velocity mapping was performed in planes perpendicular to the right and left pulmonary arteries, and absolute flow measurements were calculated from mean flow in the arteries throughout the cardiac cycle.
Results: The mean ratio of flow to the left and right lungs was 1.7 ± 1.2 (range, 1.01–4.91). The mean difference between measurements from the 2 techniques was 0.18 ± 0.01 (95% confidence interval, −0.01 to +0.36).
Conclusion: There was a good agreement without significant difference between the values measured in the group of patients studied. If quantitative pulmonary flow is required in patients for proposed lung resection or single lung transplantation, both techniques may be helpful, with MR imaging providing quantitative information and scintigraphy providing regional information.

Wednesday Morning • California Room Papers 301–308

SPECTROSCOPY II

MODERATORS: GB Matson, PhD
JA Sorenson, PhD

301 • 10:30 AM

H-1 Chemical Shift Imaging of Diffuse Brain Damage

S Furuya, S Naruse, M Ide, Y Horikawa, C Tanaka, T Yamaki, T Maeda, S Ueda
Department of Radiology, Kyoto Prefectural University of Medicine, Kyoto, Japan

Purpose: To reveal the metabolic change in diffuse brain damage by using H-1 chemical shift imaging (CSI) and to obtain understanding of the function of *N*-acetylaspartate (NAA), which is a specific metabolite of the neuron.
Methods: The system used was a Magnetom H15 (1.5 T). H-1 CSI was performed by applying 2-directional phase encoding in the field of view in which the volume of interest was selected, by using the spin-echo method with water suppression. Metabolite mapping was done by means of the curve-fitted area. Twenty-two patients with diffuse brain damage due to hypoxia, diffuse axonal injury (DAI), CO intoxication, or MELAS were studied.
Results: All cases showed decrease in NAA throughout the brain. Hypoxia and DAI patients in a vegetative state showed more decrease in NAA than did other patients. In patients with some disturbance of memory or orientation, a decrease in NAA was observed but was not so prominent compared with patients with severe damage. It is suggested that the amount of NAA may be related to the consciousness level in diffuse brain damage. In 1 case of MELAS, the recovery of the NAA peak was observed after treatment with improvement in neurologic findings. This suggested that the decrease in NAA does not indicate only neuronal loss but also reversible change in neuronal function.
Conclusion: Patients with severe neurologic damage had a tendency to show more decrease in NAA in diffuse brain damage. It is considered that the decrease in NAA indicates either neuronal loss or reversible impairment of neuronal function.

302 • 10:42 AM

Regional Differences in Infratentorial and Supratentorial Brain Sections with in Vivo Proton Chemical Shift Imaging

I Mader, M Schneider, H Kolem, K Wicklow, R Sauter, W Steinbrich

Department of Medical Radiology, University of Basel, Basel, Switzerland

Purpose: The purpose of this study was to examine regional differences in infratentorial and supratentorial brain sections in healthy volunteers with proton chemical shift imaging (CSI) and single-voxel measurements.
Methods: Measurements were performed on a 1.5-T whole-body imager (Siemens Magnetom). A hybrid CSI sequence was used that was based on an SE single-voxel sequence to preselect a large volume of interest (TE = 135 msec). A "section-shaped" transverse-oriented volume of interest was located supratentorially in gray and white matter (insular and occipital region) or infratentorially (pons, brachium pontis, cerebellar hemisphere). Within the preselected volume of interest, better spatial resolution was achieved with 2 phase-encoding gradients (supratentorial, 16×16 matrix with a resulting voxel size of 8 mL; infratentorial, 32×32 matrix with a resulting voxel size of 3 mL). For comparison, single-voxel SE measurements were performed at a TE of 135 msec in corresponding locations, with a voxel size of 8 mL.
Results: The spectra showed regional differences for the ratios of *N*-acetylaspartate (NAA: 2.01 ppm) to phosphocreatine/creatine (PCr/Cr: 3.03 ppm) and choline (Cho: 3.22 ppm). The ratio of NAA to PCr + Cr in pons (4.69 in CSI measurements and 3.22 in single-voxel measurements) was higher than in cerebellum and supratentorial parts of the brain. The ratio of Cho to PCr + Cr had in pons the highest value (2.09 in CSI measurements and 2.02 in single-voxel measurements). The ratio of PCr + Cr to the area of all peaks was less in pons (0.13 in CSI measurements and 0.16 in single-voxel measurements) than in other locations. Except for 1 temporal voxel, CSI and single-voxel techniques yield similar ratios of NAA to Cr, Cho to Cr, and Cr to the area of all peaks.
Discussion: Knowledge about regional differences in healthy volunteers is essential in the interpretation of proton spectra in pathologic stages. Simultaneous measurements of spectra from adjacent locations improve access to this information.

303 • 10:54 PM

H-1 and P-31 MR Spectroscopy of Deep White Matter Lesions

JM Constans, DJ Meyerhoff, D Norman, G Fein, MW Weiner

MR Unit, University of California San Francisco, San Francisco, CA

Purpose: To characterize metabolic changes in focal deep white matter lesions (DWML) seen on MR images and to compare them with those of the normal aging brain.
Methods: After MR imaging, 8 patients with DWML and 4 elderly controls were studied with 2D H-1 and 3D P-31 MR spectroscopy. Spectra from 25-mL volumes (for P-31) and 3-mL volumes (for H-1) were extracted with home-written MR spectroscopy display software from the lesion, the contralateral side, a normal appearing region on MR images, and from a spatially corresponding normal region in the controls. Spectra were analyzed and curve fitted to yield metabolite ratios and metabolite percentages (as percentage of total metabolite area).
Results: PME/PDE and PME in DWML were significantly (Mann-Whitney *U* test) decreased relative to elderly controls. The PDE and ATP/Pi values were not different from controls. In DWML, NAA and NAA/Cho were not significantly decreased (1.9 ± 0.3 vs 2.3 ± 0.5) and choline was not significantly increased (28 ± 3 vs 25 ± 4). The metabolite ratios in the normal appearing region contralateral to the lesion were between those of lesions and controls.
Conclusion: The results from this preliminary study suggest altered phospholipid metabolism and no neuron or axon loss in the DWML. These results are qualitatively different from metabolic changes in multiple sclerosis lesions found in this laboratory. Metabolic changes observed in normal appearing brain tissue may suggest a diffuse process underlying DWML.

304 • 11:06 AM

Integrated MR Imaging and MR Spectroscopy of Astrocytomas Treated with Gamma-Knife Radiosurgery

MM Mengeot, D Elias, P Rosel, KE Cramer, T Helenowski, J Moskal, JE Leestma, L Cerullo, et al

Siemens Medical Systems, Chicago, IL

Purpose: To evaluate the overall information afforded by a combined H-1 MR imaging and MR spectroscopy of patients with brain tumors who are receiving radiation therapy with a Leksell gamma knife, either by itself or in combination with surgery, chemotherapy, and conventional radiation therapy. The objectives were: (1) to determine whether and how MR spectroscopy complements MR imaging information with respect to tumor heterogeneity; (2) to evaluate how reliably MR spectroscopy allows differentiation between normal, malignant, and necrotic brain tissue; (3) to characterize the postradiation changes observed on MR images; (4) to study the predictive value of the MR spectroscopic data with respect to patient prognosis and treatment outcome. H-1 MR imaging and MR spectroscopy, were performed before gamma knife treatment, after treatment, and at intervals thereafter. Correlation was obtained with pathology results and clinical evaluation.
Methods: The authors used a 1.5-T whole-body system (Siemens Magnetom SP4000). A normal MR imaging examination entailed precontrast SE T1 and T2 studies, FLASH 3D, serial TurboFLASH during injection of contrast material, and postcontrast SE T1. H-1 spectra were obtained with water-suppressed single-voxel MR spectroscopy by using STEAM or SE-PRESS sequences with TEs of 20, 135, or 270 msec. The authors interrogated voxels in the tumor volume and on the contralateral side. Voxel localization was performed on the preceding imaging study with interactive display. Peak areas were determined to evaluate the metabolite ratios. A baseline study of healthy volunteers was conducted concomitantly.
Results and Conclusion: Preliminary results indicate that (1) MR spectroscopy appears to enable differentiation between healthy, malignant, and necrotic brain tissue; (2) a necrotic spectrum is associated with the nonenhancing part of the tumor; (3) in healthy volunteers, the metabolite ratios (NAA/Cho, NAA/PCr) have values of (2.9 + 0.9; 2.1 + 0.4); (4) in astrocytoma grade 4 patients, those values fall in 2 ranges: (0.45 + 0.3; 0.9 + 0.5), and (1.2 + 0.3; 1.5 + 0.3).

305 • 11:18 AM

Phosphorus Heart Spectroscopy with a Double-Oblique Chemical Shift Imaging Technique

H Kolem, K Bachmann, M Friedrich, M Schneider, K Wicklow, R Sauter

Siemens Medical Engineering Group, Erlangen, Germany

Purpose: Phosphorus heart spectroscopy was used to examine patients with coronary artery disease. The major aims were (1) the detection of well-separated spectra from

different parts of the myocardium with low blood contamination and (2) the reproducible detection of the inorganic phosphate peak in disease.
Methods: Measurements were performed by using a 1.5-T whole-body MR system (Siemens Magnetom) equipped with an experimental second RF channel, which was used for nuclear Overhauser enhancement and proton decoupling. Localization was performed with a chemical shift resolved spectroscopic imaging technique by using phase-encoding gradients in all 3 dimensions. To reduce blood contamination of the spectra, a voxel size of 2.5 × 2.5 × 5 cm was used; the voxels were oriented parallel to the long axis of the heart. Total acquisition time was typically 25 minutes.
Results: The method resulted in spectra from the left ventricular anterior wall and from the septum, with reasonable signal-to-noise ratio for quantitation. The contamination by blood was low. In most volunteer spectra, the inorganic phosphate could be detected; the typical PCr/Pi ratio was 5 for volunteers (spectra not corrected for saturation). In patients, the PCr/Pi ratios varied from 2 to 4. Signal-to-noise ratio from the left ventricular side wall was low; spectra from the left ventricular posterior wall were not detectable.
Conclusion: The double-oblique chemical shift imaging technique provides helpful metabolic information on the status of the heart muscle. Limitations are the problems of absolute quantitation and the difficulty of getting spectra from the posterior wall.
H. Kolem is an employee of Siemens AG.

306 • 11:30 AM

Functional Citrate Imaging of the Human Prostate with 3D Proton MR Spectroscopy with 0.4–1.0-cm^3 Spatial Resolution

J Kurhanewicz, DB Vigheron, SJ Nelson, H Hricak, A Kosco, P Carroll, P Narayan
Department of Pharmaceutical Chemistry, University of California, San Francisco, CA

Purpose: Recent studies have demonstrated the potential of MR spectroscopy for differentiating benign prostatic hypertrophy (BPH) from prostate cancer based on the significantly lower citrate levels in adenocarcinomas. By using novel techniques, the authors imaged the 3D distributions of citrate in normal and pathologic human prostates at a spatial resolution of 0.4–1.0 cm^3 and correlated this functional data both with morphology identified on high-resolution fast SE images and with histopathology.
Methods: Fifteen patients with well-defined BPH and prostate cancer were studied by using an endorectal coil on a 1.5-T GE Signa clinical imager. With the STEAM localization technique, H-1 MR spectroscopic excitation was restricted to the prostate. From the 30–60 cm^3 selected voxel, an 8 × 8 × 8 phase-encode array was acquired in 17 minutes. All MR data were analyzed and corrected for the reception profile of the coil by using software developed in the authors' laboratory.
Results: High-quality 3D citrate metabolite images of the prostate were obtained in 30 minutes. Citrate signal-to-noise ratio was 50–60 close to the coil and 10–30 in anterior regions. Resonances due to creatine, choline, glutamine, glutamate, and polyamines were also observed. Clear differences in citrate levels corresponding to different regions of zonal anatomy and pathology were observed. Citrate levels corresponding to regions of cancer were reduced by 55% ± 11 and 44% ± 10 relative to regions of normal and BPH tissue, respectively.
Conclusion: Three-dimensional MR spectroscopic citrate imaging can be performed in a clinical examination (1–1.5 hours) and can depict abnormal glandular function in cancerous prostates.

307 • 11:42 AM

Multisection Proton Spectroscopic Imaging with Outer Volume Presaturation

JH Duyn, CTW Moonen, PCM Van Zijl, G Sobering, J Gillen
Diagnostic Radiology Research Program, National Institutes of Health, Bethesda, MD

Purpose: To develop multisection proton spectroscopic imaging to simultaneously measure metabolite distributions in multiple sections through the brain and to improve localization by using outer volume presaturation.
Methods: The pulse sequence consisted of an SE spectroscopic imaging experiment, combined with CHESS water suppression and multiple-section outer volume presaturation. The section-selective 90° and 180° RF pulses of the SE sequence excite approximately the same (axial) section. The nominal section thickness is 13–14 mm, with an intersection gap of 2.5 mm. A 256-msec echo was symmetrically acquired at a TE of 272 msec. TR is 2.2 sec (4 sections), with 32 × 32 (circular) phase encodings, for an acquisition time of 28 minutes. The outer volume presaturation consisted of 8 sinc-gauss section-selective pulses following the outline of the skull.
Results: Metabolic images obtained from studies in volunteers demonstrated the capability of measuring multiple sections simultaneously without reduction in signal-to-noise ratio. The spectra show greatly reduced water and lipid suppression, not only in spectra from regions close to the skull but throughout the sections. Within the brain, lipid signals were below the noise level. This finding is explained by the fact that slight patient movements can cause a sizable spatial scattering of signals. The presaturation helped to reduce this effect.
Conclusion: Multisection proton spectroscopic imaging of the brain provides metabolic information from multiple sections simultaneously, and volume presaturation greatly improves the suppression of water and lipid signals.

308 • 11:54 AM

Lactate-Lipid Separation with Simultaneous Subcutaneous Fat and Water Suppression

S Singh, WR Brody
Department of Radiology, The Johns Hopkins University School of Medicine, Baltimore, MD

Purpose: Previous in vivo studies have indicated that in an ischemic tissue both lactate and lipid increase, and, in that respect, measurement of both lactate and lipid may be useful for assessing the metabolic state of tissue. The J-coupling approach has recently been applied to observe lactate and lipid separately; however, the problem of good suppression of water and subcutaneous fat signals should be more efficiently handled. Here the authors describe a composite pulse sequence for lactate-lipid separation, while simultaneously suppressing the water and subcutaneous fat resonances robustly.
Methods: The composite sequence contains 4 segments: (*a*) A water-selective RF pulse is applied to presaturate the water signal. (*b*) A 2D or 3D projection presaturation (PP) technique is used to spatially presaturate the subcutaneous fat in the outer region/volume. (*c*) A nonselective inversion pulse is then applied and the water-selective pulse is repeated (if needed) to presaturate and null the residual water signal simultaneously with inversion nulling of subcutaneous fat signal. (*d*) Immediately after null time, a double-resonance sequence, $90°_{sel}$-τ-$180°_{sel/nonsel}$-τ-acquire, where $\tau = 1/2J = 68$ msec, is applied to acquire 2 SE signals, 1 with 180° pulse selective and the other with 180° nonselective when steps *a–d* are repeated. Addition and subtraction of these 2 acquisitions separate lactate and lipid resonances, with water and subcutaneous fat

signals robustly suppressed. With phase encoding along the orthogonal directions, the composite sequence will provide a data set for spectroscopic images.
Results: The authors tested the accuracy of their method on a 4.7-T GE chemical shift imaging system by using animals and a phantom containing a combination of aqueous solution of lactate bottle and oil. Additional oil was placed around the phantom to mimic the subcutaneous fat. All water saturation, 90°, and 180° pulses were sinc, although Meyer's pulse can also be used for the latter 2. Phantom and in vivo data show lactate-lipid separation, with water and subcutaneous fat well suppressed.
Conclusion: The composite sequence is a robust method for lactate-lipid separation, with water and subcutaneous fat suppressed.

Wednesday Morning • Balboa Room Papers 309–316

MRI: General

MODERATORS: MR Fisher, MD • NJ Pelc, ScD

309 • 10:30 AM

MR Microimaging of the Resected Stomach with a 4.7-T Superconductive Magnet System

YH Auh, TH Lim, DH Lee, CW Mun, MG Lee, YH Kim
Asan Medical Center-University of Ulsan, Seoul, Korea

Purpose: As a preliminary step before in vivo use, surgical specimens of the resected stomach were imaged. In vitro image quality and image resolution were evaluated.
Methods: A new method for MR microimaging was developed in a 4.7-T superconductive magnet system by using a gradient field of 10 G/cm and an RF coil with 3.5-cm internal diameter. Images were obtained from 23 specimens of normal stomach and 9 specimens of the resected gastric cancer. Image resolution was 100 μm, and image acquisition time was 34 minutes for T1-weighted images and 128 minutes for T2-weighted images. MR microscopic images were compared with histologic slides, which were prepared such that each slide was exactly matched with the MR image at the level and orientation.
Results: MR microscopic images clearly showed 3 layers of normal stomach, namely, mucosal, submucosal, and muscular layers, and this was validated by means of statistical analysis of signal intensity difference in 3 layers. Tumor invasion into the submucosal layer can be distinctly identified on T1- and T2-weighted images and tumor invasion into the muscle layer on T2-weighted images. This finding was also validated with statistical analysis of measured signal intensity. Other findings suggesting cancer involvement were thickening of the gastric wall, irregularity of signal intensity, loss of interface between layers, and loss of mucosal layer due to ulceration.
Conclusion: Spatial resolution of 100 μm generated in this study was sufficient to visualize 3 distinct layers of the stomach. Gastric cancer and depth of tumor invasion were clearly identified on microimages.

310 • 10:42 AM

MR Microscopy of Articular Cartilage

LL Tyson, D Lee, E McFarland, JV Crues
Cottage Community MRI Center, Santa Barbara, CA

Purpose: The accuracy of MR imaging in the evaluation of articular cartilage is suboptimal because of inadequate spatial resolution. The authors have developed a technique for obtaining images with resolution of 20–50 μm by using a standard 1.5-T clinical instrument.
Methods: Adequate signal-to-noise ratio and tissue contrast is achieved by using local gradient coils with high gradient field strengths and specially designed receiver coils. T1-weighted (500/20), intermediate (2,000/20), T2-weighted (2,000/80), and magnetization transfer (60/15, flip angle = 20°, off-resonance pulse width = 0.4 msec) contrast images of bovine cartilage have been acquired.
Results: High-resolution images with good T1, T2, and magnetization transfer contrast show 4 or 5 different layers within articular cartilage. On the T2-weighted images, increased signal intensity in the superficial layers and decreased signal intensity in the deeper layers correlates with the known distribution of water in articular cartilage.
Conclusion: Early biochemical alterations in injured cartilage cause a change in the water content of certain layers, possibly due to changes in the proteoglycan substrate. With these high-resolution imaging techniques, changes in water content of cartilage may be detectable before routine images show abnormalities. The ability to obtain high-resolution microscopic images of articular cartilage should lead to improved understanding of the pathologic processes causing its degeneration and to earlier detection of disease. Similar protocols will be developed to evaluate human articular cartilage in vivo and ex vivo.

311 • 10:54 AM

Characterization and Localization of Volt-evoked potential Signals with Functional MRI

KK Kwong, CE Stern, JW Belliveau, JR Baker,
RBH Tootell, H-M Cheng, TJ Brady, BR Rosen
NMR Center, Massachusetts General Hospital, Charlestown, MA

Purpose: To use functional MR imaging (1) for identifying the underlying neuroanatomic location and distribution of volt-evoked-potential (VEP) signal changes. Specific hypotheses: (*a*) VEP measures of visual functions (fusion, suppression, and stereopsis) reflect anatomically distinct patterns of activation with MR imaging. (*b*) VEP signal reflects the involvement of higher order visual areas in addition to V1 and can be anatomically localized by using functional MR imaging.
Methods: Functional MR imaging (Instascan echo-planar gradient echo: 1,000/50, up to 512 images collected sequentially) was used to obtain temporal and spatial frequency responses to goggle and checkerboard stimuli. By using 4 volunteers, functional MR imaging studies have examined binocularity with goggles and stereopsis with random dot stereograms. Spatial frequency VEP studies were performed separately in 3 volunteers. Other corresponding VEP results were taken from the literature.
Results: Temporal and spatial frequency responses of VEP to visual stimuli matched well with that of functional MR imaging. Temporal frequency response peaks were between 8 and 12 Hz and spatial frequency response peaks around 20 minutes of arc. Both MR and VEP showed that the binocular responses were larger. For binocularity and stereopsis tests, MR imaging also demonstrated that a significant change occurred at extrastriate higher-visual-function centers in addition to V1. In addition, MR imaging showed preliminary evidence of V2, which includes centers of disparity.
Conclusion: Functional MR imaging localizes VEP signals and should become an important diagnostic and research tool for the study of visual cortex functions.

1. Kwong, et al, PNAS, June 1992.

312 • 11:06 AM

MR Imaging of Retinoblastoma: Role of Pulse Sequence Selection and Contrast Agent

DF Frei, KL Gupta, DJ Ainbinder, BG Haik
Department of Radiology, Tulane University Medical Center, New Orleans, LA

Purpose: To determine the most sensitive pulse sequence and to clarify the role of each pulse sequence in the MR imaging diagnosis and staging of retinoblastoma, T1, T2, and contrast-enhanced T1-weighted images were compared blindly and independently by 2 experienced neuroradiologists.

Methods: Seventeen patients with pathologically proved retinoblastoma were examined with US and a 1.5-T GE Signa MR imager with an orbital surface coil. Eleven studies were performed after the injection of Gd-DTPA. Tumor detection rate and the ability to detect tumor extension were compared between unenhanced T1, T2, and postcontrast T1-weighted SE images.

Results: Postcontrast T1-weighted images were most sensitive in detecting tumor extension. The contrast-to-noise ratio between retinoblastoma and vitreous fluid was greatest on postcontrast T1-weighted images, followed by T2, then unenhanced T1-weighted SE images. Postcontrast T1-weighted images also proved useful in differentiating retinoblastoma from subretinal fluid collections.

Conclusion: Postcontrast T1-weighted SE sequences contribute to a higher sensitivity in the detection of retinoblastoma by increasing the contrast-to-noise ratio of tumor to vitreous fluid and are most sensitive in detecting tumor extension.

313 • 11:18 AM

High-Resolution Neuroimaging at 4.1 T

HP Hetherington, JT Vaughan, JW Pan, PJ Noa, DB Twieg, RK Kuzniecky, GM Pohost
Center for Nuclear Imaging Research, University of Alabama, Birmingham, AL

Purpose: The goal of this work was to evaluate the unique anatomic information available from high-resolution neuroimaging at 4.1 T.

Methods: High-resolution images (512 × 512 and 1,024 × 1,024 matrices, 240-mm field of view, 3- and 5-mm sections) of 20 volunteers were obtained at 4.1 T by using a multisection inversion-recovery gradient-echo (IRGE) sequence (TR/TE/TI = 2,500/17.5/1,200) with a quadrature head coil.

Results: Despite decreasing T1 differences, the inversion-recovery sequence provides excellent contrast and signal-to-noise ratio, 50:1 and 30:1 for gray and white matter, respectively, on 3-mm 512 × 512 images. The gray/white matter contrast and high spatial resolution helps visualize the gray/white junction, subcortical structures including basal ganglia and thalamus, commissural tracts, internal capsule, and optic radiations. Small cerebral vessels not seen on lower field images are well defined within the basal ganglia as well as medullary veins draining white matter tracts into the internal cerebral veins. Furthermore, definition of the major thalamic groups appears possible. Finally, the red nuclei and substantia nigra are easily resolved at 4.1 T due to the enhanced T2* contrast at high field strength.

Conclusion: Structures not routinely seen on lower field images, such as small vessels in the thalamus and white matter, are easily resolved at 4.1 T. The fine detail available suggests that evaluation of small lacunes, tumors, berry aneurysms, and demyelinating diseases may be significantly improved at 4.1 T. Visualization of epileptic foci in the temporal lobe and alterations in substantia nigra (due to changes in iron content in Parkinson disease) may be possible to better understand the progression and etiology of these diseases.

314 • 11:30 AM

RF Limitations to High-Field-Strength Clinical Imaging

JT Vaughan, J Harrison, HP Hetherington, GM Pohost
University of Alabama, Birmingham, AL

Purpose: Past predictions have maintained that B_1 penetration, RF heating, and signal-to-noise ratio (S/N) degradation would limit the B_0 field strength at which clinical imaging could be "optimally" performed. Recent successes with high resolution and functional imaging at clinical 4-T sites prompt the important question, What are the RF limitations to safe and successful imaging at 4T? The answer is the goal of this study.

Methods: B_1 penetration, RF heating, and S/N were predicted, measured in phantom and animal models, and verified in humans. The 3D time-dependent B_1 field predictions were verified with field probing of phantoms and with MR generated B_1 maps from phantoms and human subjects. B_1-dependent RF power loss in tissue models was substituted into the bioheat equation to predict RF heating. RF heating was then measured in phantoms and in 12 anesthetized pigs in vivo and in vitro with fluoroptic thermometry. S/N was similarly predicted and measured.

Results: At 4.1 T (175 MHz), B_1 distribution is highly dependent on tissue type (conductivity, σ/permitivity, ϵ) and geometry. Depending on σ/ϵ, B_1 penetration was slightly attenuated or slightly enhanced as in the human head. RF heating, also tissue dependent, produced temperature maxima in subcutaneous (1–2 cm deep) hot spots near the coil elements. Heating at 175 MHz was approximately twice that at 71 MHz. The 3W heating at either frequency did not exceed Food and Drug Administration guidelines for well-perfused tissue but resulted in excessive heating for nonperfused tissues at both frequencies. S/N at 4.1 T was measured to be about 2.7 times that at 1.5 T.

Conclusion: B_1 penetration has not been found to limit successful 4.1-T clinical imaging. For a constant power and the experimental conditions noted, the risk of excessive heating of local regions at 4 T may be twice that of 1.5 T. S/N at 4 T exhibits a linear dependence on B_0. High field B_1 penetration, heating, and S/N can be described with 3D time-dependent models.

315 • 11:42 AM

Functional Mapping of the Motor Cortex in the Human Brain with Conventional MR Imaging at 1.5 T

Y Cao, VL Towle, DN Levin, JM Balter
Department of Radiology, University of Chicago Hospitals, Chicago, IL

Purpose: To study task-related changes in the signal intensity of motor cortex with conventional gradient-echo MR imaging at 1.5 T.

Methods: Gradient-echo pulse sequences (GRASS) on a GE Signa imager were modified to obtain T2*-weighted images of thick (8–15-mm) axial sections with long TE (38–52 msec), coarse matrices (128 × 64 or 128 × 128), and low bandwidth (±4 kHz or ±8 kHz). Each image was obtained in 3–7 seconds. Each subject's motor cortex was imaged 48–80 times during a control period, a task performance period, a resting period, and a second task performance period. Successive images were registered with 2D cross correlation to correct for possible subject motion. Functional images were created by subtracting the control images from images during task performance. In some cases, functional data were mapped onto MR imaging-derived 3D models of the subject's gyral anatomy. Ten volunteers were studied during finger motion protocols, and 3 subjects were imaged while performing lateral tongue movements.

Results: Images during finger motion showed changes (3%–7%) in signal intensity of contralateral motor cortex as well as signal intensity changes in frontal and sensory areas. Tongue movements caused 6% signal intensity changes in bilateral motor areas in two subjects and 10%–18% changes in left motor cortex in 1 subject.

Conclusion: Noninvasive functional brain imaging, originally demonstrated on an echo-planar imager (1), can also be performed with a conventional 1.5-T machine.

1. Kwong KK, et al. Proc Natl Acad Sci USA 1992 (in press).

316 • 11:54 AM

MR Imaging in the Pregnant Patient: Proposed Guidelines for Rational Use

PM Colletti, PB Sylvestre, A Maderas, MR Terk, HD Segall, LD Platt

Department of Radiology, University of Southern California School of Medicine, Los Angeles, CA

Purpose: The use of MR imaging in pregnant patients remains controversial. The authors propose guidelines for rational use of MR imaging based on experience in 100 patients.

Methods: Forty-eight pregnant patients with maternal abnormalities (17 pelvic, 20 brain, 11 others) and 52 patients with sonographically detected fetal anomalies were studied.

Results: Of these, 28/48 (58%) had significant maternal abnormalities defined with MR imaging. Examples include medulloblastoma, sagittal sinus thrombosis, abdominal pregnancy, unstable spinal fracture, pancreatic phlegmon, and pelvic and nonpelvic neoplasm. Known gross fetal anomalies were readily identified. Additional information was seen in 5/52 (9.6%) of these patients.

Conclusions: The following guidelines for use of MR imaging in pregnancy are proposed: (1) MR imaging is reserved for suspected abdominal and pelvic abnormalities in which US is unsuccessful. (2) MR imaging should not be withheld in suspected acute brain and spine abnormalities during pregnancy. (3) MR imaging may be used to evaluate the extent of malignancies during pregnancy. (4) While MR imaging confirms fetal abnormalities detected with US, additional information is usually not obtained.

Wednesday Morning • Plaza A
Papers 317–324

FLOW VELOCITY II

MODERATORS: RS Hinks, PhD • SR Thomas, PhD

317 • 10:30 AM

Modulus Threshold Method to Minimize Interuser Variability of in Vivo Phase-Contrast Flow Measurements

DJ Burkart, JP Felmlee, RL Wolf, RL Ehman

MR Research Laboratory, Mayo Clinic, Rochester, MN

Purpose: Theoretically, cine phase-contrast (CPC) flow measurements should not require exact vessel edge detection for accurate flow measurement; however, in practice, precise segmentation of the vessel is essential. The purpose of this study was to construct a method of vessel edge detection that correctly identifies vessel pixels and minimizes interuser variability of in vivo volumetric flow rates.

Methods: A modulus threshold method (MTM) of vessel edge detection was developed in which vessel pixels were assumed to have a higher intensity relative to nonvessel pixels in modulus images, and a threshold value was determined as the average of the 3 highest intensities in a region-of-interest (ROI) in background on the modulus image. The MTM was compared with the conventional user-specified ROI method (CRM) in a flow phantom (3 users per method) and in the portal venous system (5 users per method) of 6 volunteers.

Results: With phantom flow rates ranging from 0.4 to 2 L/min, the MTM was within 10% of the known flow rate while the CRM was within 35%. The maximum interuser variability was 4% and 24%, respectively. For the in vivo measurements, the standard deviation of the mean flow rate ranged from 20 to 54 mL/min for the MTM, whereas it was larger, 63–138 mL/min, with the CRM.

Conclusion: The results indicate that the MTM has substantially less interuser variability of flow measurements, in a phantom and in vivo, compared with the CRM.

318 • 10:42 AM

MR Velocity Mapping of Complex Flow: Is Ultrashort TE Necessary?

C Thomsen, L Søndergaard, F Ståhlberg, O Henriksen

Danish Center for Magnetic Resonance, Hvidovre Hospital, Hvidovre, Denmark

Purpose: When using MR velocity mapping for quantification of complex flow (eg, flow consisting of linear velocity, acceleration, and jerk) the linearity between flow and phase signal have been preserved by using ultrashort TEs at the cost of spatial resolution. However, basic theory behind MR velocity mapping states that the nth order motion phase dependence is proportional to the time integral of the motion-encoding gradient multiplied by time to the nth power. Hence, a mere change in TE without subsequent variation of gradient time pattern variation is not efficient for lowering the sensitivity to higher-order-motion terms. The aim of the present study was to demonstrate this relation.

Methods: The study was performed by using a Siemens SP 63/84 whole-body unit with a standard gradient system (10 mT · m^{-1} and 10 T/m^{-1} · sec^{-1}) and a head coil. Through-plane MR velocity mapping of steady flow (15 L/min) through an 80% stenosis in a Plexiglas tube (ID, 21 mm) was performed with 8 pulse sequences with variable TE (5–40 msec) but with a constant-motion–encoding gradient pattern (2 lobes with reversed polarity in each of the 2 basic sequences, 1.5-msec gradient duration, 0.6 rad · sec · m^{-1} encoding). By temporal separation of all 3 gradients, a 350-mm field-of-view, 256^2 matrix size, and an 8-mm section thickness were obtained.

Results: No significant loss ($<$ 10%) of the average phase signal in the tube was seen for TE $\leq$ 25 msec, whereas a randomized phase shift was present with further increase in TE, probably because the excited spins in the stenotic jet in this case have left the head coil before data sampling.

Conclusion: This investigation shows that ultrashort TE is not necessary to inhibit breakdown of the flow/phase relation in the presence of a complex motion pattern. The important factor is the duration of the motion-encoding gradient. By selecting the present pulse sequence with a TE of 5 msec, the position of the flow information was preserved, and, furthermore, the spatial resolution was reduced by a factor of 8 compared with the initial pulse sequence.

319 • 10:54 AM

Rapid MR Velocity Measurements of Pulsatile Flow

D Saloner, K Selby, RU Weir, D Chien

Radiology Services, University of California, VA Medical Center, San Francisco, CA

Purpose: Pulsatile flow velocities are conventionally measured in cine mode by using cardiac triggering. The authors demonstrate that accurate MR velocity measurements can be obtained with much reduced imaging times by applying cardiac-phase synchronization to only the low-frequency phase-encoding lines.

Methods: Cardiac-phase-selective prospective gating (1) was used with a bolus tagging sequence (54/8, 30° flip angle) to measure in-plane flow velocities in a pulsatile phantom. For the low-frequency phase-encoding lines, data were acquired only within a controlled time window corresponding to a chosen portion of the pulsatility cycle. During the remainder of the cycle, phase-encoding steps were not advanced, and echoes were discarded. The high-frequency phase-encoding lines were acquired continuously throughout the pulsatility cycle. Velocities were measured by varying the fraction of the phase-encoding lines acquired in phase-specific mode and also the duration of the time window and its position within the pulsatility cycle. The values were compared with laser Doppler velocimetry (LDV).

Results: Agreement between MR and LDV was excellent even when only 20% of the phase-encoding lines were acquired in phase-specific mode. Best results were obtained with a 50-msec time window, encompassing 1 phase-encoding line. This gave an imaging time of 30 seconds, a fourfold reduction over cardiac triggering.

Conclusion: Our technique gives accurate measurements of pulsatile flow velocities with reduced imaging times. This approach should be valuable for breath-hold studies where short acquisition times are essential.

1. Selby K, Saloner D, Anderson CM, Chien D, Lee RE. JMRI (in press).

320 • 11:06 AM

MR Volume Flow and Jet Velocity Mapping in Aortic Coarctation

RH Mohiaddin, PJ Kilner, S Rees, DB Longmore

Magnetic Resonance Unit, Royal Brompton Hospital, London, England

Purpose: MR velocity mapping was used to characterize flow waveforms and to measure volume flow in the ascending and descending thoracic aorta in patients with aortic coarctation and in healthy volunteers. The authors present the method and discuss the relation between these measurements and aortic narrowing assessed with MR imaging. Finally, they compare coarctation jet velocity measured with MR velocity mapping with that obtained from continuous-wave Doppler echocardiography.

Methods: MR phase-shift velocity mapping was used to measure ascending and descending aortic volume flow in 39 patients with aortic coarctation and in 12 healthy volunteers. MR was also used for anatomic and peak jet velocity measurements. The latter was compared with those from continuous-wave Doppler in 40% of the patients.

Results: Whereas ascending aortic volume flow measurement did not show significant differences between the patient and healthy control groups, volume flow curves in the descending aorta did show significant differences between the 2 groups. Peak volume flow (mean ± standard deviation) was 10.6 L/min ± 5.3 in patients and was 19.6 L/min ± 4.7 in controls ($P < .001$). Time-averaged flow was 2.5 L/min ± 0.9 in patients and 3.9 L/min ± 1.1 in controls ($P < .05$). The descending/ascending aortic flow ratio was 0.47 ± 0.19 in patients and 0.64 ± 0.08 in controls ($P < .05$). These parameters correlate well with the degree of aortic narrowing. MR peak coarctation jet velocity is comparable with that obtained from continuous-wave Doppler ($r = .95$).

Conclusion: The authors have established normal ranges for volume flow in the descending aorta and have demonstrated abnormalities in patients with aortic coarctation. These abnormalities are likely to be related to resistance to flow imposed by the coarctation and could represent an additional index for monitoring patients.

321 • 11:18 AM

3D Velocity Mapping of Left Atrial Flow

PG Walker, MB Scheidegger, R Schwab, AP Yoganathan, GM Pohost, R Grimes

School of Chemical Engineering, Georgia Institute of Technology, Atlanta, GA

Purpose: Blood hemodynamics is known to play an important role in a number of diseases. The purpose of this study was to use MR phase velocity mapping to measure the time dependent flow in the left atrium and to assess the accuracy and viability of this type of measurement.

Methods: Seven sagittal imaging planes, 1 cm apart, were obtained through the left atrium of a healthy 27-year-old man. In each plane, 3 perpendicular velocity components were measured. A 1.5-T Philips system S-15 and the FLAG sequence were used with the following parameters: velocity range, ± 50 cm/sec; section thickness, 6 mm; resolution = 128, field of view = 400, TE = 11 msec, 24 heart phases 35 msec apart.

Results: Velocity vectors were plotted on top of the modulus image to produce an image of blood flow in relation to the physical structure of the atrial wall. By considering these images at the same cardiac time, in each of the 7 imaging planes, a good understanding of the 3D flow in the left atrium was obtained. Animation of the data gave an impression of the time course of the flow. It was found that left atrial flow is complex, involving multiple counter rotating vortices and high velocity streams.

Conclusion: MR phase velocity encoding enabled measurement of the complex left atrial flows and is therefore a valuable tool in the investigation of the relationship between disease and blood flow hemodynamics.

322 • 11:30 AM

MR Flow Quantification with the RACE Sequence: Clinical Application to the Carotid Arteries

HE Moeller, G Bongartz, HK Klocke, PE Peters

Department of Clinical Radiology, University of Muenster, Muenster, Germany

Purpose: Temporal-resolved quantitative flow measurements combined with MR angiographic techniques have various clinical applications. This study examined the diagnostic potential of a projective 1D RACE sequence applied to the carotid arteries.

Methods: Quantitative flow patterns of 68 vessels showing various degrees of carotid artery occlusive disease were obtained by using a 1.5-T system. Axial sections were positioned 2 cm proximal to the carotid bifurcation (TH = 3 mm, TE = 10 msec, TA = 10.26 sec, 0.90-mm spatial and 20-msec temporal resolution). Gradient calibration with a flow phantom resulted in a phase shift of π for a linear velocity of 1 m/sec.

Results: No statistically significant differences of flow parameters could be found between groups of subjects without carotid artery narrowing, plaques, and low-grade stenosis ($\langle v_{vol} \rangle = 4.0$ mL/sec ± 2.0). However, in cases of high-grade stenosis or occlusion, markedly reduced flow rates were found ($\langle v_{vol} \rangle = 1.89$ mL/sec ± 0.96). In addition, those vessels showed typical deviations from normal

flow patterns indicated by flat profiles without good separation of diastolic and systolic peaks.
Conclusion: The method consumes less than 5 minutes of additional time and can easily be combined with MR angiography, extending the diagnostic capability of MR imaging for a reliable assessment of intracerebral vascular diseases.

323 • 11:42 AM

Compensation for the Partial-Volume Effect in Phase-Contrast Flow Measurements

C Tang, DL Parker
University of Utah, Salt Lake City, UT

Purpose: Because of the low resolution of MR images and the relatively small blood vessel size, volume flow rate (VFR) measurements obtained with phase-contrast techniques are overestimated, especially in the case of high contrast between blood and stationary tissues. The authors present a method for improving VFR measurement accuracy by correcting the quantitative errors in partially occupied voxels (POV).
Methods: Phase-contrast VFR measurements use the linear relationship between the phase and flow velocity of spins in the flow-encoding direction. In a real vessel, the flow in boundary voxels is slow, and the resulting phase shift in the boundary POV is small. By using a small phase approximation, the true VFR can be obtained from the measured VFR by a correction, which depends on the relative signal in fully and partially occupied voxels. The technique was verified with simulation and phase-contrast studies in flow phantoms.
Results: Simulation shows that the accuracy of the corrected VFR measurement will be within 5% and 15% if the phase shift in POV is less than 30° and 60°, respectively. Without correction, the VFR will be overestimated by a factor that depends on the occupancy in the POV. In in vitro experiments, correction reduced the VFR measurement error in a 2-mm-radius tube from 40% to 7%.
Conclusion: The correction to VFR effectively compensates for the partial volume effect in phase-contrast flow measurements.

324 • 11:54 AM

Comparison of Ultrafast Techniques for Blood Flow Imaging

DN Firmin, PD Gatehouse, JP Konrad, DB Longmore
Magnetic Resonance Unit, Royal Brompton National Heart and Lung Hospital, London, England

Purpose: The purpose of this study was to compare methods of ultrafast flow imaging to identify the relative problems and the best method to use in particular situations.
Methods: The study was performed on a 0.5-T system with a reduced diameter (53 cm) gradient set and an SMIS console to drive the system. Echo-planar imaging (EPI), spiral imaging, and subsecond FLASH were compared in vitro and in vivo. Flow maps were obtained in the same manner as in conventional phase velocity mapping. The effects of altering various imaging parameters were investigated. Phantom experiments included flow through tubes for velocity validation and flow through a "vortex phantom," generating turbulence, to study sensitivity to signal loss. In vivo images were acquired of the heart and great vessels.
Results: All methods proved accurate when tested in phantoms. Results from the vortex phantom showed a range of sensitivity to signal loss. Subsecond FLASH and spiral imaging were less sensitive than the EPI methods, and as with conventional methods, shortening the TE reduced the effect. Subsecond FLASH and EPI had better resolution than the spiral imaging, which was particularly sensitive to poor shimming and tuning. EPI and spiral methods followed pulsatile flow much better than subsecond FLASH, for which the relatively long acquisition time resulted in an averaging effect.
Conclusion: The methods studied all have limitations for routine imaging of pulsatile flow. The technique of choice will depend on the particular clinical requirement.

Wednesday Morning • Plaza B
Papers 325–332

MRA: Clinical II

MODERATORS: C Dumoulin, PhD
TR McCauley, MD

---

325 • 10:30 AM

MR Imaging and MR Angiography of Skull Base Tumors

TJ Vogl, M Juergens, J Balzer, M Mack, S Ihrler, J Lissner
Department of Radiology, University of Munich, Munich, Germany

Purpose: To map characteristics of glomus tumors of the skull base in MR imaging and MR angiography with regard to morphology, signal behavior, and changes in the arterial and venous vessel system.
Methods: In 26 patients, MR imaging and arterial and venous MR angiography were performed with a 1.5-T MR unit (Magnetom 63SP, Siemens). The examination protocol comprised axial T2 and plain and enhanced T1-weighted SE sequences (Gd-DTPA, 01. mmol/kg) as well as MR angiography to visualize arterial (FISP 3D) and venous blood flow (FLASH 2D). In 7 patients, the results of DSA studies were compared with those of MR angiography. All patients with tumorous lesions underwent histopathologic correlation.
Results: Type A ($n = 9$), type B ($n = 4$), and type C ($n = 8$) glomus tumors could be assessed true-positive. Skull base glomus tumors were found to be related with displacement ($n = 3$) and occlusion ($n = 5$) of the internal jugular vein and showed inhomogeneous signal intensity and vascularization-related contrast agent uptake ranging from 80% to 140%. In 6 cases with high ipsilateral flow reduction, the contralateral sinus system showed an enlarged transverse and sigmoid sinus. Tumorous lesions could be ruled out by visualizing a superior jugular bulb ($n = 5$) on venous MR angiograms. In 4 cases, arterial MR angiography could delineate supplying vessels in correlation with DSA.
Conclusion: The authors recommend MR imaging and venous MR angiography for differentiating precisely between an asymmetry of the jugular bulb and tumorous lesions.

326 • 10:42 AM

MR Angiography of the Aortic Arch and the Carotid Artery

TJ Vogl, MF Juergens, J Balzer, B Anton, A Rademacher, J Lissner
Department of Radiology, University of Munich, Munich, Germany

Purpose: Evaluation of axial triple-slab 3D time-of-flight MR angiography and Doppler sonography for suspected arteriosclerotic disease of the carotid artery from the origin at the aortic arch to the syphon.
Methods: Sixty patients and 20 volunteers underwent Doppler sonography and MR angiography (Magnetom 63SP at 1.5 T, neck coil) of the carotid artery. Maximum-intensity projections were compared with raw data of axial

triple-slab FISP 3D MR angiography (overlap: 30%–45%) and results of Doppler sonography.

Results: Thirty-seven patients showed a stenosis of the proximal segment of the internal carotid artery in the direct vicinity of the carotid bifurcation. In 88% of patients, MR angiography was able to reproduce the eccentric contour of stenoses caused by atheromatous plaques. Stenosis of the external carotid artery was found in 7 patients. The stenotic segments were located exclusively in the course near the carotid bifurcation. In all cases, the evaluation of the MR angiogram showed a high correlation (92%) with the Doppler scan. In 1 case, a sonographically suspected aneurysm of the internal carotid artery could be ruled out by documenting coiling in the MR angiographic data set. Axial triple-slab MR angiography allowed a reliable depiction of the supraaortic arteries from the aortic arch to the syphon.

Conclusion: Analysis of both modalities indicated that technically adequate triple-slab MR angiography may be a sensitive screening method for lesions of the carotid artery.

327 • 10:54 AM

Acute Posterior Fossa Stroke in Children: Evaluation with MR Angiography

ST Bradshaw, CM Glasier, CA James, EJ Angtuaco
Department of Radiology, Arkansas Children's Hospital, Little Rock, AR

Purpose: To present MR angiographic findings in 4 children with posterior fossa stroke and to correlate the results of MR angiography with those of MR imaging and conventional angiography.

Methods: Four children aged 5–15 years were diagnosed with acute posterior fossa strokes. One child had a history of trauma. The other patients had no known etiology. All 4 patients underwent conventional MR imaging and time-of-flight MR angiography. Three also underwent conventional angiography.

Results: MR imaging showed focal areas of infarction in a posterior circulation distribution in all 4 children. Initial MR imaging in 1 patient showed abnormal flow in the basilar artery. Conventional angiography showed bilateral vertebral dissection in 1 patient and posterior circulation vascular occlusions in 2 others. MR angiography showed vascular occlusions corresponding to areas of infarction in all 4 patients. MR angiographic findings correlated well with conventional angiographic findings in 3 patients. All 4 children were treated with anticoagulation therapy. Follow-up MR angiography showed progressive vascular occlusion in 1 patient and recanalization in the other 3.

Conclusion: The findings of MR angiography correlated well with those of conventional angiography in the evaluation of posterior fossa stroke. MR angiography was valuable in follow-up, showing progressive occlusion in 1 patient and recanalization in the other 3.

328 • 11:06 AM

Apparent Vascular Occlusion on MR Angiograms Due to Proximity of Lateral Presaturation Bands

SA Mirowitz
Department of Radiology, Jewish Hospital at Washington University, St Louis, MO

Purpose: Spatial RF bands are frequently prescribed laterally when performing time-of-flight MR angiography, to reduce the signal intensity of fat and thereby improve vessel conspicuity. The objective of this study is to describe the potential for lateral presaturation bands to result in apparent occlusion of patent vessels.

Methods: Intracranial MR angiography was performed on a 1.5-T unit in 3 patients by using a 3D time-of-flight technique. Flow-compensated spoiled GRASS images were acquired (48/4.6, 25° flip angle, 64 partitions, and 1 excitation in the transaxial plane). Presaturation was applied superiorly to reduce venous signal intensity as well as around the periphery of the head in a "picture-frame" format. The sequence was then repeated in each patient after lateral presaturation bands were sequentially retracted and finally removed.

Results: Apparent occlusion of 1 carotid siphon was present in each patient on initial MR angiograms obtained with the lateral presaturation band. Progressive increased signal intensity within the vessel was demonstrated with retraction of the ipsilateral lateral presaturation band, and with the band removed, each vessel was documented to be patent.

Conclusion: The use of lateral presaturation bands in time-of-flight MR angiography may result in apparent occlusion of patent vessels. This is due to imperfections in the section profile of the administered RF pulses, so that the effect of such pulses may inadvertently contaminate adjacent tissue, leading to saturation of flowing spins. If the lateral presaturation method is to be utilized, it must be used with caution so that serious misdiagnosis does not occur.

329 • 11:18 AM

Gadolinium-enhanced MR Angiography of the Brain

DM Murakami, NR Bucciarelli, SR Kapelov, WJ Mullin, K Yan, WG Bradley, Jr
Memorial Magnetic Resonance Center, Long Beach Memorial Medical Center, Long Beach, CA

Purpose: At present, gadolinium is not used routinely in time-of-flight MR angiography due to background enhancement. However, with new techniques to minimize saturation effects, the use of contrast material is feasible. The newer nonionic agents such as gadodiamide injection (Gd-DTPA BMA, Omniscan; Sterling-Sanofi-Winthrop) also offer higher concentrations not previously available. To address the utility of gadodiamide in clinical practice, the authors tested routine MR angiography against gadodiamide-enhanced MR angiography.

Methods: Thirty-two patients were imaged through the circle of Willis with 3D time-of-flight MR angiography by using the Siemens 63SP. The sequence parameters used were either FISP (40/7, 15°) before injection and FISP (29/7, 50°) after injection or, later, a FISP (42/7) with a ramped flip angle from 10° (entry, lower surface) to 30° (exit, upper surface) and magnetization transfer contrast, both before and after injection. All patients were given a "triple dose" of 0.3 mmol/kg Gd-DTPA-BMA. Due to the intense enhancement of overlapping normal vessels, selectively targeted maximal-intensity projections with reduced numbers of partitions were obtained in some cases. All angiograms were reviewed by 3 reviewers who judged vessel enhancement, confidence of abnormality, and additional information not on routine MR angiograms.

Results: In several clinical situations the gadodiamide-enhanced MR angiograms distinguished pathology not revealed on routine MR angiograms. With Gd-DTPA-BMA it was possible to distinguish slow flow from occlusion in vessels that were not visualized with routine MR angiography. The vascular enhancement was crucial in diagnosing slow flow due to lupus vasculitis with asymmetric flow in the middle cerebral vessels. Gd-DTPA-BMA was also essential in demonstrating slow flow (as opposed to occlusion) due to vascular insufficiency in 1 patient while it confirmed acute occlusion in another with stroke. Slow flow (vs occlusion) within the venous system was diagnosed on the basis of enhancement of the transverse and sigmoid sinuses, which were compressed by tumor (me-

ningioma). Intense enhancement of unsuspected cerebral metastases led to a diagnosis in a patient with an occult malignancy referred only for MR angiography.
Conclusion: The strong contribution of Gd-DTPA-BMA to MR angiography is the ability to enhance vessels with slow flow and therefore distinguish them from occluded vessels whether in the arterial or venous system. While gadolinium is not necessary for every MR angiogram, the authors believe that the added information in selected cases may be crucial in the treatment of some patients.

330 • 11:30 AM

Preoperative Evaluation of Abdominal Aortic Aneurysm with MR Imaging

LG Martin, S Sheppard, GM Sherbourne, S Mukundan, SL Kaufman, AM Zuckerman
Department of Radiology, Emory University Hospital, Atlanta, GA

Purpose: Preoperative evaluation of an abdominal aortic aneurysm (AAA) frequently requires CT or US in addition to angiography. The authors have retrospectively studied 18 consecutive patients who were evaluated with T1 weighted SE and 2D and 3D fast field echo MR angiography, to determine whether operative outcome was affected by the lack of information from angiography, CT, or US.
Methods: The MR images were evaluated to determine the size and extent of the AAA; the levels necessary for the proximal and distal surgical anastomoses; renal, iliac, and common femoral artery patency; and the condition of the distal thoracic and upper abdominal portions of the aorta.
Results: Seven patients were operated on without angiography and 11 with only limited additional angiographic information necessary. In none was information from CT or US necessary. There was no significant increase in duration of the operation or recovery or in morbidity compared with patients operated on after conventional evaluation. False-positive diagnoses of common iliac artery stenosis and renal artery stenosis occurred 3 and 2 times, respectively. Angiography was necessary an additional 3 times to evaluate renal blood flow.
Conclusion: A high percentage of patients with AAA can be evaluated with MR imaging alone, and only limited angiography may be necessary for supplemental information in the remainder.

331 • 11:42 AM

Time-of-Flight MR Angiography at Field Strengths of 0.2–1.5 T: Comparison of Parameters, Sequences, and Results

U Boettcher, R Hausmann
Medical Engineering Group, Siemens AG, Erlangen, Germany

Purpose: Time-of-flight (TOF) MR angiography is the most widely used MR angiographic technique today, and results have been obtained from systems with field strengths down to 0.1 T. The field strengths, the resulting signal-to-noise ratio (S/N), and saturation effects have to be considered and are compared in this study.
Methods: Measurements were performed on Siemens Magnetom systems operating at 0.2, 1.0, and 1.5 T. FLASH and FISP sequences were used for the measurements.
Results: The most important factor for parameter considerations is the S/N. The smaller S/Ns at low field strengths can be partially compensated with high flip angles and reduced bandwidths. Higher flip angles lead to unacceptable saturation in some situations. At 0.2 T, lower bandwidths and thereby longer TEs have to be used, sometimes causing problems in the presence of turbulent flow. The longitudinal relaxation times depend on the field strength. The signal intensity from flowing blood is mainly determined by the number of RF pulses applied to the blood during its transition through the excited volume and the flip angle used. The saturation of the stationary tissue is a function of T1, TR, and the flip angle. Therefore, the signal intensity of stationary tissue is less saturated due to the reduced T1 at low field strength. Calculations show that the contrast is reduced at low field strength.
Conclusion: TOF MR angiography is useful from 0.2 to 1.5 T. According to the reduced S/N at low field strength, compromises have to be accepted. This limits the application of TOF MR angiography at low field strength.
U. Boettcher is an employee of Siemens, AG.

332 • 11:54 AM

Implications of Brain MR Imaging and MR Angiography in Endovascular Treatment for Acute Intracranial Venous Sinus Thrombosis

AM Wang, AN Shetty, FY Tsai, M Goetting, DP Wesolowski, W Yuh
William Beaumont Hospital, Royal Oak, MI

Purpose: The early clinical diagnosis of acute thrombosis of intracranial dural venous sinuses is difficult, and the prognosis is usually unfavorable. The use of brain MR imaging and 2D sequential MR angiography of venous circulation may provide the diagnosis early enough to lead to a successful endovascular thrombolytic treatment and improvement of clinical outcome.
Methods: Six consecutive patients with acute dural venous sinus thrombosis were treated with endovascular thrombolytic treatment. SE brain MR imaging and 2D sequential time-of-flight MR angiography with presaturation of the arterial blood flow were performed prior to and after treatment in all 6 patients.
Results: Resolution of blood clots ($n = 6$), resolution of interstitial brain edema ($n = 2$), and persistent ischemic infarct ($n = 1$) were found on SE MR images. Occlusion of venous sinuses ($n = 5$) and defects in the dural sinuses ($n = 1$) were found on MR angiograms with recanalization and improvement of the blood flow after treatment in all 6 patients. Five patients were completely recovered, and 1 patient improved clinically after the treatment.
Conclusion: Although this study is limited to a small patient population, the following points were noted: (1) SE brain MR imaging can help identify and monitor the status of blood clots and brain parenchymal changes prior to and after the treatment. (2) Two-dimensional sequential time-of-flight MR angiography can help identify the occluded venous sinuses and provide guidance for successful endovascular thrombolytic treatment.

Wednesday Morning
Imperial Ballroom
Papers 333–340

CONTRAST AGENTS IV: Brain and Miscellaneous

MODERATORS: SB Peterman, MD • GK Sze, MD

---

333 • 10:30 AM

Correlation of the Rate of Contrast Enhancement with Capillary Count in Breast Cancer: Implications for the Determination of Malignant Potential

RS Mezrich, N Barnard, D Devereaux, M Nissenblatt
Laurie Imaging Center, Robert Wood Johnson Medical School, New Brunswick, NJ

Purpose: To examine the ability of dynamic contrast-enhanced MR imaging to determine the malignant potential of breast cancer. Recent studies have shown a correlation between capillary count and the probability that a breast cancer will metastasize. This relationship is mediated by a proliferation of hyperpermeable capillaries. The increased vessel permeability, necessary for cells to metastasize, should also lead to increases in the rise time of contrast enhancement.
Methods: Patients with suspected breast lesions were imaged in the supine position on a 1.5-T Signa system. Surface coils were used, and the breast was compressed against the chest wall. An injection of 0.1 mmol/kg Gd-DTPA was performed, and 16 sagittal sections spanning the breast were obtained repetitively at a rate of 3 per minute for 320 seconds by using the fast SPGR technique. The images were transferred to a Macintosh workstation and displayed as a montage in a cine loop, and analyzed with region-of-interest cursors to create time-intensity profiles and measure rise time and magnitude.
Results: Fifteen patients, 6 with breast cancer, were imaged before surgery. The rise time of contrast enhancement in the cancers was greater than in benign lesions in all cases. There was moderate correlation ($P = .05$, Spearman rank test) between rise time and capillary count. There was poor correlation between maximum or equilibrium signal intensity and the presence of cancer.
Conclusions: These preliminary results indicate that the rise time of contrast enhancement can be a sensitive discriminant of tumor pathology and furthermore may be able to predict the invasive potential of breast cancers.

334 • 10:42 AM

Dextran-covered Superparamagnetic Iron Oxide: Assessment of Cervical Lymph Nodes in Humans

Y Anzai, RB Lufkin, MR Morris, SJ McLachlan, RE Saxton, WN Hanafee
Department of Radiology, UCLA Medical Center, Los Angeles, CA

Purpose: The presence of lymph node metastases has a strong influence on treatment planning and prognosis in patients with head and neck cancer. Current radiologic criteria for lymph node metastases include size, presence of central necrosis, and extracapsular spread. It is difficult, however, to distinguish small metastatic lymph nodes or large reactive lymph nodes containing no metastatic diseases. Animal studies that use superparamagnetic iron oxide particles have shown that these agents are phagocytized by elements of the reticuloendothelial system, including lymph nodes. The authors investigated a new MR contrast agent, dextran-covered superparamagnetic iron oxide particles (BMS 180549: Squibb Diagnostics), to assess cervical lymph nodes in humans.
Methods: MR imaging was performed before, and at 1, 4, and 24 hours after administration of contrast material in 5 healthy volunteers. The signal intensity of cervical lymph nodes was measured and analyzed as a function of dose, pulse sequence, and imaging time after injection.
Results: The intravenous injection of BMS 180549 dramatically decreased signal intensity of the cervical lymph nodes due to a strong magnetic susceptibility effect. T2*-weighted gradient-echo images as well as T2-weighted SE images showed significant decrease in signal intensity of normal lymph nodes at 24 hours after injection of contrast material at a dose of 1.7 mg Fe/kg.
Conclusion: Intravenous administration of BMS 180549 decreases the signal intensity of normal lymph nodes on T2- and T2*-weighted images. This agent may have the potential for discriminating normal lymph nodes from metastatic nodes and warrants further investigation.
M.R. Morris and S.J. McLachlan are employees of Squibb Diagnostics.

335 • 10:54 AM

Comparison of Triple-Dose Gadoteridol with Standard Dose Gadopentetate Dimeglumine in the Evaluation of Intracranial Lesions

MJ Kuhn, HT Youssef, LC Swenson, TJ Gleason
Department of Radiology, St. John's Hospital, Springfield, IL

Purpose: The sensitivity and safety of triple-dose gadoteridol in the evaluation of various intracranial disorders was compared with that of standard dose gadopentetate dimeglumine.
Methods: Twelve patients with various intracranial lesions (including neurofibromatosis, multiple sclerosis, and various neoplasms) were studied prospectively with both 0.3 mmol/kg Gd–HP-DO3A and 0.1 mmol/kg gadopentetate dimeglumine. Images were acquired before and immediately after administration of contrast material. The two studies were performed within 2 and 6 days of each other. Imaging parameters and injection rates were identical on both occasions. Patient monitoring for the gadoteridol study included physical examination, vital signs, and laboratory tests at several predetermined times.
Results: Thirty-five total lesions were demonstrated on the images after gadoteridol administration, while 22 lesions were demonstrated with gadopentetate dimeglumine. Additional lesions were seen with gadoteridol in 7 of the 12 patients. In 4 patients, 2 lesions were demonstrated with gadoteridol compared with only 1 on the gadopentetate dimeglumine studies, and this was of definite clinical significance. No patient had any laboratory or vital sign change secondary to contrast material injection.
Conclusion: On the basis of these preliminary results, 0.3 mmol/kg gadoteridol appears to be safe and more sensitive than 0.1 mmol/kg gadopentetate dimeglumine in the evaluation of various intracranial lesions.

336 • 11:06 AM

MR Imaging with High-Dose Gadodiamide of Soft-Tissue Tumors of the Head and Neck: Results of a Phase III Trial

TJ Vogl, M Mack, M Juergens, S Ihrler, J Lissner
Department of Radiology, University of Munich, Munich, Germany

Purpose: To evaluate high-dose gadodiamide injection with regard to safety, tolerance, and contrast enhancement in MR imaging of patients with soft-tissue tumors of the head and neck.
Methods: Fifty adult patients with soft-tissue tumors of the skull base ($n = 16$), neck ($n = 17$), and face region

($n = 17$) were examined with an intravenous injection of 0.3 mol/kg gadodiamide injection (Nycomed AS; Sanofi Winthrop). MR imaging was performed with a Magnetom 63SP (1.5 T, Siemens, Erlangen) with T2-, T1-, and fat-saturated T1-weighted SE sequences, before and after administration of gadodiamide injection. Slope of uptake of contrast material was obtained by using dynamic MR imaging over 10 minutes p.i. (TurboFLASH; TR/TE/TI = 6.5/3/300). Safety and tolerance were measured by registration of adverse events and discomfort during injection.
Results: The preliminary results show an increase in enhancement after administration of gadodiamide injection. Muscle tissue showed about 60% mean increase in enhancement and fat tissue about 15% increase. Soft-tissue tumors showed about 160% mean enhancement; on the average, there was a 2.7-fold increase in enhancement of tumors compared with muscle. Evaluating the degree of gadodiamide injection enhancement over time, the authors found a more rapid enhancement in highly vascularized lesions such as meningiomas, neurinomas, and glomus tumors in comparison with mesenchymal tumors. Fat-saturation sequences proved optimal in the demarcation and characterization of lesions with skull base infiltration ($n = 15$). Gadodiamide enhancement was most helpful in the delineation of small lesions near cranial nerves, vessel sheaths, and the parapharyngeal spaces.
Conclusion: These preliminary results indicate that high-dose gadodiamide injection is well tolerated and safe to use for MR imaging of the head and neck. An increased uptake in tumorous lesions could be demonstrated, resulting in increased contrast and better delineation of lesions in the head and neck.

337 • 11:18 AM

Tissue Characterization of Intracranial Tumors with MR Imaging

JC Böck, B Sander, J Haustein, R Felix
Strahlenklinik and Poliklinik, Klinikum Rudolf Virchow, Berlin, Germany

Purpose: To characterize intracranial tumors and surrounding brain tissue on the basis of Gd-DTPA–enhanced MR imaging. The authors hypothesized that typical constellations of signal intensity (SI) on T2-weighted images, degree of blood-brain barrier (BBB) disruption, and regional cerebral blood volume (rCBV) might be useful for describing the tissue alterations observed in brain tumors.
Methods: In 45 patients with intracranial tumors, proton density-, T2-, and T1-weighted images were obtained. During and after intravenous injection of 0.1 mmol/kg Gd-DTPA, fast T2*-weighted images were acquired, followed by postcontrast T1-weighted images. rCBV was calculated in selected regions of interest as the integral of the concentration-time curve (gamma-variate fit) after bolus injection.
Results: In low-grade intraaxial tumors, SI was increased, BBB was intact, and rCBV was low. In malignant intraaxial tumors, SI was increased, BBB was disrupted, and rCBV was high. Malignant intraaxial tumors often demonstrated signs of marked heterogeneity with central necrosis (SI increased, no contrast enhancement, rCBV = 0) and perifocal edema (SI increased, BBB intact, rCBV decreased). In extraaxial tumors, SI was intermediate, the BBB was disrupted, and rCBV was high. Central necrosis or perifocal edema, when present, showed the same characteristics as in malignant intraaxial tumors.
Conclusion: The results show that intracranial tumors possess tissue characteristics that can be used for differential diagnosis. While signal intensity alterations on T2-weighted images are quite nonspecific, the assessment of the BBB and of rCBF are useful for the characterization of intracranial tumors and surrounding brain tissue.

338 • 11:30 AM

Detection of Brain Metastases with MR Imaging Enhanced with High-Dose Contrast Agent

VM Runge, JE Kirsch, JW Wells, MH Awh, DF Bittner
MRISC, University of Kentucky, Lexington, KY

Purpose: The use of high-dose contrast material for improved detection of brain metastases on MR images is examined in an ongoing clinical trial.
Methods: Patients ($n = 13$ to date) with a high suspicion of brain metastases are imaged at 2 examinations, separated by more than 24 hours and less than 7 days. A dose of 0.1 mmol/kg Gd-HP-DO3A is administered for the first and 0.3 mmol/kg for the second MR imaging examination. Results are compared with those of 2 previous studies ($n = 31$ and $n = 12$), in which both images (standard and high-dose) were obtained in 1 session.
Results: The number of metastatic lesions detected increased from 26 at 0.1 mmol/kg to 33 at 0.3 mmol/kg (27%). Of patients with confirmed metastatic disease to the brain, 33% demonstrated an increase in the number of lesions detected at high dose.
Conclusion: With 0.3 mmol/kg Gd-HP-DO3A administered as a single dose, increased lesion enhancement is consistently seen. This permits identification of brain metastases that would otherwise go unrecognized on conventional pre- and postcontrast MR images, with therapeutic implications. These findings document the difference between doses without influence due to delayed enhancement or washout, a possible source of error in previous studies. Prior work compared 0.1 and 0.3 mmol/kg by performing an initial examination at 0.1 mmol/kg followed by a supplemental injection of contrast material at 30 minutes of 0.2 mmol/kg, failing to separate out possible temporal effects.
This research was in part supported by a scientific grant from Squibb Diagnostics.

339 • 11:42 AM

Safety and Efficacy of High Dose Gd-DTPA-BMA in the Central Nervous System

CG Torres, R Svihus, DT Kristoffersen
Nycomed Imaging AS, Oslo, Norway

Purpose: Gd-DTPA-BMA (Omniscan; Sanofi Winthrop, New York, NY; 0.5 mmol/mL) is a new nonionic paramagnetic contrast agent for MR imaging. The purpose of the present study was to compare the safety, efficacy, and possible additional diagnostic yield of a higher dose (0.3 mmol/kg) of Gd-DTPA-BMA compared with the standard dose of 0.1 mmol/kg.
Methods: A double-blind randomized parallel phase III trial was conducted to compare intravenously administrated Gd-DTPA-BMA at 0.1 mmol/kg with 0.3 mmol/kg. Safety was assessed by evaluating clinical chemical parameters in blood and serum, vital signs, neurologic status, and adverse events. Efficacy was evaluated by comparing images of the central nervous system (CNS) for diagnostic information and changes in signal intensity.
Results: Thirty-nine adult patients entered the study. The majority of the patients had suspected space-occupying lesions in the CNS or a question of recurrence of herniated disk in patients operated on in the lumbar spine. No changes of clinical concern were observed in either dose group regarding vital signs and clinical chemical parameters in blood and serum. No serious adverse events occurred; 1 mild event (sting in an eyelid lasting for 3 minutes) with uncertain relationship to the contrast medium was reported in the standard-dose group. In 7 of 19 patients receiving the high dose, new information that af-

fected patient management was reported, while the same was reported in 8 of 20 patients receiving the standard dose.
Conclusion: This trial indicates that the safety of Gd-DTPA-BMA administered intravenously at a high dose (0.3 mmol/kg) is similar to that of the standard dose of 0.1 mmol/kg. Efficacy was good for both doses.
C.G. Torres and D.T. Kristoffersen are employees of Nycomed Imaging.

340 • 11:54 AM

Accumulation of White Matter Abnormalities during a 3-Year Longitudinal Follow-up of Patients with Multiple Sclerosis

LA Stone, H McFarland, ME Smith, P Albert,
M Armstrong, DE McFarlin, JA Frank
Diagnostic Radiology Research Program, National Institutes of Health, Bethesda, MD

Purpose: The authors examined white matter (WM) abnormalities on T2-weighted MR images in 7 patients with multiple sclerosis (MS) and compared them with other MR imaging and clinical parameters.
Methods: Monthly MR imaging was performed at 1.5 T in 6 relapsing-remitting (RR) and 1 chronic-progressive MS patients. T1-weighted (SE 600/20) images were obtained before and after administration of Gd-DTPA as well as T2-weighted images (SE 2,000/100) over more than 36 months. Areas of enhancement and WM abnormalities were calculated by using Analyze-5.0.1 (Mayo Foundation). The area of WM disease on T2-weighted images was measured by taking the total area of WM abnormality including the lateral ventricles (LV) and subtracting the area of the LV on T1-weighted images.
Results: All 6 of the RR patients showed increases in the amount of T2-weighted WM abnormalities. In 3 patients, the increase was associated with a sustained increase in the Expanded Disability Scale Score (EDSS). The patient with the least change in T2-weighted parameters had the lowest average number and area of Gd-enhanced lesions on T1-weighted images, and the least change clinically. Correlation between the area and number of Gd-enhanced lesions and T2-weighted parameters was not identified, but this may be due to the small sample size.
Conclusion: This study documents the accumulation of diseased WM in patients with mild RR MS. Comparison of the MR imaging parameters and clinical status provides insight into the pathophysiology of MS. The mechanisms that control opening of the blood-brain barrier differ from those affecting WM abnormality.

Wednesday Afternoon • California Room
Papers 341–348

CHEST/CARDIAC

MODERATORS: JL Duerk, PhD • RD White, MD

341 • 2:45 PM

Identification of Rupture and/or Residual Silicone in Patients with Breast Implant

MS Middleton, R Mattrey, MK Dobke, R Vokoff
Department of Radiology, University of California, San Diego, CA

Purpose: To determine whether MR imaging can depict rupture of silicone gel-filled breast implants and/or residual silicone after explantation, and to study patterns of migration of silicone in patients who had silicone directly injected into their breast soft tissues.
Methods: The authors performed 133 MR imaging examinations on a 1.5-T GE MR imager in women who have or had silicone implants and/or direct silicone injections. In many of the more recent studies, the authors used a prototype bilateral breast surface coil (Medical Advances). Ninety-four subjects had silicone implants (average subject age, 40.3 years; average implant age, 8.1 years), 22 had been explanted (average age, 46.9 years), and 5 had been directly injected with silicone in the middle 1960s to the early 1970s (average age, 57.2 years). As of the date of submission of this abstract, 15 have undergone surgery: 13 for explantation and 2 to remove possible residual silicone after explantation. T2-weighted imaging with water and silicone suppression was used to identify silicone.
Results: The criteria for rupture were the presence of 1 or more of the following signs: (1) a thin, long extension of silicone away from the implant; (2) multiple wavy, continuous thin lines within an implant; or (3) a very irregular contour possibly accompanied by thin, irregular lines near the surface of the implant. The criteria for residual or migrated silicone were the presence of high signal intensity on a water-suppression T2-weighted image that turns to low signal intensity on a T2-weighted silicone-suppression image. On the basis of these criteria, the authors' preoperative predictions (4 rupture, 9 nonrupture, 1 residual silicone, 1 postoperative nonsilicone fluid collection) have been correct. The 5 cases of directly injected silicone showed variable migration to locations as distant as the low neck, back, and anterior wall of the abdomen and pelvis.
Conclusion: The initial results in identifying rupture in its various presentations are encouraging, but estimates of sensitivity and specificity for this small number of patients with operative follow-up would be premature. The authors are confident of their ability to distinguish silicone from naturally occurring soft tissue, which is useful in the identification of residual silicone after explantation and the migration of silicone in directly injected patients.

342 • 2:57 PM

Electrocardiogram-triggered RARE (Turbo SE) Imaging of the Chest

JL Haddad, JC Weinreb, NM Rofsky
MRI-Radiology, New York University Medical Center, New York, NY

Purpose: Conventional T2-weighted electrocardiogram (ECG)-triggered imaging of the chest is time consuming and often results in poor image quality due to respiratory and flow artifacts and variations of the RR interval over the 9–12 minutes usually required for data acquisition. Conventional T2-weighted RARE (Turbo SE) sequences decrease data acquisition time but are still suboptimal in the chest. The authors investigated the use of an ECG-triggered T2-weighted RARE sequence for evaluation of the chest.
Methods: Conventional ECG-triggered T2-weighted SE, nontriggered T2-weighted RARE, and ECG-triggered T2-weighted RARE sequences were employed to image the chest and/or liver in 30 subjects. The nontriggered and ECG-triggered RARE sequences each took under 2 minutes to image the chest.
Results: The ECG-triggered RARE sequence consistently resulted in a marked decrease in flow-related artifacts and improved overall image quality, especially in the mediastinum and heart.
Conclusion: ECG-triggered RARE imaging provides improved T2-weighted images of the chest in less time compared with conventional SE and RARE sequences.

343 • 3:09 PM

Regional Long-Axis Ventricular Wall Velocity Measured with MR Velocity Mapping: Comparison with M-Mode Echocardiography

SP Karwatowski, SJ Brecker, GZ Yang, M St John Sutton, DN Firmin, SR Underwood, DB Longmore
Magnetic Resonance Unit, Royal Brompton Hospital, London, England

Purpose: Long-axis ventricular wall motion is dependent on subendocardial myocyte function. It is an early marker of disease, often becoming impaired prior to short-axis parameters. M-mode echocardiographic measures can measure long-axis function at 3 points, and MR velocity mapping can document true regional long-axis function in all areas; the authors compared the 2 techniques.
Methods: Twelve patients with ischemic heart disease were studied off cardiac medication (1 woman; 4 with a previous infarct). Long-axis M-mode echocardiograms were acquired from the left and central fibrous bodies. These were analyzed to measure peak early diastolic velocity. On the same day, patients underwent an MR velocities mapping study. Velocity information was acquired through a basal short-axis plane. Peak early diastolic velocities in segments corresponding to those studied with M-mode were measured and compared.
Results: The mean velocity in millimeters per second (± standard deviation, range) for the left fibrous body was 65.8 (31.7, 22–125) with M-mode echocardiography and 62.3 (22.6, 28–98) with MR velocity mapping. The central fibrous body values were 53.4 (27.2, 19.6–120) for M-mode echocardiography and 54.4 (13.9, 29–80) for MR velocity mapping. Correlation coefficient for the left fibrous body was 0.85 ($P < .01$) and for the central body 0.65 ($P < .05$).
Conclusions: MR measurements of long-axis wall motion correlate well with those of M-mode echocardiography. Abnormalities of timing with respect to delay and duration are better examined with M-mode echocardiography; MR velocity mapping provides greater spatial information. The 2 techniques provide complementary information.

344 • 3:21 PM

Left Ventricular Regional Long-Axis Wall Motion Assessed with MR Velocity Mapping: A Comparison with Doppler Echocardiographic Transmitral Filling in Ischemic Heart Disease

SP Karwatowski, SJ Brecker, GZ Yang, M St John Sutton, DN Firmin, SR Underwood, DB Longmore
Magnetic Resonance Unit, Royal Brompton Hospital, London, England

Purpose: Abnormal ventricular relaxation is an early marker of ischemic heart disease. The authors used MR velocity mapping of long-axis myocardial wall motion as a means of assessing impaired diastolic function, comparing this new technique with Doppler ultrasound measurements of mitral flow.
Methods: Twenty patients (mean age, 62 years; range, 42–78 years; 18 men) with coronary artery disease (12 with previous myocardial infarction) were studied off cardiac medication. Doppler indices measured were peak mitral flow velocity during early diastole (E vel) and atriosystolic contraction (A vel). The velocity ratio (E/A) and early deceleration (E dec) were derived. Cine MR mapping of myocardial velocity perpendicular to a basal short-axis plane was performed on the same day. Velocity-time curves were constructed in each of 16 sectors, with measurement of the peak and mean early diastolic velocity (mean vel) and the number of segments with maximum velocity less than 50% of peak velocity (N).
Results: E vel was strongly correlated with both N and mean vel ($r = -.72$ and .82, respectively). E dec also had a strong correlation with both N and mean vel ($r = -.77$ and +.83; $P < .001$). A vel was less well correlated ($r = .47$ for N and −.36 for mean vel).
Conclusion: The authors have defined a new measure of regional diastolic ventricular function and have demonstrated that regional abnormalities of wall motion during early diastole have a significant effect on left ventricular filling.

345 • 3:33 PM

MR Assessment of Regional Long-Axis Myocardial Velocity during Dobutamine Stress: Comparison of Healthy Controls and Patients with Ischemic Heart Disease

SP Karwatowski, SM Forbat, RH Mohiaddin, GZ Yang, DN Firmin, SR Underwood, DB Longmore
Magnetic Resonance Unit, Royal Brompton Hospital, London, England

Purpose: Rest abnormalities of ventricular wall motion may be present in ischemic heart disease (IHD). Stress may exacerbate existing abnormalities and provoke new ones. The authors used symptom-limited dobutamine infusion and MR velocity mapping to study regional ventricular long-axis function.
Methods: Sixteen patients with IHD (6 with prior infarction; 3 women; age range, 30–69 years) and 8 healthy subjects were studied. MR cine velocity maps were acquired through a basal short-axis plane and divided into 16 sectors to provide regional long-axis myocardial velocity. After a resting study, dobutamine was infused at 5, 10, and 15 μ/kg per minute if tolerated, and the study was repeated. Early diastolic long-axis velocity was standardized to the peak circumferential value to permit comparison.
Results: Controls showed an increase in peak long-axis velocity ($P = .0002$) and a decreased time to peak velocity ($P = .0036$) during stress compared with baseline. At rest, all 6 patients with prior infarction and 3 without had impaired long-axis function. All patients showed increased absolute long-axis velocity during stress in at least 1 segment. Eleven developed areas of reduced relative velocity during stress; 2 showed no change. Two developed global reductions in velocity despite increases in the rate-pressure product. One showed an increase in velocity in an area abnormal at rest. The patient with triple vessel disease had the greatest change during stress. All patients tolerated the procedure well.
Conclusion: Low-dose dobutamine stress during MR velocity mapping of regional ventricular function is a useful technique for studying the effects of stress and induced ischemia on ventricular function.

346 • 3:45 PM

Ultrafast MR Imaging of the Major Pulmonary Vessels with Gd-DOTA

PC Douek, P Loubeyre, A Delignette, M Amiel, D Reuel
Hôpital Cardiovasculaire et Pneumologiene, Lyon, France

Purpose: To evaluate an MR pulmonary angiography imaging technique by combining ultrafast data acquisition with intravenous bolus injection of Gd-DOTA.
Methods: Thirty-five patients with suspected acute pulmonary emboli of the major pulmonary arteries ($n = 22$), hilar lung carcinoma with suspected infiltrated pulmonary artery ($n = 4$), or tetralogy of fallot with Blalock-Taussig shunts ($n = 9$) underwent MR imaging at 1.5 T (Siemens) and selective pulmonary DSA, 2D Doppler echocardiography, or surgery. After SE transverse sections, non-respiratory-gated or cardiac-trigerred oblique views were obtained along the main axis of the vessels (section thickness = 20 mm) by using a T1-weighted ultrafast gradient-echo sequence (TR/TE/TI = 6.5/3/300, $\alpha = 11°$).

Typical imaging times were 832 msec per image for a 128 × 128 matrix. After a single 0.1 mmol/kg intravenous bolus injection of Gd-DOTA, a series of 15 images were obtained simultaneously in the previously selected plane in less than 1 minute with a delay of approximately 1 second between images.
Results: Before injection of Gd-DOTA, the ultrafast image exhibited no signal intensity from the blood pool. After bolus injection, there was sequential pronounced signal enhancement from pulmonary to systemic circulation. All major pulmonary vessels were consistently and clearly visualized on ultrafast contrast-enhanced MR images. In some cases, subsegmental branches up to the sixth to seventh order branches could be depicted. All the 8 major pulmonary artery thrombi or tumoral processes ($n = 4$) detected with DSA were identified with ultrafast contrast-enhanced MR angiography. Distal thrombi were not visualized ($n = 8$). All obstructions of systemic-to-pulmonary shunts were identified ($n = 2$). Patency of a previously ligated Potts shunt was demonstrated.
Conclusion: Contrast-enhanced MR angiography allows reproducible, fast, dynamic, and multiplanar good-quality imaging of the major pulmonary vessels and their proximal branches. This technique may be useful in patients with pulmonary hypertension in whom DSA is dangerous, in patients with congenital obstruction of the right ventricular outflow tract, or in patients with abnormal pulmonary venous return when 2D Doppler echocardiography is limited.

347 • 3:57 PM

Chest MR Imaging in Staging of Non–Small Cell Bronchogenic Carcinoma: Evaluation of 500 Consecutive Patients

JD Tesoro Tess, A Amoruso, E Turrini, E Civelli, L Balzarini, E Ceglia, R Musumeci
Istituto Nazionale Tumori, Milan, Italy

Purpose: Preoperative assessment is an important clinical and radiologic problem in planning treatment in lung cancer. The purpose is to determine the value of MR imaging in staging of tumor (T) and node (N) at disease presentation.
Methods: From 1986 through 1991, in 500 consecutive, unselected, previously untreated patients with histologically proved non-small-cell bronchogenic carcinoma, chest MR imaging was performed with a 1.5-T Siemens Magnetom. T1-weighted, 8-mm-thick images with a 1.5-mm gap were obtained in the axial plane with electrocardiogram gating. The presence, size, and location of the primary tumor and the findings of mediastinal fat or vascular as well as pleural or chest wall invasion were recorded. Similarly, the presence, site, and size of hilar or mediastinal nodes were evaluated according to the ATS lymph node station mapping system, and a 10-mm diameter was used to distinguish normal from abnormal nodes. The T and N MR imaging classifications were compared with the definitive pathologic and surgical findings. For estimating overall accuracy, sensitivity, and specificity, T stages were grouped into T0–T2 and T3–T4 and N stages into N0–N1 and N2–N3.
Results: Of the 500 examined patients, 275 (55%) underwent surgery while 183 were considered not eligible for surgery due to extensive disease and 42 were not suitable for surgery because of anesthesiologic high risk. After surgery, 73 patients (26.5%) were considered to have T3–T4 tumors, while 202 (73.5%) had T0–T2 tumors. The overall accuracy in distinguishing T0–T2 from T3–T4 disease was 77.8%, with 52.9% sensitivity and 86.3% specificity. The overall accuracy of MR imaging in detecting N0–N1 from N2–N3 disease was 70.3%, sensitivity 75.7%, and specificity 67.7%. Node sampling was performed in 244 cases (average, 2.6 node groups), and histology disclosed metastases in 208/636 node sites (32.7%).
Conclusion: The staging of bronchogenic carcinoma and mainly of mediastinal lymph node diffusion can be usefully done with MR imaging, which demonstrated good diagnostic accuracy.

348 • 4:09 PM

MR Velocity Mapping of Aortic Stenosis: Estimation of Pressure Gradient, Aortic Valvular Area, and Flow Rate

L Søndergaard, P Hildebrandt, K Lindvig, C Thomsen, F Ståhlberg, E Kassis, O Henriksen
Danish Center for Magnetic Resonance, Hvidovre Hospital, Hvidovre, Denmark

Purpose: While the use of peak pressure gradients (ΔP) alone is an inaccurate way of assessing the severity of aortic stenosis, especially when cardiac output decreases, the aortic valvular area (AVA) and the cardiac index (CI) give important information as to the prognosis. Therefore, the aim of this study was to estimate ΔP, AVA, and CI simultaneously by using MR velocity mapping.
Methods: The authors examined 13 patients with aortic stenosis. MR velocity mapping was performed perpendicular to the aortic jet at the valvular level. ΔP was calculated by inserting the maximum velocity (v_{max}) of the stenotic jet into the modified Bernoulli equation ($P = 4 \cdot v_{max}^2$). AVA was measured in the peak systole image by using $v_{max}/2$ as the threshold for pixels included in the orifice. The flow rate was calculated as the product of area and mean velocity in the valvular area. As reference, all patients underwent heart catheterization to determine ΔP, and AVA was estimated from the Gorlin formula by using the mean systolic pressure gradient and the stroke volume found by a simultaneously performed right-heart thermodilution measurement. Flow rate was found by means of the indicator dilution technique performed simultaneously with MR velocity mapping.
Results: The results showed good agreement between MR velocity mapping and catheterization in determination of ΔP up to about 80 mm Hg, whereas MR velocity mapping underestimated higher values. Significant agreement was found between MR velocity mapping and the reference techniques in estimation of AVA and flow rate.
Conclusion: The 2 important parameters in aortic stenosis, AVA and flow rate, may be quantified with MR velocity mapping. The underestimation of the highest ΔP with MR velocity mapping may be explained by the fact that the modified Bernoulli equation omits the viscous loss, which may not be valid for small AVA, a problem also known from Doppler US. Hence, this study suggests that MR velocity mapping may become an important clinical tool for evaluation of aortic stenosis.

Wednesday Afternoon • Franciscan A
Papers 349–356

RELAXOMETRY

MODERATORS: GD Fullerton, PhD • SW Young, MD

349 • 2:45 PM

Discrimination of Muscle Pathology in the Rat with Relaxometry Imaging

JW Carlson, DM Goldhaber, A Brito, L Kaufman
Radiologic Imaging Laboratory, University of California, San Francisco, South San Francisco, CA

Purpose: Localized T1 dispersion measurements obtained from imaging procedures may be an indicator of

pathology. Particularly, quantitative measurements of the peaks in relaxation rates probe the coupling to nitrogen in proteins.
Methods: A clinical imager equipped with a field cycling electromagnet was used to image rats with a saturation recovery sequence. Tissue was prepared with a 90° pulse, then recovered when the field was cycled to a value between 300 and 1,000 G. Data from operator drawn regions of interest (typical volume, 2 cm^3) were extracted and fit to a monoexponential. Rats used were implanted with mammary adenocarcinomas or infarcted with absolute alcohol injected into the external iliac artery. The contralateral leg was used as normal muscle.
Results: The overall trend of relaxation rates for normal muscle show a decrease from 5 sec^{-1} at 300 G to 3 sec^{-1} at 1,000 G. Peaks in the rate occur at 500 and 660 G, with rates 0.5 and 1.0 sec^{-1} above the baseline. Infarcted muscle showed reduced rate and a reduced dispersive component: from 2.75 sec^{-1} at 300 G to 2 sec^{-1} at 1,000 G. Peaks at 500 and 660 G were also smaller: 0.5 and 0.75 sec^{-1}. Implanted tumor showed a nearly flat relaxation rate behavior at 2 sec^{-1}, with no significant change at 500 and 660 G.
Conclusion: As is well known, both infarct and tumors show increased T1 due to higher water content. Nitrogen peaks in infarcted muscle show that the underlying proteinous matrix is preserved in infarcted muscle, while their absence in tumor shows an alteration in that underlying structure. The exact cause of that alteration, whether it is from the growth of the tumor or its subsequent necrosis, is not fully understood at this time.

350 • 2:57 PM

Collagen in Aneurysmal Aorta: MR Study

P Vinee, B Meurer, A Constantinesco, KH Hauenstein, J Laubenberger, S Petkov, B Eisenmann
Radiologische Uni-Klinik Freiburg, Abteilung Röntgendiagnostik, Freiburg, Germany

Purpose: To study and compare the H-1 MR relaxation characteristics of collagen in normal aortic tissue and in abdominal aortic aneurysm with special attention paid to the second moment (M2) of the collagen line shape.
Methods: H-1 MR in vitro measurements were made at 60 MHz (Bruker SXP). The M2 and the T2 of the line shape of collagen ($T2 < 20\ \mu sec$) were measured in 14 abdominal aortic aneurysmal walls and 13 age-matched fresh cadavers. M2 is used in polymer science to characterize the molecular motion determining physical properties, especially the viscoelastic behavior.
Results: The percentage of collagen (9.4% ± 1.9 vs 7.3% ± 1.2) and M2 (5.3 ± 0.6 vs 4.8 ± 0.6 G^2) were found to be significantly ($P < .01$) higher in aneurysms (9.4% ± 1.9 vs 7.3 ± 1.2%). T2 was lower in aneurysms (16.3 ± 0.9 vs 17.7 ± 1.2 μsec; $P < .01$).
Conclusion: Aneurysmal dilatation (increased aortic radius and decreased wall thickness) leads to the rise of wall tension, consistent with the higher M2 found for aneurysm. This rise again leads to a recruitment of collagen fibers, explaining the found increase in collagen content. Aneurysms are considered biomechanical in origin, but recent evidence implies a biochemical dimension to their etiology. The increase in M2 indicates structural changes in collagen in aneurysms. The high M2 values in aneurysms are due to reduced molecular mobility of the collagen in aneurysms, possibly by site binding or intercalation in the complex helices or by electric dipolar interactions taking place in the less mobile side groups of the collagen macromolecule.

351 • 3:09 PM

Analysis of Relaxivity and Magnetization Transfer of the Major Lipid Components of White Matter

W Kucharczyk, P MacDonald, G Stanisz, RM Henkelman
Department of Radiology, University of Toronto, Toronto, Ontario, Canada

Purpose: To measure the MR relaxation times and magnetization transfer (MT) properties of the major lipid constituents of white matter.
Methods: Multilamellar phospholipid vesicles were synthesized by using varying amounts of phospholipid, cholesterol, sphingomyelin, and cerebroside. The lipids were dispersed in physiologic buffer at concentrations varying from 0% to 25% by weight. T1, T2, and MT were measured in a relaxometer operating at 60 MHz, using 300 mM physiologic buffer as a control.
Results: All lipids reduced the relaxation times. The maximum effect of pure phospholipid occurred at 25% concentration. T1 was reduced from 2.8 to 1.6 seconds, and T2 from 2.2 to 0.57 seconds. No MT effect was observed. The addition of equimolar amounts of cholesterol or sphingomyelin to the phospholipid did not cause significant changes in relaxivity, but an MT effect became apparent. The addition of cerebroside caused by far the greatest change in relaxation times, reducing T1 to 0.99 seconds and T2 to 0.24 seconds, and caused the most marked MT of all the lipids tested. The MT observed with cerebroside was 2.5 times greater than with either cholesterol or sphingomyelin.
Conclusion: Cerebroside has a much greater effect on MR relaxation and MT than any of the other major lipid classes in white matter. The effect of cerebroside is large enough to approximate the short T1 and strong MT observed in white matter. The authors hypothesize that the 4 hydroxyl groups on the galactose side chain of the cerebroside molecule are responsible for these properties.

352 • 3:21 PM

Fast Spin Echo: Shortcut to Accurate T1 Characterization

CRG Guttmann, K Oshio, FA Jolesz, RV Mulkern
Department of Radiology, Brigham and Women's Hospital, Boston, MA

Purpose: Rapid quantification of T1 from images is useful when monitoring dynamic processes, such as perfusion with contrast agents or heating of tissues (eg, laser surgery). Fast spin echo (FSE) has high temporal and spatial resolution and has been shown to be well suited for qualitatively monitoring dynamic T1 changes. The authors address the accuracy of T1 values obtained from FSE images.
Methods: Phantoms consisting of $MnCl_2$ and $NiCl_2$ solutions with a wide range of T1, T2, and T1/T2 ratios were prepared. On a 1.5-T GE Signa, images were obtained by using partial saturation (PS) with 4-echo FSE sequences and inversion recovery (IR) SE sequences. TR values used for T1 calculation were adjusted to account for the last refocusing pulse. T2 values were calculated from 64-echo Carr-Purcell-Meiboom-Gill studies.
Results: A linear least-squares fit yielded excellent correlation ($r^2 = 1.0$, slope = 1.04) between T1 values calculated from the IR and FSE sequences.
Conclusion: On the basis of the IR and FSE results, it appears that accurate T1 measurements with FSE are quite feasible. Considering the high speed and image quality of this sequence, the authors suggest its use for dynamic studies in which accurate T1 measurements are required.

353 • 3:33 PM

Interaction of Phosphonate-modified Gadolinium Complexes with Serum Albumin

IK Adzamli, V Brown, MA Davis
Department of Radiology, University of Massachusetts Medical Center, Worcester, MA

Purpose: Previous evaluation of paramagnetic phosphonates indicated enhanced in vivo relaxivities not explained by demetallation (1). Since there is a paucity of data on relaxivity enhancement from electrostatic interactions between molecules and proteins (2), this study explores the interactions between phosphonates (−3) and protein residues (+ve), because of the implications for agent development (better agents in vivo vs inhibition of serum enzymes).

Methods: The association of bovine serum albumin (BSA) with 2 phosphonates (Gd-DTPA-BDP [4-aminobutane-1,1-diphosphonate–modified DTPA], a free diphosphonate, and Gd-DOTP [the tetraphosphonate analog of DOTA], a bound phosphonate) was studied with relaxometry (3). Solutions with varying amounts of complexes and BSA were studied at pH 7, 20 MHz (H-1), 40°C, and the data (T1, T2) fitted to: $1/T_{1,\mathrm{observed}} - 1/T_{1,0} = k[\mathrm{BSA}]\{K[\mathrm{agent}]/(1 + K[\mathrm{agent}])\}$, where $1/T_{1,0}$ represents intrinsic relaxation rates.

Results: Derived association constants (K) and relaxivities (k) are as follows: Gd-DTPA-BDP: BSA $K(\mathrm{M}^{-1}) = 300 \pm 20$; $k(\mathrm{mM}^{-1}\mathrm{s}^{-1}) = 25 \pm 4$. Gd-DOTP:BSA $K(\mathrm{M}^{-1}) = 1{,}400 \pm 50$; $k(\mathrm{mM}^{-1}\mathrm{s}^{-1}) = 30 \pm 4$. The high association constant obtained for Gd-DOTP (4 bound phosphonates) could result from a configuration of Gd-DOTP where 4 phosphonates on 1 face of a prismatic arrangement will concentrate negative charge on that face. Relaxivities are identical for both adducts.

Conclusion: Nonspecific associations are possible between highly charged complexes and protein residues to yield species with enhanced relaxivities. The implications for enzyme activity are yet to be explored.

1. Adzamli IK, et al. Invest Radiol 1991; 26:143–148.
2. Koenig SH, et al. Magn Reson Med 1986; 3:791–795; ibid 1986; 3:541–548. 3. Connors KA. Binding constants. New York: Wiley-Interscience, 1987.

354 • 3:45 PM

Early Detection of Denervation in Rat Muscle: MR Imaging versus Electromyography

ME Sweet, AR Cross, C Lemaire, ML Wood, PA Ashby
Department of Neurology, Toronto Hospital, Western Division, Toronto, Ontario, Canada

Purpose: Needle electromyography (EMG), the standard method for detecting denervation in human muscles, has several deficiencies: It is invasive, painful, and restricted to small areas of accessible muscles. MR imaging is not hampered by these deficiencies. A preliminary report suggests that MR imaging can depict denervation through changes in T2 (1). The authors' aim was to test the hypothesis that T2 changes allow the detection of denervation earlier with MR imaging than with EMG.

Methods: The left sciatic nerve was lesioned in 6 female 120-g Wistar rats. MR images were obtained in 4 rats 1, 8, 15, and 29 days after surgery. The MR images were acquired with a 2.0-T CSI Omega system. An SE pulse sequence with 16 echoes at 10-msec delays was used to produce axial images with TR = 500, 1,000, 2,000, and 4,000 msec. Fat-suppressed images were acquired under similar conditions by using a 1,331 frequency-selective inversion pulse followed by a 140-msec delay before each excitation. The T2 measured in the denervated muscles was compared with the T2 in the unaffected leg, which served as the control. The two remaining rats underwent nerve conduction studies and EMG on days 1, 8, and 15 after surgery.

Results: At 15 days after surgery, the T2 of sciatic-innervated muscles on images with and without fat suppression was elevated by approximately 15% relative to the control. The elevated T2 persisted for at least 30 days. Nerve conduction studies of the sciatic nerve in the 2 rats demonstrated normal nerve conduction below the lesion 1 day after surgery but not on days 8 and 15 after surgery. EMG depicted fibrillation potentials in the sciatic-innervated muscles 8 days after surgery.

Conclusion: EMG can facilitate detection of denervation in sciatic-innervated muscles of the rat 8 days after surgery. T2 does not become elevated significantly until 15 days after surgery.

1. Pollak JF, Jolesz FA, Adams DF. Invest Radiol 1988; 23:107.

355 • 3:57 PM

T1 in the Diagnosis of Squamous Cell Carcinoma Lymph Nodes and as a Predictive Assay for Radiochemotherapy

C Wagner-Manslau, P Lukas, M Herzog, RJ Kau
Nuklearmedizin Klinik, TU München, Munich, Germany

Purpose: To prove that relaxometry is reliable in tumor diagnosis, as a predictive parameter in therapy, and for differentiation of residual or recurrent tumor.

Methods: The authors investigated 91 patients (median age, 53 years) with different head and neck tumors. Thirty-eight underwent operation and 53 radiochemotherapy. All were studied before therapy, 53 after the first and second courses of radiochemotherapy. T1 was evaluated with τ0 (IE-mode TR/TE/TI = 1,400/30/120, 300, 400, 500).

Results: Histologic validation of T1: In the group of hypothetically not malignant lymph nodes (T1 < 800 msec) 108/116 were hyperplastic (T1 = 549 msec ± 181) and 8/116 tumor infiltrated (T1 = 783 msec ± 10). In the group of hypothetically malignant lymph nodes (T1 > 800 msec), histology proved tumor in 23/28 (T1 = 935 msec ± 122) and infection in 5/28 (T1 = 854 msec ± 23). Eighteen percent false-positive ($n = 5$), 7% false-negative ($n = 8$), sensitivity 82%, specificity 93%. T1 changes during radiochemotherapy: T1 of 55 hypothetically malignant lymph nodes was 949 msec ± 129. After the first course of radiochemotherapy, 36 lymph nodes were left with a significantly ($P < .01$) reduced T1 (801 msec ± 156); after the second course, 26 were left with also significantly ($P < .01$) reduced T1 (733 msec ± 105); and 8 weeks after therapy, 13 were still left with T1 = 731 msec ± 84.

Conclusion: T1 improves N classification; malignant and hyperplastic lymph nodes can be diagnosed with a sensitivity of 82% and a specificity of 93%. T1 can be considered a predictive assay showing favorable therapeutic changes such as fibrosis proved with histology (in animal study).

356 • 4:09 PM

Magnetostatic 3D Model of Vertebral Trabecular Bone and Relationship to T2*

JC Ford, FW Wehrli, H Chung
Department of Radiology, University of Pennsylvania Medical Center, Philadelphia, PA

Purpose: The objective was to develop a computer-based mathematical model of the magnetic field distribution (MFD) in trabecular bone. T2* is reciprocally related to the width of the MFD and is believed to depend on the density of trabeculation (1,2). This model may assist in predicting the relative sensitivity of T2* to specific architectural parameters (bone volume, trabecular plate density, thickness, etc).

Methods: The model chosen is a 3D lattice of interconnected struts, similar to one used in bone mechanics (3). The magnetic field perturbation was derived analytically from the induced magnetic surface charge density. MFD was calculated for 2,000 randomly placed locations within a unit cell and included contributions from 65 nearest neighbor struts. T2* was calculated for (*a*) constant strut thickness (200 μm) while varying strut density (number of struts per unit length) from 0.5 to 1.1 mm^{-1}, (*b*) constant strut density (0.83 mm^{-1}) while varying strut thickness from 140 to 250 μm, and (*c*) constant "bone" fraction (8%) while varying density and thickness.
Results: T2* is predicted to increase both with (*a*) decreasing strut thickness (−0.06 ms/μm) and (*b*) decreasing strut density (−30 ms/mm^{-1}). For the same change in bone volume, T2* is more sensitive to strut density. Finally, T2* is predicted to be invariant when both strut thickness and density are varied such that bone volume is held constant (*c*).
Conclusion: The model shows that T2* is sensitive to microarchitectural changes, supporting earlier hypotheses (1,2) that MR imaging-based T2* reflects trabecular thinning and thus may serve as a predictor of fracture risk.

1. Ford JC, Wehrli FW. Magn Reson Med 1991; 17:543.
2. Wehrli FW, Ford JC, Attie M, et al. Radiology 1991; 179:615. 3. Gibson LJ. J Biomechanics 1985; 18:317.

Wednesday Afternoon • Franciscan B Papers 357–364

PULSE SEQUENCE II

MODERATORS: W Sattin, PhD • FG Shellock, PhD

357 • 2:45 PM

Fat-Suppression MR Imaging of the Pancreas

A Shirkhoda, KG Bis, AN Shetty
William Beaumont Hospital, Royal Oak, MI

Purpose: To evaluate a new SE fat-suppression (FS) technique in the MR imaging assessment of the pancreas.
Methods: A prospective MR imaging study of the pancreas was done in 7 volunteers and 8 patients by using an FS technique that uses a broader fat RF pulse with a flip angle of 130°. In addition, conventional T1- and T2-weighted SE and breath-hold T1-weighted FLASH sequences were used. T1-weighted breath-hold FLASH and T1-weighted FS sequences were repeated after intravenous injection of Gd-DTPA. All patients underwent CT within 1 week of MR imaging. The MR imaging findings were compared with each other and correlated with findings from CT.
Results: On the T1 FS image, the normal pancreas was seen as a homogeneous well-defined structure displaying high signal intensity. It was rated superior to the conventional SE sequences with regard to overall image quality, lack of artifacts and pitfalls from adjacent bowel loops, and the specificity of diagnosis. Among the 6 patients with CT findings suspected of having pancreatic pathology, in 1 there was focal fatty infiltration of the pancreas, in a second case there was an a nonopaque stone impacted in the distal common bile duct, and in the third and fourth cases, there was normal variation of the tail of the pancreas in 1 and a splenic mass in another, both mimicking a pancreatic tumor on CT scans. In the fifth case, there was partial thrombus in the portal vein confluence that mimicked a pancreatic tumor on CT scan, and in the sixth case, there was a small 1-cm pancreatic insulinoma. In 2 patients, a normal pancreas was found, confidently excluding a mass suspected with CT.
Conclusion: The FS sequence provides the highest image quality and soft-tissue contrast resolution for detection of normal pancreas and diagnosis of normal variations and benign conditions and probably neoplasms of pancreas.

358 • 2:57 PM

Magnetization Transfer Pulse Power for 2DFT Gradient-Echo Imaging of the Knee

GC Hurst, CW Gardner, AD Motta, DA Finelli, JM Lieberman, R Yagan, EM Bellon, J Hua
Department of Radiology, MetroHealth Medical Center, Cleveland, OH

Purpose: Preliminary to a study of the efficacy of magnetization transfer (MT) imaging of the knee, the authors sought to determine appropriate levels of MT power. Published work emphasizes MT excitation that maximally suppresses the cartilage signal intensity, corresponding to the largest cartilage-fluid contrast. From this, the authors hypothesized that preferred conditions would include maximum saturation, with SAR restrictions as a limiting factor.
Methods: Sagittal 2D Fourier transform gradient-echo images of the knee were obtained with Picker Vista HPQ 1.5-T and 1.0-T MR imagers, with healthy volunteers as subjects. MT sequences were constructed by adding an MT pulse (10-msec duration, Gaussian, truncated at 3σ, offset 1.6 kHz) to each section imaging cycle of the authors' standard knee gradient-echo sequence (12 sections, 600/13). Section excitation was 30°. Images were collected by using a range of MT pulse amplitudes, from 0 to a limit due to SAR at 1.5 T (14 μT) or system maximum (23 μT). Image preferences were chosen by 6 experienced radiologists in the context of expected overall utility for a specified "family" of common knee problems.
Results: The average preferred parameter configuration was 7-μT MT pulse peak amplitude, with a range from 0 to 12 μT. This average preference corresponds to only 0.4 W/kg SAR at 1.5 T, well below suggested safety limits. Preliminary findings in an ongoing patient trial do suggest improved detectability of cartilage lesions with these parameters.
Conclusion: "Optimum" gradient-echo MT imaging of the knee does not appear to be limited by SAR, because complete saturation of cartilage is not required.

359 • 3:09 PM

Power Efficiency of On- and Off-Resonance Magnetization Transfer Methods

J Hua, GC Hurst
Department of Radiology, MetroHealth Medical Center, Cleveland, OH

Purpose: Methods used for magnetization transfer (MT) saturation on whole-body imaging systems include off-resonance continuous-wave (CW) excitation, on-resonance binomial pulses, and off-resonance shaped pulses. It has been proposed elsewhere that on-resonance MT excitation is fundamentally more efficient than off-resonance excitation. The authors believe this is not true and report here their findings relating to that suggestion.
Methods: The authors consider simple gradient-echo MT sequences with MT excitation (plus gradient spoilers) at the beginning of the imaging pulse sequence. Computer simulations were based on a generalized form of the Bloch equations, including cross relaxation. Whole-body MT experiments, with the pulsed MT approaches, were performed on a Picker 1.5-T Vista whole-body imaging system. Samples included boiled eggs, $MnCl_2$-doped water, and human volunteers. The RF of the system was calibrated, and RF amplitude and power compressions were considered.
Results: Simulations show similar power efficiency over reasonable ranges of contrast and acquisition parameters, if each method is used near its "optimum" conditions. The

pulsed MT experimental results generally agreed with the trends indicated by simulations. The largest discrepancies were found for binomial MT pulses, for which the experimental direct saturation was much higher than expected from simulations; this is not well understood but may be due to extreme fidelity requirements for the binomial pulses. The off-resonance shaped pulse MT results are consistent with published results from another laboratory that used CW MT at similar power levels.

Conclusion: The power efficiency of on- and off-resonance MT saturation is nominally equivalent.

360 • 3:21 PM

Use of GRASS Pulse Sequence to Detect in Vivo Temperature Changes Noninvasively

A Darkazanli, KH Hynynen, EC Unger, AF Gmitro, TA Fritz, RW Ziolkowski, CA Damianou

Department of Radiology-MRI, Arizona Health Sciences Center, Tucson, AZ

Purpose: MR imaging has been used for noninvasively monitoring in vivo tissue changes. Monitoring in vivo local temperatures is particularly important in localized hyperthermic and heat surgeries. The results of the sensitivity of the GRASS pulse sequence to T1 changes due to thermal effects are presented.

Methods: A set of 11 phantom tubes of 2% agar gel and saline with various Gd-DTPA concentrations was prepared. T1 and T2 of the tubes were measured with SE pulse sequences. GRASS pulse sequences with TR of 50, 100, 200, and 300 msec, TE of 5 msec, and flip angle of 60° were used. The equation for the GRASS pulse sequence was examined against experimental results. The T1 sensitivity of the pulse sequence was then determined and used to estimate the changes in T1 due to the thermal changes caused by immersing the tubes in a thermally controlled water bath. Ten rabbits were used to confirm the consistency of the GRASS sequence.

Results: The GRASS pulse sequence showed consistent sensitivity to temperature changes. An increase in T1 led to a reduction in signal intensity. The percentage change in signal intensity depended on the actual percentage change in T1. An increase in temperature by 40° led to a reduction in signal intensity to 60%. Computer simulations were used to predict the changes in the T1 of the phantom. Animal results correlated well with phantom studies. When heat was applied by using ultrasound energy, there was a reduction in signal intensity by 30%–40%.

Conclusion: In vivo temperature changes can be successfully monitored with the GRASS pulse sequence. Sensitivity of approximately 1% per degree celsius can be used as a rule of thumb. Due to the use of a very short TE, diffusion effects are minimal.

361 • 3:33 PM

Intravoxel Phase Cancellation Effect between Water and Lipid Protons in STIR Sequence

H Sugimoto, T Kimura, O Sakai, T Shinozaki, T Ohsawa

Department of Radiology, Jichi Medical School, Kawachi-Gun, Tochigi-Ken, Japan

Purpose: Because of the inherent sensitivity of the inversion recovery sequence to phase term and the presence of water (15%) in adipose tissue, an intravoxel phase cancellation effect between water and lipid protons is thought to affect fat suppression in the STIR sequence. The purpose of this study was to investigate the phase effect on fat suppression in the STIR sequence.

Methods: By using STIR combined with the Dixon method (oppose phase STIR [OPIR]) and conventional STIR (in-phase STIR [IPIR]), the authors measured the signal intensity of adipose tissue in volunteers and plotted it as a function of TI. In patients, they measured the signal difference-to-noise ratio (SD/N) in the same plane by using OPIR and IPIR at a variety of TIs. All studies were done with a 1.5-T superconducting magnet.

Results: The profiles of the signal intensities crossed each other between 150.2 and 157.1-msec TI (average, 154.0 msec ± 2.9). The TI-dependent phase cancellation effect was confirmed in patients. SD/N of OPIR was superior to that of IPIR when TI was shorter than 160 msec.

Conclusion: The results indicated that water protons rather than olecinic protons (–CH=CH–) play a major role in the opposed phase effect in vivo. It is concluded that profound fat suppression in STIR is derived from the inherent phase-contrast effect between water and lipid protons, and that the most effective fat suppression can be achieved when the intravoxel phase-cancellation effect between water and lipid protons is maximal, rather than when longitudinal magnetization of lipid protons is minimal.

362 • 3:45 PM

Magnetization Transfer Contrast MR Imaging of Tumor Necrosis in Rats

KC Li, RB Jeffrey, S Ning, A Kandil, G Hahn, B Pike, G Glover, J Kosek

Department of Radiology, Stanford University Medical Center, Stanford, CA

Purpose: To compare the ability of magnetization transfer contrast (MTC) MR imaging and conventional SE MR imaging in detecting necrosis in adenocarcinomas implanted in rat livers.

Methods: Adenocarcinoma cells were transplanted in 10 syngeneic BDIX rats. To induce various degrees of tumor necrosis, the rats were randomly assigned to (1) control ($n = 2$), (2) localized hyperthermia ($n = 3$), (3) intralesional cisplatin ($n = 2$), (4) hyperthermia plus intralesional cisplatin ($n = 3$). At day 7 after treatment, the rats were imaged with a Signa 1.5-T MR imager with (1) GRASS 500/8, 20° with and without the 0° binomial pulse, (2) SE 2,500/20, 80, and (3) SE 300/20 pulse sequences. The rats were then killed, and pathologic specimens were prepared with MR images as guidance. T2 and Ms/Mo ratios of the necrotic and granulation tissues and viable tumors were determined.

Results: Compared with standard GRASS images, GRASS images with the 0° binomial pulse provided better contrast between the pathologic tissues and normal liver. However, T2 values were more useful than Ms/Mo ratios in distinguishing necrotic from viable tumors.

Conclusion: MTC MR imaging was inferior to SE MR imaging in distinguishing necrotic from viable tumors in rat livers by using the pulse sequences described.

363 • 3:57 PM

SE and STIR Sequences in the Assessment of Brain Myelination

DM Wimberger, KJ Hittmair, THW Rand, J Kramer, H Imhof

Department of Neuroradiology, University of Vienna, Vienna, Austria

Purpose: MR imaging is of demonstrated diagnostic importance in the assessment of brain myelination. However, the relative value of T1- and T2-weighted SE sequences compared with STIR sequences is unclear. The aim of this study was to evaluate which sequences would provide the clearest anatomic information about ongoing myelination during various stages of neonatal development.

Method: Twenty-seven infants and young children with normal neurologic development were examined with a 1.5-T superconducting system (Siemens 63P). T1-

weighted (700/15), T2-weighted (2,500–3,000/15, 90) SE sequences and STIR (2,500/20/40) sequences were obtained. White matter age was determined by using a flow chart diagram (1). Classification of signal intensity of white matter was performed with reference to established intracerebral landmarks.
Results: During the first 6 months of age, T1-weighted sequences were most useful for assessing myelination of deep supratentorial white matter, while infratentorial white matter changes could be followed better with T2-weighted images. From 6 to 14 months, STIR images provided optimal contrast in supratentorial regions; after 14 months, T2-weighted images mirrored the myelinating process better than other sequences.
Conclusion: The usefulness of T1- and T2-weighted SE and STIR sequences in the assessment of myelination depends on the state of brain maturation and thus may vary during the first 2 years of life.

1. Barkovich AJ, et al. MRI Decisions 1989, May/June, 17–26.

364 • 4:09 PM

Development and Value of Fast STIR for Musculoskeletal MR Imaging

M Vahlensieck, F Träber, J Gieseke, K Seelos, M Reiser
Department of Radiology, University of Bonn, Bonn, Germany

Purpose: One disadvantage of the STIR sequence is its long acquisition time. The purpose of this investigation was to develop a fast STIR sequence at 0.5 T and to compare its diagnostic reliability with SE and gradient-echo sequences for musculoskeletal applications.
Methods: To find the null point of fat for an inversion-recovery sequence with a particular short TR, the authors calculated the TI for different TRs ($TI = T1_{fat} \times \{\ln 2 - \ln[1 + \exp(-TR/T1_{fat})]\}$) and performed measurements on a fat phantom. They used TRs from 800 to 1200 msec, a matrix of 256 × 128, and 2 excitations. Measurements were performed at 0.5 T (T5, Philips). They then compared the lesion conspicuity and detail perceptibility of this optimized fast STIR sequence with T2-weighted SE and T2*-weighted gradient-echo sequences in 22 patients with inflammatory and neoplastic musculoskeletal disorders.
Results: A combination of TR/TE/TI = 1,000/30/100 yielded best contrast with good nulling of fat and allowed for a sufficient number of sections in less than 5 minutes. The conspicuity of lesions on fast STIR images was superior to T2-weighted SE images in 80% and to T2*-weighted gradient-echo images in 40%.
Conclusion: The STIR sequence can easily be accelerated by using short TR/ideal TI combinations. These combinations can be predicted mathematically for different magnetic field strengths. This fast STIR sequence can aid in diagnostic sensitivity of musculoskeletal MR imaging.

Wednesday Afternoon • Plaza A
Papers 365–373

IMAGE PROCESSING

MODERATORS: LP Clarke, PhD
DN Levin, MD, PhD

365 • 2:45 PM

3D Reconstruction of Subtraction Images in Female Breast Imaging

HJ Oellinger, B Sander, U Quednau, J Hadijuana, W Schoenegg, F Felix
University Hospital Rudolf Virchow, Universität Berlin, Berlin, Germany

Purpose: Basically, with MR female breast imaging, it is possible to detect small malignant lesions that will often not be seen with conventional mammography. It is difficult to make a safe diagnosis for poorly enhancing lesions. After compiling subtraction images, the application of the maximal-intensity projection (MIP) method can be diagnostically helpful.
Methods: Thirty-three patients (age range, 18–85 years; median, 50 years) with clinical and/or suspicious signs at mammography were investigated with MR imaging. A 1.5-T MRT and a double breast coil (Siemens, Erlangen, Germany) were used. The contrast agent Magnevist (Schering, Berlin, Germany) was administered at a dose of 0.1 mmol/kg. The sequence used was FLASH 3D, 22/4, 40° flip angle. It was applied once before and twice after administration of contrast material in a transverse plane. All MR imaging results were histologically verified.
Results: By using the MIP technique in 2 cases, 1 carcinoma and 1 fibroadenoma could be detected that conventional MR images and mammograms did not show. Furthermore, among 10 multicentric carcinoma female breast MR images, it was possible to detect 8; mammography gave the right answer only once.
Conclusion: Female breast MR imaging proved in the past to be probably the best method for detection of breast cancer. For detecting poorly enhancing lesions, the MIP technique may contribute to a more certain diagnosis.

366 • 2:57 PM

Semiautomatic Quantitation of Cerebral Ventricles and White Matter Lesions in Dementia

RA Margolin, AP Zijdenbos, BM Dawant, MC Burger, AC Palmer
Vanderbilt University Medical Center, Nashville, TN

Purpose: The quantitative analysis of MR image volumes requires a computer-aided approach, especially since modern fast volumetric acquisition sequences produce vast data sets. The authors have developed a semiautomatic, multimodal image segmentation system based on artificial neural networks (MIDAS) to perform such tasks, and they are currently validating this technique in dementia.
Methods: T1-, T2-, and proton-density–weighted axial brain images of 6 patients with Alzheimer disease (AD) were acquired with a Siemens 1.5-T Magnetom imager. From each of these sets, 6 registered sections were selected for analysis. Ventricular cerebrospinal fluid (CSF) and white matter lesion (WML) areas were determined on these images by using MIDAS. In parallel, regions of interest (ROIs) for the same tissues were manually drawn by experts, and the results were compared. Both methods were repeated twice by 2 operators, resulting in a total of 8 measurements per section.
Results: The areas of ventricular CSF and WML obtained manually and with MIDAS were compared section by section. The correlation coefficients for WML and CSF, calcu-

lated over all measurements on all sections used in the experiment, are 0.87 and 0.99, respectively. Both correlations were statistically significant ($P = .001$).

Conclusion: Measurements obtained with MIDAS show a good correlation with those obtained from manually drawn ROIs, especially for ventricular CSF. MIDAS will therefore be a valuable tool in quantitative morphometric MR imaging studies, such as the differential diagnosis of AD and multiinfarct dementia.

367 • 3:09 PM

Gd-DOTA Dynamic MR Imaging of Transplanted Kidneys Processed with Factor Analysis of Medical Image Sequences

J Chabriais, JM Correas, O Helenon, H Benali, F Frouin, C Legendre, JF Moreau, R Di Paola

Department of Radiology, Necker Hospital, Paris, France

Purpose: To visualize and evaluate the different components of Gd-DOTA pharmacokinetics to assess renal transplant perfusion with dynamic MR imaging sequences processed with factor analysis of medical image sequences (FAMIS).

Methods: Sixty hydrated patients underwent 62 MR imaging studies of their transplanted kidney (1.5-T GE Signa) with an SPGR sequence. Twenty-five coronal transsinus sections were acquired every 10 seconds during a breath hold, within 6 minutes after bolus intravenous injection of Gd-DOTA (0.1 mL/kg if serum creatinine level was <300 μmol/L and 0.2 mL/kg if not). Image sequences were then processed with FAMIS, which estimates by means of orthogonal and oblique multivariate analysis, physiologic time-concentration functions (factors) and their spatial distribution (factor images).

Results: In normal kidneys, 4 factors were exhibited: cortical, pyramidal, medullary, and excretory. For patients having chronic rejection and renal insufficiency, the cortical factor was modified, whereas for patients with only histologic changes, the patterns were near normal. In cases of acute rejection, all components were modified. In cases of cortical necrosis, FAMIS exhibited a specific factor related to the infarcted area. In cases of renal artery stenosis and of histologic cyclosporin toxicity, the factors showed a normal pattern. In the cases of chronic rejection with other associated complications, the patterns were close to those of chronic rejection.

Conclusion: FAMIS allowed extraction of physiologic information about the pharmacokinetics of the paramagnetic agent, from dynamic MR imaging sequences of transplanted kidneys. Several qualitative patterns were depicted and have to be further studied.

368 • 3:21 PM

Different Bone Marrow MR Imaging Patterns in Multiple Myeloma with Spin-Echo and Gradient-Echo Sequences with Opposed-Phase Fat Suppression

AA Alim, MK Razavi, JR Berenson, RC Udkoff

Center for the Health Sciences, UCLA-VA Wadsworth, Los Angeles, CA

Purpose: Accurate detection of multiple myeloma bone lesions improves staging of the disease. MR imaging has been shown to be superior to other imaging modalities for detection of marrow lesions. The authors investigated the value of a gradient-recalled echo (GRE) imaging technique with fat suppression to improve the detection of focal myelomatous lesions.

Methods: Thirty patients with histologically proved multiple myeloma were imaged on a 1.5-T Siemens Magnetom SP. GRE (T1 FLASH) MR images with a TE value chosen to cause fat-water phase opposition were compared with conventional SE T1- and T2-weighted sequences. A body coil and large field of view were used to visualize the entire spine in a sagittal plane. The pelvis and proximal femurs were imaged in the coronal plane. Gadolinium was used in some cases.

Results: Different patterns of myelomatous involvement of the bone marrow including diffuse and focal patterns were recognized. GRE with fat suppression was superior to T2-weighted SE for visualization of the lesions. The GRE sequences had much shorter acquisition time, less motion artifact, and increased sensitivity for the detection of focal lesions.

Conclusion: The GRE image sequences with fat suppression based on optimized TE value offer an improved assessment of lesions in the entire spine, pelvis, and proximal femur when compared with T1- and T2-weighted SE sequences. Delineation of focal lesions was also improved.

369 • 3:33 PM

Reconstructed MR Angiography of Human Coronary Arteries

JD Pearlman, W Li, WJ Manning, RR Edelman

Departments of Radiology and Cardiology, Beth Israel Hospital, Boston, MA

Purpose: To produce diagnostic coronary angiograms of a substantive portion of the coronary tree noninvasively by using a novel image reconstruction and to compare the results with those of x-ray angiography.

Methods: Ten subjects (age range, 24–65 years) were recruited for coronary MR angiography within 2 weeks of x-ray angiography, with a commercial MR imager (1.5-T Magnetom, Siemens Medical Systems, Iselin, NJ). Data were acquired with segmented TurboFLASH during breath hold, gated to middiastole. Fat suppression and incrementing flip angle produced contiguous sections with $1.1 \times 0.9 \times 4.9$-mm resolution and $18 \times 21 \times 3$-cm field of view. Misregistration and signal intensity overlay were corrected with custom software. Local signal intensity characteristics defined borders automatically on multiple frames, accounting for variations where a threshold technique would fail, so 3D ray casting reliably reconstructed coronary MR angiograms with the obstructing ventricular signal intensity eliminated. The resulting images were mapped to an x-ray angiography projection so that lengths of the visualized coronary artery could be compared directly.

Results: Complete processing and analysis of patient data were accomplished in less than 20 minutes. Angiograms were successfully reconstructed in all cases. For the 10 matching arteries without critical narrowing, visualized length with MR angiography was 108.5 mm ± 28.6 versus 121.2 mm ± 28.6 with x-ray angiography (mean ± SE). Linear regression indicated that x-ray angiography = $1.031 \times$ MR angiography with good correlation ($r = .8$). MR angiography explained 98.6% of the x-ray angiography variance in length ($P < .0001$).

Conclusion: The authors have demonstrated the feasibility of reconstructing noninvasively from MR coronary angiograms in healthy subjects and patients with coronary artery stenoses. The length of the visualized coronary artery is now comparable to that obtained with routine x-ray angiography in the absence of critical narrowing.

370 • 3:45 PM

Simulated Annealing Technique for Selection of Optimal Phase Encoding in Constrained MR Image Reconstruction

Y Cao, DN Levin
Department of Radiology, University of Chicago, Chicago, IL

Purpose: High-resolution MR images can be reconstructed from a subset of the usual phase-encoded signals by means of the feature-recognizing MR imaging algorithm (1), which uses prior knowledge from a collection of training images. This study describes a simulated annealing technique for deriving the optimal phase encodings, which are usually scattered nonuniformly in k space.
Methods: The optimal phase encodings minimize a cost function representing the average error encountered when a set of phase encodings is used to reconstruct the training images. The system was annealed 10 times to seek the best 4, 6, or 8 phase encodings for reconstruction of simulated training images with 16 phase-encoded lines as well as experimental 16-line training images of oil-filled phantoms. The results were compared with the known best phase encodings, found by simply calculating the cost function for all 1,820, 8,008, and 12,870 choices, respectively. Large (64-line) brain images will also be reconstructed from annealed subsets of phase encodings. The results will be compared with those of reconstructions from phase encodings obtained with conventional "downhill" ("quenched") optimization methods as well as with the results of reconstructions from the full set of 64 phase encodings.
Results: For the simulated images, 60% of the annealed phase-encoding sets were among the best 3 choices. The remaining 40% of the annealing "experiments" led to phase encodings among the best 12 choices. The annealing technique was 60%–70% more efficient than the "brute force" optimization method.
Conclusion: Simulated annealing can be used to find nearly optimal phase encodings for feature-recognizing acquisition and reconstruction of MR images.
1. Cao Y, Levin DN. Proc of SMRM 1992; p 4235.

371 • 3:57 PM

Cranial MR Imaging, CT, and US of Neonates and Young Infants: Relative Diagnostic Accuracy

MA Mikhael, MT Gorey, MM Mikhael
Department of Radiology, Northwestern University, Evanston Hospital, Evanston, IL

Purpose: Evaluation of relative accuracy of cranial US, CT, and MR imaging in detecting brain abnormalities in neonates and young infants.
Methods: Two hundred one neonates and young infants were studied with cranial US; 32 also underwent CT and 25 MR imaging. The findings from various imaging procedures were retrospectively evaluated with the final clinical diagnosis. US, CT, and MR imaging were done within 1–10 days of each other.
Results: Disorders detected included hydrocephalus ($n = 12$), parenchymal ($n = 9$), extraparenchymal ($n = 12$) and ventricular hemorrhage ($n = 15$), vascular and other developmental malformations ($n = 18$), inflammatory changes and abscess formation ($n = 2$), and ischemia and infarctions ($n = 9$). Significant failure of US was in detecting acute subarachnoid hemorrhage and small subdural collections (0% vs 100% with CT and MR imaging) and focal and diffuse parenchymal abnormalities such as ischemia (25% vs 75% with CT and 100% with MR imaging). MR imaging was the study of choice (100%) in delineating congenital parenchymal and structural abnormalities (T1-weighted images) and inflammatory and vascular lesions including ischemia and bleed (T2-weighted images).
Conclusion: Results suggest that US will still play the dominant role as the initial screening modality for newborns. It is less expensive and simpler to perform even in sick neonates. Portable US machines can be moved to the patients. CT scans are for cases in which US fails to reveal enough information to explain neurologic abnormalities and for follow-up. MR imaging, being more expensive and difficult to perform in newborns, should be preserved for more accurate delineation of small cranial bleed, small infarctions, and congenital abnormalities before considering corrective surgery.

372 • 4:09 PM

Adaptive Weighted Ray Sum Projection Techniques as an Improvement to Maximum-Intensity Projection for MR Angiography

PM Margosian, H Liu
Picker International, Inc, Highland Heights, OH

Purpose: To optimize projection views of "bright blood" vessel images by using a histogram weighted ray sum technique.
Methods: Volunteers were imaged by using 3D time-of-flight MR angiography acquisitions on a Picker HPQ imager. Conventional maximum-intensity projection (MIP) views were calculated for reference. In the basic "weighted ray sum" method, all voxels along a ray are summed after raising their intensity to the Nth power, then dividing by the sum of the same values raised to the (N-1)th power (for normalization). Image quality is improved if a low exponent (eg, 2) is used for the brightest voxels (vessels), a high exponent (eg, 12) for the midrange intensities, which mix small vessels and background tissue, and a low exponent for dimmer (background) voxels. Use of a volume histogram to guide the choice of exponent makes this adaptive.
Results: MR angiography projection images made by the adaptive version of this method exhibit lower background noise than the MIP versions, as well as showing large crossing vessels in a much more realistic way than does MIP.
Conclusion: A projection technique that consistently provides more realistic appearance of blood vessels against a lower noise background than does MIP has been demonstrated. Clinical tests will reveal whether the improvement is sufficient to warrant the additional computation needed.
P. Margosian is an employee of Picker International.

373 • 4:21 PM

Inter- and Intraoperator Variability in the Quantitative Volumetric Measurements of Multiple Sclerosis Lesions

PA Narayana, EF Jackson, JS Wolinsky
Radiology Department, University of Texas Medical School, Houston, TX

Purpose: Image segmentation based on multispectral analysis has recently been proposed as a robust technique for quantitative volumetric analysis. In this method, the initial identification of different tissues of interest can introduce significant intra- and interoperator variability. The purpose of these studies was (*a*) to evaluate the inter- and intraoperator variability in the determination of volumes of multiple sclerosis (MS) lesions in patient volunteers and (*b*) to examine the effect of image preprocessing prior to segmentation on these variabilities.
Methods: Five patients with clinically definite MS were recruited for these studies. All MR imaging studies were performed on a GE 1.5-T whole-body imager. Contiguous, dual-echo, 3-mm-thick axial images were acquired at TEs

of 20 and 70 msec and a TR of 2,500 msec. With a nonparametric feature map, segmentation was performed both prior to and following image preprocessing. This preprocessing consisted of (*a*) application of an anisotropic diffusion filter and (*b*) stripping of all extrameningeal tissues by using 3D connectivity. Images were segmented by five observers on four different occasions into gray matter, white matter, cerebrospinal fluid, and MS lesions. At least 30 representative pixels from each tissue of interest were sampled.
Results: The mean inter- and intraoperator coefficients of variation for MS lesions without image preprocessing were 21.2% and 20.3%, respectively. The corresponding coefficients of variation after preprocessing were 6.0% and 10.2%, respectively. These studies demonstrate that image processing prior to segmentation greatly improves with inter- and intraoperator reproducibility. These studies also indicate that semiautomatic segmentation based on multispectral analysis after appropriate image preprocessing is a robust technique that should be useful in longitudinal patient studies.

Wednesday Afternoon • Plaza B
Papers 374–381

MUSCULOSKELETAL III: Spine

MODERATORS: B Flannigan-Sprague, MD
E Kanal, MD

---

374 • 2:45 PM

MR Imaging Appearances of Patellar Retinacular Injuries

TR Brown, SF Quinn, TA Demlow
Department of Radiology, OHSU, Portland, OR

Purpose: Although the patellar retinacular ligaments are important stabilizers of the knee and patella, little information is available regarding MR imaging appearances. This report describes the MR imaging appearances of patellar retinacular ligaments that have been injured and reviews the types of trauma and related injuries.
Methods: Sixteen patients with patellar retinacular ligament injuries were evaluated with axial T1-, proton-density–, and T2-weighted MR imaging sequences. The MR imaging findings were correlated with the clinical histories and correlative surgery.
Results: The injuries involved the medial retinacular ligament in 93.8% (15/16) and the medial and lateral retinacular ligament in 6.3% (1/16). In 62.5% (10/16), there was evidence of a patellar dislocation on MR images. The stigmata of patellar dislocations on MR images were focal impaction injuries involving the lateral femoral condyle ($n = 10$), osteochondral injuries of the medial patellar facet ($n = 10$), loose ($n = 1$) or partially attached medial patellar fracture fragments ($n = 5$), and injuries of the medial retinacular ligament ($n = 10$). The injured retinaculum had indistinct, irregular appearances associated with edema and hemorrhage. In 37.5% (6/16), the mechanism of injury was a patellar tendon tear ($n = 1$) or hyperextension valgus injuries ($n = 5$).
Conclusion: MR imaging can depict disruptions of the patellar retinacular ligaments, which occur with patellar dislocation injuries, hyperextension valgus injuries, and patellar tendon disruptions. With patellar dislocations, osteochondral fractures of the medial patellar facet are common.

375 • 2:57 PM

High-Resolution MR Imaging of the Wrist: Optimization of Techniques

SF Quinn, J Szumowski, TKF Woo, J Nye, TA Domlow
Department of Radiology, Good Samaritan Hospital, Portland, OR

Purpose: To assess the clinical utility of high-spatial-resolution MR imaging sequences and to optimize imaging protocols for evaluation of ligamentous and cartilaginous abnormalities of the wrist.
Methods: In the first part of the study, 40 patients and volunteers were imaged with multiple sequences. A prototype birdcage quadrature receive-only coil on a 1.5-T MR unit was used. Sequences that provide a pixel resolution on an order of 0.1 mm were used: 2D interleaved multisection gradient-echo (GRE) SPGR/GRASS, SE, and 3D GRE. The TR/TE, flip angle, field of view (FOV), bandwidth, matrix, and section thickness were systematically varied. In the second part of the study, 40 patients with complaints of carpal instability and unexplained pain were imaged with what were felt to be optimal parameters. The images were analyzed for conspicuity of intrinsic and extrinsic ligaments and the triangular fibrocartilage. When available, the MR images were compared with arthroscopy and arthrography.
Results: With 3D GRE sequences, the conspicuity of the structures of interest were diminished. The optimal 2D GRE sequence was TR/TE 400/min msec, flip angle 60°, FOV 6 cm, 256 × 256, 3.0-mm thickness. The image sequence that provided the best contrast resolution was a high-resolution SE sequence: 2,000/20, FOV 6 mm, 256 × 192, 3.0-mm thickness.
Conclusion: High-resolution images that confidently identify the principal wrist ligaments and the triangular fibrocartilage were obtained. The best GRE sequences incorporate a relatively long TR (400 msec). Overall, high-resolution proton-density SE sequences had the best contrast resolution.

376 • 3:09 PM

MR Imaging Evidence of Bone Marrow Response to Hematopoietic Growth Factors

BD Fletcher, JE Wall
Department of Diagnostic Imaging, St Jude Children's Research Hospital, Memphis, TN

Purpose: Colony-stimulating factors (CSF) activate myeloid hematopoietic cells and reduce the duration and severity of neutropenia, permitting more intensive cancer chemotherapy. The authors observed bone marrow signal intensity changes simulating metastases in a patient receiving CSF during chemotherapy. Consequently they evaluated bone marrow signal intensity in children receiving initial chemotherapy, with or without CSF, for malignant musculoskeletal tumors.
Method: Short TR/TE and STIR images of the pelvis and/or uninvolved femurs obtained at diagnosis and on 2 subsequent examinations during neoadjuvant chemotherapy were assessed in 9 patients ages 9–16 years. Six patients also received granulocyte (G) or granulocyte-macrophage (GM) CSF. Marrow was independently scored as predominately fatty (high signal intensity on short TR/TE, absent on STIR) or hematopoietic (low signal intensity on short TR/TE, intermediate on STIR). Findings were correlated with CSF administration and absolute neutrophil count (ANC).
Results: In 4 of 6 patients receiving CSF, change in MR marrow signal intensity from fatty to hematopoietic accompanied a large increase in ANC (maximum ANC range at post-CSF MR imaging = 4,310–45,657). Two patients who did not respond to CSF (maximum ANC = 90 and 1,771) had no change in initially hematopoietic marrow.

The 3 patients who did not receive CSF had a maximum ANC range equal to 4,720–5,248 and no change in initially fatty marrow. Tc-99m-MDP bone scintigrams were normal except for a solitary vertebral metastasis in 1 patient. ***Conclusion:*** These preliminary results suggest CSF-induced hematopoietic activity may be detected with MR imaging. Accompanying changes in marrow signal intensity may simulate disseminated bone marrow disease.

377 • 3:21 PM

Is T2*-weighted MR Imaging Better than Arthrography for Diagnosis of the Perforation of Triangular Fibrous Cartilage?

T Nakamura, E Nakamura, K Ahsoh, K Uchida, S Masumi
Department of Orthopedic Surgery, Oita Medical University, Oita, Japan

Purpose: Perforation of triangular fibrous cartilage (TFC) is a painful malady of the wrist joint, the diagnosis of which has heretofore depended, primarily, on arthrography. There has recently been some experimentation with the use of MR imaging in the diagnosis of TFC perforation. However, to our knowledge, there has been no report examining the effectiveness of T2-weighted MR imaging in comparison with arthrography in this ailment. The following is a report of such an examination.
Methods: An experiment was performed with 22 wrists from 11 cadavers (5 male, 6 female; age range, 61–92 years; mean age, 78.8 years). The MR imaging device used was Resona 0.5-T by Yokogawa Medical. The authors attached an 8-cm surface coil disk on the dorsal side of the wrist joint and took coronal sections in T2*-weighted imaging (500/20, flip angle = 35°). Then, they performed arthrography of the radiocarpal joint. Further, they dissected the wrists and compared macroscopic observations with the 2 imaging methods. Also, in 3 clinical cases in which TFC perforation was suspected, they performed the above 2 methods of imaging and compared the results with observations during surgery.
Results: The same correct diagnosis was derived from both methods in 19 of 21 cadaveric wrists (90%), though slit-type perforations were poorly diagnosed with both methods. In all 3 clinical cases, the same diagnosis was derived from both methods, which was subsequently confirmed during surgery.
Conclusion: T2*-weighted MR imaging is equally effective as arthrography in the diagnosis of TFC perforation.

378 • 3:33 PM

Clinical Utility of Cervical Spine MR Imaging in Patients with Multiple Sclerosis and Cervical Myelopathy

JJ Baka, EM Spickler, B Koffman, S Elias
Department of Diagnostic Radiology, Henry Ford Hospital, Detroit, MI

Purpose: To evaluate the practical usefulness of cervical spine MR imaging in patients with multiple sclerosis (MS) and cervical myelopathy.
Methods: Forty-one cervical spine MR images of 36 patients with previously established (16 images) or subsequently confirmed (25 images) MS and clinical evidence of cervical myelopathy were retrospectively reviewed. The presence of cord signal intensity abnormalities, extradural or intradural disease, and coexisting intracranial disease was determined.
Results: Twenty-four (59%) studies demonstrated focal intramedullary hyperintensities suggestive of demyelination, 17 (41%) studies demonstrated a normal cord, and 20 (49%) studies demonstrated extradural disease, including spondylosis without cord compression (n = 17), spondylosis with cord compression (n = 2), and epidural lipomatosis (n = 1). None of the patients with extradural disease, including those with cord compression, underwent surgery. Thirty-five studies were performed in conjunction with cranial MR imaging. Demyelination was present in both the cord and brain in 16 (45%), the cord alone in 3 (9%), and brain alone in 16 (45%). There were 14 focal cervical cord plaques in patients with spondylosis (none with cord compression): 10 (71%) occurred at sites remote from spondylosis, and 4 (29%) occurred at sites of osteophytes.
Conclusion: (1) Demonstration of lesions other than cervical cord plaques in MS patients with cervical myelopathy did not have a major effect on patient management. (2) Spondylotic spurs probably do not contribute to the formation of MS plaques. (3) In 40% of our patients, cervical myelopathy was present clinically despite the absence of positive MR imaging findings.

379 • 3:45 PM

MR Imaging of Spinal Perineural Cysts: Role of Cerebrospinal Fluid Flow Analysis

LM Levy, S Davis, D LeBihan, S Rajan, D Schellinger
Georgetown University Hospital, Columbia, MD

Purpose: To evaluate patients with spinal perineural (Tarlov) cysts by using MR imaging flow-sensitive pulse sequences and to correlate flow characteristics with clinical symptoms.
Methods: All images were obtained with a 1.5-T system by using both conventional SE acquisitions and a slow flow (SFMR) pulse sequence. The SFMR is based on a 3D steady state free precession scheme with additional gradients on the readout axis to provide increased flow sensitivity down to velocities of 0.5 mm/sec. MR imaging was performed in healthy subjects as well as in 19 patients with lumbar perineural Tarlov cysts (24 cysts). In a few cases, myelograms were also obtained. The patient's symptoms were then correlated with neurologic examinations and MR imaging findings.
Results: There was no significant difference in size between symptomatic and asymptomatic cysts. However, 5/5 asymptomatic cysts showed internal flow patterns on MR flow studies, while 7/7 symptomatic cysts failed to show any internal flow. In some cases with internal flow, a communicating channel could sometimes be observed, and myelography also showed communication.
Conclusion: MR imaging is useful in demonstrating which spinal perineural cysts have absence of internal flow or of communication with the subarachnoid space and may thereby provide a means of identifying lesions likely to be symptomatic.

380 • 3:57 PM

Cinematic MR Imaging of the Cervical Spine

M Naegele, R Bruening, V Kunze, B Woell, M Reiser
Department of Radiology, University of Bonn, Bonn, Germany

Purpose: To develop a cinematic system for examining the cervical spine in dynamic function.
Methods: Five volunteers and 31 patients were examined with MR imaging (herniated disk [n = 5], spinal trauma [n = 4], rheumatoid arthritis [n = 2], spinal stenosis [n = 6], laminectomy [n = 9], ventral fusion [n = 5]). MR imaging was performed with a Philips T5. Dynamic sequence: TR/TE 320/11, 40, and 60/18, sagittal, flexible surface coil (diameter, 8 cm), section thickness of 5 mm, total examination time of 20 minutes. Cinematic system: flexible surface (head), 5 sagittal flexion positions of cervical spine (0°, 25°, 35°, 42°, 48°, 54°). Image evaluation: staging of spinal canal and cord compression performed in various positions of flexion.
Results: A significant change in spinal canal and cord compression depending on flexion or extension of cervi-

cal spine was observed in patients with herniated disk (n = 2), spinal stenosis (n = 3), spinal trauma (n = 2), laminectomy (n = 5), and ventral fusion (n = 3).
Conclusion: Dynamic MR imaging does not substitute for but supplements static MR imaging information. Indications for dynamic function MR imaging of cervical spine are evaluation of spinal stenosis and postoperative cases.

381 • 4:09 PM

MR Evaluation of Gadolinium in the Evaluation of the Unoperated Patient with Clinical Lumbosacral Radiculopathy: Comparison of 0.1 mmol/kg Intravenous Gadopentetate Dimeglumine with 0.3 mmol/kg Intravenous Gadoteridol

JR Jinkins, GT Gee, RA Rauch, C Bazan
Department of Radiology, University of Texas Health Science Center, San Antonio, TX

Purpose: The objective of this clinical study was to evaluate the efficacy of low-dose intravenous gadopentetate dimeglumine versus high-dose intravenous gadoteridol in the demonstration of abnormal nerve root enhancement in unoperated patients with lumbosacral neural plexus radiculopathy.
Methods: Twelve unoperated patients (10 men and 2 women) between the ages of 21 and 64 with clinical lower extremity radiculopathy were studied. Initial MR imaging without intravenous contrast material was performed and was followed by a 0.1 mmol/kg intravenous gadopentetate dimeglumine–enhanced acquisition. After a 1–6 day delay, MR imaging was then repeated after 0.3 mmol/kg intravenous gadoteridol administration. The MR imaging results were subsequently reviewed and compared in a double-blind fashion.
Results: Unenhanced MR imaging showed disk herniations at the level of L-5 to S-1 in 8 patients and disk herniations at the level of L-4 to L-5 in 4 patients. Associated intrathecal nerve root enhancement was present in 7 (58%) studies in the low-dose intravenous gadopentetate dimeglumine group and in 9 (75%) studies in the high-dose intravenous gadoteridol group. In addition, the enhancement was relatively greater in degree and more extensive in coverage in the high-dose gadoteridol enhancement group.
Conclusion: Overall, with intravenous gadoteridol administered at 0.3 mmol/kg, there was superior demonstration of abnormal enhancement of nerve roots as compared with the 0.1 mmol/kg intravenous gadopentetate dimeglumine group. This improved enhancement is thought to be due to the increased dose rather than to any inherent difference in the chemical nature of the 2 contrast agents. Such neural enhancement is believed to occur as a result of direct local neural trauma or inflammation and to indirect distant wallerian degeneration of axons within injured nerve roots.

This research was supported in part by an educational grant from Squibb Diagnostics.

Wednesday Afternoon
Imperial Ballroom
Papers 382–388

PERFUSION/DIFFUSION III

MODERATORS: S Majumdar, MD • VM Runge, MD

382 • 2:45 PM

MR Imaging Characterization of Anisotropic Water Self-Diffusion in Experimental Spinal Cord Injury

JC Ford, DB Hackney, DC Alsop, H Jara, PM Joseph, SL Tabor, CM Hand, RS Markowitz, P Black
Department of Radiology, University of Pennsylvania Medical Center, Philadelphia, PA

Purpose: To characterize the apparent diffusion coefficients (ADC) in normal rat spinal cord and to quantitate white matter damage by observing ADC changes after injury.
Methods: The authors employed a weight drop spinal cord injury model (1). Control (n = 3) and injured cords (n = 4) were formalin-fixed in situ. The authors used multisection, axial, SE imaging on a 1.9-T magnet: 1,200/43, field of view of 20 mm, 256 × 128, section thickness of 1 mm, 2 excitations. Four diffusion strengths (b_{max} = 475 s/mm^2) were applied parallel and then perpendicular to the cord. Long TR multiecho images were also acquired to provide an estimate of T2. Longitudinal ADC (LADC), transverse ADC (TADC), and T2 maps were generated for subsequent region-of-interest analysis.
Results: Control cords: TADC/LADC, an index of diffusion anisotropy (2), for lateral and anterior funiculus (LWM), dorsal column (DCWM), and gray matter (GM) were (mean ± standard error) 0.278 ± 0.007, 0.291 ± 0.010, 1.03 ± 0.024, respectively. No significant correlations (t test) were observed between ADC and T2 values. Injured cords: TADC/LADC for LWM, DCWM, and GM in apparently normal sections remote from the lesion were 0.487 ± 0.044, 0.711 ± 0.104, 0.921 ± 0.053, respectively. In the lesion (no recognizable GM or WM), TADC/LADC was 1.017 ± 0.088.
Conclusion: Consistent with previous work (3), considerable diffusion anisotropy is observed in normal WM of control cords. In injured cords, this anisotropy decreases significantly both in the lesion itself and in the normal-looking WM remote from the lesion.

1. Black P, Markowitz RS, Damjanov I, et al. Neurosurgery 1988; 22:51. 2. Douek P, Turner R, Pekar J, Patronas N, Le Bihan D. J Comput Assist Tomogr 1991; 15:923. 3. Ford JC, Jara H, Hackney DB, et al. JMRI 1991; 1:202.

383 • 2:57 PM

Apparent Diffusion Coefficient Mapping with Diffusion-weighted Echo-Planar Imaging to Study Ischemic Brain Damage in Rats

BJ Dardzinski, K Minematsu, L Li, CH Sotak, M Fisher
Department of Biomedical Engineering, Worcester Polytechnic Institute, Worcester, MA

Purpose: To spatially map the apparent diffusion coefficient (ADC) by using diffusion-weighted echo-planar images (DWEPI) of ischemic brain damage in experimental temporary middle cerebral artery occlusion (MCAO) in rats. The goals of this work are to establish the correspondence between pre-reperfusion ADC values and postmortem studies to delineate between irreversibly injured tissues and ischemic regions that will recover.
Methods: Sixteen DWEPI were obtained in 32 seconds with either x, y, or z diffusion sensitivity in rats undergoing MCAO with the suture-occlusion method. The 16 im-

ages were presmoothed, and the ADCs were calculated on a pixel-by-pixel basis with linear regression. The correlation coefficient (0.95) was used to filter the final ADC maps.
Results: Lesions, 1 hour after MCAO, with diffusion sensitivity in the x direction have average ADCs of 0.39×10^{-5} cm^2 sec^{-1} while the contralateral side has an average value of 0.55×10^{-5} cm^2 sec^{-1}. Contralateral ADCs with diffusion sensitivity in the y or z direction average 0.67×10^{-5} cm^2 sec^{-1}. Regions with irreversible ischemic lesions were infarcted on postmortem TTC studies.
Conclusion: ADC maps provide better visualization and calculation of lesion areas and correspond to postmortem staining studies. The use of 16 DWEPI provides better accuracy, and correlation coefficient filtering provides a method to isolate proton self-diffusion in the ischemic region. Changes in lesion areas (based on a narrow range of ADCs) are being monitored during the evolution of ischemia and compared with postmortem TTC results.

384 • 3:09 PM

Biodistribution and Kinetics of Gd-153 DTPA in C3H Mice Hosting a Mammary Adenocarcinoma

C Laubenbacher, C Wagner-Manslau, J Griebel, E van de Flierdt, S Möllenstädt, R Senekowitsch, HR Langhammer, HW Pabst
Nuklearmedizin Klinik, TU München, Munich, Germany

Purpose: Despite the widespread use of Gd-DTPA for MR imaging, there have been only few reports on its biodistribution. Therefore, the authors used a well-established radiotracer technique to evaluate the kinetics of Gd-153 DTPA in C3H mice with mammary adenocarcinomas (AT 17).
Methods: Gd-153 DTPA was injected intravenously in tumor-bearing C3H mice. Whole-body retention was measured, and biodistribution data, expressed in percentage of injected dose per gram tissue and as tissue/tumor ratios, were obtained by killing and dissecting animals at time points from 20 seconds to 1,440 minutes after injection (p.i.).
Results: Fifty percent of the injected Gd-153 DTPA was excreted within 65 minutes p.i. The highest activity was found in the kidneys 2 minutes p.i. (24.9% of injected dose per gram). The activity concentration in the tumor was highest 3 minutes p.i. The tumor/blood ratio reached values about 1 (steady state) between 30 and 60 minutes p.i. and was highest 6 hours p.i. The biodistribution of Gd-153 DTPA was similar to published data in other animals or man.
Conclusion: To the authors' knowledge, they are the first to describe the kinetics of Gd-DTPA in tumors by means of radiotracer techniques. With exact knowledge of the kinetics of Gd-DTPA in malignant tissue they should be able to optimize their MR parameters for a better evaluation of tumor perfusion with MR imaging. Further studies in man and with other tumors should be initiated to prove whether imaging in the steady-state phase could help in the evaluation of tumor perfusion.

385 • 3:21 PM

Effects of an NMDA Antagonist on Perfusion Deficit in Rat Focal Brain Ischemia as Evaluated with Dynamic Contrast-enhanced MR Imaging

CH Sotak, K Minematsu, L Li, M Fisher, M Meadows, AG Knapp, RN McBurney
Department of Biomedical Engineering, Worcester Polytechnic Institute, Worcester, MA

Purpose: To evaluate the effects of an *N*-methyl-D-aspartate (NMDA) receptor antagonist on cerebral perfusion during focal ischemia with dynamic contrast-enhanced (DCE) MR imaging.
Methods: Focal brain ischemia was achieved with an intraluminal suture middle cerebral artery occlusion (MCAO) model in rats. Fifteen minutes after MCAO, the animals were treated with either an NMDA antagonist, CNS-1102, or saline control. For DCE MR imaging, echo-planar imaging (EPI) was used at 2.0 T to monitor bolus passage of iron particles through the brain. The animals were reperfused after 3 hours, and the cerebral perfusion state was evaluated just before and 30 minutes after reflow. Lesion size was measured by using diffusion-weighted (DW) MR imaging.
Results: During occlusion, the perfusion of the ischemic area was significantly better in the treated ($n = 10$) than in the control rats ($n = 6$), based on the relative changes in signal intensity and the time delay of the bolus passage between the ischemic and contralateral hemispheres. The treated animals also showed a marked reduction in lesion size (with DW MR imaging) compared with controls.
Conclusion: These studies suggest that the protective effects of CNS-1102, as evidenced by reduced lesion size, may in part be due to increased cerebral blood flow due to an improvement in collateral circulation.

386 • 3:33 PM

Measurement of Background Magnetic Field Gradients with Diffusion MR Imaging

H Jara, H Chung, FW Wehrli, JC Ford
Department of Radiology, University of Pennsylvania Medical Center, Philadelphia, PA

Purpose: The purpose of this work was to design and validate a quantitative diffusion-based MR imaging method for measuring internal magnetic field gradients in heterogeneous systems.
Methods: Two STEAM (1) diffusion image data sets with opposite polarities of the applied diffusion sensitizing gradients are shown to simultaneously yield the diffusion coefficient D_{loc} and the intrinsic gradient G_{loc} on a pixel-by-pixel basis. The method has been validated at 1.5 T by measuring the spatial distribution of the background gradients induced by a paramagnetic cylinder oriented orthogonal to B_0 and surrounded by water.
Results: Semilogarithmic plots of region-of-interest signal amplitudes versus applied gradient factor deviate from linearity in regions with background gradients. The local gradients thus obtained at multiple locations in the x-z plane were in good agreement with those predicted by the Maxwell equations. Analogous behavior was observed for trabecular bone specimens immersed in water for which an average local gradient G_{loc} of approximately 40 mG/cm was obtained. At the pixel size used ($\Delta r = 0.78$ mm), this value corresponds to $T2' = (\gamma \Delta r\, G_{loc})^{-1} \sim 15$ msec in good agreement with previous results (2–4). Regardless of the strength of the local gradient, the local water diffusion coefficient derived from these measurements was within the range of $2.0–2.2 \times 10^{-5}$ cm^2/sec.
Conclusion: The method has implications for microscopic MR imaging of trabecular bone and other magnetically inhomogeneous systems. The technique gives simul-

taneously accurate values for D_{loc} and G_{loc} and therefore may lend itself for testing the accuracy of solutions to the Bloch-Torrey equation for nonlinear field gradients.

1. Tanner JE. J Chem Phys 1970; 52:2523–2526.
2. Wehrli FW, Ford JC, Attie M, Kressel HY, Kaplan FS. Radiology 1991; 179:615–621. 3. Ford JC, Wehrli FW. Magn Reson Med 1991; 17:543–551. 4. Majumdar S, Genant HK. JMRI 1992; 2:209–219.

387 • 3:45 PM

Susceptibility-Sensitive Perfusion Imaging of the Rat Brain with 4 Different Contrast Agents

H Vogler, H Baker, HY Weinmann
Schering AG, Berlin, Germany

Purpose: Bolus injection of contrast medium enables measurement of relative perfusion of the brain due to the susceptibility effects occurring because of the heterogeneous distribution of the contrast agent in the brain. In this study, 4 different substances (superparamagnetic iron oxides [SPIO], Dy-DTPA, Gd-DTPA, and Gd-DTPA-polylysine) were compared concerning their effect on signal reduction due to perfusion of the rat brain.

Methods: T_2*-weighted FLASH images, each lasting 1.6 seconds, were acquired with a 2-T imager. The contrast agents were applied via the tail vein within 3 seconds. Doses of 0.3 mmol/kg Dy-DTPA, Gd-DTPA, and Gd-DTPA-polylysine and 0.01–0.1 mmol Fe/kg SPIO in were given.

Results: Dy-DTPA caused a decrease in the signal intensity to 60% of the baseline. Gd-DTPA and GD-DTPA-polylysine had a somewhat smaller effect, nearly corresponding to the difference in the magnetic moments of gadolinium and dysprosium. As expected, the SPIO are the most potent agents. A dose of 0.03 mmol Fe/kg gives the same effect as a dose of 0.3 mmol/kg Gd-DTPA.

Conclusion: All of the substances examined are applicable for perfusion studies. Although gadolinium has the smallest effect, it is the only compound that enhances, in additional T1-weighted imaging studies, a lesion with a damaged blood-brain barrier.

H. Vogler is an employee of Schering AG.

388 • 3:57 PM

Dynamic MR Contrast Bolus Tracking of Cerebral Microcirculation with Standard Hardware: Optimization of Experimental Techniques

RW Hynes, RM Thompson, CR Jack, NJ Hangiandreou, RK Butts, RL Ehman, SJ Riederer
Mayo Clinic, Rochester, MN

Purpose: Many studies demonstrating the ability to perform functional MR imaging have used equipment with limited commercial availability (4-T magnets, modified receiver coils, or special gradient subsystems). These experiments were designed to optimize a technique for dynamic MR imaging of cerebral microcirculation with standard 1.5-T equipment.

Methods: Experiments were performed with an unmodified 1.5-T GE Signa imager and Sprague-Dawley rats. Gadolinium boluses were injected through a femoral venous catheter, and serial coronal brain images were acquired. Signal intensity data were used to generate time-intensity curves, and gamma variate fits were performed. The integral of the time-intensity curve (ITIC) was used as a figure of merit to compare various techniques. Several variables were evaluated: (1) dose of gadolinium, (2) bolus interval, (3) flip angle, (4) temporal offset in the echo-planar imaging (EPI) refocusing pulse, (5) EPI offset variations (EPI implemented on standard hardware). Optimized gradient-echo (GRE) and EPI techniques were then compared.

Results: The ITIC was directly proportional to the gadolinium dose; however, the shape of the TIC depended on the injection order. There was no significant difference in the ITIC obtained by using different bolus intervals. ITIC was maximized with a flip angle of 30°. A GRASS technique tended to produce a greater ITIC than did SPGR. Variations in the offset with EPI resulted in no significant differences; however, the ITIC tended to be greatest with a 2-msec offset.

Conclusion: An optimized contrast bolus tracking technique was established for GRE and EPI. The results indicate there was no significant difference in power or utility between the 2.

Notes

Notes

MR 1993

SCIENTIFIC POSTERS

The Scientific Poster Exhibits offer **SMRI** attendees an opportunity to examine and discuss scientific material in a more intimate atmosphere.

Discussion periods, moderated by individual Scientific Poster presenters, are scheduled daily throughout the Meeting. A schedule of the discussion times follow:

Section: **Physics I: Flow, Motion, Perfusion, Artifacts**
Day, Date: Sunday, March 28
Time: 12:15 PM - 1:30 PM

Section: **Clinical MRI: Head, Spine, Body**
Day, Date: Monday, March 29
Time: 12:30 PM - 1:30 PM

Section: **Physics II: Rapid Imaging, Pulse Sequences, Image Processing**
Day, Date: Tuesday, March 30
Time: 12:15 PM - 1:30 PM

Section: **Contrast Agents, Spectroscopy, Other Nuclei**
Day, Date: Wednesday, March 31
Time: 12:15 PM - 1:00 PM

SCIENTIFIC POSTER EXHIBIT AREA

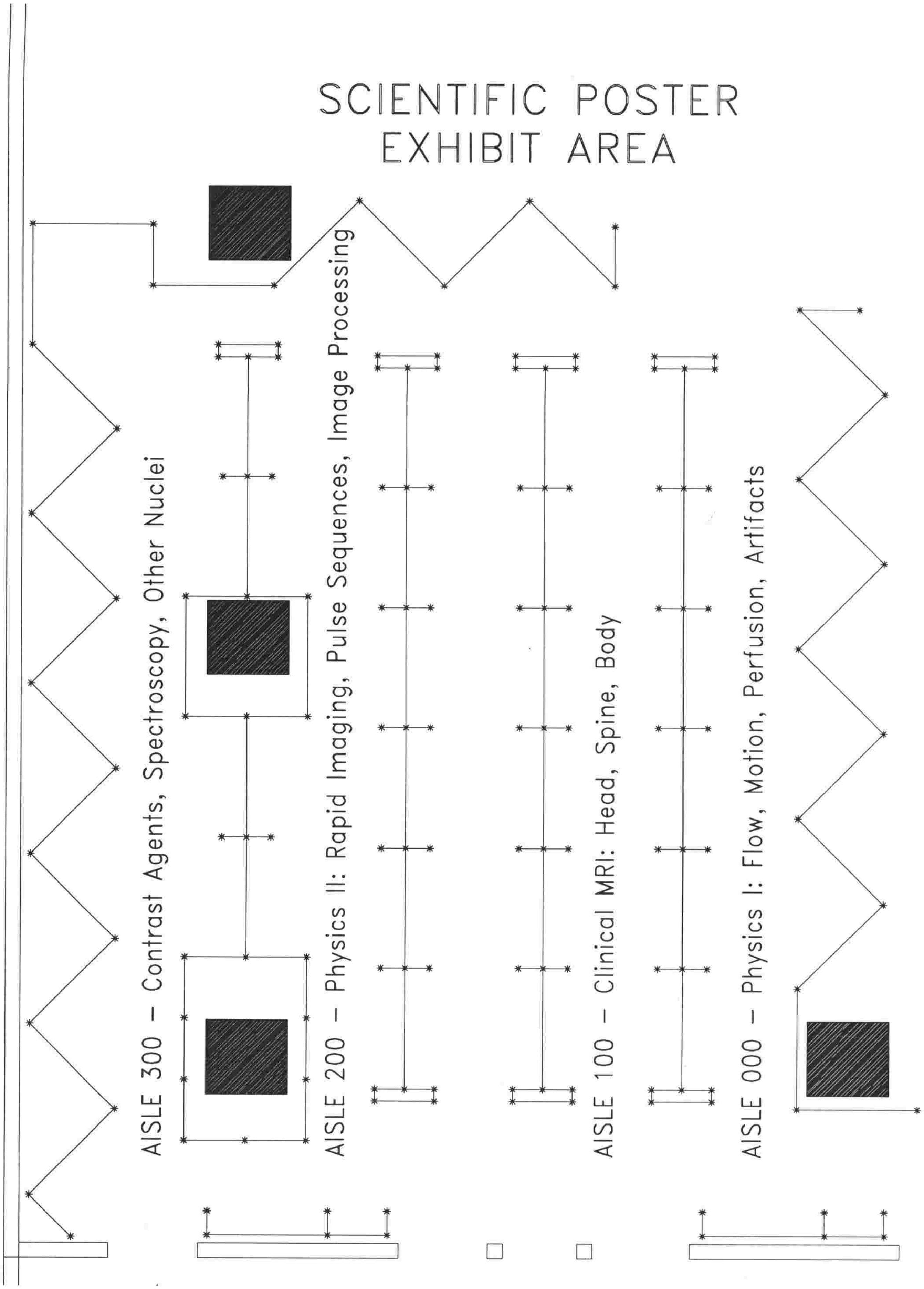

SMRI '93 Eleventh Annual Meeting Poster Abstracts

Sunday, March 28, 12:15 PM–1:30 PM
PHYSICS I: Flow, Motion, Perfusion, Artifacts
Posters P001–P038

P001

MR Imaging Thresholded Signal Obliteration from Motion Blur

PR Moran, CA Hamilton, O Nalcioglu
Department of Radiology, Bowman Gray School of Medicine, Winston-Salem, NC

Purpose: The authors attempt to explain laboratory observations of abrupt MR signal intensity disappearance in preturbulent flows with residual motion phase contrast. This occurs especially in oblique motion, is visually obvious once recognized, and is inexplicable with current MR imaging theory intravoxel incoherent (IVI) models. This effect changes with image reconstructions, indicating the importance of enhanced Gibbs oscillation from motion blurring.
Methods: Cumulative MR imaging encoding theory predicts acquired data:

$$A^{-}(k)\int_R \int_V M\,[R + \delta R\,(k)]\,\exp\,(2\pi ik \cdot R)$$

$$\times\ p\,(\delta R,\, u_n)\,\exp\,(2\pi i\,[f_n \cdot u_n)\,dV^3\,dR^3, \quad (1)$$

where $\delta R(k)$ is datagate TOF travel, u_n is specific phased motion, and $p(\delta R, u_n)$ is intravoxel dispersion. Equation (1) implies TOF elongates voxels along readout and cross-couples other phasing via the intravoxel distribution. With "u_n" phase shear, $PS(u) \cdot x$, image reconstruction is easily evaluated.
Results: The local voxel phase-shear evaluation gives

$$A(r) = M\,\{TRUE[-(1/2a) < PS < (1/2a)]$$

$$\times\ \exp\,(\pi i\,[PS_x\,(r)^2\,(d_G \cdot a)])\}, \quad (2)$$

where d_G is TOF travel during the datagate, and a is the normal "x-readout" pixel size. The TRUE-square is the normal sinc(x) blur cutoff. The question is how both motion blur and motion phase shear occur along the same axis. $\delta R(k)$ blurring itself has negligible phase effects.
Conclusion: The $(d_G \cdot a)^{-1}$ value is a critical phase-shear limit, past which the complex exponential drops abruptly to 0 in voxel-average amplitude. $(d_G \cdot a)$ can be 10 times greater than (a^2). Motion blur substantially elongates the pixel size, giving exaggerated phase-shear IVI occurring abruptly versus velocity. Velocity and phase shear along the same axis can be obliquely strong.

P002

MR Imaging of the Breast Implant: Normal Variants That Masquerade as Intracapsular Rupture

CS Moss, P Pugh, RB Lufkin, B Hayden
West Los Angeles MRI, Los Angeles, CA

Purpose: Interpretation of MR imaging of breast implants is not yet well established. In the case of implant rupture, false positives and negatives can affect patient care. This pictoral essay will address the anatomic and design pitfalls of MR implant imaging that may cause misinterpretation, when ruling out rupture.
Methods: Imaging was performed in 15 patients with suspected implant rupture with whole-body MR instruments, in the decubitus position, by using a local elliptical coil. The average age was 43 years. The patients were imaged with a T1-/T2-weighted sagittal acquisition and an axial T1-weighted acquisition with fat suppression. The MR imaging results were reviewed by 2 radiologists who evaluated the images for rupture, contour deformities, and type of implant. These findings were coupled with surgical and/or clinical data.
Results: Many normal variants were observed to mimic prosthetic rupture. These included anatomic entities such as cysts (n = 3), vessels and adjacent muscles (n = 3), contour deformities such as implant envelope folds (n = 4) and diverticula (n = 2), and design variants such as filling devices (n = 3) and double-lumen implants.
Conclusion: MR imaging for evaluation of silicone breast implant rupture has introduced an array of pitfalls in interpretation. Deceptive appearances mimicking implant rupture can relate to construction of the implant, anatomic structures, and protocols. Patient positioning and imaging parameters are important, as they can contribute to artifacts. Various implant devices may be mistaken for implant rupture. Anatomic structures such as parenchymal cysts or axillary vessels can mimic extracapsular rupture. Implant envelope wrinkling and diverticuli can mimic intracapsular rupture.

P003

Stimulated-Echo Contributions to the Bright Fat Phenomenon in Fast Spin-Echo Sequences

RV Mulkern, CRG Guttmann, K Oshio
Department of Radiology, Children's Hospital, Boston, MA

Purpose: To determine if bright fat signal in fast spin-echo (FSE) is a consequence of off-resonance spins and nonideal refocusing pulses.
Methods: Bloch equation analyses of CPMG sequences, including relaxation, off-resonance, and imperfect 180° pulses, were used to calculate echo maxima. Experiments were performed with a 1.5-T imaging system by using materials covering a wide range of T1, T2, and T1/T2 ratios, including those of fat, but with no J-coupling interactions. CPMG imaging sequences underlying FSE were used to image the phantoms. The effects of reduced 180° section-selective RF pulse amplitudes, echo spacings (2τ), and resonance frequency w on "apparent" T2 decays were evaluated. In vivo FSE studies of knees were also performed.
Results: Simulations reveal that for a single line 220 Hz off resonance and relaxation parameters similar to those of fat (T1 = 200 msec, T2 = 125 msec), 135° refocusing pulses yield "apparent" T2 decay rates ranging from 88 to 250 msec, the actual value depending critically on the

product $w\tau$. No such effects were observed experimentally. Apparent T2 decay rates were remarkably stable to variations in RF amplitudes, applied w, and 2τ values. Bone marrow signal intensity on T2-weighted FSE images varied less than 3% when RF was applied on water or fat frequencies.

Conclusion: Apparent lengthening of T2 and concomitant bright fat due to off-resonance effects and imperfect 180° pulses is possible in pure CPMG sequences. In CPMG/FSE imaging, the effect is washed out by the frequency distribution imposed by imaging gradients and is not responsible for bright fat in FSE.

P004

Inversion Recovery Fast Spin-Echo Imaging

S Vinitski, FB Mohamed, ME Schweitzer, DG Mitchell, AE Flanders, HV Ortega, SG Einstein

Department of Radiology, Thomas Jefferson University Hospital, Philadelphia, PA

Purpose: Inversion recovery (IR) imaging has been shown to be sensitive to a variety of pathologies. Utility of this technique, based on conventional IR spin-echo (IR-SE) data acquisition, is limited due to the excessive imaging times, susceptibility to motion, and low signal-to-noise ratio (S/N). In this work, the authors investigate the feasibility of the IR technique based on fast spin-echo (1) data acquisition (IR-FSE).

Methods: First, MR imaging (both IR-SE and IR-FSE) was performed by using phantoms (doped water solution and oil). Second, neuro, musculoskeletal, and upper abdominal imaging in volunteers was also performed. To improve spatial resolution and reduce motion artifacts, the echo space was shortened up to 6 msec (2). TR was 2.5–5 msec, TI was 50–2500 msec, and TE was 15–18 msec. A 1.5-T Signa (GE) imager was used.

Results: Signal behavior of IR-FSE, expressed as a function of T1 and TR, was very similar to that of IR-SE, with identical null points for both doped water and fat. The results remained the same with a change in the number of echoes per train or type of RF pulse. In vivo experiments showed that IR-FSE and IR-SE exhibited almost identical tissue contrast behavior. Acquisition speed was 4 times faster, however, and image resolution was twice as good on IR-FSE images. In the upper abdomen, respiratory ghosts were suppressed up to 3 times. Further, we obtained 13-second breath-hold IR-FSE images. They were characterized by high S/N and good tissue contrast. Musculoskeletal IR-FSE was highly sensitive to subtle edema and bone marrow infiltration.

Conclusion: IR-FSE shows the same contrast behavior as IR-SE, but with much faster speeds of acquisition, greater resolution, and suppression of motion artifacts. The technique warrants further clinical evaluation.

1. Melki PS, Mulkern RV, Panych LP, Jolesz FA. JMRI 1991; 1:319–326. 2. Vinitski S, Mitchell DG, Rao VM, Ortega HV, Mohamed FB, Einstein S. JMRI 1992; 2(P):54.

P005

Removal of the Effects of Global Magnetic Field Inhomogeneity in Heavily T2*-weighted MR Images

RJ Ordidge, C Branch, J Ewing, V Nagesh

Department of Neurology, Henry Ford Hospital, Detroit, MI

Purpose: T2*-weighted images may be greatly distorted by the magnetic effects of tissue interfaces and field inhomogeneities. The exploration of T2* contrast in normal and impaired brain (eg, in stroke patients) would be greatly enhanced by the removal of these global field inhomogeneity effects, so that local inhomogeneity effects could be studied in greater detail.

Methods: Global inhomogeneity effects introduce fields that are approximately linear over the dimensions of image voxels. Inhomogeneities that produce gradients along readout and phase-encoding directions produce MR signals that are effectively shifted in 2D k-space but still appear in their correct location in the 2D image (1). Inhomogeneities that produce gradients along the section-selection axis, however, cause signal loss due to dephasing. This signal may be recovered by obtaining a series of images with incremented phase encoding along the section-selection axis so that signals experiencing magnetic inhomogeneity-induced gradients are progressively refocused in successive images. Co-addition of image sections leaves T2* contrast, which is solely a function of local (eg, within a voxel) inhomogeneity effects.

Results: Human head imaging was performed at 3 T by using the FLASH technique with α = 10°, TE = 40 msec, and TR = 50 msec. Sixteen images were obtained with progressive phase-encoded steps along the section-selection axis. The magnitude of the phase-encoding increment was chosen to balance global inhomogeneity gradient steps corresponding to 0.0016 G/cm when integrated over the 40-msec experimental duration.

Conclusion: A method has been developed and successfully applied to extend the usefulness of T2*-weighted MR image contrast by separation of the effects of global and local field inhomogeneities.

1. Posse S. Direct imaging of magnetic field gradients by group spin-echo selection. Magn Reson Med 1992; 25:12–29.

P006

MR Image Reconstruction with Data Interpolation in Time for the Segmented K-Space Data Acquisition Method

E Atalar, ER McVeigh

Department of Biomedical Engineering, Johns Hopkins University, Baltimore, MD

Purpose: Recently, the segmented k-space cine MR data acquisition method has been proposed (1). With very short TR, multiple phase-encoding views per cine frame are acquired. The standard image reconstruction method used for the segmented k-space data acquisition method assumes that there is no motion during each cine frame. Here the authors present a new image reconstruction method that is designed to remove the image distortion in moving objects such as the heart.

Methods: The proposed new MR image reconstruction method does a raw data interpolation before the image reconstruction. The segmented k-space imaging method samples a given point in k space with the regular time intervals, but with a time shift with respect to other k-space points. In this new method, before calculating the inverse Fourier transform, the time shifts are corrected by interpolation in time.

Results: The new interpolation method was tested in a flow phantom. A flow of 2 cm/sec was observed with the aid of tag lines. The segmented k-space data with time segments of 48 msec and TR of 6 msec were collected. The images reconstructed by using the standard and new image reconstruction methods were compared. Significant reduction in motion distortion was observed. Similar data sets were obtained for the human heart. Image quality improvement in the heart images was also observed.

Conclusion: This new image reconstruction method decreases the image distortion due to the nature of the segmented k-space data acquisition method. In addition, since data at any given time point can be interpolated, cine movies with an arbitrary frame rate can be achieved.

1. Atkinson, D, Edelman, R. Radiology 1991; 178:357.

P007

Aliasing Zone Analysis for MR Angiographic Phase Contrast

PR Moran, CA Hamilton
Department of Radiology, Bowman Gray School of Medicine, Winston-Salem, NC

Purpose: How basic geometry limits velocity information from 3D phase-contrast MR angiography is not yet understood. MR angiography can use the 4-point (tetrahedral: 4pT), 6-point (octahedral:6pO), and 8-point (simple-cubic:8sC) methods, but concern arises for artifact/aliasing instability of such sparse-sample modes. We aim at rigorous specifications for noise-limited sensitivity in velocity imaging, antialiasing in 3D, and to determine whether 1D modeling may be used in computer studies.
Methods: Crystallography codifies principles relating phase-space and lab-space properties. These identify primitive vectors for the 4pT, the 6pO, and 8sC methods, and their sample space cells. Then characteristic "flow vectors" map reciprocal space size, measurement pairs, surfaces, and geometry of the V-antialiasing (Brillouin) zone. The 8sC and 6pO methods have defined inversion flow vectors, but the 4-point tetrahedron does not.
Results: MR angiography models validly in 1D by using flow vectors. 4pT (strictly) lacks aliasing protection retrograde to its 3D flow vectors. This traces to tetrahedral inversion nonsymmetry, with extraneous phase errors. However, tolerance limits can be estimated. Compared for equal velocity antialiasing volume, the (4pT:6pO:8sC) $(S/N)^2$ shows (1:2:4) against imaging times of (4:6:8). For principal directions, 8sC offers 4 determinations,; 6pO offers 2, and 4pT offers only 1. Analysis discovers a new 4-point MR angiography method with exceptional antialiasing.
Conclusion: The price for short image time of 4p-tetrahedral, small aliasing protection, is surprising. Images demonstrating a new 3D 4-point encoding for phase-contrast MR angiography, using a 7-point Fourier algorithm, show remarkable properties.

P008

Turbo Spin Echo in Neuroradiologic Applications: Evaluation of Differences from Conventional Spin-Echo Imaging

G Bomgartz
Institut für Klinische Radiologie des Westfälischen Wilhelms-Universität, Münster, Germany

Purpose: Contributions to turbo spin echo (TSE) imaging mostly refer to benefits in economics and to certain disadvantages in image quality (weaker GWM contrast, lipid enhancement, contour blurring) when compared to conventional spin echo (CSE) imaging. Further positive effects of the TSE sequence on image quality have been disregarded so far. The influence of flow artifacts on TSE and CSE imaging was compared in this study.
Methods: Images of 60 patients (heads, $n = 40$; spines, $n = 20$) were obtained with CSE (TR = 2000–2800; TE = 15–90; SL = 4–6 mm) and TSE (TR = 4000–5000; TE = 19–90; SL = 4–6 mm) imaging with a 1.5-T Magnetom. Proton-density–weighted and T2-weighted sequences were acquired consecutively with TSE imaging. Axial orientation was chosen in cranial studies, and sagittal orientation was chosen in spinal studies. Images were compared by 2 blinded radiologists regarding artifacts, contrast, and diagnostic value.
Results: All lesions detected at CSE imaging were also indetified at TSE imaging. A reduction in flow artifacts was seen in 30% of the cases, predominantly at the brainstem and in the spinal canal. Bone structures of the skull base or vertebral column were more reliably defined in approximately 70%. A slight but not significant reduction in GWM contrast was found without affecting diagnostic reliability.
Conclusion: Improved image quality of TSE imaging is based on the repetitive 180° pulses leading to a pronounced even echo rephasing and a decreased sensitivity to susceptibility artifacts.

P009

Three-dimensional Time-of-Flight MR Angiography: Applications in the Pulmonary Vessels

T Nakada, M Hatanaka, Y Suda, T Kuramitsu, T Nakanishi
School of Medicine, Yamaguchi University, Ube, Japan

Purpose: The goals were to compare the usefulness of 2D and 3D time-of-flight MR angiography in the pulmonary vessels and to evaluate the clinical application.
Methods: MR imaging was performed in 12 healthy male volunteers with a 1.5-T whole-body imaging system (Siemens, Erlangen, Germany). The image parameters were 40/8/40° (TR/TE/flip angle), 256 × 256 acquisition matrix, 4-mm section thickness, 40-cm field-of-view, and 13-sec imaging time for each breath-hold acquisition in 2D FLASH and 10/4/16°, 128 × 256, 2-mm, 35-cm and 22-sec in 3D Super FLASH. In 12 patients with pulmonary disease, the above-mentioned parameters were applied.
Results: Pulmonary vessels were visualized and graded as follows: clear and consecutively (2+), clear but partly (1+), and not shown (−). In 2D FLASH, (2+) and (1+) were 12 volunteers (100%) at pulmonary trunk, 10 (83.3%) at upper pulmonary veins and 11 (91.7%) at lower pulmonary veins on the right side, and 12 (100%), 2 (18.2%), and 11 (91.7%) on the left side. In 3D Super FLASH, (2+) and (1+) were 12 (100%), 10 (83.3%), and 12 (100%) on the right side, and 12 (100%), 10 (83.3%), and 10 (83.3%) on the left side. Comparing 2D FLASH and 3D Super FLASH showed that 3D Super FLASH was better than 2D FLASH in left upper pulmonary veins. Some interesting cases of diseases are demonstrated.
Conclusion: MR angiography with 3D Super FLASH could be done with high spatial resolution and short image times during a breath hold. These results suggest that the method may be useful in imaging the pulmonary vessels.

P010

Three-dimensional Time-of-Flight MR Angiography in 35 Patients with Internal Carotid Artery Occlusion

H Hoshino, M Takagi, I Takeuchi, Y Takagi, I Hayakawa
Department of Neurology, Tokyo Saiseikai Central Hospital, Tokyo, Japan

Purpose: We evaluated 3D time-of-flight (TOF) MR angiography of the circle of Willis in 35 patients with internal carotid artery occlusion.
Methods: The patients, 30 men and 5 women, ranged in age from 34 to 78 years. The sites of occlusion were at the origin in 31 patients and at the supraclinoid portion in 4 patients. Conventional angiography was used to examine 20 patients, and duplex carotid sonography was used to examine all patients. MR angiography was performed with a 3D Fourier transformation spoiled GRASS sequence at 28–45/4.3–5.1/20–30° (TR/TE/flip angle). The volume slab was oriented axially to cover the circle of Willis. Imaging volume ranged in thickness from 42 to 60 mm, with 60 partitions ranging in thickness from 0.7 to 1.0 mm. Field of view was 12–22 cm with a 256 × 128 matrix. Angiographic images were obtained by using a maximum intensity projection algorithm.
Results: The imaging with 60 partitions at a thickness of 0.7 mm at 34/5.1/25° in 12 cm field of view was consid-

ered adequate for evaluating the intracranial circulation. The site of occlusion was accurately diagnosed. MR angiography demonstrated the collateral circulation through the circle of Willis in 26 patients. In 8 of 9 patients without collateral circulation through the circle of Willis, MR angiography did not demonstrate the middle cerebral artery. The pattern of cerebral infarction was not correlated with the type of collateral circulation.

Conclusion: MR angiography could demonstrate the site of occlusion and the collateral circulation through the circle of Willis noninvasively. Use of MR angiography as the primary diagnostic tool for patients with internal carotid artery occlusion should be considered.

P011

Strategies for MR Angiography of the Upper Extremities

PM Colletti, JM Tyszka, SE Hanks, MR Terk
Department of Radiology, School of Medicine, Los Angeles, CA

Purpose: To develop techniques for MR angiography of the upper extremities.

Methods: Two-dimensional time-of-flight (TOF), 2D phase-contrast (PC), and cine 2D PC variations of MR angiography were applied to volunteers and patients with atherosclerosis, vasculitis, graft evaluation, gunshot wound, stab wound, and dog bite of the upper extremity. A variety of surface coils were used, including a knee coil, a 12-inch posterior neck coil, and a 3-inch round coil positioned to show the area of interest.

Results: Two-dimensional TOF MR angiography with selective saturation was best suited for the relatively straight vessels at the brachial trifurcation. Cine 2D PC was best for nonlinear areas, such as the subclavian arteries. Delay in pulse transmission is seen in intimal injury, and rapid venous flow is seen in AV fistula.

Conclusion: Proper choice of technique and surface coil is required for optimal MR angiography of the upper extremities.

P012

Optimization of Vessel Boundary Detection in MR Angiography

H Mathura, AP Crawley, RJ Sevick, LJ Hahn
Department of Radiology, University of Calgary, Calgary, Alberta, Canada

Purpose: To grade stenoses accurately, high vessel boundary contrast is required. The authors have investigated boundary contrast versus velocity for the time-of-flight (TOF) and phase-contrast (PC) methods.

Methods: Computer simulations of laminar flow perpendicular to the section were performed. Therefore, a TOF effect is inherent in the PC results. Vessel boundary contrast was defined as CNR/$\sqrt{\text{imaging time}}$ at an edge pixel. The optimal flip angle (α_{opt}) and flow-encoding gradient amplitude were calculated as a function of velocity. The PC data were processed by complex subtraction (CS) or phase subtraction (PS). Comparison of experimental and simulated data was performed by using the total distribution of edge pixels.

Results: The TOF method performs better than the CS method above a certain velocity. This arises from the intravoxel dephasing inherent in the PC method. The PS method is the best at all velocities, due to the higher signal-to-noise ratio (S/N) that can be obtained in a phase image. At high velocities, α_{opt} for all methods approaches approximately 90°. At low velocities, α_{opt} for the PC method tends toward the Ernst angle, whereas the TOF method requires a higher flip angle. For the CS method, the optimal phase accrued at the peak velocity is approximately 180°, but it is considerably higher for the PS method.

Conclusion: Given a prior knowledge of the mean velocity, the boundary contrast can be optimized by choice of technique, flip angle, and flow-encoding gradient. Even with a 20% error in velocity estimate, the best choice seems to be the PS method.

P013

Dynamic MR Angiography of the Abdomen and Pelvis with Gated Segmented K-Space Techniques

PM Margosian
Picker International, Inc, Highland Heights, OH

Purpose: The goal was to improve the quality of MR angiographic images of vessels, such as renal vessels and femoral vessels, which move considerably during a heart cycle, by using gated phase-encoded grouping methods (PEGs) to provide cardiac-cycle synchronization within a reasonable examination time.

Methods: Numerous gated studies were done by using a Picker HPQ imager equipped with software to support PEG acquisitions and cine maximum intensity projections (CINE MIPs). For renal imaging, images of volunteers were obtained as a series of 10–15 contiguous 2D axial sections, acquired sequentially, and structured as cine loops having 3–5 frames, with the PEG technique to keep measurement time below 30 seconds per section. For femoral imaging, coronal orientations were used. CINE MIP provided volume views of vessels.

Results: It was possible to image renal and femoral vessels routinely with these simple and fast techniques and to obtain good quality time-of-flight cines, both with and without MIP. With the acquisition of cines having as few as 3 frames, image quality was made repeatable. Observed vessel motion varied from almost no motion to more than a centimeter.

Conclusion: These synchronized segmented raw data methods provided consistently good quality images of renal and femoral vessels in 10–15 minutes. Clinical evaluation is in progress.

P.M. Margosian is an employee of Picker International.

P014

Method for Combining Raw Data from Thin Slab MR Angiographic Acquisitions for Fourier Reconstruction

PM Margosian
Picker International, Inc, Highland Heights, OH

Purpose: To improve the quality of blood vessel images made from several thin-slab 3D MR angiographic acquisitions by properly combining the various raw data subsets, then using the reconstruction to make images of the entire volume covered all at once.

Methods: Volunteers were imaged with a Picker HPQ imager equipped with software to support maximum intensity projection (MIP) and stacking of thin-slab acquisitions by combining images prior to projection. Composite volume MR angiographic projections were made with the conventional techniques. Next, the various raw data subsets were combined by (1) attaching a linearly varying phase (section direction) to each data segment whose transform positions the corresponding images; (2) convolving each data subset with an apodizing function (section direction), which would in effect remove unwanted images and properly weight overlapping images; (3) adding the processed data subsets; and (4) reconstructing.

Results: Projections of images made from combined processed raw data sets exhibited reduced conspicuity of dark lines at acquisition boundaries relative to conventional methods, as well as smoother appearance.

Conclusion: The raw data combination method leads to improved MR angiographic image quality for stacked 3D slab acquisitions. Clinical studies will test the diagnostic importance of this improvement.

P.M. Margosian is an employee of Picker International.

P015

Diagnostic Significance of Gd-DTPA–enhanced MR Imaging in Hypertrophic Cardiomyopathy

S Okamoto, T Konishi, T Nakano, H Sakuma
First Department of Internal Medicine, Mie University School of Medicine, Tsu, Mie, Japan

Purpose: The authors evaluated the diagnostic value of Gd-DTPA-enhanced MR imaging in patients with hypertrophic cardiomyopathy (HCM).
Methods: Gd-DTPA-enhanced MR imaging was performed in 18 patients with HCM at an operating field of 1.5 T.
Results: The intensive enhancement was found in 7 patients in the ventricular septum and in 4 patients in the entire left ventricular (LV) wall. The patients were divided into 3 groups, according to the morphologic appearance of the Gd-DTPA–enhanced MR images: group N, no enhancement ($n = 7$); group S, enhancement only within the ventricular septum ($n = 7$); and group D, diffuse enhancement ($n = 4$). Clinical characteristics and thallium-201 myocardial scintigraphic, echocardiographic, and microscopic findings of the endocardium were evaluated in 3 groups. For clinical characteristics and degree of echocardiographic hypertrophy, there was no significant difference between the groups. The LV diastolic and systolic diameter in group D was significantly larger than in the other 2 groups ($P < .05$). Left ventricular ejection fraction values were significantly different between the groups (N = 0.84; S = 0.67; D = 0.38). The microscopic findings of endocardial biopsy in the LV wall showed marked interstitial fibrosis in group D. Thus, these findings in group D showed features similar to HCM and suggested diffuse myocardial degeneration.
Conclusion: Gd-DTPA-enhanced MR imaging may be useful for the early detection of myocardial degeneration in HCM and follow-up of patients with HCM.

P016

Quantification of Regional Left Ventricular Myocardial Thickness, Thickening and Motion with Cine MR Imaging: Development of a Technique and Comparison with Qualitative Reporting

MA Sakrana, GZ Yang, DN Firmin, SP Karwatowski, FM El-Demerdash, SR Underwood, DB Longmore
Magnetic Resonance Unit, Royal Brompton Hospital, London, England

Purpose: Cine MR imaging is an established method for assessment of global and regional left ventricular function. An advantage over other techniques is that myocardial thickness, thickening, and wall motion can be assessed. These parameters are frequently reported qualitatively, and the authors have therefore developed a quantitative method, have established normal values, and have tested the method in patients with myocardial infarction.
Methods: The authors studied 20 patients (mean age, 52 years; range, 34–73 years; 15 men) 6 months after myocardial infarction and 10 healthy men (mean age, 40 years; range, 28–51 years) by using cine MR imaging in vertical and horizontal long-axis planes and in basal and apical short-axis planes. Endocardial and epicardial boundaries were defined manually in end-diastolic and end-systolic frames and circumferential profiles of diastolic myocardial thickness, systolic wall thickening, and wall motion were generated in each plane. Categories for each variable were assigned according to the number of standard deviations from the mean of the normal group in each of 9 segments. The results were compared with subjective assessment.
Results: One hundred eighty segments were assessed. Agreement of the 2 methods for wall motion (normal, hyper-, hypo-, a-, dyskinetic) was good, differing by 1 category or less in 166 segments (92%, $\kappa_w = 0.72$). Agreement for wall thickness and thickening (normal or abnormal) was moderate (77%, $\kappa_w = 0.53$, and 70%, $\kappa_w = 0.41$, respectively).
Conclusion: The authors have therefore developed an objective method of assessing 3 aspects of regional myocardial function, which agrees well with subjective reporting. It is expected to improve reproducibility and accuracy, and more widespread experience of its use in patients with reversible ischemia and other disorders is warranted.

P017

Improved Segmented 2D Breath-Hold MR Imaging of the Coronary Arteries

CB Paschal, D Li, EM Haacke
Magnetic Resonance Imaging, University Hospitals of Cleveland, Cleveland, OH

Purpose: To greatly improve a published segmented 2D breath-hold coronary artery imaging technique (1) by incorporating shorter TE and optimized variable flip angle series and by using segmented reverse centric phase encoding, RF spoiling, preparation image, and an automated sequential image procedure.
Methods: A segmented 2D FLASH-like sequence with a short TE of 3.712 msec was used. Data was acquired in 12, 12-line segments during 150 msec of successive diastolic periods. The flip angle series was 15, 16, 16, 17, 17, 18, 19, 20, 21, 22, 23, and 25 degrees. Segmented reverse centric reordering was used to optimize signal from inflowing blood. To RF spoil, the RF phase was incremented by 117°. For each segment, a fat-saturation pulse was applied, and the gradient waveform of the sequence was repeated several times to stabilize any eddy currents. Transverse, 2–3-mm-thick sections with 220–256 field of view and 1 acquisition and 3 preparation cycles were used. Total breath hold was 15 heartbeats long. An automated procedure incremented the section position and repeated the acquisition after a fixed resting interval for 25–40 repetitions.
Results: The technique produced 25–40 images, with the coronary arteries visible as bright blood against darker myocardium and fat. The optimized flip angle series produced a more uniform signal. The short TE and RF spoiling reduced smearing and ghosting. Image sets were postprocessed to visualize sections of the coronary arteries in various planes, though section misregistration was a problem.
Conclusion: Two-dimensional segmented breath-hold imaging of the coronary arteries has been improved by incorporating the features tested in this work. The automated procedure required no a priori knowledge of coronary artery anatomy and enabled the subjects to develop a consistent breath hold and normal breathing pattern. Misregistration of the images, however, remained a substantial limitation.

1. Edelman, et al. Radiology 1991; 181:641.

P018

3D MR Imaging of the Coronary Arteries with Retrospective Respiratory Gating

MB Hofman, CB Paschal, D Li, EM Haacke
Magnetic Resonance Imaging, University Hospitals of Cleveland, Cleveland, OH

Purpose: The purpose of this work was to improve image quality in 3D MR imaging of the coronary arteries by incorporating retrospective respiratory gating.

Methods: The motion of the heart as a result of respiration causes blurring and ghost artifacts in the images of the coronary arteries. Acquisition of 3D data takes too long for a breath-hold approach. Averaging can reduce ghosting but does not remove blurring. Respiratory gating can reduce both. To accomplish this, a craniocaudal projection spin-echo signal from a column passing through the diaphragm is obtained once each cardiac cycle and is used as a reference for the respiratory cycle. The basic 3D imaging sequence is a triggered 3D magnetization-prepared rapid gradient echo sequence. After magnetization preparation and a delay time, all k_z lines and the projection echo are then acquired. This is repeated for the same k_y line for more than 4 to 8 successive cardiac cycles to ensure adequate sampling of the respiratory cycle. Retrospective respiratory gating limits were set for a narrow range of diaphragmatic positions. Images were then reconstructed from data acquired when the diaphragm position fell within the gate limits. For comparison, nongated images were reconstructed by averaging all the data collected. Image sets were evaluated subjectively for conspicuity and sharpness of the coronary arteries.
Results: To date, 8 patients underwent imaging with this technique. In more than half of the cases, the retrospectively respiratory gated images were deemed to be sharper, with better definition of coronary arteries, than the ungated, completely averaged images.
Conclusion: Retrospective respiratory gating produced sharper 3D images of the heart and coronary arteries than did straight averaging of data. There is no difference in acquisition time between the 2 approaches, and retrospective respiratory gating does not preclude the option of averaging instead.

P019

Automated Myocardial Edge Detection in MR Images: Accuracy in Consecutive Subjects

SR Fleagle, DR Thedens, W Stanford, BH Thompson, JM Weston, PP Patel, DJ Skorton
Cardiovascular Center, College of Medicine, University of Iowa, Iowa City, IA

Purpose: In the initial feasibility studies, to permit comparison of automated myocardial borders to manually traced borders in spin-echo MR images, the authors evaluated only images with at least 75% of each myocardial border clearly visible. The purpose of this study was to assess the utility of the automated method in consecutive subjects, without excluding less optimal studies.
Methods: The authors analyzed all images from apex to left ventricular outflow tract obtained in all subjects who had short-axis spin-echo images during a 1-year period. One hundred forty-two images were analyzed from these 11 subjects, yielding an unbiased image set with a wide range of quality. Using an edge operator, the method constructed a map of edge likelihood. The map was then searched for optimal epicardial and endocardial borders by using a graph-searching algorithm. Computer borders were compared to those traced by a blinded observer using a previously validated, systematic procedure.
Results: The program correctly identified endocardial and epicardial edges in 121 of 142 images (85%). The computer method failed to correctly identify at least 75% of the endocardium in 3 images, at least 75% of the epicardium in 11 images, and at least 75% of both edges in 7 images. The computer-derived epicardial and endocardial areas correlated well with observer data (epicardium, $r = .71, y = .76x + 6.2$, SEE = 8.6 cm^2; endocardium, $r = .83, y = .84x + 0.02$, SEE = 4.6 cm^2). In a subset ($n = 63$) of higher quality images in which the tracer was confident of at least 75% endocardial and epicardial visibility, endocardial r was .92 and epicardial r was .82, similar to our earlier studies.
Conclusion: The method permits accurate identification of myocardial borders in the great majority of consecutive subjects and may facilitate quantitation of cardiac magnetic resonance image data.

P020

Multisection Breath-hold Imaging in the Lung with Multisection Excitation Pulses and Hadamard Processing

GD Clarke, WA Erdman, M NessAiver, H Liu, JB Murdoch, RM Peshock
Department of Radiology, Southwestern Medical Center, University of Texas, Dallas, TX

Purpose: Single breath-hold phase-encode grouping (PEG) with 3 or 4 phases allows good identification of the pulsatile nature of the pulmonary arteries and accounts for the displacement of the pulmonary vessels due to heart motion. A method for reducing imaging time by using special RF pulses that excite 4 sections at 1 time, each with differing RF phases, has been investigated.
Methods: Six normal volunteers were studied by using a Picker 1.5-T HPQ imaging system. The signals from a total of 4 excitations are added or subtracted (as in a simple Hadamard transform) to separate the signals from each of the 4 sections. A 3-frame cine loop from each of 4 sections was obtained in a single breath hold. Between each section was a gap equal to twice the section thickness.
Results: The images were shown to produce twice the signal-to-noise ratio of normally excited pulmonary cine images, since each image is effectively due to 4 excitations. A lung was completely imaged in 3 breath holds, allowing the production of 12 section × 3-frame cine loops with 6–10 mm sections. Image quality was generally good, but presaturation of large cardiopulmonary structures was necessary to eliminate artifacts due to quickly flowing blood.
Conclusion: Hadamard imaging can be used to improve signal-to-noise ratios and facilitate rapid imaging of the pulmonary vasculature.
M. Ness Aiver, H. Liu, and J.B. Murdoch are employees of Picker International.

P021

Use of Striped Radial Tagging to Measure Three-dimensional Endocardial and Epicardial Deformation throughout the Canine Left Ventricle during Ischemia

CC Moore, ER McVeigh, A Mebazaa, EA Zerhouni
Department of Biomedical Engineering, Johns Hopkins University, Baltimore, MD

Purpose: The goal was to develop a tagging and data analysis method for measuring transmural gradients of strain throughout the left ventricle (LV).
Methods: We implemented a striped radial tagging protocol for the LV that produced clearly resolved tag points at spacings as close as 4 mm across the wall at 12 circumferential positions. The LAD coronary artery of a dog was occluded after the first diagonal before imaging in a Signa 1.5-T imager (spin-echo, multisection-multiphase, head coil, 18-cm field of view, 256 × 192, number of signals averaged = 1, TR = 2 RR). Five short-axis sections were acquired having 12 radial tags, each with 3–5 radial points spaced at 4.6 mm. An orthogonal set of 6 radially oriented long-axis sections with parallel tags was also taken. The images were processed by using a semiautomated tag and heart contour detection algorithm. Material points were defined from the positions of the short-axis tag points before deformation and tracked by using an iterative interpolation algorithm to reconstruct 3D motions.

Results: By end-systole in the normal region, which spanned 180° circumferentially, the most endocardial material points separated by 6.1–7.2 mm, and the most epicardial ones by 5.7–6.5 mm. At the center of the affected region in the anteroseptal wall, however, endocardial points closed to 4.0-mm spacing, and epicardial point separation remained at 4.6 mm.

Conclusion: Transmural gradients in myocardial deformation were measured during ischemia throughout the canine LV by using striped radial tagging. This method will be used to quantify the effects of locally graded perfusion.

P022

Phase-Contrast Method in Turbulent Flow Velocity Measurement

J Gao, DO Kuethe, LJ Neuringer
Francis Bitter National Magnet Laboratory, Massachusetts Institute of Technology, Cambridge, MA

Purpose: Flow velocities have been measured successfully by several investigators for laminar flow (1–3). The authors tried to determine if the time-averaged velocities in turbulent flow could also be measured by imaging the phase of MR spins.

Methods: Images of the longitudinal component of velocity were made of laminar flow (Reynolds number 1197 ± 10) and turbulent flow (Reynolds number 2903 ± 18) in well-developed flow in a pipe with circular cross section. The flow rate through the pipe as measured by imaging (the average velocity of the pixels in the cross section multiplied by the area of the cross section) was compared to the flow rate exiting the pipe (the volume of water collected in a graduated cylinder divided by the time to collect it) to test the validity of the method.

Results: For laminar flow (Re = 1197 ± 10, flow rate = 48.19 ± 0.41 mL/s), the flow rate measured from MR imaging was 44.72 ± 3.27 mL/s. For turbulent flow (Re = 2903 ± 18, flow rate = 116.59 ± 0.82 mL/s), the flow rate measured from MR imaging was 115.97 ± 1.43 mL/s.

Conclusion: The image of velocities in turbulent flow appeared uneven (noisy), but the flow rate measured from the image was correct. The noise is to be expected from the chaotic nature of turbulent flow.

1. Moran PR, Magn Reson Imaging 1982; 1:197–203.
2. Bryant DJ, Payne JA, Firmin DN, Longmore DB. J Comput Assist Tomogr 1984; 8:588–593. 3. O'Donell M, Med Phys 1984; 12:59–64.

P023

Computer Algorithm for Determining Ascending Aorta Blood Flow Patterns and Estimation of Total Coronary Artery Flow

MH Buonocore
Division of Diagnostic Radiology, University of California Davis Medical Center, Sacramento, CA

Purpose: Using multisection velocity data obtained from the base of the ascending aorta, the computer algorithm constructs a self-consistent picture of the flow patterns in the ascending aorta and an estimate of total coronary artery flow.

Methods: The algorithm uses axial-oblique, cardiac-gated velocity data of the ascending aorta blood flow. Velocity data is needed from below the coronary ostia in systole to above the ostia in diastole. The computer model uses the histograms of transverse velocity data at each section and time step. The algorithm propagates the velocity histogram at each section and time step to the next time step. The propagated histograms are compared to those acquired in the scans, and a global least-squares correction of the acquired data is made so that the propagated and acquired histograms show the same net flow. If a coronary artery ostia is present within or between the sections, inconsistencies in net flow are attributed to coronary artery flow. The algorithm also uses spatial information and in-plane velocity measurements.

Results: Recirculation of blood flow in the ascending aorta ranges from 5% to 30% of the net flow, being largest in sections lying entirely above the aortic valve in late systole. Total coronary artery flow reproducibility is approximately 30%.

Conclusion: Multisection measurements of velocity in the ascending aorta can be used to estimate total coronary artery flow. A computer algorithm for determining ascending aorta flow patterns is necessary to make the best possible estimate.

P024

Measurement of Coronary Artery Flow from Multisection Measurements of Flow in the Ascending Aorta

MH Buonocore
Division of Diagnostic Radiology, University of California Davis Medical Center, Sacramento, CA

Purpose: Total (left plus right) coronary artery flow is estimated by using phase-contrast measurements of velocity in the ascending aorta and aortic root.

Methods: The protocol for obtaining aortic velocity measurements is: (1) axial gated multisection spin-echo sequence (field of view [FOV] = 24 cm, matrix = 128 × 256, 3-mm section) timed so that the ostia of both vessels are visualized in systole; (2) 3 short TE coronal VINNIE (GE Medical Systems) sequences (FOV = 20 cm, matrix = 128 × 256, 7-mm section, flow compensation on, 200 cm/sec velocity encoding) to establish the motion of the left coronary artery through the cardiac cycle; and (3) 5 or more short TE axial oblique VINNIE sequences (FOV = 24 cm, matrix = 128 × 256, 5-mm section, flow compensation on, 200 cm/sec transverse velocity encoding in systole, 40 cm/sec in diastole) at successive levels through the ascending aorta, from below the coronary ostia in systole to above the ostia in diastole. Velocity data are then used in a custom least-squares algorithm to compute a consistent picture of forward and backward flow patterns in the aorta and an estimate of flow into the coronary arteries.

Results: Net flow measurements obtained through the aortic valve are typically reproducible to within 10% standard deviation, and backward flow to within 20%. Velocities are adjusted about 5%–15% by the least-squares algorithm, and the total coronary artery flow estimate has a standard deviation of about 30%.

Conclusion: Total coronary artery flow estimation is feasible by using multisection measurements of flow in the ascending aorta.

P025

Dynamic Monitoring of Blood Flow by Spiral Scan Velocity Mapping

PD Gatehouse, DN Firmin, JP Konrad, RH Mohiaddin, SP Karwatowski, DB Longmore
Magnetic Resonance Unit, Royal Brompton National Heart and Lung Hospital, London, England

Purpose: To develop an ultrafast method of imaging flow velocities in rapid succession so that rapid changes in flow can be monitored.

Methods: The study was performed on a 0.5-T magnet with a reduced diameter (53 cm) gradient set and an SMIS console used to drive the system. Each image was acquired by the spiral scanning of k space after a section excitation and velocity phase encoding. Data were acquired over 40 msec while spiraling out from the center of k space. Phantom experiments were used to validate the technique. To monitor flow over a series of successive cardiac cycles, images were triggered off each R wave of the electrocardiogram and repeated every 50 msec throughout each cycle. Reference images were acquired during the first cardiac cycle, then encoded images on those following. This method was used to study changes in flow in normal subjects at rest and while performing Valsalva's maneuver.

Results: Phantom studies proved the technique to be accurate and relatively insensitive to phase-dispersive signal loss. In vivo measurements of aortic flow compared well with the time-averaged measurements obtained by using a conventional velocity-mapping technique. When used to dynamically monitor flow, a relationship was shown between the aortic flow and the duration of the previous R-R interval; the longer this interval, the faster the flow.

Conclusion: Phase-contrast velocity mapping with spiral scanning of k space is a promising new approach to rapid flow imaging; it enables sudden variations in blood flow to be monitored.

P026

Pulmonary Vein Flow in Ischemic Heart Disease: a Comparison between MR Imaging and Doppler Echocardiography

SI Mavrogeni, MA Sakrana, RH Mohiaddin, DJ Pennell, MY Henein, SR Underwood, DB Longmore
Magnetic Resonance Unit, Royal Brompton Hospital, London, England

Purpose: Abnormal ventricular relaxation occurs in coronary artery disease, which causes changes in mitral valve flow in diastole. Therefore, pulmonary vein flow might be similarly affected. The authors compared MR velocity mapping and Doppler echocardiography in the estimation of mitral valve and pulmonary vein flow in ischemic patients.

Methods: Fifteen patients were recruited, but Doppler measurements were possible only in 10. Nine had a history of myocardial infarction, and 6 had stable chronic angina. All patients (mean age, 63 years; range, 59–72 years; 9 men) stopped cardiac medication prior to study. Doppler and MR variables measured were peak mitral valve flow (E_{vel}), atriosystolic contraction (A_{vel}), peak systolic pulmonary vein (x_{vel}), peak diastolic pulmonary vein (y_{vel}) and peak reverse (rv_{vel}) flow velocities. Echocardiography measurements and MR velocity mapping of the right upper pulmonary vein and of mitral valve flow were performed on the same day and at the similar heart rates.

Results: The results, shown as the difference between the 2 techniques were the following: E_{vel}: mean value = 59.9; mean difference (mean averages of the differences between the 2 techniques [cm/s] = 3.1; standard deviation (SD) difference (standard deviations of the differences between the 2 techniques = 4.32; 95% confidence interval (CI) = −5.3 + 11.5. A_{vel}: mean value = 41.9; mean difference = 26.6; SD difference = 17.77; 95% CI = −8.2 + 61.4. X_{vel}: mean value = 41.9; mean difference = 2.4; SD difference = 1.9; 95% CI = −1.32 + 6.12. Y_{vel}: mean value = 25.1; mean difference = 2.4; SD difference = 4.86; 95% CI = −7.12 + 11.92. rv_{vel}: mean value = 9.75; mean difference = 12.33; SD difference = 5.18; 95% CI = +2.17 + 22.48. The E wave measured by MR was correlated with the X and Y wave ($r^2 = 0.139$, $P < .001$ and $r^2 = 0.722$, $P < .001$ respectively). Thus, MR may be used as a noninvasive technique for the estimation of pulmonary venous flow, with good correlation to Doppler measurements. MR measurements were possible in 5 patients in whom adequate Doppler interrogation of flow was not possible.

Conclusion: Such techniques may find application in coronary artery disease.

P027

Pressure Gradient Measurement across Stenotic Valves in a Pulsatile Flow Aorta Phantom Using Phase Velocity Mapping

SP Loehr, KM Link, NM Lesko
Bowman Gray School of Medicine, Winston-Salem, NC

Purpose: To determine the accuracy of coronal and oblique axial-plane MR imaging phase-velocity mapping in assessing pressure gradient across in vitro stenotic valves compared to catheter-generated pressure gradients.

Methods: A low-flip-angle phase-velocity mapping (VINNIE) sequence was performed on a 1.5-T GE Signa imager to assess poststenotic jet velocities across 86% and 75% central and 81% eccentric (15° angulation) acrylic stenosis at a pulsatile flow rate of 15 L/m and 20 L/m in each case. The MR imaging-derived pressure gradients were compared to catheter-generated pressures generated under the same experimental conditions.

Results: The MR imaging-assessed pressure gradients in the coronal plane across the 75% central stenosis at flow rates of 15 L/m and 20 L/m (velocity range, 1.93–2.43 m/s) yielded an 84.0% and 88.1% correlation, respectively, with the catheter pressures. With the oblique transaxial plane, MR imaging yielded an 87.5% and 98.3% correlation, respectively. With the 86% central stenosis in the coronal plane, MR imaging correlated to 94.3% and 93.6%, respectively. In the oblique transaxial plane, MR imaging pressure measurements correlated to 94.9% and 98.0%, respectively. With the 81% eccentric stenosis, the MR imaging coronal plane pressure gradients correlated to 51.2% and 79.5% (average, 65.4%), respectively. There was some improvement in the transaxial plane as the MR imaging pressures compared to 72.2% and 86.3% (average, 79.2%) of the catheter values.

Conclusion: Phase mapping appears accurate in assessing pressure gradients across centrally oriented stenoses. Eccentric stenoses appear to produce complex flow phenomena, which may diminish the ability of MR imaging to produce consistently accurate pressure gradients.

P028

Investigation of Time-of-Flight MR Angiography in the Presence of Pulsatile Turbulent Flow

S Vinitski, HV Ortega, FB Mohamed, S Seshagiri, AE Flanders, DG Mitchell
Department of Radiology, Thomas Jefferson University Hospital, Philadelphia, PA

Purpose: The authors previously investigated the effect of physiologically complex, but not yet pulsatile, turbulent flow on MR angiography. To better understand the relationship between turbulent flow and signal alterations in MR imaging, a study was performed to produce images of flow in the presence of stenosis and to compare them with computer simulation.

Methods: MR angiography was performed in vitro by using 2D and 3D time-of-flight (TOF) sagittal acquisition. Color Doppler was also used. Experimental fluid (carboxymethylcellulose) with relaxation times and viscosity similar to that of blood was prepared. The experiments were performed by using a Plexiglas phantom with a 2-cm-diameter tube with varying degrees of stenosis (50%, 75%, and 90%) and a cardiac pump that was set to generate high-velocity pulsatile flow with Reynolds numbers ranging from 200 to 10,000. Images were obtained by TOF using flip angles varying from 20°–50° and TR of 50 msec with a minimum TE of 5–8 msec. Computer simulation of fluid flowing through the model was performed by (1) solving the Navier-Stokes equation for nonturbulent flow

and (2) by using an eddy viscosity/diffusivity model for turbulent flow. Finite element analysis was utilized. A SUN 3 computer was used.
Results: Two-dimensional and 3D in-plane TOF images demonstrated marked hemodynamic dependability expressed as a change in signal intensity as the velocities and/or degree of stenosis increased. Computation time was between 1 and 7 days, depending on the type of flow. Computer simulation depicted spatial distribution of losses in kinetic energy, degree of vortices, and the jet elongation as a function of Reynolds numbers, type of flow, and stenotic vessel geometry. Increase in viscosity resulted in stagnation of poststenotic fluid. These results correlated well with both MR angiography and color Doppler flow imaging.
Conclusion: The appearance of MR angiographic images strongly correlates with the authors' mathematical model of pulsatile turbulent flow.

P029

Improving the Accuracy of Flow Measurements with a Threshold Technique

C Tang, DL Parker
University of Utah, Salt Lake City, UT

Purpose: The partial volume effect (PVE), in which more than 1 type of tissue is included in 1 voxel, causes quantitative errors in phase-contrast volume flow rate (VFR) measurements. In this study, the authors demonstrate how thresholding based on the magnitude image can improve VFR accuracy.
Methods: In this technique, velocity measurement for voxels in the region of interest are included in the VFR calculation. The authors demonstrate that the optimal threshold is a function of the saturation ratio, which is the ratio of image intensity between the stationary tissue and flowing blood. A computer program has been written to choose the threshold automatically. The technique was verified by using phase-contrast studies in flow phantoms.
Results: Computer simulations demonstrate that the application of an appropriate threshold can significantly reduce the error in VFR measurements. The experimental results show that the VFR measurement error is reduced from 40% to 10% in a 4.5-mm-diameter tube. The magnitude of the VFR error and magnitude of the corresponding correction decreases as tube size increases, reaching only a few percent in a 12-mm-diameter tube.
Conclusion: The threshold technique provides a simple and effective compensation for the PVE.

P030

Effect of Field Susceptibility on MR Microvascular Flow Measurements

M Su, O Nalcioglu
Department of Radiological Sciences, Division of Physics and Engineering, University of California, Irvine, CA

Purpose: When the spin-phase analysis technique is used for flow quantification, the correct measurement of the spin phase is important. The field inhomogeneity due to the susceptibility variations in the medium may affect the spin-phase measurement, especially in the case of microvascular flow. The authors propose a method for studying the effect of susceptibility on the measurement of microvascular flow with MR.
Methods: A phantom made out of glass beads in a tube was used in the experiments. The first (90°-2τ-180°-2τ) and second RF echo (90°-τ-180°-2τ-180°-τ) pulse sequences were used to measure the signal. The local field distribution was calculated from the susceptibility differences between the glass beads and water. As a water molecule flows through the medium, its spin experiences the field gradient and accumulates a velocity phase. The signal attenuation can then be estimated from the velocity phase distribution in the voxel.
Results: As expected, the signal of the second RF echo pulse sequence was much higher, because of the velocity compensation effect in the internal field gradient. From the experimental and simulation results, the susceptibility variations in the medium were successfully extracted. For example, the susceptibility variation for the 1.5-mm bead phantom was 1.4×10^{-6} emu/cm^3.
Conclusion: The authors have shown that the signal attenuation due to microvascular flow in a heterogeneous medium can be estimated. This should help in investigating the effect of susceptibility on the MR flow measurements.

P031

Kinetic Parameter Maps from Dynamic Gd-DTPA Studies: Application to a Tumor Model in Mice

S Nekolla, T Gneiting, J Griebel, C Wagner-Manslau, A Haase
Physikalisches Institut (EPV), Universität Würzburg, Würzburg, Germany

Purpose: With high spatial and temporal resolution, T1 maps allow the observation of kinetic events in normal and tumor tissue after the application of paramagnetic contrast agents. The purpose of the study is to demonstrate the feasibility of using T1 maps to calculate kinetic parameter maps from dynamic Gd-DTPA studies.
Methods: Evaluation of kinetic parameter maps must use model functions fitted on a pixel-by-pixel base. But the mostly nonlinear functions demand numerical techniques that are difficult to run in an automatic procedure for 128 × 128 data points. Using a priori information about Gd-DTPA kinetics, we decomposed the problem, allowing the use of local but linear functions for the calculation of perfusion and wash-out maps. T1 maps were computed from 16 T1-weighted inversion recovery snapshot FLASH images (matrix: 64 × 128; in-plane resolution: 0.25 mm; section thickness: 1.5 mm; acquisition time: 2.5 sec; Bruker Biospec 4.7T/20cm). Both processing and postprocessing were performed parallel to the image acquisition on an IBM RS/6000 workstation. Gd-DTPA was injected as a bolus into the tail veins of the tumor-bearing mice. Up to 20 postcontrast T1 maps were obtained, starting with intervals of 12 sec.
Results: The application of dynamic T1 mapping is a fast, reliable, and sensitive technique for mapping Gd-DTPA kinetics in normal and tumor tissue. Compared to the use of direct nonlinear models, the authors' method yields perfusion and washout maps, with drastically increased homogeneity and sensitivity.
Conclusion: Dynamic T1 mapping allows the evaluation of kinetic parameter maps with a temporal and spatial resolution superior to that of most other digital imaging techniques.

P032

Important Role of MR in Radiologic Detection of Lesions in Patients with Hearing/Vestibular Problems

MT Gorey, AP Wolff, CZ Weingarten, MM Mikhael
Department of Radiology, Evanston Hospital, Evanston, IL

Purpose: To determine the optimum radiologic study for the detection of lesions of the 8th cranial nerve (hearing/vestibular).
Methods: Two hundred seventy-one patients (195 women, 76 men) (age, 25–78 years) with hearing/vestibular problems were evaluated during the last 7.5 years: polytomography ($n = 42$), routine CT ($n = 92$), CT com-

bined with cisternography ($n = 20$), and MR images ($n = 82$). Fifty-two patients were studied with MR images before and after enhancement. Seventy-eight tumors were diagnosed and surgically removed; 62 were acoustic neuromas and 16 were meningiomas. Other lesions discovered in the brain stem included lymphoma ($n = 3$), multiple sclerosis ($n = 2$), brain stem glioma ($n = 2$), small AVM lesions ($n = 4$), and posttraumatic small hematoma ($n = 1$). Extraaxial lesions seen on enhanced MR included inflammatory changes (labyrinthitis: $n = 2$), cerebellopontine angle (CPA) vascular loop ($n = 2$), cholesteatomas ($n = 6$), meningeal carcinomatosis ($n = 6$), and Bell palsy ($n = 2$).
Results: Polytomography helped to detect 10 of 15 lesions (66.7%) with 5 false-negative (33.3%) and 4 false-positive (26.7%) studies. Routine CT images visualized large and enhancing lesions (37 of 52) but missed 15 small intracanalicular tumors that were only visualized by CT images combined with cisternography or MR. Enhanced MR helped to diagnose 34 of 34 lesions (100%), with no false-positive or -negative studies, including 10 intracanalicular small tumors missed on routine CT and nonenhanced MR images. Enhanced MR also detected brain stem tumors and lesions in the temporal bone that can be present with hearing/vestibular problems.
Conclusion: The present study has shown that, although routine CT can visualize large and enhancing CPA tumors, MR can replace both routine CT images and CT combined with cisternography, for diagnosis of extra- and intracanalicular lesions. Enhanced MR imaging is the standard for the radiologic diagnosis of lesions and hearing/vestibular problems. MR angiography is helpful for vascular lesions. Neuroradiologic study of patients with hearing/vestibular problems should also include MR evaluation of the brain stem.

P033

Imaging Cerebral Activation with BOLD Contrast at 1.5 T: Optimizing a Technique for Conventional Hardware

RM Thompson, CR Jack, RW Hynes, RK Butts, NJ Hangiandreou, SJ Riederer, RL Ehman
MR Research Laboratory, Mayo Clinic, Rochester, MN

Purpose: Functional cerebral imaging can be performed by using T2*-weighted MR sequences that are sensitive to changes in blood oxygenation. The goal was to examine several of the parameters used to generate such images and optimize a technique with standard hardware at 1.5 T.
Methods: All experiments were performed in volunteers with an unmodified 1.5-T General Electric Signa imager. Photic stimulation consisted of flashing red light at 8 Hz. A gradient-recalled-echo (GRE) imaging sequence was used. Sagittal scouts were acquired to select an oblique plane through the primary visual cortex for functional images. The following parameters were modified in serial fashion: field of view (FOV), TE, flip angle, RF spoiling, section thickness, frame rate, matrix size, type of receiver coil, stimulus duration, and method of averaging data.
Results: The percent change in signal intensity (PCSI) was slightly greater with an FOV of 24 cm compared to 20 cm. A longer TE (up to 38 msec) resulted in a slightly greater PCSI. A 30° flip angle was optimal. SPGR tended to give better results than GRASS. The optimum section thickness was 5–8 mm. The PCSIs, using both surface and head coils, were in the 1%–4% range, but slightly better signal-to-noise ratio was achieved with the surface coil.
Conclusion: Activation of the visual cortex resulted in consistent 1%–4% PCSI at 1.5 T. An optimized GRE sequence for performing functional experiments on standard hardware is outlined.

P034

Correction of Motion Artifacts in Diffusion-weighted MR Images with Navigator Echoes

RJ Ordidge, JA Helpern, Z Qing, RA Knight
Department of Neurology, Henry Ford Hospital, Detroit, MI

Purpose: Patient motion seriously degrades the quality of MR images during diffusion-weighted MR imaging procedures that use strong gradient pulses of long duration. This arises from an MR signal phase-shift error that is proportional to the magnitude of the random motion. Fourier transformation of the data set causes severe "ghosting" artifacts and loss of image detail. A pulse sequence has been developed that uses the phase information from navigator echoes to remove these errors.
Methods: The effect of this random patient motion can be minimized by a modification to the MR imaging procedure which acquires an additional spin echo (navigator echo) that is not subjected to a phase-encoding gradient and has the same phase as the spin echo used for imaging (1). The data are then processed with a computer algorithm that corrects the MR image spin echo by using a calculated phase angle obtained by comparison of the correction echo phase for each phase-encoding step with the phase of the first correction echo in the imaging sequence. The correction is based on the fact that linear motion of the subject along the axis of the applied diffusion-weighted gradient produces a uniform phase shift of the MR signal.
Results: Diffusion-weighted MR of the human head was performed with a 3-T 80-cm-bore magnet (Magnex Scientific) with b values in the range 100–1000 s/mm^2 (TR = 3 s; TE = 144 msec; 128 × 128 image matrix; section thickness = 5 mm). The phase-correction approach was used in conjunction with ECG triggering (with a Nonnin pulse oximeter) to minimize brain pulsation motion.
Conclusion: The new procedure greatly reduces image ghosting and related distortions in diffusion-weighted MR images and may have applications in other high-resolution MR imaging studies.

1. Ehman RL, Felmlee JP. Radiology 1989; 173:255.

P035

Rapid Measurements of ADC$_w$ with a Spin-Echo Imaging Technique

RA Knight, RJ Ordidge, JA Helpern
Department of Neurology, Henry Ford Hospital, Detroit, MI

Purpose: The mechanism responsible for changes reported in the "apparent" diffusion coefficient of water protons (ADC$_w$) within minutes after the onset of focal cerebral ischemia in experimental animals is currently unknown. A technique capable of producing rapid, reliable ADC$_w$ measurements, without the complicating T2* effects caused by other currently available techniques, would be useful for investigating such mechanisms. This work presents a spin-echo method for producing relatively fast ADC$_w$ measurements.
Methods: ADC$_w$-weighted images were produced on a 7-T system by using a standard Stejskal-Tanner pulsed gradient spin-echo (PGSE) imaging sequence (TR = 1.5 s, TE = 43 msec) and a modified PGSE sequence (TR = 200 msec, TE = 43 msec), in which the selective 90° RF pulse is replaced by a low flip angle RF pulse, and the acquisition period is followed by a nonselective 180° RF pulse centered between 2 gradient crusher pulses. Images (64 × 64, 5 cm field of view) were obtained from middle cerebral artery-occluded rat brains ($n = 11$) by using gradient b values of 0, 200, 400, 600, 800, and 1200 s/mm^2. ADC$_w$ measurements, obtained by using both techniques, were taken from regions of interest (3 × 3 pixels) in the

control side of the brain and were compared by using a paired *t* test.
Results: The modified PGSE method is an implementable and relatively straightforward technique that can provide diffusion-weighted images within seconds. Although the modified PGSE technique suffers from an overall loss in signal to noise as compared to the standard PGSE technique, the quality of the images is sufficient to calculate the value of ADC_w and thus distinguish between ischemic and normal brain tissue. As expected, comparison of ADC_w values obtained by using the standard (7.405 ± 0.677 mm²/s) and modified (7.298 ± 0.903 mm²/s) PGSE techniques failed to demonstrate any significant difference between the 2 methods ($P > .15$).
Conclusion: This new technique can provide a fast and accurate assessment of ADC_w values.

P036

Anisotropically Restricted Diffusion (ARD) Imaging with Fast Acquisition Multiecho (FAME)

RP Gullapalli, L Kasuboski
Picker International, Highland Heights, OH

Purpose: It has been shown that diffusion studies can be performed with a conventional human imager with normal gradient strengths of 1 G/cm. High motion sensitivity is a well known drawback of this technique, with imaging times on the order of 5–6 minutes. Faster techniques, such as CE-FAST diffusion, give information about isotropic diffusion rather than anisotropically restricted diffusion (ARD). The authors propose here the use of FAME to produce ARD images with a substantial reduction in motion artifacts and image times.
Methods: Images of water and acetone phantoms and a normal human brain were obtained by using a 1.5-T Picker HPQ MR imaging system. A 4-echo FAME sequence, with an effective echo time of 130 msec, and a normal spin echo, with an echo time of 130 msec, were used to produce the normal and ARD images. Diffusion sensitization ($b = 550$ s/mm²) in the section direction was applied in both the sequences.
Results: The diffusion coefficients obtained for the water and acetone phantom ($D_{water} = 2.4E^{-3}$ mm²/s, $D_{acetone} = 4.2E^{-3}$ mm²/s) from the standard spin-echo sequence were comparable to the FAME sequence. The resulting diffusion coefficients obtained from the diffusion map by using the 2 sequences were comparable.
Conclusion: Substantial reduction in image times (4-fold in this case), and hence a reduction in motion artifacts, can be obtained by using this technique. Both normal and diffusion-weighted FAME images can be obtained within 4 minutes to produce the diffusion maps. Much shorter imaging times can be obtained with longer echo trains.

P037

Diffusion Imaging with Generalized Series Reconstruction

S Chandra
Biomedical Magnetic Resonance Laboratory, University of Illinois, Urbana, Il

Purpose: The aim of this study is to demonstrate the gain in temporal resolution that can be achieved in diffusion-weighted MR imaging by using a generalized series (GS) reconstruction algorithm. This algorithm can incorporate a priori information from a high-resolution image to reconstruct high-resolution diffusion images from data acquired quickly with a few phase encodings.
Methods: A volume coil RF transmit and surface coil signal receive set-up was used at 4.7 T. Sprague-Dawley rats were anesthetized with 2% halothane. A high-resolution basis image (128 × 128 SE; TR/TE = 5000/97; section thickness = 2.0 mm) was collected. Reduced-encoding diffusion-weighted images (128 × 32; gradient (G/cm): 1.0, 1.1, 1.2, 1.3, 1.4, 1.5, 1.6; corresponding b factors: 105.78, 127.99, 152.32, 178.77, 201.33, 238.01, 270.8) were collected with 4 signal averages. The reduced encoding images were reconstructed with GS by using the high-resolution basis image to generate high-resolution diffusion-weighted images.
Results: The mean value of the diffusion coefficient in a 40-pixel-deep brain region was found to be $0.71 \pm 0.02 \times 10^{-5}$ cm²/sec (mean ± SEM). Anatomic details remained sharp.
Conclusion: The GS algorithm allows the number of phase encodings used in diffusion imaging to be reduced, without sacrificing structural clarity. The time saved can be used to follow fast processes or to enhance signal-to-noise ratios by additional signal averaging.

P038

Cumulative Formulation of MR Image Formation Theory

PR Moran
Department of Radiology, Bowman Gray School of Medicine, Winston-Salem, NC

Purpose: To find whether an elemental MR imaging gradient that phase-sensitizes motion is characterized by many higher-motion-order phasings, or by 1 unique order of motion, over a specific intrasequence interval.
Methods: When flow encounters an abrupt bend (remaining nonturbulent) higher-order vector motion derivatives are substantial until $[(\text{flow speed}]/(\text{radius-curvature})]^n \le (1/n!)T^n$, where T^n is the waveform nth moment. A phantom can be constructed and imaged in lab experiments. Current theory implies a nexus of higher-order phase-shift interference, increasing rapidly with flow speed. A cumulative phasing theory of MR image formation predicts simple imaged properties from 1 sensitized motion.
Results: Cumulant theory describes an abrupt and narrow phase band along flowlines, propagating downstream to be imaged as a phase-signature profile in the vessel. The phase amplitude increases only linearly with speed, regardless of the sensitized motion, and its parabolic time-of-flight signature elongates. Moment theory predicts a region of many admixed higher-order phase-shift effects. The experiments show a clear simple pattern: the narrow band phase discontinuity predicted by the cumulative formulation.
Conclusion: An MR imaging gradient phase-sensitizes specifically to the motion (d^nR/dt^n), with a value averaged over a specific interval of action, when its waveform is (2^n)-polar. No higher moments play a role in motion phasing. Oblique bend experiments confirm a new cumulative motion theory of MR image formation, but not the older moments formulation.

The author gratefully acknowledges experimental collaborations with Dr C. A. Hamilton.

Monday, March 29, 12:30 PM–1:30 PM
CLINICAL MRI: Head, Spine, Body

Posters P101–P142

P101

Clinical Application of Ferric Pyrophosphate as a Contrast Agent for MR Imaging of Obstructive Jaundice

H Yokota, H Tonami, T Okimura, I Yamamoto
Department of Radiology, Kanazawa Medical University, Kahoku, Ishikawa, Japan

Purpose: Aiming to visualize the lesion causing obstructive jaundice, a ferric pyrophosphate soluble as a contrast medium was injected into the common bile duct in patients who were treated for obstructive jaundice by percutaneous transhepatic cholangial drainage (PTCD). In this report, all MR findings were correlated with surgical confirmation.

Methods: Twenty patients who had PTCD for the treatment of obstructive jaundice were enrolled in this study. The causes of biliary tract obstruction were cancer of the pancreatic head ($n = 9$), cancer of the biliary tract ($n = 7$), metastatic lymphadenopathy ($n = 4$), and choledocholithiasis ($n = 1$). By the SE method of T1- and T2-weighted imaging, MR images of axial and coronal sections were obtained.

Results: With ferric pyrophosphate at 1.0 mmol/L, the most clear and highest intensity T1-weighted images were obtained. After injecting ferric pyrophosphate into the biliary tract through the PTCD tube, its capability of visualizing the intrahepatic bile duct at MR imaging was investigated. The dilated biliary tract was clearly seen in all 21 cases. In the patients with pancreas head cancer, both invasion to the common bile duct and tumor extent at the end of the stenotic site could be visualized simultaneously. In the patients with common bile duct cancer, the tumors were visualized as a low-signal-intensity area at the end of the common bile duct.

Conclusion: This approach was considered to produce a further improvement in the diagnosis of obstructive lesions in the biliary tract and the degree of invasion into the surrounding tissue.

P102

MR Imaging Versus CT for the Diagnosis of Renal Angiomyolipomas

MA Amendola, G Morillo, M Schnall, P Dickson, M Glickstein, R Joseph, S Brown
Department of Radiology, Jackson Memorial Hospital, Miami, FL

Purpose: Renal angiomyolipomas (AML) are benign tumors comprising a variable mixture of abnormal blood vessels, smooth muscle, and mature adipose tissue. CT has been described as the modality of choice for the detection of fat within the AML. MR imaging may be even more sensitive than CT in identifying fat. Only anecdotal cases of AML imaged with MR, however, have been reported in the literature. We compared the findings at CT and MR imaging in 20 patients with fatty renal masses consistent with AML.

Methods: The CT and MR imaging studies performed in 20 patients with fat-containing renal masses, 5 of them pathologically proved renal AML, were reviewed. CT scans were obtained with intravenous contrast enhancement. MR imaging examinations were performed by using T1- and T2-weighted spin-echo pulse sequences. In some patients, additional gradient-echo, echo-offset, and spectroscopy techniques were used.

Results: At CT, density measurements consistent with fat were obtained in some areas within the lesions, ranging from −10 to −85 Hounsfield units. Typical MR imaging findings of a fatty renal mass were present in all cases, irrespective of field strength. In 8 cases, MR imaging clearly displayed the abnormally enlarged vessels commonly present in renal AML. MR imaging findings were confirmed by renal arteriography in the 6 patients in whom this study was obtained. Although CT scans showed enhancement in some of these lesions, this was only an indirect indication of the nature of the abnormality.

Conclusion: The accuracy of MR imaging appears to be similar to that of CT for demonstration of renal angiomyolipomas. In addition, MR imaging can display the increased vascularity commonly present in renal AML better than CT.

P103

MR Imaging of Crohn Disease with Perfluorooctylbromide (PFOB)

CM Anderson, JJ Brown, DM Balfe, JP Heiken, RE Clouse, JA Borrello
Mallinckrodt Institute of Radiology, Washington University School of Medicine, St Louis, MO

Purpose: To evaluate the use of PFOB as an oral contrast agent for MR imaging of Crohn disease.

Methods: MR examinations were performed before and after PFOB ingestion in 12 patients with documented Crohn disease. Glucagon (1 mg IM) was administered prior to the post-PFOB examinations. Each patient also underwent abdominal CT scanning within 48 hours of the MR examinations. All images were analyzed for effectiveness of bowel wall marking with the oral contrast agent, clarity of bowel wall visualization, thickness of the bowel wall, and presence of abdominal abscess, fistula, mesenteric fat inflammation, and lymphadenopathy. The accuracy of the MR examinations was judged on the basis of the CT findings, which served as the standard.

Results: There was improved effectiveness of bowel wall opacification, clarity of bowel wall visualization, and confidence of diagnosing bowel wall thickening on the post-PFOB images compared to the precontrast MR images. The percentage of opacified bowel loops and clarity of bowel wall visualization was similar for CT and post-PFOB MR imaging. Detection of abdominal abscess, fistulas, mesenteric fat inflammation, and lymphadenopathy was not substantially improved at post-PFOB MR examinations.

Conclusion: The use of PFOB as an oral contrast agent for MR imaging improved bowel opacification and clarity of bowel wall visualization. There was no substantial improvement in the detection of bowel wall thickening or the complications of Crohn disease.

J.J. Brown is a consultant to Alliance Pharmaceutical Company.

P104

Comparison of Fast Spin Echo versus Routine Spin Echo in MR Imaging of the Liver

RS Sherry, TW Chan, G Lee
Department of Radiology, University of Chicago, Chicago, IL

Purpose: Fast spin echo (FSE) imaging is becoming increasingly important in clinical MR imaging because of the savings in imaging time. Previous reports have raised the problems of contrast difference between FSE and conventional spin echo (SE) due to a variety of factors. The authors compared both sequences in MR imaging of the liver.

Methods: Seven separate MR liver examinations were performed with a 1.5-T imager. T2-weighted SE (2500/80) with respiratory compensation signals averaged, and FSE (2500/85), ETL 8, 4 signals averaged without respiratory compensation, and otherwise the same imaging parameters were compared retrospectively. In 4 cases, a heavily T2-weighted (2500/160) sequence was also compared.

Results: Lesion conspicuity was considered superior in FSE sequences in 6 of 7 cases and the same in 1 case, even though FSE showed more respiratory motion artifacts than SE in 5 of 7 cases. In 2 cases, FSE helped to detect more lesions; in the remaining cases, there was no difference in the number of lesions detected. In all cases, intrahepatic vessels were less intense with the FSE sequence and eliminated a potential confusion with pathology. Lesion-to-liver contrast-to-noise ratios (C/N) of 17 comparable lesions for the FSE sequence averaged 15.6 versus 11.2 for SE sequences. In 3 of 4 hemangiomas, there was a substantial increase in C/N in the FSE sequence, possibly due to a difference of incidental magnetization transfer effect on the lesion versus the liver.

Conclusion: FSE is at least equal to, if not better than, SE in T2-weighted MR imaging of the liver because of increased lesion conspicuity.

P105

In Vitro Study of Gallstone Fragmentation with Extracorporeal Shock Waves: Correlation with Characteristics at MR Imaging, Ultrafast CT, and US

H Tonami, H Yokota, T Okimura, I Yamamoto, I Kita, S Takashima

Department of Radiology, Kanazawa Medical University, Kahoku, Ishikawa, Japan

Purpose: To determine whether in vitro MR imaging, ultrafast CT, and US could help predict the outcome of gallstone fragmentation after extracorporeal shock waves.

Methods: In vitro 1.5-T MR, ultrafast CT, and US images were obtained of gallstones removed from 70 patients at surgery. The patterns of the gallstones seen with each imaging modality were categorized in 3–5 groups. The calcium score of each stone was calculated from CT scans. After imaging, gallstones underwent in vitro extracorporeal shock wave fragmentation. Following lithotripsy at 2,000 shock waves, the fragments were dried and analyzed for chemical composition.

Results: MR signal patterns on T1-weighted SE images correlated well with the degree of fragmentation of the stones. No substantial correlation was found between the imaging characteristics of ultrafast CT, US, or the calcium score and the results of shock wave fragmentation.

Conclusion: These data show that MR imaging may play an important role in the prediction of gallstone fragmentation after extracorporeal shock wave.

P106

MR Cholangiography with a Fast Spin-Echo Sequence

EK Outwater

Department of Radiology, Thomas Jefferson University Hospital, Philadelphia, PA

Purpose: Previous methods of MR cholangiography utilizing gradient-echo techniques have been limited in the depiction of the normal or nondilated biliary tree. The authors sought to assess the ability of heavily T2-weighted fast spin-echo sequences to visualize the biliary tree in normal volunteers and in patients with biliary disorders.

Methods: Five healthy volunteers and 16 patients were studied. Ten patients underwent contrast cholangiography and 6 patients had CT documentation of the presence or absence of biliary obstruction. MR cholangiography was performed at 1.5 T with fast spin-echo sequences with TR of 4,000 msec and effective TE of 160 msec. Three-mm-thick contiguous interleaved sections with a 256 × 256 acquisition matrix (4 signals averaged) allowed 3D reconstructions with MIP or traced-ray by array processor (TRAP) algorithms for multiple projections.

Results: In normal volunteers ($n = 5$) and patients without biliary obstruction ($n = 4$), the common bile duct, the common hepatic duct, the right and left hepatic ducts, and the distal pancreatic ducts were visualized, whereas intrahepatic ducts were not. In contrast, dilated intrahepatic ducts in those patients with obstruction ($n = 12$) were clearly seen. The level of obstruction was accurately depicted in all cases of obstruction.

Conclusion: MR cholangiography can depict the major normal biliary ducts and assess the level of stricture in patients with obstruction.

P107

MR Imaging Evaluation of Acute Hydrocephalus in Dogs

T Vullo, V Deo-Narine, DG Gomez, A Tankhiwale, RD Zimmerman, RP Manzo, PT Cahill

Cornell Medical Center, New York, NY

Purpose: Immediate changes in ventricular cerebrospinal fluid (CSF) pressure and volume that occur in the early stages of hydrocephalus are of major clinical concern. To investigate these dynamic effects, acute noncommunicating hydrocephalus was first induced in canines with the placement of a balloon catheter in the aqueductal recess, followed with MR imaging.

Methods: The atlantooccipital dura was surgically exposed, and a Lincoff polyethylene ophthalmology balloon catheter (O.D. 2 mm) was inserted into the aqueductal recess. An 18-gauge angiocatheter was then placed into the body of 1 lateral ventricle so that CSF pressure measurements could be obtained via a manometer. The balloon was inflated to a diameter of approximately 4 mm, which was sufficient to totally occlude the aqueductal recess. Serial 1-mm-thick T1-weighted (TR/TE = 500/25) MR images were acquired at 2.0 T.

Results: A midline sagittal MR image obtained after inflation of the balloon demonstrated its appropriate placement in the aqueductal recess. Ventricular pressure measurements increased from an initial 14 cm H_2O to more than 50 cm H_2O. Infusion of Gd-DTPA into the lateral ventricles demonstrated no leakage past the balloon catheter. Changes in ventricular volume, as seen at MR imaging, could be observed over time.

Conclusion: The use of a balloon catheter is a practical technique for the induction of acute hydrocephalus. In addition, MR imaging is particularly useful for studying the dynamic changes in ventricular volume associated with this animal model.

P108

Radiologic Evaluation of Cerebrovascular Malformations

CH Hoffman, RB Dietrich, M Pritz, D Sklar, D Butler, WG Bradley, Jr, HF Pribram

Department of Radiological Sciences, University of California, Irvine, Orange, CA

Purpose: The purpose of this exhibit is to demonstrate the MR imaging, MR angiography, CT, and conventional angiographic characteristics of the various types of cerebrovascular malformations and to discuss the different roles of these modalities in their evaluation.

Methods: The radiologic studies of patients with cerebrovascular malformations from 2 institutions were retrospectively reviewed and findings correlated with clinical histories and surgical reports. Cases included 5 different types of cerebrovascular malformations: arteriovenous, venous, cavernous, and capillary malformations, as well as arteriovenous fistulas.

Results: Both MR images and CT scans helped to detect the presence of arteriovenous, cavernous, and venous malformations, as well as arteriovenous fistulas. The multiplanar capabilities of MR imaging better mapped the anatomy of malformations than did CT. Parenchyma within the vascular nidus and aging of hemorrhage was better detected with MR imaging. Differentiation of hemorrhage, flow, and calcification within arteriovenous malformations, however, was sometimes difficult with MR imaging. MR angiography supplied additional information by better visualizing and delineating the extent of the supplying arteries and draining veins. Areas of turbulent flow, however, were difficult to assess with this modality. Conventional angiography was still required to completely evaluate the hemodynamics of the vascular anatomy, particularly in cases of arteriovenous malformation. Although lesions such as cavernous hemangiomas and thrombosed arteriovenous malformations may be angiographically occult, they are well visualized with MR imaging.

Conclusion: Multiple modalities may be frequently needed to evaluate cerebrovascular malformations and delineate their unique characteristics. In this exhibit, the specific roles of the different modalities are demonstrated.

P109

Usefulness and Limitation of MR Imaging and MR Angiography in Diagnosis of Juvenile Moyamoya Disease

T Aoki, K Houkin, Y Iwasaki, H Abe, M Koiwa,
S Kawaguchi, T Kashiwaba, H Saitou, K Miyasaka
Kashiwaba Neurosurgical Hospital, Sapporo, Japan

Purpose: In the diagnosis of juvenile moyamoya disease, MR images and MR angiograms were studied to evaluate their accuracy in the assessment of moyamoya vessels in the basal ganglia, carotid occlusive lesions, and postoperative collateral arteries.

Methods: Routine T1- and T2-weighted SE MR imaging and phase-contrast or time-of-flight MR angiography were performed in 21 children and in 14 patients with surgical treatment.

Results: Both MR imaging and MR angiography depicted moyamoya vessels in the basal ganglia in all cases, with a positive but not definite correlation to the conventional angiographic findings. MR imaging depicted the stenotic or occlusive lesions of the carotid fork and horizontal portion of the middle cerebral artery effectively. MR angiography depicted the lesions that MR imaging failed to show, and it tended to overestimate the lesions. The postoperative state of collateral flow and the patency of extracranial-intracranial (EC-IC) arterial bypass could be evaluated as well with MR angiography as with conventional angiography, although MR angiography was limited in spatial resolution and evaluation of flow direction.

Conclusion: MR imaging and MR angiography were considered to be reliable noninvasive modalities in the diagnosis of moyamoya disease in stages 3 and 4, but were less effective in the evaluation of the angiographic stage. MR angiography also could be a useful examination in the follow-up study of postoperative patients with EC-IC bypass surgery.

P110

Transient Hyperintensities on T1-weighted MR Images in a Patient with Acute Autoimmune Hepatic Failure

RS Boulos, JJ Baka, N Spripathi, N Ramadan
Division of Neuroradiology, Department of Diagnostic Radiology, Henry Ford Hospital, Detroit, MI

Purpose: (1) To report the occurrence and complete resolution of abnormal hyperintensities in the basal ganglia, mesencephalon, and cerebellum on T1-weighted MR images in a patient with acute liver failure. (2) To compare the findings with reports of MR abnormalities in chronic hepatic failure. (3) To discuss possible etiologies and clinical significance.

Methods: A 19-year-old woman was hospitalized with acute liver failure secondary to autoimmune hepatitis. After initial deterioration, the patient showed rapid improvement. MR imaging was performed on the 2nd and 12th days of hospitalization. Follow-up MR imaging was performed 80 days and 1 year after hospitalization.

Results: Initial MR images showed hyperintensity symmetrically in the globus pallidus, midbrain, and dentate nuclei on T1-weighted images. Follow-up MR images showed complete resolution of all abnormal signal intensities. Descriptions of similar signal abnormalities in patients with chronic liver failure report such findings as mild or absent in acute disease. Our case presents unique features that raise questions about the suggested etiologies of these changes: (1) a patient had acute hepatic failure, (2) MR abnormalities were more extensive, and (3) MR abnormalities showed complete resolution.

Conclusion: Extensive, reversible MR abnormalities were seen in a patient with encephalopathy secondary to acute liver failure, suggesting that the "gliopathy" stipulated as the mechanism for the MR abnormalities in chronic liver failure might be a reversible process.

P111

Clinical and Pathologic Significance of Enhanced Nerve Roots of Cauda Equina in MR Studies

MA Mikhael, MT Gorey, MM Mikhael
Department of Radiology, Evanston Hospital, Evanston, IL

Purpose: To study the significance of the enhanced nerve roots of the cauda equina and their correlation with clinical and pathologic diagnosis.

Methods: Fifty-eight cases of enhanced nerve roots of the cauda equina seen at MR imaging were retrospectively studied, and the radiologic diagnosis was correlated with final clinicopathologic diagnosis. Cases included Guillain-Barre syndrome (GBS) ($n = 2$), subarachnoid hemorrhage ($n = 20$), meningeal carcinomatosis ($n = 23$), primary recurrent conus tumors ($n = 2$), lymphoma ($n = 8$), infection ($n = 10$), postsurgical change ($n = 12$), and postradiation changes ($n = 5$).

Results: MR images of the lumbodorsal spine (TR = 600 msec, TE = 20 msec) were obtained with sagittal and coronal sections before and after contrast enhancement. Enhancement of the nerve roots of the cauda equina is a nonspecific finding. The nature of the underlying lesion can be understood only in the light of clinical information and the nature of enhancement. Nodular enhancement is seen more frequently with mets and recurrent conus tumors. Diffuse enhancement is more common in inflammatory lesions (GBS) and post subarachnoid hemorrhage. Enhancement with matting of nerve roots is seen with postradiation, postsurgical changes, and meningeal carcinomatosis. With infections, enhancement is usually accompanied with thickened enhanced dura. Follow-up imaging is sometimes helpful for a differential diagnosis and the effectiveness of treatment.

Conclusion: Enhancement of the nerve roots of the cauda equina is nonspecific but is a substantial MR finding. The underlying diagnosis can be reached in the light of the clinical information and the nature of enhancement seen on MR studies.

P112

Phase III Multicenter Trial of High-Dose-Gadolinium MR Imaging in the Evaluation of Brain Metastases

WTC Yuh, DJ Fisher, SE Harms, KR Maravilla, AC Proce, VM Runge
Department of Radiology, MR Division, University of Iowa, Iowa City, IA

Purpose: To study the efficacy and safety profile of high-dose gadoteridol in patients with suspected central nervous system metastatic disease (phase III multicenter clinical trials).

Methods: Patients were studied by using an incremental dose technique consisting of an initial bolus injection of 0.1 mmol/kg gadoteridol (standard dose), followed by an additional bolus injection of 0.2 mmol/kg (cumulative high dose, 0.3 mmol/kg). Images were analyzed quantitatively and also by unblinded and blinded reviewers.

Results: Sixty-seven patients received gadoteridol and were included in the safety analysis. Forty-nine patients were included in the efficacy analysis. Three adverse effects in 2 patients were considered to be related to gadoteridol administration. The adverse effects were not serious and were self-resolving. Both unblinded and blinded reviewers noted that the high doses of gadoteridol allowed detection of approximately 50% more lesions than did the standard doses. Both noted 2 patients with lesions identified on high-dose studies who had negative standard-dose examinations. Five patients (blinded) or 8 patients (unblinded) with a single lesion at the standard-dose study had multiple lesions identified at the high-dose study. Quantitative analysis (133 lesions, 45 patients) demonstrated that lesion signal intensity increased significantly on the high-dose studies when compared to the standard-dose studies ($P < .001$).

Conclusion: Gadoteridol administered at a dose of 0.3 mmol/kg does not appear to have adverse effects. The high-dose study allowed improved lesion detectability and provided additional diagnostic information, which led to improved treatment in some patients.

P113

Lung Signal Intensity and Dimensions Measured with MR Imaging in Patients with Chronic Lung Disease before and after Single Lung Transplantation

RH Mohiaddin, G Notohamiprodjio, K Schoser, RS Underwood, DB Longmore
Magnetic Resonance Unit, Royal Brompton Hospital, London, England

Purpose: Retrospective analysis was done of lung signal intensity normalized for fat and lung cross-sectional area normalized for body surface area, in patients with advanced pulmonary diseases before and after a single lung transplantation.

Methods: Twelve patients with pulmonary airway disease (emphysema, $n = 7$; bronchiectasis, $n = 2$; obliterative bronchiolitis, $n = 3$), and 14 patients with interstitial lung disease (pulmonary fibrosis, $n = 3$; fibrosing alveolitis, $n = 4$; lymphangioleiomyomatosis, $n = 7$) were reviewed. Nine healthy volunteers were studied for comparison. Data were obtained from cardiac-gated transverse SE (TE = 40 msec) images.

Results: The native lung in pulmonary airway disease has signal intensity (79% ± 12) similar to that of control (100% ± 6), and interstitial lung disease has a higher signal intensity (172% ± 33; $P < .05$). The transplanted lungs had normal signal intensity (103% ± 12), except 1 patient had a rejection reaction and 2 patients had infection. The cross-sectional area of the native lung was smaller than normal in pulmonary fibrosis (50% ± 8) and fibrosing alveolitis (78% ± 8) and larger in lymphangioleiomyomatosis (136% ± 6) and pulmonary airway disease (165% ± 8). The area of the transplanted lung was comparable to that of control (100% ± 13).

Conclusion: Variations of lung signal intensity and dimensions in various lung diseases were demonstrated retrospectively by using data acquired for other purposes. This indicates that with optimized pulse sequences, MR imaging could be useful in assessing lung pathology.

P114

Evaluation of Discrete Membranous Subaortic Stenosis with MR Imaging

KM Link, SP Loehr, NM Lesko
Department of Radiology, Bowman Gray School of Medicine, Winston-Salem, NC

Purpose: The purpose of this study was to investigate the potential advantages of MR imaging in diagnosing discrete subaortic membranous stenosis.

Methods: Six patients with known or suspected aortic stenosis were evaluated with a 1.5-T GE Signa imager by using standard SE and gradient-echo (GRE) sequences. Of these, 3 patients were also evaluated by using an oblique axial phase-velocity mapping (VINNIE) technique. The anatomic location of the lesions was evaluated with SE studies. Qualitative and quantitative assessment of the severity of the stenosis was made with GRE and phase-velocity-mapping techniques, respectively. The accuracy of MR imaging in detecting the position of the subaortic membrane and in qualitatively grading the severity of stenosis was compared to that of echocardiography and angiography. Qualitative MR assessment of the flow velocity and pressure gradient across the stenosis was compared to the reported angiocatheter pressure gradient valves.

Results: MR imaging was accurate in identifying the presence and extent of the discrete subaortic membrane in all 6 cases. Echocardiography correctly established the diagnosis in 50%. The qualitative assessment of the subaortic stenosis with MR imaging correlated well ($r > .90$) with the echocardiographic assessment. Phase-velocity MR imaging proved 94% accurate when compared to angiocatheter values in quantifying the transstenotic pressure gradients.

Conclusion: We conclude that MR imaging has substantial advantages and versatility in accurately assessing membranous subaortic stenosis.

P115

MR Imaging and PET Correlation of Head and Neck Cancer with 2-[18F] Fluoro-2-Deoxy-D-Glucose (FDG)

Y Anzai, S Rege, L Chaiken, E Abemayor, U Sinha, C Ho, B Jabour, R Hawkins, R Lufkin
Radiology Department, UCLA Medical Center, Los Angeles, CA

Purpose: Although MR imaging can clearly delineate head and neck pathology and has been the imaging modality of choice, MR images that suggest the presence of tumors are still based on morphology. This causes problems in post-surgical and/or radiation therapy cases in which fascial planes have been distorted, or in small primary tumors that do not demonstrate deep fascial plane destruction. The authors summarize their experiences of PET and MR imaging correlation of head and neck cancer.

Methods: PET images were obtained by using a Siemens/CTI 931/08-12 scanner. After 4 hours of fasting, patients were injected with 10 mCi of FDG intravenously. Images were reconstructed by employing a Shepp-Logan 0.3 filter. MR imaging was performed with a 0.3-T permanent unit and 1.5-T superconducting units. T1- and T2-weighted axial images were mainly used for PET correlation. Twenty-one patients were examined with both FDG and MR imaging. Correlation was made with surgical findings and/or clinical outcomes.

Results: FDG imaging demonstrated abnormal uptake of primary tumors in all cases. PET imaging could detect the presence of tumor in 3, which were difficult to determine only with MR imaging. Two of these 3 cases represented recurrent tumors following surgery and radiation. PET imaging with FDG is extremely sensitive in detecting recurrent tumors in patients after surgery or radiation therapy.

Conclusion: PET imaging with FDG is a promising adjunct to MR imaging in situations that distort normal anatomic planes, especially as in postsurgical or radiation therapy.

P116

MR Imaging of the Parotid Gland

AI Shedden, MH Johnson, W Kubal, AJ Kuta
Department of Radiology, Medical College of Virginia, Richmond, VA

Purpose: Radiologic evaluation of the parotid gland includes plain radiographs, sialography, and CT. MR imaging has become an increasingly popular modality for evaluation of parotid space lesions. The authors discuss the utility of MR in the evaluation of parotid lesions and optimization of pulse sequences.

Methods: The variable fat content of the parotid gland may make the identification of lesions difficult and demands the use of multiple sequences and planes. Each sequence has advantages and disadvantages dependent on the pathology of the lesion. The authors reviewed MR examination results of parotid lesions over the past 3 years at their institution. Images were obtained with 3 separate high-field MR units. T2, pre- and postcontrast T1, and fat-suppression techniques were used.

Results: A variety of MR sequences help identify and characterize parotid gland lesions. Examples of normal parotid anatomy and pathologic lesions are presented. Specific sequences that optimize the visualization and characterization of lesions are discussed. Images are included that allow differentiation of parotid hemangioma from lymphangioma and differentiation of lymphoepithelial cysts from neoplasm, as well as other pathologic processes.

Conclusion: Specific pulse sequences are useful in MR evaluations of parotid glands. A tailored examination of the parotid gland will provide the most valuable evaluation of parotid gland lesions.

P117

Intraocular Silicone Oil: in Vitro and in Vivo MR and CT Characteristics

VP Mathews, AD Elster, PB Barker, WL Buff, JA Haller, CM Greven
Department of Radiology, Bowman Gray School of Medicine, Winston-Salem, NC

Purpose: To describe the CT and MR characteristics of intraocular silicone oil (polydimethylsiloxane).

Methods: CT was performed in a silicone oil/water phantom and in a patient with CMV retinitis-related retinal detachments treated by bilateral intraocular silicone oil injections. CT appearance and the CT number of silicone oil were evaluated. Proton MR spectroscopy was performed in a sample of polydimethylsiloxane within a tube of D_2O by using a 200 MHz spectrometer. MR imaging was performed in a silicone oil/water phantom and in 2 patients with retinal detachments treated with silicone oil injection.

Results: Silicone oil is relatively radiodense, having a CT number of approximately 130 HU. At spectroscopy, silicone oil gave a single peak at 0.33 ppm. Silicone oil was hyperintense on T1-weighted images and hypointense on spin-density and T2-weighted images relative to water. Estimated T1 and T2 were 716 msec and 68 msec, respectively. Chemical shift artifacts were noted on MR images and were exaggerated by using a narrow bandwidth on the second echo of the long TR sequence. In clinical cases, silicone oil could be selectively saturated such that only signal from fat and soft tissues remained.

Conclusion: Since intraocular silicone oil is frequently used to treat complicated retinal detachments, radiologists must be familiar with its imaging appearance. The authors have summarized not only the CT and MR imaging features of silicone oil but have also presented specific measurements of this substance, such as MR resonant frequency, T1 and T2 values, and CT number.

P118

Trauma of the Eye and Orbit: Evaluation with MR Imaging

H Tonami, H Yokota, T Okimura, I Yamamoto, K Sasaki, S Tsukada
Department of Radiology, Kanazawa Medical University, Kahoku, Ishikawa, Japan

Purpose: To study the utility of MR imaging in evaluation of trauma of the eye and orbit.

Methods: Forty-five patients with ocular and orbital trauma were examined with MR imaging. The types of trauma were blow-out fractures ($n = 21$), maxillofacial complex fractures ($n = 12$), and ocular injuries ($n = 12$). MR examinations were performed at 0.5 or 1.5 T by using SE pulse sequences, and both T1- and T2-weighted images were available for each examination.

Results: In all patients with blow-out fractures, the location of fracture was precisely detected by the presence of prolapsed orbital fat. MR imaging also offered useful information about the status of extraocular muscles. Orbital fat prolapsed in a saccular shape indicated a poor prognosis with restriction of ocular motility. Evaluation of maxillofacial fractures on MR imaging still remains a limitation. Absence of prolapsed orbital fat made the detection of the fracture site difficult. MR imaging was useful, however, in assessing soft-tissue involvement. In patients with ocular injuries, MR imaging offered useful information about the pathologic intraocular conditions, including intraocular hemorrhages, lens abnormalities, and detached lesions.

Conclusion: Although a strict comparison with high-resolution CT and US should be made, the results suggest that MR imaging is an important adjunct in evaluating patients with ocular and orbital trauma.

P119

MR Imaging of the Cruciate Ligaments: Functional Study

F Aparisi
Valencia, Spain

Purpose: The purpose was to show the differences in the cruciate ligaments when the knee is flexed. The MR imaging examination allows an in vivo study of the cruciate ligaments better than any other radiologic procedure. The normal MR imaging examination shows the knee in full extension. In this position, the anterior cruciate ligament (ACL) is seen as a dark straight line, and the posterior cruciate ligament (PCL) has a semicircular appearance. The difference in the shape suggests a different tensional behavior. The straight ACL seems taut, but the folded PCL is relaxed. When the knee is flexed, differences are seen in the shape of the cruciate ligaments.

Methods: To obtain images with the knee flexed 90°, a special articulated device made of plastic can be used that allows imaging with a surface coil arranged around the joint. Twenty normal knees were studied with this system. This MR image was compared with the same section image of a frozen knee.

Results: At 90° of flexion, the ACL shows the undulating contour of a loose structure, and the PCL shows a straight profile, indicating that it is taut.

Conclusion: The cruciate ligaments can be studied with this system as a functional test, and it is possible to obtain an early diagnosis of knee instability.

P120

MR Imaging of Cartilage-forming Bone Tumors: Radiologic-Pathologic Correlation

H Mizutani, S Ohba, M Mizutani, M Ito, M Koyama, S Otake
School of Medicine, Nagoya City University, Nagoya, Japan

Purpose: The radiologic-pathologic correlation of cartilage-forming bone tumors and the value of intravenously administrated Gd-DTPA-enhanced MR imaging were studied.

Methods: The MR studies were retrospectively reviewed. Twenty-nine cases were examined with a 0.5-T imager and were pathologically proved. MR examinations included T1-weighted (350–500/30) and T2-weighted (1800–2000/100) SE sequences. Enhanced MR images were obtained in 12 cases. The study comprised 7 enchondromas, 8 osteochondromas, 3 chondroblastomas, 1 chondromyxoidfibroma, 8 chondrosarcomas, and 2 dedifferentiated chondrosarcomas.

Results: One chondromyxoidfibroma, 7 enchondromas, and 7 low-grade chondrosarcomas showed low signal intensity (SI) on T1-weighted images and homogeneous hyperintensity on T2-weighted images. Three chondroblastomas demonstrated cystic components. Their tumor matrices showed low SI with both sequences. Cartilage caps of 8 osteochondromas demonstrated the same signal pattern as the enchondromas. One high-grade chondrosarcoma and 2 dedifferentiated chondrosarcomas showed mixed SI on T2-weighted images. On Gd-DTPA-enhanced images, 3 enchondromas, 4 chondrosarcomas, and 1 dedifferentiated chondrosarcoma demonstrated lobulated marginal enhancement. One chondroblastoma and 1 chondromyxoidfibroma were entirely enhanced.

Conclusion: The difference in SI between hyaline cartilage matrix tumor (enchondroma and low-grade chondrosarcoma) and chondroid matrix tumor (chondroblastoma) depends on the volume of free water in hyaline cartilage and chondroid matrix. Lobulated marginal enhancement is a characteristic finding of a hyaline-cartilage-forming tumor (including dedifferentiated chondrosarcoma) and may be pathologically compared with the fibrovascular bundle and the enchondral ossification area. Enhanced MR studies are useful in differentiating cartilage-forming tumors.

P121

Aneurysmal Bone Cysts: MR Features

J Golzarian, C Matos, V Caucheteur, J Struyven
Hôpital Erasme, Brussels, Belgium

Purpose: To report MR imaging features of 5 cases of aneurysmal bone cysts (ABCs).

Methods: All patients had a histologically confirmed diagnosis. There were 3 male and 2 female patients, 11–71 years old. The most frequent symptoms were pain and swelling. In 1 patient, the ABC was an incidental finding. MR images were obtained with either at 1.5-T or 0.5-T imager (Philips Medical Systems). SE T1- and T2-weighted images were obtained in all patients. Intravenous contrast medium was injected in 2 patients.

Results: All the lesions were lobulated. In 4 cases, the tumor was hypointense and heterogeneous on T1-weighted images, with slightly hyperintense areas. These lesions were hyperintense on T2-weighted images. Four of the cysts were surrounded by a thin, well-defined hypointense rim. Fluid levels were observed in 1 case. In 1 case, the plain film examination suggested an enchondroma. MR imaging demonstrated a small, rounded hyperintense lesion within the mass on T2-weighted images, corresponding to a vascular lac. The extent of the tumors was well demonstrated by MR imaging. In 4 patients, a curettage was performed. Two of these patients underwent embolotherapy before surgery. In 1 case (a spinal ABC), embolotherapy was used alone, and there was substantial tumoral regression.

Conclusion: MR imaging is a sensitive but not specific method for the detection of an ABC, and the extent of the lesion is well demonstrated. The presence of an expansile lobulated lesion that is bordered by a low-signal-intensity rim and is hypointense on T1-weighted images and contains slightly hyperintense areas suggests an ABC, especially when it occurs in youth.

P122

Malignant Bone and Soft-Tissue Tumors: Conventional and Dynamic MR Imaging for Detection of Local Recurrence after Surgery

M Uchida, H Nishimura, T Abe, K Kojima, H Ueda, K Fujimoto, I Kawahara, T Kumabe, N Hayabuchi
Department of Radiology, Kurume University School of Medicine, Kurume, Fukuoka, Japan

Purpose: Malignant bone and soft-tissue tumors are known to have a high tendency for local recurrence after surgery. Clinical detection of these recurrent tumors is difficult, however. The authors evaluated the detectability of local recurrence by using conventional and dynamic MR imaging.

Methods: Twenty-one patients with malignant primary bone and soft-tissue tumors with various histologic features were examined. Conventional MR imaging was performed in 36 studies, and dynamic MR imaging was performed in 10 studies. Conventional MR imaging was performed by using SE T1-weighted (TR/TE = 400–460/35) and T2-weighted (1500–2000/80–100) or short TI inversion recovery (STIR) (1500/100/40 [TR/TI/TE]) sequences. Dynamic studies were performed with SE T1-weighted (120–150/20) sequences. After the first SE sequence, a bolus injection of Gd-DTPA (0.1 mmol/kg body weight) was administered into the vein, and 7 more SE sequences were then acquired. The entire dynamic MR imaging required approximately 8 minutes. All images were obtained with a 0.5-T superconductive magnet system (SMT-50).

Results: The sensitivity and specificity for the detection of local recurrences were 82% and 71%, respectively, for conventional MR imaging and 100% and 83%, respectively, for dynamic MR imaging. The accuracy for local recurrence was 78% for conventional MR imaging and 90% for dynamic MR imaging.

Conclusion: MR imaging proved to be a valuable technique in the evaluation of local recurrence of malignant bone and soft-tissue tumors after surgery. In particular, dynamic MR imaging was useful in distinguishing local recurrence from reactive change after surgery.

P123

Early Central Enhancement Sign on Dynamic Gd-DTPA-enhanced MR Images of Soft-Tissue Tumors

H Nishimura, M Uchida, T Abe, K Kojima, F Nishi, O Edamitsu, S Meno, N Hayabuchi, K Hiraoka

Department of Radiology, Kurume University School of Medicine, Kurume, Fukuoka, Japan

Purpose: For improvement of tumor characterization, more than 150 cases of soft-tissue lesions were studied since 1987 by using dynamic MR imaging. In an early phase of dynamic MR imaging, some soft-tissue tumors showed central enhanced areas that were designated "early central enhancement sign." The authors attempted to correlate the 21 tumors that showed this sign with histopathologic findings.

Methods: Histologically, the 21 tumors were 11 schwannomas, 5 neurofibromas, and 5 myxoid liposarcomas. MR imaging examinations were performed with a 0.5-T superconducting magnet. All patients initially underwent conventional MR imaging. Dynamic Gd-DTPA–enhanced MR imaging (SE 150–200/20–29) was subsequently performed.

Results: At radiologic-pathologic correlation, tumors with this sign contained a myxoid matrix in the peripheral zone, with several masses of tumor cells in the central zone, seen as floating islands. The shape (round, amorphous) of this sign was helpful in differentiating benign from malignant myxoid-containing tumors.

Conclusion: This sign may be helpful in identifying myxoid-containing tumors. The results indicate the advantage of using dynamic MR imaging for qualitative lesion characterization.

P124

MR Imaging of Adult and Pediatric Hip Disorders

H Gabriel, SW Fitzgerald, MT Myers, JS Donaldson, AJ Poznanski

Northwestern Memorial Hospital, Chicago, IL

Purpose: MR imaging of the hips has been emphasized primarily for the evaluation of avascular nec[illegible] The authors demonstrate their experience with [illegible] in a wide spectrum of adult and pediatric [illegible]rs of the hip.

Methods: Four hundred MR exam[illegible] of the hip for a broad range of clinical indicat[illegible] reviewed. The diagnostic advantages of surfac[illegible]imaging, STIR imaging, 3D gradient-echo (GRE) [illegible], and the utility of intravenous gadolinium com[illegible] conventional body coil sequences were as[illegible].

Results: Su[illegible]imaging, in conjunction with STIR or 3D G[illegible], was superior to SE body coil studies in a w[illegible]e of adult and pediatric hip disorders. Specific exa[illegible]les in the evaluation of hip trauma, hip prostheses, marrow disorders, and congenital anomalies will be illustrated. The utility of intravenous gadolinium in the evaluation of arthritides, hip neoplasms, and inflammation will be presented. A review of normal hip anatomy will also be included.

Conclusion: This exhibit will illustrate the application of alternative MR sequences and MR imaging strategies in a wide range of adult and pediatric hip disorders. Examples of the role of MR imaging in the evaluation of congenital anomalies, marrow disorders, traumatic lesions, neoplasms, and arthropathies will be presented.

P125

Posterior Cruciate Ligament Injury: MR Diagnosis and Injury Patterns

SW Fitzgerald, AH Sonin, H Friedman, FL Hoff, LF Rogers, RH Hendrix

Northwestern Memorial Hospital, Chicago, IL

Purpose: The posterior cruciate ligament (PCL) is less frequently injured than the anterior cruciate ligament (ACL). Clinical and arthroscopic identification of PCL injury can be difficult. The MR findings in PCL injury are not as well established compared to ACL injury. The authors review the mechanisms of PCL injury and present their experience with MR imaging in the evaluation of PCL injury and associated knee injury.

Methods: MR examinations of 1,450 knees were reviewed, and 62 patients with clinically confirmed PCL injury were identified. The findings of PCL injury were evaluated on sagittal, coronal, and axial SE images. Associated MR findings of joint effusion, bone marrow contusion, and meniscal and ligamentous injury were identified. Patient histories were correlated to determine the mechanism of knee injury.

Results: Posterior cruciate ligament injuries can be accurately identified by MR imaging. The spectrum of intrasubstance injury, complete PCL tear, and avulsion of the tibial PCL insertion will be illustrated. Associated meniscal and ligamentous injury will also be presented. The presence of bone marrow injury in PCL injury and correlation with the mechanism of injury will be discussed. Potential pitfalls in the diagnosis of PCL injury will be reviewed.

Conclusion: MR imaging is a valuable diagnostic tool in the evaluation of PCL injury, which may not be suspected clinically. Although less common than ACL injury, an understanding of PCL injury mechanisms and the associated MR findings is important in the treatment of patients with knee trauma.

P126

MR Imaging Findings in Psoriatic Arthritis of the Hand

A Giovagnoni, W Grassi, F Terilli, N Danese

NMR Center, University of Ancona, Ancona, Italy

Purpose: The aim of this work is to evaluate the diagnostic possibilities of MR imaging in defining psoriatic arthritis (PA) lesions of the hand.

Methods: Twenty-one selected patients (9 men, 12 women) with PA lesions of the hands proved by clinical-laboratory and radiographic examinations underwent MR imaging of the hands and wrists. The hands of 25 patients with rheumatoid arthritis and 25 healthy subjects were also studied as a control group. MR imaging examinations were performed with a superconductive 1.0-T imager (Magnetom, Siemens) with a round surface coil. SE T1-weighted and GE (FLASH) T2*-weighted images of the hands and wrists were obtained in coronal, sagittal, and, if necessary, axial planes. MR images of the hands were evaluated by blinded examiners, and soft tissues, joints, and skeletal abnormalities were recorded and compared with radiographic data.

Results: Three groups of MR imaging findings were identified: (1) normal findings ($n = 26$); (2) periarticular effusion, no capsule distention, no severe skeletal changes ($n = 18$); (3) periarticular effusion with capsule distention, synovial pannus hypertrophy, and multiple skeletal lesions ($n = 23$). The distribution of patients relating to the groups identified was (1) 22 healthy subjects, 3 patients with PA, 1 patient with rheumatoid arthritis; (2) 16 patients with PA, 2 healthy subjects; (3) 1 healthy subject, 2 patients with PA, 20 patients with rheumatoid arthritis. MR imaging helped to identify a particular and massive distribution of effusion in soft tissue, with no involvement of interphalangeal and metacarpal phalangeal joints, in 16 patients with PA. In particular, the effusions appeared to involve the subcutaneous fat. The joints appeared involved by the effusion in the late phase of disease. Moreover, in 6 cases of PA, patients' focal ischemic areas of the metacarpal head were recorded.

Conclusion: MR imaging demonstrated specific soft-tissue changes in patients with PA and appears to be a useful imaging modality for pathogenesis evaluation of joint damage in psoriatic disease.

P127

Rheumatoid Arthritis: Comparison of MR Imaging and Joint Counts—Preliminary Results of a Longitudinal Study

MB Rominger, WK Bernreuter, PJ Kenney, SL Morgan, GS Alarcon

Department of Radiology, University of Alabama, Birmingham, AL

Purpose: MR imaging has been proposed as an objective method of assessing therapeutic response in rheumatoid arthritis (RA). MR helps to distinguish synovial proliferation (Sy) and fluid within tendon sheaths (Ts), while still imaging cortical erosions (Er). Joint Counts (JCs) for pain/tenderness (Pt) and swelling (Sw) are standard measurements of disease activity in RA. The authors thus hypothesized that MR images should correlate with JCs.

Methods: Eighteen examinations in 11 patients with RA were performed. Coronal T1-weighted SE/proton density images, T2-weighted SE images with fat-suppression (FS), and coronal SPGR images with FS and intravenous injection of Gd-DTPA were obtained. Each sequence was scored for Sy, Ts, and Er; the mean of these 3 scores was designated MR-total (MRT). JCPt, JCSw and JC-total (JCT) were obtained in 60 diarthodial joints. In 7 of 11 patients, repeated assessments were obtained 3 months after initiation of a drug therapy.

Results: FS SPGR with Gd-DTPA was the best sequence. Correlations between JCs for hands (Pt, Sw, JCT) and MR Sy and MRT were found to be nonsignificant (r = .009–.273). The differences between final and initial JC scores (Pt, Sw, JCT), and MR Sy and MRT were likewise found to be nonsignificant (r = .098–.651).

Conclusion: The lack of correlation between JCs and MR findings is puzzling. MR seems to more precisely help determine the presence and amount of Sy, Ts, and cortical Er than JCs. A larger sample size and a longer observation may be necessary before definitive conclusions can be established about the relationship between these 2 assessment methods.

P128

MR Imaging of Bone Contusions of the Knee: Comparison of Routine Spin-Echo versus Fat-suppressed T2-weighted Sequences

YH Hahn, TW Chan, T Kim, G Lee, RS Sherry

Department of Radiology, University of Chicago, Chicago, IL

Purpose: Bone contusions are commonly seen in MR imaging of the knee. Previous studies have suggested that fat-suppression techniques can better evaluate marrow signal abnormality. In this study, the authors examined this hypothesis by using receiver operating characteristic (ROC) analysis.

Methods: MR examinations to assess internal derangement of 25 knees were performed on a 1.5-T magnet by using T1-weighted coronal, T2-weighted sagittal, and T2-weighted coronal SE with chemical-shift-selective fat suppression. The knee was separated into 4 zones (medial and lateral halves of the tibia and femur), thus giving 100 data values. Bone contusion was defined by signal intensity consistent with edema seen with all 3 pulse sequences when reviewed together by 2 radiologists. The discrimination capacity of each pulse sequence was determined with ROC analysis by 3 other reviewers. Each reviewed an individual sequence independently, using a continuous confidence-rating scale of 0%–100% for the presence of contusion.

Results: The fat-suppressed T2-weighted sequence was superior in detection of bone contusion, compared with the non-fat-suppressed T2-weighted sequence when Az was compared (2-tailed P level = .0005). Similarly, it was superior to the T1-weighted sequence (P level = .0021). Comparison of the non-fat-suppressed T2-weighted and T1-weighted sequences showed no substantial difference.

Conclusion: Bone contusions may not be seen on conventional SE T1-weighted and T2-weighted images of the knee. On the basis of ROC analysis, the T2-weighted sequence with fat suppression was superior in detecting bone contusions and, in our opinion, should be included at all routine MR examinations of the knee.

P129

Gadolinium-enhanced MR Imaging Evaluation of a Percutaneous Needle-free Jet Injection System

DA Clunie

Radiology Department, Royal Adelaide Hospital, Adelaide, Australia

Purpose: To use MR imaging with gadopentetate dimeglumine to evaluate depth of penetration and dispersion pattern of injectate delivered with a pneumatically powered needle-free percutaneous jet injection system. Jet injection devices have many advantages, including less pain and reduced risk of needle injuries, compared to the conventional needle and syringe. Disposable jet injection syringes minimize the risk of cross-infection.

Methods: Healthy adult volunteers were injected intramuscularly or subcutaneously in 2 sites in the arm with diluted gadopentetate dimeglumine by using a jet injector (Bioject) with various orifice sizes. Depth of penetration was observed and quantitated. An appropriate dilution of contrast (1:64) was determined by preliminary in vitro experiments.

Results: No substantial morbidity was observed. Intramuscular delivery in the deltoid was achieved with a .008-inch orifice diameter syringe. A .006-inch diameter orifice delivered an intramuscular injection 17% of the time (χ^2 = 8.57; P = .003). Subcutaneous delivery into the lateral triceps region was achieved with both .004-inch and .006-inch orifices, though significantly deeper penetration (t = 4.2; P = .001) and occasional intramuscular injection (13% of the time) was observed with the .006-inch orifice.

Conclusion: MR imaging with a diluted gadolinium chelate is a safe and effective means of assessing the depth and pattern of dispersion of parenteral injectates. Consistent subcutaneous or intramuscular injection can be achieved by using a jet injection system when the appropriate orifice size and injection site are selected.

The author is a consultant to Bioject.

P130

MR Imaging during Postoperative Follow-up after Carpal Tunnel Release

W Buchberger, W Judmaier, G Birbamer, C Schmidauer, K Hasenöhrl
Department of Radiology, University of Innsbruck, Innsbruck, Austria

Purpose: Although surgical release of the transverse carpal ligament results in a high ratio of success, recurrent or unrelieved carpal tunnel syndrome (CTS) is not infrequently observed. To provide a rational basis for reexploration, determination of the cause of persistent symptoms is necessary. The purpose of the study was to evaluate MR imaging in the postoperative follow-up after carpal tunnel release, and to assess its ability to identify possible causes of treatment failure or recurrence.

Methods: Ten wrists of 9 patients (3 men, 6 women) with unrelieved carpal tunnel syndrom were reexamined 13–24 months after surgery. In addition, 10 patients with complete relief of symptoms and normal postoperative EMG were also examined. All 19 patients had undergone MR imaging preoperatively. All imaging was done with a 1.5-T superconducting system (Magnetom, Siemens) and a surface coil. The imaging protocol included axial T1-weighted (450–550/15 [TR/TE]), proton-density–, and T2-weighted (2400/90, 15) SE images.

Results: Complete incision of the transverse carpal ligament and normal shape of the median nerve was demonstrable in all asymptomatic wrists. Findings in 10 wrists with persistent symptoms included incomplete sectioning of the transverse carpal ligament ($n = 3$), extensive postsurgical scarring ($n = 2$), and synovitis ($n = 3$). Increased flattening of the median nerve, suggesting persistent compression, was shown in 5 cases. Increased signal intensity of the median nerve on T2-weighted images, suggesting chronic neuritis, was present in 3 cases.

Conclusion: Preliminary findings suggest that MR imaging can be used successfully for postoperative follow-up after carpal tunnel release.

P131

Impingement Syndrome of the Shoulder: Geometric Evaluation of the Subacromial Space with MR Imaging

W Judmaier, M Lener, G Sperner, AH Dessl, GG Birbamer
Department of Magnetic Resonance Imaging, University of Innsbruck, Innsbruck, Austria

Purpose: Twenty-five patients with clinically suspected impingement syndrome were evaluated with MR imaging to detect specific form variants of the scapula that might contribute to the occurrence of the disease.

Methods: Matching the plane of the scapula, paracoronal and parasagittal sections were obtained by using T2*-weighted gradient-echo sequences on a 1.5-T superconductive magnet (Magnetom, Siemens). A total of 17 different parameters were obtained, including an area measurement between the supraglenoid tuberculum, the coracoid process, the acromioclavicular (AC) joint, and the dorsal edge of the acromion (acromial angle). All measurements were compared to those of 25 age- and sex-matched asymptomatic volunteers. For statistical evaluation, the Student t test was used.

Results: There was no statistically significant difference between the patients and the control group in the height of the subacromial space measured between the highest point of the glenoid labrum and the AC joint. Introducing a second dimension to the measurement by evaluating the subacromial area, a difference of over 30% was found between the 2 groups, with a statistical correlation coefficient of $P < 0.0001$.

Conclusion: Mainly because of the multiplanar capability of MR imaging, it became possible to evaluate geometric parameters of the scapula that accord with the onset of subacromial impingement. We found evidence that certain variations in the shape of the scapula are an indication of this syndrome. Because of an overlap in the measurements in healthy volunteers and patients, these parameters cannot solely be used to diagnose primary impingement syndrome with MR imaging.

P132

Traumatic Injuries of the Extensor Mechanism of the Knee: MR Diagnosis

AH Sonin, SW Fitzgerald, FL Hoff, M Kirsch, H Friedman
MR Imaging Facility, Northwestern Memorial Hospital, Chicago, IL

Purpose: The extensor mechanism is an important component of normal knee function and gait. Extensor mechanism injury can mimic more common intraarticular injury and may not be suspected prior to MR evaluation. Appropriate conservative or surgical management of extensor mechanism injury requires accurate and timely diagnosis. In this exhibit, the authors present [illegible] experience with the MR diagnosis of the complete spectrum of injury to the extensor mechanism.

Methods: MR examinations in 95 patients with surgically or clinically correlated injuries of the extensor mechanism were reviewed. MR examinations consisted principally of sagittal and axial SE sequences. MR studies were performed with a surface coil and, occasionally, the body coil to adequately demonstrate the extensor mechanism. A review of the normal anatomy and the normal MR appearance of the extensor mechanism will be provided.

Results: MR imaging can detect a wide range of muscular, tendinous, and osseous injury of the extensor mechanism. Common injuries of the extensor mechanism, including patellar tendinitis, spontaneous patellar dislocation and retinacular injury, patellar fracture, quadriceps and patellar tendon tears, and quadriceps muscular injury will be illustrated. The role of MR imaging in grading tendon injury will be discussed. Important injuries of the extensor mechanism that are frequently clinically or radiographically occult will be demonstrated. Potential imaging pitfalls will be presented.

Conclusion: MR imaging can provide important diagnostic information in the evaluation and therapy of a wide range of traumatic injuries of the extensor mechanism.

WITHDRAWN

P133

MR Imaging of the Foot and Ankle

BC Horvath
Imaging Science Center, University of Southern California Hospital, Los Angeles, CA

Purpose: MR imaging of the foot and ankle is not a common examination in community imaging centers. The purpose of this study is to increase examination quality by increasing technologist familiarity with foot and ankle protocols, and to be a guide in the establishment of protocols.

Methods: Seventy-five examinations of the foot and ankle were performed to evaluate tendon and ligament injury and to determine the existence of neuromas and avascular necrosis. The technologists familiarized themselves by reading books on anatomy, by experimentation, and by questioning radiologists, referring physicians, and equipment manufacturer representatives.

Results: High-quality examinations of the foot and ankle were accomplished through the use of fat suppression, contrast enhancement, and 3D protocols.

Conclusion: To accomplish a high-quality examination of the foot and ankle, the technologist should be familiar with the protocols used. The purpose of the examination, as indicated by the referring physician, should be understood; the performance of the examination should then fit the purpose.

P134

MR Imaging of Endometriosis

WN Snearly, BJ Wagner, TE Farley, FL Videla, PJ Woodward
United States Air Force Medical Center, San Antonio, TX

Purpose: Endometriosis is a disease affecting a large portion of the menstruating population; histologic detection occurs in approximately 10% of pelvic laparotomy specimens. With the increasing use of MR imaging in various disorders of the pelvis, the preoperative radiologic detection of this condition has increased. The authors were interested in correlating MR imaging with other imaging modalities and pathologic results in this condition.

Methods: A retrospective review was done of MR imaging and US findings in cases in which endometriosis was detected at laparotomy. Also reviewed were those cases in which endometriosis was suspected based on imaging findings, but where there was no histologic evidence of the disease.

Results: Over a 24-month period, 122 surgical specimens were submitted that contained histologic evidence of endometriosis. Among these, 14 patients had undergone preoperative evaluation with pelvic MR imaging. Preoperative US was performed in 37 patients and computed tomography was performed in 12.

Conclusion: The MR imaging features of endometriosis are reviewed. Correlative US and CT images, as well as gross and microscopic pathologic specimens, are shown. Imaging pitfalls, with illustrative false-positive cases, are discussed.

P135

Application of MR Imaging in Radiation Therapy for Gynecologic Malignancies

NA Mayr, ET Tali, WTC Yuh, BP Brown, H Nguyen, DH Hussey
Department of Radiology, University of Iowa Hospitals and Clinics, Iowa City, IA

Purpose: To evaluate the usefulness of MR imaging for planning of radiation therapy for gynecologic malignancies and to assess tumor response.

Methods: Forty-one MR examinations were performed in 11 women: 8 with squamous cell carcinomas (cervix, 7; urethra, 1; vulva, 1) and 2 with adenocarcinomas (cervix). The MR images were reviewed, with attention to tumor extension, pelvic anatomy, bone landmarks, and the MR-detectable skin markings for assessment of the adequacy of the radiation port placement. Tumor response was assessed by sequential computerized digital measurements of tumor volume.

Results: All tumors were easily related to pelvic structures (bone, bladder, rectum) used for radiation therapy planning and to the external skin markings. In 7 patients, the MR studies showed more extensive tumor involvement than suggested by clinical and CT findings. These findings resulted in a modification of the radiation fields in 6 of the 11 patients. Tumor regression rate was dependent on growth pattern rather than tumor volume. One group of patients (4) with exophytic tumors showed rapid regression to 40% or less of the initial tumor volume at dose levels of 20–25 Gy; the other group (7) with endophytic infiltrative tumors showed a more protracted response rate. Three of the 7 slowly responding patients had tumor recurrence to date.

Conclusion: MR imaging may provide additional information to improve the placement of the radiation ports and quantitative assessment of tumor volume and response. Further follow-up is needed to evaluate any prognostic significance of the findings.

P136

Normal Imaging and Functional Anatomy of the Posterior Paraspinal Muscles

JJ Baka, VV Chundi, EM Spickler
Department of Diagnostic Radiology, Henry Ford Hospital, Detroit, MI

Purpose: To review the imaging and functional anatomy of the posterior paraspinal musculature, or deep back muscles.

Methods: MR and CT images are used to demonstrate in detail the anatomy of the posterior paraspinal muscles of the cervical, thoracic, and lumbar spine. Tables and diagrams outline their functional anatomy, including muscle origins and insertions and muscle actions.

Results: The superficial layer, or the transversocostal group, consists of the splenius capitis, splenius cervicis, and erector spinae, which include the iliocostalis, longissimus, and spinalis muscle groups. The deep layer, or the transversospinal group, consists of the semispinalis, multifidus, rotatores, interspinalis, and intertransverse muscle groups. The suboccipital muscles constitute a separate group of muscles at the craniovertebral junction that help control head movements, consisting of the rectus capitis posterior and obliquus capitis muscles. Innervation is by the posterior primary divisions of the spinal nerves.

Conclusion: The posterior paraspinal muscles provide stability to the spine and help control its movements. Knowledge of their anatomy is of value in assessing disorders involving the spine and its supporting soft tissues.

P137

Enhanced MR Imaging Evaluation of Solidity of Anterior Cervical Spine Fusions and Correlation with MR Imaging of Fusion of Spine in 8 Dogs

KL Gupta, KE Legendre, EH Tan
Department of Radiology, Tulane University Medical Center, New Orleans, LA

Purpose: To evaluate the solidity of the anterior cervical spine fusion.

Methods: MR imaging was utilized to help evaluate patients who had undergone prior anterior cervical spine fusion but who reported recurrent symptomatology. Two neuroradiologists independently evaluated the postoperative MR imaging examination results of 68 such patients, comparing the signal characteristics of fused disk levels with those of the adjacent vertebral bodies and uninvolved cervical disks above and below. Sequences used included precontrast T1, postcontrast T1, proton density, T2, and MPGR. The patients' charts and plain radiographs were also reviewed to assess by conventional methods the presence or absence of a solid fusion.

Results: Correlation between these 2 methods demonstrated that the solidity of a fusion may be accurately assessed with MR imaging, as fusions appearing indeterminate or with no union were found to yield inconsistent signals with various sequences, while those thought to be solid were hypointense with all sequences obtained. Therefore, in addition to revealing information regarding disk herniations or osteophyte formation, MR imaging of the fused cervical spine may become useful in assessing the solidity of prior fusion sites as well.

Conclusion: Although the results are preliminary for cervical fusion, these signal characteristics will be compared with experimental studies in dogs, and the results will be presented.

P138

Use of Fluid-attenuated Inversion Recovery (FLAIR) Pulse Sequences for Imaging of the Spinal Cord in Multiple Sclerosis

IR Young, JV Hajnal, DJ Thomas, JM Pennock, GM Bydder
MRI Unit, Hammersmith Hospital, London, England

Purpose: Although heavily T2-weighted SE pulse sequences (eg, SE = 2500/80 at 1.0 T) are the mainstay of MR imaging diagnoses in the brain, their use in the spinal cord is problematic. The high signal from cerebrospinal fluid (CSF) creates artifacts due to partial volume effects and CSF motion that obscure lesions. By applying an inversion pulse and then allowing sufficient time (2,000–2,500 msec at 1.0 T) for the CSF magnetization to recover to its null point before proceeding with the SE sequence, difficulties with CSF artifacts can be reduced. Because the T1 of the spinal cord is short, it largely recovers its magnetization during the time the CSF takes to reach its null point, and subsequent use of a long TE (60–120 msec) provides heavy T2 weighting.

Methods: To assess the potential of this approach, the authors examined the cervical spinal cord of 15 patients with probable or definite multiple sclerosis (MS). The results were compared with the use of fluid-attenuated inversion recovery (FLAIR) sequences (as described above) to those obtained with a T1-weighted (SE = 700/20) sequence (with and without intravenous Gd-DTPA) and a T2-weighted gradient moment nulled (SE = 2500/80) sequence. All studies were performed with 3-mm sections in the sagittal plane on a Picker HPQ Vista system.

Results: Two contrast-enhancing lesions were seen on the T1-weighted images. One of these was seen on the SE = 2,500/80 images, which also showed 5 additional lesions in a total of 4 patients. Over 60 lesions were identified with the FLAIR sequence in 13 of the 15 patients.

Conclusion: The FLAIR sequences provide a substantial improvement over conventional sequences for detecting plaques in the cervical spinal cord in patients with MS.

I.R. Young is an employee of Picker International.

P139

MR Imaging of Suspected Spinal Metastasis: An Efficacy Study

HJ Siegel, PM Colletti, HY Young
School of Medicine, University of Southern California, Los Angeles, CA

Purpose: MR imaging is frequently used for the assessment of metastatic disease of the spine. The efficacy of the procedure, however, in terms of indicating redirection of patient treatment, is not well documented. The authors evaluated the efficacy of MR imaging for investigating the effects of this tool on treatment planning in patients suspected of metastatic disease of the spine.

Methods: One hundred forty-two patients with primary tumors and suspected metastatic spinal involvement were evaluated. Symptoms of back pain, weakness, incontinence, and parasthesia were present; following MR imaging, changes resulted in radiation therapy, chemotherapy, and surgery and were documented. The therapeutic effect of MR imaging was examined by type of primary cancer and by symptoms, and the overall effect was evaluated.

Results: Of the 142 patients, 64 had changes in therapy directed by MR findings. Forty-three of the 64 (67%) were changes in radiation therapy, 17 (24%) were changes in chemotherapy, and 7 (11%) resulted in surgical intervention. Among the 6 most common primary cancers, therapy was changed in the following percentages—17 of 28 (61%) patients with breast cancer, 7 of 14 (50%) with prostate cancer, 9 of 17 (53%) with lung cancer, 7 of 12 (58%) with lymphoma, 5 of 10 (50%) with melanoma, and 6 of 13 (46%) with bladder cancer. Fifty-eight of 120 (48%) patients with 1 or more of the symptoms, and 27 of 54 (50%) patients with 2 or more of the symptoms had changes in therapy. Only 6 of 22 (27%) patients who did not have any of the selected symptoms had changes in therapy.

Conclusion: MR imaging of the spine appears to be an efficacious study in this population, regardless of the primary pathology, and particularly in patients with 1 or more of the above symptoms. The focal findings at MR imaging most often influence the course of radiation therapy treatment.

P140

MR Imaging of Spinal Cord Radiation Damage in a Simian Model

JD Hazle, NE Leeds, RE Price, KK Ang
Department of Diagnostic Radiology, University of Texas M.D. Anderson Cancer Center, Houston, TX

Purpose: The goal of this work is to determine if MR imaging can quantitate residual radiation injury to the spinal cord and predict radiation retreatment tolerance by following the animals longitudinally during radiation retreatment studies in rhesus monkeys.

Methods: Twelve retired breeder rhesus monkeys (*Macaca mulatta*) were included. Simulation films were used to determine the anatomic location of the radiation fields for comparison with the MR imaging findings. Six animals each were included from groups initially receiving fractionated doses of 22 Gy and 44 Gy, respectively. MR studies were performed with a 1.5-T Signa whole-body imager. A 7.6-cm (3-inch) diameter surface coil was used. Animals were immobilized in a vacuum pad and were anesthetized with ketamine hydrochloride. MR images were obtained before and 6 weeks (acute) and 6 months after irradiation.

Results: All 12 animals were imaged prior to irradiation to characterize the MR imaging appearance of the normal spinal cord. Excellent gray/white matter contrast was seen from cervical level 1 through thoracic level 4 on proton density (PD)-weighted images. Good gray/white matter contrast was seen on T1-weighted images, and poor-to-no contrast on T2-weighted images. Gray/white contrast was preserved on contrast-enhanced (Gd-DPTA) T1 images in control subjects. Six weeks after therapy, only subtle changes in gray/white matter contrast were seen in any animal at either 22- or 44-Gy doses. Some loss of gray/white matter contrast was noted in the lower cervical and upper thoracic levels on T1 images, both pre- and postcontrast. Minimal swelling of the cord was noted in most animals. Bone marrow content in the vertebral bodies showed generally homogeneous fatty changes with both doses. Nominal changes were noted 6 months after irradiation on T1 and T2 images. Gray/white matter contrast increased in all levels of the cord, most obviously on T2-weighted images and at higher doses in about half of the animals. Bone marrow changes became more pronounced in a minority of individual vertebral bodies. Cord changes in symptomatic animals (total doses of 84 Gy to 110 Gy) included hyperintense lesions on T1 images. Bone marrow showed homogenous and heterogeneous changes in lipid content. Fibrotic muscular changes were also noted.

Conclusion: MR imaging can successfully demonstrate early, presymptomatic changes in the spinal cord of monkeys irradiated with doses of 22 to 44 Gy. Late changes associated with clinical radiation myelopathy were also observed with MR imaging and correlated with somatosensory-evoked potential deficiencies and histopathology.

Because of the phylogenic proximity of these animals to man, the results of these studies may be used to initiate clinical trials in this area.

P124

Two Types of Flexion Myelopathy: Correlation of MR and Clinical Findings

H Fukatsu, Y Takeuchi, T Ando, N Kamata, T Ishigaki
Department of Radiology, Nagoya University, Nagoya, Japan

Purpose: The purpose of this study is to analyze the similarity and difference in 2 types of flexion myelopathy: so-called Hirayama disease and unilateral proximal arm myoatrophy, which is not yet generally recognized as such.

Methods: A 1.5-T superconducting MR unit was used for the study. Sagittal T1-weighted images were obtained in neutral and flexed neck positions. Four patients with so-called Hirayama disease and 2 patients with proximal arm myoatrophy underwent clinical and imaging examinations.

Results: All 4 patients with so-called Hirayama disease showed unilateral distal arm myoatrophy with muscle weakness, without any sensory disturbance. The other 2 patients showed unilateral proximal arm myoatrophy with muscle weakness and mild sensory disturbance. MR imaging performed in the neutral position in both groups depicted no abnormalities, but it showed anterior shift of the dura in the flexion position, causing spinal cord compression between itself and the vertebra in all 6 patients. Also, dilated extradual venous space appeared only in the flexion position in all patients, perhaps secondary to the dural shift. Spinal cord compression was most prominent at the C5/6 level in the former group, and at C4/5 level in the latter group, which is consistent with the neurologic difference in the 2 conditions.

Conclusion: The authors conclude that so-called Hirayama disease and proximal arm myoatrophy can be included within the same category of flexion myelopathy, with a different affected level.

P132

MR Imaging of Spinal Infection: Prospective Comparison of Selected Sequences

WS Kubal, RA Blinder
Department of Radiology, Medical College of Virginia, Richmond, VA

Purpose: High sensitivity and a noninvasive nature have made MR imaging the study of choice in the diagnosis of spinal infection. A prospective study is presented, designed to compare the conspicuity and extent of disease as seen with 4 MR imaging sequences.

Methods: Seven adult patients were imaged with a high-field (1.5-T) system. T1-weighted, T2-weighted, contrast-enhanced T1-weighted, and contrast-enhanced T1-weighted images with spectral fat saturation were obtained. The epidural spaces, vertebral bodies, intervertebral disk spaces, and paraspinous spaces were analyzed for conspicuity and extent of disease.

Results: Spinal infection could be depicted on standard T1- and T2-weighted images. Sensitivity was increased by the addition of gadolinium contrast; conspicuity was increased by fat saturation. In the epidural space, enhancing phlegmon was best distinguished from normal fat with fat-saturation images (7 of 7). In the intervertebral space, both contrast-enhanced sequences were equivalent. To evaluate vertebral body involvement, the noncontrast T1-weighted images (3 of 7), and the postcontrast fat-saturation images (4 of 7) showed the best delineation from normal marrow fat. In the paraspinous space, each sequence was successful in demonstrating mass, but the fat-saturation images (5 of 7) were best at separating mass from normal fat.

Conclusion: Fat-saturation, postcontrast sequences offer high conspicuity of the epidural, intervertebral, vertebral, and paraspinal components of infection. Quick evaluation of these often uncomfortable patients should include precontrast and postcontrast fat saturation T1-weighted imaging. The authors are currently testing the efficacy of these sequences in the follow-up of spinal infection.

Tuesday, March 30, 12:15 PM–1:30 PM
PHYSICS II: Rapid Imaging, Pulse Sequences, Image Processing

Posters P201–P240

P201

Algorithms for Improving Calculated Streamlines in 3D Phase-Contrast MR Angiography

MH Buonocore
Division of Diagnostic Radiology, University of California Davis Medical Center, Sacramento, CA

Purpose: Development of algorithms that modify 3D phase-contrast velocity data by imposing boundary constraints and fluid dynamics conservation laws to improve the realism of calculated streamlines.

Methods: Algorithms based on least-squares estimation and cost function reduction were applied in sequence to (1) iteratively adjust the velocity field to reduce temporal and spatial fluid density variations, (2) determine a linear correction of the phase background to equalize the calculated flow through multiple cross-sectional surfaces, and (3) iteratively reduce the normal component of the velocity to 0 at the vessel wall. Streamline realism was quantitated by the percentage of lines that exited the vessel or tube lumen through its wall. The algorithms were developed and tested by using 3D phase-contrast MR angiograms of flow in a curved tube and subsequently applied to gated velocity-encoded images of the ascending aorta. Spatial resolution was a 14-cm field of view, 256 matrix, 1.2-mm thickness, 32 cm/sec velocity encoding. Mean flow velocity was approximately 8 cm/sec.

Results: The background correction algorithm was essential to have streamlines remain within the curved tube boundaries through the entire length. Algorithms for divergence and wall boundary constraint reduced the number of errant streamlines by a factor of 2–3.

Conclusion: When the velocities are slow (1 cm/sec) or the geometry simple (nearly straight tubes), calculated streamlines may be realistic without postprocessing. For higher flows or curved tubes, postprocessing is important.

P202

Use of Constrained Image Reconstruction in Fast T1 Mapping

S Chandra, A Webb, PC Lauterbur
Biomedical Magnetic Resonance Laboratory, University of Illinois, Urbana, IL

Purpose: To demonstrate that a large reduction in acquisition time is possible in T1 imaging by using a phase-encoded look-locker (LL) imaging sequence with a generalized series (GS) reconstruction algorithm to combine T1 information with a high-resolution reference image.

Methods: Phantoms consisted of water and agar gels with different T1 values. Twelve T1-weighted images were acquired at 4.7 T in 7 hours with a saturation recovery sequence (SE 1,600/25; 128 phase-encoding steps). The T1 calculations used a Newton-Raphson algorithm. Another high-resolution (128 × 128) data set was then acquired with the LL sequence in only 25.6 minutes. With the last image of the high-resolution LL data set as the basis image, each of the other images was reconstructed by using GS and only the central 32 phase-encoding steps taken from its corresponding k space. The total time required, if only 32 encodings had been used, would have been 6.4 minutes.

Results: Subtraction of the GS from the LL images yielded intensities near noise level. This confirmed that GS does not introduce significant image artifacts, even while reducing acquisition time by a factor of 4. The T1s obtained from the GS-LL data set were within 8% of those obtained with the long saturation recovery experiment. It is thus possible to save a factor of at least 60 in time over an IR-SE sequence by using the LL-GS method, without loss of T1 accuracy.

Conclusion: GS reconstruction can be used in combination with optimized single-shot pulse sequences to significantly reduce data acquisition times in T1 imaging.

P203

Motion Correction in Fast Spin-Echo Imaging

J Wilbrink, IH Zang, J Fielden, H Koizumi, A Takane
Hitachi Instruments, Inc, San Jose, CA

Purpose: The purpose of this study was to reduce motion artifacts on fast SE (FSE) images, by using only the data and no external markers. The authors accomplished this by using a method developed for multisection SE imaging, in which echoes with low-order phase encoding were used to measure the position. This scheme was made possible by using phase-encoding offsets in the different sections in the multisection sequence so that at all times at least 1 section uses a low-order phase encoding. On the same data, they also applied another motion correction method, the Gerchberg-Saxton algorithm, to further improve image quality. This method also made use of the phase-encoding offsets used in the experiment. Both methods work only for translational motion within the imaging plane. In FSE, each echo within an echo train has a different phase encoding; therefore, just as in the authors' multisection sequence, there is always an echo with a low-order phase encode that can be used for measuring the position. This position can be used to correct the other echoes that were acquired in the same echo train.

Methods and Results: A standard FSE sequence was used on a prototype Hitachi MRH-1500. No modifications to the pulse sequence have to be made for this motion-correction scheme. Significant reduction in the motion artifacts is achieved. In this sequence, motion in the phase-encode direction is corrected by using a version of the Gerchberg-Saxton algorithm especially modified for the FSE sequence. In their earlier experiments, the authors also alternated the readout and phase-encode directions to be able to measure motion in both directions by using the self-calibration method. For FSE this is also possible. The FSE pulse sequence has to be changed to have half of the sections with the readout and phase-encode directions switched. Then translational motion in 2 directions can be measured and compensated for.

Conclusion: By using a standard FSE sequence, the authors are able to reduce motion artifacts substantially with a combination of self-calibration and the Gerchberg-Saxton algorithm. With a modified FSE sequence, even better results are obtained.

The authors are employees of Hitachi Medical.

P204

Analytical Correction of MR Images Obtained with Endorectal or Surface Coils

DB Vigneron, SJ Nelson, S Moyher, DAC Kelley, J Kurhanewicz, H Hricak
Department of Radiology, University of California, San Francisco, CA

Purpose: To develop an accurate and robust method for correcting MR images for the intensity variations due to the inhomogeneous reception profile of endorectal and surface coils. This is extremely important for quantitative image analysis and for endorectal prostate T2-weighted imaging in which hypointense regions in the peripheral zone are often associated with cancer. Without the image correction, signal intensity is strongly dependent on the distance from the small endorectal coil.

Methods: With software developed in the authors' laboratory, a theoretical B1 field map is calculated for each coil geometry by using the Biot Savart law. After aligning this reception profile to the MR images by using MR-visible coil markers, either all signal intensities or those selected by spatial or intensity criteria are divided by the field map. In most cases, a 2% threshold prevented the amplification of image noise far from the coil.

Results: This correction procedure provided a dramatic improvement in uniformity for prostate, leg, and spine images. Correction of a phantom image with initially a 95% decrease in signal intensity resulted in only a 4% deviation in local mean values. This method greatly facilitated the interpretation of clinical prostate images by effectively removing the spatial dependence on signal intensity. After correction, normal peripheral zones appeared uniform and windowing or leveling of the images was made easier.

Conclusion: The authors anticipate that this correction procedure will be extremely beneficial for prostate cancer detection and staging and for all studies in which the quantitation of relative image intensities is a critical factor in image interpretation.

P205

Multisection Reconstruction from Motion-Corrupted Single-Section Data

JK Riek, AM Tekalp, WE Smith
Department of Electrical Engineering, University of Rochester, Rochester, NY

Purpose: Motion artifacts in MR imaging greatly reduce the diagnostic content of the image. Many researchers have discussed how to correct for in-plane block motion, but no one has truly addressed the problems associated with the correction of out-of-plane block motion. The difficulty that arises is that all the lines of raw data are not from the same image. As one moves into and out of the imaging plane, new information is introduced that corresponds to different sections along the section-selection axis. With knowledge of the motion, the authors were able to reconstruct multiple sections along the section-selection axis from the motion-corrupted single-section data.

Methods: To compensate for the motion, we used a reconstruction method known as projection onto convex sets (POCS). We basically apply all the constraints we know in an iterative manner. For example, by looking at the motion-corrupted image, we can roughly estimate the support of the object. Outside this region, we assume that there should be no signal intensity. Also, the image should be real and positive after appropriate phase adjustments. The image itself should be fairly smooth both within the plane and between sections. In the raw data domain, we know that each line came from 1 of the reconstruction images, and we can enforce this knowledge accordingly. To obtain acceptable results, we iteratively enforce the constraints on the image and raw data.

Results: All experiments were performed on a 1.5-T GE Signa. Five axial sections of a wrist were used to simulate out-of-plane motion. From the resulting raw data set, the 5 original sections were successfully reconstructed, and motion artifacts eliminated. A single-section axial head image was then obtained with the table rocking back and forth. Three sections were reconstructed, and there were no motion artifacts present in any of the sections.

Conclusion: This algorithm is a novel approach to artifact reduction along the section-selection axis, since we are attempting to reconstruct a volume from planar data. Preliminary results suggest that we can eliminate artifacts due to motion along the section-selection axis while at the same time providing the radiologist with more information about the object being imaged.

P206

Flow Artifact Reduction with a Phase-Corrected Real Reconstruction

JK Riek, S Totterman, AM Tekalp, WE Smith
Department of Electrical Engineering, University of Rochester, Rochester, NY

Purpose: Flow artifacts in MR imaging present themselves as streaks along the phase-encoding axis of the image. Several methods are currently in use to reduce the artifacts caused by flow, such as gradient moment nulling, presaturation pulses, and cardiac gating. We present a postprocessing routine to reduce flow artifacts that produces the most dramatic results when used in conjunction with one of the previously mentioned methods. In lieu of displaying the magnitude image, we propose a simple method to correct for the phase in the image and display the real positive image that discards the contributions of the imaginary channel (noise and artifacts).

Methods: To correct for the shifts in the raw data, the magnetic inhomogeneities, and the nonlinearity of the gradients, we assume that it can be modeled as a constant, linear, and quadratic phase across the image. We then locate the largest point in the raw data set. This corresponds to DC (both the phase- and frequency-encoding gradients are 0). Next, we take a small square of data points centered around DC and take the inverse Fourier transform of that square. This gives a small, low-resolution estimate of the image from which the quadratic polynomial can be estimated after unwrapping the phase. Finally, we multiply the whole image by the inverse of the detected quadratic phase and display the real part of the image.

Results: All experiments were performed on a 1.5-T GE Signa machine. Axial head images with severe flow artifacts were used. The best results were obtained by using both the proposed algorithm and the FLOWCOMP sequence, in which virtually all flow artifacts were removed. Also, an axial wrist image with flow artifacts in an 8-cm field of view was used because the FLOWCOMP sequence works only down to a field of view of 16 cm.

Conclusion: This algorithm adds no time to patient imaging, and it significantly reduces flow artifacts, especially when used in conjunction with flow-compensating pulse sequences. It also provides flow reduction for images in which it is impossible to use other flow-compensation techniques. Therefore, it seems likely that in time it could become standard practice in clinical MR imaging.

P207

Phase Unwrapping of MR Phase Images with the Poisson Equation

SM Song, SA Napel, GH Glover
Department of Radiology, Stanford University, Radiological Sciences Laboratory, Stanford, CA

Purpose: We have developed a phase-unwrapping technique based on a solution of the Poisson equation to unwrap the phase in MR phase images.

Methods: The technique is based on the assumption that the magnitude of the interpixel phase change is less than π. Therefore, we obtain an estimate of the phase gradient by wrapping the gradient of the original phase image. The problem is then to obtain the true phase given the estimate of the phase gradient. The least-squares (LS) solution to this problem is a solution of the Poisson equation; thus, the LS phase may be obtained by using a fast Poisson solver. The true phase can then be obtained from the LS phase by computing the nearest multiple of 2π from the original phase.

Results: We have applied the algorithm to unwrap phase difference images of the 3-point Dixon method. The algorithm has been effective in a number of images that we have considered thus far.

Conclusion: The proposed algorithm robustly creates unwrapped phase difference images for field mapping applications such as 3-point Dixon water/fat reconstruction. It may also have an application in increasing the dynamic range of phase-contrast velocity images.

P208

Displacement Field Fitting Approach for Calculating 3D Deformations from Parallel-tagged MR Images

WG O'Dell, CC Moore, ER McVeigh
Department of Biomedical Engineering, Johns Hopkins University, Baltimore, MD

Purpose: To develop a 3D motion reconstruction method for MR images that uses the entire lengths of tag lines and is applicable to parallel-tagged cardiac images.

Methods: Three multiphasic sets of images are obtained, each with 1 of 3 mutually orthogonal sets of parallel tags. Every point along each tag line in an image contains displacement information in the direction normal to the point's original tag plane. By using all tag points with the same displacement direction, the authors reconstruct the displacement field in that direction over the entire heart. This is done by using a basis set spanning the 3D space, such as a power series in x, y, and z, and solving via least squares for a series of coefficients. The 3 orthogonal displacement fields are determined independently and then combined to perform the reconstruction of the 3D field. Finally, local deformations can be computed from the myocardial 3D displacement field, whose boundary is defined by heart contours.

Results: Bulk motions and deformations simulating those expected in the living heart were reconstructed with displacement error less than 0.1 mm for computer-generated model spheres and cylinders.

Conclusion: The authors have demonstrated a continuous field fitting approach to analyze tagged cardiac MR images that (1) uses all available tag data, (2) gives the 3D deformation at any point, (3) does not rely solely on sparse tag-tag or tag-contour intersections, and (4) can be used for grid or parallel tag data sets.

P209

Automatic Brightness and Contrast Adjustment of MR Images by Using Viewer's Preferences and Image Acquisition Information

RE Wendt, DE King
Department of Radiology, Baylor College of Medicine, Houston, TX

Purpose: Automatic, robust adjustment of the hyperintensity and contrast ("windowing") of MR images is 1 feature of a low-cost, easy-to-use MR imaging viewing station being developed for referring physicians. A method was developed and tested that uses the median and standard deviation of all pixels within a central subregion of the image that exceed a threshold intensity in conjunction with rules incorporating the image orientation and various acquisition parameters.

Methods: The images from routine head and MR angiographic examinations of 11 patients were individually adjusted for satisfactory appearance on the workstation screen. The window parameters were compared with a variety of pixel statistics from the images. Image acquisition parameters were extracted from the headers of the images. Initial rules were developed from this data base and applied to 4 more studies, which produced minor refinements. Ten studies were then processed completely automatically.

Results: The linear combination of the median and the standard deviation statistics yields a reliable windowing algorithm. The best coefficients are different for different contrast weightings. All 10 evaluation studies were entirely satisfactory.

Conclusion: This method works well when the background pixels and artifacts are automatically excluded from the calculations. The setup procedure for a particular workstation includes a training set of images that is adjusted by the user to accommodate personal preference and variations in monitor characteristics and ambient lighting. Unlike the routine filming of studies in the authors' institution, which requires the technologist to adjust the hyperintensity and contrast frequently, this automatic windowing approach is quite robust.

P210

Stereoscopic Display of MR Angiograms

RE Wendt, K von Gynz, ME Mawad
Department of Radiology, Baylor College of Medicine, Houston, TX

Purpose: A method of processing MR angiograms as stereoscopic pairs and of displaying the stereoscopic maximum-intensity projections statically and as cine loops was developed and evaluated.

Methods: MR angiographic studies were performed on Magnetom 63SP imagers (Siemens Medical Systems, Iselin, NJ). The raw MR angiographic data were processed into maximum-intensity projections on a Sun-4/470VX workstation by using SunVision software (Sun Microsystems, Mountain View, CA). The authors wrote programs to convert the Magnetom data to SunVision format and to control the Sun Voxel tool of SunVision to produce stereoscopic pairs of images as 24-bit color composite images suitable for viewing with colored filters. These were then dithered to 8-bit color and concatenated into movie loops. The MR angiograms of 7 patients with disease of the carotid artery or the intracranial circulation, as documented with x-ray angiograms, were retrospectively selected for this evaluation.

Results: There was no loss of information in the stereoscopic processing. High-grade stenoses that are evident as wisps are better appreciated in the stereoscopic, cine display than they are on 2D static images. Very small defects detected in the movie were confirmed on static, 24-bit color stereoscopic displays of the appropriate frames from the movie because dithering slightly reduces the image quality of the movie frames.

Conclusion: Stereoscopic display of MR angiograms is very helpful in studies with many small vessels, in the evaluation of ateriovenous malformations and aneurysms and in locating a vessel with respect to other organs.

P211

Rectangular Bird-Cage Coil for MR Imaging of the Hand

T Vullo, R Pascone, A Tankhiwale, PT Cahill
Cornell Medical Center, New York, NY

Purpose: A new type of low-pass bird-cage coil with a rectangular geometry was developed for MR imaging of the hand. This geometry has the advantage of a reduced coil volume compared with analogous cylindrical bird-cage coils, resulting in an increased signal-to-noise ratio (S/N).

Methods: The electrical behavior of the rectangular coil was theoretically analyzed by using a lumped element transmission line model that had previously been validated for cylindrical low- and high-pass bird-cage resonators. The effective inductance elements of the coil were determined, and coil "compensation" was performed to achieve the mode 1 column currents characteristic of all standard cylindrical bird-cage coils. RF field plots were calculated with the Biot-Savart law, and MR hand images were acquired at 0.6 T.

Results: The S/N of the rectangular coil was 240% greater than that of a comparable cylindrical version. This was consistent with a reduction of noise due to decreased volume, and, from the calculated field plots, a 22% greater sensitivity of the rectangular coil compared with that of an equivalent cylindrical version. Furthermore, high-resolution hand images confirmed the clinical utility and advantage of this type of coil for MR imaging.

Conclusion: A lumped-element transmission line model provided a unique evaluation of the electrical nature of the rectangular bird-cage coil. Increased coil sensitivity and S/N for this coil compared with that of the cylindrical version demonstrated the benefits of this rectangular bird-cage resonator for MR imaging of the hand.

P212

Analysis of Switched-Field MR Imaging

DM Goldhaber, JW Carlson, L Kaufman
Radiologic Imaging Laboratory, University of California, South San Francisco, CA

Purpose: In switched-field MR imaging (1,2), a relatively inhomogeneous field is applied during times when neither encoding nor sampling occurs. For sufficiently large boosted fields, the unit-time signal-to-noise ratio (S/N) increases. The authors have calculated the effect of the boost on S/N and contrast for a wide range of sequence parameters in a low-field (0.064-T) imager.

Methods: The Bloch equations are solved for 2D and 3D imaging sequences in which a fraction of each TR is used for the boosted field. The unit-time S/N is computed and compared with the best achievable S/N in an unswitched experiment. The authors' calculations are compared with experimental results from their switched-field system (3).

Results: In general, the unit-time S/N is maximized for boosted field duty-cycles near 50%. The break-even point occurs for a ratio of boosted to base fields (f) equal to 1.4. For 3D, optimal TR (for S/N) is about T1, somewhat lower for smaller values of f and larger for larger f. For 2D multisection, above the break-even point, the optimal TR is about T1 times the number of sections. For a given boost ratio, the unit-time S/N increase is larger for 3D experiments than for 2D. For both 3D and 2D, the T1 contrast is similar to that obtained in an unswitched experiment with a shorter TR. Experiments imaging the head and knee of a healthy volunteer confirm the general features of the authors' calculations for a boost ratio f = 2.

Conclusion: Switched-field MR imaging can provide a substantial improvement in S/N.

1. Carlson JW, Crooks LE, Arakawa M, et al. Switched field magnetic resonance imaging. SPIE Medical Imaging VI: Instrumentation 1992; 1651:22–27. 2. Conolly S, Macovski A. Feasibility study of prepolarized MRI. SMRM Eleventh Annual Meeting 1992; 2:689. 3. Carlson JW, Goldhaber DM, Brito A, Kaufman L. MR relaxometry imaging. Radiology 1992; 184:635–639.

D.M. Goldhaber is an employee of Toshiba America MRI, Inc. J.W. Carlson and L. Kaufman are consultants to Toshiba America MRI, Inc.

P213

Noise Aliasing at the Input of Analog-to-Digital Converters in MR Systems

LE Crooks, JC Hoenninger, J Jones
Radiologic Imaging Laboratory, University of California, South San Francisco, CA

Purpose: Analog receivers in MR systems quadrature demodulate the RF signal into I and Q channels. These are amplified, filtered, and digitized by analog-to-digital converters (ADCs). The filtering, provided by programmable active "antialiasing" low-pass filters (LPFs), eliminates noise above the Nyquist frequency of the ADC. The ADC samples this band-limited noise and signal, plus any noise added by the LPF over the frequency response range of the ADC. This last point is critical because ADCs have a broadband small-signal (noise) frequency response. The filters used by the authors generate 50 μV of noise over 0–100 kHz and 70 μV over 0–1 MHz.

Methods: The noise level was measured with high S/N, three-dimensional head imaging on the Toshiba MRT-35A and ACCESS imagers, with and without 28-kHz low-pass RC filters added to the ADC inputs to eliminate excess noise. The MRT-35A protocol is sagittal, with 32 × 5-mm-thick sections, TR of 80 msec, TE of 20 msec, 27° flip angle, 0.95-mm resolution with 256 lines, and an LPF of 3.3 kHz. Total imaging time is 11 minutes. The ACCESS protocol is similar with an LPF of 1.0 kHz.

Results: The MRT-35A shows a 7% improvement in S/N from 39.4 to 42.3. There is no change in the S/N of the ACCESS. It uses a slower ADC.

Conclusion: This example shows that the imager collects excess noise when the ADC has broadband small-signal capability, the system operates with a narrow bandwidth LPF, and the sampling rate of the ADC matches the LPF. The effect of the excess noise depends on the amount of noise in the actual signal, so the excess noise is a greater problem when S/N is high. Three-dimensional imaging and proton spectroscopy will be most sensitive to the extra noise.

P214

Performance of Some Analog-to-Digital Converters used in MR Systems

LE Crooks, M Arakawa, JC Hoenninger, J Jones, E Tapio, S Krasnor
Radiologic Imaging Laboratory, University of California, South San Francisco, CA

Purpose: Analog-to-digital converters (ADCs) are the final analog component in an MR receiver system. Their linearity is an important determinant of receiver dynamic range. The dynamic range of the sample-and-hold in an ADC decreases with increasing frequency. A digital receiver (DR) requires good ADC performance at high frequencies because the ADC must quantize the MR signal modulating a nonzero intermediate frequency (IF). In our DR, this carrier frequency is 125 kHz (the required test frequency) and the ADC operates at 500 kHz. Two tone tests are an effective alternative to single-frequency tests for comparison of the linearity of various ADCs at these frequencies.

Methods: Two test frequencies are generated by using the IF section of our DR. The tones come from a pair of PTS 160 frequency synthesizers combined to give 2.0 MHz ± 1,356 Hz. The IF section mixes this down to 125 kHz ± 1,356 Hz and gives a peak level of 2.4 V. The ADC performance is evaluated by comparing the DR's output of the tones at ±1,356 Hz with the spurious responses at ±4,068 Hz. The analog portion of the IF section has less distortion than any of the ADCs tested, but sets the ultimate limit of this approach. Five ADCs were tested: Analog Devices ADC1382 and ADC1385 and Analogic ADC41116, ADC4344, and ADC4345.

Results: The spurious signal levels were ADC1382: −74.1 dBc, ADC1385: −77.9 dBc, ADC41116: −76.9 dBc, ADC4344: −80.3 dBc, and ADC4345: −78.1 dBc.

Conclusion: The ADC4344 and ADC4345 were the best performers of the units tested. The extra speed of the ADC4344 provides better linearity at 125 kHz at the cost of additional noise related to its wider bandwidth.

P215

Performance of a Digital Receiver with a Floating Point Digital Signal Processor

JC Hoenninger, LE Crooks, J Jones
Radiologic Imaging Laboratory, University of California, South San Francisco, CA

Purpose: A digital receiver (DR) has well known advantages: elimination of DC and low-frequency noise, perfect matching of I and Q channels, high performance filters, and finer quantization. We have implemented a digital reception channel with an AT&T DSP32C floating point processor.

Methods: The DR channel uses a 16-bit, 500-kHz ADC to quantize a 125-kHz IF signal. The DSP32C immediately floats, then demodulates and filters this data. Multirate FIR filters decimate and low-pass-filter the I and Q channels. The authors insert the DR into the ADC data path of a Toshiba MRT-35A, so the floating point results are rounded to 16-bit integers. They compare the DR's 124-tap filter with an active 8-pole Butterworth filter set to 7 kHz. The duration of the 256-point sample window is 18.432 msec. The DSP32C is programmed in C with in-line assembly language for speed-critical pipelined sections.

Results: The DR's frequency response drops from −3 dB at 6,673 Hz to −50 dB above 7,161 Hz. The 20-MHz DSP32C requires 61 msec to input, process, and output the data. Processing overlaps data acquisition. DC is eliminated and body imaging shows an improved alias rejection along the readout direction.

Conclusion: The DR provides all of the expected improvements available with 16-bit data. The floating point calculations eliminate programming concerns with overflow/truncation and coefficient sizes. The mixed C and assembly language support is the first step to a more open programming environment. The single 20-MHz DSP's long processing time can be reduced with faster DSPs. Multiple DSPs can also be applied to parallel parts of the problem.

P216

Surface Gradient Coil Assembly for MR Imaging and Microscopy of Skin

H Jin, JI Shapiro, MS Brown, ER Hendrick
Department of Radiology, University of Colorado Health Sciences Center, Denver, CO

Purpose: An interest in MR microscopic imaging of primary skin tumors (melanoma) and infiltrative disorders of skin has motivated the construction and testing of a unique gradient coil set designed for placement on a patient's skin and capable of producing strong linear gradients in 3 dimensions.

Methods: The coils were designed by using first-order perturbation theory so that the region of linearity is toward the top surface of the coil assembly and to handle currents of up to 20 A. They are constructed by using 18-gauge magnet wire wound on a delrin form. Shifting of the coil windings is prevented by using Super Glue and wax. Testing and characterization of the coils were performed on a Bruker 1.9-T Biospec system.

Results: The gradient fields are linear in a region of 3 cm^3. Typical gradient strengths obtained are 8 G/cm at 15 A for x, 13 G/cm at 10 A for y, and 7.5 G/cm at 10 A for z. The coils have rise and fall times of less than 500 μsec at 10 A. The small size of the coil assembly (20 × 19 × 8 cm) minimizes coupling to the magnet for negligible eddy current production. Images with a voxel size of 78 μm × 78 μm × 0.5 mm have been obtained.

Conclusion: The surface coil nature of the set is suitable for MR microscopy of skin at any location on a patient and can be adapted for use on a clinical whole-body system.

P217

Thin-Film High-Temperature Superconductor Surface Coils for Low-Field-Strength MR Imaging

JG van Heteren, LC Bourne, TW James, L Kaufman
University of California, South San Francisco, CA

Purpose: To investigate the use of thin-film high-temperature superconductor (HTS) material to improve the signal-to-noise ratio (S/N) of small volumes in low-field-strength MR imaging (0.064 T). In MR areas such as microscopy, spectroscopy of nonconducting samples, and low-field-strength MR imaging, the sample noise is so low that RF conductor losses become significant. The use of HTS in RF coils should reduce these losses and improve S/N. Although limited by wafer size (5.0–7.5 cm diameter), thin-film HTS is not significantly degraded by exposure to the static magnetic field as bulk HTS is.

Methods: A 5-cm diameter thin-film HTS coil was compared with a similar geometry copper coil at 300K and 77K. The HTS coil had 15 spiral turns of 100-μm-wide windings and was coarsely tuned with an HTS interdigital capacitor on the same wafer. Varactors performed fine tuning and matching.

Results: The 77K HTS coil had 1.3× S/N of 77K copper coil on saline and human hand images. The HTS coil S/N with 4 mm of insulation equalled the 300K copper coil S/N with no insulation gap. HTS coil Q was unaffected by a 0.064-T field. Loaded Qs were $Q_{HTS} = 800$, $Q_{77KCu} = 300$, $Q_{300KCu} = 124$.

Conclusion: HTS did improve S/N over 77K copper, but the advantage was lost over 300K copper due to insulation thickness. Future work will use larger coils in which insulation thickness will not be as significant.

J.G. van Heteren is a part-time employee of Toshiba America MRI, Inc.

P218

Biplanar Gradient-Coil Imaging and Geometric Distortion Correction

H Liu, M Morich
Picker International, Highland Heights, OH

Purpose: In present-day MR imaging, ultrafast echo-planar imaging and diffusion mapping are placing greater demands on gradient strength and fast switching times.

Methods: To fulfill these demands and meet the constraints imposed by the human body, a single-axis biplanar insertable gradient coil (1) was recently chosen for cardiac imaging applications (2). In this case, the geometric distortion in the reconstructed image is dominated by the nonlinearity of the gradient field. For the same reason, the actual image section position and shape are distorted as well. Correction can be achieved by performing a coordinate mapping transformation, which is defined by the nonlinearity of the biplanar gradient system. The distortion characteristic of the biplanar design differs from the traditional cylindrical shape design in the basis function to be used to represent the nonlinearity of the resultant gradient field. In this work, the nonlinearity of a gradient system is decomposed into a Taylor series. In the corresponding distortion correction, a section position tracking algorithm was developed and used to determine the exact imaging section position before performing the in-plane geometric distortion correction. The image intensity modulation can be corrected with the Jacobean of the transformation.

Results and Conclusion: With this correction scheme, the corrected phantom and human images showed a remarkable improvement in the reduction of geometric distortion even at a relatively large distance away from the imaging isocenter.

1. Martens, et al. Rev Sci Instrum 1991; 62:2639.
2. Clark, et al. SMRM 11th annual meeting 1992; 581.

H. Liu is an employee of Picker International.

P219

MR Imaging–guided Thermal Surgery

HE Cline, JF Schenck, RD Watkins
GE Corporate Research and Development, Schenectady, NY

Purpose: To model and measure the thermal distributions in minimally invasive surgical treatment of deep-lying lesions by using either focused US or interstitial laser surgery guided with MR imaging.

Methods: A hydraulic focused US apparatus was constructed for experiments in a 1.5-T MR system to acquire images. Both the heat distribution and the creation of focused US lesions in gel phantoms, in vitro bovine muscle, and in vivo rabbit muscle were monitored with MR imaging. Thermal surgical procedures were modeled by using an elongated Gaussian heat source controlled with tissue thermal properties.

Results: Heat flow is controlled by tissue-specific heat, radial thermal conduction, and tissue perfusion with increasing pulse duration. Temperature profiles measured with thermocouples or calculated from MR imaging are in agreement with the model. A 2-second gradient refocused acquisition (TE/TR = 3/11, 60° flip angle) gave T1-weighted images giving an effective thermal diffusion coefficient of 0.015 cm^2/sec in gel and 0.033 cm^2/sec in muscle. The lesions were detected by using a 2-minute T2-weighted SE or 30-second fast SE (RARE) pulse sequence and resembled a muscle tissue section at the focal plane.

Conclusion: The thermal profiles generated with focused US and measured with MR imaging are in accord with a thermal model that uses elongated Gaussian sources. Future clinical applications of thermal surgery guided with MR imaging may include the prostate, breast, liver, kidney, eye, and brain.

P220

Phantoms for MR Imaging of Laser Interactions

SG Hushek, V Date, PR Morrison, MP Fried, FA Jolesz
Radiology Department-MRI, Brigham and Women's Hospital, Boston, MA

Purpose: Phantoms have been developed to study MR imaging of laser tissue interactions. A combination of dopants was used to independently control the T1 and T2 imaging parameters as well as the optical scattering and absorption coefficients.

Methods: Polyacrylamide gels were made with an 80:1 monomer:comonomer ratio and 10% dry gel by weight. The MR parameters were controlled by varying the concentrations of $MnCl_2$, $CuCl_2$, and dextran. The optical parameters were controlled with polystyrene microspheres (Duke Scientific) and India ink (Faber-Castell). T2 values were determined by fitting the signal intensities from a 64-echo, 15-msec echo spacing Carr-Purcell-Meiboom-Gill sequence on a 1.5-T Signa (GE Medical Systems) to an exponential decay curve. T1 values were determined by fitting the signal intensities from a partial saturation series with TRs ranging from 50 msec to 6 seconds to a recovering exponential. The reduced absorption and scattering coefficients were obtained at 1,064 nm on a photospectrometer.

Results: Appropriate doping of the gels allows simulation of a wide variety of tissues, including gray matter, white matter, fat, and select tumor models. To our knowledge, reasonable independence of the MR and optical parameters was achieved for the first time.

Conclusion: Development of phantoms for MR imaging of laser tissue interactions is significant in the development of MR-controlled therapeutic laser treatments. The phantoms will allow study of the underlying physical interactions involved in these procedures and lead to new understandings of the critical parameters in control and optimization of these techniques.

P221

Morphologic Characterization of Carotid Atherosclerotic Plaque with MR Imaging

A Sarram, C Yuan, JS Tsuruda, DE Strandness, M Ferguson
Department of Radiology, University of Washington, Seattle, WA

Purpose: Atherosclerosis and its associated complications are the leading cause of mortality in the United States. It has been suggested that plaque composition is in direct correlation with eventual clinical outcome. Therefore, the authors have attempted to show that MR imaging can be used effectively to identify plaque composition.

Methods: High-resolution MR images were acquired from carotid atherosclerotic plaques by using a GE 1.5-T Signa imager. After MR imaging, the specimens were prepared for histologic examination under a light microscope. Outlines of the fibrous plaque, fibrous cap, calcification, loose necrosis, hemorrhage, foam cells, and cholesterol were drawn on digitized pictures of the histologic sections. The authors then used these outlines as well as direct microscopic examination to identify corresponding regions on the MR images, noting signal intensity and contrast.

Results: The results indicate that high-resolution MR images are capable of outlining the fibrous plaque and the lumen. In 1 case, the authors were able to visualize the thinning of regions within the fibrous cap. This has particular clinical relevance, since it may predict future events such as ulceration and embolism. Calcium deposits give little to no signal intensity, showing up as black regions within the plaque. Regions of amorphous, pink material (loose necrosis) have signal intensity characteristics similar to the background. While thrombotic regions in the fixed specimen appear similar to the fibrous plaque, the contrast is markedly enhanced in the fresh specimen.

Conclusion: These preliminary results have shown that MR imaging has the potential to enable identification of atherosclerotic plaque composition. The authors project that this technique can be developed into the method of choice for diagnosing plaque presence and predicting clinical outcome.

P222

Added-Gradient-Echo Pulse Sequence Technique: Application to Spine MR Imaging

KD Miller, R Restrepo, JP Jones, JA Kalmar, RH Tutton, JJ Eick
Department of Radiology, Ochsner Clinic, Ochsner Medical Institutions, New Orleans, LA

Purpose: To assess the value of combining an added gradient spin echo (SE) echo (AGE) with a T1-weighted spin echo (SE) in the same pulse sequence to determine the value of AGE in detecting spinal abnormalities without adding to the imaging time.

Methods: To the standard T1-weighted sequence used in spine MR imaging, a readout gradient reversal was added and the resulting gradient echo collected. This image was compared with standard T1- and T2-weighted sequences, a gadolinium-enhanced T1-weighted sequence, and a small-flip-angle FLASH gradient-echo sequence.

Results: The T1-weighted SE preceding the AGE was not affected by the gradient reversal, but the additional gradient echo adds T2* contrast information, resulting in low-signal-intensity bone, high-signal-intensity disk, and intermediate-signal-intensity cerebrospinal fluid while preserving contrast enhancement. Osteophytes and herniated disk material as well as herniation beyond osteophytes may be more easily determined. Bone marrow replacement by tumor and osseous, epidural, intradural-extramedullary, and intramedullary enhancement may be more readily identified. The AGE sequence also aids recognition of osteopenia and helps to confirm or reinforce the absence of contrast enhancement.

Conclusion: The AGE technique adds sensitivity for the detection of spinal abnormalities without adding to the overall imaging time of a routine T1-weighted sequence.

P223

Magnetization Transfer Gradient-Echo Imaging of the Cervical Spine

CR Timberlake-Kwit, HA Reiss, DA Finelli, BA Karaman, JE Simon, J Hua, GC Hurst
Department of Radiology, MetroHealth Medical Center, Cleveland, OH

Purpose: Magnetization transfer (MT) is known to decrease the image intensity of gray and white matter relative to clear fluid such as cerebrospinal fluid. The authors hypothesized that addition of this source of contrast might allow a higher excitation flip angle than they currently use for gradient-echo cervical spine MR imaging, with concomitant advantage in image quality due to increased contrast-to-noise ratios. They therefore examined cervical spine gradient-echo MT images by using a range of MT pulse amplitudes and excitation flip angles.

Methods: Experiments were performed with a standard 1.5-T clinical MR imager (Picker Vista), with healthy volunteers as subjects. Acquisitions were sagittal 2D FT gradient-echo sequences with TE/TR = 13/500 with 1 MT pulse (10-msec duration, Gaussian, truncated at 3σ, offset 1.6 kHz) per section excitation. MT pulse peak amplitude was varied from 0 to a limit (set by SAR) of 14 μT. Section excitation amplitude was varied from 15° to 50°. Images were subjectively evaluated by experienced neuroradiologists.

Results: The apparently "best" parameter configuration, within the above range, is 12 μT MT pulse amplitude with 30° section-select excitation; this excitation pulse is indeed larger than the 20° pulse used in our non-MT gradient echo (similarly chosen by reader preference). There was consensus that these sequences were at worst equal to, and usually better than, our standard, non-MT gradient-echo sequence.

Conclusion: Our preliminary experience with MT sequences shows promise for improved "myelographic effect" in gradient-echo cervical spine imaging. An "optimum" parameter set seems to be within current SAR limits.

P224

Selective T1 Suppression Imaging

C Labadie

Department of Chemistry, State University of New York at Stony Brook, Stony Brook, NY

Purpose: A method is proposed to achieve T1-selective water suppression that allows relaxation measurements of other isochronous water signals that have either shorter or longer T1 than the one being suppressed. The method takes advantage of the inversion recovery null point by applying increasing inversion pulses from 90° to 180° preceding TI of 0 to a fraction of the suppressed T1 (0.69). An application to T1-weighted imaging of biexponential processes is presented.

Methods: The selective T1 suppression imaging was adapted from the FLASH sequence with a strong spoiler gradient following the variable inversion pulses. The suppression technique was illustrated with 2 phantoms composed of 7 tubes of different $CuSO_4$ solutions. A third phantom was prepared with yeast resuspended in 3 mM extracellular Gd-DTPA, which simulated an in vivo biexponential signal.

Results: The $CuSO_4$ phantoms showed that the suppression is very dependent on the homogeneity of the B_1 field. The biexponential yeast signal intensity agreed with the theoretical curve. The yeast water signal intensity was increased at early TI by the presence of shorter T1 (90 msec, extracellular water encountering Gd-DTPA) than the one suppressed ($T1_{sup}$, 130 or 149 msec); it then decreased at long TI as longer T1 signals (400 msec, intracellular water) recovered.

Conclusion: The proposed selective T1 suppression imaging corresponds to the residuals obtained after a monoexponential deconvolution of a conventional T1-weighted data set. Appearance of a systematic pattern on those images (ie, positive at first followed by negative intensities) is the signature of a biexponential signal intensity. The direct imaging of biexponential processes appears to be possible with this approach provided that the B_1 field is sufficiently homogeneous.

P225

Large-Flip-Angle Spin-Echo Imaging

G DiIorio, WH Perman, JJ Brown, JA Borrello, HH Shu

Mallinckrodt Institute of Radiology, Washington University School of Medicine, St Louis, MO

Purpose: To determine the optimal flip angle for spin-echo (SE) imaging with short TR values.

Methods: The Bloch equations were used to predict signal intensities derived from single-echo SE pulse sequences by using excitation flip angles of 90°–180° (in 10° increments) for TR values of 50–275 msec. These values were compared with experimental signal intensities derived from water, mineral oil, and $MnCl_2$ phantoms by using the same imaging parameters. The concentrations of the $MnCl_2$ phantoms were varied to approximate the T1 of liver parenchyma and liver metastases.

Results: Calculated signal intensity values were maximal at excitation angles of 101°–158° for TR values of 50–275 msec ($167 \text{ msec} \leq T1 \leq 661 \text{ msec}$). These angles are the complements of the Ernst angles derived for gradient-echo imaging. Liver-lesion contrast calculations were predicted to be maximal at excitation flip angles of 115°–120° for TR values of 50–275 msec. Experimental signal intensities derived from phantom imaging agreed with calculated values except that maximal signal intensities occurred at slightly smaller flip angles and were of lower amplitude than calculated values.

Conclusion: A theoretical advantage of using excitation pulses greater than 90° for SE imaging with 1 refocusing pulse and short TR values was demonstrated based on the Bloch equations. The theory is supported by experimental data derived from phantom imaging.

P226

Fat Suppression with an Adiabatic Excitation Pulse

H Liu, RP Gullapalli

Picker International, Highland Heights, OH

Purpose: Fat suppression methods have proved highly desirable for a variety of diagnostic cases. An adiabatic pulse that is both amplitude and phase modulated was used as a chemical shift selective excitation pulse for fat suppression at fields ranging from 0.5 to 1.5 T.

Methods: Appropriate choice of the tip angle and frequency offset for the pulse enable the suppression of the desired component. Both fat and water signals in the steady state are determined by these 2 parameters, which can be optimized for fat suppression. By the proper choice of these 2 parameters, the fat magnetization can be put back to the z axis, while leaving the water magnetization in the transverse plane. With this adiabatic pulse used as an excitation pulse, a relatively short TE can be achieved in a sequence. Steady-state acquisition allows a short TR as well, which also translates into reduced motion artifact.

Results: A 3D FE6 TR20 image was obtained with a 0.5- and 1.5-T Picker HPQ MR imaging system in both a fat-water phantom and a human brain. The resulting images showed a marked reduction of fat signal intensity. Short TE as low as 3 msec can be achieved with this technique. Images from both low and high field strengths will be shown.

Conclusion: The RF pulse has the potential of producing fat-water images at high field strength as well as low field strength, which has been particularly difficult to obtain with any other imaging techniques.

H. Liu is an employee of Picker International.

P227

Effective Rotation Axis Analysis of Multiple-Echo Pulse Sequences

JB Murdoch

Picker International, Highland Heights, OH

Purpose: Multiple-echo pulse sequences are of interest both for imaging and for measuring dipolar couplings. The usual way to think about the associated spin dynamics is in terms of coherence pathways: primary echoes, stimulated echoes, and so on. This quickly gets complicated: the number of pathways associated with the N^{th} echo is roughly $3^{N-1}/(N\pi/3)^{1/2}$. An alternative is to consider the refocusing pulse cycle ($\tau/2$-α_x-$\tau/2$ for a Carr-Purcell sequence with tip angle α and pulse spacing τ; $\tau/2$-α_x-τ-α_y-$\tau/2$ for an XY sequence, etc) and to calculate the effective rotation per cycle for each contributing isochromat *k*. Magnetization parallel to the effective rotation vector $\mathbf{n}_k$ remains invariant from echo to echo (neglecting relaxation and diffusion); magnetization perpendicular to $\mathbf{n}_k$ is spun from echo to echo and tends to average away. Hence, to estimate the "steady-state" Nth echo amplitude, we project the initial magnetization vector onto $\mathbf{n}_k$, project $\mathbf{n}_k$ onto a "detection axis," and average over isochromats.

Methods: Mathematica software (Wolfram Research) is used to generate analytic expressions for $\mathbf{n}_k$, and for comparison, "exact" echo amplitudes based on sums over pathways.

Results: A number of sequences (X, XY, $XX\overline{XX}$, $XY\overline{YXXY}YX$, etc) have been examined as a function of tip angle for both hard and soft refocusing pulses. For Carr-Purcell, amplitude $\propto$ sin ($\alpha/2$), as Hennig found numerically. Curiously, pulse cycles designed for RF-spoiled rapid imaging show promise in multiple-echo applications.

Conclusion: This is a physically insightful way to estimate Nth echo amplitudes for a variety of sequences.

P228

Magnetization Transfer Contrast–FLAIR Technique

RP Gullapalli, H Liu, L Kasuboski
Picker International, Highland Heights, OH

Purpose: There has been some interest in the ability to better diagnose various diseases by using cerebrospinal fluid (CSF)-nulled T2-weighted imaging with fluid attenuated inversion recovery (FLAIR) (1). The long TEs and the reduced bandwidth used in this technique limit the number of sections that can be obtained within a single TR. The authors propose here a technique that combines FLAIR with magnetization transfer contrast (MTC) imaging.

Methods: All images were obtained in a normal brain by using a standard 1.0-T Picker HPQ MR system. A standard field echo sequence with a TE of 15 msec was used as the imaging sequence. This was preceded by both a section-selection inversion pulse and a nonselective off-resonance RF irradiation pulse offset by 1 kHz from the center frequency. As many as 16 sections were interleaved within the TI after the inversion pulses. Off-resonance irradiation was also applied between the inversion pulses to maintain saturation of the bound pool. The sequence time was further shortened by minimizing the TI and optimizing the combination of repeat time and inversion flip angle used to suppress CSF signal intensity.

Results: The images obtained with the MTC-FLAIR technique were comparable to those obtained from the standard FLAIR sequence.

Conclusion: The MTC-FLAIR technique produces images comparable to the images produced by the FLAIR technique in healthy volunteers. Further, a significant reduction in imaging time as well as more sections per TR are obtained.

1. Hajnal JV, et al., J Comput Assist Tomogr 1992; 16(4).

P229

Parametric Study of Magnetization Transfer Contrast in the Human Brain

RP Gullapalli, HT Friel, PM Margosian
Picker International, Highland Heights, OH

Purpose: The ability to saturate protons in macromolecules and bring about a new type of contrast, namely magnetization transfer contrast (MTC), has been well established. The images obtained with this technique have a T2-weighted appearance, although the underlying mechanism for the obtained contrast is different. The authors exploit this property to obtain images of the brain with a T2-like contrast in far shorter time than with conventional T2 imaging.

Methods: All images were obtained on a standard 1.0-T Picker HPQ MR system with the quadrature head coil, in healthy volunteers. A systematic study was done to determine the parameters that affect image contrast, namely $T1_{sat}$ for individual tissues in the brain, the power, frequency offset, the bandwidth of the off-resonance irradiation, and the flip angle of the imaging sequence. A standard 2D field echo sequence with a TE of 15 msec was used as the imaging sequence. A standard T2-weighted image (2,500/90) was also obtained for comparison.

Results: Comparable images were obtained by using the MTC technique that produced the apparent contrast of a standard T2-weighted image (2,500/90). The off-resonance irradiation was 800 Hz from center frequency with a B_1 approximately equal to 11 μT and a bandwidth of approximately 400 Hz. Images obtained from the MTC studies by varying the above parameters and the standard T2-weighted images will be shown.

Conclusion: Substantial time savings can be obtained with proper use of field echo parameters along with the relevant magnetization transfer parameters to obtain T2-like images.

P230

Clinical Evaluation of Superheavy T2-weighted Images ($\geq$ 6,000/$\geq$ 80) with a Fast SE Method

Y Imanishi, H Mitsuhashi, M Masuoka, H Suzuki, R Igarashi, M Yoneda, M Fujikawa, K Yamaguchi, T Gorou
St Marianna University, Tohyoko Hospital, Kawasaki, Japan

Purpose: A pure T2 image will depict T2 times slightly different between some lesions and the surrounding tissue even if they have similar long T1 times. By using a fast SE method, we have been able to obtain superheavy T2-weighted images (TR msec/TE msec = 6,000/80) easily, which is probably very close to the pure T2 image. In this study, we tried to evaluate superheavy T2-weighted images clinically by comparison with conventional T2-weighted images.

Methods: In 81 patients, both conventional T2-weighted images (SE 2,500/80) and superheavy T2-weighted images (fast SE $\geq$6,000/80 or 100) were obtained with a 1.5-T system (MRT-200/FX IIIsv, Toshiba) at the same sites, which included the upper abdomen in 45 patients, the pelvic cavity in 19 patients, and other sites in 17 patients.

Results: The superheavy T2-weighted images depicted normal anatomy better in 65 of the 81 patients than did the conventional T2-weighted images, although the former had more motion artifact in 51 of the 81 patients. Also, the superheavy T2-weighted images depicted various lesions, especially hepatocellular carcinoma and ovarian tumors, better in 37 of the 57 patients, with some lesions in the upper abdomen or pelvic cavity, than did the conventional T2-weighted images.

Conclusion: The superheavy T2-weighted image is clinically useful for evaluation of lesions in the abdomen.

P231

Ultrafast MR Imaging of Gd-DTPA Bolus Transit in Human Renal Transplants

T Vestring, KH Dietl, S Heidenreich, U Stöber, I Braun-Anhalt, S Maurer, G Bongartz, E Rummeny, B Buchholz
Institut für Klinische Radiologie, Westfälische Wilhelms-Universität, Münster, Germany

Purpose: To determine the value of ultrafast snapshot FLASH MR imaging in monitoring Gd-DTPA bolus passage through human renal transplants.

Methods: One hundred five patients were evaluated at 1.5 T. Eighty-five patients showed impaired renal function due to acute rejection ($n = 56$), acute tubular necrosis ($n = 9$), chronic rejection ($n = 10$), cyclosporin A nephrotoxicity ($n = 5$), and cytomegalovirus infection ($n = 5$). To define the baseline normal values, 20 transplants without any sign of acute or chronic disease were investigated. The diagnosis was confirmed with biopsy ($n = 70$) and clinical course ($n = 35$), respectively. One hundred consecutive transverse snapshot FLASH images (TI/TR/TE = 27/7/4, 8°) through the transplant were obtained at 1 every 2 seconds after an intravenous low-dose bolus of 1.5-mmol Gd-DTPA (3 mL Gd-DTPA solution). The relative increase in signal intensity ($RSI = SI_{post} - SI_{pre}/SI_{pre}$) in the iliac arteries, the cortex, and medulla was calculated over time. The cortex perfusion index [$CPI = (RSI_{max})^2/RSI_{15\,seconds\,after\ RSImax}$] was used for mathematical description of cortical bolus transit.

Results: In all cases, arteries presented a sharp signal intensity peak confirming the shape of the bolus given. Median CPI in patients with acute rejection (1.8; range, 7.2) was significantly lower compared with all other transplants (8.1; range, 9.6, Kruskal-Wallis analysis, $P < .001$). However, CPI values were unable to differentiate between acute tubular necrosis, chronic rejection, cyclosporin A nephrotoxicity, and cytomegalovirus infection. A good correlation was found between the slope of medullary enhancement and serum creatinine ($r = -.72$, Spearman rank correlation coefficient) and also creatinine clearance ($r = .68$).

Conclusion: Low-dose Gd-DTPA–enhanced snapshot FLASH MR imaging can separate acute rejection from other causes of renal transplant dysfunction.

P232

Use of Fast Spin Echo in the Dynamic Study of the Pituitary Gland

Y Kawamura, GK Sze
Yale University School of Medicine, New Haven, CT

Purpose: To determine if the fast-spin-echo (FSE) technique used in dynamic fusion could increase the detectability of pituitary microadenomas, phantom experiment and dynamic pituitary imaging were performed with both FSE and conventional SE (CSE) techniques.

Methods: MR imaging of agar gel phantoms containing different concentrations of Gd-DTPA was performed with FSE (550/14, matrix 192, echo train 8, and echo spacing 14) and CSE technique (200/23, matrix 128). Thirty-six cases of suspected pituitary lesions were studied with FSE technique and 20 cases with CSE technique. After bolus injection of Gd-DTPA, 8 sequential acquisitions of 26 seconds each were obtained. Dynamic signal intensity change, image quality, and lesion detection were evaluated separately by 2 neuroradiologists. Contrast-to-noise ratios (C/N) were calculated in the phantom and in 17 definite adenoma cases.

Results: Dynamic signal intensity change was identical with both sequences. Readers preferred the FSE technique due to better resolution and less susceptible artifact. Although lesion detection was similar, lesion borders were better evaluated with CSE. Better C/Ns were also seen with CSE in 77.8% of cases due to larger signal intensity differences between the adenoma and the pituitary gland and lower background noises. The phantom study supported clinical results.

Conclusion: Although the dynamic FSE technique had superior resolution and was preferred for image quality, contrast between the normal pituitary gland and the adenoma was greater with the dynamic CSE technique.

P233

Evaluation of a Fast Spin-Echo Sequence for the Liver

EK Outwater, DG Mitchell
Department of Radiology, Thomas Jefferson University Hospital, Philadelphia, PA

Purpose: Fast spin-echo (FSE) pulse sequences have the potential to provide T2-weighted images with higher signal per unit time for imaging of the abdomen. In this report, the authors provide a quantitative assessment of an FSE imaging strategy for imaging the upper abdomen, that of using high-resolution matrices and very long TR, with a comparison with conventional SE sequences.

Methods: Twenty patients with known or suspected liver disease were imaged with conventional SE sequences (dual echo 2,500–3,000/50, 100, 128 × 256 acquisition matrix, 2 excitations) and FSE sequences (6,000–8,000/102, 512 × 256 acquisition matrix, 4 excitations, 16-echo train length) at identical field of view and section positions. Signal intensity measurements were made for liver, spleen, pancreas, kidney, muscle, fat, noise, and liver lesions for the 2 sequences.

Results: Mean signal-to-noise ratio (S/N) for the normal organs (excluding fat) for FSE sequences bore a linear relationship to the mean S/N for the SE sequences. Despite having a nominal predicted S/N advantage of 2.8:1 (based on differences in voxel size and number of excitations) compared with FSE, the empirical S/N advantage was 1.2–1.5 for normal tissues (excluding fat). The mean signal intensity ratios (compared with that of liver) for the tissues were all higher for the FSE sequences than the SE sequences. FSE sequences also produced higher mean SIR for cysts (20 cysts in 2 patients) and hemangiomas (12 hemangiomas in 3 patients), but not malignant liver tumors (26 tumors in 6 patients).

Conclusion: Although many mechanisms act to alter contrast of FSE compared with SE, normal abdominal tissues, except fat, show similar contrast with the 2 imaging sequences.

P234

Fat and Water Quantification in Spine and Knee with Inner Volume Spectroscopic CPMG Sequences and Automated Postprocessing

RV Mulkern, J Meng, D Jaramillo, K Oshio
Department of Radiology, Harvard Medical School, Boston, MA

Purpose: To demonstrate efficient acquisition and postprocessing methods for quantifying intravoxel relative fat-water contents and spectral T2 values in bone marrow of spine and knee.

Methods: Section-selective Carr-Purcell-Meiboom-Gill (CPMG) trains use an inner volume excitation scheme to acquire echoes from 5 × 5 mm columns. Echo readouts without imaging gradients provide a spectral resolution of 32 Hz per pixel. Spatial encoding along columns is performed with standard phase encoding. With a 2-sec TR, data from 128 5 × 5 × 1.2-mm voxels along each of 5 columns at 8 TEs (43-msec echo spacing) are collected in 4 minutes and 16 seconds. Automated postprocessing serves to (1) fit the 5,120 spectra to 2-peak Gaussians; (2) fit resulting area versus TE curves with monoexponential functions to obtain spectral T2 values and relative fat-water concentrations at 0 TE; (3) redisplay calculated parameters as a function of position along columns.

Results: Tested in fat-water phantoms of known mixtures of mayonnaise and agar gels, the methods yielded an excellent correlation between MR-measured fat-water percentages and true percentages (slope = 1.03, cc = 0.99). Data sets of lumbar spines from healthy adult volunteers revealed vertebral body fat contents of 60% ± 3 and fat-water T2 values of 93 msec ± 9 and 57 msec ± 8, respectively. Knee marrow in healthy adults had 91% ± 6 fat, with fat-water T2 values of 114 msec ± 10 and 90 msec ± 36, respectively.

Conclusion: An efficient method for extracting relative fat-water content and spectral T2 values throughout extensive regions of bone marrow in spine and knee has been demonstrated. The first clinical application will be in leukemic patients undergoing chemotherapy.

P235

Breath-Hold 2D T1-weighted MP-RAGE Imaging of Focal Liver Lesions: Comparison with Conventional T2-weighted SE Imaging

EE de Lange, JP Mugler, JE Bosworth, GA DeAngelis, JM Rosenblatt, LW Merickel, EK Harris
Department of Radiology, University of Virginia Health Sciences, Charlottesville, VA

Purpose: The authors developed a 2D T1-weighted MP-RAGE technique with a section-selective preparation pulse that allows the acquisition of multiple images during a single breath hold. This technique was compared with conventional T2-weighted SE imaging in detecting liver lesions.

Methods: The liver MR images of 68 consecutive patients with proved disease were reviewed. In each patient, 4 sets of 15 sections were obtained: coronal, sagittal, and axial T1-weighted MP-RAGE (TI/TR/TE = 200–350/9/4, 10°) images (each set in a 19–20-second breath hold), and axial T2-weighted SE (2,500/120) images (in 12 minutes during breathing). The sets were pooled and reviewed in random order by 4 independent reviewers. A fifth set of images was also reviewed consisting of the coronal, sagittal, and axial (3-plane) T1-MP-RAGE images combined. The number and size of lesions were determined as well as reviewer confidence. All images were also reviewed by 3 reviewers in consensus. Statistical evaluation was performed by using fuzzy-set logic receiver operating characteristic analysis.

Results: The total number of lesions, and particularly the number of small (< 1.0 cm) lesions detected on all T1-MP-RAGE image sets was greater than on T2-SE images ($P < .01$). The diagnostic accuracy of the 3-plane T1-MP-RAGE images was significantly better than that of the 1-plane T1-MP-RAGE techniques and much better than that of T2-SE imaging. Reviewer confidence in detecting lesions was significantly greater for the 3-plane T1-MP-RAGE method than with 1-plane T1-MP-RAGE and T2-SE imaging ($P < .01$). Motion artifacts influenced reviewer confidence most on T2-SE images ($P < .01$).

Conclusion: Detection of liver lesions, particularly small ones, was significantly better on breath-hold T1-MP-RAGE than on T2-SE images. The diagnostic accuracy in detecting lesions, as well as reviewer confidence, were significantly greater with 3-plane T1- MP-RAGE imaging.

P236

Contrast-to-Noise Ratio Efficiency of T1-weighted 3D Gradient Echo versus 2D Multisection Spin Echo

AP Crawley, CJ Wallace, LJ Hahn
Department of Radiology, University of Calgary, MRI Center, Calgary, ALberta, Canada

Purpose: Three-dimensional gradient-echo (GRE) images produce T1-weighted images with excellent contrast-to-noise ratio (C/N). However, conventional spin-echo (SE) images are often still used as the method of choice. The purpose of this work was to compare the C/N efficiency of these methods.

Methods: The authors compared a 3D GRE (35/5, 35°) and 2D SE (600/17) sequence. To separate the effect of different TRs from the effect of gradient versus spin echoes, a 2D GRE (600/5, 90°) sequence was evaluated. SNR efficiency was defined as $\mathrm{SNR}/\sqrt{\mathrm{TR}}$, for optimal $\alpha = \alpha_{\mathrm{opt}}(\mathrm{TR}/\mathrm{T1})$. C/N efficiency was defined equivalently. The SNR and C/N efficiencies were calculated over a range of TRs.

Results: The SNR efficiency of the 3D GRE images was higher than that of an SE image by a factor of 1.3–1.5 (white-gray matter) at equal resolution and section thickness. The C/N efficiency for white-gray matter was higher by a factor of 2.7. The SNR efficiency of the 3D GRE image was only slightly higher than that of the 2D GRE (TR = 600) image by a factor of 1.0–1.1 (gray-white matter), in agreement with theoretical calculations. Experiments using various concentrations of gadolinium confirmed a minor dependence on TR but demonstrated a 1.4 times higher SNR efficiency for the 2D GRE (TR = 600) image compared with that of the SE image.

Conclusion: The higher SNR and C/N efficiencies of GRE images are due primarily to the use of GRE rather than SE. The large difference cannot be explained by the shorter TE (given known T2 and $T2^*$) and appears to be primarily due to the absence of a section-selective refocusing pulse.

P237

Improved Fast Spin-Echo Imaging with Data Conjugation

HE Avram, L Kaufman
Toshiba America, South San Francisco, CA

Purpose: To improve the efficiency of fast spin-echo (FSE) techniques by acquiring about half of k space along the phase-encoding direction. FSE techniques acquire a train of individually encoded spin echoes. The typical number of echoes acquired can be as high as 16. For such a long echo train and for a typical brain T2 of 70 msec at middle field strength and a TE per echo of 15 msec, the last echo amplitude is 3% of the signal intensity of the first. For muscle (T2 = 26 msec), this number is less than 0.01%. This figure is even lower if we consider that there is an extra signal loss with increasing number of echoes caused by section selection. These 2 factors reduce the efficiency of FSE for a large number of echoes. In addition, an increase in the number of echoes is followed by a broadening of the point spread function with the consequent loss of spatial resolution. A way to reduce the effect of these 2 factors is to reduce the TE per echo, thereby acquiring the echoes in a shorter time. This approach is limited by hardware, and a TE of 15 msec is a standard value for commercial imagers today.

Methods: A realistic approach is to acquire about half the phase-encoding steps and generate the rest of k space by conjugation. The latter also offers the advantage of more coverage by reducing the time per section. This approach was used with 3 different phase-encoding schemes: low pass (emphasizes low frequencies), high pass (emphasizes high frequencies), and Ramp, which is an intermediate case. The parameters used were TE per echo = 18 msec, TR = 2 seconds, N = 1, gradient duty cycle 50%, resolution 0.95 × 0.95 × 10 mm (256 × 256) at 0.35 T. Groups of 5, 8, 16, 4 + 4, and 8 + 8 echoes were used. The latter for double-echo mode. Conjugation is used to either reduce imaging time or increase coverage.

Results: In the brain, compared with standard FSE single-echo mode, 91% of the time data conjugation of 57% of k space increases coverage by 60%, with an S/N drop of 12% for same TE_{eff}. Water experiments show that conjugation introduces about a 15% drop in S/N. For a double-echo scheme in 113% of the time, coverage could be increased by 100%.

Conclusion: Data conjugation can be applied to FSE sequences. It provides clinically useful images with increased coverage.

P238

Whole-Head High-Resolution T2-weighted 3D MP-RAGE Imaging in under 10 Minutes

JP Mugler, JR Brookeman

MRI Facility, University of Virginia Health Sciences Center, Charlottesville, VA

Purpose: To develop and implement a 3D pulse sequence based on the magnetization-prepared rapid gradient-echo (MP-RAGE) technique, capable of acquiring high-resolution (128 × 128 × 256) T2-weighted image sets of the whole head in under 10 minutes.

Methods: The feasibility of acquiring 32 × 128 × 256 T2-weighted data sets in 4.3 minutes has been demonstrated by using a driven equilibrium pulse set (90°-180°-90°) for the preparation in a 3D MP-RAGE sequence. Extending this implementation, a 128 × 128 × 256 acquisition would require over 17 minutes. Recent improvements in imager software have allowed the maximum number of phase encodes per prepare-acquire-recover sequence cycle to be increased from 32 to 128 when preparatory gradients are required to compensate for preparation pulse imperfections and eddy currents. We implemented T2-weighted 3D MP-RAGE on a 1.5-T whole-body imager (Siemens Magnetom 63SP), by using a driven equilibrium preparation (TE = 50 ms), 128 phase encodes per sequence cycle with gradient preparation (5° FLASH acquisition, TR/TE = 12/5, centric phase encoding), and a 2-second recovery period. The sequence was tested in volunteers.

Results: High-resolution 3D data sets demonstrating good image quality and T2-weighted contrast were obtained in imaging times of 7.5 minutes. Image contrast was similar to that obtained with long TR/TE SE.

Conclusion: High-resolution T2-weighted 3D data sets of the whole head were acquired in under 10 minutes with 3D MP-RAGE. The authors are currently investigating potential clinical applications and the use of shaped signal responses for achieving increased signal-to-noise ratios.

P239

Breath-hold Interleaved Spin-Echo Echo-Planar Imaging of the Abdomen

K Butts, SJ Riederer

MR Research Laboratory, Mayo Clinic, Rochester, MN

Purpose: Conventional T2-weighted spin-echo (SE) images of the abdomen give excellent liver-lesion contrast but are susceptible to respiratory artifacts due to long imaging times. The purpose of this work was to implement on a commercial imager a multisection interleaved SE echo-planar imaging (EPI) sequence that acquires T2-weighted images (2,000/85) within a breath hold.

Methods: The pulse sequence acquires 8 shots of 16 echoes with 256 points each over a field of view of 32 × 24 cm, thereby producing in-plane resolution of 1.25 × 1.875 mm in an imaging time of 16 seconds. The sampling bandwidth used is 64 kHz. Fat saturation and spatial saturation of flowing spins are both used.

Results: Results in healthy volunteers show excellent spleen-liver contrast, comparable to that on standard T2-weighted SE images. The anatomy is well depicted with no degradation due to respiratory motion. The in-plane vasculature is also well defined, although vessels appear slightly larger on the interleaved EPI image than on a standard SE image, due to previously described flow effects (1).

Conclusion: Imaging of the abdomen within a breath hold increases lesion conspicuity by alleviating respiratory artifacts. The use of standard gradient hardware makes this technique accessible to standard imaging systems. More important, the approximate 8-fold reduced bandwidth provides improved signal-to-noise ratio compared with that obtained with customized EPI systems. Future work will include studies on the image quality of interleaved EPI in the clinical arena.

1. Butts RK, Riederer SJ. JMRI 1992; 2(3).

P240

Adaptive MR Imaging with Wavelet Transform Encoding

LP Panych, FA Jolesz

Radiology Department-MRI Division, Brigham and Women's Hospital, Boston, MA

Purpose: New applications of MR imaging such as the monitoring of surgical processes necessitate the rapid refreshing of image data in time. The authors have recently succeeded in implementing wavelet encoding of images and are now investigating its usefulness for adaptive imaging of such time-varying processes. Because wavelet transform encoding provides the capability of selectively resolving images in space, it may provide a more optimal approach to imaging in these applications.

Methods: Low-resolution wavelet coefficients can be used to determine if the denser high-resolution data need to be collected and thereby derive a data compression algorithm. The authors exploit the unique noise characteristics in MR wavelet encoding and designed a filter to adapt this algorithm for MR data encoding. Specifically, the weight, k_l, given to a new measurement of a wavelet-encoded value at the resolution level l is $k\_l = V/(V + N\_l)$, where N_l is the measurement noise power at the level of resolution and V is the signal power of the wavelet value at the lower resolution. Wavelet data is encoded from low to high resolution until V reaches the noise level. Because N_l increases with resolution, the algorithm is stable.

Results and Conclusion: Simulations of imaging experiments of dynamic, time-varying processes show that less than one-third of the data normally acquired in Fourier transform encoding may be all that is necessary to acquire if wavelet encoding is used to update the image. The amount of data compression is greatest when change is confined to 1 region of the imaged volume.

Wednesday, March 31, 12:15 PM–1:00 PM
CONTRAST AGENTS, SPECTROSCOPY, OTHER NUCLEI

Posters P301–P335

P301

Utility of Motor Coordination Tasks to Assess the Neurotoxicity of Intracisternally Injected Paramagnetic Chelates in Rats

WH Ralston, KP Galen, MD Adams
Mallinckrodt Medical, Inc, St Louis, MO

Purpose: Previous intracisternal median lethal dose (LD50) studies showed a disparity between the comparative morbidity and mortality of 2 paramagnetic chelates, Gd-DTPA and Gd-DTPA-BMEA. The objective of the present study was to examine the utility of motor coordination tasks, as an alternative to lethality estimates, to assess the relative neurotoxicity of intracisternally injected paramagnetic chelates at sublethal doses.

Methods: Lightly etherized, task-acclimated rats were injected intracisternally, at 5 per dose, with 50, 100, or 150 μmol/kg (0.5 mol/L) Gd-DTPA or Gd-DTPA-BMEA. Control rats received 0.03 mL/kg 0.9% saline. Prior to and at 0.5, 1, 2, 4, and 24 hours and at 4 and 7 days after injection, the rats were evaluated for motor coordination deficits in hind-limb grasp reflex, inclined-screen orientation, and balance-beam tasks.

Results: As the test substance doses and complexity of the tasks increased, there were more significant decreases in task scores. In general, test animal performance scores were lower than saline controls over the first 4 hours, then eventually returned to control levels between 24 hours and 4 days. A biphasic response, evidenced by an initial deficit followed by recovery and latent deficit after 24 hours, occurred with 150 μmol/kg Gd-DTPA. The latent deficit, at 150 μmol/kg Gd-DTPA, was consistent with the development of a progressive hind-limb paralysis between 1 and 4 days after injection.

Conclusion: Neurobehavioral tests provided a quantitative method by which to examine dose-related and contrast agent-related effects at sublethal doses of intracisternally injected MR contrast media.

The authors are employees of Mallinckrodt, Inc.

P302

Microencapsulation of Fluorinated Hydrocarbons for MR Contrast Agents

AG Webb, RL Magin, MW Grinstaff, KS Suslick
Bioacoustics Research Laboratory, Department of Electrical and Computer Engineering, University of Illinois, Urbana, IL

Purpose: The detection of tumors in the liver and spleen is enhanced by using particulate MR contrast agents that reduce the proton T2. The authors have developed a more direct approach by using fluorocarbon-filled microcapsules, where now the particle itself is the source of the signal.

Methods: Experiments were performed at 4.7 T with a double-tuned RF coil. Rats were injected intravenously 12 hours before imaging with 2 mL of microcapsules containing perfluorinated nonane (7 g/kg F-19 nonane). Microencapulation used high-intensity ultrasound irradiation of a 1:3 (v/v) mixture of F-19 nonane with 5% (w/v) aqueous BSA solutions. Particle size distribution was determined with an Elzone particle counter, showing an average diameter of 2.5 μm with narrow size distribution.

Results: Proton images were sited through the liver. Selective excitation of the methylene fluorines was used with a TE of 6 msec and a TR of 2 seconds to obtain fluorine projection images. Total imaging time was 8.5 minutes. Exact correspondence was found between the images, showing high fluorine signal intensity from the liver and spleen. The expected distribution of the microcapsules was confirmed by F-19 spectra from excised organs.

Conclusion: Proteinaceous microspheres filled with F-19 nonane have been formulated with physical and chemical properties suitable for their use as a contrast agent, targeting the liver and spleen in sufficient concentration to allow F-19 MR imaging.

P303

Gd-DOTA–enhanced Subsecond FLASH MR Imaging of the Postoperative Aorta

A Deligvette, D Reuel, P Loubeyre, C Baldy-Poucher, P Douek, M Amiel
Hôpital Cardiologie, Lyon, France

Purpose: Subsecond MR imaging with intravenous bolus injection of Gd-DOTA (Dotarem; Laboratoire Guerbet) allows the detection of postoperative complications after thoracic aortic surgery.

Methods: Seventeen patients were studied after surgery for aortic dissection ([AD] $n = 13$) and for aortic valve replacement ([AVR] $n = 4$) on a 1.5-T Magnetom SP 63 Magnet (Siemens, Erlangen). After SE transverse section localization, sagittal images were obtained with a strongly T1-weighted TurboFLASH sequence (TR/TE/TI = 6.5/3/300, 11°) and compared with cine MR images of the aorta obtained with a FLASH sequence in the same plane (left anterior oblique projection).

Results: Among the 13 patients followed after AD surgery, in 5 cases Gd-DOTA–enhanced TurboFLASH MR imaging was more appropriate than cine MR imaging to detect persistent perfusion in the false channel or abnormal perfusion surrounding the prosthetic tube. Among the 4 patients followed up after AVR, only Gd-DOTA–enhanced MR imaging was able to demonstrate a circulating aortic false aneurysm at the site of the aortotomy in 1 case.

Conclusion: For the postsurgical follow-up of aortic diseases, Gd-DOTA–enhanced subsecond (TurboFLASH) MR imaging seems to be appropriate in addition to cine MR imaging for the diagnosis of potential complications.

P304

MR Imaging Contrast Enhancement of Dopamine Derivatives of Gd-DTPA

DL White, RG Eason, R Lin
Department of Radiology, University of California, San Francisco, CA

Purpose: As part of a continuing investigation of the effect of chemical structure on the enhancement pattern of MR contrast agents, the authors have prepared the DTPA-bis(amide) of both dopamine [2-(3,4-dihydroxyphenyl)-ethylamine] [$(\text{DHPE})_2$] and methyl-protected dopamine [2-(3,4-dimethoxyphenyl)ethylamine] [$(\text{DMPE})_2$] and examined the MR imaging contrast enhancement behavior of their gadolinium (III) chelates.

Methods: DTPA-$(\text{DHPE})_2$ and DTPA-$(\text{DMPE})_2$ were prepared from DTPA-bis(anhydride) and 2 equivalents of the corresponding amine. The gadolinium (III) chelates were prepared by reaction of each ligand with 1 equivalent of GdCl_3. The identities of ligand and chelates were confirmed with mass spectrometry. Nongated, T1-weighted MR images were obtained with a GE CSI 2-T imager: SE 300/6; 4 NEX; 128 × 256; 3-mm section; 90-mm field of view. Sprague-Dawley rats (250–350 g; $n = 4$) received intravenously 0.1 mmol/kg contrast agent. Relaxivities were measured at 0.25 T and 37°C in pH 7.4 aqueous 0.1 mol/L HEPES buffer.

Results: R1 values for Gd-DTPA-(DHPE)$_2$ and Gd-DTPA-(DMPE)$_2$ were 4.5 and 4.4, respectively. Gd-DTPA-(DHPE)$_2$ gave significantly higher enhancement in the heart for up to 20 minutes after injection relative to Gd-DTPA-(DMPE)$_2$ (at 10 minutes: 64% ± 23 vs 29% ± 5). Lung enhancement also appeared to be higher for the former compound (at 5 minutes: 188% ± 50 vs 141% ± 5), but the variances were high. Liver, muscle, and kidney enhancements were not significantly different for the 2 agents at any point during the 90-minute course of the experiment.

Conclusion: Gd-DTPA-(DHPE)$_2$ displays potentially useful contrast enhancement in the heart. The mechanism of this apparent localization is as yet undetermined. The increased heart enhancement produced by Gd-DTPA-(DHPE)$_2$ may be due to its binding to dopamine receptors, but any significant binding might be expected to cause more profound physiologic effects (eg, death) than those observed. The catechol derivative is easily oxidized compared with its methylated analog. The different pattern of enhancement may be related to this difference in oxidative stability and concomitant changes in coordination of the gadolinium.

The support of this work by Molecular Biosystems, Inc, is gratefully acknowledged. D.L. White has a research contract with Molecular Biosystems.

P305

Evaluation of BMS 180549, an Ultrasmall Superparamagnetic Iron Oxide Particle, as a Contrast Agent in Liver MR Imaging: Results in an Abscess Model

VM Runge, JE Kirsch, JN Dunworth, JW Wells, CE Woolfolk
MRISC, University of Kentucky, Lexington, KY

Purpose: An ultrasmall superparamagnetic iron oxide particle (BMS 180549), previously investigated for lymph node imaging, was evaluated as a liver contrast agent for MR imaging in an abscess model.

Methods: Nine rabbits with a liver abscess were studied with MR imaging at 1.5 T prior to and at 10 and 60 minutes after intravenous injection. T2-weighted SE and fast SE techniques were used for contrast agent visualization. Five animals were evaluated at 0.8 mg Fe/kg, with a dose range study ($n = 1$ at each dose) performed to include 0.3, 0.6, 1.1, and 1.7 mg Fe/kg. Lesion detectability was assessed by means of region-of-interest measurements, with results compared with those from 24 animals studied by using dynamic gadoteridol-enhanced T1-weighted imaging.

Results: At 0.8 mg Fe/kg, liver signal intensity decreased by 79% ± 5 at 10 minutes and 82% ± 6 at 60 minutes after injection with SE imaging. No statistically significant change in lesion signal intensity was observed after injection. A 94% increase in liver-lesion contrast was observed after injection with breath-hold fast SE imaging. No dose effect was demonstrated within the range evaluated, indicating liver saturation. In comparison, enhancement with gadoteridol at 0.5 mmol/kg resulted in a 130% increase in liver-lesion contrast, with this result strongly dose dependent.

Conclusion: BMS 180549 substantially improves lesion detection in an experimental liver abscess model, with results comparable to those with high-dose gadoteridol.

This research was supported in part by a scientific grant from Squibb Diagnostics.

P306

Tumor-specific Boronated Metalloporphyrin for MR Imaging Contrast Enhancement

LR Huang, RM Straubinger, SB Kahl, R Mazurchuk, SJ Thamer, RI Chau, RJ Fiel
Department of Biophysics, Roswell Park Cancer Institute, Buffalo, NY

Purpose: Contrast agents currently in use or under clinical investigation do not localize specifically in tumors. In this report, the authors show that the manganese chelate of a boronated porphyrin, tetrakiscarborane carboxylate ester of 2,4-(α,β-dihydroxyethyl)deuteroporphyrin IX (Mn-BOPP), originally designed for boron neutron capture therapy (BNCT), is an effective tumor-specific contrast agent in rat 9L glioma and may therefore serve as an agent for both contrast enhancement and BNCT.

Methods: SE images (400/20) before and after injection of Mn-BOPP (0.02 mmol/kg) were obtained at different time points over a period of 4 days by using a custom-built stereotaxic head coil at 1.5 T. Postcontrast high-resolution (0.3 × 0.3 × 0.7-mm voxel size) T1-weighted volume images (spoiled-gradient-recalled sequence, 240/9, and flip angle 85°) were also obtained.

Results: The immediate postcontrast SE images (3.0-mm section thickness) showed the tumor as slightly enhanced and the blood pool significantly enhanced. At 24 hours, the tumor-normal brain contrast reached the maximum ($SI_{tumor}/SI_{normal} = 1.6$), but tumor enhancement was sustained up to 92 hours. A hypointense border anterior to the tumor shown on SE and volume images was determined to be a region of the anterior cortex compressed by the tumor. Greater morphologic details of the tumor and the normal brain were revealed by the thin-section (0.7 mm) volume images.

Conclusion: Mn-BOPP is an effective tumor-specific contrast agent in the rat 9L glioma even at a very low dose and is the first example of a potential dual-function agent for cancer diagnosis and therapy.

P307

MR Contrast Enhancement of 9L Glioma with Low-Dose Mn-TPPS$_4$ at 1.5 T

LR Huang, RM Straubinger, R Mazurchuk, RI Chau, SL Thamer, RJ Fiel
Department of Biophysics, Roswell Park Cancer Institute, Buffalo, NY

Purpose: In spite of its ability to localize in tumors and enhance the signal intensity on MR images, the limitation of manganese-(III)tetraphenylporphine sulfonate (Mn-TPPS$_4$) appears to be its relatively poor ratio of effective-to-toxic dose. This study was designed to investigate the effectiveness of Mn-TPPS$_4$ contrast enhancement on images of rat 9L glioma at a dose as low as 15 times less than the highest dose employed previously by these authors and others.

Methods: SE images (400/20) and volume images (spoiled-gradient-recalled sequence, 240/9, flip angle 85°, and 0.3 × 0.3 × 0.7-mm voxel size) before and after injection of Mn-TPPS$_4$ (at doses of 0.01, 0.02, and 0.04 mmol/kg) were obtained at 1.5 T by using a custom-built stereotaxic head coil.

Results: The tumor showed only a slight degree of enhancement on the SE images at 0.01 mmol/kg. At 0.02 mmol/kg, however, as early as 5 minutes after injection, the tumor was clearly delineated from normal tissue as a hyperintense region. Mn-TPPS$_4$ was well tolerated at this dose with no notable side effects. Contrast enhancement was maximal at 5 minutes (38% difference in tumor-normal tissue signal intensity); however, tumor enhancement was still apparent at 24 hours. The postcontrast volume imaging at 0.02 and 0.04 mmol/kg doses showed the tumor to be hyperintense and heterogeneous, with necrotic regions.

Conclusion: $Mn\text{-}TPPS_4$ is an effective tumor-specific contrast agent at doses significantly lower than previously thought. The authors believe this results in part from a combination of the high field strength used (1.5 T) and the high selectivity of $Mn\text{-}TPPS_4$ for the 9L glioma relative to normal brain tissue.

P308

Clinical Application of Superparamagnetic Iron Oxide for Evaluation of Hilar Cholangiocarcinoma

T Takahara, M Saeki, K Imamura, T Ishikawa
Department of Radiology, St Marianna University School of Medicine, Kawasaki, Japan

Purpose: To evaluate the potential of MR imaging with superparamagnetic iron oxide (AMI-25) in patients with hilar cholangiocarcinoma.

Methods: The authors analyzed MR images with and without AMI-25 in 3 patients with hilar cholangiocarcinoma and compared them with CT scans. The pulse sequences for SE images were 2,000/100 and 600/15. Breath-hold gradient-echo (GRE) images were used for evaluation of vascular invasion of the tumor. In each patient, 10 μmol Fe/kg of AMI-25 was administered intravenously for 30 minutes.

Results: Tumors were demonstrated on MR images in all 3 patients. However, only 1 tumor was identified on CT scans. On conventional MR images, cholangiocarcinomas were of low signal intensity on T1-weighted images and high signal intensity on T2-weighted images. Tumors were more clearly seen on AMI-25–enhanced MR images than on conventional MR images. Two cases of portal vein invasion were diagnosed with GRE images and confirmed with follow-up angiography.

Conclusion: MR imaging was superior to CT in detection and localization of tumors. Some reports said that bile duct dilatation, periportal abnormal intensity, and pseudoinfarction prevented the tumor from being seen on conventional MR images, especially T2-weighted images. AMI-25 showed a remarkable reduction of the signal intensity of the liver parenchyma; the areas of pseudoinfarction or edema that were hyperintense on T2-weighted images were enhanced with AMI-25. These preliminary results suggest that AMI-25–enhanced MR images are useful for evaluation of hilar cholangiocarcinoma.

P309

Tolerance and Pharmacokinetic Evaluation of Gd-BOPTA/Dimeg at High Doses in Healthy Volunteers

G Pirovano, V Lorusso, P Tirone, G Rosati
Research and Development Division, Bracco SpA, Milan, Italy

Purpose: Gd-BOPTA/Dimeg, a polyvalent intravascular MR contrast agent, has been proved to be well tolerated in man at intravenous doses ranging from 0.005 to 0.2 mmol/kg. The aim of this study was to evaluate the pharmacokinetics, safety, and tolerance of Gd-BOPTA/Dimeg, 0.5 mol/L solution at doses up to 0.4 mmol/kg.

Methods: Twelve healthy male volunteers received intravenously Gd-BOPTA/Dimeg (0.5 mol/L) at 0.2, 0.3, and 0.4 mmol/kg dose levels. Blood, urine, and feces samples were collected during 24–96 hours for the Gd-BOPTA/Dimeg assay. Meanwhile Gd-BOPTA/Dimeg safety and tolerance were studied.

Results: Plasmakinetics of Gd-BOPTA/Dimeg was well described with a biexponential function (distribution and elimination phases). At different dose levels, the main pharmacokinetic parameters were in the range of 0.45 to 0.65 hours for distribution half-life, 1.97–1.99 hours for elimination half-life, 0.259–0.269 $L \cdot kg^{-1}$ for apparent total volume of distribution, 0.090–0.096 $L \cdot kg^{-1}$ for total clearance, and 0.080–0.087 $L \cdot kg^{-1}$ for renal clearance. Gd-BOPTA/Dimeg was recovered unchanged in urine, corresponding to 89%–95% of the injected dose within 24 hours; 0.6%–3.5% of the dose was recovered in the feces. Vital signs, electrocardiograms, and laboratory tests did not show any clinically remarkable change. Three mild adverse events consisting of transient myalgia, cold sensation, giddiness, and nausea and an episode of diarrhea were observed (2 in the 0.3 mmol/kg dose group and 1 in the 0.4 mmol/kg dose group).

Conclusion: Gd-BOPTA/Dimeg is rapidly distributed and eliminated from plasma compartment. It is well tolerated and can be proposed as a safe MR contrast agent also for examinations where a high dose of contrast medium is required.

P310

Application of Delayed Imaging and Dose Increment in the Evaluation of Central Nervous System Metastatic Disease

ET Tali, WTC Yuh, H Nguyen, NA Mayr-Yuh, GP Farrar, DP Mueller, F Gao, TM Simonson, DJ Fisher
Department of Radiology, MR Division, University of Iowa Hospitals and Clinics, Iowa City, IA

Purpose: Detection of brain metastasis depends on reasonably high signal intensity of the lesion in relation to surrounding background, which can be improved with either a higher dose of contrast material or delayed imaging. The authors compared the effect of these 2 methods on the detection rate of central nervous system lesions of various sizes.

Methods: MR images enhanced with gadoteridol (ProHance; Squibb Diagnostics, Princeton, NJ) were obtained in 45 patients with brain metastases. Each patient received an initial bolus injection of either 0.05 (cumulative standard dose [CSD]) or 0.1 (cumulative high dose [CHD]) mmol/kg gadoteridol and was imaged immediately and at 10 and 20 minutes. At $t = 30$ minutes, an additional bolus injection of 0.05 (CSD) or 0.2 (CHD) mmol/kg was administered, and images were acquired immediately.

Results: There was no difference in the detection rate of lesions larger than 10 mm in both study groups with time delayed and higher dose criteria. T2-weighted images showed the same detection rate as the contrast-enhanced studies. For lesions less than 10 mm, improved detection was achieved in the delayed studies in both groups; however, delayed image acquisitions still depicted fewer lesions than did higher dose immediate studies.

Conclusion: Large lesions (> 10 mm) showed no difference in detection rate with either higher dose or delayed acquisition time in both groups. Delayed imaging and higher dose did affect the detection rate for the lesions that measured less than 10 mm in both groups, but higher dose immediate studies still remained superior to delayed studies for detecting small lesions.

P311

Sequential MR Imaging Enhancement Pattern in Normal Pituitary Gland and Pituitary Ademona

WTC Yuh, ET Tali, H Nguyen, DJ Fisher, GF Gao,
JP Turk, TM Simonson, JA Schlechte
Department of Radiology, MR Division, University of Iowa Hospitals and Clinics, Iowa City, IA

Purpose: To evaluate the enhancement characteristics of the normal pituitary gland and pituitary adenomas with improved time resolution.

Methods: Thirty-five healthy subjects and 10 patients with sellar pituitary adenomas were prospectively studied with dynamic contrast-enhanced MR imaging (spoiled gradient-echo, 25/13, 1–2 NEX, flip angle 50°) with a 5- or 10-second temporal resolution. Imaging was initiated 30–45 seconds before bolus injection of 0.1 mmol/kg Gd-DTPA by using either hand injection or an MR compatible injector (Medrad, Pittsburgh, PA) and continued for a total of 180 seconds. The images were reviewed visually and analyzed quantitatively.

Results: Qualitative visual analysis of the normal pituitary gland demonstrated a consistent sequential pattern of enhancement in which the posterior lobe enhanced earlier than the anterior lobe by an average of 35 seconds. Quantitative analysis revealed that in 35 healthy subjects posterior lobe enhancement occurred 10.9 seconds ± 1.83 (mean ± standard error) before the anterior lobe, whereas in patients with adenomas, tumor enhancement was noted to occur significantly ($P = .0001$, paired Student t test) before anterior lobe enhancement and slightly before posterior lobe enhancement.

Conclusion: The sequential enhancement pattern of the normal pituitary gland was found to be consistent with its vascular anatomy. The finding that enhancement of sellar pituitary adenomas occurred slightly before posterior lobe and significantly before anterior lobe enhancement contradicts previous reports. These findings suggest that sellar pituitary adenomas may have a direct arterial blood supply (neovasculature).

P312

MR Imaging and CT Findings of Brain Abscess in Patients with Bone Marrow Transplant

F Gao, WTC Yuh, ET Tali, H Nguyen, NA Mayr-Yuh,
DP Mueller, LJ Burn
Department of Radiology, MR Division, University of Iowa Hospitals and Clinics, Iowa City, IA

Purpose: To investigate MR imaging and CT findings of brain abscess in patients with bone marrow transplants (BMTs) and to correlate them with laboratory findings.

Methods: Eight BMT patients with MR imaging evidence of brain abscesses were reviewed retrospectively.

Results: Forty-two lesions were detected in 8 patients with documented infectious foci outside the brain, 6 patients had low and 2 patients had normal white blood cell counts (WBC) and/or lymphocyte counts. Thirty-eight lesions were detected in 6 patients with low WBC, and 28 lesions (4 patients) were studied with contrast-enhanced MR imaging. The majority of lesions (96%) demonstrated no appreciable edema or contrast enhancement. One patient who underwent 5 serial MR imaging and CT examinations showed progressive development of vasogenic edema and ring enhancement that correlated with the recovery of WBC to a normal level. A total of 4 lesions were detected in the 2 patients with normal WBC. All lesions had distinct vasogenic edema and ring enhancement. In 1 patient with normal WBC who underwent 4 serial examinations, the degree of enhancement and vasogenic edema was proportional to the WBC.

Conclusion: Brain abscesses in BMT patients exhibited negligible amounts of vasogenic edema and contrast enhancement during low WBC and lymphocyte count states. This may be related to a diminished immunologic or inflammatory response and relatively intact blood-brain barrier. With the rise in WBC and lymphocyte counts, suggestive of the recovery of the immunologic or inflammatory response, the abscesses developed vasogenic edema and contrast enhancement typically seen in immunocompetent patients.

P313

MR Imaging of Liver with AMI-25: Potential Pitfalls and Benefits in Differential Diagnosis

TW Chan, CS Leong
Department of Radiology, University of Chicago, Chicago, IL

Purpose: AMI-25 (Ferumoxides), a superparamagnetic iron oxide contrast agent, has previously been shown to be useful in liver MR imaging. The authors report their experience with a recent clinical trial of the new formulation (code 7035) with emphasis on the potential pitfalls as well as benefits in differential diagnosis.

Methods: Thirteen patients with focal liver lesions were imaged with a 1.5-T imager by using T1-weighted SE 300/12 and proton-density– and T2-weighted SE 2,500/40, 80 sequences. A slow infusion of 10 μmol/kg AMI-25 was administered, followed by postcontrast MR imaging 1–4 hours later.

Results: Of a total of 29 lesions that were hypointense to liver on the precontrast T1-weighted images, 8 (27.6%) became isointense (ie, not detectable) while 3 (10.3%) appeared hyperintense on the contrast-enhanced T1-weighted images. Furthermore, 4 of the remaining 18 hypointense lesions became less conspicuous. With the T2-weighted sequences, 2 hypointense, hemorrhagic metastases became isointense on the postcontrast images. One low-signal-intensity lesion in the spleen on precontrast images appeared hyperintense on the postcontrast T2-weighted images. In 2/2 hemangiomas, the postcontrast signal intensity decreased by 31%, possibly due to residual contrast material in the blood pool. Of 2 cirrhotic patients with suspicious heterogeneous signal intensity, 1 showed uptake of contrast material, suggesting regenerating nodules, while the other did not, suggesting diffuse hepatocellular carcinoma.

Conclusion: Evaluation of the precontrast MR images is important, as lesions can become isointense or take on apparently different signal intensity characteristics on the AMI-25–enhanced MR images. Furthermore, the change in signal intensity of lesions after administration of contrast material may potentially aid in differential diagnosis.

P314

Serial Contrast-enhanced MR Images in Multiple Sclerosis of Brain and Spinal Cord: Radiologic and Clinical Importance

MA Mikhael, MT Gorey, MM Mikhael
Department of Radiology, Evanston Hospital, Evanston, IL

Purpose: Radiologic detection of active multiple sclerosis (MS) disease, which necessitates treatment, and the correlation between the efficiency of treatment and the regression of the disease. What is the optimum neuroimaging study?

Methods: Fifty-eight cases of suspected MS were studied with MR imaging before and after gadolinium enhancement. Serial studies for positive cases (22 cases) were obtained every 2 weeks. Of the 22 cases, 15 showed active disease in the brain and spinal cord, 2 cases in cervical cord only, and 5 cases in the brain only.

Results: For confirmation of clinical diagnosis of MS, a T2-weighted image (2000/70) of brain and spinal cord was needed. For differentiation of old from active acute plaques that require aggressive medical treatment, it was important to obtain contrast-enhanced MR images (600/20). Active acute plaques showed enhancement with Gd-DTPA injection. Serial contrast-enhanced MR images in patients receiving no treatment showed active plaque to gradually lose its clearly delineated margins and high signal intensity after the 4th week and to completely lose enhancement after 8 weeks. The segment of spinal cord that showed enhancement was usually swollen. Swelling of spinal cord lags behind loss of enhancement of the plaque. Enhanced active plaque on top of chronic disease in the brain had a characteristic location most of the time, at the margin of an old nonenhanced lesion, an important finding for differentiation from infarctions. With successful treatment, periods of regression of enhancement are shortened.

Conclusion: For confirmation of clinical diagnosis of MS, a T2-weighted MR image is needed to visualize the plaques. Gadolinium is useful as a marker for new and clinically active lesions and should be used to follow up the efficiency of medical treatment. In this series, the correlation between symptomatology and enhancement showed that the disappearance of enhancement slightly lags behind clinical improvement.

P315

Use of Gd-DTPA to Improve Lesion Visibility in Ultrasound Surgery

A Darkazanli, KH Hynynen, EC Unger, CA Damianou, JF Schenck
Department of Radiology-MRI, Arizona Health Sciences Center, University of Arizona, Tucson, AZ

Purpose: MR imaging has been successful in monitoring lesion creation in rabbit hind muscle during localized ultrasound sonication. It is desirable to accurately determine the extent of the damage caused by sonication. Gd-DTPA was used as a contrast agent to improve the edge definition of the lesions.

Methods: Four rabbits were used in this experiment. Experiments were carried out inside a clinical MR imager. Ultrasound was used to induce in vivo lesions under the guidance of MR imaging. Gd-DTPA was then administered intravenously at a dose of 0.6 mmol/kg. Lesions were created at 15-minute intervals. Signal intensities were then examined statistically, and a time constant was determined to describe the contrast agent washout and its effect on visibility of lesions. The GRASS pulse sequence (100/5, 60° flip angle) was used in these imaging experiments.

Results: Signal intensity of the muscle was reduced by 25% on the application of heat prior to administering the contrast agent and by 35% after administration of the contrast agent. The washout time constant of the contrast agent was 28 minutes ± 2 in the hind muscle fibers. The lesions were visible faster when produced after administration of contrast agent. Gd-DTPA also improved the edge definition of the extent of the damage.

Conclusion: The use of contrast agent gave positive results in improving the visibility of lesions due to ultrasound heating. The agents can be used either prior to sonication to improve the localization of the focal point or after sonication to determine the boundaries of the treated area. Use of the contrast agent twice (before and after) proved to be useless, as an increase in signal intensity of the muscle would make the lesion invisible and isointense with background muscle.

P316

Monitoring Sodium Flux during Focal Ischemia in the Rat Brain with Triple-Quantum Filtered Spectroscopic Imaging

L Li, CH Sotak, K Minematsu, M Fisher
Department of Biomedical Engineering, Worcester Polytechnic Institute, Worcester, MA

Purpose: The differential MR visibility between intra- and extracellular sodium observed with multiple-quantum MR methods can potentially be used to monitor sodium flux during ischemia. Triple-quantum filtered (TQF) spectroscopic imaging was used to monitor changes in sodium signal intensity in the ischemic region with the goal of studying the role of sodium in stroke.

Methods: Focal brain ischemia was achieved by using an intraluminal suture MCA-occlusion model in rats. An H-1/Na-23 surface coil was placed over the surgically exposed skull for H-1 diffusion-weighted imaging (DWI) and sodium TQF spectroscopic imaging. Data were obtained at 2.0 T.

Results: Sections (2 mm) from sagittal 1D TQF spectroscopic imaging in the ischemic region (visualized with DWI) showed an average 40% increase in the TQF sodium signal intensity at 1.5 hours after occlusion, compared with that of the contralateral side. After the rats were killed, the contralateral TQF sodium signal intensity was equal to the level in the ischemic region, which remained unchanged after death.

Conclusion: Increased TQF sodium signal intensity in the ischemic region is consistent with increased intracellular sodium, which is thought to contribute to cytotoxic edema. This model should allow the study of therapeutic interventions that prevent the influx of sodium during ischemia or reverse the process.

P317

In Vivo Oxygenation Mapping with Inversion-Recovery Echo-Planar Imaging and F-19 Relaxometry of Perfluorocarbon Emulsions

BJ Dardzinski, CH Sotak
Department of Biomedical Engineering, Worcester Polytechnic Institute, Worcester, MA

Purpose: To map oxygen tension in vivo by using F-19 echo-planar imaging (EPI) of sequestered perfluorocarbon (PFC) emulsions. This technique allows rapid spatial mapping of oxygen tension. Preliminary validation of this method was performed in the liver and spleen in mice breathing air and pure oxygen.

Methods: Sagittal projection EPI of F-44E PFC emulsions sequestered in the liver and spleen of C3H mice was performed at 2.0 T. A 3-parameter nonlinear fitting algorithm was used to calculated the relaxation rate (R1) on a pixel-by-pixel basis. The R1 values and the corresponding Po_2 values were then displayed as an image (map) that allows the spatial distribution of oxygen tension to be visualized.

Results: Mice liver and spleen Po_2 maps were obtained in 2.5 minutes when two 10 g/kg doses of PFC were administered. Preliminary oxygen tension maps indicated a Po_2 of 40 torr ± 10 when the animal breathes air and a Po_2 of 90 torr ± 20 when the animal breathes pure oxygen.

Conclusion: Inversion-recovery EPI of PFCs provides a fast and accurate method for spatially mapping in vivo oxygenation in mice liver and spleen. This work is being extended to mapping oxygen tension of RIF-1 tumors in the response to chemical adjuvants and radiation therapy. *Funding for this work by The Whitaker Foundation is gratefully acknowledged.*

P318

Evaluating Areas under MR Spectroscopic Peaks without Phasing

WR Riddle, DR Pickens, SJ Gibbs, MR Willcott, RR Price
Department of Radiology, and Radiological Sciences, Vanderbilt University Medical Center, Nashville, TN

Purpose: To provide a reliable and reproducible method of evaluating the area under peaks in MR spectroscopy that does not require phasing.

Methods: A deconvolution algorithm was developed that accepts a free induction decay (FID), applies a line-broadening filter, transforms the data to the frequency domain, then fits the magnitude mode spectrum. The fitting process uses a Levenberg-Marquardt method for nonlinear least squares to determine the best-fit parameters of Lorentzian functions. For each peak in the spectrum, the algorithm requires estimates of the following: (*a*) peak location (Hz), (*b*) peak magnitude (A/D units), (*c*) the full width at half maximum of the magnitude of the peak (Hz). After the parameters of each Lorentzian are determined with the algorithm, the absorption mode spectrum, the individual peaks, and peak areas are defined.

Results: The algorithm was able to correctly fit both the absorption mode spectrum and the magnitude mode spectrum of software-generated FIDs that were correctly phased. The algorithm was also able to correctly fit the magnitude mode spectrum of a software-generated FID that was not phased. The algorithm has been used to evaluate the areas under peaks in P-31 spectra and H-1 spectra.

Conclusion: The algorithm provides an accurate and reproducible method for evaluating peak areas without phasing spectra into absorption and dispersion modes.

P319

Comparison of the Performance of ISIS for Volume-selected Phosphorus Spectroscopy on Three Clinical MR Systems

SF Keevil, CM Segebarth, R Longo, MA Smith
Division of Radiological Sciences, United Medical and Dental Schools, Guy's Hospital, London, England

Purpose: Many factors influence the performance of MR spectroscopic localization techniques implemented on commercial imagers, including site-specific variations not apparent from computer simulations (1). Performance assessment techniques have been developed (2) and used to examine image-selected in vivo spectroscopy (ISIS) on clinical (3) and experimental (4) spectrometers. The authors report the result of a comparison of ISIS on 3 similar clinical MR systems at different sites in Europe. This study was sponsored by the European Community Concerted Action on MR.

Methods: Selection efficiency, suppression efficiency, and contamination (2) were measured by using a 2-compartment Perspex phantom filled with suitable test materials (5). Three Philips Gyroscan S15 systems with standard head coils were used. The version of ISIS studied employs Silver-Hoult inversion pulses and conventional hard 90° detection pulses. One site had a spectroscopy upgrade not available elsewhere. Fully relaxed measurements were made for volumes of interest of various sizes concentric with the inner compartment of the phantom.

Results: Variations in behavior observed between the 3 sites can be understood in terms of differences in instrumental and software performance.

Conclusion: Interlaboratory comparisons of this sort have an important role in ensuring the performance of commercial spectroscopy systems and comparability of clinical results from different sites.

1. Lawry TJ, et al. Magn Reson Med 1989; 9:299. 2. Keevil SF, et al. Phys Med Biol 1990; 35:821. 3. Keevil SF, et al. NMR Biomed 1992; 5:200. 4. Howe F, Griffiths JR. SMRM Book of Abstracts 1991; 1174. 5. Collins DJ, et al. SMRM Book of Abstracts 1992; 3826.

P320

In Vivo P-31 MR Spectroscopy of the Spleen in Patients with Hematologic Malignancy

M Saeki, K Ishizuka, K Imamura, T Ishikawa, H Nagoshi
Department of Radiology and 3rd Internal Medicine, St Marianna University School of Medicine, Kawasaki, Japan

Purpose: To assess malignant cell proliferation or extramedullary hematopoiesis, P-31 MR spectroscopy was performed in patients with hematologic disorders.

Methods: The authors evaluated localized in vivo spectra from the spleen in patients with hematologic disorders (11 myeloproliferative disorders [MPD], 3 lymphoproliferative disorders [LPD], 1 infectious disease) and in 4 healthy volunteers. P-31 MR spectroscopy was performed with an MR system (Gyroscan S15, Philips) at 1.5 T. The 3D localized spectra of the spleen were obtained with the image-selected in vivo spectroscopic method with a TR of 2,000 msec. Evaluated parameters were PME/βATP ratio, chemical shift between PME and Pi (δ[PME/Pi]), and phosphorylethanolamine/phosphorylcholine (PE/PC) ratio.

Results: Four of 6 patients with chronic myelogenous leukemia (CML) and splenomegaly revealed prolonged δ[PME/Pi] larger than 1.4 ppm. Three of the 4 showed PE/PC ratio larger than 1.0. Another 2 patients with polycythemia vera and non-Hodgkin lymphoma showed a similar pattern. However, no specific MR spectroscopy pattern was observed in patients with essential thrombocythemia, myelodysplastic syndrome, and non-Hodgkin lymphoma without splenomegaly. Follow-up studies were performed in 3 of 4 CML patients during chemotherapy, which represented a reduced PE/PC ratio and/or δ(PME/Pi) with good correlation of clinical data. The PME/βATP ratio was not a good indicator.

Conclusion: These results suggest that MR spectroscopy data reflect the occurence of cell proliferation in the spleen of MPD and LPD patients. P-31 MR spectroscopy was thought to be useful for the therapeutic effect and discrimination of the grade of cell proliferation.

P321

P-31 MR Spectroscopy of Bone and Soft-Tissue Tumors

A Kitagawa, M Saeki, K Imamura, T Watanabe,
T Ishikawa, M Soh, H Nakajima, K Kageyama
Departments of Radiology and Orthopedics, St Marianna University School of Medicine, Kawasaki, Japan

Purpose: The purpose of this study was to assess the capability of P-31 MR spectoroscopy in the differential diagnosis of benign and malignant bone and soft-tissue tumors.

Methods: The authors analyzed 18 patients with histologically proved bone and soft-tissue tumors. The patients underwent P-31 MR spectroscopy preoperatively with an MR system (Gyroscan S15, Philips) at 1.5 T. The 3D localized spectra of the tumor were obtained with the image-selected in vivo spectroscopic method with a TR of 2,000 msec. The authors evaluated the PME/βATP ratio, chemical shift of PME from Pi δ(PME-Pi), and pH of the tumor.

Results: Low content of PCr in the localized spectra suggested a good suppression of muscle signal intensity. All malignant tumors (11 patients) revealed excellent spectral resolution with high intensity of PME. In 8 patients, PME/βATP was over 1.0, and the range of δ(PME-Pi) was between 1.20 and 2.49. Ten malignant tumors showed pH higher than 7.0. Six benign tumors showed no definite peaks of phosphorus compounds.

Conclusion: These results reveal that bone or soft-tissue malignancies, like other malignant tumors, have definite phosphorus peaks with a large amount of PME, which is the same as in other malignant tumors. The main component of PME in malignant tumors is thought to be phosphoethanolamine because δ(PME-Pi) is greater than 1.4 ppm. The authors stress that P-31 MR spectroscopy is a useful modality for the evaluation of patients with bone or soft-tissue tumors.

P322

P-31 MR Spectroscopy of Muscle in Patients with Peripheral Vascular Disease before and after Bypass Surgery

C Dewey, G Timm, B Schnackenburg*, J Sauer, M Laning, H Hirsche†

*Institute of Diagnostic Radiology, Charité Humboldt-University, Berlin, Germany; *Philips Medical Systems; and †University of Essen, Germany*

Purpose: P-31 MR spectroscopy was performed to analyze changes in phosphate metabolites before and after femoropopliteal bypass surgery in patients with peripheral vascular disease (stage III).

Methods: The authors investigated 2 groups of healthy volunteers (group 1 [$n = 11$]: average age, 25 years; group 2 [$n = 11$]: average age, 54 years) and 9 patients (group 3: average age, 57 years). In vivo P-31 MR spectroscopy was performed at 1.5 T (Philips) with a double-tuned surface coil (diameter = 14 cm). The spectra were obtained by using the following parameters: TR = 3 seconds, adiabatic pulse, 8 or 16 measurements. Twenty-four sequential spectra during muscle exercise (beyond the pain point) and time of recovery were measured. Evaluation of phosphocreatine (PCr) to inorganic phosphate (Pi) was used to analyze metabolic changes. The course of PCr/Pi can be described by a Bateman function.

Results: The PCr/Pi ratio decreased during exercise in all groups to a minimum of about 25% of the rest value. There were no differences between groups 1 and 2. There were significant differences between group 2 (old volunteers) and the group of preoperative patients during recovery and between pre- and postoperative patients. The comparison of patient results postoperatively and those of healthy volunteers in the same age group did not show any significant differences. Dynamic behavior of PCr/Pi of postoperative results in group 3 demonstrated a positive effect of bypass surgery in patients with peripheral vascular disease.

Conclusion: MR spectroscopy is a simple and fast method for quantifying the success of femoropopliteal bypass surgery.

P323

Unruptured Cerebral Aneurysms at Clinical Examination of the Brain: Evaluation with MR Angiography

M Kojima, E Tsuda, N Mabuchi, T Tsuda

Soseikai General Hospital, Kyoto, Japan

Purpose: In this study, the authors report the effectiveness of MR angiography for the screening of unruptured cerebral aneurysms (UCAs) and discuss the problems in its treatment.

Methods: For 2 years, the authors examined the circle of Willis with MR angiography in 4,293 subjects participating in a medical checkup. The equipment used in this study consisted of a 1.5-T system (Signa Advantage; GE Medical Systems). The MR angiogram was obtained in the axial plane with a 3D Fourier transform SPGR sequence.

Results: Of the 4,293 subjects, 122 were suspected of having UCA at MR angiography, and conventional cerebral angiography (CCA) was performed in 31 subjects. Twenty-nine UCAs were revealed with CCA in 23 cases, and the other 8 cases were false-positive. These false-positive cases resulted in limitations of MR angiography due to insufficient spatial resolution and loss of visualization of small vessels.

Conclusion: Eleven patients with 15 UCAs detected in our medical checkup underwent craniotomy, 11 by neck clipping and 3 by coating. Mild cerebral contusion with thin subdural hematoma occurred in 1 case as an operative complication, but there was no serious operative morbidity. Unlike with ruptured cases, operations for UCAs may bring about much better results, with no occurrence of vasospasm and/or hydrocephalus. However, because some risks are involved in craniotomy under general anesthesia, it is proposed that operative indications for UCAs should be limited to the cases in which a safe operation would be expected because of the patient's age and the location, size, and shape of the aneurysms.

P324

Focal Lesions of the Spine Assessed with Chemical Shift Imaging and H-1 Localized Spectroscopy

F Schick, WJ Jung, S Duda, K Aicher, M Skalej, O Lutz, M Laniado, CD Claussen

Department of Diagnostic Radiology, Institute of Physics, University of Tübingen, Tübingen, Germany

Purpose: MR images of the spine obtained with proton-density–, T1-, and T2-weighted sequences are often used to determine the involved areas in cases of plasmacytoma, lymphoma, metastases, or osteogenic tumors of the spine. Unfortunately, signals from vertebral bone marrow stem from lipid and water protons in variable fractions. Therefore, a clear delineation of the tumor areas in cases with high cellularity of the bone marrow is difficult. Fatty degeneration of tumors under cytotoxic treatment cannot be clearly assessed with standard imaging techniques. Therefore, examinations with chemical shift selective methods are promising.

Methods: SENEX (1,2) frequency selective chemical shift imaging and PRESS (3–5) volume selective H-1 spectroscopy were tested in examinations of focal lesions of the spine (7 plasmocytoma or lymphoma, 2 osteogenic tumors, 3 metastases). Chemical shift selective imaging allows determination of the distribution of water and fat separately. Volume selective spectroscopy gives the Larmor frequency distribution in a volume element of 2 cm^3.

Results: The areas of the tumors were given with improved contrast by using fat-selective imaging. Chemical shift selective imaging reveals fatty degeneration of the tumors and effects of radiation-therapy within the bone marrow. H-1 spectroscopy provides quantification of the fat and water fractions and changes in the microscopic field distribution within the involved bone marrow.

Conclusion: Chemical shift imaging and H-1 spectroscopy give additional information about the areas involved by focal lesions of the spine. The changes in the lesions due to chemotherapy or radiation therapy are shown with better contrast than with standard images.

1. Braun M, Jung WI, Lutz O, Oeschej R. Z Naturforsch 1987; 42a:1391. 2. Schick F, Bongers H, Jung WI, Skalej

M, Lutz O. Magn Reson Imaging 1991; 9:509. 3. Gordon RE, Ordidge RJ (abstr). In: Book of abstracts. SMRM, New York 1984; 272. 4. Bottomley PA. Ann New York Acad Sci 1987; 508:333. 5. Jung WI, Grodd W, Lutz O, Petersen D. Magn Reson Med 1990; 15:320.

P325

Uncertainties of P-31 MR Spectroscopy of the Human Brain

CM Segebarth

Unité De Résonance Magnétique, Hôpital Erasme, Brussels, Belgium

Purpose: To predict the statistical uncertainties of the estimates of spectral parameters derived from P-31 MR signals of the human brain.

Methods: Five P-31 MR signals (256 averages) from a large volume (200 cm^3) centered in the brain were measured sequentially in a healthy volunteer. The signals were combined to generate, in addition, sets of signals averaged respectively 512, 768, and 1,024 times, and 1 set containing a signal averaged 1,280 times. All signals were fitted in the time domain by means of a fully automated maximum-likelihood fitting technique, and the standard deviations of the estimates of the various spectral parameters were approximated with the Cramer-Rao (CR) standard deviations. The ratios of the CR standard deviations to the corresponding parameter estimates were averaged within each of the 5 signal sets. The set averages of the relative CR standard deviations were expressed as a function of the number of averages (NAV), and these data points were eventually least squares fitted by $C/\sqrt{NAV}$.

Results: Within each set of signals, significant variations were observed in the relative CR standard deviations. The lower NAV, the larger these variations. An excellent agreement was observed between the variation with NAV of the set averages of the relative CR standard deviations and the theoretical variation with NAV of the relative standard deviations.

Conclusion: In P-31 MR spectroscopy of the human brain, it is possible to predict the average values of the relative CR standard deviations of the spectral parameters, provided the relative CR standard deviations are known for 1 reference signal obtained under sufficient conditions of signal-to-noise ratio.

P326

Reproducibility of Coil Loading in Repeated MR Spectroscopy in Clinical Settings

K Imamura, M Saeki, K Ishizuka, H Ashida, K Ohashi, M Endo, T Ishikawa, H Nakajima

Departments of Radiology and Orthopedics, St Marianna University School of Medicine, Kawasaki, Japan

Purpose: In vivo phosphorus spectroscopy is a noninvasive and useful technique in monitoring the effect of therapy or the disease processes. MR spectroscopy will be performed repeatedly in a patient, and quantitativeness is strongly required. The aim of this study was to evaluate the intrapatient variation of coil loading that will possibly cause a sensitivity deviation.

Methods: Patients with liver disease ($n = 14$) or malignant extremity tumor ($n = 7$) were examined repeatedly 2–5 times with a 1.5-T MR system (Gyroscan S15, Philips) by using a 14-cm surface coil. Localized spectra were obtained with ISIS. Signal of a solution of methylphosphonic acid (MPA) at the center of the coil was acquired in all studies as a reference standard. Signal intensity of MPA was measured on unlocalized spectra and that of metabolites on localized spectra.

Results: The intrapatient variation was averaged to be 7.8% (maximum, 25.4%) in the liver examination and 6.6% (maximum, 10.9%) in the extremity tumors. Sensitivity correction was performed for signal intensity of metabolites in a proportional way to MPA intensity. Spectroscopic signal reduction coincided well with histologic findings in extremity tumors.

Conclusion: The results demonstrate that intrapatient variation of coil loading is within 10% on average. Therefore, the possible variation of sensitivity will be that much, which is fairly good for follow-up in routine clinical settings.

P327

In Vivo Observation of Changes Due to Temperature Variations with Inversion-Recovery and Magnetization Transfer Sequences

IR Young, JW Hand, JV Hajnal, MV Prior

NMR Unit, Royal Postgraduate Medical School, Hammersmith Hospital, London, England

Purpose: T1 measurement has been previously described as a means of observing temperature changes in vivo (1). The method used was based on saturation recovery, and the near order of magnitude difference in TR between the pair of sequences used to calculate T1 (1,500 and 200 msec) meant that if there were unintentional magnetization transfer effects in the tissue studied (muscle) (more likely with the short TR sequence) inaccuracies in the temperature results would follow. Here, the authors investigate the possibility in a parallel study employing inversion recovery (IR) and multiple magnetization transfer experiments in volunteer peripheral muscle tissue.

Methods: Volunteer calf tissue temperature was varied over a range of 20°C to 38°C by using pads through which water at controlled temperature was passed. Temperatures were monitored by 3–5 surface thermocouples and by 1 implanted through a cannula into the muscle beneath 1 of the pads. The work was performed at 0.15 T with conventional single-section IR sequences, while magnetization transfer images were acquired with varying durations of RF pulses (0, 80, 160, 320, 640 msec). Data were acquired at 3 temperatures differing by 9°–10° and analyzed as described by Hajnal et al (2) by using the 2-pool model applied by Wolff and Balaban (3).

Results and Conclusion: The magnitude of the temperature changes noted before (1) using IR were rather less than those previously obtained with saturation recovery. Changes in the equilibrium magnitude of the free water pool were observed, as well as changes in its T1 and the rate constant of transfer from it to the hidden pool.

1. Dickinson RJ, et al. J Comput Assist Tomogr 1976; 10:468. 2. Hajnal JV, et al. J Comput Assist Tomogr 1992; 16. 3. Wolff SD, Balaban RS. Magn Reson Med 1989; 10:135.

I.R. Young is an employee of Picker International.

P328

Metabolic Findings in Patients with Treated Hyperphenylalaninemia with in Vivo Proton MR Spectroscopy

HE Moeller, U Bick, U Stoeber, P Vermathen, G Schuierer, K Ullrich

Department of Clinical Radiology, University of Muenster, Muenster, Germany

Purpose: In hyperphenylalaninemia (HPA), conversion of phenylalanine to tyrosine is disturbed. The purpose of this study was to further clarify the pathogenesis and clinical significance of MR imaging white matter abnormalities in treated HPA.

Methods: Ten patients (6 type I HPA, 2 type II, and 2 type III) and 11 healthy volunteers underwent H-1 spectroscopy with a 1.5-T MR unit. For all patients, at least 1 spectrum was recorded by applying the STEAM technique (1,500/270). Six patients tolerated additional MR spectroscopy at different TEs, which could be used for an estimate of metabolite T2. In 1 case, repeated MR spectroscopy with varying TR served to calculate T1 of the major peaks. In all cases, voxels of 8 or 27 mL were positioned within the left or right parietooccipital periventricular white matter.

Results: Contrary to MR imaging results, H-1 spectra of all patients showed no significant abnormal findings. Elevated cerebral lactate could not be detected in any case. There was no correlation of the measured ratios of NAA/PCr, NAA/Cho, and Cho/PCr with plasma Phe levels or severity of MR imaging white matter abnormalities. All 3 ratios as well as T1 and T2 did not vary from age-matched controls within the experimental errors.

Conclusion: From the MR spectroscopy results, the authors conclude that the observed white matter changes in treated HPA probably represent reversible structural myelin changes rather than permanent demyelination.

P329

In Vivo H-1 MR Spectroscopy of the Brain after Temporary Ischemia

G Timm, L Harms, S Enchtuja, B Schnackenburg*
*Institute of Diagnostic Radiology, Charité Humboldt-University, Berlin, Germany, and *Philips Medical Systems.*

Purpose: An increasing concentration of lactate and *N*-acetylaspartate (NAA) is assumed to be a result of reduced cerebral blood flow causing transient ischemic attacks (TIA) and reversible ischemic neurologic deficits (RIND). To prove this hypothesis, we estimated the differences in this hydrogen metabolite between patients with ischemic insult and healthy volunteers by using H-1 MR spectroscopy.

Methods: The data of the spectroscopic examinations of 25 patients with ischemic insults were compared with the results of 10 healthy volunteers (group 3). Fifteen patients with TIAs (group 1) and 10 patients with RINDs (group 2) were examined. Furthermore, all patients were evaluated in the region of reduced cerebral blood flow and in the contralateral area of the brain. In vivo H-1 MR spectroscopy was performed at 1.5 T (Philips). The volume selective (20 × 20 × 40-mm) spectroscopy was performed with water suppression by using selective inversion pulses. Evaluation of the ratios of phosphocholine (PCh) to phosphocreatine (PCr), NAA to PCh, and NAA to lactate was used to describe metabolic changes mathematically.

Results: At least 4 weeks after the acute event, the authors detected lactate of the pathologic hemisphere in 80% of patients in group 2 and 50% of group 3. In addition, they estimated considerable differences between the pathologic area and contralateral hemisphere in group 2. These differences were not established in patients with TIAs. As a result, they could not find substantial changes of PCh/PCr and NAA/PCr ratios in all 3 groups.

Conclusion: In summary, the detection of lactate in both patient groups was significantly higher than in the healthy volunteers group. Furthermore, the lactate concentration is increased in the whole brain after temporary cerebral ischemia. After RIND, the authors found high differences in lactate between the affected region and contralateral hemisphere.

P330

MR Imaging and H-1 MR Spectroscopy of the Brain after Cardiac Resuscitation

SR Felber, P Lechleitner, GG Birbamer, A Schinnerl, G Luef, FT Aichner
Department of Magnetic Resonance Imaging, University of Innsbruck, Innsbruck, Austria

Purpose: This ongoing study was designed to evaluate prospective criteria for determination of outcome after cardiac resuscitation.

Methods: At present, 30 consecutive patients (7 women, 23 men; mean age, 63.5 years) were included. All were successfully resuscitated after cardiac arrest (mean anoxia time, 6.7 minutes) and coma rated. The protocol consisted of laboratory and electrophysiologic investigations and sequential MR imaging and MR spectroscopy examinations of the brain. MR imaging and MR spectroscopy were performed with a 1.5-T system (Siemens, Germany). T1- and T2-weighted SE images were followed by localized H-1 MR spectroscopy (volume of interest = 27 mL, 1,500/270, 384 excitations), of the deep white matter by using stimulated echo sequences.

Results: MR imaging and MR spectroscopy were performed in 21 patients who survived day 1. The localized spectra showed elevated cerebral lactate in 14/21 patients; 12 of them died, and 2 had neurologic sequelae. Spectra did not show lactate in 7 patients who survived without (n = 5) or with minimal (n = 2) neurologic deficit. Lactate on localized spectra correlated to the mean anoxia time (4.7 minutes in lactate-negative and 7.8 minutes in lactate-positive patients) and lactate elevation in blood samples.

Conclusion: These preliminary data indicate that localized proton MR spectroscopy of the brain may become a powerful tool for predicting outcome after cardiac resuscitation.

P331

MR Studies of Perfused, Immunoprotected, Insulin-secreting Endocrine Cells in a 4.7-T Horizontal Magnet

I Constantinidis, A Sambanis, RC Long
Department of Radiology, Emory University, Atlanta, GA

Purpose: A promising method for the treatment of diabetes consists of implantating immunoisolated pancreatic β cells or whole islets. Although feasibility has been demonstrated, optimization of such a system is far from accomplished. Specifically, it is unknown whether immobilized cells express, to sufficient levels, important differentiated properties pertaining to regulated insulin secretion. The overall purpose of this study was to monitor the biochemistry of endocrine cells spectroscopically with MR and correlate the changes to insulin secretion.

Methods: Mouse pituitary AtT-20 cells genetically engineered to secrete human insulin and proinsulin were used as an endocrine model. Cells were grown as spheroids and immobilized in an alginate-polylysine-alginate copolymer for immunoprotection. MR experiments were performed with a horizontal SISCO 4.7-T spectrometer. A homemade transmit-receive loop-gap resonator probe, tuned to both P-31 and H-1, was used. The bioreactor containing immunoprotected spheroids had a volume of 20 mL.

Results: The cell preparation was monitored with MR for a period of 70 days. H-1 multisection SE images were obtained periodically to determine the homogeneity of packing. P-31 1D-CSI spectra along the axial and radial directions were acquired to evaluate the bioenergetic status of cells at different places within the bioreactor. Single-pulse

P-31 MR spectra, and glucose, lactate, and insulin assays were performed daily.

Conclusion: The authors have developed an MR-compatible perfusion system for the long-term study of immunoisolated preparations of genetically engineered cells exhibiting uniform distribution and metabolism in the perfusion vessel.

P332

High-Field-Strengh Proton T1 Studies of Water Exchange Parameters in Red Cell Suspensions

RV Mulkern, J Bowers, RH Sadowski
Department of Radiology, Children's Hospital, Harvard Medical School, Boston, MA

Purpose: To compare available analyses of T1 data of paramagnetically doped red cell suspensions for the extraction of water exchange parameters.

Methods: Red cells from freshly drawn blood of 8 adult male volunteers were washed 3 times in 30 mmol/L $MnCl_2$ and 110 mmol/L NaCl solutions. Individual MR samples were prepared with resuspension at 50% hematocrit in the wash solution. T1 decay curves were obtained at 7 T with an inversion recovery sequence (24–32 time points from 0.5–750 msec). Results were fit with mono-, bi-, and triexponential functions with a nonlinear least-squares algorithm. Water exchange analyses were performed by using the best fit parameters, and an independent measure of the intracellular water relaxation rate was obtained from packed red cells.

Results: Intra- to extracellular water exchange rates calculated from monoexponential fits were significantly lower ($P < .05$) than those calculated from 2-site exchange analyses of the 2 quickly relaxing components in the triexponential fits (73.2 Hz ± 11.7 vs 88.9 Hz ± 15.2). Interindividual correlation between intra- to extracellular exchange rates calculated with mono- versus triexponential analyses was poor (cc = 0.66). The triexponential analyses yielded additional exchange parameters, including intracellular water fractions and extracellular relaxation rates in good agreement with those measured independently. Biexponential fit parameters were widely varying and yielded unrealistically small exchange rates (45.0 Hz ± 37.1).

Conclusion: Triexponential analyses of high field strength T1 data account for nonexchanging hemoglobin protons and yield internally consistent water exchange parameters. Intra- to extracellular exchange rates obtained from triexponential analyses are not in accord with the monoexponetial analyses of the data.

P333

Evaluating Cardiac Allograft Rejection with P-31 MR Spectroscopy

WR Riddle, JH Wudel, JB Atkinson, H Lee, SJ Gibbs, MR Willcott
Department of Radiology, and Radiological Sciences, Vanderbilt University Medical Center, Nashville, TN

Purpose: To evaluate whether P-31 MR spectroscopy can provide a signature for cardiac allograft rejection.

Methods: Laboratory rats were surgically prepared with an abdominal allograft. At day 7 after transplantation, the rats were killed and the native and allograft hearts were harvested and immediately plunged into 4°C saline. The cold heart, cold saline, and ice were packed into a chilled glass vial, then placed in a 4.7-T spectrometer. The resulting spectra were deconvolved into Lorentzian peaks to give areas for phosphomonoesters (PME), inorganic phosphate (Pi), phosphocreatine (PCr), and adenosine triphosphate (ATP). Ratios of areas were calculated, and a t statistic was used to compare means between groups of native and allograft hearts. Hearts were also histologically evaluated for rejection.

Results: The native hearts showed no histologic evidence of rejection. The allograft hearts showed severe acute rejection. The PCr/Pi and PCr/ATP ratios of the allograft hearts were not significantly different from the ratios of the native hearts ($P > .1$). The PME/Pi and PME/ATP ratios of the allograft hearts were significantly greater than the ratios of the native hearts ($P < .005$).

Conclusion: The ratios related to the bioenergetics of cardiac metabolism (PCr ratios) were not significantly different with rejection. The ratios related to membrane phospholipids (PME ratios) were significantly different with severe rejection.

P334

Ex Vivo P-31 MR Spectroscopy of Human Kidneys for the Assessment of Renal Viability before Transplantation

HE Moeller, T Vestring, A Gaupp, KH Dietl, P Vermathen, E Rummeny, B Buchholz, PE Peters
Department of Clinical Radiology, University of Muenster, Muenster, Germany

Purpose: Noninvasive prediction of renal viability before transplantation is one of the most promising potential clinical uses for MR spectroscopy. The purpose of the present study was to investigate the use of P-31 MR spectroscopy in a clinical transplant setting.

Methods: Thirty cadaveric human kidneys derived from different donors were studied during simple hypothermic storage by using a 1.5-T system (image-selected in vivo spectroscopic or free induction decay sequences, TR = 8,000 msec, AC = 256, volume of interest = 64 mL). Twenty organs were preserved in HTK (histidine-tryptophane-α-ketoglutamate), 8 in UW (University of Wisconsin), and 2 in EC (EuroCollins) solution. Spectral parameters were correlated with postoperative transplant function determined by the change of serum creatinine level and creatinine clearance and the results of Tc-99m MAG3 renography performed on the fifth postoperative day. All transplant recipients underwent the same immunosuppressive treatment. During the first 10 days after transplantation, no transplant showed any sign of acute rejection.

Results: PME/Pi ratios showed a lower correlation with postoperative function compared with PDE/(PME + Pi). In addition, intensities of ATP and/or NAD(H) signals correlated with postoperative transplant function, but accurate quantification was difficult and was impossible for organs flushed with inorganic phosphate containing UW or EC solution.

Conclusion: P-31 MR spectroscopy provides a noninvasive means of predicting final renal viability before transplantation. The preservation solution may influence the spectra.

P335

Sodium Transport in Cardiomyocytes of Aging Rats

MD Osbakken, T Ivanics, D Zhang, K Wroblewski
University of Pennsylvania School of Medicine, Philadelphia, PA

Purpose: Studies were designed to determine whether aging cardiomyocytes have progressive changes in sodium transport that might explain altered mechanical function. To this end, the bioenergetics of sodium transport, with special reference to the [Na,K]-ATPase system, were studied in isolated cardiomyocytes from rats, 2, 6, and 11 months of age, by using Na-23 (132.2 MHz) and P-31 (202.5 MHz) MR.

Methods: Dysprosium tripolyphosphate (6 mmol/L) was used to identify intra- and extracellular sodium (Na_i, Na_e). 2-deoxyglucose (2-DOG, 10 mmol/L), replacing glucose as substrate, was used to inhibit glycolysis. Ouabain (Oua, 100 µm) was used to inhibit [Na,K]-ATPase. Combined agents were used to uncover non-Oua–inhibited ATPase function.

Results: The following age related changes in sodium transport function were found. (1) Dependence on glycolysis to maintain Na_i progressively increased with age. (2) [Na,K]-ATPase activity decreased with age. (3) Non-Oua–inhibited [Na,K]-ATPase was found in all age groups. (4) Myocytes from older rats took longer to respond to any intervention. (5) Glucose, but not acetate, pyruvate or butyric acid, reversed the 2-DOG–produced inhibition of glycolysis in sodium transport. (6) Global ATP did not change significantly during any intervention.

Conclusion: The present data demonstrate that there are age-related changes in glycolysis-supported sodium transport. Because global ATP did not change during 2-DOG administration, a localized (possibly sarcolemmal) glycolytic process to maintain sodium transport is suggested in all age groups. In addition, [Na,K]-ATPase–supported sodium transport diminishes with age.

1993 ANNUAL MEETING COMMENTS

The 1993 Annual Meeting Organizing Committee would appreciate receiving your comments regarding the 1993 Annual Meeting in San Francisco. Those comments will be collated and forwarded to the 1994 Annual Meeting Organizing Committee for possible incorporation in next year's educational programming. While your comments may also be provided on the Evaluation/CME Accreditation Form distributed at each session, please let us know your thoughts regarding the following:

1. Which Program did you attend? ____________________

2. Did it meet its stated objectives? ______ Yes ______ No. Why? ____________________

____

____

3. What should have been included in the Program that was not? ____________________

____

4. What should have been excluded from the Program? ____________________

____

5. What Program revisions would you like to see implemented next year? ____________________

____

____

____

6. General Comments: ____________________

____

____

Please return this form to the **SMRI** Registration Area, Ballroom Level, of the San Francisco Hilton and Towers by Wednesday, March 31, or mail it to the **SMRI** Central Office at the following address:

Society for Magnetic Resonance Imaging
213 West Institute Place, Suite 501
Chicago, Illinois 60610 USA

Notes

Notes

MR 1993

INDICES AND INFORMATION

- Technical Exhibits Floorplan
- 1993 Annual Meeting Acknowledgements
- Author Index
- SMRT Membership Information
- **SMRI** Membership Information

PLAN YOUR INDIVIDUAL ITINERARY

To help you plan your week at **SMRI**, the Printed Program index lists all plenary sessions, proffered papers and scientific poster presentations. All papers are categorized by author with the abstract number of each symposium, paper, or exhibit found following the author name. The first eight co-authors are listed individually.

The type of work is indicated by one of three abbreviations preceding the abstract number. An abbreviation key appears opposite the Author Index. All numbers listed in the index reference the paper number and not the page number on which the abstract may be found.

Please note that other pertinent information regarding the Technical Exhibits Program, Annual Meeting Acknowledgements, and **SMRI** and SMRT membership information may also be found in this section.

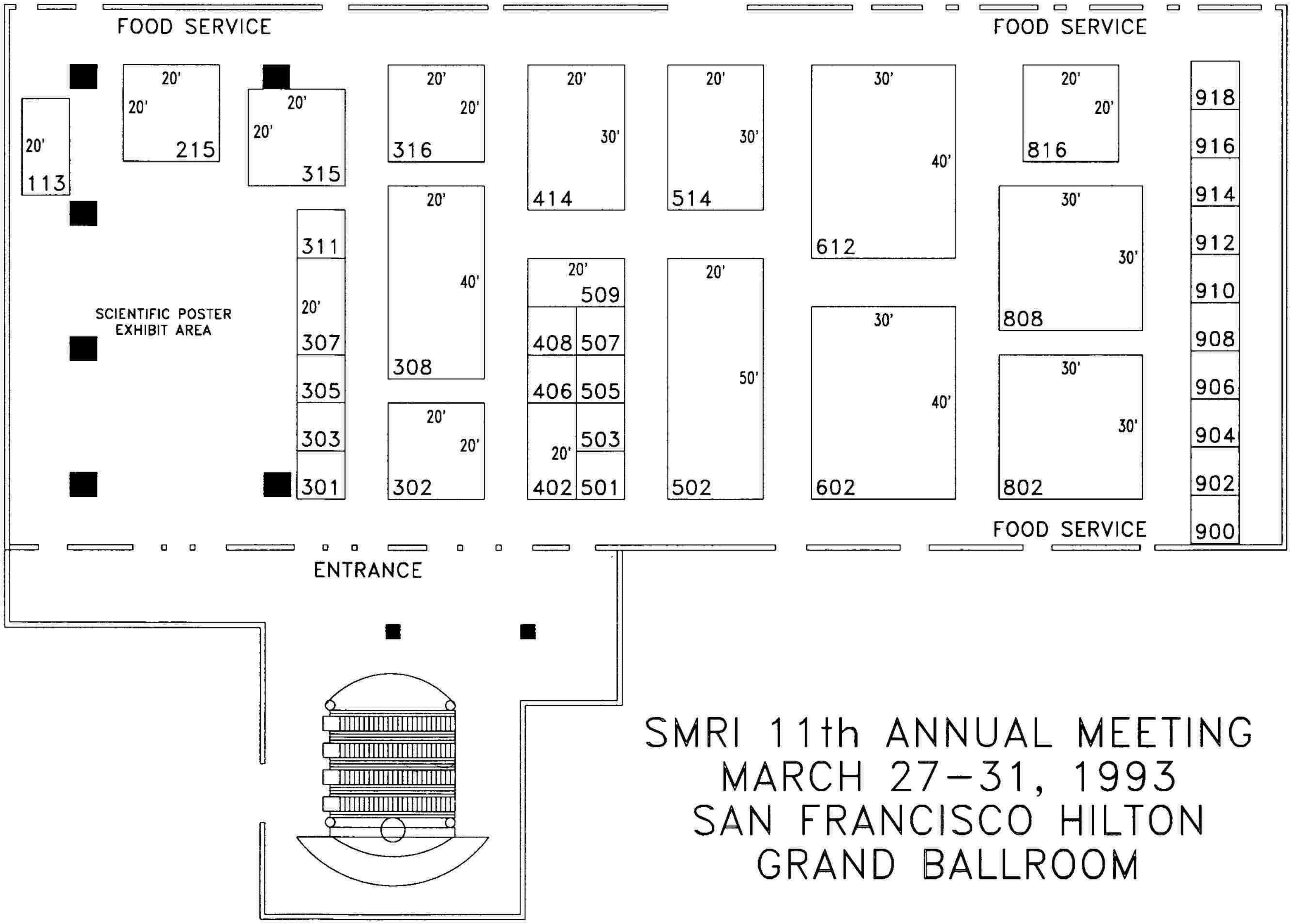

SMRI 11th ANNUAL MEETING
MARCH 27–31, 1993
SAN FRANCISCO HILTON
GRAND BALLROOM

SMRI 1993 Technical Exhibitors

Alliance Pharmaceutical Corporation
3040 Science Park Road
San Diego, CA 92121
619/558-4300

Analogic Corporation (Medical Division)
8 Centennial Drive
Peabody, MA 09160
508/977-3000

Applied Radiology
80 Shore Road
Port Washington, NY 11050
516/883-0164

Avotec
P.O. Box 1777
Jensen Beach, FL 34958
407/692-4405

Berlex Laboratories
300 Fairfield Road
Wayne, NJ 07470
201/305-5082

CompHealth
4021 S. 700 East, Suite 300
Salt Lake City, UT 84107
800/328-3085

Diagnostic Imaging Magazine
600 Harrison Street
San Francisco, CA 94107
415/905-2671

Eastman Kodak Company
343 State Street
Rochester, NY 14650-0801
716/724-5985

Elscint Inc.
505 Main Street
Hackensack, NJ 07601
201/342-2020

E-Z-EM, Inc.
717 Main Street
Westbury, NY 11590
516/333-8230

General Electric Medical Systems, Inc.
P.O. Box 414-W439
Milwaukee, WI 53201
414/544-3424

Hitachi Medical Systems America, Inc.
1963 Case Parkway
Twinsburg, OH 44087
800/800-3106

ICON Medical Systems, Inc.
1901 South Baxom Avenue, 9th Floor
Campbell, CA 95008
408/879-1900

Instrumentarium Imaging Inc.
300 West Edgerton
Milwaukee, WI 53207
414/747-1030

Journal of Magnetic Resonance Imaging (JMRI)
213 West Institute Place, Suite 501
Chicago, IL 60610
312/751-2590

Medical Advances, Inc.
10431 West Watertown Plank Road
P.O. Box 26425
Milwaukee, WI 53226
414/258-3808

Medrad, Inc.
271 Kappa Drive
Pittsburgh, PA 15238
412/967-9700

Newmatic Sound Systems
237 Redwood Circle
Petaluma, CA 94954
707/763-1428

Otsuka Electronics (USA), Inc.
2555 Midpoint Drive
Fort Collins, CO 80525
303/484-0428

Pergamon Press Inc.
660 White Plains Road
Tarrytown, NY 10591
914/524-9200

Philips Medical Systems
North America Co.
710 Bridgeport Avenue
Shelton, CT 06484
203/926-7475

Picker International, Inc.
595 Miner Road
Cleveland, OH 44143
216/473-3000

Radiological Society of North America (RSNA)
2021 Spring Road, Suite 600
Oak Brook, IL 60521
708/571-2670

Raven Press
1185 Avenue of the Americas
New York, NY 10036
212/930-9500

Resonance Technology Co.
22647 Ventura Boulevard
Woodland Hills, CA 91364
818/764-5885

Resonex, Inc.
720 Palomar Avenue
Sunnyvale, CA 94086
408/720-8600

R Squared Scan Systems, Inc.
1611 Pomona Road
Corona, CA 91720
714/736-3700

Sanofi Winthrop Pharmaceuticals
90 Park Avenue
New York, NY 10016
212/907-3221

Shimadzu Medical Systems
101 West Walnut Street
Gardena, CA 90248
800/228-1429

Siemens Medical Systems, Inc.
186 Wood Avenue South
Iselin, NJ 08830
908/321-4654

SLACK Inc.
6900 Grove Road
Thorofare, NJ 08086
609/848-1000

S.M.I.S.
Alan Turing Road
Guildford, Surrey, UK
44/48-350-6611

Society of Magnetic Resonance in Medicine (SMRM)
1918 University Avenue, Suite 3C
Berkeley, CA 94704
510/841-1899

Squibb Diagnostics
P.O. Box 4500
Princeton, NJ 08543
609/897-3748

Toshiba America Medical Systems, Inc.
2441 Michelle Drive
Tustin, CA 92680
714/669-4118

Universal Shielding Corp.
20 West Jefryn Boulevard
Deer Park, NY 11729
516/667-7900

Published based on information available January 28, 1993.

Luncheon Service

The Society gratefully acknowledges a generous contribution received in support of Monday's Luncheon from **Berlex Imaging.**

Scientific Poster Exhibits Reception

The Society gratefully acknowledges a generous contribution received in support of this event from **Toshiba America Medical Systems, Inc.**

BERLEX IMAGING®

Kodak

PICKER

TOSHIBA

SQUIBB™
Diagnostics

MR

1993 Annual Meeting Acknowledgements

Educational Grants

The Society gratefully acknowledges the generous grants received in support of educational and scientific programs at the Annual Meeting from the following corporate sponsors:

Fischer Imaging Corp.

General Electric Medical Systems, Inc.

Hitachi Medical Systems America, Inc.

Mallinckrodt Medical, Inc.

Philips Medical Systems North America Co.

Picker International, Inc.

Resonex, Inc.

Sanofi Winthrop Pharmaceuticals

Siemens Medical Systems, Inc.

Squibb Diagnostics, Inc.

sanofi WINTHROP

Annual Meeting Totes

The Society gratefully acknowledges a generous contribution received in support of Annual Meeting tote distribution from **Squibb Diagnostics, Inc.**

Audiovisual Services

The Society gratefully acknowledges a generous contribution received in support of audiovisual services from **Eastman Kodak Company.**

MALLINCKRODT
MEDICAL

HITACHI

GE Medical Systems

SIEMENS

PHILIPS

RESONEX

FISCHER IMAGING
CORPORATION

1993 ANNUAL MEETING COMMENTS

The 1993 Annual Meeting Organizing Committee would appreciate receiving your comments regarding the 1993 Annual Meeting in San Francisco. Those comments will be collated and forwarded to the 1994 Annual Meeting Organizing Committee for possible incorporation in next year's educational programming. While your comments may also be provided on the Evaluation/CME Accreditation Form distributed at each session, please let us know your thoughts regarding the following:

1. Which Program did you attend? ____________________

2. Did it meet its stated objectives? ______ Yes ______ No. Why? ____________________

3. What should have been included in the Program that was not? ____________________

4. What should have been excluded from the Program? ____________________

5. What Program revisions would you like to see implemented next year? ____________________

6. General Comments: ____________________

Please return this form to the **SMRI** Registration Area, Ballroom Level, of the San Francisco Hilton and Towers by Wednesday, March 31, or mail it to the **SMRI** Central Office at the following address:

Society for Magnetic Resonance Imaging
213 West Institute Place, Suite 501
Chicago, Illinois 60610 USA

Key to Abbreviations in Author Index

A–award presentations

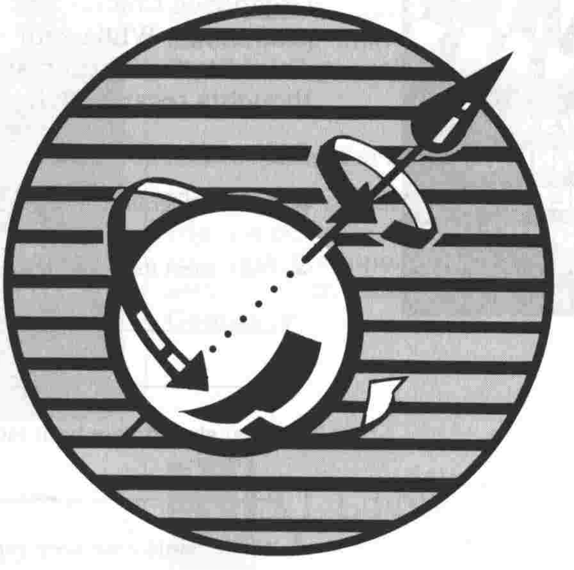

#–proffered papers

PS–plenary symposia

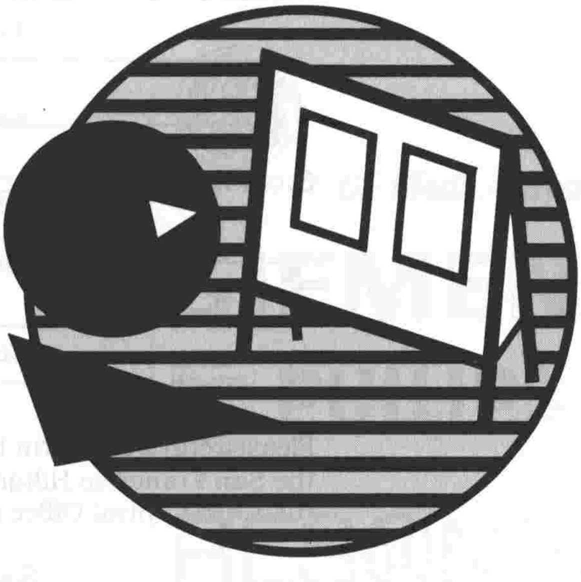

P–scientific poster presentations

Key to abbreviations:
A–award presentations
PS–plenary symposia
#–proffered papers
P–scientific poster presentations

Author Index

DALLAS

SMRI

Society for Magnetic Resonance Imaging

MARCH 5-9, 1994

1994 ANNUAL MEETING

Future Meetings

1995 • March 25-29 • Washington, DC
1996 • April 20-26 • Vancouver, BC

SMRI

Society for Magnetic Resonance Imaging
213 West Institute Place
Suite 501
Chicago, IL 60610
312/751-2590

COMBINED SECTION FOR MAGNETIC RESONANCE TECHNOLOGISTS
SMRT

Membership Application

The Society of Magnetic Resonance in Medicine, Inc., and the Society for Magnetic Resonance Imaging, Inc., non-profit professional associations, combined efforts in 1991 and formed the Section for Magnetic Resonance Technologists. SMRT is devoted to advancing the education, training and quality of Magnetic Resonance Technologists, to promoting world-wide communication of information in the field of Magnetic Resonance, and to establishing a forum for dissemination of this information.

Annual Meetings of SMRT

San Francisco (1991)
New York (1992)
New York (1993)

____
Sponsor #1 Name (please print)

____
Sponsor #1 Signature

____
Sponsor #1 Society Affiliation

____
Sponsor #2 Name (please print)

____
Sponsor #2 Signature

____
Sponsor #2 Society Affiliation

Membership Benefits

Technologist Membership in the Society of Magnetic Resonance in Medicine and the Society for Magnetic Resonance Imaging.

The journals, Magnetic Resonance in Medicine (published monthly) and/or Journal of Magnetic Resonance Imaging (published bimonthly) at a special SMRT member's rate. Subscriptions begin with the January issue for applications **completed** January 1 through September 30 and with the January issue of the following year for applications **completed** October 1 through December 31. Subscription to the journal(s) is optional.

SMRT Newsletter, *Signals*, (published biannually) will bring you the latest technical and educational news breakthroughs, as well as information on upcoming SMRT events.

SMRT Membership Directory, published annually.

Advance notice and substantially reduced registration fees for the Annual Meeting and SMRT workshops, as well as SMRM and SMRI meetings and workshops.

Membership Categories and Qualifications (please check one category). Prior to final acceptance by the SMRT Policy Board, each application is reviewed by the Membership Committee for verification of eligibility.

☐ **Technologist (Voting) Member:**

An individual who (i) shares the stated purposes of the SMRT, (ii) is (A) certified by the American Registry of Radiologic Technologists, (B) a Registered Diagnostic Medical Sonographer, (C) a Certified Nuclear Medicine Technologist, (D) or certified by an equivalent professional certifying organization; and (iii) has practiced as a technologist in the field of magnetic resonance for a minimum of one year. Members have the right to vote and hold office. The applicant must submit a current resume and verification of the above qualifications. Sponsorship: Endorsement of two or more voting members of the SMRT, of the SMRM or of the SMRI; OR if the individual (i) shares the stated purposes of the SMRT, (ii) can demonstrate appropriate equivalent professional competence in radiologic practice or in work in support of biochemical, biophysical or biological programs, (iii) and has practiced as a magnetic resonance technologist for a minimum of two years. The applicant must submit a current resume, as well as a letter of verification from their department head or administrator verifying two years practice in an NMR modality. Sponsorship: Endorsement of two or more voting members of the SMRT, of the SMRM or of the SMRI.

☐ **Technologist (Non-Voting) Member:**

An individual who shares the stated purposes of the SMRT, but does not meet the qualifications for voting membership. The applicant must submit a current resume. Sponsorship: Endorsement of one or more voting members of the SMRT, of the SMRM or of the SMRI.

ID # FOR OFFICE USE ONLY

Please mail your completed application, membership fee, current resume and, if applicable, letter of verification to:

SMRT
Combined Section for Magnetic Resonance Technologies

Membership Coordinator
1918 University Avenue
Suite 3C
Berkeley, CA 94704 U.S.A.
Telephone (510) 841-1899
Fax (510) 841-2340

(Please Print Legibly) Date ____________

Name ____________

Degree ____________ Title ____________

Address (**Check preferred journal mailing address**)

☐ Office ____________
____
Country ____________ Telephone ( )
Fax ( )

☐ Home ____________
____
Country ____________ Telephone ( )
Fax ( )

ALL APPLICANTS, please answer the following:

Are you currently working in the field of MRI? ☐ yes ☐ no Date you were registered as an R.T. ___ / ___ / ___

Please list the type of scanners used: ____________
____

Other Professional Affiliations: ☐ AAN ☐ AAPM ☐ ACR ☐ ARRS ☐ ASNR ☐ ASRT
☐ ESMRMB ☐ RSNA ☐ SMRI ☐ SNM ☐ Other

Dues Payment

$70.00 per year for Technologist [ ] Voting [ ] Non-Voting
$125.00 per year for Technologist [ ] Voting [ ] Non-Voting with Journal, **Magnetic Resonance in Medicine**
$120.00 per year for Technologist [ ] Voting [ ] Non-Voting with Journal, **Journal of Magnetic Resonance Imaging**
$175.00 per year for Technologist [ ] Voting [ ] Non-Voting with Both Journals

Payment Methods:

Check: Must be payable "to" (not "through") a U.S. Bank in U.S. dollars and must be imprinted with the computer encoding and routing information authorized by the American Banking Association Please make checks payable to SMRT.

Travelers check: Travelers' checks in U.S. dollars for the exact amount, properly countersigned are acceptable.

International Money Order: Must be in U.S. dollars and must be imprinted with the computer encoding and routing information as authorized by the American Banking Association. U.S. dollar International Postal Money Orders imprinted as stated above are acceptable.

Credit Cards: Visa, Mastercard and Eurocard are accepted. To pay by card, please check: Visa ☐ Mastercard ☐ Eurocard ☐

Card #: ____________ Expiration Date ___ /___ Signature: ____________

DO NOT PAY BY WIRE.

MEMBERSHIP APPLICATION

SMRI

Society for Magnetic Resonance Imaging

The organizational goals of this Society are to:

- Provide an equal opportunity to physicians and basic scientists to contribute to the development of MRI.
- Provide an international multidisciplinary forum for the advancement of magnetic resonance imaging.
- Promote the applications of magnetic resonance techniques to medicine and biology, with special emphasis on imaging.
- Prepare and disseminate technical and product information related to research techniques, equipment and clinical applications of magnetic resonance.
- Develop educational and training material and methods for the application of magnetic resonance to medicine and biology.

All individuals involved in the field of magnetic resonance imaging are invited to join the Society.

The classifications of membership are defined as follows:

FULL: A person who shares the stated purpose of the Society, who is involved in the field of magnetic resonance imaging, and who has completed postgraduate studies or equivalent training in any subject or work of significant merit in the area of magnetic resonance.

TECHNOLOGIST: A person who shares the stated purpose of the Society and who has technical or professional background in the area of magnetic resonance imaging or an allied field.

STUDENT: A person who shares the stated purpose of the Society and who is engaged in full-time study, graduate or undergraduate.

CORPORATE: A corporate entity that has a major interest in the development and application of NMR instrumentation in MRI or MRS for medical or biological purposes. Selection to corporate membership must be confirmed by 2/3 vote of the Board members present at the meeting following application for such membership.

ASSOCIATE: A person who shares the stated purpose of the Society, but does not qualify for other categories of membership.

The Full, Associate and Corporate membership rates include a subscription to the bimonthly journal, **Journal of Magnetic Resonance Imaging**. Those applying for membership categories of Technologist and Student may obtain a subscription to the Journal by remitting an additional $50. In order to be considered for MEMBERSHIP, please provide the information requested on the reverse side. Please note: two sponsors, either **SMRI**-member or non-member collegues, must be listed on each application.

PLEASE SEND THESE THREE IMPORTANT ITEMS WITH THIS APPLICATION:

1. **Completed Candidate Information Form** (see reverse),
2. **Your curriculum vitae; and,**
3. **Appropriate remittance to:**

Membership Department
Society for Magnetic Resonance Imaging
213 West Institute Place, Suite 501
Chicago, Illinois 60610

SMRI

SOCIETY FOR MAGNETIC RESONANCE IMAGING

CANDIDATE INFORMATION FORM

In order to be considered for MEMBERSHIP, please provide the information requested below. A complete curriculum vitae of your education, employment and publications MUST accompany this application.

1. Name: (first)

(middle)

(last)

Degree:

2. Address:

City/State/Zip/Country:

Tel. ( )

Fax ( )

This information is your (☐ office or ☐ home) address, telephone and fax number.

Employed By/Affiliated With:

Title/Job Position:

3. Sponsor I (mandatory*):
Name:

Tel. No.:

Sponsor II (mandatory*):
Name:

Tel. No.

*does not need to be a **SMRI** member

SMRI

4. Classification Codes: (Enter code which best describes your professional classification.)

A. Clinical scientist (specialty)

B. Basic scientist (specialty)

C. Resident/trainee (specialty)

D. Radiology Support Personnel and Hospital Staff:
(a) technologist,
(b) engineer,
(c) radiology business manager,
(d) radiology administrator,
(e) nurse,
(f) hospital administrator,
(g) radiology educator,
(h) hospital purchasing agent.

E. Qualified Non-Health Sciences Personnel:
(a) architect,
(b) computer analyst,
(c) investment banker.

F. Non-Hospital-Based Medical Care Provider:
(a) purchasing consultant,
(b) equipment consultant,
(c) imaging center entrepreneur.

5. Professional Affiliations:

(a) AAN
(b) AAPM
(c) ACR
(d) ARRS
(e) ASNR
(f) ASRT
(g) ESMRM3
(h) JMRM
(i) RSNA
(j) SMRM
(k) SNM

6. Please check your area of specialty from the following fields of study:
☐ **M.D.**: Radiology, Neurology, Cardiology, Other:
☐ **Ph.D.**: Physics, Bio-Chemistry, Spectroscopy, Biology, Other:
☐ **Other:**

7. Please check your primary workplace from those listed below:
☐ University Hospital/Medical School
☐ Industry
☐ Private Hospital/Clinic
☐ Hospital/Clinic:
☐ Number of Beds
☐ Government Lab
☐ Other:

8. Please check appropriate Membership Classification:
☐ Full($100)
☐ Technologist($25)
☐ Student($25)
☐ Associate($100)

☐ I am applying for Student or Technologist Membership and am enclosing an additional $50.00 for a subscription to the **Journal of Magnetic Resonance Imaging**.

Signature:

Date

(**SMRI** C/O)

Extremely Important

REMEMBER!
Your application package MUST include all of the following elements before approval procedures may begin:

Completed Application, with two sponsors listed (**SMRI**-member or non-member collegues required)
Curriculum Vitae
Membership Fee

SMRI

SOCIETY FOR MAGNETIC RESONANCE IMAGING

MR

1993 ANNUAL MEETING COMMENTS

The 1993 Annual Meeting Organizing Committee would appreciate receiving your comments regarding the 1993 Annual Meeting in San Francisco. Those comments will be collated and forwarded to the 1994 Annual Meeting Organizing Committee for possible incorporation in next year's educational programming. While your comments may also be provided on the Evaluation/CME Accreditation Form distributed at each session, please let us know your thoughts regarding the following:

1. Which Program did you attend? ______________________________

2. Did it meet its stated objectives? ______ Yes ______ No. Why? ______________________________

____

____

3. What should have been included in the Program that was not? ______________________________

____

4. What should have been excluded from the Program? ______________________________

____

5. What Program revisions would you like to see implemented next year? ______________________________

____

____

____

6. General Comments: ______________________________

____

____

Please return this form to the **SMRI** Registration Area, Ballroom Level, of the San Francisco Hilton and Towers by Wednesday, March 31, or mail it to the **SMRI** Central Office at the following address:

Society for Magnetic Resonance Imaging
213 West Institute Place, Suite 501
Chicago, Illinois 60610 USA

Finally.
Total
abdominal
screening
in less
than
2 minutes.

MR

At Philips, the measure of a system is not only how fast it obtains an image. But also how much it improves diagnostic confidence. Expands clinical applications. And enhances throughput and efficiency. ▪ By all measures, GYROSCAN S15/ACS is setting the standard in MR today. And in the process, expanding MR's role from advanced problem-solver to screening modality of choice. ▪ Evaluate the S15/ACS for yourself. See how it eliminates motion artifacts in abdominal studies. Notice the superior contrast and resolution of its head and joint studies. And pay particular attention to today's most advanced cardio, angio and FAST Scan packages. ▪ You'll understand why GYROSCAN S15/ACS is today's most promising platform for future MR developments. ▪ For all the details, just call **1-800-999-5883, ext. 26.**

GYROSCAN S15/ACS will quickly and economically incorporate new applications and advances in technology thanks, in part, to this unique removable body coil.

FINDING THE ANSWER. MAKING IT WORK.

LIFETIME MEDICAL TELEVISION

Sponsor of Lifetime's
Radiology Update
Sundays at 2 pm, ET/PT.
Check local listings.

CT • PACS • DIGITAL • VASCULAR • MR • ULTRASOUND • R/F • RADIOGRAPHY • MAMMOGRAPHY • CARDIOVASCULAR • COMPUTED RADIOGRAPHY • THERAPY • SURGERY • UROLOGY • CT • PACS • DIGITAL • VASCU

Philips Medical Systems

PHILIPS

PHILIPS

JMRI • SMRI 1993 PRINTED PROGRAM ■ Volume 3 (P)

PAGES 1–182